NASA Technical Memorandum 106825

Turbulent Fluid Motion V—Fourier Analysis, the Spectral Form of the Continuum Equations, and Homogeneous Turbulence

Robert G. Deissler
Lewis Research Center
Cleveland, Ohio

August 1996

National Aeronautics and
Space Administration

TURBULENT FLUID MOTION V—

Fourier Analysis, The Spectral Form of The Continuum Equations, and Homogeneous Turbulence

Robert G. Deissler
National Aeronautics and Space Administration
Lewis Research Center
Cleveland, Ohio 44135

SUMMARY

Background material on Fourier analysis and on the spectral form of the continuum equations, both averaged and unaveraged, are given. The equations are applied to a number of cases of homogeneous turbulence with and without mean gradients. Spectral transfer of turbulent activity between scales of motion is studied in some detail. The effects of mean shear, heat transfer, normal strain, and buoyancy, are included in the analyses.

INTRODUCTION

In chapter I it was pointed out that turbulence is multiscaled. That is, it consists of small eddies (small-scale motion) superimposed on larger-scale motion. In order to proceed with our study of the dynamics of turbulence, we should consider how the turbulent activity is distributed among the various scales of motion, together with the interaction, if any, of those scales.

One possible (the usual) way of representing scales of motion is by means of a series of trigonometric functions, that is, by a Fourier series. For example, one might write a turbulent velocity u as

$$u = \sum_{\kappa=1}^{\infty} \left(A_\kappa \cos \kappa x + B_\kappa \sin \kappa x \right),$$

where x is a distance, κ is known as the wavenumber (with dimension 1/length), and the values of the coefficients A_κ and B_κ depend on the turbulence. For simplicity the system is assumed here to be one-dimensional. Larger values of κ correspond to smaller eddies (smaller spatial scales) and vise versa.

Basis functions other than trigonometric are sometimes used to represent turbulence, particularly in numerical simulations with boundary conditions other than periodic (ref. 1). Moreover, attempts are sometimes made to represent the turbulence by functions whose shape is closer to that of a typical eddy (if such can be defined) than is that of trigonometric functions (refs. 2 and 3). For instance the steep instantaneous gradients which are known to occur in turbulent flows, particularly at high Reynolds numbers, might be incorporated into the basis function. However, most of the work on turbulence has used trigonometric basis functions (see e.g., ref. 4), and those will be adequate for our purposes.

In addition to using Fourier analysis for instantaneous turbulent quantities, one can use it to analyze averaged quantities, such as those in the two-point correlation equations (section 4.3.4). Since the latter are easier to deal with than unaveraged quantities, which may require the use of generalized functions, they will be considered first.

5.1 FOURIER ANALYSIS OF THE TWO-POINT AVERAGED CONTINUUM EQUATIONS

5.1.1 Analysis of Two-Point Averaged Quantities

One can decompose the two-point velocity correlation $\overline{u_i\, u_j'}\,(\mathbf{r})$ into a three-dimensional series of trigonometric functions (eddy sizes) as follows:

$$\overline{u_i\, u_j'}(\mathbf{r}) = \sum_{\kappa=-\infty}^{\infty} \left(\varphi_{ij}\right)_{\kappa} e^{i\kappa\cdot\mathbf{r}}, \tag{5-1}$$

where the trigonometric series has been written in complex notation by using the Euler relation

$$e^{i\kappa\cdot\mathbf{r}} = \cos\kappa\cdot\mathbf{r} + i\sin\kappa\cdot\mathbf{r}, \tag{5-2}$$

and where u_i and u_j' are velocity components at two points which are separated by the vector $\mathbf{r}$, κ is a wavevector, $\kappa\cdot\mathbf{r} = \kappa_k r_k = \kappa_1 r_1 + \kappa_2 r_2 + \kappa_3 r_3$ is the dot product of the vectors κ and $\mathbf{r}$, and the $(\varphi_{ij})_{\kappa}$ are called Fourier coefficients. The $(\varphi_{ij})_{\kappa}$ are complex because of the presence of the complex exponential in equation (5-1), and because $\overline{u_i\, u_j'}\,(\mathbf{r})$ is real. To simplify the notation, possible dependencies on $\mathbf{x}$ and time have been omitted. The summation in equation (5-1) is taken separately over each component of κ.

To determine the coefficients $(\varphi_{ij})_{\kappa}$ multiply both sides of equation (5-1) by $e^{-n\cdot\mathbf{r}}$ and by $d\mathbf{r} = dr_1 dr_2 dr_3$. Then, integrating over the period 2π for each component of $\mathbf{r}$, we get

$$\left(\varphi_{ij}\right)_{\kappa} = \frac{1}{(2\pi)^3} \int_{-\pi}^{\pi} \overline{u_i\, u_j'}(\mathbf{r})\, e^{-\kappa\cdot\mathbf{r}}\, d\mathbf{r}, \tag{5-3}$$

since terms for which $n_k \neq \kappa_k$ are zero because of the periodicity of $e^{(\kappa-n)\cdot\mathbf{r}}$. Equation (5-1) gives the three- dimensional Fourier-series expansion of $\overline{u_i\, u_j'}\,(\mathbf{r})$, where the $(\varphi_{ij})_{\kappa}$ are given by equation (5-3). Since $\overline{u_i\, u_j'}$ is a second-order tensor (section 2.4.1), equation (5-3) will have meaning only if $(\varphi_{ij})_{\kappa}$ is a second-order tensor (section 2.9).

If the period over which r_k is defined is R_k rather than 2π, where the three R_k are not necessarily equal, equations (5-1) and (5-3) become respectively,

$$\overline{u_i\, u_j'}(\mathbf{r}) = \sum_{\kappa=-\infty}^{\infty} \left(\varphi_{ij}\right)_{\kappa} e^{i2\pi\kappa_k r_k/R_{(k)}}, \tag{5-4}$$

and

$$\left(\varphi_{ij}\right)_{\kappa} = \frac{1}{R_1 R_2 R_3} \int_{-R_k/2}^{R_k/2} \overline{u_i\, u_j'}(\mathbf{v})\, e^{-i2\pi\kappa_k r_k/R_{(k)}} d\mathbf{v}, \tag{5-5}$$

where the dummy variable $\mathbf{r}$ on the right side of equation (5-3) has been changed to $\mathbf{v}$ to avoid later confusion.

Consider now the case where $R_k \to \infty$. To that end, substitute equation (5-5) into (5-4). That gives

$$\overline{u_i\, u_j'}\,(\mathbf{r}) = \sum_{\kappa=-\infty}^{\infty} \frac{1}{R_1 R_2 R_3}\, e^{i2\pi\kappa_k v_k/R_{(k)}} \int_{-R_k/2}^{R_k/2} \overline{u_i\, u_j'}\,(\mathbf{v})\, e^{-i2\pi\kappa_k v_k/R_{(k)}} d\mathbf{v}, \tag{5-6}$$

Next let

$$\frac{2\pi}{R_k} \equiv \Delta s_k, \tag{5-7}$$

where s_k is given by

$$s_k \equiv \kappa_k \Delta s_{(k)}, \tag{5-7a}$$

(no sum on k), and Δs_k is an increment of s_k. From equations (5-7) and (5-7a),

$$s_k = \frac{2\pi\kappa_k}{R_{(k)}}, \tag{5-7b}$$

showing that s_k varies linearly with κ_k for a given period R_k. Equation (5-6) can then be written as

$$\overline{u_i\, u_j'}(\mathbf{r}) = \sum_{s=-\infty}^{\infty} \left[\int_{-R_k/2}^{R_k/2} \overline{u_i\, u_j'}(\mathbf{v})\, e^{-is_k v_k} d\mathbf{v} \right] e^{is_k v_k} \frac{\Delta s_1 \Delta s_2 \Delta s_3}{(2\pi)^3}, \tag{5-8}$$

where Δs_k is given by equation (5-7). For $R_k \to \infty (\Delta s_k \to 0$, see equation (5-7)), equation (5-8) becomes

$$\overline{u_i\, u_j'}(\mathbf{r}) = \int_{-\infty}^{\infty} \left[\frac{1}{(2\pi)^3} \int_{-\infty}^{\infty} \overline{u_i\, u_j'}(\mathbf{v})\, e^{-i\mathbf{s}\cdot\mathbf{v}} d\mathbf{v} \right] e^{i\mathbf{s}\cdot\mathbf{r}} d\mathbf{s} \tag{5-9}$$

since, for each value of k (k = 1,2,3),

$$\lim_{\Delta s_k \to 0} \sum_{s_k=-\infty}^{\infty} f_{s_k} \Delta s_{(k)} = \int_{-\infty}^{\infty} f(s_k)\, ds_{(k)} \tag{5-10}$$

(no sum on k). Equation (5-10) can be considered a defintion of the definite integral $\int_{-\infty}^{\infty} f(s_k)\, ds_{(k)}$. Equation (5-9) gives the Fourier-integral representation of $\overline{u_i\, u_j'}(\mathbf{r})$.

If we let the quantity in brackets in equation (5-9) be equal to φ_{ij}, and replace the dummy variables **s** and **v** by $\boldsymbol{\kappa}$ and **r** respectively, we get

$$\overline{u_i\, u_j'}(\mathbf{r}) = \int_{-\infty}^{\infty} \varphi_{ij}(\boldsymbol{\kappa})\, e^{i\boldsymbol{\kappa}\cdot\mathbf{r}} d\boldsymbol{\kappa}, \tag{5-11}$$

and

$$\varphi_{ij}(\boldsymbol{\kappa}) = \frac{1}{(2\pi)^3} \int_{-\infty}^{\infty} \overline{u_i\, u_j'}(\mathbf{r})\, e^{-i\boldsymbol{\kappa}\cdot\mathbf{r}} d\mathbf{r}. \tag{5-12}$$

The quantity $\varphi_{ij}(\boldsymbol{\kappa})$ is the three-dimensional Fourier transform of $\overline{u_i\, u_j'}(\mathbf{r})$. Like $(\varphi_{ij})_\kappa$ in equation (5-3), it shows how spectral contributions to $\overline{u_i\, u_j'}(\mathbf{r})$ are distributed in wavenumber space. The difference between the two is that $(\varphi_{ij})_\kappa$ applies when $\overline{u_i\, u_j'}(\mathbf{r})$ is defined over a finite part of physical space (**r**-space), whereas $\varphi_{ij}(\boldsymbol{\kappa})$ applies when $\overline{u_i\, u_j'}(\mathbf{r})$ is defined over all of **r**-space. The quantity $\varphi_{ij}(\boldsymbol{\kappa})$ exists, of course, only if the integral in equation (5-12) exists, or if $\overline{u_i\, u_j'}(\mathbf{r})$ in equation (5-12) is absolutely integrable over **r** (ref. 5), but that is usually the case (see e.g., fig. 4-16). By analogy with $\varphi_{ij}(\boldsymbol{\kappa})$ (eq. (5-12)), $(\varphi_{ij})_\kappa$ (eq. (5-3)) is sometimes called the finite Fourier transform of $\overline{u_i\, u_j'}(\mathbf{r})$ (applicable when **r** remains finite (ref. 6). The treatment of the other two-point

correlations is similar. For example, the Fourier transform of the two-point (mechanical) pressure-velocity correlation $\overline{\sigma u_i'}(\mathbf{r})$ is given by the vector

$$\lambda_j(\boldsymbol{\kappa}) = \frac{1}{(2\pi)^3}\int_{-\infty}^{\infty} \overline{\sigma u_j'}(\mathbf{r})\, e^{-i\boldsymbol{\kappa}\cdot\mathbf{r}} d\mathbf{r}, \tag{5-13}$$

in place of equation (5-12), and , in place of equation (5-11), we have

$$\overline{\sigma u_j'}(\mathbf{r}) = \int_{-\infty}^{\infty} \lambda_j(\boldsymbol{\kappa})\, e^{i\boldsymbol{\kappa}\cdot\mathbf{r}} d\boldsymbol{\kappa}. \tag{5-14}$$

It is easy to show that taking the derivative of a quantity with respect to r_k multiplies its Fourier transform by $i\kappa_k$. Thus,

$$\frac{\partial}{\partial r_k}\ \overline{\sigma u_j'}(\mathbf{r}) = \int_{-\infty}^{\infty} i\kappa_k \lambda_j(\boldsymbol{\kappa})\, e^{i\boldsymbol{\kappa}\cdot\mathbf{r}} d\boldsymbol{\kappa}, \tag{5-15}$$

or

$$i\kappa_k \lambda_j(\boldsymbol{\kappa}) = \frac{1}{(2\pi)^3}\int_{-\infty}^{\infty} \frac{\partial}{\partial r_k}\ \overline{\sigma u_j'}(\mathbf{r})\, e^{-i\boldsymbol{\kappa}\cdot\mathbf{r}} d\mathbf{r}. \tag{5-16}$$

Next we obtain the spectral form of the two-point averaged continuum equations.

5.1.2 Analysis of the Two-Point Correlation Equations

To convert to spectral form the two-point correlation equations obtained in the last chapter (eqs. (4-147) to (4-150)), we multiply those equations through by $[1/(2\pi)^3]e^{-i\kappa\cdot r}dr$ and integrate from $-\infty$ to $+\infty$. That gives

$$\frac{\partial}{\partial t}\varphi_{ij}+\varphi_{kj}\frac{\partial U_i}{\partial x_k}+\varphi_{ik}\frac{\partial U_j'}{\partial x_k'}+(U_k'-U_k)i\kappa_k\varphi_{ij}+\left[(1-n)U_k+nU_k'\right]\frac{\partial}{\partial(x_k)_n}\varphi_{ij}$$

$$+\frac{1}{\rho}\left[\frac{\partial}{\partial(x_i)_n}\lambda_j+\frac{\partial}{\partial(x_j)_n}\lambda_i'\right]+\frac{\partial}{\partial(x_k)_n}\left[n\varphi_{ijk}'+(1-n)\varphi_{ikj}\right]+i\kappa_k\left(\varphi_{ijk}'-\varphi_{ikj}\right) \tag{5-17}$$

$$=\frac{1}{\rho}\left[n\frac{\partial}{\partial(x_i)_n}\lambda_j+(1-n)\frac{\partial}{\partial(x_j)_n}\lambda_i'-i\kappa_j\lambda_i'+i\kappa_i\lambda_j\right]$$

$$+\left(1-2n+2n^2\right)\nu\frac{\partial^2\varphi_{ij}}{\partial(x_k)_n\,\partial(x_k)_n}-2(1-2n)\nu i\kappa_k\frac{\partial\varphi_{ij}}{\partial(x_k)_n}-2\nu\kappa^2\varphi_{ij},$$

$$\frac{1}{\rho}\left[n^2\frac{\partial^2\lambda_i'}{\partial(x_j)_n\,\partial(x_j)_n}+2ni\kappa_j\frac{\partial\lambda_i'}{\partial(x_j)_n}-\kappa^2\lambda_i'\right]=-2\frac{\partial U_j'}{\partial x_k'}\left[n\frac{\partial\varphi_{ik}}{\partial(x_j)_n}+i\kappa_j\cdot\varphi_{ik}\right] \tag{5-18}$$

$$-n^2\frac{\partial^2\varphi_{ijk}'}{\partial(x_j)_n\,\partial(x_k)_n}-ni\kappa_k\frac{\partial\varphi_{ijk}'}{\partial(x_j)_n}-ni\kappa_j\frac{\partial\varphi_{ijk}'}{\partial(x_k)_n}+\kappa_j\kappa_k\varphi_{ijk},$$

and

$$\frac{1}{\rho}\left[(1-n)^2\frac{\partial^2\lambda_j}{\partial(x_i)_n\,\partial(x_i)_n}-2(1-n)i\kappa_i\frac{\partial\lambda_j}{\partial(x_i)_n}+\kappa^2\lambda_j\right]=-2\frac{\partial U_i}{\partial x_k}\left[(1-n)\frac{\partial\varphi_{kj}}{\partial(x_i)_n}-i\kappa_i\varphi_{kj}\right] \tag{5-19}$$

$$-(1-n)^2\frac{\partial^2\varphi_{ikj}}{\partial(x_i)_n\,\partial(x_k)_n}+(1-n)i\kappa_k\frac{\partial\varphi_{ikj}}{\partial(x_i)_n}+(1-n)i\kappa_i\frac{\partial\varphi_{ikj}}{\partial(x_k)_n}+\kappa_i\kappa_k\varphi_{ikj},$$

where φ_{ij} and λ_j are given respectively by equations (5-12) and (513). Similarly,

$$\lambda_i'(\kappa)=\frac{1}{(2\pi)^3}\int_{-\infty}^{\infty}\overline{u_i\sigma'}(r)\,e^{-i\kappa\cdot r}dr, \tag{5-20}$$

$$\varphi_{ikj}(\kappa) = \frac{1}{(2\pi)^3}\int_{-\infty}^{\infty} \overline{u_i u_k u_j'}(\mathbf{r})\, e^{-i\kappa\cdot\mathbf{r}} d\mathbf{r}, \tag{5-21}$$

and

$$\varphi'_{ijk}(\kappa) = \frac{1}{(2\pi)^3}\int_{-\infty}^{\infty} \overline{u_i u_j' u_k'}(\mathbf{r})\, e^{-i\kappa\cdot\mathbf{r}} d\mathbf{r}, \tag{5-22}$$

where n and $\mathbf{x}_n$ are defined in figure (4-17), and functional dependencies on $\mathbf{x}_n$ and t are understood. Finally, the equation for the mean velocity (eq. (4-151)) can be written in spectral form as

$$\frac{\partial U_i}{\partial t} + U_k \frac{\partial U_i}{\partial x_k} = -\frac{1}{\rho}\frac{\partial P}{\partial x_i} + \frac{\partial}{\partial x_k}\left[\nu \frac{\partial U_i}{\partial x_k} - \int_{-\infty}^{\infty} \varphi_{ik}(\kappa) d\kappa\right], \tag{5-23}$$

where $\overline{u_i u_k}$ has been eliminated by letting $\mathbf{r} = 0$ in equation (5-11).

Equations (5-17) to (5-19), and equation (5-23), constitute the two-point spectral equations for inhomogeneous turbulence with mean-velocity gradients. Note that these equations have a simpler form than the correlation equations, because derivatives with respect to $\mathbf{r}$ or κ are absent. However, the introduction of spectral quantities does not alleviate the closure problem. As was the case for the correlation equations, these spectral equations do not form a complete set; the Fourier transforms of the triple correlations are left undetermined. If the turbulence is sufficiently weak, and/or some of the mean gradients are sufficiently large, it may be possible to neglect the triple-correlation terms.

As was the case for the Poisson equations (4-149) and (4-150), the terms on the right side of equations (5-18) and (5-19) are source terms associated with the mean velocity and triple correlations. The interpretation of most of the terms in equation (5-17) is also similar to that of terms in the two-point correlation equations. Thus, equation (5-17) contains turbulence-production, convection, viscous, diffusion, and directional-transfer terms.

5.1.2.1 *The spectral-transfer terms in equations (4-147) or (5-17).*—It was indicated in section 4.3.4 that the two-point equation (4-147) contains, in addition to the terms mentioned in the last paragraph, the new terms $-\partial\left(\overline{u_i u_j' u_k'} - \overline{u_i u_k u_j'}\right)/\partial r_k$ and $\left(U_k' - U_k\right)\partial\overline{u_i u_j'}/\partial r_k$ which do not have counterparts in the one-point equation (4-140), and which require spectral analysis for their interpretation. The Fourier transforms of those terms, as given in the spectral equation (5-17) are, respectively,

$$-i\kappa_k\left(\varphi'_{ijk} - \varphi_{ikj}\right) \equiv T_{ij}(\kappa, \mathbf{x}_n) = \frac{1}{(2\pi)^3}\int_{-\infty}^{\infty}\left[-\partial\left(\overline{u_i u_j' u_k'} - \overline{u_i u_k u_j'}\right)/\partial r_k\right] e^{-i\kappa\cdot\mathbf{r}} d\mathbf{r}, \tag{5-24}$$

and

$$-\left(U_k' - U_k\right)i\kappa_k\varphi_{ij} \equiv T'_{ij}(\kappa, \mathbf{x}_n) = \frac{1}{(2\pi)^3}\int_{-\infty}^{\infty}\left[-\left(U_k' - U_k\right)\partial\overline{u_i u_j'}/\partial r_k\right] e^{-i\kappa\cdot\mathbf{r}} d\mathbf{r}, \tag{5-25}$$

where $\mathbf{x}$ is included in the functional designations for T_{ij} and T'_{ij} to emphasize that the turbulence can be inhomogeneous.

Consider first the term $T_{ij}(\kappa, \mathbf{x}_n)$, which is the three-dimensional Fourier transform of the turbulence self-interaction term $-\partial\left(\overline{u_i u_j' u_k'} - \overline{u_i u_k u_j'}\right)/\partial r_k$. That term should be absolutely integrable over $\mathbf{r}$ in order for its Fourier transform to exist (ref. 5). Moreover, if a wall is present in the flow, a finite Fourier transform with respect to the component of $\mathbf{r}$ normal to the wall would be appropriate (eq. (5-3)) (see discussion following eq. (5-12) and ref. 6).

We want to interpret the term $T_{ij}(\kappa, \mathbf{x}_n)$. To that end, referring to figure 4-17, one notes that

$$\mathbf{x} + \mathbf{r} = \mathbf{x}', \qquad \mathbf{x} + n\mathbf{r} = \mathbf{x}_n$$

from which

$$\mathbf{x}_n + n\mathbf{x}' + (1-n)\mathbf{x}.$$

In subscript notation,

$$r_k = x_k' - x_k, \tag{5-26}$$

and

$$\left(x_k\right)_n = nx_k + (1-n)x'_k, \tag{5-27}$$

where n is a number between 0 and 1. By using eqs. (5-26) and (5-27) and the rules for partial differentiation, one obtains

$$\frac{\partial}{\partial x_k} = (1-n)\frac{\partial}{\partial\left(x_k\right)_n} - \frac{\partial}{\partial r_k}, \tag{5-28}$$

and

$$\frac{\partial}{\partial x'_k} = n\frac{\partial}{\partial\left(x_k\right)_n} + \frac{\partial}{\partial r_k}. \tag{5-29}$$

Taking the transform of equation (5-24), and solving (5-28), and (5-29) for $\partial/\partial r_k$, one can write

$$\int_{-\infty}^{\infty} T_{ij}\left(\kappa, x_n\right)e^{i\kappa\cdot r}d\kappa = -\frac{\partial}{\partial r_k}\overline{u_i u'_j u'_k} + \frac{\partial}{\partial r_k}\overline{u_i u_k u'_j}$$

$$= \left(-\frac{\partial}{\partial x'_k} + n\frac{\partial}{\partial\left(x_k\right)_n}\right)\overline{u_i u'_j u'_k} + \left(-\frac{\partial}{\partial x_k} + (1-n)\frac{\partial}{\partial\left(x_k\right)_n}\right)\overline{u_i u_k u'_j} \tag{5-30}$$

$$= -\overline{u_i u'_k\frac{\partial u'_j}{\partial x'_k}} - \overline{u'_j\frac{\partial}{\partial x_k}u_i u_k} + \frac{\partial}{\partial\left(x_k\right)_n}\left(n\overline{u_i u'_j u'_k} + (1-n)\overline{u_i u_k u'_j}\right),$$

where the continuity condition $\partial u_k/\partial x_k = 0$ and the fact that quantities at one point are independent of the position of the other point were used. Equation (5-30) becomes, for $\mathbf{r} = 0$,

$$\int_{-\infty}^{\infty} T_{ij}\left(\kappa, x_n\right)d\kappa = -\left(\overline{u_i u_k\frac{\partial u_j}{\partial x_k} + u_j\frac{\partial}{\partial x_k}u_i u_k}\right) + \frac{\partial}{\partial x_k}\overline{u_i u_j u_k} \tag{5-31}$$

$$= -\frac{\partial}{\partial x_k}\overline{u_i u_j u_k} + \frac{\partial}{\partial x_k}\overline{u_i u_j u_k} = 0,$$

since, for $\mathbf{r} = 0$, $x_k = x'_k = (x'_k)_n$. Therefore, even for a general inhomogeneous turbulence, T_{ij}, when integrated over all wavenumbers, gives zero contribution to the rate of change of $\overline{u_i u_j}$ (see eqs. (4-147) and (5-30)). Thus, $T_{ij}(\kappa, x_n)$ can only transfer Fourier components of $\overline{u_i u_j}$ (energy for i = j) from one part of wavenumber space to another.

The quantity $T'_{ij}(\kappa, x_n)$ (see eq. (5-25)), in contrast to $T_{ij}(\kappa, x_n)$ (which produces turbulence self-interaction), is associated with the interaction of the turbulence with the mean flow. However, both terms are related to transfer terms. We can write

$$-\left(U'_k - U_k\right)\frac{\partial}{\partial r_k}\overline{u_i u'_j} = \int_{-\infty}^{\infty} T'_{ij}\left(\kappa, x_n\right)e^{i\kappa\cdot r}d\kappa \tag{5-32}$$

where $T'_{ij}(\kappa, x_n)$ is the Fourier transform of $-(U'_k - U_k)(\partial/\partial r_k)\overline{u_i u'_j}$. Letting $r = 0$, equation (5-32) becomes

$$\int_{-\infty}^{\infty} T'_{ij}(\kappa, x_n) d\kappa = 0 \qquad (5-33)$$

since, for $r = 0$, $U'_k = U_k$. Thus, as in the case of $T_{ij}(\kappa, x_n)$, $T'_{ij}(\kappa, x_n)$ gives zero total contribution to the rate of the change of $\overline{u_i u_j}$ (energy for i = j) and can only alter the distribution in wavenumber space of contributions to $\overline{u_i u_j}$. We first interpreted and calculated $T'_{ij}(\kappa)$ as a transfer term for homogeneous turbulence in reference 7. (Craya (ref. 8) also discusses, in a general way, the modification of homogeneous turbulence by uniform mean gradients, but does not show that T'_{ij} is specifically a spectral-transfer term.)

The quantities T_{ij} and T'_{ij}, defined respectively in equations (5-24) and (5-25), appear to be the only terms in the evolution equation (5-17) which can be interpreted as spectral-transfer terms. As mentioned earlier, the other terms are interpretable as production, convection, directional-transfer, diffusion, and dissipation terms.

The transfer of turbulent activity from one part of wavenumber space to another, or from one eddy size to another, produces a wide range of scales of motion in most turbulent flows. The state of affairs is neatly summarized in a nonmathematical way by a poem written long before equations (5-17), (5-31), or (5-33) were known (ref. 9):

Big whorls have little whorls,
Which feed on their velocity;
And little whorls have lesser whorls,
And so on to viscosity.

As will be seen later (e.g., sections 5.3.2.2 and 5.4.2.1), both T_{ij} and T'_{ij} generally (although not always (see fig. (5.61)) transfer turbulent activity from larger to smaller scales of motion, where it can be dissipated more readily. Thus, T_{ij} and T'_{ij} ordinarily have stabilizing effects.

5.2 FOURIER ANALYSIS OF THE UNAVERAGED (INSTANTANEOUS) CONTINUUM EQUATIONS

5.2.1 Analysis of Instantaneous Quantities

Consider now the Fourier (spectral) analysis of an instantaneous quantity such as the velocity $u_i(\mathbf{x})$. If u_i is defined only for x_k between $-\pi$ and π, one can represent $u_i(\mathbf{x})$ by means of a Fourier series (finite Fourier transform (ref. 6)). Then, in place of equations (5-1) and (5-3) one has, respectively

$$u_i(\mathbf{x}) = \sum_{\boldsymbol{\kappa}=-\infty}^{\infty} (\varphi_i)_{\boldsymbol{\kappa}}\, e^{i\boldsymbol{\kappa}\cdot\mathbf{x}} d\boldsymbol{\kappa}, \tag{5-34}$$

and

$$(\varphi_i)_{\boldsymbol{\kappa}} = \frac{1}{(2\pi)^3} \int_{-\pi}^{\pi} u_i(\mathbf{x})\, e^{-i\boldsymbol{\kappa}\cdot\mathbf{x}} d\mathbf{x}. \tag{5-35}$$

If, instead of being defined over a finite portion of physical space, $u_i(\mathbf{x})$ is defined for x_k from $-\infty$ to $+\infty$, one might suppose that equations (5-34) and (5-35) would become a Fourier-transform pair such as that given by equations (5-11) and (5-12). Thus, one might write

$$u_i(\mathbf{x}) = \int_{-\infty}^{\infty} \varphi_i(\boldsymbol{\kappa}) e^{i\boldsymbol{\kappa}\cdot\mathbf{x}} d\boldsymbol{\kappa}, \tag{5-36}$$

and

$$\varphi_i(\boldsymbol{\kappa}) = \frac{1}{(2\pi)^3} \int_{-\infty}^{\infty} u_i(\mathbf{x}) e^{-i\boldsymbol{\kappa}\cdot\mathbf{x}} d\mathbf{x}, \tag{5-37}$$

where $\varphi_i(\boldsymbol{\kappa})$ is the Fourier transform of $u_i(\mathbf{r})$. However, $\varphi_i(\boldsymbol{\kappa})$ as given by equation (5-37) may not exist in the ordinary sense, since the integral in that equation can be infinite (in contrast to the integral in equation (5-12)). That happens when the strength of the velocity fluctuation $u_i(\mathbf{x})$ in equation (5-37) does not approach zero sufficiently fast as $|\mathbf{x}| \to \infty$ (for example, when $u_i(\mathbf{x})$ is a stationary random function). The problem is sometimes solved by replacing the integral in equation (5-36) by a stochastic Fourier-Stieltjes integral, as in references 4 and 10. But it may be simpler to consider $\varphi_i(\boldsymbol{\kappa})$ as a generalized function (refs. 11 to 13).

Probably the simplest generalized function is the Dirac delta (or impulse) function $\delta\left(\kappa_k - q_k^m\right)$ which can, for our purposes, be defined as

$$\delta\left(\kappa_k - q_k^m\right) \equiv \lim_{g\to\infty} \frac{\sin\left[g\left(\kappa_k - q_k^m\right)\right]}{\pi\left(\kappa_k - q_k^m\right)} \tag{5-38}$$

for k = 1, 2, or 3 (no sum on k), and where q_k^m is a particular value of κ_k. Since $\delta\left(\kappa_k - q_k^m\right) \to \infty$ as $q_k^m \to \kappa_k$, it has the property that

$$\int_{-\infty}^{\infty} \delta\left(\kappa_k - q_k^m\right) a_i\left(\kappa_k\right) d\kappa_k = a_i\left(q_k^m\right), \tag{5-39}$$

where $a_i(\kappa_k)$ is a continuous function. Note also that (for one dimension),

$$\int_{-\infty}^{\infty} \delta(\kappa) d\kappa = \lim_{g\to\infty} \int_{-\infty}^{\infty} \frac{\sin g\kappa}{\pi\kappa} d\kappa = 1, \tag{5-40}$$

$$\int_{-\infty}^{\infty} e^{i\kappa x} dx = \lim_{g\to\infty} \int_{-g}^{g} (\cos\kappa x + i\sin\kappa x) dx = 2\pi\delta(\kappa), \tag{5-41}$$

and

$$\int_{-\infty}^{\infty} e^{-i\kappa x} dx = 2\pi\delta(\kappa). \tag{5-42}$$

Thus, although the integrals in equations (5-41) and (5-42) do not exist in the sense of being ordinary functions, they are equal to the generalized function $2\pi\delta(\kappa)$.

Returning now to the problem of the existence of the Fourier transform $\varphi_i(\kappa)$, as given by equation (5-37), we try replacing $u_i(x)$ by the trigonometric function $2^3 a_i e^{q^m \cdot x}$. That gives

$$\varphi_i\kappa = \frac{1}{\pi^3}\int_{-\infty}^{\infty} a_i e^{i(q^m-\kappa)\cdot x} dx = \frac{1}{\pi^3} a_i \lim_{g\to\infty} \frac{\sin\left[g\left(\kappa_1 - q_1^m\right)\right]}{\kappa_1 - q_1^m} \frac{\sin\left[g\left(\kappa_2 - q_2^m\right)\right]}{\kappa_2 - q_2^m} \frac{\sin\left[g\left(\kappa_3 - q_3^m\right)\right]}{\kappa_3 - q_3^m}$$

$$= a_i \delta\left(\kappa_1 - q_1^m\right)\delta\left(\kappa_2 - q_2^m\right)\delta\left(\kappa_3 - q_3^m\right) \equiv a_i \delta\left(\kappa - q^m\right), \tag{5-43}$$

where, as before q_k^m is a particular value of κ_k, and where equations (5-38) and (5-41) were used. Thus, by replacing $u_i(x)$ in equation (5-37) by a trigonometric function proportional to $e^{q^m \cdot x}$, we obtained an expression for $\varphi_i(\kappa)$ in terms of generalized functions. The turbulent velocity $u_i(x)$ is, in fact similar to $e^{q^m \cdot x}$, inasmuch as both quantities fluctuate as x varies. Moreover, one can allow for the fact that $u_i(x)$ varies irregularly and that it may include a mean velocity, by using a *series* of trigonometric functions. Thus, let

$$u_i(x) = \sum_{m=1}^{\infty} 2^3 a_i\left(q_k^m\right) e^{iq^m \cdot x}, \tag{5-44}$$

where the q^m and $a_i(q^m)$ are random vectors (which may include regular components). Then, instead of equation (5-43), we have

$$\varphi_i(\kappa) = \frac{1}{\pi^3}\int_{-\infty}^{\infty} \sum_{m=1}^{\infty} a_i\left(q^m\right) e^{i(q^m-\kappa)\cdot x} dx, = \frac{1}{\pi^3} \sum_{m=1}^{\infty} a_i\left(q^m\right) \lim_{g\to\infty} \frac{\sin\left[g\left(\kappa_1 - q_1^m\right)\right]}{\kappa_1 - q_1^m} \frac{\sin\left[g\left(\kappa_2 - q_2^m\right)\right]}{\kappa_2 - q_2^m} \frac{\sin\left[g\left(\kappa_3 - q_3^m\right)\right]}{\kappa_3 - q_3^m}, \tag{5-45}$$

or

$$\varphi_i(\kappa) = \sum_{m=1}^{\infty} a_i\left(q^m\right)\delta\left(\kappa_1 - q_1^m\right)\delta\left(\kappa_2 - q_2^m\right)\delta\left(\kappa_3 - q_3^m\right) \equiv \sum_{m=1}^{\infty} a_i\left(q^m\right)\delta\left(\kappa - q^m\right). \tag{5-46}$$

So, although the turbulent velocity $u_i(x)$ can be nonzero over all of x-space, its Fourier transform can exist as a generalized function; it can be written as an infinite row of deltas with random coefficients. By virtue of equation (5-38), the operations of differentiation, integration, multiplication, etc. can be applied to $\varphi_i(\kappa)$. That is, $\varphi_i(\kappa)$ can be treated much like an ordinary function. The same can be said about the Fourier transform of the turbulent pressure. It makes sense, therefore, to write the unaveraged equations of fluid motion in spectral form by considering their Fourier transforms as generalized functions, even though those transforms may not exist as ordinary functions.

5.2.2 Analysis of The Instantaneous Continuum Equations

The instantaneous equations (4-11) to (4-13) can be written, for $g_i = 0$ (no buoyancy), as

$$\frac{\partial \tilde{u}_i}{\partial t} = -\frac{\partial\left(\tilde{u}_i \tilde{u}_k\right)}{\partial x_k} - \frac{1}{\rho}\frac{\partial \tilde{\sigma}}{\partial x_i} + \nu \frac{\partial^2 \tilde{u}_i}{\partial x_k \partial x_k}, \tag{5-47}$$

$$\frac{\partial \tilde{T}}{\partial t} = -\frac{\partial\left(\tilde{T}\,\tilde{u}_k\right)}{\partial x_k} + \alpha \frac{\partial^2 \tilde{T}}{\partial x_k \partial x_k}, \tag{5-48}$$

and

$$\frac{1}{\rho}\frac{\partial^2 \tilde{\sigma}}{\partial x_1 \partial x_1} = -\frac{\partial^2\left(\tilde{u}_i \tilde{u}_k\right)}{\partial x_i \partial x_k}, \tag{5-49}$$

where ~ over a quantity indicates a total instantaneous value (mean plus fluctuating), and where the quantity σ_e drops out of the set of equations for $g_i = 0$ (see equation following (3-22)).

In order to convert equations (5-47) to (5-49) to spectral form, we write the three following Fourier-transform pairs:

$$\tilde{u}_i(\mathbf{x}) = \int_{-\infty}^{\infty} \tilde{\varphi}_i(\boldsymbol{\kappa}) e^{i\boldsymbol{\kappa}\cdot\mathbf{x}} d\boldsymbol{\kappa}, \tag{5-50}$$

$$\tilde{\varphi}_i(\boldsymbol{\kappa}) = \frac{1}{(2\pi)^3}\int_{-\infty}^{\infty} \tilde{u}_i(\mathbf{x}) e^{-i\boldsymbol{\kappa}\cdot\mathbf{x}} d\mathbf{x}; \tag{5-51}$$

$$\tilde{\sigma}(\mathbf{x}) = \int_{-\infty}^{\infty} \tilde{\lambda}(\boldsymbol{\kappa}) e^{i\boldsymbol{\kappa}\cdot\mathbf{x}} d\boldsymbol{\kappa}, \tag{5-52}$$

$$\tilde{\lambda}(\boldsymbol{\kappa}) = \frac{1}{(2\pi)^3}\int_{-\infty}^{\infty} \tilde{\sigma}(\mathbf{x}) e^{-i\boldsymbol{\kappa}\cdot\mathbf{x}} d\mathbf{x}; \tag{5-53}$$

$$\tilde{T}(\mathbf{x}) = \int_{-\infty}^{\infty} \tilde{\gamma}(\boldsymbol{\kappa}) e^{i\boldsymbol{\kappa}\cdot\mathbf{x}} d\boldsymbol{\kappa}, \tag{5-54}$$

$$\tilde{\gamma}(\boldsymbol{\kappa}) = \frac{1}{(2\pi)^3}\int_{-\infty}^{\infty} \tilde{T}(\mathbf{x}) e^{-i\boldsymbol{\kappa}\cdot\mathbf{x}} d\mathbf{x}. \tag{5-55}$$

The $\boldsymbol{\kappa}$-space Fourier transforms in equations (5-50) to (5-55) are, of course, generalized functions, as discussed in the last section.

As in the case of averaged quantities, differentiation of an unaveraged quantity in $\mathbf{x}$-space with respect to x_k multiplies its Fourier transform in $\boldsymbol{\kappa}$-space by $i\kappa_k$. For example, from equation (5-50), one obtains

$$\frac{\partial}{\partial x_k}\tilde{u}_i(\mathbf{x}) = \int_{-\infty}^{\infty} i\kappa_k\, \tilde{\varphi}_i(\boldsymbol{\kappa}) e^{i\boldsymbol{\kappa}\cdot\mathbf{x}} d\boldsymbol{\kappa}, \tag{5-56}$$

or

$$i\kappa_k\, \tilde{\varphi}_i(\boldsymbol{\kappa}) = \frac{1}{(2\pi)^3}\int_{-\infty}^{\infty} \frac{\partial}{\partial x_k}\tilde{u}_i(\mathbf{x})\, e^{-i\boldsymbol{\kappa}\cdot\mathbf{x}} d\mathbf{x}. \tag{5-57}$$

Finally, in order to take the Fourier-transforms of equations (5-47) to (5-49), one must consider the Fourier transforms of the products $\tilde{u}_i\tilde{u}_k$ and $\tilde{T}\tilde{u}_k$. Thus, writing the Fourier transform of $\tilde{u}_i\tilde{u}_k$ as $\tilde{\zeta}(\boldsymbol{\kappa})$, one has

$$\tilde{\zeta}_{ik}(\kappa)=\frac{1}{(2\pi)^3}\int_{-\infty}^{\infty}\tilde{u}_i(x)\,\tilde{u}_k(x)e^{-i\kappa\cdot x}\,dx=\frac{1}{(2\pi)^3}\int_{-\infty}^{\infty}\tilde{u}_i(x)\int_{-\infty}^{\infty}\tilde{\varphi}_k(\kappa')e^{i\kappa'\cdot x}\,d\kappa'\,e^{-i\kappa\cdot x}\,dx$$

$$=\frac{1}{(2\pi)^3}\int_{-\infty}^{\infty}\int_{-\infty}^{\infty}\tilde{u}_i(x)\tilde{\varphi}_k(\kappa')e^{-i(\kappa-\kappa')\cdot x}\,d\kappa'\,dx=\frac{1}{(2\pi)^3}\int_{-\infty}^{\infty}\int_{-\infty}^{\infty}\tilde{u}_i(x)\tilde{\varphi}_k(\kappa')e^{-i(\kappa-\kappa')\cdot x}\,dx\,d\kappa' \qquad (5-58)$$

$$=\frac{1}{(2\pi)^3}\int_{-\infty}^{\infty}\tilde{\varphi}_k(\kappa')\int_{-\infty}^{\infty}\tilde{u}_i(x)e^{-i(\kappa-\kappa')\cdot x}\,dx\,d\kappa'=\int_{-\infty}^{\infty}\tilde{\varphi}_k(\kappa')\tilde{\varphi}_i(\kappa-\kappa')d\kappa',$$

where use was made of the relation

$$\int_{-\infty}^{\infty}\int_{-\infty}^{\infty}f(x,\kappa')\,d\kappa'dx=\int_{-\infty}^{\infty}\int_{-\infty}^{\infty}f(x,\kappa')\,dx\,d\kappa'.$$

Inasmuch as $\tilde{\zeta}_{ik}(\kappa)=\tilde{\zeta}_{ki}(\kappa)$ (see first equality in eq. (5-58)), one could just as well write the alternate form

$$\tilde{\zeta}_{ik}(\kappa)=\frac{1}{(2\pi)^3}\int_{-\infty}^{\infty}\tilde{u}_k(x)\tilde{u}_i(x)e^{-i\kappa\cdot x}dx=\int_{-\infty}^{\infty}\tilde{\varphi}_i(\kappa')\varphi_k(\kappa-\kappa')d\kappa'. \qquad (5-58a)$$

Similarly, the Fourier transform of $\tilde{T}\tilde{u}_k$, call it $\tilde{\eta}_k(\kappa)$, can be written as

$$\tilde{\eta}_k(\kappa)=\int_{-\infty}^{\infty}\tilde{\varphi}_k(\kappa')\tilde{\gamma}(\kappa-\kappa')d\kappa'. \qquad (5-59)$$

As shown by equations (5-56) and (5-57), differentiating a quantity in x-space by x_k multiplies its Fourier transform in κ-space by $i\kappa_k$. Applying this to a product, that in equation (5-58) for example, shows that

$$i\kappa_k\tilde{\zeta}_{ik}=\frac{1}{(2\pi)^3}\int_{-\infty}^{\infty}\left[\partial(\tilde{u}_i\tilde{u}_k)/\partial x_k\right]e^{-i\kappa\cdot x}dx=\int_{-\infty}^{\infty}i\kappa_k\tilde{\varphi}_k(\kappa')\tilde{\varphi}_i(\kappa-\kappa')d\kappa', \qquad (5-60)$$

or, using the alternate form for $\tilde{\zeta}_{ik}(\kappa)$ (eq. (5-58a)), one obtains

$$i\kappa_k\tilde{\zeta}_{ik}=\frac{1}{(2\pi)^3}\int_{-\infty}^{\infty}\left[\partial\left(\tilde{u}_k\tilde{u}_i\right)/\partial x_k\right]e^{-i\kappa\cdot x}dx=\int_{-\infty}^{\infty}i\kappa_k\tilde{\varphi}_k(\kappa-\kappa')\tilde{\varphi}_i(\kappa')d\kappa'. \qquad (5-60a)$$

The unaveraged equations (5-47) to (5-49) can now be written in spectral form by taking their Fourier transforms. Thus, multiplying those equations through by $[1/(2\pi)^3]e^{-\kappa\cdot x}dx$, integrating over x from $-\infty$ to $+\infty$, and replacing the subscripts i by j's, we get

$$\frac{\partial}{\partial t}\tilde{\varphi}_j(\kappa)=-\int_{-\infty}^{\infty}i\kappa_k\,\tilde{\varphi}_k(\kappa')\tilde{\varphi}_j(\kappa-\kappa')d\kappa'-\frac{1}{\rho}i\kappa_j\tilde{\lambda}(\kappa)-\nu\kappa^2\tilde{\varphi}_j(\kappa), \qquad (5-61)$$

$$\frac{\partial}{\partial t}\tilde{\gamma}(\kappa)=-\int_{-\infty}^{\infty}i\kappa_k\tilde{\varphi}_k\,(\kappa')\tilde{\gamma}(\kappa-\kappa')d\kappa'-\alpha\kappa^2\,\tilde{\gamma}(\kappa), \qquad (5-62)$$

and

$$-\frac{1}{\rho}\kappa^2\tilde{\lambda}(\kappa)=\int_{-\infty}^{\infty}\kappa_j\kappa_k\,\tilde{\varphi}_k(\kappa')\tilde{\varphi}_j(\kappa-\kappa')d\kappa' \qquad (5-63)$$

where $\kappa^2=\kappa_\ell\kappa_\ell$ and equations (5-50) to (5-60) were used. Combining equations (5-61) and (5-63) gives

$$\frac{\partial}{\partial t}\tilde{\varphi}_j(\kappa)=-i\kappa_k\left(\delta_{j\ell}-\frac{\kappa_j\kappa_\ell}{\kappa^2}\right)\int_{-\infty}^{\infty}\tilde{\varphi}_k(\kappa')\tilde{\varphi}_\ell(\kappa-\kappa')d\kappa'-\nu\kappa^2\,\tilde{\varphi}_j(\kappa). \qquad (5-64)$$

The evolution equation for $\tilde{\varphi}_j$, when written in the form of (5-64), emphasizes the similarity of the first two terms on the right side of equation (5-47); the spectral equivalents of those terms are both nonlinear inertia terms which are second degree in $\tilde{\varphi}_k(\kappa')$ and $\tilde{\varphi}_\ell(\kappa-\kappa')$. As was the case for the unaveraged equations in physical space, equation (5-64) does not require a closure assumption for its solution. In fact, it is often used in discrete form for numerical solutions of turbulence (ref. 1).

Equations (5-62) and (5-64) can be written in terms of complex conjugates by using the relations $\tilde{\varphi}_j(\kappa)=\left(\tilde{\varphi}_j\right)_R(\kappa)+i\left(\tilde{\varphi}_j\right)_I(\kappa)$, $\tilde{\varphi}_i^*(\kappa)=\left(\tilde{\varphi}_i\right)_R(\kappa)-i\left(\tilde{\varphi}_i\right)_I(\kappa)$, $\tilde{\gamma}(\kappa)=\tilde{\gamma}_R(\kappa)+i\tilde{\gamma}_I(\kappa)$, and $\tilde{\gamma}^*(\kappa)=\tilde{\gamma}_R(\kappa)-i\tilde{\gamma}_I(\kappa)$, where the stars designate complex conjugates, and the subscripts R and I refer respectively to real and imaginary parts. Thus, we get

$$\frac{\partial}{\partial t}\tilde{\varphi}_i^*(\kappa)=-i\kappa_k\left(\delta_{i\ell}-\frac{\kappa_i\kappa_\ell}{\kappa^2}\right)\int_{-\infty}^{\infty}\tilde{\varphi}_k^*(\kappa')\tilde{\varphi}_\ell^*(\kappa-\kappa')d\kappa'-\nu\kappa^2\,\tilde{\varphi}_i^*(\kappa), \qquad (5-65)$$

and

$$\frac{\partial}{\partial t}\tilde{\gamma}^*(\kappa)=i\kappa_k\int_{-\infty}^{\infty}\tilde{\varphi}_k^*(\kappa')\tilde{\gamma}^*(\kappa-\kappa')d\kappa'-\alpha\kappa^2\,\tilde{\gamma}^*(\kappa). \qquad (5-66)$$

Multiplying equation (5-64) by $\tilde{\varphi}_i^*(\kappa)$ and equation (5-65) by $\tilde{\varphi}_j(\kappa)$, we get, after adding the two equations,

$$\begin{aligned}\frac{\partial}{\partial t}\left[\tilde{\varphi}_i^*(\kappa)\tilde{\varphi}_j(\kappa)\right]&=i\kappa_k\left(\delta_{i\ell}-\frac{\kappa_i\kappa_\ell}{\kappa^2}\right)\int_{-\infty}^{\infty}\tilde{\varphi}_j(\kappa)\tilde{\varphi}_k^*(\kappa')\tilde{\varphi}_\ell^*(\kappa-\kappa')d\kappa'\\&-i\kappa_k\left(\delta_{j\ell}-\frac{\kappa_j\kappa_\ell}{\kappa^2}\right)\int_{-\infty}^{\infty}\tilde{\varphi}_i^*(\kappa)\tilde{\varphi}_k(\kappa')\tilde{\varphi}_\ell(\kappa-\kappa')d\kappa'-2\nu\kappa^2\tilde{\varphi}_i^*(\kappa)\tilde{\varphi}_j(\kappa).\end{aligned} \qquad (5-67)$$

Equation (5-67) gives the evolution of the total (mean plus turbulent) spectral energy tensor (at a particular κ). Contracting the indices i and j we get, for the total spectral energy (at a particular κ)

$$\begin{aligned}\frac{\partial}{\partial t}\left[\tilde{\varphi}_i^*(\kappa)\tilde{\varphi}_i(\kappa)\right]&=\frac{\partial}{\partial t}\left[\left(\tilde{\varphi}_i\right)_R\left(\tilde{\varphi}_i\right)_R+\left(\tilde{\varphi}_i\right)_I\left(\tilde{\varphi}_i\right)_I\right]=\left|\tilde{\varphi}_i(\kappa)\tilde{\varphi}_i(\kappa)\right|=i\kappa_k\int_{-\infty}^{\infty}\left[\tilde{\varphi}_i(\kappa)\tilde{\varphi}_k^*(\kappa')\tilde{\varphi}_i^*(\kappa-\kappa')\right.\\&\left.-\tilde{\varphi}_i^*(\kappa)\tilde{\varphi}_k(\kappa')\tilde{\varphi}_i(\kappa-\kappa')\right]d\kappa'-2\nu\kappa^2\tilde{\varphi}_i^*(\kappa)\tilde{\varphi}_i(\kappa)\end{aligned} \qquad (5-67a)$$

Note that the spectral-pressure terms (those divided by κ^2) drop out of the contracted equation because of continuity (see eqs. (4-10) and (5-57)). That is, the spectral pressure terms can transfer total (mean plus turbulent) energy between directional components, but do not change the sum of the three directional components at any κ. Similarly, from equations (5-62), (5-66), and (5-65), we get

$$\frac{\partial}{\partial t}\left[\tilde{\gamma}(\kappa)\tilde{\gamma}^*(\kappa)\right]=\frac{\partial}{\partial t}\left|\tilde{\gamma}^2(\kappa)\right|=-i\kappa_k\int_{-\infty}^{\infty}\left[\tilde{\varphi}_k(\kappa')\tilde{\gamma}(\kappa-\kappa')\tilde{\gamma}^*(\kappa)-\tilde{\varphi}_k^*(\kappa')\tilde{\gamma}^*(\kappa-\kappa')\tilde{\gamma}(\kappa)\right]d\kappa-2\alpha\kappa^2\tilde{\gamma}(\kappa)\tilde{\gamma}^*(\kappa) \qquad (5-68)$$

and

$$\frac{\partial}{\partial t}\left[\tilde{\gamma}(\kappa)\tilde{\varphi}_i^*(\kappa)\right] = -i\kappa_k\int_{-\infty}^{\infty}\left[\tilde{\varphi}_k(\kappa')\tilde{\gamma}(\kappa-\kappa')\tilde{\varphi}_i^*(\kappa) - \left(\delta_{i\ell} - \frac{\kappa_i\kappa_\ell}{\kappa^2}\right)\tilde{\varphi}_k^*(\kappa')\tilde{\varphi}_\ell^*(\kappa-\kappa')\tilde{\gamma}(\kappa)\right]d\kappa - (\alpha+\nu)\kappa^2\tilde{\gamma}(\kappa)\varphi_i^*(\kappa). \tag{5-69}$$

The presence of the integrals in equations (5-61) to (5-69) reveals that the Fourier components at each κ depend nonlinearly on Fourier components at every other point in wavenumber space. An important deduction from those equations is the triad nature of the nonlinear interaction of the Fourier components. For instance, equation (5-64) shows that the evolution of the component $\tilde{\varphi}_i$ at wavevector κ depends on components at wavevectors κ' and $\kappa - \kappa'$. That is, there is an interaction among components at those three wavevectors. Equation (5-67) shows that the evolution of $\tilde{\varphi}_i(\kappa)\tilde{\varphi}_j^*(\kappa)$ also depends on the interaction among components at the three wavevectors κ, κ', and $\kappa - \kappa'$.

The last terms in equations (5-64), (5-65), (5-67), and (5-69), which are multiplied by $\nu\kappa^2$, are viscous dissipation terms. The presence of κ^2 in those terms shows that the viscous dissipation occurs at higher wavenumbers than does the bulk of the activity. Similar comments apply to the terms in equations (5-62), (5-66), (5-68), and (5-69) which are multiplied by $\alpha\kappa^2$. Those terms cause a reduction of activity by thermal conduction or thermal smearing. Note that equation (5-69) contains both thermal-smearing and viscous-dissipation terms.

Although equations (5-61) to (5-69) have rather compact forms, they are general, applying to both homogeneous and inhomogeneous turbulence. But since they are written in terms of total instantaneous quantities, it is hard to identify the various turbulence processes. For instance, the nonlinear term in equation (5-64), besides containing spectral-transfer and directional-transfer effects, may contain turbulence production by mean gradients. Thus, further interpretations are postponed to the next section, where mean velocities are absent (or uniform), and the turbulence is homogeneous.

5.3 HOMOGENEOUS TURBULENCE WITHOUT MEAN VELOCITY OR TEMPERATURE (SCALAR) GRADIENTS

A (statistically) homogeneous turbulence is defined as one in which averaged turbulence quantities are not functions of position. For instance, for homogeneous turbulence

$$\overline{u_i\, u_j} \neq \overline{u_i\, u_j}\ (\mathbf{x}),$$

$$\overline{u_i\, u_j u_k} \neq \overline{u_i\, u_j u_k}\ (\mathbf{x})$$

and

$$\overline{\sigma\, \partial u_i / \partial x_j} \neq \overline{\sigma\, \partial u_i / \partial x_j}\ (\mathbf{x}),$$

where $\mathbf{x}$ is the position vector. Similar statements apply to other averaged turbulence quantities in a homogeneous turbulence.

Homogeneous turbulence without mean gradients is attractive as an area of study because of its conceptual simplicity. Production and diffusion terms, for example, are absent in the equations for that type of turbulence. The absence of those terms, however, may not always be helpful for getting solutions. The *presence* of large mean-gradient and/or diffusion effects may, in fact, be an advantage, since a solution will depend to a lesser extent on the difficult-to-determine nonlinear self-interaction terms. In this section we are not interested in mitigating the effects of those terms. Rather we consider homogeneous turbulence without mean gradients mainly as a vehicle for studying the nonlinear self-interaction and/or dissipation effects.

First we will consider the basic equations for homogeneous turbulence without mean velocity or temperature gradients. Then we will give some illustrative solutions. In most cases the *analytical* solutions considered will be of the simplest kind, in order to avoid mathematical complexity. Somewhat more widely applicable *numerical* solutions will also be discussed where available and appropriate.

5.3.1 Basic Equations

For homogeneous turbulence without mean velocity gradients, the averaged two-point flow equations in $\mathbf{r}$-space (eqs. (4-147) to (4-150) in the last chapter) simplify to

$$\frac{\partial}{\partial t}\overline{u_i u_j'}(\mathbf{r}) + \frac{\partial}{\partial r_k}\left(\overline{u_i u_j' u_k'} - \overline{u_i u_k u_j'}\right) = \frac{1}{\rho}\left(\frac{\partial}{\partial r_i}\overline{\sigma u_j'} - \frac{\partial}{\partial r_j}\overline{u_i \sigma'}\right) + 2\nu\frac{\partial^2 \overline{u_i u_j'}}{\partial r_k \partial r_k}, \tag{5-70}$$

$$\frac{1}{\rho}\frac{\partial^2 \overline{u_i \sigma'}}{\partial r_j \partial r_j} = -\frac{\partial^2 \overline{u_i u_j' u_k'}}{\partial r_j \partial r_k}, \tag{5-71}$$

and

$$\frac{1}{\rho}\frac{\partial^2 \overline{\sigma u_j'}}{\partial r_i \partial r_i} = -\frac{\partial^2 \overline{u_i u_k u_j'}}{\partial r_i \partial r_k}. \tag{5-72}$$

The corresponding spectral equations in the $\boldsymbol{\kappa}$-space (eqs. (5-17) to (5-19)) become

$$\frac{\partial}{\partial t}\varphi_{ij}(\boldsymbol{\kappa}) + i\kappa_k\left(\varphi_{ijk}' - \varphi_{ikj}\right) = \frac{1}{\rho}\left(i\kappa_i\lambda_j - i\kappa_j\lambda_i'\right) - 2\nu\kappa^2\varphi_{ij}, \tag{5-73}$$

$$-\frac{1}{\rho}\kappa^2\lambda_i' = \kappa_j\kappa_k\varphi_{ijk}', \tag{5-74}$$

and

$$-\frac{1}{\rho}\kappa^2\lambda_j = \kappa_i\kappa_k\varphi_{ikj}. \tag{5-75}$$

Combining equations (5-73) to (5-75), we get

$$\frac{\partial}{\partial t}\varphi_{ij}(\kappa) = -i\kappa_k\left(\delta_{j\ell} - \frac{\kappa_j\kappa_\ell}{\kappa^2}\right)\varphi'_{i\ell k} + i\kappa_k\left(\delta_{i\ell} - \frac{\kappa_i\kappa_\ell}{\kappa^2}\right)\varphi_{\ell kj} - 2\nu\kappa^2\varphi_{ij}. \tag{5-76}$$

One could, of course, obtain equations (5-70) to (5-76) directly from the instantaneous equations (5-47) and (5-49), and from similar equations written at a point P′ with the subscript i replaced by j. The ¯'s over the instantaneous quantities would be omitted, since mean gradients are absent. So instead of starting with the general equations (4-145), (4-146), and (4-148), and then simplifying the final two-point equations, one could start with the simpler equations for homogeneous turbulence without mean gradients. Then, multiplying the unprimed equations by u'_j, the primed equations by u_i, using the fact that quantities at one point are independent of the location of the other point, adding and space averaging the equations, letting $\partial/\partial x'_k = \partial/\partial r_k$ and $\partial/x_k = -\partial/\partial r_k$, and using the Fourier transforms given by equations (5-12), (5-13), and (5-20) to (5-22), one obtains equations (5-70) to (5-76).

Equations (5-64), (5-62), and (5-65) to (5-69) become, for homogeneous turbulence without mean gradients,

$$\frac{\partial}{\partial t}\varphi_j(\kappa) = -i\kappa_k\left(\delta_{j\ell} - \frac{\kappa_j\kappa_\ell}{\kappa^2}\right)\int_{-\infty}^{\infty}\varphi_k(\kappa')\varphi_\ell(\kappa-\kappa')d\kappa' - \nu\kappa^2\varphi_j(\kappa), \tag{5-77}$$

$$\frac{\partial}{\partial t}\gamma(\kappa) = \int_{-\infty}^{\infty} i\kappa_k\varphi_k(\kappa')\gamma(\kappa-\kappa')d\kappa' - \alpha\kappa^2\gamma(\kappa), \tag{5-78}$$

$$\frac{\partial}{\partial t}\varphi_i^*(\kappa) = i\kappa_k\left(\delta_{i\ell} - \frac{\kappa_i\kappa_\ell}{\kappa^2}\right)\int_{-\infty}^{\infty}\varphi_k^*(\kappa')\varphi_\ell^*(\kappa-\kappa')d\kappa' - \nu\kappa^2\varphi_i^*(\kappa), \tag{5-79}$$

$$\begin{aligned}\frac{\partial}{\partial t}\left[\varphi_i^*(\kappa)\varphi_j(\kappa)\right] = &-i\kappa_k\left(\delta_{j\ell} - \frac{\kappa_j\kappa_\ell}{\kappa^2}\right)\int_{-\infty}^{\infty}\varphi_i^*(\kappa)\varphi_\ell(\kappa-\kappa')\varphi_k(\kappa')d\kappa' \\ &+i\kappa_k\left(\delta_{i\ell} - \frac{\kappa_i\kappa_\ell}{\kappa^2}\right)\int_{-\infty}^{\infty}\varphi_\ell^*(\kappa-\kappa')\varphi_k^*(\kappa')\varphi_j(\kappa)d\kappa' - 2\nu\kappa^2\varphi_i^*(\kappa)\varphi_j(\kappa),\end{aligned} \tag{5-80}$$

$$\begin{aligned}\frac{\partial}{\partial t}\left[\varphi_i^*(\kappa)\varphi_i(\kappa)\right] &= \frac{\partial}{\partial t}\left[\left(\varphi_i\right)_R\left(\varphi_i\right)_R + \left(\varphi_i\right)_I\left(\varphi_i\right)_I\right] = \left|\varphi_i(\kappa)\varphi_i(\kappa)\right| \\ &= -i\kappa_k\int_{-\infty}^{\infty}\left[\varphi_i^*(\kappa)\varphi_k(\kappa')\varphi_i(\kappa-\kappa') - \varphi_i(\kappa)\varphi_k^*(\kappa')\varphi_i^*(\kappa-\kappa')\right]d\kappa' - 2\nu\kappa^2\varphi_i^*(\kappa)\varphi_i(\kappa),\end{aligned} \tag{5-80a}$$

$$\frac{\partial}{\partial t}\left[\gamma(\kappa)\gamma^*(\kappa)\right] = \frac{\partial}{\partial t}\left|\gamma^2(\kappa)\right| = -i\kappa_k\int_{-\infty}^{\infty}\left[\varphi_k(\kappa')\gamma(\kappa-\kappa')\gamma^*(\kappa) - \varphi_k^*(\kappa')\gamma^*(\kappa-\kappa')\gamma(\kappa)\right]d\kappa' - 2\alpha\kappa^2\gamma(\kappa)\gamma^*(\kappa), \tag{5-81}$$

and

$$\begin{aligned}\frac{\partial}{\partial t}\left[\gamma(\kappa)\varphi_i^*(\kappa)\right] = &-i\kappa_k\int_{-\infty}^{\infty}\left[\varphi_k(\kappa')\gamma(\kappa-\kappa')\varphi_i^*(\kappa) - \left(\delta_{i\ell} - \frac{\kappa_i\kappa_\ell}{\kappa^2}\right)\varphi_k^*(\kappa')\varphi_\ell^*(\kappa-\kappa')\gamma(\kappa)\right]d\kappa' \\ &-(\alpha+\nu)\kappa^2\gamma(\kappa)\varphi_i^*(\kappa).\end{aligned} \tag{5-82}$$

Note that equations (5-77) to (5-82) are the same as the corresponding equations in the last section, except that the ~'s over the dependent variables have been omitted for homogeneous turbulence without mean velocity or temperature gradients (see eqs. (4-14) to (4-20)).

5.3.1.1 *Equivalence of equations (5-76) and (5-80).*—To show the equivalence of the subject equations we first relate $\varphi_i^*(\kappa)\,\varphi_j(\kappa)$ to $\varphi_{ij}(\kappa)$. To that end, we write

$$\overline{u_i u_j'}(\mathbf{r}) = \overline{u_i(\mathbf{x})u_j(\mathbf{x}+\mathbf{r})} = \frac{1}{R_1R_2R_3}\int_{-R_k/2}^{R_k/2} u_i(\mathbf{x})u_j(\mathbf{x}+\mathbf{r})d\mathbf{x}, \tag{5-83}$$

where the overbar desginates a space average and R_k is the spatial period in the k-direction. Space averages can, of course, be used because the turbulence is homogeneous. Since the period is, at this point, finite, we represent u_i by a Fourier series (finite Fourier transform) (see, e.g., eq. (5-4)). Thus,

$$u_i(\mathbf{x}) = \sum_{\kappa=-\infty}^{\infty} \left(\varphi_i\right)_\kappa e^{i2\pi\kappa_k x_k/R_{(k)}}, \tag{5-84}$$

or

$$u_j(\mathbf{x}+\mathbf{r}) = \sum_{\kappa=-\infty}^{\infty} \left(\varphi_j\right)_\kappa e^{i2\pi\kappa_k (x_k+r_k)/R_{(k)}}. \tag{5-85}$$

Then equation (5-83) becomes

$$\begin{aligned}
\overline{u_i(\mathbf{x})u_j(\mathbf{x}+\mathbf{r})} &= \frac{1}{R_1R_2R_3}\int_{-R_k/2}^{R_k/2} u_i(\mathbf{x}) \sum_{\kappa=-\infty}^{\infty} \left(\varphi_j\right)_\kappa e^{i2\pi\kappa_k (x_k+r_k)/R_{(k)}} d\mathbf{x} \\
&= \frac{1}{R_1R_2R_3}\int_{-R_k/2}^{R_k/2} \sum_{\kappa=-\infty}^{\infty} u_i(\mathbf{x})\left(\varphi_j\right)_\kappa e^{i2\pi\kappa_k (x_k+r_k)/R_{(k)}} d\mathbf{x} \\
&= \frac{1}{R_1R_2R_3}\sum_{\kappa=-\infty}^{\infty} \int_{-R_k/2}^{R_k/2} u_i(\mathbf{x})\left(\varphi_j\right)_\kappa e^{i2\pi\kappa_k (x_k+r_k)/R_{(k)}} d\mathbf{x} \\
&= \frac{1}{R_1R_2R_3}\sum_{\kappa=-\infty}^{\infty} \left(\varphi_j\right)_\kappa e^{i2\pi\kappa_k r_k/R_{(k)}} \int_{-R_k/2}^{R_k/2} u_i(\mathbf{x}) e^{i2\pi\kappa_k x_k/R_{(k)}} d\mathbf{x} \\
&= \sum_{s=-\infty}^{\infty} \left(\varphi_j\right)_s e^{is_k r_k} \int_{-R_k/2}^{R_k/2} u_i(\mathbf{x}) e^{is_k x_k} d\mathbf{x} \frac{\Delta s_1 \Delta s_2 \Delta s_3}{(2\pi)^3},
\end{aligned} \tag{5-86}$$

where equations (5-7) and (5-7b) were used. Note that Δs_k is given by equation (5-7). Passing to the limit as $R_k \to \infty$ ($\Delta s_k \to 0$), and using equation (5-10), one obtains

$$\overline{u_i(\mathbf{x})u_j(\mathbf{x}+\mathbf{r})} = \frac{1}{(2\pi)^3}\int_{-\infty}^{\infty} \varphi_j(\mathbf{s}) e^{i\mathbf{s}\cdot\mathbf{r}} \int_{-\infty}^{\infty} u_i(\mathbf{x}) e^{i\mathbf{s}\cdot\mathbf{x}}\, d\mathbf{x}d\mathbf{s}. \tag{5-87}$$

But,

$$\frac{1}{(2\pi)^3}\int_{-\infty}^{\infty} u_i(\mathbf{x}) e^{i\mathbf{s}\cdot\mathbf{x}} d\mathbf{x} = \varphi_i^*(\mathbf{s}), \tag{5-88}$$

since, for $R_k \to \infty$, equation (5-84) becomes

$$u_i(\mathbf{x}) = \int_{-\infty}^{\infty} \varphi_i(\mathbf{s}) e^{i\mathbf{s}\cdot\mathbf{x}} d\mathbf{s}. \tag{5-89}$$

Substituting equation (5-88) into (5-87) and changing the dummy variable from s to κ, one has

$$\overline{u_i u_j'}(\mathbf{r}) = \overline{u_i(\mathbf{x})u_j(\mathbf{x}+\mathbf{r})} = \int_{-\infty}^{\infty} \varphi_i^*(\boldsymbol{\kappa})\varphi_j(\boldsymbol{\kappa})e^{i\boldsymbol{\kappa}\cdot\mathbf{r}}\,d\boldsymbol{\kappa}, \tag{5-90}$$

showing that $\varphi_i^*(\boldsymbol{\kappa})\,\varphi_j(\boldsymbol{\kappa})$ is the Fourier transform (from r-space to κ-space) of $\overline{u_i\,u_j'}\,(\mathbf{r})$. Since $\varphi_{ij}(\boldsymbol{\kappa})$ is also the Fourier transform of $\overline{u_i\,u_j'}\,(\mathbf{r})$ (see eqs. (5-11) and (5-12)),

$$\varphi_{ij}(\boldsymbol{\kappa}) = \varphi_i^*(\boldsymbol{\kappa})\varphi_j(\boldsymbol{\kappa}). \tag{5-91}$$

That is, $\varphi_{ij}(\boldsymbol{\kappa})$ in equation (5-76) is equal to $\varphi_i^*(\boldsymbol{\kappa})\,\varphi_j(\boldsymbol{\kappa})$ in equation (5-80). The tensor $\tilde{\varphi}_i^*(\boldsymbol{\kappa})\,\tilde{\varphi}_j(\boldsymbol{\kappa})$ is often written as $\overline{\varphi_i^*(\boldsymbol{\kappa})\varphi_j(\boldsymbol{\kappa})}$, where the overbar could represent, say, an ensemble average. However, the overbar does not seem to be strictly necessary because $\varphi_i^*(\boldsymbol{\kappa})\,\varphi_j(\boldsymbol{\kappa})$ is already the Fourier transform of a space-averaged quantity (eq. (5-90)).

Consider next the equivalence of the nonlinear terms in equations (5-76) and (5-80). To that end, we relate the tensor $\varphi_{\ell kj}(\boldsymbol{\kappa})$ in equation (5-76) to $\varphi_\ell^*(\boldsymbol{\kappa}-\boldsymbol{\kappa}')\varphi_k^*(\boldsymbol{\kappa}')\varphi_j(\boldsymbol{\kappa})$ in equation (5-80). Note first that $\varphi_{\ell kj}(\boldsymbol{\kappa})$ is the Fourier transform of $\overline{u_\ell u_k u_j'}(\mathbf{r})$ (see eq. (5-21)), where the overbar again designates a space average. Then, carrying out a development similar to that in the last paragraph,

$$\begin{aligned}
\overline{u_\ell u_k u_j'}(\mathbf{r}) &= \overline{u_\ell(\mathbf{x})u_k(\mathbf{x})u_j(\mathbf{x}+\mathbf{r})} = \frac{1}{R_1R_2R_3}\int_{-R_k/2}^{R_k/2} u_\ell(\mathbf{x})\,u_k(\mathbf{x})u_j(\mathbf{x}+\mathbf{r})dx_1dx_2dx_3 \\
&= \frac{1}{R_1R_2R_3}\int_{-R_k/2}^{R_k/2} u_\ell(\mathbf{x})\,u_k(\mathbf{x})\sum_{\kappa=-\infty}^{\infty}\left(\varphi_j\right)_{\boldsymbol{\kappa}} e^{i2\pi\kappa_k(x_k+r_k)/R_{(k)}}dx \\
&= \frac{1}{R_1R_2R_3}\int_{-R_k/2}^{R_k/2}\sum_{\kappa=-\infty}^{\infty} u_\ell(\mathbf{x})u_k(\mathbf{x})\left(\varphi_j\right)_{\boldsymbol{\kappa}} e^{i2\pi\kappa_k(x_k+r_k)/R_{(k)}}dx \\
&= \frac{1}{R_1R_2R_3}\sum_{\kappa=-\infty}^{\infty}\int_{-R_k/2}^{R_k/2} u_\ell(\mathbf{x})u_k(\mathbf{x})\left(\varphi_j\right)_{\boldsymbol{\kappa}} e^{i2\pi\kappa_k(x_k+r_k)/R_{(k)}}dx \\
&= \frac{1}{R_1R_2R_3}\sum_{\kappa=-\infty}^{\infty}\left(\varphi_j\right)_{\boldsymbol{\kappa}} e^{i2\pi\kappa_k r_k/R_{(k)}}\int_{-R_k/2}^{R_k/2} u_\ell(\mathbf{x})u_k(\mathbf{x})e^{i2\pi\kappa_k r_k/R_{(k)}}dx.
\end{aligned} \tag{5-92}$$

Using equations (5-7) to (5-7b), and passing to the limit as $R_k \to \infty$,

$$\begin{aligned}
\overline{u_\ell u_k u_j'}(\mathbf{r}) &= \overline{u_\ell(\mathbf{x})u_k(\mathbf{x})u_j(\mathbf{x}+\mathbf{r})} = \frac{1}{(2\pi)^3}\int_{-\infty}^{\infty}\varphi_j(\mathbf{s})e^{i\mathbf{s}\cdot\mathbf{r}}\int_{-\infty}^{\infty} u_\ell(\mathbf{x})\,u_k(\mathbf{x})e^{i\mathbf{s}\cdot\mathbf{x}}dxds \\
&= \frac{1}{(2\pi)^3}\int_{-\infty}^{\infty}\varphi_j(\boldsymbol{\kappa})e^{i\boldsymbol{\kappa}\cdot\mathbf{r}}\int_{-\infty}^{\infty} u_\ell(\mathbf{x})\,u_k(\mathbf{x})e^{i\boldsymbol{\kappa}\cdot\mathbf{r}}dxd\boldsymbol{\kappa} \\
&= \int_{-\infty}^{\infty}\varphi_j(\boldsymbol{\kappa})e^{i\boldsymbol{\kappa}\cdot\mathbf{r}}\zeta_{\ell k}^*(\boldsymbol{\kappa})d\boldsymbol{\kappa} = \int_{-\infty}^{\infty}\varphi_j(\boldsymbol{\kappa})e^{i\boldsymbol{\kappa}\cdot\mathbf{r}}\int_{-\infty}^{\infty}\varphi_k^*(\boldsymbol{\kappa}')\varphi_\ell^*(\boldsymbol{\kappa}-\boldsymbol{\kappa}')d\boldsymbol{\kappa}'d\boldsymbol{\kappa} \\
&= \int_{-\infty}^{\infty}\left[\int_{-\infty}^{\infty}\varphi_\ell^*(\boldsymbol{\kappa}-\boldsymbol{\kappa}')\varphi_k^*(\boldsymbol{\kappa}')\varphi_j(\boldsymbol{\kappa})d\boldsymbol{\kappa}'\right]e^{i\boldsymbol{\kappa}\cdot\mathbf{r}}\,d\boldsymbol{\kappa},
\end{aligned} \tag{5-93}$$

where $\zeta_{\ell k}^*(\boldsymbol{\kappa})$ was calculated from equation (5-58) ("'s omitted). Equation (5-93) shows that $\int_{-\infty}^{\infty}\varphi_\ell^*(\boldsymbol{\kappa}-\boldsymbol{\kappa}')\varphi_k^*(\boldsymbol{\kappa}')\varphi_j(\boldsymbol{\kappa})\,d\boldsymbol{\kappa}'$ in equation (5-80) is the Fourier transform (from r-space to κ-space) of $\overline{u_\ell u_k u_j'}(\mathbf{r})$. Since $\varphi_{\ell kj}(\boldsymbol{\kappa})$ in equation (5-76) is also the Fourier transform of $\overline{u_\ell u_k u_j'}$,

$$\varphi_{\ell kj}(\boldsymbol{\kappa}) = \int_{-\infty}^{\infty}\varphi_\ell^*(\boldsymbol{\kappa}-\boldsymbol{\kappa}')\varphi_k^*(\boldsymbol{\kappa}')\varphi_j(\boldsymbol{\kappa})d\boldsymbol{\kappa}'. \tag{5-94}$$

Finally, we relate $\varphi'_{i\ell k}(\boldsymbol{\kappa})$ in equation (5-76) to $\varphi_i^*(\boldsymbol{\kappa})\varphi_\ell(\boldsymbol{\kappa}-\boldsymbol{\kappa}')\varphi_k(\boldsymbol{\kappa}')$ in equation (5-80). The Fourier transform of $\varphi'_{i\ell k}$ is, according to equation (5-22), $\overline{u_i u'_\ell u'_k}(\mathbf{r})$. Carrying out a development similar to those in the last two paragraphs, with overbars designating space averages,

$$\overline{u_i u'_\ell u'_k}(\mathbf{r}) = \overline{u_i(\mathbf{x})u_\ell(\mathbf{x}+\mathbf{r})u_k(\mathbf{x}+\mathbf{r})} = \frac{1}{R_1R_2R_3}\int_{-R_k/2}^{R_k/2} u_i(\mathbf{x})\,u_\ell(\mathbf{x}+\mathbf{r})u_k(\mathbf{x}+\mathbf{r})d\mathbf{x}$$

$$= \frac{1}{R_1R_2R_3}\int_{-R_k/2}^{R_k/2} u_i(\mathbf{x})\sum_{\boldsymbol{\kappa}=-\infty}^{\infty}(\zeta_{\ell k})_{\boldsymbol{\kappa}}e^{i2\pi\kappa_k(x_k+r_k)/R_{(k)}}d\mathbf{x}$$

$$= \frac{1}{R_1R_2R_3}\int_{-R_k/2}^{R_k/2}\sum_{\boldsymbol{\kappa}=-\infty}^{\infty} u_i(\mathbf{x})(\zeta_{\ell k})_{\boldsymbol{\kappa}}e^{i2\pi\kappa_k(x_k+r_k)/R_{(k)}}d\mathbf{x}$$

$$= \frac{1}{R_1R_2R_3}\sum_{\boldsymbol{\kappa}=-\infty}^{\infty}\int_{-R_k/2}^{R_k/2} u_i(\mathbf{x})(\zeta_{\ell k})_{\boldsymbol{\kappa}}e^{i2\pi\kappa_k(x_k+r_k)/R_{(k)}}d\mathbf{x}$$

$$= \frac{1}{R_1R_2R_3}\sum_{\boldsymbol{\kappa}=-\infty}^{\infty}(\zeta_{\ell k})_{\boldsymbol{\kappa}}e^{i2\pi\kappa_k r_k/R_{(k)}}\int_{-R_k/2}^{R_k/2} u_i(\mathbf{x})e^{i2\pi\kappa_k x_k/R_{(k)}}d\mathbf{x}.$$

Passing to the limit as $R_k\to\infty$ after using equations (5-7) to (5-7b), we get

$$\overline{u_i u'_\ell u'_k}(\mathbf{r}) = \overline{u_i(\mathbf{x})u_\ell(\mathbf{x}+\mathbf{r})u_k(\mathbf{x}+\mathbf{r})} = \frac{1}{(2\pi)^3}\int_{-\infty}^{\infty}\zeta_{\ell k}(\mathbf{s})e^{i\mathbf{s}\cdot\mathbf{r}}\int_{-\infty}^{\infty} u_i(\mathbf{x})e^{i\mathbf{s}\cdot\mathbf{x}}d\mathbf{x}\,d\mathbf{s}$$

$$= \frac{1}{(2\pi)^3}\int_{-\infty}^{\infty}\zeta_{\ell k}(\boldsymbol{\kappa})e^{i\boldsymbol{\kappa}\cdot\mathbf{r}}\int_{-\infty}^{\infty} u_i(\mathbf{x})e^{i\boldsymbol{\kappa}\cdot\mathbf{x}}d\mathbf{x}\,d\boldsymbol{\kappa}$$

$$= \int_{-\infty}^{\infty}\zeta_{\ell k}(\boldsymbol{\kappa})e^{i\boldsymbol{\kappa}\cdot\mathbf{r}}\varphi_i^*(\boldsymbol{\kappa})d\boldsymbol{\kappa} = \int_{-\infty}^{\infty}\int_{-\infty}^{\infty}\varphi_\ell(\boldsymbol{\kappa}-\boldsymbol{\kappa}')\varphi_k(\boldsymbol{\kappa}')d\boldsymbol{\kappa}'\varphi_i^*(\boldsymbol{\kappa})e^{i\boldsymbol{\kappa}\cdot\mathbf{r}}d\boldsymbol{\kappa}$$

$$= \int_{-\infty}^{\infty}\left[\int_{-\infty}^{\infty}\varphi_i^*(\boldsymbol{\kappa})\varphi_\ell(\boldsymbol{\kappa}-\boldsymbol{\kappa}')\varphi_k(\boldsymbol{\kappa}')d\boldsymbol{\kappa}\right]e^{i\boldsymbol{\kappa}\cdot\mathbf{r}}d\boldsymbol{\kappa}, \qquad (5-95)$$

where $\zeta_{\ell k}(\boldsymbol{\kappa})$ was obtained from equation (5-58) ("'s omitted). Equation (5-95) shows that $\int_{-\infty}^{\infty}\varphi_i^*(\boldsymbol{\kappa})\varphi_\ell(\boldsymbol{\kappa}-\boldsymbol{\kappa}')\varphi_k(\boldsymbol{\kappa}')d\boldsymbol{\kappa}'$ in equation (5-80) is the Fourier transform (from $\mathbf{r}$-space to $\boldsymbol{\kappa}$-space) of $\overline{u_i u'_\ell u'_k}(\mathbf{r})$. Since $\varphi'_{i\ell k}$ in equation (5-76) is also the Fourier transform of $\overline{u_i u'_\ell u'_k}$,

$$\varphi'_{i\ell k}(\boldsymbol{\kappa}) = \int_{-\infty}^{\infty}\varphi_i^*(\boldsymbol{\kappa})\varphi_\ell(\boldsymbol{\kappa}-\boldsymbol{\kappa}')\varphi_k(\boldsymbol{\kappa}')d\boldsymbol{\kappa}'. \qquad (5-96)$$

Using equation (5-91), (5-94), and (5-96), one sees that equations (5-76) and (5-80) are equivalent, since all the terms in those two equations are equivalent. The strategy for arriving at that conclusion was to show that spectral tensors in equation (5-80) are Fourier transforms from $\mathbf{r}$- to $\boldsymbol{\kappa}$-space of velocity-correlation tensors (see eqs. (5-90), (5-93), and (5-95)). It was already known that that is the case for the spectral tensors in equation (5-76); that equation was derived by transforming the evolution equation for $\overline{u_i u'_j}$ from $\mathbf{r}$- to $\boldsymbol{\kappa}$-space. That was not the case for equation (5-80), which was obtained by transforming from $\mathbf{x}$- to $\boldsymbol{\kappa}$-space (rather than from $\mathbf{r}$- to $\boldsymbol{\kappa}$-space). Hence, the need for the development in the present section.

Because of the equivalence of equations (5-76) and (5-80), the latter, like the former, is an averaged equation and thus requires a closure assumption. Note, however, that equation (5-80) could be closed deductively (without introducing additional information) by calculating the φ_i from a numerical solution of the unaveraged equations (5-77) and/or (5-79).

The demonstration of the equivalence of equations (5-76) and (5-80) (at least, according to the present method), depends on the homogeneity of the turbulence and the use of space averages in at least one direction. Also, developments similar to those

in the present section can be used to show that equations (5-81) and (5-82) are Fourier transforms from $\mathbf{r}$- to $\boldsymbol{\kappa}$-space of evolution equations for temperature or temperature-velocity correlations.

5.3.1.2 *Further discussion of the equations for homogeneous turbulence without mean gradients.*—Consider first the spectral-transfer term. It has already been shown in section 5.1.2.1 that for a general Navier-Stokes turbulence the spectral terms associated with triple correlations can, except for the pressure terms, be considered as spectral-transfer functions or terms. However, for homogeneous turbulence, the demonstration is much simpler. For that case $\partial/\partial r_k = \partial/\partial x'_k = -\partial/\partial x_k$. Then, in equation (5-70), the term

$$-\frac{\partial}{\partial r_k}\left(\overline{u_i u'_j u'_k} - \overline{u_i u_k u'_j}\right) = \frac{\partial}{\partial x_k}\overline{u_i u'_j u'_k} + \frac{\partial}{\partial x'_k}\overline{u_i u_k u'_j}$$

$$= \overline{u'_j u'_k \frac{\partial u_i}{\partial x_k}} + \overline{\frac{\partial\left(u'_j u_k\right)}{\partial x'_k} u_i} = \int_{-\infty}^{\infty} T_{ij}(\boldsymbol{\kappa}) e^{i\boldsymbol{\kappa}\cdot\mathbf{r}} d\boldsymbol{\kappa}, \qquad (5-97)$$

where $T_{ij}(\boldsymbol{\kappa})$ is the Fourier transform of $-\partial\left(\overline{u_i u'_j u'_k} - \overline{u_i u_k u'_j}\right)/\partial r_k$.

Then, for $\mathbf{r} = 0$,

$$\int_{-\infty}^{\infty} T_{ij}(\boldsymbol{\kappa}) d\boldsymbol{\kappa} = \overline{u_j u_k \frac{\partial u_i}{\partial x_k}} + \overline{\frac{\partial\left(u_j u_k\right)}{\partial x_k} u_i} = \frac{\partial\left(\overline{u_i u_j u_k}\right)}{\partial x_k} = 0 \qquad (5-98)$$

for homogeneous turbulence. Referring to equation (5-70) and letting $\mathbf{r} = 0$ in that equaiton, we see that T_{ij}, when integrated over all $\boldsymbol{\kappa}$, gives zero contribution to the rate of change of $\overline{u_i u_j}$. It can, however, transfer spectral components of $\overline{u_i u_j}$ from one part of wavenumber space to another. So we interpret T_{ij} as a spectral transfer term associated with turbulence self-interaction. The term $-\partial\left(\overline{u_i u'_j u'_k} - \overline{u_i u_k u'_j}\right)/\partial r_k$ in equation (5-70) is therefore the Fourier transform from $\boldsymbol{\kappa}$- to $\mathbf{r}$-space of a self-interaction spectral-transfer term.

Some detail about the spectral transfer of turbulent activity (and about the other turbulence processes) is obtainable from the evolution equation for $\varphi_i^* \varphi_j$ (eq. (5-80)).[1] The spectral energy tensor $\varphi_i^* \varphi_j$ is the Fourier transform from $\mathbf{r}$- to $\boldsymbol{\kappa}$-space of the turbulent-energy tensor $\overline{u_i u'_j}$, and φ_j is the Fourier transform from $\mathbf{x}$- to $\boldsymbol{\kappa}$-space of u_j. Letting $\mathbf{r} = 0$ in equation (5-90) shows that $\varphi_i^* \varphi_j$ gives spectral contributions to $\overline{u_i u_j}$ from various wavevector bands.

The spectral transfer term in equation (5-80) is

$$T_{ij}(\boldsymbol{\kappa}) = \int_{-\infty}^{\infty} P_{ij}(\boldsymbol{\kappa}, \boldsymbol{\kappa}') d\boldsymbol{\kappa}', \qquad (5-99)$$

where

$$P_{ij}(\boldsymbol{\kappa}, \boldsymbol{\kappa}') = i\left[\kappa_k \varphi_i^*(\boldsymbol{\kappa} - \boldsymbol{\kappa}')\varphi_j(\boldsymbol{\kappa})\varphi_k^*(\boldsymbol{\kappa}') - \kappa_k \varphi_i^*(\boldsymbol{\kappa})\varphi_j(\boldsymbol{\kappa} - \boldsymbol{\kappa}')\varphi_k(\boldsymbol{\kappa}')\right]. \qquad (5-100)$$

Equations (5-99) and (5-100) show that contributions from various wavevectors $\boldsymbol{\kappa}'$ between $-\infty$ to $+\infty$ make up the total turbulent transfer at $\boldsymbol{\kappa}$. In particular they show that the net transfer into a wavevector band at $\boldsymbol{\kappa}$ takes place by the interaction of triads of Fourier components at the wavevectors $\boldsymbol{\kappa}$, $\boldsymbol{\kappa}'$, and $\boldsymbol{\kappa} - \boldsymbol{\kappa}'$. That is a hallmark of the turbulence spectral-transfer process and is an important deduction from the Navier-Stokes equations. But it only became evident through the Fourier analysis of the unaveraged velocities $u_i(\mathbf{x})$ in those equations.

[1] One should note that the discussion preceding section 5.3 was not strictly for turbulence, because the velocity components $\tilde{u}_i$ and their Fourier transforms could include mean components. Thus, the terms in the equations discussed there, unlike those considered in the present section, were not identified as turbulence terms.

By using equation (5-60a) in place of (5-60) and omitting the ~'s for homogeneous turbulence, we get the alternate form

$$P_{ij}(\kappa,\kappa') = i\left[\kappa_k \varphi_k^*(\kappa-\kappa')\varphi_i^*(\kappa')\varphi_j(\kappa) - \kappa_k \varphi_k(\kappa-\kappa')\varphi_i^*(\kappa)\varphi_j(\kappa')\right]. \tag{5-101}$$

Equation (5-101) becomes, on using continuity in the form $(\kappa_\kappa - \kappa_{\kappa'})\,\varphi_{k(\kappa-\kappa')} = 0$ (see eqs. (4-21) and (5-36)),

$$P_{ij}(\kappa,\kappa') = i\left[\kappa'_k \varphi_k^*(\kappa-\kappa')\varphi_i^*(\kappa')\varphi_j(\kappa) - \kappa'_k \varphi_k(\kappa-\kappa')\varphi_i^*(\kappa)\varphi_j(\kappa')\right]. \tag{5-102}$$

Interchanging κ and κ' in equation (5-101), and noting that $\varphi_k^*(\kappa'-\kappa) = \varphi_k(\kappa-\kappa')$ and $\varphi_i(\kappa'-\kappa) = \varphi_i^*(\kappa-\kappa')$ since **u** is real, we get

$$P_{ij}(\kappa',\kappa) = i\left[-\kappa'_k \varphi_k^*(\kappa-\kappa')\varphi_i^*(\kappa')\varphi_j(\kappa) + \kappa'_k \varphi_k(\kappa-\kappa')\varphi_i^*(\kappa)\varphi_j(\kappa')\right]. \tag{5-103}$$

Comparison of equations (5-102) and (5-103) shows that

$$P_{ij}(\kappa,\kappa') = -P_{ij}(\kappa',\kappa). \tag{5-104}$$

Thus, P_{ij} is antisymmetric in κ and κ'. That is a condition which must be satisfied by any expression (assumed or calculated) for P_{ij}. Another condition, obtained by letting $\kappa = \kappa'$ in equation (5-104), is

$$P_{ij}(\kappa,\kappa) = 0. \tag{5-105}$$

That is, there is no spectral transfer between Fourier components (eddies) with the same wavevector. This result shows that spectral transfer can take place only between wavevectors that, at least to some extent, are separated.

One can also get the spectral-transfer condition (5-98) from equation (5-104). Thus, using equation (5-104) in (5-99) and integrating from $\kappa = -\infty$ to $+\infty$, there results

$$\int_{-\infty}^{\infty} T_{ij}(\kappa) = \int_{-\infty}^{\infty}\int_{-\infty}^{\infty} P_{ij}(\kappa,\kappa')d\kappa'\,d\kappa = -\int_{-\infty}^{\infty}\int_{-\infty}^{\infty} P_{ij}(\kappa',\kappa)d\kappa\,d\kappa'. \tag{5-106}$$

Since κ and κ' are dummy varibables in the integrals in equation (5-106), those variables can be interchanged without changing the values of the integrals. Thus, equations (5-106) can be true only if

$$\int_{-\infty}^{\infty} T_{ij}(\kappa)\,d\kappa = 0, \tag{5-107}$$

showing again that $T_{ij}(\kappa)$ gives zero contribution to the rate of change of turbulent-velocity correlation $\overline{u_i u_j}$, but it can transfer turbulent spectral components of $\overline{u_i u_j}$ from one part of wavenumber space to another.

Terms in equations (5-81) and (5-82) analogous to $P_{ij}(\kappa, \kappa')$ are, respectively,

$$S(\kappa,\kappa') = -i\left[\kappa_k \varphi_k(\kappa')\gamma(\kappa-\kappa')\gamma^*(\kappa) - \kappa_k \varphi_k^*(\kappa')\gamma^*(\kappa-\kappa')\gamma(\kappa)\right] \tag{5-108}$$

and

$$V_i(\kappa,\kappa') = -i\left[\kappa_k \varphi_k(\kappa')\gamma(\kappa-\kappa')\varphi_i^*(\kappa) - \kappa_k \varphi_k^*(\kappa')\varphi_i^*(\kappa-\kappa')\gamma(\kappa)\right]. \tag{5-109}$$

By using developments similar to those for $P_{ij}(\kappa, \kappa')$ and $T_{ij}(\kappa)$ in equations (5-99) to (5-107), one can show that

$$S(\kappa, \kappa') = -S(\kappa', \kappa). \tag{5-110}$$

and

$$V_i(\kappa, \kappa') = -V_i(\kappa', \kappa). \tag{5-111}$$

For $\kappa' = \kappa$, equations (5-110) and (5-111) show that, like equation (5-105),

$$S(\kappa, \kappa) = V_i(\kappa, \kappa) = 0. \tag{5-105a}$$

Then, letting

$$W(\kappa) = \int_{-\infty}^{\infty} S(\kappa, \kappa')d\kappa' \tag{5-112}$$

and

$$X_i(\kappa) = \int_{-\infty}^{\infty} V_i(\kappa, \kappa')d\kappa', \tag{5-113}$$

one obtains

$$\int_{-\infty}^{\infty} W(\kappa)d\kappa = \int_{-\infty}^{\infty} X_i(\kappa)d\kappa = 0. \tag{5-114}$$

Thus, $W(\kappa)$ and $X_i(\kappa)$ can be given interpretations which are analogous to that given for $T_{ij}(\kappa)$. That is, $W(\kappa)$ gives zero contribution to the rate of change of turbulent temperature correlation $\overline{\tau\tau}$, but it can transfer spectral components $\gamma(\kappa)\gamma^*(\kappa))$ of $\overline{\tau\tau}$ from one part of wavenumber space to another. Similarly, $X_i(\kappa)$ gives zero contribution to the rate of change of temperature-velocity correlation $\overline{\tau u_i}$, but it can transfer spectral components $\gamma(\kappa)\varphi_i^*(\kappa)$ of $\overline{\tau u_i}$ from one part of wavenumber space to another.[2]

Consider next the turbulent spectral-pressure terms in equations (5-80) and (5-82). Those are the terms with κ^2 in the denominator. Like the other inertia terms (the spectral-transfer terms), the spectral-pressure terms contain integrations over wavenumber space from $-\infty$ to $+\infty$. Thus, the spectral-pressure components at κ can be affected by turbulent activity at all parts of wavenumber space. We do not identify them as spectral-transfer terms because, unlike the latter, they can give contributions to the rate of change of $\overline{u_i u_j}$ or of $\overline{u_i \tau}$. The turbulent spectral-pressure terms drop out of the contracted equation (5-80a) because of continuity, so that they make no contribution to the rate of change of $\varphi_i^*(\kappa)\varphi_i(\kappa)$. But at each κ they can transfer turbulent energy among the three directional components of $\varphi_i^*\varphi_i$. The spectral-pressure term in equation (5-82), however, does not seem to have a clear physical significance, other than that it can contribute to the rate of change of $\overline{u_i \tau}$ or of $\gamma(\kappa)\,\varphi_i^*(\kappa)$.

Finally, consider the turbulent-dissipation and turbulent thermal-smearing terms in equations (5-80) to (5-82). Those are the terms multiplied by κ^2, the turbulent-dissipation and turbulent thermal-smearing terms being additionally multiplied respectively by ν and α. They always act in a direction such that the turbulent quantities which evolve according to equations (5-80) to (5-82) are brought closer to zero. The fact that the terms are multiplied by κ^2 means that Fourier components at larger wavenumbers (the smaller eddies) will be viscously dissipated or thermally smeared more effectively than will those at smaller wavenumbers (the larger eddies). However, just how much more effectively depends on the shapes of the turbulent spectra, as will be seen later.[3] To illustrate the turbulence processes and turbulence quantities, we will next obtain solutions of the continuum equations for several solvable cases.

---

[2]Note, however, that although all of equations (5-104) to (5-114) are true, $\overline{\tau u_i}$ (proportional to the turbulent heat transfer) is zero in the present case where mean gradients are absent. The same can be said about $u_i u_j$ for $i \neq j$ (see section 4.3.1.1). (Note that the corresponding spectral quantities $\gamma\varphi_i^*$ and $\varphi_i^*\varphi_j$ for $i \neq j$ are not zero.) Spectral transfer related to $\overline{\tau u_i}$ and to $u_i u_j$ for $i \neq j$ for cases where mean gradients are not absent will be considered in section 5.3.

[3]An analogous situation occurs for the transmission of sound in a gas. The shorter higher-frequency waves tend to be attenuated more rapidly by viscous dissipation (and by thermal smearing) than the longer lower-frequency ones.

5.3.2 Illustrative Solutions of the Basic Equations

Since we are considering a homogeneous turbulent field without mean gradients or external forces, the turbulence will decay with time, no energy being added to the system. Thus we have an initial-value problem for which, in lieu of boundary conditions, we specify statistical uniformity.

5.3.2.1 Low turbulence Reynolds number.—The simplest analytical solution of the equations for homogeneous turbulence is that for low Reynolds numbers. Low Reynolds-number turbulence is identified as weak turbulence, the Reynolds number being proportional to a ratio of inertia to viscous forces. It should occur in the final period of decay. The solution might be used to study to some extent the viscous dissipation, that being the only turbulence process accounted for in the analysis.

For homogeneous turbulence without mean gradients the instantaneous equations (5-47) and (5-49) become, respectively,

$$\frac{\partial u_i}{\partial t} = -\frac{\partial\left(u_i u_k\right)}{\partial x_k} - \frac{1}{\rho}\frac{\partial \sigma}{\partial x_i} + \nu\frac{\partial^2 u_i}{\partial x_k \partial x_k} \tag{5-115}$$

and

$$\frac{\partial^2 \sigma}{\partial x_\ell \partial x_\ell} = -\frac{\partial^2\left(u_i u_k\right)}{\partial x_i \partial x_k}, \tag{5-116}$$

where the ~'s have been omitted beacuse mean quantities are zero or uniform. Examination of equations (5-115) and (5-116) shows that the pressure term in equation (5-115) and the first term on the right side of that equation are both nonlinear and second-order in **u**. Thus, as **u** becomes small, the nonlinear terms in equation (5-115) approach zero faster than the viscous dissipation term, which is first-order in **u**. Then, for weak turbulence, equations (5-115), (5-77), (5-76), and (5-80) become, respectively,

$$\frac{\partial u_i}{\partial t} = \nu\frac{\partial^2 u_i}{\partial x_k \partial x_k}, \tag{5-117}$$

$$\frac{\partial}{\partial t}\varphi_j(\boldsymbol{\kappa}) = -\nu\kappa^2\varphi_j(\boldsymbol{\kappa}), \tag{5-118}$$

$$\frac{\partial}{\partial t}\varphi_{ij}(\boldsymbol{\kappa}) = -2\nu\kappa^2\varphi_{ij}(\boldsymbol{\kappa}), \tag{5-119}$$

and

$$\frac{\partial}{\partial t}\left[\varphi_i^*(\boldsymbol{\kappa})\varphi_j(\boldsymbol{\kappa})\right] = -2\nu\kappa^2\left[\varphi_i^*(\boldsymbol{\kappa})\varphi_j(\boldsymbol{\kappa})\right]. \tag{5-119a}$$

Neglecting nonlinear terms at low Reynolds number has resulted in the *closed averaged* equations (5-119) and (5-119a). (The *unaveraged* equations from which (5-117) and (5-118) were obtained were, of course already closed.) As shown in section 5.3.1.1, the equations from which (5-119) and (5-119a) were obtained are equivalent, and thus so are equations (5-119) and (5-119a).

Equations (5-118) to (5-119a) can be solved to give

$$\varphi_j(\boldsymbol{\kappa}, t) = \varphi_j(\boldsymbol{\kappa}, 0)e^{-\nu\kappa^2 t} \tag{5-120}$$

and

$$\varphi_{ij}(\boldsymbol{\kappa}, t) = \left[\varphi_i^*(\boldsymbol{\kappa}, t)\varphi_j(\boldsymbol{\kappa}, t)\right] = \varphi_{ij}(\boldsymbol{\kappa}, 0)e^{-2\nu\kappa^2 t} = \left[\varphi_i^*(\boldsymbol{\kappa}, 0)\varphi_j(\boldsymbol{\kappa}, 0)\right]e^{-2\nu\kappa^2 t}. \tag{5-121}$$

Equations (5-120) and (5-121) show that Fourier components of $u_j(\mathbf{x}, t)$ and of $\overline{u_i u_j'}(\mathbf{r}, t)$ are attenuated strongly as (κ) or t becomes large. That attenuation is produced by the viscous dissipation terms in equations (5-118) and (5-119), both of which are multiplied by κ^{2}. Thus, the terms $\partial\varphi_i/\partial t$ and $\partial\varphi_{ij}/\partial t$ in those equations tend to bring φ_i and φ_{ij} close to zero at large κ or t. As a result, with increasing time the turbulent activity (energy for j = i) shifts to lower wavenumbers, or to larger eddy sizes. The physical interpretation of this shift is that the smaller eddies die out faster than the larger ones because of the larger velocity gradients (larger shear stresses) between the smaller eddies. The essence of the turbulence dissipation is that it always tends to bring the turbulence activity closer to zero, and that it affects mainly the smaller eddies.

Consider next an illustrative solution for the two-point velocity correlation. To simplify the problem, we look only at the contracted quantity $\overline{u_i u_i'}$, a scalar.

Using equation (5-121) in (5-11), we get

$$\overline{u_i u_i'}(\mathbf{r}) = \int_{-\infty}^{\infty} A\kappa^2 \cos \boldsymbol{\kappa}\cdot\mathbf{r}\, e^{-2\nu\kappa^2 t}\, d\boldsymbol{\kappa}, \tag{5-122}$$

where we have replaced $e^{i\boldsymbol{\kappa}\cdot\mathbf{r}}$ by $\cos \boldsymbol{\kappa}\cdot\mathbf{r}$, since $\int_{-\infty}^{\infty} i \sin \boldsymbol{\kappa}\cdot\mathbf{r}\, e^{-2\nu\kappa^2 t}\, d\boldsymbol{\kappa} = 0$. Also, continuing to work toward a one-dimensional scalar solution, we have let $\varphi_{ii}(\boldsymbol{\kappa}, 0) = A\kappa^2$. Introducing spherical coordinates $\begin{pmatrix} r_1 \\ \kappa_1 \end{pmatrix} = \begin{pmatrix} r \\ \kappa \end{pmatrix} \cos\varphi \sin\theta$, $\begin{pmatrix} r_2 \\ \kappa_2 \end{pmatrix} = \begin{pmatrix} r \\ \kappa \end{pmatrix} \sin\varphi \sin\theta$, and $\begin{pmatrix} r_3 \\ \kappa_3 \end{pmatrix} = \begin{pmatrix} r \\ \kappa \end{pmatrix} \cos\theta$, one obtains $\boldsymbol{\kappa}\cdot\mathbf{r} = \kappa r$. Then, integrating over all directions in $\boldsymbol{\kappa}$-space, equation (5-122) becomes

$$\overline{u_i u_i'}(r, t) = \int_0^{\infty} A\kappa^2 \cos(\kappa r) e^{-2\nu\kappa^2 t} \int_0^{\pi}\int_0^{2\pi} \kappa^2 \sin\theta\, d\varphi\, d\theta\, d\kappa, \tag{5-123}$$

or

$$\overline{u_i u_i'}(r, t) = 4\pi A \int_0^{\infty} \kappa^4 \cos r\kappa\, e^{-2\nu\kappa^2}\, d\kappa.$$

Carrying out the integration in equation (5-123) (see, e.g., ref. 14) results in

$$\overline{u_i u_i'}(r, t) = \frac{3}{2}\pi^{3/2} A (2\nu t)^{-5/2} \left[1 - (2\nu t)^{-1} r^2 + \frac{1}{12}(2\nu t)^{-2} r^4\right] e^{-r^2/(8\nu t)} \tag{5-124}$$

or, evaluating A in terms of $\overline{u_i u_i'}(0, t_0)$ and t_0, where t_0 is an initial time, we get[4]

$$\overline{u_i u_i'}(r, t) = \overline{u_i u_i'}(0, t_0) \left(\frac{t}{t_0}\right)^{-5/2} \left(1 - \frac{r^2}{2\nu t} + \frac{r^4}{48\nu^2 t^2}\right) e^{-r^2/(8\nu t)}. \tag{5-125}$$

Equation (5-125) satisfies the weak-turbulence equation

$$\frac{\partial \overline{u_i u_i'}(r, t)}{\partial t} = 2\nu \frac{\partial^2 \overline{u_i u_i'}(r, t)}{\partial r_k \partial r_k}, \tag{5-126}$$

[4]A more general expression for the two-point velocity correlation in the final period has been obtained by Batchelor and Proudman (ref. 15, eq. (7-7)).

which is obtained from equation (5-70). For the present case, where $\overline{u_i u_i'}$ is a function only of r and t, equation (5-126) becomes[5]

$$\frac{\partial \overline{u_i u_i'}(r,t)}{\partial t} = 2\nu \frac{\partial^2 \overline{u_i u_i'}(r,t)}{\partial r^2}, \tag{5-127}$$

Equation (5-125) shows that just as φ_{ii} was strongly attenuated as κ increases, so $\overline{u_i u_i'}$ is strongly attenuated with increasing r, as indicated by the negative argument of the exponential. That may seem surprising because at large r, where length scales are large, the viscous effects tend to be small. However, the fact that t appears in the denominator of the argument of the exponential means that $\overline{u_i u_i'}$ decreases less rapidly with time at large r in the region of smaller viscous effects. That is, of course, as it should be. Perhaps the attenuation of $\overline{u_i u_i'}$ with increasing r is best explained by a physical argument. Thus, since a turbulent velocity tends to be a random function of position, the fluid at a point x will, so to speak, lose touch with that at x + r as r increases, so that the correlation between u_i and u_i' will decrease with increasing r.

One can define characteristic length scales for $\overline{u_i u_i'}(r)$ as

$$\lambda^2 = -\frac{2\,\overline{u_i u_i'}(0,t)}{\left(\partial^2 \overline{u_i u_i'}(r,t)/\partial r^2\right)_{r=0}}, \tag{5-128}$$

and

$$L(t) = \frac{\int_0^\infty \overline{u_i u_i'}(r,t)\,dr}{\overline{u_i u_i'}(0,t)}, \tag{5-129}$$

where λ is a microscale, a measure of the size of the small eddies of the turbulence, and L is a macroscale, a measure of the size of the energy-containing eddies. The former of these is obtained by inscribing a parabola in the curve for $\overline{u_i u_i'}(r)$ versus r at r = 0. The microscale λ is then the value of r where the parabola intersects the r axis. When $\overline{u_i u_i'}(r,t)$ is given by equation (5-125), where $\overline{u_i u_i'}(0,t_0)(t/t_0)^{-5/2} = \overline{u_i u_i'}(0,t)$, we have $\lambda/\sqrt{\nu t} = 2\sqrt{2/5}$ and $L/\sqrt{\nu t} = 0$! The perhaps unexpected value for $L/\sqrt{\nu t}$ means that $\overline{u_i u_i'}$ must go negative for some values of r, as confirmed in figure 5-1. The value of zero calculated for L means, of course, that the definition of L given by equation (5-128) is not realistic when $\overline{u_i u_i'}$ goes appreciably negative for some values of r. Possibly a better definition for the macroscale would be

$$L' = \frac{\int_0^\infty \left|\overline{u_i u_i'}(r,t)\right| dr}{\overline{u_i u_i'}(0,t)}. \tag{5-129a}$$

For $\overline{u_i u_i'}$ given by equation (5-125), we find $L'/\lambda = 2.34$ for all times in the final period.

---

[5]The equality of $\partial^2 \overline{u_i u_i'}/\partial r_k\,\partial r_k$ and $\partial^2 \overline{u_i u_i'}/\partial r^2$ for $\overline{u_i u_i'} = \overline{u_i u_i'}(r,t)$ can be shown as follows: First, note that

$$\frac{\partial}{\partial r_k}\overline{u_i u_i'}(r,t) = \frac{\partial \overline{u_i u_i'}(r,t)}{\partial r}\frac{\partial r}{\partial r_k} = \frac{\partial \overline{u_i u_i'}}{\partial r}\frac{\partial (r_\ell r_\ell)^{1/2}}{\partial r_k} = \frac{\partial \overline{u_i u_i'}}{\partial r}\frac{r_\ell}{r}\frac{\partial r_\ell}{\partial r_k} = \frac{\partial \overline{u_i u_i'}}{\partial r}\frac{r_\ell}{r}\delta_{\ell k} = \frac{\partial \overline{u_i u_i'}}{\partial r}\frac{r_k}{r}.$$ Then,

$$\frac{\partial^2 \overline{u_i u_i'}(r,t)}{\partial r_k \partial r_k} = \overline{u_i u_i'}\left(-\frac{r_k}{r^2}\frac{\partial r_k}{\partial r} + r^{-1}\right) + \frac{r_k r_k}{r^2}\frac{\partial^2 \overline{u_i u_i'}}{\partial r^2} = \overline{u_i u_i'}\left(-\frac{r_k}{r^2}\frac{r}{r_k} + \frac{1}{r}\right) + \frac{\partial^2 \overline{u_i u_i'}}{\partial r^2} = \frac{\partial^2 \overline{u_i u_i'}(r,t)}{\partial r^2}.$$ (This of course, has nothing to do with transforming from x_i to (r,θ,φ) coordinates where, for spherical symmetry, $\partial^2/\partial x_k \partial x_k$ is replaced by $(1/r^2)(\partial/\partial r)(r^2\partial/\partial r)$; $\overline{u_i u_i'}$ is a function of r_i (or of r for spherical symmetry), not of x_i.)

One might ask how there could be a negative correlation between u_i and u_i'. Evidently the negative and oscillating correlations shown in figure 5-1 might be obtained when there is some nonrandom (possibly periodic) structure in a flow superimposed on random turbulent flow that tends to make the correlation go to zero at large r. Incidentally, there is nothing unusual about correlations in turbulent flow which go negative and/or oscillate (see, e.g., fig. 4-16).

5.3.2.2 *Turbulence at various times before the final period of decay.*—Unless the turbulence level is very low, as in the final period of decay (or the decay times are very short (see section 5.3.2.1)), the inertial or spectral-transfer effects will not be negligible ($T_{ij} \neq 0$), and so we would like to be able to take them into account in some way. A large number of proposals for calculating the spectral transfer have been given, including those of Heisenberg, Kovasznay, and Kraichman, to name a few (refs. 16 to 18). The number of proposals for calculating the spectral transfer effects appears, in fact, to approach the number of workers in the field. Reviews of the proposals are given, for instance, in references 4, 19, and 20. Here we will consider a simple deductive approach which is essentially a perturbation on the solution for the final period of decay considered in the last section. That is by far the simplest deductive approach and will be sufficient for our purpose, which is to illustrate spectral transfer by a comparatively simple solution.

We consider a correlation-term discard closure. In using that (systematic) procedure, the infinite set of multipoint correlation equations is made determinate by neglecting the highest-order terms in the highest-order equations considered (refs. 21 and 22). The procedure can be shown to be equivalent to a formally exact expansion in powers of Reynolds number (or of time) (refs. 23 and 24). It has been speculated that the scheme may be divergent and may give negative spectral energies (refs. 10 and 25), although the results in references 21 and 22 showed no such tendencies.[6] Even though the expansion may be divergent, the truncated series should give a reasonable approximation as an asymptotic expansion (ref. 24). That may be the saving feature of the present scheme as well as of other approximations.[7] A more serious problem might be that the calculations are likely to become hopelessly complicated (or impossible) if higher Reynolds-number turbulence is to be represented.

Several other schemes, such as the cumulant-discard closure and the direct-interaction approximation, which are essentially partial summations of the expansion in powers of Reynolds number (ref. 23), have been proposed. Both of those are much more complex than the method considered here. Although at least the latter of those schemes appears to give some realistic results, the problem in their justification is that there seems to be no way of knowing whether the additional terms retained (to all orders in Reynolds number) are more important than those still neglected. In this connection, note that although cumulant-discard approximations retain terms of all orders in Reynolds number or time, the domains of validity of the cumulant-discard approximations and the simpler power-series truncations (correlation-term discard schemes) are apparently the same (small Reynolds number or small time (refs. 23 and 24)).

Consider first the two-point correlation equations—equations that involve product mean values or correlations between velocities or between velocities and pressures at two points. Those equations could be obtained by simplification of equations (4-147), (4-149), and (4-150) in the last chapter, but it may be instructive to obtain them directly from the Navier-Stokes equations.

The incompressible Navier-Stokes or momentum equations written for the points P and P′ separated by the vector r are

$$\frac{\partial u_i}{\partial t} + \frac{\partial (u_i u_k)}{\partial x_k} = -\frac{1}{\rho}\frac{\partial \sigma}{\partial x_i} + \nu \frac{\partial^2 u_i}{\partial x_k \partial x_k} \tag{5-130}$$

and

$$\frac{\partial u_j'}{\partial t} + \frac{\partial (u_j' u_k')}{\partial x_k'} = -\frac{1}{\rho}\frac{\partial \sigma'}{\partial x_j'} + \nu \frac{\partial^2 u_j'}{\partial x_k' \partial x_k'}, \tag{5-131}$$

[6]Perhaps it is too much to expect an approximate (truncated) representation to be good (e.g., that it produces positive energy) at all Reynolds numbers, times, and wavenumbers. (Of course, the wider the range of applicability, the better.) A more realistic expectation might be that it be good for limited ranges of those parameters. For example, it seems unreasonable to discard a representation solely because the energy goes negative for a range of wavenumbers at large times. It may be perfectly satisfactory at earlier times. (Note that Newtonian mechanics has not been thrown out because it breaks down as the speed of light is approached!)

[7]Other, more sophisticated approximations, appear also to work because they are kinds of asymptotic expansions. For example, higher-order expansions related to the direct-interaction approximation appear to give less reasonable results than those of lower-order (refs. 24 and 26).

where, as usual, the subscripts can take on the values 1, 2, or 3, and a repeated subscript in a term indicates a summation. The quantities u_i and u'_j are instantaneous velocity components, x_i is a space coordinate, t is the time, ρ is the density, ν is the kinematic viscosity, and σ is the instantaneous mechanical pressure (see eq. (3-14)). Multiplying the first equation by u'_j and the second by u_i, adding, and taking space averages, result in

$$\frac{\partial \overline{u_i u'_j}}{\partial t} + \frac{\partial}{\partial x_k}\left(\overline{u_i u'_j u_k}\right) + \frac{\partial}{\partial x'_k}\left(\overline{u_i u'_j u'_k}\right) = -\frac{1}{\rho}\left(\frac{\partial \overline{\sigma u'_j}}{\partial x_i} + \frac{\partial \overline{\sigma' u_i}}{\partial x'_j}\right) + \nu\left(\frac{\partial^2 \overline{u_i u'_j}}{\partial x_k \, \partial x_k} + \frac{\partial^2 \overline{u_i u'_j}}{\partial x'_k \, \partial x'_k}\right) \tag{5-132}$$

where the fact that quantities at x_i are independent of x'_i and quantities at x'_i are independent of x_i was used. Equation (5-132) can be written as

$$\frac{\partial \overline{u_i u'_j}}{\partial t} + \frac{\partial}{\partial r_k}\left(\overline{u_i u'_j u'_k} - \overline{u_i u'_j u_k}\right) = -\frac{1}{\rho}\left(\frac{\partial \overline{\sigma' u_i}}{\partial r_j} - \frac{\partial \overline{\sigma u'_j}}{\partial r_i}\right) + 2\nu \frac{\partial^2 \overline{u_i u'_j}}{\partial r_k \, \partial r_k} \tag{5-133}$$

where the relations $(\partial/\partial x_i) = -(\partial/\partial r_i)$ and $(\partial/\partial x'_i) = (\partial/\partial r_i)$ were used, and the correlations are functions only of $\mathbf{r}$ and t. Equation (5-133) was first obtained by Kármán and Howarth (ref. 27). It is desirable to write equation (5-133) in spectral form in order to reduce it to an ordinary differential equation and because of the physical significance of spectral quantities. For this purpose we use the three-dimensional Fourier transforms (from $\mathbf{r}$- to $\boldsymbol{\kappa}$-space):

$$\overline{u_i u'_j(\mathbf{r})} = \int_{-\infty}^{\infty} \varphi_{ij}(\boldsymbol{\kappa}) e^{i\boldsymbol{\kappa}\cdot\mathbf{r}} d\boldsymbol{\kappa} \tag{5-134}$$

$$\overline{u_i u_k u'_j(\mathbf{r})} = \int_{-\infty}^{\infty} \varphi_{ikj}(\boldsymbol{\kappa}) e^{i\boldsymbol{\kappa}\cdot\mathbf{r}} d\boldsymbol{\kappa} \tag{5-135}$$

and

$$\overline{\sigma u'_j(\mathbf{r})} = \int_{-\infty}^{\infty} \lambda_j(\boldsymbol{\kappa}) e^{i\boldsymbol{\kappa}\cdot\mathbf{r}} d\boldsymbol{\kappa} \tag{5-136}$$

where $\boldsymbol{\kappa}$ is a wavevector and $d\boldsymbol{\kappa} = d\kappa_1 d\kappa_2 \, d\kappa_3$. The magnitude of $\boldsymbol{\kappa}$ has the dimension 1/length and can be considered to be the reciprocal of an eddy size. From equation (5-135)

$$\overline{u_i u_k u'_j(-\mathbf{r})} = \int_{-\infty}^{\infty} \varphi_{ikj}(\boldsymbol{\kappa}) e^{-i\boldsymbol{\kappa}\cdot\mathbf{r}} d\boldsymbol{\kappa} = \int_{-\infty}^{\infty} \varphi_{ikj}(-\boldsymbol{\kappa}) e^{-i\boldsymbol{\kappa}\cdot\mathbf{r}} d\boldsymbol{\kappa}$$

where the last step can be seen more clearly by writing the inverse transform. Interchanging the subscripts i and j and then interchanging the points P and P′ give

$$\overline{u_i u'_j(\mathbf{r}) u'_k(\mathbf{r})} = \overline{u_j u_k u'_i(-\mathbf{r})} = \int_{-\infty}^{\infty} \varphi_{jki}(-\boldsymbol{\kappa}) e^{i\boldsymbol{\kappa}\cdot\mathbf{r}} d\boldsymbol{\kappa}. \tag{5-135a}$$

Similarly

$$\overline{u_i \sigma'(\mathbf{r})} = \overline{\sigma u'_i(-\mathbf{r})} = \int_{-\infty}^{\infty} \lambda_i(-\boldsymbol{\kappa}) e^{i\boldsymbol{\kappa}\cdot\mathbf{r}} d\boldsymbol{\kappa}. \tag{5-136a}$$

Substituting equations (5-134) to (5-136a) into equation (5-133) gives

$$\frac{d\varphi_{ij}}{dt} + i\kappa_k\left[\varphi_{jki}(-\boldsymbol{\kappa}) - \varphi_{ikj}\right] = -\frac{1}{\rho}\left(i\kappa_j \lambda_i(-\boldsymbol{\kappa}) - i\kappa_i \lambda_j\right) - 2\nu\kappa^2 \varphi_{ij} \tag{5-137}$$

where the functional designations (κ) are omitted for brevity. The tensor equation (5-137) becomes a scalar equation by contraction of the indices i and j. Thus,

$$\frac{d\varphi_{ii}}{dt} + 2\nu\kappa^2\varphi_{ii} = i\kappa_k\varphi_{iki} - i\kappa_k\varphi_{iki}(-\kappa). \tag{5-138}$$

The pressure terms drop out of equation (5-138) because of the continuity relation $\partial u_i / \partial x_i = \partial u_i' / \partial x_i' = 0$ (see eq. (5-133)).

The terms on the right side of equation (5-138) are collectively proportional to what is known as the energy-transfer term. They account for the transfer of energy from one wavenumber to another or from one eddy size to another, but their total contribution to $d\overline{u_i u_i}/dt$ is zero (see section 5.3.1.2). Equation (5-138) applies to homogeneous as well as to isotropic turbulence. However, in order to obtain a solution an expression for the transfer or inertia term on the right side must be obtained. Kármán and Howarth neglected that term and obtained a solution applicable in the final period of decay (ref. 27). In the present investigation it is proposed to obtain an expression for the transfer term applicable at times before the final period from the three-point correlation or spectral equations. To obtain the three-point equation, write the Navier-Stokes equation at the points P, P′, and P″ separated by the vectors **r** and **r**′. The vector configuration is shown in figure 5-2. The first two equations are the same as equations (5-130) and (5-131), with the dummy subscripts k replaced by ℓ. The third equation is

$$\frac{\partial u_k''}{\partial t} + \frac{\partial}{\partial x_\ell''}\left(u_k'' u_\ell''\right) = -\frac{1}{\rho}\frac{\partial \sigma''}{\partial x_k''} + \nu\frac{\partial^2 u_k''}{\partial x_\ell'' \partial x_\ell''}. \tag{5-139}$$

Multiplying the first equation by $u_j' u_k''$ the second by $u_i u_k''$, and the third by $u_i u_j'$, adding the three equations, and taking space averages, result in

$$\frac{\partial}{\partial t}\overline{u_i u_j' u_k''} + \frac{\partial}{\partial x_\ell}\overline{u_i u_j' u_k'' u_\ell} + \frac{\partial}{\partial x_\ell'}\overline{u_i u_j' u_k'' u_\ell'} + \frac{\partial}{\partial x_\ell''}\overline{u_i u_j' u_k'' u_\ell''} = -\frac{1}{\rho}\left(\frac{\partial\overline{\sigma u_j' u_k''}}{\partial x_i} + \frac{\partial\overline{\sigma' u_i u_k''}}{\partial x_j'} + \frac{\partial\overline{\sigma'' u_i u_j'}}{\partial x_k''}\right)$$

$$+ \nu\left(\frac{\partial^2\overline{u_i u_j' u_k''}}{\partial x_\ell \partial x_\ell} + \frac{\partial^2\overline{u_i u_j' u_k''}}{\partial x_\ell' \partial x_\ell'} + \frac{\partial^2\overline{u_i u_j' u_k''}}{\partial x_\ell'' \partial x_\ell''}\right). \tag{5-140}$$

Equation (5-140) can be written in terms of the independent variables **r** and **r**′ as

$$\frac{\partial}{\partial t}\overline{u_i u_j' u_k''} - \frac{\partial}{\partial r_\ell}\overline{u_i u_j' u_k'' u_\ell} - \frac{\partial}{\partial r_\ell'}\overline{u_i u_j' u_k'' u_\ell} + \frac{\partial}{\partial r_\ell}\overline{u_i u_j' u_k'' u_\ell'} + \frac{\partial}{\partial r_\ell'}\overline{u_i u_j' u_k'' u_\ell''} = -\frac{1}{\rho}\left(-\frac{\partial}{\partial r_i}\overline{\sigma u_j' u_k''} - \frac{\partial}{\partial r_i'}\overline{\sigma u_j' u_k''} + \frac{\partial}{\partial r_j}\overline{\sigma' u_i u_k''}\right.$$

$$\left. + \frac{\partial}{\partial r_k'}\overline{\sigma'' u_i u_j'}\right) + 2\nu\left(\frac{\partial^2\overline{u_i u_j' u_k''}}{\partial r_\ell \partial r_\ell} + \frac{\partial^2\overline{u_i u_j' u_k''}}{\partial r_\ell \partial r_\ell'} + \frac{\partial^2\overline{u_i u_j' u_k''}}{\partial r_\ell' \partial r_\ell'}\right). \tag{5-141}$$

Where the following relations were used:

$$\frac{\partial}{\partial x_\ell'} = \frac{\partial}{\partial r_\ell}, \quad \frac{\partial}{\partial x_\ell''} = \frac{\partial}{\partial r_\ell'}, \quad \frac{\partial}{\partial x_\ell} = -\frac{\partial}{\partial r_\ell} - \frac{\partial}{\partial r_\ell'}.$$

In order to convert equation (5-141) to spectral form, one can define the following six-dimensional Fourier transforms:

$$\overline{u_i u'_j(\mathbf{r}) u''_k(\mathbf{r}')} = \int_{-\infty}^{\infty}\int_{-\infty}^{\infty} \beta_{ijk}(\boldsymbol{\kappa}, \boldsymbol{\kappa}')\, e^{i(\boldsymbol{\kappa}\cdot\mathbf{r}+\boldsymbol{\kappa}'\cdot\mathbf{r}')} d\boldsymbol{\kappa} d\boldsymbol{\kappa}', \tag{5-142}$$

$$\overline{u_i u_\ell u'_j(\mathbf{r}) u''_k(\mathbf{r}')} = \int_{-\infty}^{\infty}\int_{-\infty}^{\infty} \beta_{i\ell jk}(\boldsymbol{\kappa}, \boldsymbol{\kappa}')\, e^{i(\boldsymbol{\kappa}\cdot\mathbf{r}+\boldsymbol{\kappa}'\cdot\mathbf{r}')} d\boldsymbol{\kappa} d\boldsymbol{\kappa}', \tag{5-143}$$

$$\overline{\sigma u'_j(\mathbf{r}) u''_k(\mathbf{r}')} = \int_{-\infty}^{\infty}\int_{-\infty}^{\infty} \alpha_{jk}(\boldsymbol{\kappa}, \boldsymbol{\kappa}')\, e^{i(\boldsymbol{\kappa}\cdot\mathbf{r}+\boldsymbol{\kappa}'\cdot\mathbf{r}')} d\boldsymbol{\kappa} d\boldsymbol{\kappa}'. \tag{5-144}$$

By using the method for obtaining equation (5-135a) the following relations result from equations (5-143) and (5-144):

$$\overline{u_i u'_\ell(\mathbf{r}) u'_j(\mathbf{r}) u''_k(\mathbf{r}')} = \overline{u_j u_\ell u'_i(-\mathbf{r}) u''_k(\mathbf{r}'-\mathbf{r})} = \int_{-\infty}^{\infty}\int_{-\infty}^{\infty} \beta_{j\ell ik}(-\boldsymbol{\kappa}-\boldsymbol{\kappa}', \boldsymbol{\kappa}')\, e^{i(\boldsymbol{\kappa}\cdot\mathbf{r}+\boldsymbol{\kappa}'\cdot\mathbf{r}')} d\boldsymbol{\kappa} d\boldsymbol{\kappa}', \tag{5-143a}$$

$$\overline{u_i u'_j(\mathbf{r}) u''_k(\mathbf{r}') u''_\ell(\mathbf{r}')} = \overline{u_k u_\ell u'_i(-\mathbf{r}') u'_j(\mathbf{r}-\mathbf{r}')} = \int_{-\infty}^{\infty}\int_{-\infty}^{\infty} \beta_{k\ell ij}(-\boldsymbol{\kappa}-\boldsymbol{\kappa}', \boldsymbol{\kappa})\, e^{i(\boldsymbol{\kappa}\cdot\mathbf{r}+\boldsymbol{\kappa}'\cdot\mathbf{r}')} d\boldsymbol{\kappa} d\boldsymbol{\kappa}', \tag{5-143b}$$

where the points P and P′ were interchanged to obtain equation (5-143a). For obtaining (5-143b), P is replaced by P′, P′ is replaced by P″, and P″ is replaced by P. Similarly,

$$\overline{u_i \sigma'(\mathbf{r}) u''_k(\mathbf{r}')} = \overline{\sigma u'_i(-\mathbf{r}) u''_k(\mathbf{r}'-\mathbf{r})} = \int_{-\infty}^{\infty}\int_{-\infty}^{\infty} \alpha_{ik}(-\boldsymbol{\kappa}-\boldsymbol{\kappa}', \boldsymbol{\kappa}')\, e^{i(\boldsymbol{\kappa}\cdot\mathbf{r}+\boldsymbol{\kappa}'\cdot\mathbf{r}')} d\boldsymbol{\kappa}\, d\boldsymbol{\kappa}', \tag{5-144a}$$

and

$$\overline{u_i u'_j(\mathbf{r}) \sigma''(\mathbf{r}')} = \overline{\sigma u'_i(-\mathbf{r}) u''_j(\mathbf{r}-\mathbf{r}')} = \int_{-\infty}^{\infty}\int_{-\infty}^{\infty} \alpha_{ij}(-\boldsymbol{\kappa}-\boldsymbol{\kappa}', \boldsymbol{\kappa})\, e^{i(\boldsymbol{\kappa}\cdot\mathbf{r}+\boldsymbol{\kappa}'\cdot\mathbf{r}')} d\boldsymbol{\kappa}\, d\boldsymbol{\kappa}'. \tag{5-145}$$

Substituting the preceeding relations into equation (5-141) gives

$$\frac{d}{dt}\beta_{ijk} + 2\nu\left(\kappa^2 + \kappa_\ell \kappa'_\ell + \kappa'^2\right)\beta_{ijk} = \left[i\left(\kappa_\ell + \kappa'_\ell\right)\beta_{i\ell jk} - i\kappa_\ell \beta_{j\ell ik}(-\boldsymbol{\kappa}-\boldsymbol{\kappa}', \boldsymbol{\kappa}') - i\kappa'_\ell \beta_{k\ell ij}(-\boldsymbol{\kappa}-\boldsymbol{\kappa}', \boldsymbol{\kappa})\right]$$

$$-\frac{1}{\rho}\left[-i\left(\kappa_i + \kappa'_i\right)\alpha_{jk} + i\kappa_j \alpha_{ik}(-\boldsymbol{\kappa}-\boldsymbol{\kappa}', \boldsymbol{\kappa}') + i\kappa'_k \alpha_{ij}(-\boldsymbol{\kappa}-\boldsymbol{\kappa}', \boldsymbol{\kappa})\right]. \tag{5-146}$$

Equation (5-146) agrees with equation (2.11) in reference 28.

The expression in the first bracket on the right side of equation (5-146) can be interpreted as a transfer term similar to that on the right side of equation (5-138). Using an argument similar to that given for equation (5-138) (see section 5.3.1.2), one can obtain an expression for the quadruple correlation terms in equation (5-141) for $\mathbf{r}$ and $\mathbf{r}' = 0$ by allowing the points x_i, x'_i, and x''_i in equations (5-130), (5-131), and (5-139) to coincide. Then the terms involving quadruple correlations become

$$\overline{u_j u_k \frac{\partial\left(u_i u_\ell\right)}{\partial x_\ell}} + \overline{u_i u_k \frac{\partial\left(u_\ell u_j\right)}{\partial x_\ell}} + \overline{u_i u_j \frac{\partial\left(u_k u_\ell\right)}{\partial x_\ell}} = \overline{u_\ell u_j u_k \frac{\partial u_i}{\partial x_\ell}} + \overline{u_\ell u_i u_k \frac{\partial u_j}{\partial x_\ell}} + \overline{u_\ell u_i u_j \frac{\partial u_k}{\partial x_\ell}} = \frac{\partial}{\partial x_\ell}\left(\overline{u_i u_j u_k u_\ell}\right) = 0, \tag{5-147}$$

where the conditions of homogeneity and continuity were used. From equation (5-143) for $\mathbf{r} = \mathbf{r}' = 0$, and equation (5-147),

$$\int_{-\infty}^{\infty}\int_{-\infty}^{\infty}\left[\beta_{ijk}\right] d\boldsymbol{\kappa}\, d\boldsymbol{\kappa}' = 0 \tag{5-148}$$

where the expression in the first bracket in equation (5-146) was set equal to $[\beta_{ijk}]$. Thus $[\beta_{ijk}]$ gives zero total contribution to $d\,\overline{u_i u_j u_k}/dt$. However it can alter the distribution in wavenumber space of contributions to $\overline{u_i u_j u_k}$. It appears that similar transfer terms occur in all higher-order equations.

The tensor equation (5-146) can be converted to a scalar equation by contraction of the indexes i and j and inner multiplication by κ_k:

$$\frac{d}{dt}(\kappa_k \beta_{iik}) + 2\nu\left(\kappa^2 + \kappa_\ell \kappa'_\ell + \kappa'^2\right)\kappa_k\,\beta_{iik} = i\kappa_k(\kappa_\ell + \kappa'_\ell)\beta_{i\ell ik} - i\kappa_k\kappa_\ell\beta_{i\ell ik}(-\boldsymbol{\kappa}-\boldsymbol{\kappa}',\boldsymbol{\kappa}') - i\kappa_k\kappa'_\ell\beta_{k\ell ii}(-\boldsymbol{\kappa}-\boldsymbol{\kappa}',\boldsymbol{\kappa})$$

$$-\frac{1}{\rho}\left[-i\kappa_k(\kappa_i + \kappa'_i)\alpha_{ik} + i\kappa_k\kappa_i\alpha_{ik}(-\boldsymbol{\kappa}-\boldsymbol{\kappa}',\boldsymbol{\kappa}') + i\kappa_k\kappa'_k\alpha_{ii}(-\boldsymbol{\kappa}-\boldsymbol{\kappa}',\boldsymbol{\kappa})\right]. \qquad (5-149)$$

To obtain a relation between the terms on the right side of equation (5-149) which are derived from the quadruple correlation terms and from the pressure terms in equation (5-141), take the divergence of the Navier-Stokes equation and combine the result with the continuity equation to give

$$\frac{1}{\rho}\frac{\partial^2\sigma}{\partial x_\ell\,\partial x_\ell} = -\frac{\partial^2(u_\ell u_m)}{\partial x_\ell\,\partial x_m}. \qquad (5-150)$$

Multiplying equation (5-150) by $u'_i u''_k$, taking space averages, and writing the resulting equation in terms of the independent variables $\mathbf{r}$ and $\mathbf{r}'$, give

$$\frac{1}{\rho}\left(\frac{\partial^2\overline{\sigma u'_i u''_k}}{\partial r_\ell\,\partial r_\ell} + 2\frac{\partial^2\overline{\sigma u'_i u''_k}}{\partial r_\ell\,\partial r'_\ell} + \frac{\partial^2\overline{\sigma u'_i u''_k}}{\partial r'_\ell\,\partial r'_\ell}\right) = -\frac{\partial^2\overline{u_\ell u_m u'_i u''_k}}{\partial r_m\,\partial r_\ell} - \frac{\partial^2\overline{u_\ell u_m u'_i u''_k}}{\partial r_m\,\partial r'_\ell} - \frac{\partial^2\overline{u_\ell u_m u'_i u''_k}}{\partial r'_m\,\partial r_\ell} - \frac{\partial^2\overline{u_\ell u_m u'_i u''_k}}{\partial r'_m\,\partial r'_\ell}. \qquad (5-151)$$

The Fourier transform of equation (5-151) is

$$-\frac{1}{\rho}\left(\kappa^2 + 2\kappa_\ell\kappa'_\ell + \kappa'^2\right)\alpha_{ik} = \left(\kappa_\ell\kappa_m + \kappa'_\ell\kappa_m + \kappa_\ell\kappa'_m + \kappa'_\ell\kappa'_m\right)\beta_{\ell mik}$$

or

$$-\frac{1}{\rho}\alpha_{ik} = \frac{\kappa_\ell\kappa_m + \kappa'_\ell\kappa_m + \kappa_\ell\kappa'_m + \kappa'_\ell\kappa'_m}{\kappa^2 + 2\kappa_\ell\kappa'_\ell + \kappa'^2}\beta_{\ell mik}. \qquad (5-152)$$

Equation (5-152) can be used to eliminate the quantities α_{ik}, $\alpha_{ik}(-\boldsymbol{\kappa}-\boldsymbol{\kappa}', \boldsymbol{\kappa}')$, etc., from equation (5-149). In order to solve equations (5-138), (5-149), and (5-152) simultaneously a relation between β_{iik} and φ_{iki} is required. Letting $\mathbf{r}'=0$ in equation (5-142) and comparing the result with equation (5-135) shows that

$$\varphi_{iki}(\boldsymbol{\kappa}) = \int_{-\infty}^{\infty}\beta_{iik}(\boldsymbol{\kappa},\boldsymbol{\kappa}')\,d\boldsymbol{\kappa}'. \qquad (5-153)$$

The set of equations (5-138), (5-149), (5-152), and (5-153) is still not determinate inasmuch as there are more unknowns than equations. It is proposed to obtain a solution applicable at times before the final period, as well as during the final period of decay, by neglecting the terms in equations (5-149) and (5-152) corresponding to quadruple correlation terms. Corresponding to the case of the final period, where a solution was obtained by neglecting the triple correlation terms in the two-point equation, it should be possible to obtain a solution for times before the final period by neglecting the quadruple correlation terms in the three-point equations. If a solution applicable at still earlier times were desired it would be necessary to consider four or five point equations. In each case the set of equations would be made determinate by neglecting terms containing the highest-order correlations.

Equation (5-152) shows that if terms containing quadruple correlations are neglected, then the terms containing pressure correlations must also be neglected. Thus, neglecting all the terms on the right side of equation (5-149), the equation can be integrated between t_0 and t to give

$$\kappa_k \beta_{iik} = \kappa_k (\beta_{iik})_0 \exp\left[-2\nu(t-t_0)\left(\kappa^2 + \kappa\kappa' \cos\theta + \kappa'^2\right)\right], \tag{5-154}$$

where $(\beta_{iik})_0$ is the value of β_{iik} at $t = t_o$ (an initial time or virtual origin), and θ is the angle between κ and κ'. Note that $(\beta_{ijk})_0$ also equals β_{iik} for small values of κ and κ' at various times, so that β_{ijk} has a stationary form at small values of κ and κ', at least for times when the quadruple correlations are negligible. Substitution of equations (5-154) and (5-153), in equation (5-138) results in

$$\frac{d\varphi_{ii}}{dt} + 2\nu\kappa^2\varphi_{ii} = \int_0^\infty 2\pi i\kappa_k \left[\beta_{iik} - \beta_{iik}(-\kappa,-\kappa')\right]_0 \kappa'^2 \left[\int_{-1}^{1} \exp\left[-2\nu(t-t_0)\left(\kappa^2 + \kappa\kappa'\cos\theta + \kappa'^2\right)\right] d(\cos\theta)\right] d\kappa', \tag{5-155}$$

where $d\kappa' = d\kappa_1'\, d\kappa_2'\, d\kappa_3'$ is written in terms of κ' and θ as $-2\pi\kappa'^2 d(\cos\theta)\, d\kappa'$.

In order to make further calculations it is necessary to assume a relation which gives $[\beta_{iik} - \beta_{iik}(-\kappa,-\kappa')]_0$ as a function of κ and κ'. The theory itself will not, of course, supply this relation; it gives only the state of the turbulence at various times when the initial state is known. The relation assumed here is

$$i\kappa_k \left[\beta_{iik} - \beta_{iik}(-\kappa,-\kappa')\right]_0 = -\beta_0\left(\kappa^m \kappa'^n - \kappa^n \kappa'^m\right), \tag{5-156}$$

where β_0 is a constant determined by the initial conditions, so that its value will in general depend on m and n. As will be seen later, this expression gives a transfer term which satisfies equation (5-98). Here we choose m = 4 and n = 6. Later we will investigate the effect of the choices for m and n on some of the results. The negative sign is placed in front of β_0 in order to make the transfer of energy from small to large wavenumbers for positive values of β_0. By virtue of equations (5-155) and (5-156) one can write $\varphi_{ii} = \varphi_{ii}(\kappa)$.

Energy spectrum and spectral transfer. Substituting equation (5-156) in (5-155), writing φ_{ii} in terms of the energy spectrum function,

$$E(\kappa) = 2\pi\kappa^2 \varphi_{ii}(\kappa) \tag{5-157}$$

(ref. 4), and carrying out the integration with respect to θ in equation (5-155), result in

$$dE(\kappa)/dt + 2\nu\kappa^2 E(\kappa) = T(\kappa), \tag{5-158}$$

where $T(\kappa)$ is the energy transfer term and is given by

$$T(\kappa) = -\frac{\beta_0}{2\nu(t-t_0)} \int_0^\infty \left(\kappa^5\kappa'^7 - \kappa^7\kappa'^5\right)\left\{\exp\left[-2\nu(t-t_0)\left(\kappa^2 - \kappa\kappa' + \kappa'^2\right)\right] - \exp\left[-2\nu(t-t_0)\left(\kappa^2 + \kappa\kappa' + \kappa'^2\right)\right]\right\} d\kappa'. \tag{5-159}$$

On multiplying each term in equation (5-158) by $d\kappa$ it is seen that the first term represents the rate of change of energy in the wavenumber band $d\kappa$, the second term is the energy dissipated within the band, and $T(\kappa)$ is the net energy transferred into the band.

Equation (5-159) can also be given an interesting physical interpretation. Letting the integrand in the equation be $P(\kappa, \kappa')$, we have

$$T(\kappa) = \int_0^\infty P(\kappa,\kappa')\, d\kappa'. \tag{5-160}$$

Multiplying both sides of equation (5-160) by $d\kappa$, we note that, as in equation (5-158), $T(\kappa)d\kappa$ is the the net energy flowing into the wavenmuber band $d\kappa$ from all other wavenumbers. The quantity $P(\kappa, \kappa')d\kappa' d\kappa$ is the energy flowing from the wavenumber band $d\kappa'$ into the band $d\kappa$. It might be called the distribution function for contributions to $T(\kappa)$ from various wavenumbers or eddy sizes.

Carrying out the integration indicated in equation (5-159), that is, summing up the contributions to T(κ) from all wavenumber bands, gives

$$T(\kappa) = -\frac{(\pi/2)^{1/2}}{256}\beta_0 \exp\left[-(3/2)\kappa^2\nu(t-t_0)\right]\left[105\frac{\kappa^6}{(t-t_0)^{9/2}} + 45\frac{\kappa^8}{(t-t_0)^{7/2}} - 19\frac{\kappa^{10}}{(t-t_0)^{5/2}} - 3\frac{\kappa^{12}}{(t-t_0)^{3/2}}\right]. \qquad (5-161)$$

If we integrate equation (5-161) over all wavenumbers we find that

$$\int_0^\infty T(\kappa)\, d\kappa = 0, \qquad (5-162)$$

indicating that the expression for T(κ) satisfies equation (5-98). This is a consequence of the antisymmetry of equation (5-156).

For obtaining the energy spectrum function E, equation (5-158) can be written in integral form as

$$E = \exp\left[-2\nu\kappa^2(t-t_0)\right]\int \exp\left[2\kappa^2\nu(t-t_0)\right]T\, dt + C(\kappa)\exp\left[-2\nu\kappa^2(t-t_0)\right], \qquad (5-163)$$

where T is given by equation (5-161). We let the constant of integration be given by

$$C(\kappa) = J_0\kappa^4/3\pi. \qquad (5-164)$$

There is some theoretical basis for equation (5-164) (ref. 15), but C(κ) for a particular flow may depend on how the turbulence is generated (ref. 29).

Carrying out the integration indicated in equation (5-163) and substituting equation (5-164) result in the following expression for the energy spectrum function:

$$E = \frac{J_0\kappa^4}{3\pi}\exp\left[-2\nu\kappa^2(t-t_0)\right] - \frac{\pi^{1/2}\beta_0}{256\nu}\exp\left[-(3/2)\kappa^2\nu(t-t_0)\right]\left[-\frac{15\sqrt{2}}{\nu^{7/2}}\frac{\kappa^6}{(t-t_0)^{7/2}} - \frac{12\sqrt{2}}{\nu^{5/2}}\frac{\kappa^8}{(t-t_0)^{5/2}} + \frac{7\sqrt{2}}{3\nu^{3/2}}\frac{\kappa^{10}}{(t-t_0)^{3/2}}\right.$$

$$\left. + \frac{16\sqrt{2}}{3\nu^{1/2}}\frac{\kappa^{12}}{(t-t_0)^{1/2}} - \frac{32}{3}\kappa^{13}F\left(\kappa\left[\frac{\nu(t-t_0)}{2}\right]^{1/2}\right)\right] \qquad (5-165)$$

where

$$F(\omega) = e^{-\omega^2}\int_0^\omega e^{x^2}\, dx,$$

$$\omega = \kappa\left[\frac{\nu(t-t_0)}{2}\right]^{1/2}.$$

Values of $F(\omega)$ are tabulated in reference 30. The first term on the right side of equation (5-165) is the usual expression for E in the final period of decay. The last term is the contribution to E due to energy transfer.

The expression for the energy decay is obtained from equation (5-134) by setting $\mathbf{r} = 0$, $j = i$, $d\kappa = -2\pi\kappa^2 \, d(\cos\theta) \, d\kappa$, and $E = 2\pi\kappa^2\varphi_{ii}$. Thus

$$\frac{\overline{u_i u_i}}{2} = \int_0^\infty E \, d\kappa. \tag{5-166}$$

Substituting equation (5-165) in (5-166) and performing the integration, that is, summing up the contributions to the energy from all wavenumbers results in the following expression for the energy decay law:

$$\frac{\overline{u_i u_i}}{2} = \frac{J_0}{32(2\pi)^{1/2}} \nu^{-5/2}(t - t_0)^{-5/2} + 0.2296\beta_0 \nu^{-8}(t - t_0)^{-7}. \tag{5-167}$$

The last term in equation (5-165) was integrated by expanding it in a series. For large times the last term in equation (5-167) becomes negligible, and the equation reduces to the well-known –5/2 power decay law for the final period. If higher-order correlation equations were considered in the analysis, that is, if the quadruple correlations were not neglected, it appears that more terms in higher powers of $(t - t_0)$ would be added to equation (5-167).[8]

Figure 5-3 shows our theoretical dimensionless energy-spectrum function $E^* = J_0^{1/3} E/\nu^{8/3}$ plotted against dimensionless wavenumber $\kappa^* = J_0^{1/3}\kappa/\nu^{2/3}$ for various dimensionless times $t^* = \nu^{7/3} t/J_0^{2/3}$. The curves were calculated from equation (5-165) after converting it to dimensionless form.

The values of the parameters $\beta_0^* = \nu^5 \beta_0 / J_0$ and $t_0^* = \nu^{7/3} t_0 / J_0^{2/3}$, which depend on initial conditions, are determined from decay data for grid-generated turbulence reported in reference 32 (see fig. 5-4). The Reynolds number MU/ν is 950, where M is the mesh size and U is the mean velocity of the fluid flowing through the grid. The corresponding microscale Reynolds number $R_\lambda = \overline{u_i u_i}^{1/2} \lambda/(3\nu)$ is between 5 and 8, where λ is the microscale (dissipation length) (ref. 4). The time t in the theory is taken to be $t = x/U$, where x is the distance downstream from the grid, and t_0 is the virtual origin of the turbulence (the time at which the turbulence intensity $\overline{u_i u_i}/3$ would become infinite if equation (5-167) applied for all times $\geq t_0$). Note that t_0 corresponds to x_0 (see fig. 5-4).

The unusual shape of the curve for $t^* = 0$ may be due to the fact that the theory is not accurate for a time that early (see fig. 5-4). The wavenumber κ has the dimension 1/length and as mentioned earlier, can be considered as the reciprocal of an eddy size. Large wavenumbers correspond to small eddies and small wavenumbers, to large eddies. Equation (5-166) shows that E represents the distribution of contributions to the total energy from various wavenumbers or eddy sizes. As time increases, the bulk of the energy moves to smaller wavenumbers or to larger eddies. The high velocity gradients and, consequently, high shear stresses occurring in the smaller eddies cause them to dissipate more rapidly than the large ones. The viscous dissipation thus produces a sink for the energy at the higher wavenumbers.

Interaction between spectral energy transfer and dissipation. Figure 5-5 gives a comparison between the spectra obtained from equation (5-165) and those for the final period obtained by retaining only the first two terms in equation (5-165). The difference between the curves is, of course, caused by the transfer of energy from low wavenumbers to higher ones. The energy transfer tends to fill the sink produced by viscous dissipation at the higher wave numbers. As a result the slopes on the high wavenumber sides of the spectra are more gradual than they would be in the absence of energy transfer. But at later times, when inertia effects become small, the spectra assume a more or less symmetrical shape.

Thus the function of the inertia terms in the equations is to excite the higher wavenumber or small-eddy regions of the spectrum by transferring energy into those regions. The high-wavenumber portion of the spectrum is thus determined primarily by the inertia effects, whereas the low-wavenumber portion is determined by the viscous terms in the equations. This may seem to be opposite to what one would expect, inasmuch as we usually consider the high wavenumber or small-eddy region to be dominated by viscous effects. It is true that viscous dissipation is highest in the high wavenumber region because of the high shear stresses between the small eddies. However, the small eddies owe their existence in the first place to the transfer of energy into that region, that is, to inertia effects.

[8] We have also carried out an analogous analysis of decaying turbulent temperature fluctuations. The analysis and results are reported in reference 31.

It is this interaction between the energy transfer and the dissipation (see eq. (5-158)) which is responsible for the high rate of dissipation in turbulence; the dissipation is high because the high wavenumber region of the spectrum is excited by the transfer of energy into that region. The shear stresses are higher there than in a region which could be excited in the absence of energy transfer. Another way of saying all this is that the energy transfer generally has a stabilizing effect on the flow.

Inertia and dissipation tend to shift the energy in opposite directions on the wavenumber scale. Moreover, the mechanisms for the two effects appear to be different. Whereas inertia tends to transfer the energy to higher wavenumbers by a breakup of large eddies into smaller ones (or by a stretching of vortex filaments), dissipation tends to shift the energy to smaller wavenumbers by selective annihilation of eddies, the small eddies being the first to go. As the turbulence decays, the dissipation effects must, of course, eventually win out, since the inertia effects become negligible at the low Reynolds numbers occurring at large times.

A solution of the Navier-Stokes equations for decaying homogeneous turbulence has been obtained numerically by Clark, Ferziger, and Reynolds (ref. 33). The resulting energy spectrum for a particular time is shown in figure 5-6. As in the case of our calculated spectra (fig. 5-5) the energy transfer to higher wavenumbers causes the slopes on the high-wavenumber side of the spectrum to be more gradual than those on the low-wavenumber side. The larger effect in figure 5-6 is apparently caused by the higher Reynolds number there. That Reynolds number ($R_\lambda = 36.6$) is evidently too high for the theory used in obtaining figure 5-5 to be applicable.

Experimental energy spectra reported in references 34 to 38 are qualitatively similar to and show the same trends as the calculated spectra in figures 5-5 and 5-6. In particular, the effect of Reynolds number is shown clearly in figure 5-7, where normalized experimental results from references 37 and 38 are compared. The shapes of the spectra again result from the energy transfer to higher wavenumbers. That energy transfer is of course greater for the higher Reynolds-number curve, where inertial effects in comparison with viscous effects are greater, and the slopes on the high-wavenumber side of the spectrum are more gradual than they are in the curve for lower Reynolds numbers.

Spectrum for infinite Reynolds number. Also shown in figure 5-7 is the spectrum for infinite Reynolds number which results from the hypotheses of Kolmogorov and dimensional considerations (refs. 39 to 42). Kolmogorov hypothesized that the physical quantity representative of the dynamics of high Reynolds-number turbulence is ε, the average rate of transfer of kinetic energy (per unit mass) between large and small scales of motion. The dimensions of ε are $(\text{length/time})^2/\text{time} = \text{length}^2/\text{time}^3$. Another quantity which is often a determining parameter for turbulence is the kinematic viscosity ν, with dimensions $\text{length}^2/\text{time}$. However, the region of wavenumber space which is affected by the action of viscous forces moves out from the origin toward a wavenumber of infinity as the Reynolds number of the turbulence increases. In the limit of infinite Reynolds number the energy sink produced by viscous dissipation is displaced to infinity, and the influence of viscous forces is negligible for wavenumbers κ of finite magnitude (ref. 4).

Thus, one can write for the energy-spectrum function E (with dimensions $\text{length}^3/\text{time}^2$),

$$E = E(\varepsilon, \kappa), \tag{5-168}$$

where the geometric quantity κ (with dimension length^{-1}) is included in the functional relationship because we want to end up with a relation between E and κ. The only dimensionally correct expression for E which can be formed from ε and κ is

$$E = \text{const.}\ \varepsilon^{2/3}\kappa^{-5/3}. \tag{5-169}$$

This is the celebrated –5/2 power Kolmogorov-Obukhov spectrum for infinite Reynolds number. It is plotted in figure 5-7, where agreement with the experimental data for high Reynolds numbers is indicated for a range of wavenumbers.

Note that the Reynolds numbers we have considered include both very low and very high ones. However, the Navier-Stokes equations were not used for the latter, as they were for low Reynolds numbers where a solution of those equations was obtained. But the spectra for low and high Reynolds numbers are qualitatively similar; the energy is just spread out over a wider range of wavenumbers as the Reynolds number increases. There are no bifurcations in going from low to high Reynolds numbers (except possibly in the transition region).

For further consideration of the energy transfer we return to the analysis for moderately low Reynolds numbers.

Further analysis of the spectral-energy transfer. Although we have considered in some detail the effect of spectral transfer on energy spectra, we have not looked at the transfer spectra themselves. Those have been calculated for the approach to the final period from equation (5-161) and are plotted in dimensionless form in figure 5-8. The quantity T^* equals $J_0 T(\kappa)/\nu^5$, where $T(\kappa)$ is the energy transfer term in equation (5-158). The transfer term gives the net energy transfer into a wavenumber band from all other wavenumbers (eq. (5-159)). The curves indicate net energy loss from energy bands at low wavenumbers and an energy gain to those at higher wavenumbers. The total area under each curve is zero, in agreement with equation (5-162), thus indicating that the total contribution of $T(\kappa)$ to $d\overline{u_i u_i}/dt$ is zero (see eqs. (5-158), (5-162), and (5-166)). It should be emphasized that $T(\kappa)$

represents a difference between the energy flowing into and out of a wavenumber band. The actual energy transfer at a point where $T(\kappa)$ is low or zero may be quite high as will be shown.

As was mentioned earlier the integrand in equation (5-159) can be interpreted as giving the distribution of contributions to $T(\kappa)$ from various wavenumbers or eddy sizes. The integrand $P(\kappa,\kappa')$ (see eqs. (5-159) and (5-160)) can be written in dimensionless form as

$$\frac{Pv^7(t-t_0)^7}{\beta_0} = -\frac{1}{2}\left[\left(\frac{\kappa'}{\kappa}\right)^7 - \left(\frac{\kappa'}{\kappa}\right)^5\right]\left\{\kappa\left[v(t-t_0)\right]^{1/2}\right\}^{12}\left(\exp\left\{-2\left\{\kappa\left[v(t-t_0)\right]^{1/2}\right\}^2\left[1-\frac{\kappa'}{\kappa}+\left(\frac{\kappa'}{\kappa}\right)^2\right]\right\}\right.$$

$$\left. - \exp\left\{-2\left[\kappa\left[v(t-t_0)\right]^{1/2}\right]^2\left[1+\frac{\kappa'}{\kappa}+\left(\frac{\kappa'}{\kappa}\right)^2\right]\right\}\right). \qquad (5-170)$$

Figures 5-9(a), (b), and (c) show $Pv^7(t-t_0)^7/\beta_0$ plotted against κ'/κ for several values of $\kappa[v(t-t_0)]^{1/2}$. In agreement with equation (5-105) (integrated over all directions in wavevector space), $P(\kappa/\kappa) = 0$. That is, energy transfer takes place only between wavenumber bands that, at least to some extent, are separated. The curves indicate that the energy entering a wavenumber band at κcomes from a range of wavenumbers κ' or eddy sizes rather than exclusively from neighboring wavenumbers. Similarly the energy passes on to a range of wavenumbers. Thus the energy in general is transported between wavenumber bands that are separated. This transport might occur by a breaking up of large eddies into small ones. The positive area under each curve corresponds to the total energy entering a wavenumber band at κ, the negative area to the total energy leaving. The curve corresponding to $T = 0$ indicates a considerable amount of energy entering and leaving at κ, although the net energy gain is of course zero. The asymmetrical curves indicate that when a small amount of energy is entering at κ and a large amount is leaving, the energy comes from wavenumbers close to κ and goes to more distant wavenumbers. The opposite is true when the energy entering at κ is comparatively large.

In order to obtain an idea of the average energy transfer for all values of κ, we can integrate equation (5-170) over κ for constant κ'/κ and obtain a quantity which we will call Q:

$$\frac{Q\left[(t-t_0)v\right]^{15/2}}{\beta_0} = -\frac{10\,395(\pi/2)^{1/2}}{16\,384}\left\{\left[\left(\frac{\kappa'}{\kappa}\right)^7 - \left(\frac{\kappa'}{\kappa}\right)^5\right]\left[\frac{1}{\left[1-(\kappa'/\kappa)+(\kappa'/\kappa)^2\right]^{13/2}} - \frac{1}{\left[1+(\kappa'/\kappa)+(\kappa'/\kappa)^2\right]^{13/2}}\right]\right\}. \qquad (5-171)$$

Equation (5-171) is plotted in figure 5-10. The curve indicates that on the average, energy enters and leaves wavenumber bands about as shown in figure 5-9(b), where the *net* energy transfer is zero.

All of the results for $T(\kappa)$, $P(\kappa/\kappa')$, and $Q(\kappa/\kappa')$ given so far were obtained by letting m=4 and n=6 in equation (5-156) for the initial conditions. There was early theoretical support for those values, but later work indicated that in the real world they may be somewhat lower. Empirically, the transfer term $T(\kappa)$ seems, in fact, to start out at the origin with a power of κclose to one (see refs. 38 and 43); that would correspond to m=0 and n=–1. Then equation (5-170) is replaced by

$$\frac{P\left[v(t-t_0)\right]^{3/2}}{\beta_0} = -\frac{1}{2}\left(\frac{\kappa'}{\kappa}-1\right)\kappa\left[v(t-t_0)\right]^{1/2}\left(\exp\left\{-2\left\{\kappa\left[v(t-t_0)\right]^{1/2}\right\}^2\left[1-\frac{\kappa'}{\kappa}+\left(\frac{\kappa'}{\kappa}\right)^2\right]\right\}\right.$$

$$\left. - \exp\left\{-2\left\{\kappa\left[v(t-t_0)\right]^{1/2}\right\}^2\left[1+\frac{\kappa'}{\kappa}+\left(\frac{\kappa'}{\kappa}\right)^2\right]\right\}\right), \qquad (5-172)$$

and equation (5-161) becomes

$$\frac{T(\kappa)\left[\nu(t-t_0)\right]^2}{\beta_0} = \frac{\sqrt{\pi/2}}{4}\kappa\left[\nu(t-t_0)\right]^{1/2}\left(2\,\mathrm{erf}\left\{\frac{1}{\sqrt{2}}\kappa\left[\nu(t-t_0)\right]^{1/2}\right\}-1\right) \tag{5-173}$$

$$\times\exp\left[-\frac{3}{2}\kappa^2\nu(t-t_0)\right],$$

where the symbol erf designates the error function. Finally, as an intermediate case, let m=0, n=2. Then

$$\frac{P\left[\nu(t-t_0)\right]^3}{\beta_0} = -\frac{1}{2}\left[\left(\frac{\kappa'}{\kappa}\right)^3-\left(\frac{\kappa'}{\kappa}\right)\right]\left\{\kappa\left[\nu(t-t_0)\right]^{1/2}\right\}^4$$

$$\times\left(\exp\left\{-2\left\{\kappa\left[\nu(t-t_0)\right]^{1/2}\right\}^2\left[1-\frac{\kappa'}{\kappa}+\left(\frac{\kappa'}{\kappa}\right)^2\right]\right\}\right. \tag{5-174}$$

$$\left.-\exp\left\{-2\left\{\kappa\left[\nu(t-t_0)\right]^{1/2}\right\}^2\left[1+\frac{\kappa'}{\kappa}+\left(\frac{\kappa'}{\kappa}\right)^2\right]\right\}\right)$$

and

$$\frac{T(\kappa)\left[\nu(t-t_0)\right]^{7/2}}{\beta_0} = \frac{3\sqrt{\pi/2}}{16}\left(\left\{\kappa\left[\nu(t-t_0)\right]^{1/2}\right\}^4-\left\{\kappa\left[\nu(t-t_0)\right]^{1/2}\right\}^2\right) \tag{5-175}$$

$$\times\exp\left[-\frac{3}{2}\kappa^2\nu(t-t_0)\right].$$

We calculated spectra for dimensionless T and P from equations (5-172) to (5-175). In figures 5-11 and 5-12 results are compared with the previous ones for m=4, n=6. Note that there is a relation between the shapes of the curves for $T(\kappa)$ and those for $P(\kappa'/\kappa)$, and that the energy-transfer is less local (the energy jumps are greater) when T starts out linearly at $\kappa=0$, as does P at $\kappa'=0$ (eqs. (5-172) and (5-173)). As mentioned earlier, that case, or a case close to it, seems to be indicated empirically.

It has been noted that the localness of the energy transfer is related to the shape of the $T(\kappa)$ spectrum, in particular to its shape near $\kappa=0$. Here we develop an approximate method for obtaining the localness of the energy transfer from the T spectrum. To that end, note that the T spectrum can often be represented by a truncated power-exponential series (or asymptotic expansion) in κ. See, for example, the theoretical spectra represented by equations (5-161) and (5-175), and the empirical equation for T in reference 38. Thus, one can write

$$T(\kappa) = \left(a_0+a_1\kappa+a_2\kappa^2+a_3\kappa^3+\ldots\right)\left(e^{-\alpha_1\kappa}+e^{-\alpha_2\kappa^2}+\ldots\right), \tag{5-176}$$

where dependencies on time are included in the a_i and α_i. Corresponding to equation (5-176) we have, for $P(\kappa,\kappa')$ the expansion

$$P(\kappa,\kappa')=\left[\left(c_{00}\right)+\left(c_{10}\kappa+c_{01}\kappa'\right)+\left(c_{20}\kappa^2+c_{11}\kappa\kappa'+c_{02}\kappa'^2\right)+\left(c_{30}\kappa^3+c_{21}\kappa^2\kappa'+c_{12}\kappa\kappa'^2+c_{03}\kappa'^2\right)\right.$$

$$+\left(c_{40}\kappa^4+c_{31}\kappa^3\kappa'+c_{22}\kappa^2\kappa'^2+c_{13}\kappa\kappa'^3+c_{04}\kappa'^4\right)+\left(c_{50}\kappa^5+c_{41}\kappa^4\kappa'+c_{32}\kappa^3\kappa'^2+c_{23}\kappa^2\kappa'^3+c_{14}\kappa\kappa'^4+c_{05}\kappa'^5\right)$$

$$\left.+\left(c_{60}\kappa^6+c_{51}\kappa^5\kappa'+c_{42}\kappa^4\kappa'^2+c_{33}\kappa^3\kappa'^3+c_{24}\kappa^2\kappa'^4+c_{15}\kappa\kappa'^5+c_{06}\kappa'^6\right)+\cdots\right]\left[e^{-\alpha_{10}\kappa-\alpha_{01}\kappa'}+e^{-\alpha_{20}\kappa^2-\alpha_{02}\kappa'^2}+\cdots\right],$$

(5-177)

where terms of the same degree in κ and κ' are grouped together in parentheses. By letting j=i in equation (5-104) and integrating over all directions in (κ, κ')–space , we get

$$P(\kappa,\kappa')=-P(\kappa',\kappa), \tag{5-178}$$

or P is antisymmetric in κ and κ'.

Then equation (5-177) becomes

$$P(\kappa,\kappa')=\left\{c_{10}\left(\kappa-\kappa'\right)+c_{20}\left(\kappa^2-\kappa'^2\right)+\left[c_{30}\left(\kappa^3-\kappa'^3\right)+c_{21}\left(\kappa^2\kappa'-\kappa\kappa'^2\right)\right]+\left[c_{40}\left(\kappa^4-\kappa'^4\right)+c_{31}\left(\kappa^3\kappa'-\kappa\kappa'^3\right)\right]\right.$$

$$\left.+\left[c_{50}\left(\kappa^5-\kappa'^5\right)+c_{41}\left(\kappa^4\kappa'-\kappa\kappa'^4\right)+c_{32}\left(\kappa^3\kappa'^2-\kappa^2\kappa'^3\right)\right]+\left[c_{60}\left(\kappa^6-\kappa'^6\right)+c_{51}\left(\kappa^5\kappa'-\kappa\kappa'^5\right)+c_{42}\left(\kappa^4\kappa'^2-\kappa^2\kappa'^4\right)\right]+\cdots\right\}$$

$$\times\left[e^{-\alpha_{12}\left(\kappa+\kappa'\right)}+e^{-\alpha_{20}\left(\kappa^2+\kappa'^2\right)}+\cdots\right]. \tag{5-179}$$

The terms retained in equation (5-179) for a particular problem must satisfy the equation given for $T(\kappa)$ (say eq. (5-175)), where $T(\kappa)$ is related to $P(\kappa, \kappa')$ by

$$T(\kappa)=\int_0^\infty P(\kappa,\kappa')\,d\kappa'. \tag{5-180}$$

Equation (5-180) is obtained by contracting the indices i and j in equation (5-99) and integrating over all directions in κ– and κ'–space. In addition, the following systematic procedure is used for truncating equation (5-179): Those terms are retained which are of the lowest possible degree in κ, κ', such that the given equation for $T(\kappa)$ is satisfied.

If, for example, T is given by equation (5-175), equation (5-176) becomes

$$T(\kappa)=\left(a_2\kappa^2+a_4\kappa^4\right)e^{-\alpha_2\kappa^2} \tag{5-181}$$

and equation (5-179) becomes

$$P(\kappa,\kappa')=c_{42}\left(\kappa^4\kappa'^2-\kappa^2\kappa'^4\right)e^{-\alpha_{20}\left(\kappa^2+\kappa'^2\right)} \tag{5-182}$$

where, according to our procedure described in the last paragraph, only the terms of the lowest possible degree in κ, κ' which satisfy equations (5-180) and (5-181) have been retained.

Substituting equations (5-175) and (5-182) into (5-180), we get

$$\frac{P\left[v(t-t_0)\right]^3}{\beta_0}=\frac{9\sqrt{3}}{16}\left\{\kappa\left[v(t-t_0)\right]^{1/2}\right\}^6\left[\left(\frac{\kappa'}{\kappa}\right)^2-\left(\frac{\kappa'}{\kappa}\right)^4\right]\exp\left\{-\frac{3}{2}\left\{\kappa\left[v(t-t_0)\right]^{1/2}\right\}^2\left[1+\left(\frac{\kappa'}{\kappa}\right)^2\right]\right\}. \qquad (5-183)$$

Figure 5-13 compares the approximate results calculated from equation (5-183) with the theoretical results from equation (5-174). The degree of localness calculated from the approximate equation is in good *qualitative* agreement with that obtained from the theoretical calculation. The agreement is particularly good in figure 5-13(b), where the energy transfer into the wavenumber band at κ equals that leaving (when κ/κ_0 for the T-spectrum equals 1).

The agreement in figure 5-13, where our approximate method is used for calculating a *known* $P(\kappa, \kappa')$, gives us some confidence in that method. Thus we use it to calculate the degree of localness of the energy transfer which corresponds to the experimental equation for $T(\kappa)$ obtained by Ling and Huang (ref. 38), where $P(\kappa, \kappa')$ is *unknown*. There, $T(\kappa)$ is given by

$$\frac{T(\kappa)\left[v(t-t_0)\right]^{5/2}}{Av^3}=\frac{10}{3}\left(2\sqrt{10}\left\{\kappa\left[v(t-t_0)\right]^{1/2}\right\}^4-3\left\{\kappa\left[v(t-t_0)\right]^{1/2}\right\}^3-\sqrt{10}\left\{\kappa\left[v(t-t_0)\right]^{1/2}\right\}^2\right.$$

$$\left.-\kappa\left[v(t-t_0)\right]^{1/2}\right)\exp\left(-\sqrt{10}\left\{\kappa\left[v(t-t_0)\right]^{1/2}\right\}\right), \qquad (5-184)$$

where A is defined by the evolution equation

$$\overline{u_1^2}=A(t-t_0)^2. \qquad (5-185)$$

Then equation (5-176) becomes

$$T(\kappa)=\left(a_1\kappa+a_2\kappa^2+a_3\kappa^3+a_4\kappa^4\right)e^{-\alpha_1\kappa} \qquad (5-186)$$

and equation (5-179) becomes

$$P(\kappa,\kappa')=\left[c_{21}\left(\kappa^2\kappa'-\kappa\kappa'^2\right)+c_{31}\left(\kappa^3\kappa'-\kappa\kappa'^3\right)+c_{41}\left(\kappa^4\kappa'-\kappa\kappa'^4\right)\right]e^{-\alpha_{12}(\kappa+\kappa')}, \qquad (5-187)$$

where again, only the terms of the lowest possible degree in κ, κ' which satisfy the determining equations (equations (5-180) and (5-186) have been retained. Substituting equations (5-184) and (5-187) into (5-180) we get

$$\frac{P\left[v(t-t_0)\right]^2}{Av^3}=\left(-\frac{10^{5/2}}{3}\left[\frac{\kappa'}{\kappa}-\left(\frac{\kappa'}{\kappa}\right)^2\right]\left\{\kappa\left[v(t-t_0)\right]^{1/2}\right\}^3-100\left[\frac{\kappa'}{\kappa}-\left(\frac{\kappa'}{\kappa}\right)^3\right]\left\{\kappa\left[v(t-t_0)\right]^{1/2}\right\}^4\right.$$

$$\left.+\frac{2(10)^{5/2}}{3}\left[\frac{\kappa'}{\kappa}-\left(\frac{\kappa'}{\kappa}\right)^4\right]\left\{\kappa\left[v(t-t_0)\right]^{1/2}\right\}^5\right)\exp\left\{-\sqrt{10}\left(1+\frac{\kappa'}{\kappa}\right)\kappa\left[v(t-t_0)\right]^{1/2}\right\}. \qquad (5-188)$$

Results calculated from equation (5-188) are plotted in figure 5-14. These plots of $P(\kappa, \kappa')$, which correspond to the experiment for $T(\kappa)$ from reference 38, are similar to the theoretical results in figure 5-12 (a different case), but the degree of nonlocalness tends to be somewhat greater. It seems better not to attempt to characterize the energy transfer as local or nonlocal, since the dividing line between the two is necessarily arbitrary. But strictly speaking, as mentioned earlier all spectral energy transfer is nonlocal because of the condition $P(\kappa, \kappa) = 0$ which follows from equation (5-105) (integrated over all directions in wavevector space with $j = i$). Thus, energy transfer can take place only between wavenumber bands that, at least to some extent, are separated.

The tendency of the energy to jump between wavenumber regions that are separated appears to be in accord with the idea that turbulence tends to form concentrated regions of large velocity gradients (ref. 4, pp. 108, 186, and 187). Thus, when a low

wavenumber eddy becomes unstable and forms a region of large velocity gradients, there will be a transfer of energy from low to significantly higher wavenumbers. The concept was further developed in section 4.3.2.3, where it was shown that in a turbulent flow there must be regions of relative quiescence interspersed with regions where the instantaneous mixing is intense and localized.

A poem due to Betchov (ref. 44) emphasizes the energy jumps occurring in spectral energy transfer more than does the one by Richardson (see section 5.1.2.1). Betchov's poem is

> Big whirls lack smaller whirls,
> To feed on their velocity.
> They crash and form the finest curls
> Permitted by viscosity.

It may seem that the equilibrium (cascade) theory (see ref. 4) could apply in the presence of a rather high degree of nonlocalness of the spectral energy transfer if the Reynolds number of the turbulence is very high (huge). In that case the energy spectrum extends over many decades of wavenumbers. Thus, there could be a cascade in which the energy is passed from low to high wavenumbers by successive moderately large jumps. However, the turbulence Reynolds number required to make the small eddies independent of the large ones would have to be larger than if the energy transfer were more local.

Note, however, that Kraichnan (ref. 45), for example, has given arguments against the independence of the motion of the very small and the very large eddies, even at large Reynolds numbers. The crux of his argument appears to be that even though the active high-wavenumber components are much smaller than the low-wavenumber ones when the turbulence Reynolds number is high, both of those often consist of long vortex filaments which are tangled together. Since the small-scale filaments can extend axially over considerable distances, it is hard to see how their motions could be independent of the motions of the large-scale components, particularly since the former are likely to be stretched or compressed by the latter. (See also refs. 44, and 46 to 48.)

As a further development of the discussion in the last paragraph, we return to spectral-energy transfer as related to the interaction in triads of Fourier components (see eq. (5-80)). The spectral-transfer term in equation (5-80) is

$$T_{ij}(\boldsymbol{\kappa}) = \int_{-\infty}^{\infty} P_{ij}(\boldsymbol{\kappa}, \boldsymbol{\kappa}')\, d\boldsymbol{\kappa}' \tag{5-189}$$

where

$$P_{ij}(\boldsymbol{\kappa}, \boldsymbol{\kappa}') = i\left[\kappa_k \varphi_i^*(\boldsymbol{\kappa}-\boldsymbol{\kappa}')\varphi_j(\boldsymbol{\kappa})\varphi_k^*(\boldsymbol{\kappa}') - \kappa_k \varphi_i^*(\boldsymbol{\kappa})\varphi_j(\boldsymbol{\kappa}-\boldsymbol{\kappa}')\varphi_k(\boldsymbol{\kappa}')\right]. \tag{5-190}$$

The stars designate complex conjugates. As mentioned earlier, the presence of the integral in equation (5-189) means that contributions from a range of wavevectors $\boldsymbol{\kappa}'$ between $-\infty$ and $+\infty$ make up the total net transfer at $\boldsymbol{\kappa}$. Moreover, according to equation (5-190), the transfer takes place by the interaction in triads of Fourier components at the wavevectors $\boldsymbol{\kappa}$, $\boldsymbol{\kappa}'$ and $\boldsymbol{\kappa}-\boldsymbol{\kappa}'$. Note that if a triad is composed of Fourier components at the wavevectors $\boldsymbol{\kappa}$, $\mathbf{p}$ and $\mathbf{q}$, then $\boldsymbol{\kappa}+\mathbf{p}+\mathbf{q}=0$ if $\mathbf{p}=-\boldsymbol{\kappa}'$ and $\mathbf{q}=-(\boldsymbol{\kappa}-\boldsymbol{\kappa}')$.

An important observation is that the triads in equation (5-190) consist of products, as opposed to say sums, of Fourier components at the three wavevectors. So all three components will have an influence on $P_{ij}(\boldsymbol{\kappa}, \boldsymbol{\kappa}')$, and thus on $T_{ij}(\boldsymbol{\kappa})$, even if one of the components is much smaller than the other two, and even if it is at a much lower wavenumber than the other two.

Thus, if it turns out that the triads having the most influence on $T_{ij}(\boldsymbol{\kappa})$ (or on $T(\boldsymbol{\kappa})$) generally consist of Fourier components at three wavevectors of approximately equal magnitude, one might conclude that the interactions between large and small eddies are relatively unimportant. If, on the other hand, the magnitude of the wavevector of one of the Fourier components in the more influential triads differs greatly from the others, then interactions between large and small eddies will have an important effect on the energy transfer. The latter was found to be the case in the direct numerical simulations of Domaradzki and Rogallo (ref. 49). They found that their energy transfer was due mainly to wavevector triads which have one leg much shorter than the other two.[9] Yeung and Brasseur, using a somewhat different approach (ref. 48), arrived at the same conclusion.

These results reinforce the physical argument considered in reference 45 and in this section, and suggest that the motion of the small eddies, even at high Reynolds numbers, may not be independent of the motion of the large ones. An important part of

[9]Reference 49 also obtained results for the localness of energy transfer. It was found, in agreement with our results from equation (5-188) and figure 5-14, that contributions to the energy transfer are spread over a range of wavenumbers. But the results from reference 49 showed somewhat more localness. However, comparison of figure 1(a) and figure 4 of reference 49 shows that the calculations for $P(\kappa,\kappa')$ are outside the range where the numerical simulations represent the experiment of reference 38. Thus the simulations are not strictly comparable with our results, which *are* for the experiment of reference 38. Also, the comments in reference 49 concerning the arbitrariness in our methodology are not well-founded, considering the restrictions we placed on $P(\kappa,\kappa')$. Note, however, that the logic used here in obtaining equation (5-188) is much improved over that in reference 50. At any rate it should be mentioned that the common practice (in ref. 49 and elsewhere) of designating energy transfers within a ratio of two as local is arbitrary. By virtue of equation (5-105) all spectral transfer is nonlocal.

this argument is the observation made here that Fourier components of the triads in equation (5-190) occur as products. Thus, even though the low wavenumber component of a triad may be weak, it will affect the energy transfer as much as will the other components, since they are multiplied by one another. This might be related to the tangledness of the small and large vortex filaments in the physical argument; noting that the small- and large-scale components are multiplied together, and that many of the triads have one leg much shorter than the other two, may be another way of looking at the fact that they are twisted together over long distances as vortex filaments. At any rate, both arguments tend to indicate the lack of independence of the large and the small eddies. So the independence hypothesis (ref. 39) seems to be open to some question, based on the results to date. Of course, these comments are not meant to detract from the agreement with experiment of the Kolmogorov-Obukov $-5/3$-power spectrum. But that spectrum may require a different foundation.

We return now to the solution of the Navier-Stokes equations for decaying homogeneous turbulence obtained numerically by Clark, Ferziger, and Reynolds (ref. 33). That solution yielded energy-*transfer* spectra in addition to energy spectra. The energy-transfer spectrum corresponding to the energy spectrum in figure 5-6 is plotted in figure 5-15. The shape of the spectrum is similar to the shapes of our theoretical spectra in figure 5-11, but as in the case of the energy (fig. 5-6), the energy transfer (at least the positive portion) is spread out over a wider range of wavenumbers. Because of the condition that the energy transfer integrated over all wavenumbers must be zero, this spreading causes the negative trough of the spectrum to become narrow and deep. The difference between the shapes of the spectra in figures 5-11 and 5-15 is apparently due to the higher Reynolds number for the latter. The effect of Reynolds number on the shape of transfer spectra is shown clearly by a comparison of experimental results from reference 37 ($300 < R_\lambda < 800$) with those from reference 38 ($3 < R_\lambda < 30$) (see fig. 5-16).

5.3.2.3 *The correlation-term-discard closure for short times of turbulence decay and comparison with experiment.*—Thus far we have refrained from comparing our analytical results with experiment. In general, the significance of such comparisons is uncertain because of lack of knowledge of the initial conditions. But it may be possible to make meaningful comparisons for at least one short-decay-time case.

Here we return to the correlation-term-discard closure (or expansion in powers of Reynolds number or time) in order to use it to calculate the decay of homogeneous turbulence for initial conditions obtained from experiment (ref. 51). (It should be noted that the previous calculations in section 5.3.2.2 were based on initial conditions that allowed the solution to approach the final period of decay at large times, rather than on experimental initial conditions.) The two-point equation (5-158), which was obtained by neglecting quadruple-correlation terms in the three-point correlation equation can be written as

$$dE/dt + 2\nu\kappa^2 E = T(\kappa) \tag{5-158}$$

where

$$T(\kappa) = \int_0^\infty P(\kappa, \kappa')\, d\kappa' \tag{5-191}$$

and where, from equations (5-191) and (5-159), one can write

$$P(\kappa, \kappa') = \frac{f_1(\kappa, \kappa')}{t - t_1}\left\{\exp\left[-2\nu(t-t_1)\left(\kappa^2 + \kappa\kappa' + \kappa'^2\right)\right] - \exp\left[-2\nu(t-t_1)\left(\kappa^2 + \kappa\kappa' + \kappa'^2\right)\right]\right\}. \tag{5-192}$$

Note that we have replaced the particular initial condition $\beta_0(\kappa^5\kappa'^7 - \kappa^7\kappa'^5)/(2\nu)$ at t_0 in equation (5-159) by the general condition $f_1(\kappa, \kappa')$ at t_1 in equation (5-192). As usual, E is the energy spectrum function, related to the total turbulent energy $\overline{u_i u_i}/2$ by

$$\frac{1}{2}\overline{u_i u_i} = \int_0^\infty E(\kappa)\, d\kappa, \tag{5-166}$$

where $T(\kappa)$ is the energy transfer function, which gives the net energy transfer into a wavenumber region at wavenumber κ from all other wavenumbers κ', $P(\kappa, \kappa')$ gives the contribution from κ' to the energy transfer at κ, t is the time, the subscript 1 designates an initial value, ν is the kinematic viscosity, and u_i is a velocity component. A repeated subscript indicates a summation, and an overbar indicates an averaged value.

The function $f_1(\kappa, \kappa')$ in equation (5-192) is evaluated by setting P equal to the initial condition $P_1(\kappa, \kappa')$ when $t = t_1$ and using the fact that

$$\lim_{t \to t_1} (t - t_1)^{-1}\left\{\exp\left[-2\nu(t-t_1)\left(\kappa^2 + \kappa\kappa' + \kappa'^2\right)\right] - \exp\left[-2\nu(t-t_1)\left(\kappa^2 - \kappa\kappa' + \kappa'^2\right)\right]\right\} = -4\nu\kappa\kappa'. \tag{5-193}$$

This gives

$$f_1(\kappa,\kappa') = -P_1(\kappa,\kappa')/(4\nu\kappa\kappa'). \qquad (5-194)$$

One of the difficulties in comparing closure schemes with experiment has been the unavailability of initial values of $P(\kappa, \kappa')$. Reasonable estimates of that quantity [P_1 in eq. (5-194)] can, however, be obtained from Ling and Huang's experiment (ref. 38) and our approximate equation (5-188). The initial condition for $E(\kappa)$ in equation (5-158) is obtained from reference 38.

Results calculated according to the present correlation-term-discard closure are compared with the experiment of Ling and Huang in figures 5-17 to 5-19. Figure 5-17 also shows results for $T = 0$ (pure viscous decay). The quantity A is the proportionality constant in the power decay law for $\overline{u_1^2}$ and has the dimensions of a length squared (eq. (5-185)). The initial conditions for the analysis were specified at $(\nu/A)t_1 = 0.037$, where the turbulence Reynolds number $R_\lambda \equiv \overline{u_1^2}^{1/2}\lambda/\nu = 12$ (λ is the Taylor microscale).

As one might have expected, the lower-order results $\overline{u_i u_i}$ and $E(\kappa)$ compare better with experiment than the higher-order one $T(\kappa)$. This is because a larger error is produced in quantities which are calculated directly from equations where quadruple-correlation terms are neglected. Agreement with experiment is indicated only for moderately small times, and none of the results are as good as those obtained for closure by specification of initial conditions (to be considered next) or for a modified Kovasznay-type closure (ref. 52) (The latter is more an intuitive than a deductive procedure.) For those closures good results for all initially specified quantities were obtained even for reductions in $\overline{u_i u_i}$ of over 80 percent. However, the present solution is well-behaved and shows no perceptible negative spectral energies even at large times [see curves for $(\nu/A)t_1$ of 0.5 and 5 in fig. 5-18]. (Some negligibly small negative values which occurred at high wavenumbers and large times were judged to be of no importance.) Improved results (for large times) could evidently be obtained by using a higher-order closure (ref. 22) but higher-order initial conditions would then have to be specified.

Calculations were also made for high Reynolds numbers and compared with high-Reynolds number data (ref. 37). Not surprisingly, the agreement was much poorer than for the low Reynolds number data shown here. If reasonable results were to be obtained for the high Reynolds numbers, the equations would have to be closed by neglecting correlations of a much higher order, and the amount of calculation would probably become prohibitive. Thus, this conceptually simplest deductive closure scheme works best for short times at moderately low Reynolds numbers, or for the approach to the final period of decay. For the latter case, the initial conditions must be chosen so that the solution approaches the final period at large times, as in references 21 and 22. Since this is the simplest scheme, it is the most convenient one for illustrating the spectral-transfer process in turbulence. Further discussion of the correlation-term-discard closure is given in reference 53.

5.3.2.4 *Closure by specification of sufficient random initial conditions.*—It was mentioned in the last section that although a low-order correlation-term-discard closure is the simplest and thus the most convenient closure for studying the processes in turbulence, serious difficulties are encountered when its extension to high Reynolds numbers or to large turbulence–decay times is attempted. There is, however, another way of looking at the problem of homogeneous turbulence. In order not to lose sight of our goal, we will first give a statement of that problem. The statement given by Batchelor is essentially the following: given the statistical state of a homogeneous turbulent field at an initial instant, the problem is to predict the evolution of the turbulence (in probability) as a function of time. Note that the initial development of turbulence from a nonturbulent state produced by, say, flow through a grid, is not considered here. Rather we are concerned with the evolution of turbulence after a time when the flow is already turbulent. In order to specify completely a turbulent field at an initial time, it is necessary to give all of the multipoint velocity correlations or their spectral equivalents at that time (ref. 4). It is not hard to show that, given these multipoint correlations and the correlation equations, all the time derivatives of the turbulent energy tensor and of other pertinent turbulence quantities can be calculated. These time derivatives can then be used in a series, for instance a Taylor series, to calculate the evolution of the turbulent energy tensor (or of the equivalent energy spectrum tensor) and of other turbulence quantities.

It is noted that when the turbulence is treated in this way, we no longer have the problem of closing the infinite set of correlation or spectral equations. The correlation equations are used only to relate the correlations at an initial time to their time derivatives, and those correlations must be given in order to have a complete specification of turbulence at that time. Of course, in practice only a small number of the correlations, and thus of their time derivatives, will ordinarily be available, but a sufficient number may be known to give a reasonably good representation. It might be pointed out that even in those analyses which require a closure assumption, the turbulence should be specified initially by its correlations or spectra since the correlation equations require initial conditions.

Kraichnan (ref. 54) has studied the convergence properties of series such as those considered here. As mentioned in another article by that author (ref. 55), it is not necessary that an expansion be convergent in order to be useful, since divergent series can provide excellent asymptotic approximations (ref. 56).

Although the present method circumvents the closure problem in the usual sense, there is still the question of the legitimate truncation of the time series to obtain explicit results. Here we are not concerned primarily with convergence questions but will use as a test the agreement of the results with experiment. Although a Taylor series might give good results if sufficient statistical

information were available at the initial time, it will be seen that an exponential series which arises in a study of the nonlinear decay of a disturbance in a fluid (ref. 57) is much more satisfactory. This is not surprising since the exponential series is an iterative solution of the Navier-Stokes equations and thus contains information which is not contained in the Taylor series. The resulting formulation gives results which are in quite good agreement with the available experimental data (refs. 58 and 59).

Initial time derivatives and simple expansions. In the preceding introductory section it was noted that if the multipoint correlations are known at an initial instant, as they must be for a complete specification of the turbulence at that instant, then the time derivatives of the correlations can be calculated from the correlation equations. For illustrative purposes we will consider the derivatives of the turbulent energy tensor $\overline{u_i u_j'}$, where u_i and u_j' are respectively velocity components at the points P and P′ separated by the vector $\mathbf{r}$, and the overbar indicates an averaged value. Then the first time derivative of $\overline{u_i u_j'}$ at $t = t_1$ is given directly by the two-point correlation equations (section 5.3.2.2) evaluated at $t = t_1$:

$$\left(\frac{\partial \overline{u_i u_j'}}{\partial t}\right)_{t=t_1} = -\frac{\partial}{\partial r_k}\left[\left(\overline{u_i u_j' u_k'}\right)_{t=t_1} - \left(\overline{u_i u_j' u_k}\right)_{t=t_1}\right] - \left[\frac{1}{\rho}\frac{\partial}{\partial r_j}\left(\overline{u_i \sigma'}\right)_{t=t_1} - \frac{\partial}{\partial r_i}\left(\overline{\sigma u_j'}\right)_{t=t_1}\right] + 2\nu \frac{\partial^2 \left(\overline{u_i u_j'}\right)_{t=t_1}}{\partial r_k \, \partial r_k}, \tag{5-195}$$

where the correlation between the (mechanical) pressure σ (eq. (3-14)) and the velocity u_j' is given by

$$\frac{1}{\rho}\frac{\partial^2 \left(\overline{\sigma u_j'}\right)_{t=t_1}}{\partial r_k \, \partial r_k} = -\frac{\partial^2 \left(\overline{u_\ell u_k u_j'}\right)_{t=t_1}}{\partial r_k \, \partial r_\ell} \tag{5-196}$$

and a similar equation for $\left(\overline{u_i \sigma'}\right)_{t=t_1}$. The pertinent solution of equation (5-196) is (ref. 4)

$$\frac{1}{\rho}\left(\overline{\sigma u_j'}\right)_{t-t_1} = \frac{1}{4\pi}\int \frac{1}{|\mathbf{r}-\mathbf{s}|}\frac{\partial^2 \left(\overline{u_i' u_k'' u_j'}\right)_{t=t_1}}{\partial s_i \, \partial s_k} ds,$$

where u_j'' is the velocity at the point $\mathbf{x}'' = \mathbf{x}' - \mathbf{s}$, and the integration is over all s-space. This solution is for an infinite fluid, for which case the boundary conditions are that $\overline{\sigma u_j'}$ is bounded for $r = 0$ and zero for $r = \infty$. The quntity ρ is the density, ν is the kinematic viscosity, and σ is the pressure. A repeated subscript in a term indicates a summation, with the subscript successively taking on the values 1, 2, and 3. The correlation equations are, of course, derived from the Navier-Stokes equations. The quantity $\partial \overline{u_i u_j'}/\partial t$ at $t = t_1$ can be calculated from equations (5-195) and (5-196) if $\overline{u_i u_j'}$ and the two-point triple correlations are known at $t = t_1$.

The second time derivative of $\overline{u_i u_j'}$ is obtained by differentiating the two-point correlation equations and evaluating the result at t_1. This gives

$$\left(\frac{\partial^2 \overline{u_i u_j'}}{\partial t^2}\right)_{t=t_1} = -\frac{\partial}{\partial r_k}\left[\left(\frac{\partial}{\partial t}\overline{u_i u_j' u_k'}\right)_{t=t_1} - \left(\frac{\partial}{\partial t}\overline{u_i u_j' u_k}\right)_{t=t_1}\right] - \frac{1}{\rho}\left[\frac{\partial}{\partial r_j}\left(\frac{\partial \overline{u_i \sigma'}}{\partial t}\right)_{t=t_1} - \frac{\partial}{\partial r_i}\left(\frac{\partial \overline{\sigma u_j'}}{\partial t}\right)_{t=t_1}\right] + 2\nu \frac{\partial^2}{\partial r_k \partial r_k}\left(\frac{\partial \overline{u_i u_j'}}{\partial t}\right)_{t=t_1} \tag{5-197}$$

and

$$\frac{1}{\rho}\frac{\partial^2}{\partial r_k \partial r_k}\left(\frac{\partial \overline{\sigma u_j'}}{\partial t}\right)_{t=t_1} = -\frac{\partial^2}{\partial r_k \partial r_\ell}\left(\frac{\partial \overline{u_\ell u_k u_j'}}{\partial t}\right)_{t=t_1} . \tag{5-198}$$

The quantity $\left[(\partial/\partial t)\left(\overline{u_i u_j' u_k'}\right)\right]_{t=t_1}$ in equation (5-197) is obtained from the three-point correlation equations (section 5.3.2.2) written for $t = t_1$ and $\mathbf{r}' = \mathbf{r}$. (The vector $\mathbf{r}'$ separates the points P and P″.) Thus,

$$\left(\frac{\partial}{\partial t}\overline{u_i u_j' u_k'}\right)_{t=t_1} = \left\{ \frac{\partial}{\partial r_\ell}\left(\overline{u_i u_j' u_k'' u_\ell}\right)_{t=t_1} + \frac{\partial}{\partial r_\ell'}\left(\overline{u_i u_j' u_k'' u_\ell}\right)_{t=t_1} - \frac{\partial}{\partial r_\ell}\left(\overline{u_i u_j' u_k'' u_\ell'}\right)_{t=t_1} - \frac{\partial}{\partial r_\ell'}\left(\overline{u_i u_j' u_k'' u_\ell''}\right)_{t=t_1} \right.$$

$$- \frac{1}{\rho}\left[-\frac{\partial}{\partial r_i}\left(\overline{\sigma u_j' u_k''}\right)_{t=t_1} - \frac{\partial}{\partial r_i'}\left(\overline{\sigma u_j' u_k''}\right)_{t=t_1} + \frac{\partial}{\partial r_j}\left(\overline{\sigma' u_i u_k''}\right)_{t=t_1} + \frac{\partial}{\partial r_k'}\left(\overline{\sigma'' u_i u_j'}\right)_{t=t_1} \right] \tag{5-199}$$

$$\left. + 2\nu\left[\frac{\partial^2\left(\overline{u_i u_j' u_k''}\right)_{t=t_1}}{\partial r_\ell \partial r_\ell} + \frac{\partial^2\left(\overline{u_i u_j' u_k''}\right)_{t=t_1}}{\partial r_\ell \partial r_\ell'} + \frac{\partial^2\left(\overline{u_i u_j' u_k''}\right)_{t=t_1}}{\partial r_\ell' \partial r_\ell'} \right] \right\}_{\mathbf{r}'=\mathbf{r}} ,$$

where $\left(\overline{\sigma u_j' u_k''}\right)_{t=t_1}$ is given by

$$\frac{1}{\rho}\left[\frac{\partial^2\left(\overline{\sigma u_j' u_k''}\right)_{t=t_1}}{\partial r_\ell \partial r_\ell} + 2\frac{\partial^2\left(\overline{\sigma u_j' u_k''}\right)_{t=t_1}}{\partial r_\ell \partial r_\ell'} + \frac{\partial^2\left(\overline{\sigma u_j' u_k''}\right)_{t=t_1}}{\partial r_\ell' \partial r_\ell'} \right] = -\frac{\partial^2\left(\overline{u_\ell u_m u_j' u_k''}\right)_{t=t_1}}{\partial r_m \partial r_\ell}$$

$$- \frac{\partial^2\left(\overline{u_\ell u_m u_j' u_k''}\right)_{t=t_1}}{\partial r_m \partial r_\ell'} - \frac{\partial^2\left(\overline{u_\ell u_m u_j' u_k''}\right)_{t=t_1}}{\partial r_m' \partial r_\ell} - \frac{\partial^2\left(\overline{u_\ell u_m u_j' u_k''}\right)_{t=t_1}}{\partial r_m' \partial r_\ell'} . \tag{5-200}$$

Similar equations are obtained for the other pressure-velocity correlations. The boundary conditions for equation (5-120) are similar to those for equation (5-196); that is, $\overline{\sigma u_j' u_k''}$ is bounded for $\mathbf{r}$ or $\mathbf{r}' = 0$ and zero for $\mathbf{r}$ or $\mathbf{r}' = \infty$. Also, an expression for $\left[(\partial/\partial t)\left(\overline{u_i u_j' u_k}\right)\right]_{t=t_1}$ in equation (5-197) is obtained by letting $\mathbf{r}' = 0$ instead of $\mathbf{r}$ in equation (5-199). Thus, if the turbulence is specified sufficiently well at $t = t_1$ that the double, triple, and quadruple velocity correlations are known, $\left(\partial^2\left(\overline{u_i u_j'}\right)/\partial t^2\right)_{t=t_1}$ can be calculated. Similarly, higher-order derivatives are obtained by considering four or more point correlations in the turbulent field (ref. 22). With the time derivatives of $\overline{u_i u_j'}$ known at $t = t_1$, a Taylor series gives $\overline{u_i u_j'}$ as a function of time as

$$\overline{u_i u_j'} = \left(\overline{u_i u_j'}\right)_{t=t_1} + \left(\frac{\partial \overline{u_i u_j'}}{\partial t}\right)_{t=t_1}(t-t_1) + \frac{1}{2!}\left(\frac{\partial^2 \overline{u_i u_j'}}{\partial t^2}\right)_{t=t_1}(t-t_1)^2 + \dots . \tag{5-201}$$

A similar analysis can be carried out in wavenumber space. For instance, the energy spectrum function $E(\kappa)$, which shows the contributions at various wavenumbers to $\overline{u_i u_j'}/2$, can be written as

$$E(\kappa) = E(\kappa)_{t=t_1} + \left(\frac{\partial E(\kappa)}{\partial t}\right)_{t=t_1}(t-t_1) + \frac{1}{2!}\left(\frac{\partial^2 E(\kappa)}{\partial t^2}\right)_{t=t_1}(t-t_1)^2 + \dots \quad , \tag{5-202}$$

where it is understood that E is a function of t as well as of κ, and where $\partial E(\kappa)\partial t$ is obtained from the Fourier transform of the two-point correlation equation (eq. (5-138)) as

$$\left(\frac{\partial E(\kappa)}{\partial t}\right) = \int_A \frac{1}{2}\left\{-2\nu\kappa^2\varphi_{ii}(\boldsymbol{\kappa}) + i\kappa_k\left[\varphi_{iki}(\boldsymbol{\kappa}) - \varphi_{iki}(-\boldsymbol{\kappa})\right]\right\} dA(\kappa), \tag{5-203}$$

where $dA(\kappa)$ is an element of surface area of a sphere of radius κ, $\boldsymbol{\kappa}$ is the wavevector corresponding to the spatial vector $\mathbf{r}$, and φ_{ii} and φ_{iki} are respectively the Fourier transforms of $\overline{u_i u_i'}$ and $\overline{u_i u_k u_i'}$. Extracting from the intergral that portion which can be written in terms of $E(\kappa)$ and setting the rest of the integral equal to $T(\kappa)$ give

$$\frac{\partial E(\kappa)}{\partial t} = T(\kappa) - 2\nu\kappa^2 E(\kappa). \tag{5-204}$$

Equation (5-204) is, of course, the scalar form of the two-point spectral equation. The transfer term $T(\kappa)$ produces energy transfer between wavenumbers and arises from the triple correlation term in equation (5-195) (with $i = j$). (Note that the pressure-velocity correlation terms in eq. (5-195) drop out for $i = j$.) The second time derivative of $E(\kappa)$ is

$$\left(\frac{\partial^2 E(\kappa)}{\partial t^2}\right)_{t=t_1} = \left(\frac{\partial T(\kappa)}{\partial t}\right)_{t=t_1} - 2\nu\kappa^2\left(\frac{\partial E(\kappa)}{\partial t}\right)_{t=t_1} = \left(\frac{\partial T(\kappa)}{\partial t}\right)_{t=t_1} - 2\nu\kappa^2 T(\kappa)_{t=t_1} + \left(2\nu\kappa^2\right)^2 E(\kappa)_{t=t_1}.$$

The quantity $\left(\partial T(\kappa)/\partial t\right)_{t=t_1}$ can be calculated from the two- and three-point spectral equations if the two- and three-point spectral quantities in those equations are known at $t = t_1$. From equations (5-149), (5-152), and (5-153) one obtains

$$\frac{\partial T(\kappa)}{\partial t} = \int_A \int_{-\infty}^{\infty} \frac{1}{2}\left(-2\nu\kappa^2\left\{i\kappa_k\left[\beta_{iik}(\boldsymbol{\kappa}) - \beta_{iik}(-\boldsymbol{\kappa})\right]\right\} + f\left(\beta_{ijk}, \beta_{ijk\ell}\right)\right) d\boldsymbol{\kappa}'\, dA(\kappa),$$

where $\boldsymbol{\kappa}'$ is the wavevector corresponding to $\mathbf{r}'$, $d\boldsymbol{\kappa} = d\kappa_1 d\kappa_2 d\kappa_3$, and β_{ijk} and $\beta_{ijk\ell}$ are respectively the Fourier transforms of $\overline{u_i u_j' u_k''}$ and $\overline{u_i u_j u_k' u_\ell''}$. If by analogy with the procedure used for obtaining equation (5-204), we extract from the integral that portion which can be written in terms of spectral quantities already defined ($E(\kappa)$ and $T(\kappa)$), we have

$$\left(\frac{\partial T(\kappa)}{\partial t}\right) 2\nu\kappa^2 T(\kappa) = \int_A \int_{-\infty}^{\infty} \frac{1}{2} f\left(\beta_{ijk}, \beta_{ijk\ell}\right) d\boldsymbol{\kappa}'\, dA(\kappa) = V\left[\beta_{ijk}(\boldsymbol{\kappa}'), \beta_{ijk\ell}(\boldsymbol{\kappa}')\right], \tag{5-205}$$

where V is a quantity related to the three-point spectral tensors β_{ijk} and $\beta_{ijk\ell}$. More precisely we can say that V is a functional of β_{ijk} and $\beta_{ijk\ell}$, since each value of V depends on values of β_{ijk} and $\beta_{ijk\ell}$ at all points of $\boldsymbol{\kappa}'$-space. With equation (5-205), the expression for $\left(\partial^2 E/\partial t^2\right)_{t=t_1}$ becomes

$$\left(\frac{\partial^2 E}{\partial t^2}\right)_{t=t_1} = V_{t=t_1} - 4\nu\kappa^2 T_{t=t_1} + \left(2\nu\kappa^2\right)^2 E_{t=t_1}. \tag{5-206}$$

The Taylor series for E then becomes

$$E(\kappa) = E_{t=t_1} + \left(T_{t=t_1} - 2\nu\kappa^2 E_{t=t_1}\right)(t-t_1) + \frac{1}{2!}\left[V_{t=t_1} - 4\nu\kappa^2 T_{t=t_1} + \left(2\nu\kappa^2\right)^2 E_{t=t_1}\right](t-t_1)^2 + \ldots \quad . \qquad (5-207)$$

Equation (5-207) was used in conjunction with available experimental data at an initial time (ref. 35) in an attempt to calculate the variation with time of $E(\kappa)$ and thus of $\overline{u_i u_i}$. However, with the available initial data $\left(E_{t=t_1}, T_{t=t_1}, \text{and } V_{t=t_1}\right)$, reasonable results were not obtained except at small times (fig. 5-21). It thus appears that, in order to obtain good results by using a simple Taylor series, initial statistical information of much higher order than that which is available would have to be given. Thus, an alternative approach which makes more efficient use of the initial statistical information and also incorporates additional information from the equations of motion will be considered.

A workable formulation for the development of turbulence from a given initial state. In order to obtain a more efficient means for calculating the evolution of turbulence than by a Taylor series in time, we consider an iterative solution of the Navier-Stokes equations similar to that in reference 57. In addition to the initial statistical information and calculated time derivatives, we will then have information about the form of the decay law from the equations of motion.

Although attention was confined to determinate initial conditions in reference 57, for the present purposes we can just as well assume the initial velocity fluctuations to be random or turbulent. Thus, we consider a field of homogeneous turbulence to be made up of a very high density of eddies or harmonic disturbances in wavenumber space. For all practical purposes then, since the density of disturbances is very high, the spectrum of the turbulence can be considered continuous. The velocity and pressure at any point in the field are given by

$$\frac{\partial u_i}{\partial t} - \nu\frac{\partial^2 u_i}{\partial x_k\,\partial x_k} = -\frac{1}{\rho}\frac{\partial \sigma}{\partial x_i} - \frac{\partial(u_i u_k)}{\partial x_k} \qquad (5-208)$$

and

$$\frac{1}{\rho}\frac{\partial^2 \sigma}{\partial x_k\,\partial x_k} = -\frac{\partial^2(u_k u_\ell)}{\partial x_k\,\partial x_\ell}. \qquad (5-209)$$

The latter equation is obtained by taking the divergence of equation (5-208) and applying the continuity equation.

From the spectrum of harmonic disturbances we arbitrarily select two cosine terms with wavevectors $\mathbf{q}$ and $\mathbf{r}$. Then, the velocity associated with those disturbances will be

$$u_i^{cc} = a_i \cos \mathbf{q}\cdot\mathbf{x} + b_i \cos \mathbf{r}\cdot\mathbf{x}, \qquad (5-210)$$

where the superscript cc on the velocity indicates that it depends on two cosine terms. The results that follow would be the same if two sine terms or a sine and a cosine term were considered. If u_i^{cc} is substituted for u_i in the right sides of equations (5-208) and (5-209), the time variations of a_i and b_i plus additional harmonic terms are obtained. If we then substitute that new expression into equations (5-208) and (5-209) another expression containing still more harmonic terms is obtained. In each approximation, the linear terms of the Navier-Stokes equations are considered as unknown and the nonlinear terms as known from the preceding approximation. As shown in reference 57, continuation of this process leads to

$$u_i^{cc} = \sum_{\boldsymbol{\kappa}}\left(A_{i,\boldsymbol{\kappa}}^{c'} \cos \boldsymbol{\kappa}\cdot\mathbf{x} + A_{i,\boldsymbol{\kappa}}^{s'} \sin \boldsymbol{\kappa}\cdot\mathbf{x}\right), \qquad (5-211)$$

where

$$A_{i,\boldsymbol{\kappa}}^{c'} = \sum_{q} a_{i,\boldsymbol{\kappa},q}^{c} \exp\left[-b_{\boldsymbol{\kappa},q}^{c}(t-t_1)\right] \qquad (5-212)$$

and

$$A_{i,\boldsymbol{\kappa}}^{s'} = \sum_{r} a_{i,\boldsymbol{\kappa},r}^{s} \exp\left[-b_{\boldsymbol{\kappa},r}^{s}(t-t_1)\right]. \qquad (5-213)$$

Comparison of equations (5-211) to (5-213) with the first and second approximations in reference 57 shows that $b^c_{\kappa,1} = b^s_{\kappa,1} = \nu\kappa^2$. Also, we note that since the two harmonic components in equation (5-210) were selected arbitrarily, expressions similar to equations (5-211) to (5-213) will be obtained for any other two components. But the nonlinear interaction of any number of harmonic components can be expressed as the sum of the interactions of pairs of components (eqs. (37) and (38) of ref. 57). Thus u_i, the velocity resulting from all the harmonic components, will be of the form of equations (5-211) to (5-213) and can be written as

$$u_i = \sum_{\kappa} \left(A^c_{i,\kappa} \cos \kappa \cdot x + A^s_{i,\kappa} \sin \kappa \cdot x \right), \tag{5-214}$$

where

$$A^{()}_{i,\kappa} = a^{()}_{i,\kappa,1} \exp\left[-\nu\kappa^2 (t - t_1)\right] + \sum_{\substack{q \\ q \neq 1}} a^{()}_{i,\kappa,q} \exp\left[-b^{()}_{\kappa,q}(t - t_1)\right]. \tag{5-215}$$

The summations in equations (5-214) and (5-215) will, of course, contain more terms by many orders of magnitude than those in equations (5-211) to (5-213). Since the initial conditions are random, the quantities $A^{()}_{i,\kappa}$, $a^{()}_{i,\kappa}$, and $b^{()}_{\kappa,q}$ are assumed to be random variables. The space-averaged value of u_i^2 (no sum on i) is obtained from equation (5-214) by squaring, integrating over a cycle, and using the orthogonality property of sines and cosines. This gives

$$\overline{u_i^2} = \sum_{\kappa} \frac{1}{2} \left[\left(A^c_{i,\kappa} \right)^2 + \left(A^s_{i,\kappa} \right)^2 \right] \tag{5-216}$$

where

$$\left[A^{()}_{i,\kappa}\right]^2 = \left[a^{()}_{i,\kappa,1}\right]^2 \exp\left[-2\nu\kappa^2 (t - t_1)\right] + \sum_{\substack{q \\ q \neq 1}} \left[a^{()}_{i,\kappa,q}\right]^2 \exp\left[-2b^{()}_{\kappa,q}(t - t_1)\right] + \sum_{\substack{q,r \\ q \neq r}} a^{()}_{i,\kappa,q} a^{()}_{i,\kappa,r} \exp\left\{-2\left[b^{()}_{\kappa,q} + b^{()}_{\kappa,r}\right](t - t_1)\right\}. \tag{5-217}$$

According to equation (5-217), $\left(A^c_{i,\kappa}\right)^2$ and $\left(A^s_{i,\kappa}\right)^2$ in equation (5-216) have the same form, so that we need not carry along the superscripts c and s.

We want to obtain an averaged form of equation (5-217) which is a smoothed function of the magnitude of the vector κ (but not of its direction). In order to do that, we divide the interval of $\kappa = (\kappa_i \kappa_i)^{1/2}$ over which disturbances occur into a large number of small increments $\Delta\kappa$. The terms in $\sum_{\kappa}$ in equations (5-216) and (5-217) are divided into groups each of which corresponds to a particular $\Delta\kappa$. Note that, while the magnitudes of the various vectors lying in a particular $\Delta\kappa$ are approximately equal, their directions can, of course, vary. The group of terms corresponding to each $\Delta\kappa$ is then subdivided into groups in each of which the values of the $b_{i,\kappa,q}$ in $\sum_{\substack{q \\ q \neq 1}}$ do not vary appreciably from a value of $b_s(\kappa)$. The index s designates a particular increment in the values of the $b_{i,\kappa,q}$. Also, for each s, $a^2_{i,\kappa,q}$ will have an average value which we designate by $\left\langle a^2_{i,\kappa} \right\rangle_s$. The summation $\sum_{\substack{q \\ q \neq 1}}$ in equation (5-217), which applies to a particular κ, is then replaced by

$$\sum_{s} n_{s,(i)} \left\langle a^2_{i,\kappa} \right\rangle_s (\kappa) \exp\left[-2b_s(\kappa)(t - t_1)\right]$$

which applies to a particular $\Delta\kappa$, and where $n_{s,(i)}$ is the number of terms in $\sum_{\substack{q \\ q \neq 1}}$ which are assigned to the group s for the component

which applies to a particular $\Delta\kappa$, and where $n_{s,(i)}$ is the number of terms in $\sum_{\substack{q \\ q\neq 1}}$ which are assigned to the group s for the component i. The parentheses around i indicate that there is no summation on that subscript. A similar regrouping can be carried out for the terms in $\sum_{\substack{q,r \\ q\neq 1}}$. However, that summation turns out to be zero, if we assume that the random $a_{i,\kappa}$ are uncorrelated, since $\langle a_{i,\kappa,q} a_{i,\kappa,r} \rangle_s$ will be zero for $q \neq r$. Then the average value of $A^2_{i,\kappa}$ in the increment $\Delta\kappa$ becomes (see eq. (5-217))

$$\left\langle A^2_{i,\kappa} \right\rangle(\kappa) = \left\langle a^2_{i,\kappa,1} \right\rangle(\kappa) \exp\left[-2\nu\kappa^2(t-t_1)\right] + \sum_s \left(\frac{n_s}{n_\kappa}\right)_{(i)} \left\langle a^2_{i,\kappa} \right\rangle_s (\kappa) \exp\left[-2b_s(\kappa)(t-t_1)\right], \tag{5-218}$$

where n_κ is the number of terms in $\sum_{\substack{q \\ q\neq 1}}$ that lie in $\Delta\kappa$. The expression for $\overline{u_i^2}$ (eq. (5-216)) then becomes

$$\overline{u_i^2} = \sum_\kappa \left\{ \left\langle a^2_{i,\kappa,1} \right\rangle(\kappa) \exp\left[-2\nu\kappa^2(t-t_1)\right] + \sum_s \left(\frac{n_s}{n_\kappa}\right)_{(i)} \left\langle a^2_{i,\kappa} \right\rangle_s (\kappa) \exp\left[-2b_s(\kappa)(t-t_1)\right] \right\} \tag{5-219}$$

To obtain an expression for the energy spectrum function E, we note that (eq. (5-166))

$$\frac{1}{2}\overline{u_i u_i} = \int_0^\infty E\, d\kappa, \tag{5-166}$$

where $\overline{u_i u_i} = \overline{u_1^2} + \overline{u_2^2} + \overline{u_3^2}$. Equations (5-219) and (5-166) then give

$$\int_0^\infty E\, d\kappa = \sum_\kappa \frac{1}{2} \left\{ \frac{\left\langle a^2_{i,\kappa,1} a_{i,\kappa,1} \right\rangle}{\Delta\kappa} \exp\left[-2\nu\kappa^2(t-t_1)\right] + \sum_s \left(\frac{n_s}{n_\kappa}\right)_i \frac{\left\langle a^2_{i,\kappa} \right\rangle_s}{\Delta\kappa} \exp\left[-2b_s(t-t_1)\right] \right\} \Delta\kappa, \tag{5-220}$$

where there is now a summation on i. If $\Delta\kappa$ is very small, we can write, to a very good approximation,

$$E(\kappa) = B^2(\kappa) \exp\left[-2\nu\kappa^2(t-t_1)\right] + \sum_s B_s^2(\kappa) \exp\left[-2b_s(\kappa)(t-t_1)\right]. \tag{5-221}$$

Equation (5-221) gives the evolution in time of the energy spectrum function from an initial state which is specified by the B's and b's in the equation.

As shown in the last section, if the turbulence is specified at an initial instant, the time derivatives of E can be calculated at that instant by using the Fourier transformed correlation equations. Thus, it is desirable to write the B's and b's in equation (5-221) in terms of E and its derivatives at the initial time. That can be done by evaluating equation (5-221) and its time derivatives at $t = t_1$ and solving the resulting system of equations for the B's and b's.

In what follows, we will first retain only two terms of equation (5-221). Equation (5-221) can then be written conveniently as

$$E = E_{t=t_1} \left\{ C(\kappa) \exp\left[-2\nu\kappa^2(t-t_1)\right] + (1-C) \exp\left[-2b(\kappa)(t-t_1)\right] \right\}, \tag{5-222}$$

where $0 \leq C \leq 1$.

For C = 1 equation (5-222) reduces to the well-known expression for the final period of decay (see eqs. (5-121) and (5-157) for $\varphi_{ii}(\kappa) = \varphi_{ii}(\kappa)$). For the general case ($C \neq 1$) we could determine C and b in terms of the first and second derivatives of equation (5-222) for $t = t_1$ and then evaluate those derivatives by using the two-point spectral equations (see eqs. (5-204) to (5-206)). The following procedure turns out to be simpler, however. By substituting equation (5-222) into the spectral equation (5-204) we get for the energy transfer term

$$T = 2(1-C)\left(\nu\kappa^2 - b\right)E_{t=t_1}\exp\left[-2b(t-t_1)\right] = T_{t=t_1}\exp\left[-2b(t-t_1)\right]. \tag{5-223}$$

Then,

$$\frac{\partial T}{\partial t} = 2bT_{t=t_1}\exp\left[-2b(t-t_1)\right] = \left(\frac{\partial T}{\partial t}\right)_{t=t_1}\exp\left[-2b(t-t_1)\right]. \tag{5-224}$$

Comparing the last two members of equation (5-224) and using equation (5-205) gives

$$b = \nu\kappa^2 - \frac{V_{t=t_1}}{2T_{t=t_1}}. \tag{5-225}$$

From equations (5-223) and (5-225) we have

$$C = 1 - \frac{T^2_{t=t_1}}{V_{t=t_1}E_{t=t_1}}. \tag{5-226}$$

Equations (5-222) and (5-223) then become

$$E = E_{t=t_1}\left\{C\exp\left[-2\nu\kappa^2(t-t_1)\right] + (1-C)\exp\left[-2\left(\nu\kappa^2 - \frac{V_{t=t_1}}{2T_{t=t_1}}\right)(t-t_1)\right]\right\} \tag{5-227}$$

and

$$T = T_{t=t_1}\exp\left[-2\left(\nu\kappa^2 - \frac{V_{t=t_1}}{2T_{t=t_1}}\right)(t-t_1)\right]. \tag{5-228}$$

From equation (5-205)

$$V = V_{t=t_1}\exp\left[-2\left(\nu\kappa^2 - \frac{V_{t=t_1}}{2T_{t=t_1}}\right)(t-t_1)\right], \tag{5-229}$$

where C is given by equation (5-226).

Equations (5-227) and (5-228) were obtained by retaining two terms on the right side of equation (5-221). We consider next a higher order approximation in which three terms are retained in that equation. If equation (5-221), with three terms retained, is substituted into equation (5-204), we get for T

$$T = 2B_1^2\left(\kappa^2 - b_1\right)\exp\left[-2b_1(t-t_1)\right] + 2B_2^2\left(\kappa^2 - b_2\right)\exp\left[-2b_2(t-t_1)\right]. \tag{5-230}$$

Equation (5-230) contains four unknown functions which are to be determined by the initial conditions. For that purpose we use equation (5-230) and its first three derivatives evaluated at $t = t_1$. Thus, we obtain

$$b_1 = -\frac{T_1T_2 - T_{t=t_1}T_3}{4\left(T_1^2 - T_{t=t_1}T_2\right)} + \left\{\left[\frac{T_1T_2 - T_{t=t_1}T_3}{4\left(T_1^2 - T_{t=t_1}T_2\right)}\right]^2 - \frac{T_2^2 - T_1T_3}{4\left(T_1^2 - T_{t=t_1}T_2\right)}\right\}^{1/2}, \tag{5-231}$$

$$b_2 = -\frac{T_1T_2 - T_{t=t_1}T_3}{4\left(T_1^2 - T_{t=t_1}T_2\right)} - \left\{\left[\frac{T_1T_2 - T_{t=t_1}T_3}{4\left(T_1^2 - T_{t=t_1}T_2\right)}\right]^2 - \frac{T_2^2 - T_1T_3}{4\left(T_1^2 - T_{t=t_1}T_2\right)}\right\}^{1/2}, \tag{5-232}$$

$$B_1^2 = \frac{2b_2T_2 + T_3}{16b_1^2\left(\kappa^2 - b_1\right)\left(b_2 - b_1\right)}, \tag{5-233}$$

and

$$B_2^2 = \frac{2b_1T_2 + T_3}{16b_2^2\left(\kappa^2 - b_2\right)\left(b_1 - b_2\right)}, \tag{5-234}$$

where T_1, T_2, and T_3 are the first, second, and third time derivatives of $T(\kappa)$ at $t = t_1$. The first derivative T_1 can be written in terms of the functional $V_{t=t_1}$, which gives a representation of three-point spectral quantities (eq. (5-205)). Equations for higher order functionals can be obtained by the procedure used for obtaining equation (5-205) for V. Thus, by using the four-point spectral equations (10), (12), and (18) of reference 22 we get

$$\frac{\partial V}{\partial t} = -2\nu\kappa^2 V + R \tag{5-235}$$

where R is a functional of three- and four-point spectral quantities. Similarly,

$$\frac{\partial R}{\partial t} = -2\nu\kappa^2 R + S \tag{5-236}$$

where S is a functional of three-, four, and five-point spectral quantities. By using equations (5-205), (5-235), and (5-236), the first, second, and third time derivatives of $T(\kappa)$ at $t=t_1$ in equations (5-231) to (5-234) can be written in terms of higher order spectral quantities as

$$T_1 = -2\nu\kappa^2 T_{t=t_1} + V_{t=t_1}, \tag{5-237}$$

$$T_2 = \left(2\nu\kappa^2\right)^2 T_{t=t_1} - 4\nu\kappa^2 V_{t=t_1} + R_{t=t_1}, \tag{5-238}$$

and

$$T_3 = -\left(2\nu\kappa^2\right)^3 T_{t=t_1} + 3\left(2\nu\kappa^2\right)^2 V_{t=t_1} - 6\nu\kappa^2 R_{t=t_1} + S_{t=t_1}. \tag{5-239}$$

Results and discussion. A comparison between the experimental data of Uberoi (ref. 35) and the present theory (eqs. (5-227) to (5-229)) is given in figures 5-20 to 5-23. (Another pertinent experimental investigation is that of Van Atta and Chen (ref. 36). They measured directly the individual terms in the two-point spectral equation; however, their data are for only one time.) The comparison in figures 5-20 to 5-23 is made for an initial time corresponding to X/M = 48 in the experiment of ref. 13 ($t^* = \left(\nu/M^2\right)t = 0.001818$, X is the distance downstream from the grid, and M is the mesh size of the gird). For the initial specification of the turbulence, values of $E(\kappa)$ and $T(\kappa)$ were obtained from figures 5, 9, and 10 of reference 35. Initial values of V were not given directly in reference 35 but were estimated from the decay data for $T(\kappa)$ and equation (5-205). Except for experimental error those values will be the same as those that might have been measured directly.

The agreement between the predicted and experimental energy spectra for the same initial conditions (fig. 5-20) appears to be quite good considering the difficulty of the measurements. The calculation of the experimental values of E required the differentiation of measured one-dimensional spectra and an assumption of isotropy.

Predicted and experimental values for the decay of $\overline{u_i u_i}$ are plotted in figure 5-21. The agreement between theory and experiment is excellent for values of t* up to about 0.006. (Note that spectra were measured only for values of t* between 0.00182 and 0.00417.) Elimination of the moderate deviation for $t^* > 0.006$ might require a higher order theory (more terms in eq. (5-221)), together with additional initial statistical information. Alternatively, the deviation might be due to the amplification at large times of slight inaccuracies in the measured initial spectra. The theoretical values for t* less than 0.00182 were calculated by working backwards from the measured initial spectra. Also included in figure 5-21 is a Taylor series solution which uses the same initial information as the exponential series and the curve for the weak turbulence approximation. It might be pointed out that the curve for the weak turbulence approximation is not the -5/2 power decay law usually given for the final period (ref. 4) but is the curve obtained by using the measured initial energy spectrum and equation (5-222) with C = 1.

Spectra for the energy transfer term $T(\kappa)$ are plotted in figure 5-22. The experimental and theoretical curves are in good agreement except near the value of κ where $T_{t=t_1}$ changes sign. The deviation there results from a mathematical singularity in equation (5-228) when $T_{t=t_1} = 0$. However, that deviation does not seem to be serious, because the real physical curve in that region can easily be estimated graphically or by using an interpolation formula. This is particularly true since it is known that the total area enclosed by the $T(\kappa)$ spectrum should be zero (eq. (5-162)). It appears likely that the difficulty could be eliminated if another term were retained in equation (5-221). (More will be said about that possibility in the next paragraph.) The deviation also carries over to some extent into the results for $E(\kappa)$ and $\overline{u_i u_i}$. However, if one does not use values of κ close to the point where $T_{t=t_1}$ changes sign for calculating $E(\kappa)$ and $\overline{u_i u_i}$, the inaccuracies in those quantities will be small. It appears that the overall agreement between theory and experiment obtained by using equations (5-226) to (5-228) should be considered encouraging.

For the sake of completeness, spectra of the functional V (eqs. (5-205) and (5-229)), the third initial condition specified for the turbulence, are plotted in figure 5-23. The agreement between theory and experiment is probably within the uncertainty in estimating V from the decay data in reference 35, except in the vicinity of the point where $T_{t=t_1}$ changes sign. Thus, the theory predicts the evolution in time of $E(\kappa)$, $T(\kappa)$, and $V(\kappa)$, when those quantities are specified at an initial time.

We have not been able to apply a higher-order theory to Uberoi's data, that is, to evaluate three instead of two terms in equation (5-221) by using the initial data given in his article. However, we can apply a higher order theory to the analysis in section 5.3.2.2, since for that analysis we can, in effect, calculate as much initial information as is desired. That analysis neglects quadruple correlation terms in the three-point correlation equations and should apply, for a particular set of initial conditions, at times somewhat before the final period of decay. The initial conditions, as well as values at later times, are given by closed-form equations in that analysis and thus are better defined than may be possible in an experiment. For the present purposes, the analytical results from section 5.3.2.2 might in fact be thought of as experimental results in which the initial conditions are specified exactly (an analytical experiment).

The case considered here corresponds to figure 5-5. Values of dimensionless $E(\kappa)$, $T(\kappa)$, and time derivatives of $T(\kappa)$ for the initial specification of the turbulence $\left(t_1^* = 0.002\right)$ are obtained from equations (5-165) and (5-161). We can eliminate the time derivatives of $T(\kappa)$ by introducing V (eq. (5-205)) and the higher-order functionals R and S (eqs. (5-235) and (5-236)). In the present case, those quantities will all be representations of correlations of order no higher than the third, since terms involving correlations of higher order than the third are assumed negligible in the analysis of section 5.3.2.2.

Figure 5-24 gives a comparison between results for $T(\kappa)$ calculated from the present theory and those from section 5.3.2.2. The quantity J_0 is a constant related to conditions at $t_0^* = -0.00633$ in the equations of section 5.3.2.2. The starred quantities in figures 5-24 to 5-26 are the same as those in figures 5-20 to 5-23 if we let $J_0 = M^3 v^2$. As expected, when $T(\kappa)$ is calculated from equation (5-228), the agreement with the results of section 5.3.2.2 is good except in the region where $T_{t=t_1}$ changes sign. However, when a higher order theory is used by retaining three terms in the expression for E (two terms in the expression for $T(\kappa)$ (eq. (5-230)) the agreement is excellent at essentially all values of κ. It might be expected that a similar improvement would be obtained in figure 5-22 if a higher order theory could be used for comparison with the experimental data of Uberoi.

Because of the good agreement obtained for T in figure 5-24, one would expect the calculated energy spectra E to also be in good agreement with those from section 5.3.2.2. Figure 5-25 shows that this is indeed the case. The energy spectrum, in this case, decays in a highly nonsimilar fashion. In order show the effects of spectral energy transfer on the energy spectrum, curves for the final period of decay (first term of eq. (5-165)) are also included in figure 5-25.

Figures 5-26 to 5-28 show plots for the decay of the higher order spectral quantities V, R, and S. The agreement between the present higher order theory and the results of section 5.3.2.2 is very good. Although the effects of the singularity at $\kappa = 15.33$

are greater for these higher order quantities than for the lower order ones, they are still not apparent unless points very close to the singularity are used in plotting the curves,. For points close to the singularity, an interpolation formula can be used. Thus, by specifying the initial conditions for E, T, V, R, and S, we can predict the evolution in time of those quantities by using the present higher order theory. That is, the required number of initial conditions is no greater than the number of quantities whose decay we can predict.

The higher order theory (three exponential terms retained in eq. (5-221) can also be compared with grid-turbulence data obtained in a water channel by Ling and Huang (ref. 38). For that comparison, the experimental input can be conveniently obtained from an empirical equation for E (eq. (5-184)). The higher order spectra were not measured directly in their experiment but could be calculated from their equation for E by using equations (5-204), (5-205), (5-235), and (5-236). Except for possible experimental error those values will be the same as those that might have been measured directly. The comparison is shown in dimensionless form in figures 5-29 to 5-34. The quantity A is an experimental constant (the proportionality constant in the power decay law for $\overline{u_1^2}$). It has the dimensions of a length squared and is related to conditions at time t_0 (eq. (5-185)). As in the preceding comparisons, unphysical singularities occurred in the theoretical spectra at certain values of κ, particularly in the higher order spectra. Thus, in the vicinity of those points, four-point interpolation formulas were used.

Figure 5-29 compares theory and experiment for the decay of turbulent energy when the initial state is specified at $(\nu/A)t_1 = 0.0075$. Theoretical curves are shown for 1, 2, and 3 exponential terms retained in equation (5-221). The curve for three terms is in good agreement with the experiment for the whole decay period. The curve for two terms is in almost as good agreement. That is not the case for the spectra, where only the curves for three terms agree closely (see the curves for E in fig. 5-30). Comparison of the curve in figure 5-29 for one term retained (weak turbulence approximation) with the experimental curve shows the effect of inertia on the decay process. As in figure 5-21, the curve for the weak turbulence approximation in figure 5-29 is not the –5/2 power decay law usually given for the final period, since measured initial energy spectra were used here.

Figures 5-30 to 5-34 give a comparison of theory and experiment for the decay of the spectra used to specify the initial state of the turbulence at t_1. The curves indicate good agreement with the higher order theory. That is, the theory is able to predict the decay of all of the spectra used to specify the initial turbulence, when three exponential terms are retained in equation (5-221).

High Reynolds-number turbulence. Thus far, we have given the basic theory for closure by specification of initial conditions and calculated results for low- and moderate-turbulence Reynolds numbers ($3 < R_\lambda < 70$). Here, we compare calculated results with the higher Reynolds-number experimental data of Ling and Saad (ref. 37). The Reynolds numbers for those data were high enough to obtain a –5/3-power region in the energy spectrum ($300 < R_\lambda < 800$). The exponential-series expression for the energy spectrum function E, an iterative solution of the Navier-Stokes equation, is given by equation (5-221):

$$E(\kappa) = B^2(\kappa)\exp\left[-2\nu\kappa^2(t-t_1)\right] + \sum_s B_s^2(\kappa)\exp\left[-2b_s(\kappa)(t-t_1)\right]. \qquad (5-221)$$

Equation (5-221) gives the evolution in time of the energy spectrum from an initial state at time t_1 which is specified by the B's and b's in the equation. The first term is the well-known expression for the decay of E in the final period (weak turbulence approximation). The rest of the terms in equation (5-221) therefore give the contribution of inertia to E. In the present paper we will retain a maximum of four exponential terms in equation (5-221). This is one more term than it was necessary to retain for the low and moderate Reynolds-number data considered in the last section.

With four terms retained in equation (5-221), we will have to specify seven spectra at t_1 in order to evaluate the functions B, B_1, B_2, B_3, and b_1, b_2, and b_3. Evidently, we need more spectra to describe the initial turbulence at higher Reynolds numbers because a wider range of eddy sizes is excited, and the turbulence structure is more complicated than at lower Reynolds numbers.

In addition to $E(\kappa,t_1)$, we will use spectrum functions designated by $T(\kappa)$, V, R, S, L, and M, all of which are specified at the initial time t_1. The quantity $T(\kappa)$ is the well-known energy-transfer function given by equation (5-204):

$$T(\kappa,t) = \frac{\partial E(\kappa,t)}{\partial t} + 2\nu\kappa^2 E \qquad (5-204)$$

The quantities V, R, S, L, and M are two-point functionals of three- to seven-point spectral quantities (see preceding sections). Each functional depends on a field of values of the multipoint spectral quantities. For instance,

$$V(\kappa) = \int_A \int_{-\infty}^{\infty} f\left[\beta_{ijk}(\kappa,\kappa'), \beta_{ijk\ell}(\kappa,\kappa')\right] d\kappa' dA(\kappa) = V\left[\beta_{ijk}(\kappa,\kappa'), \beta_{ijk\ell}(\kappa,\kappa')\right], \qquad (5-240)$$

where κ, and κ', are vectors in wavenumber space corresponding, respectively, to $\mathbf{r}$ and $\mathbf{r}'$ in physical space. The β_{ijk} and $\beta_{ijk\ell}$ are Fourier transforms of $\overline{u_i u_j' u_k''}$ and $\overline{u_i u_j u_k' u_\ell''}$, where the u_i, u_j', etc. are velocity components at various points, and the overbars indicate averaged values. The element $d\kappa = d\kappa_1 d\kappa_2 d\kappa_3$, and dA is an element of surface area of radius κ. Equations similar to (5-240), but which involve a larger number of wavevectors, can be written for the other higher-order spectra.

By integrating a three-point spectral equation over κ' and $A(\kappa)$ (see preceding sections), we get, using equation (5-240), equation (5-205):

$$V(\kappa,t) = \partial T(\kappa,t)/\partial t + 2\nu\kappa^2 T. \qquad (5-205)$$

Similarly, by performing integrations over wavenumber space of higher-order multipoint spectral equations, and using relations similar to (5-240), we get

$$R(\kappa,t) = \partial V(\kappa,t)/\partial t + 2\nu\kappa^2 V, \qquad (5-235)$$

$$S(\kappa,t) = \partial R(\kappa,t)/\partial t + 2\nu\kappa^2 R, \qquad (5-236)$$

$$L(\kappa,t) = \partial S(\kappa,t)/\partial t + 2\nu\kappa^2 S, \qquad (5-241)$$

and

$$M(\kappa,t) = \partial L(\kappa,t)/\partial t + 2\nu\kappa^2 L. \qquad (5-242)$$

Equations (5-205) and (5-235) to (5-242) can be thought of as two-point alternatives to the multipoint spectral equations. They are much easier to work with because, although conceptually the spectra contained in them are functionals of multipoint spectral quantities, they are, for purposes of computation, simply functions of κ(and t). For instance (see eq. (5-240)),

$$V[\beta_{ijk}(\kappa,\kappa'), \beta_{ijk\ell}(\kappa,\kappa')] = V(\kappa).$$

It is easy to show that V, R, etc. can be obtained from equations (5-204), (5-240), (5-205), (5-235) to (5-242), and the time derivatives of E. We thus have a simple way of calculating initial functionals for a given set of data.

The higher-order spectral quantities are somewhat similar to $T(\kappa)$, inasmuch as they contain the effects of transfer between wavenumbers. However, they differ in that they also contain other effects, so that the areas under those spectra are not necessarily zero, as in the case of $T(\kappa)$.

For comparing the theory with the experiment of Ling and Saad (ref. 37) the experimental input can be conveniently obtained from an empirical equation of E, equation (8) in their paper. The higher-order spectra were not measured directly in their experiment, but could be calculated from their equation for E and equations (5-204), (5-240), (5-205), and (5-235) to (5-242). Except for experimental error those values will be the same as those that might have been measured directly. The B's and b's in equation (5-221) can be related to the initial spectra by successive differentiations of that equation and Ling and Saad's equation (8) with respect to time, setting $t = t_1$, and using equations (5-204), (5-240), (5-205), and (5-235) to (5-242).

It might be pointed out that although we use the initial time variation of E in obtaining the initial conditions, we do so only because of the method of measurement of those conditions. Regardless of how they are measured, the initially specified spectra are, conceptually, functionals of multipoint spectral quantities which could in principle, be measured directly at one initial time. However, the method used here is much simpler. Moreover, it does not require us to know E for the whole decay period but only at enough early times to calculate the required initial conditions, the latter being a much smaller amount of information.

The amount of required initial information may still seem large, and the theory therefore somewhat uninteresting. Indeed it would, if the specification of many initial spectra were necessary to calculate the evolution of one or two lower-order quantities. The evolution of all of the initially specified spectra can however, be calculated, as will be seen. If the objective of a turbulence theory is to calculate the time evolution of as much statistical information as possible, then the structure of the present theory should be no disadvantage. Although it may not be particularly convenient from a practical standpoint, the initial specification of a number of interacting quantities appears necessary for the problem posed.

Before giving results obtained from equation (5-221), we will consider a Taylor series with a maximum of seven initial spectra [the same maximum number that will be used with equation (5-221)], and a modified Kovasznay-type closure (modified to include an effect of initial T) (ref. 52). Results for those calculations are given in figure 5-35, where the initial state is specified at $t_1^* = 0.0048$. The quantity u_i is a velocity component, the over-bar indicates an averaged value, and an asterisk on a quantity indicates that it has been nondimensionalized by the kinematic viscosity and an experimental constant A, the proportionality

constant in the power decay law for $\overline{u_1^2}$ (eq. (1) of ref. 37). In contrast to the A for lower Reynolds numbers in figures 5-29 to 5-34, (see eq. (5-185)), the A in figures 5-35 to 5-42 has the dimensions [(length)^2 (time)$^{1.3}$]. The turbulent energy (1/2) $\overline{u_i u_i}$ is obtained by integrating E over all wavenumbers. Figure 5-35 indicates that the Taylor-series results agree with experiment only for small times. Evidently, many more terms (and initial spectra) would be required in order to obtain accurate results for $\overline{u_i u_i}$ at large times. Note that even if enough terms were retained in the Taylor series to give accurate results for $\overline{u_i u_i}$, the decay of the higher-order spectra which would then have to be specified initially could not be accurately calculated. Thus, the use of a Taylor series in the present problem does not give a satisfactory solution, regardless of the number of terms retained.

The modified Kovasznay-type closure is in somewhat better agreement with experiment than the Taylor series, but at large times the agreement is still not good. This is in contrast to its good agreement at moderate and low Reynolds numbers (ref. 52). It was introduced in reference 52 in an effort to reduce the required number of initial spectra. Evidently, that effort is successful only for moderate and low Reynolds numbers. It is possible, of course, that a more sophisticated method might be more successful (e.g., see ref. 60).

A comparison between theory and experiment using the exponential series (eq. (5-221)) is given in figures 5-36 to 5-42, where the initial state is again specified at $t_1^* = 0.0048$. As was the case for the lower Reynolds numbers considered in section 5.3.2.4, unphysical singularities occasionally occurred in the present theoretical spectra. Inasmuch as the unphysical values were localized, particularly in the higher-order approximations, a smooth curve could be obtained without taking them into account.

Figure 5-36 gives a comparison between theory and experiment for the decay of turbulent energy. Theoretical curves are shown for one, two, three, and four exponential terms retained in equation (5-221). The curve for four terms is in good agreement with experiment for the whole decay period.

Comparison of the curve in figure 5-36 for one term retained (weak turbulence approximation) with the curve for four terms shows the effect of inertia on the decay process. In contrast to the results for moderate Reynolds number (fig. 5-29), where inertia and viscous effects were of the same order of magnitude, the inertia effects for the present high Reynolds number results are at least an order of magnitude greater than the purely viscous effects. Figure 5-37 compares results for the two ranges of Reynolds number. Thus, most of the decay at high Reynolds numbers is due to inertial self-interaction of the turbulence, rather than to purely viscous effects. Another (perhaps better) way of saying this is that at large Reynolds numbers most of the eddies making up the turbulence are inertial. That is, they would be absent if they were not excited (at higher wavenumbers) by the inertial or transfer term in the spectral equation. The ultimate dissipation of turbulent energy into heat is still, of course, produced by viscous action. Figures 5-38 and 5-39 show how the energy and the transfer spectra decay with time.

Figures 5-40 and 5-41 compare theory and experiment at a late time for all of the spectra which are initially specified to described the initial turbulence. The prediction of the decay of all seven of the spectra which are specified initially is rather good. Thus, the present theory appears to solve an initial-value problem for high Reynolds-number turbulence in which the decay of seven initially specified spectra is predicted. Note that the higher-order spectra occur at higher wavenumbers.

Although the initial dissipation spectrum $\kappa^2 E$ is not specified independently, because of its importance in turbulence theory it is compared with experiment and with the energy spectrum at a late time in figure 5-42. Again, good agreement is indicated. The separation of the energy and dissipation spectra is good evidence that we are dealing with high Reynolds number turbulence.

Concluding remarks—the gap problem. If a homogeneous turbulent field is specified at an initial instant by its multipoint-velocity correlations (or their spectral equivalents), the initial time derivatives of those quantities can be calculated from the correlation or spectral equations. The development of the turbulence in time can then be obtained by using those derivative in a series such as a Taylor power series. When the problem is formulated in this way, an assumption for closing the system of correlation equations is not required, since those equations are closed by the initially specified correlations or spectral quantities. A Taylor series expansion, however, did not give realistic results (except for small times) when the limited initial experimental data were used. An exponential series (eq. (5-221)), which was an iterative solution of the Navier-Stokes equations worked much better.

By specifying n spectra at an initial time, where n is an odd integer greater than or equal to 3, we have been able to predict the evolution in time of those n spectra. We have not been able to obtain determinate results for $n<3$, except for weak turbulence. From a practical standpoint it would be advantageous to calculate the evolution of the turbulent energy spectrum by specifying only that quantity initially. Unfortunately, because of the coupling between the members of the infinite hierarchy of multipoint correlation or spectral equations, it appears that we are not able to do that without making a closure assumption for the energy-transfer function, so that a satisfactory theory would seem to require the initial specification of a number of interacting quantities.

The prediction of the evolution of the energy spectrum, in fact, requires the specification of an infinite number of initial multipoint correlations or spectra (or functionals of those quantities) (ref. 4). If we were to claim that we should be able to predict the decay of the energy spectrum by specifying at an initial instant only that spectrum, we would in effect be saying that the Fourier components of the energy spectrum decay independently, as in the final period.

Of course, in practice, one can specify only a finite number of the lower-order quantities. This has been called the "gap problem" (ref. 61). It is the problem of bridging the gap between the infinite number of correlations which would theoretically be necessary to calculate the evolution of the turbulence, and a finite specifiable number of correlations. This is a difficulty which appears to be inherent in the problem of homogeneous turbulence and its initial specification. Most workers have attempted to bridge the gap by assuming that the initial distribution of turbulent fluctuations is exactly Gaussian (zero odd-order correlations). However, that is an artificial initial condition, probably never realized for real turbulence. The importance of accurate initial conditions is shown, for instance, by the data of Ling and Saad (ref. 37), where measurements were made downstream from a turbulence-producing waterfall. The turbulence decay law for the initial conditions produced by the waterfall is considerably different from that for initial conditions produced by a grid.

Here we bridged the gap simply by specifying a sufficient number of initial correlations or their spectral equivalents to calculate the evolution accurately. Fortunately, we do not have to specify the multipoint correlations or their spectral equivalents themselves (those would be extremely difficult to measure), but only two-point functionals of the multipoint spectral quantities. It was seen that the evolution of all the quantities which are specified initially can be calculated. In that sense the solution may be considered complete. If, on the other hand, a large number of initial conditions were specified in order to predict the evolution of say one quantity, it might be objected that the initial conditions were chosen to make the theory agree with experiment for that one quantity. However, that objection cannot be made if the evolution of all of the quantities which are specified initially can be calculated, as in the present theory. From a fundamental standpoint, the calculation of the evolution of those quantities is all that might be expected from a theory of evolving turbulence. Note that the present (higher-order) theory provides the only deductive procedure we have considered which works for high Reynolds-number turbulence (see figs. 35 to 42). Of course, with the continued improvement of computers and numerical methods, direct numerical simulation may offer an alternative.

5.3.2.5 A modified Kovasznay-type closure.—In the concluding remarks of the last section (section 5.3.2.4) we mentioned the "gap problem"—the problem of bridging the gap between the infinite number of correlations or spectra which would theoretically be necessary to calculate the evolution of turbulence, and a finite specifiable number of correlations (or spectra). A theory for the decay of homogeneous turbulence was given which did not require a closure assumption in the usual sense, because the spectral equations were closed by the initial specification of the turbulence. By specifying n spectra at an initial time, where n is an odd integer greater than or equal to 3, the evolution in time of those n spectra was predictable. Good agreement with experiment and previous analytical results was obtained for n = 3, 5, or 7, depending on the Reynolds number, higher Reynolds numbers requiring more specified spectra.

It may be that the nature of the problem is such that three or more spectra have to be specified initially in order to calculate the evolution of any of them (except for weak turbulence). However, particularly in an applied problem, three or more initial spectra will often not be available. In that case possible courses of action are first, the required initial spectra might be estimated from previous experimental or analytical results or second, the introduction of physical or mathematical hypotheses into the theory might be allowed. In the remainder of the paper the latter course of action will be considered.

The analysis is limited to the two-point spectral equation, since a similar analysis, which also used the three-point equation would require the specification of at least three initial spectra. The two-point spectral equation is

$$\partial E(\kappa)/\partial t = -(\partial S(\kappa)/\partial \kappa) - 2\nu\kappa^2 E(\kappa), \qquad (5-243)$$

where E is the energy spectrum function, t is the time, S is the energy transfer at wavenumber κ, and ν is the kinematic viscosity. Equation (5-243) is the same as equation (5-158) if

$$\frac{\partial S(\kappa)}{\partial \kappa} = -T(\kappa).$$

This equation ensures that equation (5-162) is satisfied if $S(0) = S(\infty) = 0$.

In order to close equation (5-243), a modification of Kovasznay's hypothesis (ref. 17) is used. This hypothesis was chosen mainly on the basis of simplicity, in order to illustrate how the initial specification of the turbulence might be simplified. Kovasznay's original hypothesis assumed that S is a function only of the energy at κ. Here, an effect of initial conditions is included. A sufficiently general functional relation for our purpose is

$$S = S(\kappa, E, I'), \qquad (5-244)$$

where $I'(\kappa)$ is a dimensionless function of initial conditions. From dimensional considerations

$$S/\left(E^{3/2}\kappa^{5/2}\right) = f[I'(\kappa)] = I(\kappa) \tag{5-245}$$

Then, the net rate of transfer of energy into a wavenumber band $d\kappa$ is

$$T\,d\kappa = -(\partial S/\partial\kappa)d\kappa \tag{5-246}$$

or, from equations (5-245) and (5-246)

$$T = -\frac{\partial}{\partial\kappa}\left(IE^{3/2}\kappa^{5/2}\right). \tag{5-247}$$

It is desired to determine $I(\kappa)$ as a function of initial conditions at $t = t_1$. Thus at t_1, equation (5-247) becomes

$$T_1 = -\frac{\partial}{\partial\kappa}\left(IE_1^{3/2}\kappa^{5/2}\right)$$

or

$$I(\kappa) = -\int_0^\kappa T_1(\kappa')d\kappa'\left[\kappa^{5/2}E_1^{3/2}(\kappa)\right]^{-1} \tag{5-248}$$

where the subscript 1 refers to values at the initial time t_1. Equation (5-247) for the energy transfer function then becomes

$$T(\kappa) = \frac{\partial}{\partial\kappa}\left\{E^{3/2}(\kappa)\int_0^\kappa T_1(\kappa')d\kappa'\left[E_1^{3/2}(\kappa)\right]^{-1}\right\}. \tag{5-249}$$

Note that this expression for $T(\kappa)$ contains no adjustable constants or functions. Equation (5-243) becomes, by using equations (5-246) and (5-249),

$$\frac{\partial E}{\partial t} - \frac{\partial}{\partial\kappa}\left\{E^{3/2}(\kappa) - \int_0^\kappa T_1(\kappa')d\kappa'\left[E_1^{3/2}(\kappa)\right]^{-1}\right\} = -2\nu\kappa^2 E. \tag{5-250}$$

Equation (5-250) has been solved numerically for the initial conditions of the decay data in reference 38, and the results for various times have been compared with the data. The comparison is shown in dimensionless form in figures 5-43 to 5-45. The quantity A is a constant with the dimensions of a length squared (ref. 38) and is related to conditions at a time t_0, u_i is a velocity component, and the overbar indicates an averaged value. The curve for $S = 0$ (weak turbulence approximation) is included in figure 5-43 in order to show the effect of inertia on the decay process. Inertial and viscous effects appear to be of the same order of magnitude.

The plots for the decay of turbulent energy, the energy spectrum, and the energy-transfer spectrum show agreement between theory and experiment which is probably within the accuracy of the data. Thus, as in the case of the theory of section 5.3.2.4 we were able to predict the evolution of the spectra which were used for specifying the initial turbulence. By introducing a simple physical assumption, it has evidently been possible to reduce the required number of initial spectra from three or more (preferably more) to two, E_1 and T_1. Moreover, as in our previous theory, the resulting equations contain no adjustable constants or functions. However, unlike the previous theory, the present equations do not predict the evolution of the higher Reynolds-number data of reference 37, except at short decay times (fig. 5-35).

5.3.2.6 Further discussion of homogeneous turbulence without mean gradients—numerical solutions of the instantaneous equations.—Additional insights into the physics of homogeneous turbulence can be obtained by studying turbulent or turbulent like numerical solutions of the unaveraged Navier-Stokes equations. We have already looked briefly at several numerical solutions for turbulence (ref. 33, and refs. 17, 49, and 50 of chapter 4); it was pointed out that numerical solutions of the unaveraged equations are, in general deductive, since no external information (modeling) is required. Here we consider several numerical solutions in somewhat greater detail (ref. 140).

The equations to be solved numerically, the incompressible Navier-Stokes equations, are

$$\frac{\partial u_i}{\partial t} + \frac{\partial (u_i u_k)}{\partial x_k} = -\frac{1}{\rho}\frac{\partial \sigma}{\partial x_i} + \nu \frac{\partial^2 u_i}{\partial x_k \partial x_k} \tag{5-130}$$

where the mechanical pressure (see eq. (3-14)) is given by the Poisson equation

$$\frac{1}{\rho}\frac{\partial^2 \sigma}{\partial x_1 \partial x_1} = -\frac{\partial^2 (u_1 u_m)}{\partial x_1 \partial x_m}. \tag{5-150}$$

and where as usual, the subscripts can take on the values 1, 2, or 3, and a repeated subscript in a term indicates a summation. The quantities u_i and u_j' are instantaneous velocity components, x_i is a space coordinate, t is the time, ρ is the density, ν is the kinematic viscosity, and σ is the instantaneous (mechanical) pressure. Equation (5-150) is obtained by taking the divergence of equation (5-130) and using continuity (eq. (3-4)).

The initial u_i in equations (5-130) and (5-150) are given at $t = 0$ by

$$u_i = \sum_{n=1}^{3} a_i^n \cos \mathbf{q}^n \cdot \mathbf{x}. \tag{5-251}$$

Equation (5-251), unlike the initial condition used for most numerical studies of turbulence, is nonrandom. But that condition might be considered comparable to the initial condition for turbulence generated experimentally by a regular grid in a wind tunnel. The quantity a_i^n is an initial velocity amplitude or Fourier coefficient of the velocity fluctuation, and $\mathbf{q}^n$ is an initial wavevector. In order to satisfy the continuity condition, we set (with a sum on i)

$$a_i^n q_i^n = 0, \tag{5-252}$$

For the present work let

$$a_i^1 = k(2,1,1),\ a_i^2 = k(1,2,1),\ a_i^3 = k(1,1,2), \tag{5-253}$$

and

$$q_i^1 = (-1,1,1)/x_0,\ q_i^2 = (1,-1,1)/x_0,\ q_i^3 = (1,1,-1)/x_0, \tag{5-254}$$

where k has the dimensions of a velocity and determines the intensity of the initial velocity fluctuation. The quantity x_0 is the single length scale of the initial velocity fluctuation (one over the magnitude of an initial wavenumber component). The quantities k and x_0, together with the kinematic viscosity ν and equations (5-253) and (5-254), then determine the initial Reynolds number $\left(\overline{u_0^2}\right)^{1/2} x_0/\nu$, since the square of equation (5-251), averaged over a spatial period, gives $\overline{u_0^2}$. In addition to satisfying the continuity equation (5-252), equations (5-251) to (5-254) give

$$\overline{u_1^2} = \overline{u_2^2} = \overline{u_3^2} = \overline{u_0^2} \tag{5-255}$$

at the initial time. Thus equations (5-251) to (5-254) give a particularly simple initial condition, in that we need specify only one component of the mean-square velocity fluctuation. Moreover, for no mean shear, they give an isotropic flow at later times, at least in the sense that $\overline{u_1^2} = \overline{u_2^2} = \overline{u_3^2}$, as will be seen. In this way the present initial conditions differ from those of Taylor and Green (ref. 62). Those initial conditions do not give isotropic results even at large times (ref. 24). Note that it is necessary to have at least three terms in the summation in equation 5-251) to satisfy equation (5-255). We do not specify an initial condition for the pressure because it is determined by equation (5-150) and the initial velocities.

In order to carry out numerical solutions subject to the initial condition given by equations (5-251) to (5-254), we use a stationary cubical grid with a maximum of 32^3 points and with faces at $x_i^* = x_i/x_0 = 0$ and 2π. For boundary conditions we assume periodicity for the fluctuating quantities; we consider turbulence (or a turbulent like flow) in a box with periodic walls. That is, let

$$(u_i)_{x_j^*=2\pi+b_j^*} = (u_i)_{x_j^*=b_j^*} \tag{5-256}$$

and

$$\sigma_{x_j^*=2\pi+b_j^*} = \sigma_{x_j^*=b_j^*}, \tag{5-257}$$

where $b_j^* = b_j/x_0, x_j^* = x_j/x_0$ and b_j is a variable length. These equations are used to calculate numerical derivatives at the boundaries of the computational grid. For most of the results the spatial- and time-differencing schemes (which numerically conserve momentum and energy) are essentially these used by Clark et al. (ref. 33). For the spatial derivatives in equations (5-130) and (5-150) we use centered fourth-order difference expressions (see, for example, ref. 63). For instance, the fourth-order difference expression used for $\partial u_i/\partial x_k$ is

$$\left(\frac{\partial u_i}{\partial x_k}\right)_n = \frac{1}{12\Delta x_k}\left[(u_i)_{n-2} - 8(u_i)_{n-1} + 8(u_i)_{n+1} - (u_i)_{n+2}\right]$$

where Δx_k is the grid-point spacing, and the subscripts n, n + 1, etc., refer to grid points in the x_k direction. Fourth-order difference expressions are often considered more efficient than the usual second-order ones (ref. 64). (Spectral methods devised by Orszag and associates are often still more efficient (ref. 64), but may be somewhat trickier to use.) Centered expressions (same number of points on both sides of n, see above expression) can be used both at interior grid points and at the boundaries of the grid; when n refers to a point on a boundary, values for u_i outside of the grid which are required for calculating the numerical derivatives at the boundary, are obtained from the boundary condition (eq. (5-256)).

For time-differencing we use a predictor-corrector method with a second-order (leapfrog) predictor and a third-order (Adams-Moulton) corrector (see ref. 65). If m represents a time step, and $(R_i)_m$ the right side of equation (5-130), then at each grid point in space, the second-order leapfrog predictor for u_i at time step m + 1 is

$$(u_i)_{m+1}^{(1)} = (u_i)_{m-1} + 2\Delta t(R_i)_m,$$

and the third-order Adams-Moulton corrector is

$$(u_i)_{m+1}^{(2)} = (u_i)_m + \frac{\Delta t}{12}\left[5(R_i)_{m+1}^{(1)} + 8(R_i)_m - (R_i)_{m-1}\right],$$

where Δt is the time increment. The quantity $(R_i)_{m+1}^{(1)}$ in the above corrector is calculated by using $(u_i)_{m+1}^{(1)}$ in the right side of equation (5-130), where $(u_i)_{m+1}^{(1)}$ is calculated from the leapfrog predictor. Note that the leapfrog method (so-called because it leaps over the time step m), although unstable for all Δt when used by itself for Navier-Stokes-type equations, is stable when used as a predictor.

The Poisson equation for the pressure (eq. (5-150)) is solved directly by a fast Fourier-transform method. This method of solution was found to preserve continuity quite well ($\nabla \cdot u \approx 0$) except near the ends of some of the runs, where the solutions began to deteriorate. [Another indication of incipient solution deterioration near the ends of some of the runs was that the first three terms of equation (5-255) were no longer accurately satisfied.

Two known types of numerical instabilities can occur in the present solutions: a viscous instability connected with the first and last terms in equation (5-130), which occurs if $\nu\Delta t/(\Delta x_k)^2$ is too large; and a convective instability connected with the first and second terms (or the first and third terms through equation (5-150)), which occurs if $u_i\Delta t/\Delta x_k$ is too large. In these criteria Δt, Δx_k, and u_i are, respectively, a time step, distance step, and velocity. Thus a particular solution should be numerically stable if, for a given Δx_k, the time step is sufficiently small. Numerical stability is typically obtained when the solution varies smoothly from time step to time step with no significant breaks in the slope from one step to the next.This is the case for all of the results given here. For the present solution very good temporal resolution is obtained automatically when Δt is sufficiently small to give numerical stability.

Temporal resolution is much easier to obtain than three-dimensional spatial resolution, which is more severely limited by the storage and power of the computer. However, as will be seen, good spatial resolution is obtained for Reynolds numbers and times not excessively large. Some of the averaged results are extrapolated to zero spatial mesh size in an effort to obtain greater accuracy. The fourth-order method of extrapolation (consistent with the fourth-order differencing used here) is given in reference 66. For the results given here the corrections are negligibly small.

Development of turbulent like fluctuations. Figure 5-46 shows the calculated evolution of velocity-fluctuation components (normalized by the initial root-mean-square velocity) at two fixed points in space for the initial Reynolds number shown. Also plotted is the evolution of space-averaged root-mean square velocity fluctuations. Since there is no input of energy, the fluctuating and space-averaged motions eventually decay to a state of rest. In spite of the nonrandom initial condition (eq. (5-251)), the velocity fluctuations have the appearance of those for a random turbulence. It is important to point out that the fluctuations are not due to numerical instability since a large number of time steps (typically about 20) lies between changes of sign of du_i/dt.

We note that the spatially averaged values in figure 5-46 follow approximately the decay law $\overline{u^2} \sim t^{-n}$, where $n \sim 3$. This lies closer to the value for n of 3.3 observed for turbulence downstream of a waterfall (ref. 37) than to the value 1.2 generally observed for turbulence generated by flow through a grid in a wind tunnel (ref. 35). The decay law is evidently very much dependent on the initial conditions for the turbulence.

Instantaneous velocity profiles on an off-center plane through the computational grid are plotted in figure 5-47 for various times. At the initial time $t = 0$ the profile is regular and has the shape given by equation (5-251). However, it rapidly develops a turbulent like (random) appearance as a result of the production of harmonics by the nonlinear self-interaction terms in equations (5-130) and (5-150). The profile shape is strongly time-dependent at early times. (Note that the vertical scale changes drastically as time increases.) The symbols are located at gird points, where the instantaneous velocities are calculated. The eddies (fluctuations) are in general well-resolved numerically, particularly since a high-order differencing scheme is used in the numerical solution. (Fewer grid points may be required with a high-order scheme.) At any rate the curves appear to be well-defined by the calculated values at the grid points. Further evidence that our calculated results are realistic will be given in figure 5-48.

Note that the smaller eddies die out faster than the larger ones because of the higher shear stresses between the smaller eddies (see also the subsection on the interaction between spectral energy transfer and dissipation in section 5.3.2.2). For very large times essentially all of the higher harmonics have died out and the motion becomes linear. Then the profile assumes a regular shape not unlike that of the initial profile.

We tried perturbing the initial condition to see if the flow in figures 5-46 and 5-47 is sensitively dependent on initial conditions, but the results were inconclusive. It appears, however, that the turbulent like appearance of the flow is not due to sensitive dependence on initial conditions. That is not to say that sensitivity to small changes in initial conditions is not present in the flow, but the turbulent like fluctuations evidently decay before such effects can be detected (before a perturbed flow has had a chance to diverge from an unperturbed one). This leads to the question as to whether an initially nonturbulent low Reynolds-number decaying flow, whether experimental or numerical, can ever show the effects of sensitive dependence on initial conditions. The turbulent like appearance of the curve in figures 5-46 and 5-47 is more likely caused by a proliferation harmonic components by the nonlinear terms in equations (5-130) and (5-150). But if the decay is prevented by a forcing term, the effects of sensitive dependence on initial conditions can become important, even at the low Reynolds number in figures 5-46 and 5-47 (see chapter VI). Moreover, we have shown that a *higher* Reynolds–number decaying flow *can* be affected by sensitive dependence on initial conditions before the turbulent fluctuations have decayed. (J. Comp. Phys., June, 1992.)

Evolution of mean-square velocity fluctuations. The effect of computational-mesh size on space-averaged values of u_1^2, u_2^2, or u_3^2 (all three space-averaged values are equal) is shown in figure 5-48. Surprisingly good results for the decay are obtained, even with coarse grids.

Figure 5-49 shows the calculated evolution of mean-square velocity fluctuations (spatially averaged) for a series of initial Reynolds numbers. As the Reynolds number increases (ν and initial length scale x_0 held constant), the rate of decay of $\overline{u^2}$ increases sharply, as in experimental turbulent flows (fig. 5.21). This can be attributed to the nonlinear excitation of small-scale turbulent like fluctuations at the higher Reynolds numbers. The high shear stresses between the small eddies cause a rapid decay.

Microscales and nonlinear transfer of energy to smaller eddies. The development of the small-scale eddies is seen more clearly in figure 5-50, where the microscale λ, normalized by its initial value, is plotted against dimensionless time. The microscale is defined by

$$\overline{\frac{\partial u_i}{\partial x_\ell}\frac{\partial u_i}{\partial x_\ell}} \propto \frac{\overline{u_i u_i}}{\lambda^2}. \tag{5-258}$$

For homogeneous turbulence with no mean gradients, λ can be calculated from equations (4-142) and (5-258):

$$\lambda^2 \propto -\nu\frac{\overline{u_i u_i}}{\overline{du_i u_i}/dt}. \tag{5-259}$$

As the Reynolds number increases, the small-scale structure becomes finer. The microscale decreases until the fluctuation level (inertial effect) is low enough so that viscous forces prevent a further decrease. After λ decreases to a minimum, it begins to grow. (Results for coarser grids were not qualitatively different from these, but the minima were somewhat higher.) The increase of λ at later times is due to the selective annihilation of eddies by viscosity, the small eddies being the first to go. Thus, at large times, only the big eddies remain. It is this period of increasing λ that is generally observed experimentally in grid-generated turbulence (turbulence observed downstream of a grid of wires or bars whose plane is normal to the flow in a wind tunnel). The increases of λ with time observed experimentally (ref. 4, fig. 7.2) are generally of the same order as those in figure 5-50 (doubling the time increases λ by a factor of about 1.5). The early period, in which λ decreases with time, is of interest as illustrative of inter-wavenumber energy transfer. In order to generate the small-scale structure, turbulent energy must be transferred from big eddies to small ones.

For homogeneous turbulence without mean gradients the equation for the rate of change of turbulent kinetic energy, equation (4-142), reduces to

$$\frac{\partial}{\partial t}\left(\frac{\overline{u_i u_i}}{2}\right) = -\nu\overline{\frac{\partial u_i}{\partial x_\ell}\frac{\partial u_i}{\partial x_\ell}}. \tag{5-260}$$

That is, only viscous dissipation contributes to the rate of change of kinetic energy, there being no indication that nonlinear transfer of energy between scales of motion is taking place. There may seem to be a paradox here in view of the large transfer of energy to small eddies indicated in figure 5-50. This is as it should be, however, since energy transfer between wavenumbers or scales of motion should not contribute to the rate of change of total energy. In order to consider inter-wavenumber energy transfer, we must use two-point equations. Thus it is shown in section 5.3.1.2 that the self-interaction transfer term $T_{ij}(\boldsymbol{\kappa})$ in the two-point spectral equation has the property that

$$\int_{-\infty}^{\infty} T_{ij}(\boldsymbol{\kappa})d\boldsymbol{\kappa} = 0, \tag{5-98}$$

as a spectral transfer term should. The quantity $\boldsymbol{\kappa}$ is the wavevector. It is the spectral transfer term $T_{ij}(\boldsymbol{\kappa})$ or its Fourier transform $-\partial\left(\overline{u_i u_j' u_k'} - \overline{u_i u_k u_j'}\right)/\partial r_k$ in equation (5-133), that is responsible for the generation of the small-scale structure in figure 5-50. Those terms come from the nonlinear term $-\partial(u_i u_k)/\partial x_k$ in the unaveraged equation (5-130).

Although equation (5-98) shows that T_{ij} can transfer energy between wavenumbers without contributing to the rate of change of total energy $\partial\overline{u_i u_j}/\partial t$, it says nothing about the *direction* of the transfer or how important it is. For that we need calculations such as those in figure 5-50, which show that significant energy is transferred to smaller eddies (see also figs. 5-15 and 5-16). The energy transfer can be thought of as due to a breakup of big eddies into smaller ones, or as a stretching of vortex filaments to smaller diameters. In spite of this transfer to smaller eddies, experimental results generally show a growth of scale (ref. 4, fig. 7.2). This is because those results are usually for the later period shown in figure 5-50 where, although energy is transferred to smaller eddies, the annihilation of small eddies by viscous action eventually wins out. The early period shown in figure 5-50 and in figure 2 of reference 62, is of particular interest, in that the nonlinear transfer effects are truly dominate there; a sharp decrease in scale actually occurs as energy is transferred to smaller eddies.

Vorticity and dissipation. For homogeneous turbulence without mean gradients one can obtain a relation between the viscous dissipation term in equation (4-142) and the vorticity or swirl in the turbulence. The vorticity $\boldsymbol{\omega}$ is defined as the curl of $\mathbf{u}$:

$$\boldsymbol{\omega}(\mathbf{x}) = \nabla \times \mathbf{u}(\mathbf{x}) \tag{5-261}$$

or

$$\omega_i = \varepsilon_{ijk} \frac{\partial u_k}{\partial x_j}, \tag{5-262}$$

where ε_{ijk} is the alternating tensor (see section 2.5.1). Then

$$\overline{\omega_k \omega_k} = \varepsilon_{ijk}\varepsilon_{\ell mk} \overline{\frac{\partial u_i}{\partial x_j}\frac{\partial u_\ell}{\partial x_m}} = \left(\delta_{i\ell}\delta_{jm} - \delta_{im}\delta_{j\ell}\right)\overline{\frac{\partial u_i}{\partial x_j}\frac{\partial u_\ell}{\partial x_m}}$$

$$= \overline{\frac{\partial u_i}{\partial x_j}\frac{\partial u_i}{\partial x_j}} - \overline{\frac{\partial u_i}{\partial x_j}\frac{\partial u_j}{\partial x_i}}. \tag{5-263}$$

But, because

$$\frac{\partial u_j}{\partial x_j} = 0, \tag{5-264}$$

$$\overline{\frac{\partial u_i}{\partial x_j}\frac{\partial u_j}{\partial x_i}} = \frac{\partial^2 \overline{u_i u_j}}{\partial x_i \partial x_j} = 0 \tag{5-265}$$

for homogeneous turbulence. Equation (5-263) then becomes

$$\overline{\omega_k \omega_k} \equiv \overline{\omega^2} = \overline{\frac{\partial u_i}{\partial x_j}\frac{\partial u_i}{\partial x_j}} \equiv \frac{\varepsilon}{\nu}. \tag{5-266}$$

Thus, for homogeneous turbulence or turbulent like fluctuations, the mean-square vorticity is just the rate of viscous dissipation ε of turbulent energy divided by the kinematic viscosity (eq. 4-142). So the more intense the swirl in the turbulence, the faster it dissipates.

Dissipation, vorticity generation, and pressure fluctuations. The energy dissipation term, the only term contributing to the rate of change of kinetic energy for homogeneous turbulence without mean gradients (eq. (5-260)) is plotted in figure 5-51. That is also the mean-square vorticity (see eq. (5-266)), but the two are distinct physical entities. Although the curve for zero Reynolds number, where nonlinear effects are absent, decreases monotonically to zero, the curves for higher Reynolds numbers increase sharply for a while and then decrease. Thus the nonlinear terms in the Navier-Stokes equations are very effective vorticity generators and greatly enhance the dissipation at small and moderate times. For large times they appear to have the opposite effect, evidently because the turbulence itself decays rapidly to zero. Nonlinear effects, although they do not appear explicitly in the evolution equation for $\overline{u_i u_i}$ (eq. (5-260)), thus alter greatly the evolution by altering the dissipation term.

Figure 5-52 shows mean-square pressure fluctuations plotted against dimensionless time. The enhancement of the pressure fluctuations, although not as great as that of the vorticity or dissipation, again is due to nonlinear effects: In this case the nonlinear terms on the right side of the Poisson equation for the pressure cause the effect.

Further discussion and summary of the processes in isotropic turbulence. Nonlinear velocity and pressure terms do not appear in the evolution equation for $\overline{u_i u_i}$ (eq. (5-260)). But we can calculate root-mean-square values of the nonlinear terms in the instantaneous evolution equation (5-130), as well as of the linear term. Three measures of the relative importance of inertial (nonlinear) and viscous effects are shown for a moderate Reynolds number in figure 5-53. The ratio of the nonlinear velocity term to the viscous term and the ratio of the pressure to the viscous term in equation (5-130), together with the microscale Reynolds number, are plotted against dimensionless time. The terms are space-averaged root-mean-square values. All of those measures show

a variation from a rather inertial to a weak fluctuating flow. For instance, R_λ varies from about 90 to 0.7. This is a much greater variation than has been obtained experimentally for a single run. The curves for the term ratios lie somewhat below that for R_λ. They indicate that except at early times the nonlinear inertial effects associated with velocity and with pressure do not differ greatly.

The appearance of both nonlinear velocity and pressure effects in equation (5-130) and figure 5-53 may seem somewhat paradoxical in view of equation (5-260), which says that neither contributes directly to $\partial\overline{u_i u_i}/\partial t$. The nonlinear velocity effects were already discussed in this section; it was pointed out that such effects should not appear in equation (5-260), since they only distribute energy in wavenumber space and so do not directly alter the total energy. Although there is no nonlinear velocity term in equation (5-260), such a term appears in the two-point equation for $\partial\overline{u_i u_i'}/\partial t$. That equation, for the present case, is obtained from equation (5-133) as

$$\frac{\partial}{\partial t}\overline{u_i u_i'} = 2\nu\frac{\partial^2\overline{u_i u_i'}}{\partial r_k \partial r_k} - \frac{\partial}{\partial r_k}\left(\overline{u_i u_i' u_k'} - \overline{u_i u_k u_i'}\right) = 3\frac{\partial}{\partial t}\overline{u_i u_{(i)}'},$$

where $\mathbf{r}$ is again the vector extending from the unprimed to the primed point, and the pressure terms drop out because of continuity. The last term, where the parenthesis indicates no sum on i, is a consequence of the isotropy of the turbulent like fluctuations. The equation for the rate of change of each component of $\overline{u_i u_i'}$ is contributed to by the nonlinear velocity term $-\left(\partial/\partial r_k\right)\left(\overline{u_i u_i' u_k'} - \overline{u_i u_k u_i'}\right)$, but there is no contribution from the pressure. The strong effect of pressure shown in equation (5-130) and figure 5-53 must be contained in higher-order equations in the hierarchy of averaged equations (moment equations) (section 5.3.2.2 and ref. 22). Thus, while two-point averaged equations contain a nonlinear effect of velocity, we must consider higher-order multipoint equations to obtain an effect of pressure. Terms in the unaveraged equations shown in figure 5-53 (averaged over space after the solution has been obtained) include effects of all orders. (Effects contained in the numerical results may, however, be limited by the fineness of the numerical grid.)

Although pressure effects appear in figure 5-53 and equation (5-130), the physical significance of those effects is somewhat elusive, in contrast to the effects of viscous dissipation and spectral energy transfer. If the turbulence or turbulent like fluctuations are anisotropic, a clear effect of pressure fluctuations is that they transfer net energy among directional components (see eqs. (4-140) and (4-142) and the discussion in section 4.3.3.1). That will be discussed further when mean gradients are considered. If, in addition, the turbulence is inhomogeneous, pressure can produce a net spatial diffusion of energy (eq. 4-142). Those are evidently the only physical effects of pressure fluctuations (at least that we know about). Thus, if the turbulence or turbulent like fluctuations are homogenous and isotropic, as they are here, it seems reasonable to attribute the observed pressure effects in the unaveraged equations (eq. (5-130)) to those processes. Even though there is no *net* interdirectional transfer or spatial diffusion of turbulence when the turbulence is isotropic, those processes can still be instantaneously or locally operative. They could, for instance, cause a diffusion of tagged particles. According to figure 5-53, they have an important indirect effect on the evolution of the turbulence.

From the findings of the present section we conclude that the following processes occur in isotropic turbulence: nonlinear radomization by proliferation of harmonic components and/or by sensitive dependence on initial conditions (to be discussed further in chapter VI), nonlinear spectral transfer of turbulence among wavenumbers or eddy sizes (mainly to smaller eddies), spatial diffusion and transfer of turbulence among directional components by pressure forces, with zero *net* diffusion and transfer into each component since the turbulence is isotropic, generation of vorticity or swirl, and dissipation of turbulence into heat by viscous action. From this description, as well as those in section 5.3.2.2 and chapter VI, isotropic turbulence appears interesting and many-faceted. (This is in contrast to the characterization sometimes given that isotropic turbulence is tired or fossil turbulence.)

5.3.2.7 Turbulent diffusion and multitime-multipoint correlations.—One of the basic characteristics of turbulence is its great diffusive power. For example, the rate of diffusion of a glob of cream into a cup of unstirred coffee by molecular action is extremely slow. However, that rate is increased by orders of magnitude by a slight stirring (turbulent) action.

The theory of turbulent diffusion was originated by G.I. Taylor in 1922 (ref. 67) and has since been studied by a number of authors (e.g., refs. 68 and 69). To illustrate turbulent diffusion, we calculate approximately the diffusion of particles originally concentrated at a source into a decaying turbulent field (ref. 70). In order to simplify the problem, assume that the velocity fluctuations are small.

The distance in the x_2–direction that a fluid particle orginally at $x_2 = 0$ travels during the time interval $t' - t_a$ is

$$Y(t') = \int_{t_a}^{t'} u_2(t)dt. \qquad (5-267)$$

Multiplication of this equation by $u_2(t') = dY/dt'$ gives

$$u_2(t')Y(t') = \frac{1}{2}\frac{dY^2}{dt'} = \int_{t_a}^{t'} u_2(t)u_2(t')dt. \tag{5-268}$$

Taking the particle average over all the "marked" particles that were originally concentrated at a source at $x_2 = 0$ and integrating with respect to t' result in

$$\overline{Y_b^2} = 2\int_{t_a}^{t_b}\int_{t_a}^{t'}\left[\overline{u_2(t)u_2(t')}\right]_L dt\, dt', \tag{5-269}$$

where the subscript L designates a Lagrangian correlation which is based on the velocity of a moving particle at different times, rather than on the velocity at a fixed point at different times. The latter is generally called the Eulerian time correlation. Since it is easier to measure or calculate than the Lagrangian correlation, we would like to be able to relate the two types of correlations. For small velocity fluctuations it has been suggested by Burgers (ref. 71) that they should not differ greatly. This can be shown as follows:

Consider first the Eulerian time correlation $\overline{u_2(t)u_2(t')}$, where u_2 is the component of the velocity in the x_2 direction; similar results could be obtained for the other velocity components. The Eulerian correlation can be expanded in a Taylor series as

$$\begin{aligned}\overline{u_2(t)u_2(t')} &= \left[\overline{u_2(t)u_2(t')}\right]_{t'=t} + \left[\frac{\partial}{\partial t'}\overline{u_2(t)u_2(t')}\right]_{t'=t}(t'-t) + \frac{1}{2}\left[\frac{\partial^2}{\partial t'^2}\overline{u_2(t)u_2(t')}\right]_{t'=t}(t'-t)^2 + \dots \\ &= \overline{u_2^2(t)} + \overline{u_2(t)\left[\frac{\partial u_2(t')}{\partial t'}\right]_{t'=t}}(t'-t) + \frac{1}{2}\overline{u_2(t)\left[\frac{\partial^2 u_2(t')}{\partial t'^2}\right]_{t'=t}}(t'-t)^2 + \dots .\end{aligned} \tag{5-270}$$

Similarly, the Lagrangian correlation is expanded as

$$\left[\overline{u_2(t)u_2(t')}\right]_L = \overline{u_2^2(t)} + \overline{u_2(t)\left[\frac{du_2(t')}{dt'}\right]_{t'=t}}(t'-t) + \frac{1}{2}\overline{u_2(t)\left[\frac{d^2u_2(t')}{dt'^2}\right]_{t'=t}}(t'-t)^2 + \dots , \tag{5-271}$$

where the substantial or particle derivative is given as

$$\frac{du_2(t')}{dt'} = \frac{\partial u_2(t')}{\partial t'} + u_k\frac{\partial u_2(t')}{\partial x_k}.$$

For small velocity fluctuations,

$$\frac{du_2(t')}{dt'} \cong \frac{\partial u_2(t')}{\partial t'}. \tag{5-272}$$

Also

$$\frac{d^2u_2(t')}{dt'^2} \cong \frac{\partial}{\partial t'}\frac{du_2(t')}{dt'} \cong \frac{\partial^2 u_2(t')}{\partial t'^2}, \tag{5-273}$$

and so on for higher-order derivatives. From eqautions (5-270) to (5-273),

$$\overline{u_2(t)u_2(t')} \equiv \left[\overline{u_2(t)u_2(t')}\right]_L \tag{5-274}$$

is obtained, which was the relation to be proved. It should be noted that relation (5-274) is most accurate for small values of $t' - t$ as well as for small velocity fluctuations, inasmuch as the approximate relation (5-273) had to be applied a greater number of times to the higher-order derivatives in equation (5-271) than to the lower-order ones (see eq. (5-273).

It should also be emphasized that equation (5-274) was obtained for the case of no mean motion. Thus, Eulerian time correlations measured with a stationary instrument in a moving stream may differ considerably from the Lagrangian correlations. However, if the instrument is moving with the stream, the two correlations will be approximately equal if the turbulence level is not too high (see ref. 72).

If the approximate relation (5-274) is introduced into equation (5-269) and it is noted that, for isotropic turbulence, $\overline{u_2(t)u_2(t')} = \overline{u_i(t)u_i(t')}/3$, we get

$$\overline{Y_b^2} = \frac{2}{3}\int_{t_1}^{t_2}\int_{t_1}^{t'} \overline{u_i(t)u_i(t')}\,dt\,dt'. \tag{5-275}$$

To obtain the time correlation $\overline{u_i(t)u_i(t')}$ in equation (5-275), first write the Navier-Stokes equations for the points P and P′ separated by the distance vector $\mathbf{r}$ and the time increment Δt:

$$\frac{\partial u_i}{\partial t} + \frac{\partial\left(u_i u_k\right)}{\partial x_k} = -\frac{1}{\rho}\frac{\partial \sigma}{\partial x_i} + \nu\frac{\partial^2 u_i}{\partial x_k \partial x_k}, \tag{5-276}$$

$$\frac{\partial u_j'}{\partial t'} + \frac{\partial\left(u_j' u_k'\right)}{\partial x_k'} = -\frac{1}{\rho}\frac{\partial \sigma'}{\partial x_j'} + \nu\frac{\partial^2 u_j'}{\partial x_k' \partial x_k'}, \tag{5-277}$$

where, as usual, the subscripts can take on the values 1, 2, 3 and a repeated subscript in a term indicates a summation. The quantities u_i and u_j' are instantaneous velocity components, x_i is a space coordinate, t is the time, ρ is the density, ν is the kinematic viscosity, and σ is the instantaneous mechanical pressure. Multiplying the first equation by u_j', the second by u_i, and taking space averages result in

$$\frac{\partial \overline{u_i u_j'}}{\partial t} + \frac{\partial\left(\overline{u_i u_j' u_k}\right)}{\partial x_k} = -\frac{1}{\rho}\frac{\partial \overline{\sigma u_j'}}{\partial x_i} + \nu\frac{\partial^2 \overline{u_i u_j'}}{\partial x_k \partial x_k} \tag{5-278}$$

and

$$\frac{\partial \overline{u_i u_j'}}{\partial t'} + \frac{\partial\left(\overline{u_i u_j' u_k'}\right)}{\partial x_k'} = -\frac{1}{\rho}\frac{\partial \overline{\sigma' u_i}}{\partial x_j'} + \nu\frac{\partial^2 \overline{u_i u_j'}}{\partial x_k' \partial x_k'}, \tag{5-279}$$

where the fact that quantities at x_i and t are independent of x_i' and t' was used. By introducing the transformations $\partial/\partial x_i = -\partial/\partial r_i$, $\partial/\partial x_i' = \partial/\partial r_i$, $(\partial/\partial t)_{t'} = (\partial/\partial t)_{\Delta t} - \partial/\partial \Delta t$, and $\partial/\partial t' = \partial/\partial \Delta t$, which are obtained by writing a correlation as a function of r_i, t, and Δt and differentiating, the following equations are obtained from (5-278) and (5-279):

$$\frac{\partial \overline{u_i u_j'}}{\partial t} + \frac{\partial}{\partial r_k}\overline{u_j u_k u_i'(-\mathbf{r}, -\Delta t, t+\Delta t)} - \frac{\partial}{\partial r_k}\overline{u_i u_k u_j'(\mathbf{r}, \Delta t, t)} = \frac{1}{\rho}\frac{\partial}{\partial r_i}\overline{\sigma u_j'} - \frac{1}{\rho}\frac{\partial}{\partial r_j}\overline{\sigma u_i'(-\mathbf{r}, -\Delta t, t+\Delta t)} + 2\nu\frac{\partial^2 \overline{u_i u_j'}}{\partial r_k \partial r_k}, \tag{5-280}$$

$$\frac{\partial \overline{u_i u_j'}}{\partial \Delta t} + \frac{\partial}{\partial r_k} \overline{u_j u_k u_i'(-\mathbf{r}, -\Delta t, t+\Delta t)} = -\frac{1}{\rho} \frac{\partial}{\partial r_j} \overline{\sigma u_i'(-\mathbf{r}, -\Delta t, t+\Delta t)} + \nu \frac{\partial^2 \overline{u_i u_j'}}{\partial r_k \partial r_k}. \tag{5-281}$$

Equations (5-280) and (5-281) are the space-time equivalents of the two-point equation (5-133). They were obtained in a slightly different form, for the case of isotropic turbulence, by Bass (ref. 73).

In order to convert equations (5-280) and (5-281) to spectral form, the following three-dimensional Fourier transforms are introduced:

$$\overline{u_i u_j'(\mathbf{r}, \Delta t, t)} = \int_{-\infty}^{\infty} \varphi_{ij}(\boldsymbol{\kappa}, \Delta t, t) e^{i\boldsymbol{\kappa}\cdot\mathbf{r}} d\boldsymbol{\kappa} \tag{5-282}$$

$$\overline{u_j u_k u_i'(\mathbf{r}, \Delta t, t)} = \int_{-\infty}^{\infty} \varphi_{jki}(\boldsymbol{\kappa}, \Delta t, t) e^{i\boldsymbol{\kappa}\cdot\mathbf{r}} d\boldsymbol{\kappa} \tag{5-283}$$

$$\overline{\sigma u_j'(\mathbf{r}, \Delta t, t)} = \int_{-\infty}^{\infty} \lambda_j(\boldsymbol{\kappa}, \Delta t, t) e^{i\boldsymbol{\kappa}\cdot\mathbf{r}} d\boldsymbol{\kappa}, \tag{5-284}$$

where $\boldsymbol{\kappa}$ is a wavevector and $d\boldsymbol{\kappa} = d\kappa_1 d\kappa_2 d\kappa_3$. By introducing these transforms, equations (5-280) and (5-281) become

$$\frac{\partial \varphi_{ij}}{\partial t} + i\kappa_k \varphi_{jki}(-\boldsymbol{\kappa}, -\Delta t, t+\Delta t) - i\kappa_k \varphi_{ikj}(\boldsymbol{\kappa}, \Delta t, t) = \frac{1}{\rho} i\kappa_i \lambda_j - \frac{1}{\rho} i\kappa_j \lambda_i(-\boldsymbol{\kappa}, -\Delta t, t+\Delta t) - 2\nu\kappa^2 \varphi_{ij} \tag{5-285}$$

$$\frac{\partial \varphi_{ij}}{\partial \Delta t} + i\kappa_k \varphi_{jki}(-\boldsymbol{\kappa}, -\Delta t, t+\Delta t) = -\frac{1}{\rho} \kappa_j \lambda_i(-\boldsymbol{\kappa}, -\Delta t, t+\Delta t) - \nu\kappa^2 \varphi_{ij}. \tag{5-286}$$

In order to convert the tensor equations (5-285) and (5-286) to scalar equations, contract the indices i and j:

$$\frac{\partial \varphi_{ii}}{\partial t} + 2\nu\kappa^2 \varphi_{ii} = i\kappa_k \varphi_{iki}(\boldsymbol{\kappa}, \Delta t, t) + i(-\kappa_k) \varphi_{iki}(-\boldsymbol{\kappa}, -\Delta t, t+\Delta t) \tag{5-287}$$

$$\frac{\partial \varphi_{ii}}{\partial \Delta t} + \nu\kappa^2 \varphi_{ii} = i(-\kappa_k) \varphi_{iki}(-\boldsymbol{\kappa}, -\Delta t, t+\Delta t). \tag{5-288}$$

The pressure terms drop out of these scalar equations because of the continuity relation $\partial u_i/\partial x_i = \partial u_i'/\partial x_i' = 0$ and the relation $\partial/\partial x_i = -\partial/\partial x_i'$ (see eqs. (5-278) and (5-279).

Equations (5-287) and (5-288), as they stand, contain too many unknowns for solutions to be obtained. For the final period of decay, however, the triple correlation or inertia terms should be negligible compared with the double correlation terms. Thus, the terms on the right sides of equations (5-287) and (5-288) are neglected, and the following solutions are obtained:

$$\varphi_{ii} = f_1(\boldsymbol{\kappa}, \Delta t) e^{-2\nu\kappa^2 (t - t_0)} \tag{5-289}$$

and

$$\varphi_{ii} = f_2(\boldsymbol{\kappa}, t) e^{-\nu\kappa^2 \Delta t}. \tag{5-290}$$

In order for these equations to be consistent,

$$E = f(\kappa) e^{-\nu\kappa^2 \Delta t} e^{-2\nu\kappa^2 (t - t_0)}, \tag{5-291}$$

where the energy spectrum function $E = 2\pi\kappa^2\varphi_{ii}$ has been introduced. Evaluate $f(\kappa)$ by letting $E = J_0\kappa^4/3\pi$ when κ is small (Lin, ref. 74). This gives

$$E = \frac{J_0\kappa^4}{3\pi} e^{-2\nu\kappa^2\left(t-t_0+\frac{1}{2}\Delta t\right)}, \tag{5-292}$$

where J_0 is a constant that depends on initial conditions. For $\Delta t = 0$, equation (5-292) reduces to the usual expression for the energy spectrum function in the final period, which involves only one time. By integrating equation (5-292) with respect to κ, the time correlation is obtained as

$$\frac{\overline{u_i u_i'}}{2} = \frac{J_0}{32(2\pi)^{1/2}} \nu^{-5/2}\left(t - t_0 + \frac{1}{2}\Delta t\right)^{-5/2}. \tag{5-293}$$

Equations (5-275) and (5-293) give, for diffusion by isotropic turbulence in the final period of decay,

$$\overline{Y_b^2} = \frac{J_0\nu^{-5/2}}{9\sqrt{\pi}}\left\{\frac{1}{\sqrt{2}}\left[\frac{1}{\left(t_a - t_0 + \Delta t_b\right)^{1/2}} + \frac{1}{\left(t_a - t_0\right)^{1/2}}\right] - \frac{1}{\left(t_a - t_0 + \Delta t_b/2\right)^{1/2}}\right\}, \tag{5-294}$$

where t_a is again the time at which diffusion begins and $\Delta t_b = t_b - t_a$ is the time during which the root-mean-square turbulent diffusion distance goes from 0 to $\overline{Y_b^2}^{1/2}$. For large diffusion times,

$$\overline{Y_b^2} = \frac{J_0\nu^{-5/2}}{9\sqrt{2\pi}\left(t_a - t_0\right)}. \tag{5-295}$$

That is, the turbulent diffusion distance reaches a constant value and becomes independent of Δt_b for large diffusion times. This differs from the case of stationary turbulence, where $\overline{Y_b^2}$ increases linearly with Δt_b for large diffusion times (ref. 67). The reason it reaches a constant value for decaying turbulence is that for large times the turbulence goes to zero, so that no more turbulent diffusion can take place. For early times (small $t_a - t_0$), both equations (5-294) and (5-295) show that the diffusion distances are much larger than those for later times because of the higher turbulence level at early times.

In reference 70 the analysis for turbulent diffusion was extended to somewhat earlier times than those for which equation (5-294) is applicable, and the analytical results were compared with the experiment of Uberoi and Corrsin (ref. 75). For the comparison, the diffusion time in the analysis is the distance downstream from the beginning of the line source (of heat) in the experiment divided by the speed of the mean stream. The agreement between theory and experiment was quite good for large decay times (low turbulence levels) and for small diffusion times; for other conditions, some deviation was indicated. The latter was apparently due to the assumed equality of Eulerian and Lagrangian correlations, that equality being the most accurate for small velocity fluctuations and short diffusion times (see discussion following eq. (5-274)).

5.4 HOMOGENEOUS TURBULENCE AND HEAT TRANSFER WITH UNIFORM MEAN VELOCITY AND/OR TEMPERATURE GRADIENTS

In section 5.3 we considered the simplest type of turbulence—statistically homogeneous turbulence without mean gradients. The turbulence processes occurring there are viscous dissipation, nonlinear directional transfer of turbulent activity, and nonlinear spectral transfer between scales of motion. The absence of other, often overshadowing processes, makes homogeneous turbulence without mean gradients an ideal vehicle for studying dissipation, nonlinear directional transfer, and nonlinear spectral transfer. Those processes, particularly nonlinear spectral transfer and its interaction with dissipation , were discussed in some detail in section 5.3.

However, real turbulence usually occurs in the presence of mean gradients, particularly in the presence of mean shear. So we consider here a slightly more complicated turbulence than that in section 5.3 by studying the effect of uniform mean gradients on homogeneous turbulence and heat transfer. In that way we introduce turbulence production and other processes which depend on mean gradients.

Following a plan similar to that in section 5.3, we first consider the basic equations for homogeneous turbulence *with* mean gradients. Then we will give some illustrative solutions. As in section 5.3 the analytical solutions considered will usually be of the simplest kind, in order to avoid excessive mathematical complexity. Somewhat more widely applicable numerical solutions will also be discussed where available and appropriate.

5.4.1 Basic Equations

The euqations for the fluctuations u_i, τ, and σ were obtained in the last chapter as equations (4-22) to (4-24):

$$\frac{\partial u_i}{\partial t} = -\frac{\partial (u_i u_k)}{\partial x_k} - \frac{1}{\rho}\frac{\partial (\sigma - \sigma_e)}{\partial x_i} + \nu \frac{\partial^2 u_i}{\partial x_k \partial x_k} - \beta g_i \tau - u_k \frac{\partial U_i}{\partial x_k} - U_k \frac{\partial u_i}{\partial x_k} + \frac{\overline{\partial u_i u_k}}{\partial x_k}, \tag{4-22}$$

$$\frac{\partial \tau}{\partial t} = -\frac{\partial (\tau u_k)}{\partial x_k} + \alpha \frac{\partial^2 \tau}{\partial x_k \partial x_k} - u_k \frac{\partial T}{\partial x_k} - U_k \frac{\partial \tau}{\partial x_k} + \frac{\overline{\partial \tau u_k}}{\partial x_k}, \tag{4-23}$$

and

$$\frac{1}{\rho}\frac{\partial (\sigma - \sigma_e)}{\partial x_i \partial x_i} = -\frac{\partial^2 (u_i u_k)}{\partial x_i \partial x_k} - \beta g_i \frac{\partial \tau}{\partial x_i} - 2\frac{\partial u_i}{\partial x_k}\frac{\partial U_k}{\partial x_i} + \frac{\partial^2 \overline{u_i u_k}}{\partial x_i \partial x_k}, \tag{4-24}$$

where the subscripts (except e) can take on the values 1, 2, or 3, and a repeated subscript in a term signifies a summation. The instantaneous velocities, temperatures, and mechanical pressures have respectively been divided into mean and fluctuating components U_i and u_i, T and τ, and P and σ. The quantity x_i is a space coordinate, t is the time, ρ is the density, ν is the kinematic viscosity, g_i is a component of the body force, and $\beta \equiv -(1/\rho)(\partial\rho/\partial T)_\sigma$ is the thermal expansion coefficient of the fluid. The quantities T_e and σ_e are respectively the equilibrium temperature and pressure. In obtaining the buoyancy term in equation (4-22), the density is assumed to depend effectively only on temperature and is not far removed from its equilibrium value (value for no heat transfer). Note that the equilibrium temperature is uniform whereas the equilibrium pressure is not. We retain buoyancy effects in equations (4-22) to (4-24) because those effects will be considered in some of the cases to follow.

Equations (4-22) to (4-24) apply at a point P in the turbulent fluid. Similar equations at another point P′ can be obtained simply by priming the variables and changing the subscript i to, say, j. Equations involving correlations between fluctuating quantities at points P and P′ can than be constructed by methods similar to those used for obtaining equation (5-133), or for equations (4-147) to (4-150) in the last chapter. The resulting equations for homogeneous turbulence with uniform velocity and temperature gradients are

$$\frac{\partial \overline{u_i u_j'}}{\partial t} + \overline{u_k u_j'}\frac{\partial U_i}{\partial x_k} + \overline{u_i u_k'}\frac{\partial U_j}{\partial x_k} + \frac{\partial U_k}{\partial x_\ell} r_\ell \frac{\overline{\partial u_i u_j'}}{\partial r_k} + \frac{\partial}{\partial r_k}\left(\overline{u_i u_j' u_k'} - \overline{u_i u_k u_j'}\right)$$

$$= -\frac{1}{\rho}\left(\frac{\partial \overline{u_i \sigma'}}{\partial r_j} - \frac{\partial \overline{\sigma u_j'}}{\partial r_i}\right) + 2\nu \frac{\partial^2 \overline{u_i u_j'}}{\partial r_k \partial r_k} - \beta g_i \overline{\tau u_j'} - \beta g_j \overline{u_i \tau'}, \tag{5-296}$$

$$\frac{\partial\overline{\tau\tau'}}{\partial t}+\overline{u_k\tau'}\frac{\partial T}{\partial x_k}+\overline{\tau u_k'}\frac{\partial T}{\partial x_k}+\frac{\partial U_k}{\partial x_\ell}r_\ell\frac{\partial\overline{\tau\tau'}}{\partial r_k}+\frac{\partial}{\partial r_k}\left(\overline{\tau\tau' u_k'}-\overline{\tau u_k\tau'}\right)=2\alpha\frac{\partial^2\overline{\tau\tau'}}{\partial r_k\partial r_k}, \tag{5-297}$$

$$\frac{\partial\overline{\tau u_j'}}{\partial t}+\overline{u_k u_j'}\frac{\partial T}{\partial x_k}+\overline{\tau u_k'}\frac{\partial U_j}{\partial x_k}+\frac{\partial U_k}{\partial x_\ell}r_\ell\frac{\partial\overline{\tau u_j'}}{\partial r_k}+\frac{\partial}{\partial r_k}\left(\overline{\tau u_j' u_k'}-\overline{\tau u_k u_j'}\right)=-\frac{1}{\rho}\frac{\partial\overline{\tau\sigma'}}{\partial r_j}+(\alpha+\nu)\frac{\partial^2\overline{\tau u_j'}}{\partial r_k\partial r_k}-\beta g_j\overline{\tau\tau'}, \tag{5-298}$$

$$\frac{\partial\overline{u_i\tau'}}{\partial t}+\overline{u_i u_k'}\frac{\partial T}{\partial x_k}+\overline{u_k\tau'}\frac{\partial U_i}{\partial x_k}+\frac{\partial U_k}{\partial x_\ell}r_\ell\frac{\partial\overline{u_i\tau'}}{\partial r_k}+\frac{\partial}{\partial r_k}\left(\overline{u_i\tau' u_k'}-\overline{u_i u_k\tau'}\right)=-\frac{1}{\rho}\frac{\partial\overline{\sigma\tau'}}{\partial r_i}+(\alpha+\nu)\frac{\partial^2\overline{u_i\tau'}}{\partial r_k\partial r_k}-\beta g_i\overline{\tau\tau'}, \tag{5-299}$$

$$\frac{1}{\rho}\frac{\partial^2\overline{u_i\sigma'}}{\partial r_j\partial r_j}=-2\frac{\partial\overline{u_i u_k'}}{\partial r_j}\frac{\partial U_j}{\partial x_k}-\frac{\partial^2\overline{u_i u_j' u_k'}}{\partial r_j\partial r_k}-\beta g_j\frac{\partial\overline{u_i\tau'}}{\partial r_j}, \tag{5-300}$$

$$\frac{1}{\rho}\frac{\partial^2\overline{\sigma u_j'}}{\partial r_i\partial r_i}=2\frac{\partial\overline{u_i u_j'}}{\partial r_k}\frac{\partial U_k}{\partial x_i}-\frac{\partial^2\overline{u_i u_k u_j'}}{\partial r_i\partial r_k}+\beta g_i\frac{\partial\overline{\tau u_j'}}{\partial r_i}, \tag{5-301}$$

$$\frac{1}{\rho}\frac{\partial^2\overline{\sigma\tau'}}{\partial r_i\partial r_i}=2\frac{\partial\overline{u_i\tau'}}{\partial r_k}\frac{\partial U_k}{\partial x_i}-\frac{\partial^2\overline{u_i u_k\tau'}}{\partial r_i\partial r_k}+\beta g_i\frac{\partial\overline{\tau\tau'}}{\partial r_i}, \tag{5-302}$$

and

$$\frac{1}{\rho}\frac{\partial^2\overline{\tau\sigma'}}{\partial r_j\partial r_j}=-2\frac{\partial\overline{\tau u_k'}}{\partial r_j}\frac{\partial U_j}{\partial x_k}-\frac{\partial^2\overline{\tau u_j' u_k'}}{\partial r_j\partial r_k}-\beta g_j\frac{\partial\overline{\tau\tau'}}{\partial r_j}, \tag{5-303}$$

where, by virtue of the uniformity of the mean velocity gradients we have set $\partial U_j'/\partial x_k'=\partial U_j/\partial x_k$ and $U_k'-U_k=r_\ell\,\partial U_k/\partial x_\ell$.

5.4.2 Cases for which Mean Gradients are large and/or the Turbulence is Weak

Equations (5-296) to (5-303) form a determinate set if we neglect terms containing triple correlations. As in section 5.3.2.1, where mean gradients are absent, those terms can be neglected if the turbulence is weak enough. However, it is important to notice that the turbulence in a flow with mean velocity or temperature gradients may not have to be as weak as that in a flow without mean gradients. If some of those gradients are large, the terms containing them can be large compared that in a flow without mean gradients. If some of those gradients are large, the terms containing them can be large compared with the triple correlation terms, even if the turbulence is moderately strong or strong. Thus the applicability of the solutions to be obtained here is much wider than that of the solutions in section 5.3.2.1. The mean-gradient term should, however, be large enough to give a sensible solution.

For converting equations (5-296) to (5-303) to spectral form, we introduce three-dimensional Fourier transforms defined as follows:

$$\overline{u_i u_j'}=\int_{-\infty}^{\infty}\varphi_{ij}e^{i\kappa\cdot r}d\kappa, \tag{5-304}$$

$$\overline{\sigma u_j'}=\int_{-\infty}^{\infty}\lambda_j e^{i\kappa\cdot r}d\kappa, \tag{5-305}$$

$$\overline{u_i\sigma'}=\int_{-\infty}^{\infty}\lambda_i' e^{i\kappa\cdot r}d\kappa, \tag{5-306}$$

$$\overline{\sigma\tau'} = \int_{-\infty}^{\infty} \zeta e^{i\kappa\cdot r} d\kappa, \tag{5-307}$$

$$\overline{\tau\sigma'} = \int_{-\infty}^{\infty} \zeta' e^{i\kappa\cdot r} d\kappa, \tag{5-308}$$

$$\overline{\tau u_j'} = \int_{-\infty}^{\infty} \gamma_j e^{i\kappa\cdot r} d\kappa, \tag{5-309}$$

$$\overline{u_i \tau'} = \int_{-\infty}^{\infty} \gamma_i' e^{i\kappa\cdot r} d\kappa, \tag{5-310}$$

and

$$\overline{\tau\tau'} = \int_{-\infty}^{\infty} \delta e^{i\kappa\cdot r} d\kappa, \tag{5-311}$$

where κ is the wavevector and $d\kappa = d\kappa_1 d\kappa_2 d\kappa_3$. The magnitude of κ has the dimension 1/length and can be considered to be the reciprocal of a wavelength or eddy size. Then, from equation (5-304),

$$r_\ell \frac{\partial \overline{u_i u_j'}}{\partial r_k} = \int_{-\infty}^{\infty} \left(\kappa_k \frac{\partial \varphi_{ij}}{\partial x_\ell} + \delta_{\ell k} \varphi_{ij} \right) e^{i\kappa\cdot r} d\kappa, \tag{5-312}$$

where, as usual, $\delta_{\ell k}$ is the Kronecker delta. Equation (5-312) can be obtained by differentiating equation (5-304) with respect to r_k, writing the inverse transform, and then differentiating with respect to κ_ℓ. Taking the Fourier transforms of equations (5-296) to (5-303) results in

$$\frac{\partial \varphi_{ij}}{\partial t} + \varphi_{kj} \frac{\partial U_i}{\partial x_k} + \varphi_{ik} \frac{\partial U_j}{\partial x_k} - \frac{\partial U_k}{\partial x_\ell} \left(\kappa_k \frac{\partial \varphi_{ij}}{\partial \kappa_\ell} + \delta_{\ell k} \varphi_{ij} \right) = -\frac{1}{\rho} \left(i\kappa_j \lambda_i' - i\kappa_i \lambda_j \right) - 2\nu\kappa^2 \varphi_{ij} - \beta g_i \gamma_j - \beta g_j \gamma_i', \tag{5-313}$$

$$\frac{\partial \delta}{\partial t} + \left(\gamma_k' + \gamma_k \right) \frac{\partial T}{\partial x_k} - \frac{\partial U_k}{\partial x_\ell} \left(\kappa_k \frac{\partial \delta}{\partial \kappa_\ell} + \delta_{\ell k} \delta \right) = -2\alpha\kappa^2 \delta, \tag{5-314}$$

$$\frac{\partial \gamma_j}{\partial t} + \varphi_{kj} \frac{\partial T}{\partial x_k} + \gamma_k \frac{\partial U_j}{\partial x_k} - \frac{\partial U_k}{\partial x_\ell} \left(\kappa_k \frac{\partial \gamma_j}{\partial \kappa_\ell} + \delta_{\ell k} \gamma_j \right) = -\frac{1}{\rho} i\kappa_j \zeta' - (\alpha + \nu)\kappa^2 \gamma_j - \beta g_j \delta, \tag{5-315}$$

$$\frac{\partial \gamma_i'}{\partial t} + \varphi_{ik} \frac{\partial T}{\partial x_k} + \gamma_k' \frac{\partial U_i}{\partial x_k} - \frac{\partial U_k}{\partial x_\ell} \left(\kappa_k \frac{\partial \gamma_i'}{\partial \kappa_\ell} + \delta_{\ell k} \gamma_i' \right) = -(\alpha + \nu)\kappa^2 \gamma_i' + \frac{1}{\rho} i\kappa_i \zeta - \beta g_i \delta, \tag{5-316}$$

$$-\frac{1}{\rho} \kappa^2 \lambda_i' = -2i\kappa_j \varphi_{ik} \frac{\partial U_j}{\partial x_k} - \beta g_j i\kappa_j \gamma_i', \tag{5-317}$$

$$-\frac{1}{\rho} \kappa^2 \lambda_j = 2i\kappa_k \varphi_{ij} \frac{\partial U_k}{\partial x_i} + \beta g_i i\kappa_i \gamma_j, \tag{5-318}$$

$$-\frac{1}{\rho}\kappa^2\zeta = 2i\kappa_k \gamma_i' \frac{\partial U_k}{\partial x_i} + \beta g_i i\kappa_i \delta, \tag{5-319}$$

and

$$-\frac{1}{\rho}\kappa^2\zeta' = -2i\kappa_j \gamma_k \frac{\partial U_j}{\partial x_k} - \beta g_j i\kappa_j \delta. \tag{5-320}$$

Equations (5-313) to (5-320) can be used to study a number of cases in which homogeneous turbulence is acted on by large mean gradients and/or for which the turbulence is weak. Some of those cases are considered in the following sections.

5.4.2.1 Uniformly and steadily sheared homogeneous turbulence.—The effect of a uniform transverse velocity gradient on a homogeneous turbulent field has been considered by a number of authors (e.g., refs. 7, 8, and 76 to 78). The treatment here parallels that in reference 7. That reference carried the problem to the point of calculating spectra and of studying the processes associated with the turbulence.

Equations (5-313), (5-317), and (5-318) become, for a uniform transverse velocity gradient dU_1/dx_2 and no buoyancy ($g_i = 0$),

$$\frac{\partial}{\partial t}\varphi_{ij} + \delta_{i1}\varphi_{2j}\frac{dU_1}{dx_2} + \delta_{j1}\varphi_{i2}\frac{dU_1}{dx_2} - \kappa_1 \frac{\partial \varphi_{ij}}{\partial \kappa_2}\frac{dU_1}{dx_2} = -\frac{1}{\rho}\left(-i\kappa_i\lambda_j + i\kappa_j\lambda_i'\right) - 2\nu\kappa^2\varphi_{ij}, \tag{5-321}$$

$$-\frac{1}{\rho}i\kappa_j\lambda_i' = 2\frac{\kappa_1\kappa_j}{\kappa^2}\varphi_{i2}\frac{dU_1}{dx_2}, \tag{5-322}$$

and

$$\frac{1}{\rho}i\kappa_i\lambda_j = 2\frac{\kappa_1\kappa_i}{\kappa^2}\varphi_{2j}\frac{dU_1}{dx_2}. \tag{5-323}$$

Substituting equations (5-322) and (5-323) into (5-321) gives

$$\frac{\partial}{\partial t}\varphi_{ij} = -\left(\delta_{i1}\varphi_{2j} + \delta_{j1}\varphi_{i2}\right)\frac{dU_1}{dx_2} + \kappa_1\frac{\partial\varphi_{ij}}{\partial\kappa_2}\frac{dU_1}{dx_2} + \left(2\frac{\kappa_1\kappa_i}{\kappa^2}\varphi_{2j} + 2\frac{\kappa_1\kappa_j}{\kappa^2}\varphi_{i2}\right)\frac{dU_1}{dx_2} - 2\nu\kappa^2\varphi_{ij}. \tag{5-324}$$

Equation (5-324) indicates that φ_{ij} is a function of the components of $\boldsymbol{\kappa}$ as well as of its magnitude. One can obtain a quantity that is a function only of κ by writing φ_{ij} in terms of spherical coordinates and integrating over the surface of a sphere of radius κ, as suggested by Batchelor (ref. 4). This gives

$$\psi_{ij}(\kappa) = \int_A \varphi_{ij}(\boldsymbol{\kappa})dA(\boldsymbol{\kappa}). \tag{5-325}$$

The quantity ψ_{ij} is the value of φ_{ij} averaged over all directions and multiplied by A. Similarly, each term of equation (5-324) can be averaged. If we denote the average of the second term (multiplied by A) by $P_{ij}(\kappa)\,dU_1/dx_2$, the average of the third term by $T_{ij}'(\kappa)\,dU_1/dx_2$, and the average of the fourth term by $Q_{ij}(\kappa)\,dU_1/dx_2$, then the averaged equation becomes

$$\frac{\partial}{\partial t}\psi_{ij}(\kappa) = P_{ij}(\kappa)\frac{dU_1}{dx_2} + T_{ij}''(\kappa)\frac{dU_1}{dx_2} + Q_{ij}(\kappa)\frac{dU_1}{dx_2} - 2\nu\kappa^2\psi_{ij}. \tag{5-326}$$

Contraction of the indices i and j in equation (5-326) gives

$$\frac{\partial}{\partial t}\psi_{ii} = P_{ii}\frac{dU_1}{dx_2} + T_{ii}''\frac{dU_1}{dx_2} - 2\nu\kappa^2\psi_{ii}, \tag{5-327}$$

where $\frac{1}{2}\psi_{ii} = E$, the energy spectrum function.

Interpretation of terms in spectral equations. The quantity $Q_{ij}\,(dU_1/dx_2)$, which corresponds to the pressure-force term in equation (5-296), does not appear in the contracted equation (5-327) as pointed out in reference 76. That this is the case can be seen by substituting $\partial/\partial r_i = \partial/\partial x_i'$ and $\partial/\partial r_j = -\partial/\partial x_j$ in the pressure-force term in equation (5-296) and applying continuity to the contracted equation. Thus, as in the case of homogeneous turbulence without a mean velocity gradient, the pressure-force term exchanges energy between the directional components of the energy but makes no contribution to $\partial\psi_{ii}/\partial t$.

In order to interpret the quantity T_{ii}'' or T_{ij}'', it is noted that $r_2\partial\overline{u_iu_j'}/\partial r_1$ in equation (5-296) and $\kappa_1\left(\partial\varphi_{ij}/\partial\kappa_2\right)$ in equation (5-324) are related by

$$r_2\frac{\partial\overline{u_iu_j'}}{\partial r_1} = -\int_{-\infty}^{\infty}\kappa_1\frac{\partial\varphi_{ij}}{\partial\kappa_2}e^{i\boldsymbol{\kappa}\cdot\mathbf{r}}\,d\boldsymbol{\kappa}. \tag{5-328}$$

Evaluating this equation for $\mathbf{r} = 0$ gives

$$\int_{-\infty}^{\infty}\kappa_1\frac{\partial\varphi_{ij}}{\partial\kappa_2}\,d\boldsymbol{\kappa} = 0, \tag{5-329}$$

and thus

$$\int_0^{\infty}T_{ij}''(\kappa)\,d\kappa = 0. \tag{5-330}$$

Thus, T_{ij}'' gives zero contribution to $\partial\overline{u_iu_j}/\partial t$. However, it can alter the distribution in wavenumber space of contributions to $\partial\overline{u_iu_j}/\partial t$ and thus can be interpreted as a transfer function. The quantity T_{ij}'' was evidently first interpreted as a transfer function in our reference 7. More will be said about it later when spectra of T_{ii}'' are computed. The quantity T_{ii}'', which arises because of the velocity gradient, has a function similar to that of the transfer term arising from triple correlations (neglected here), but should not be confused with the latter. The transfer term $T_{ii}''\,(dU_1/dx_2)$ can be important even in the final period, whereas that arising from the triple correlations is absent in that case. Note that in the general case, where the velocity gradient is not uniform, the transfer term will be associated with an average velocity gradient $\left(U_1' - U_1\right)/r_2$ (see the fourth term in equation (4-147)).

In order to complete the interpretation of terms in equation (5-327), we note that $P_{ii}\,(dU_1/dx_2)$, which corresponds to the second and third terms in equation (5-296), represents the production of turbulent energy at wave number κ by work done on the turbulence by the velocity gradient. Finally, the term $-2\nu\kappa^2\psi_{ii}$ is the usual dissipation term.

Solutions of spectral equations. Next, solutions will be given for some of the components of the tensor φ_{ij} in equation (5-324). The nine equations represented by equation (5-324) are simultaneous first-order partial differential equations in the independent variables t and κ_2 and can be solved by methods given, for instance, in reference 79.

The component of φ_{ij} most easily obtained is φ_{22}, inasmuch as it is independent of the other components. Thus, the expression for φ_{22} is obtained by solution of equation (5-324) as (ref. 79)

$$\varphi_{22} = \left\{f\left[\kappa_1, a_{12}\kappa_1(t-t_0)+\kappa_2, \kappa_3\right]/\kappa^4\right\}\exp\left\{-2\nu(t-t_o)\left[\kappa^2 + \frac{1}{3}\kappa_1^2a_{12}^2(t-t_0)^2 + a_{12}\kappa_1\kappa_2(t-t_0)\right]\right\}, \tag{5-331}$$

where

$$a_{12} \equiv \partial U_1/\partial x_2, \tag{5-332}$$

and f is a function of integration that depends on initial conditions. In order to evaluate f, it is assumed that the turbulence is isotropic at $t = t_0$ (but not at other times). This is a possible assumption because the effect of the velocity gradient on the turbulent quantities becomes negligible as $t \to t_0$ (see eq. (5-331)]. Thus, $(\varphi_{ij})_0$ is given by equation (3.4.12) in reference 4, where, as in equation (5-164), we set $E_0 = C(\kappa) = J_0\,\kappa^4/3\pi$. So

$$\left(\varphi_{ij}\right)_0 = \frac{J_0}{12\pi^2}\left(\kappa^2\delta_{ij} - \kappa_i\kappa_j\right). \tag{5-333}$$

Inspection of equation (5-333) shows that rotations and reflections (in wave number space) of the vector $\boldsymbol{\kappa}$ do not affect $(\varphi_{ij})_0$, provided the same rotations and reflections are given to the coordinate axes to which $\boldsymbol{\kappa}$ is referred. Thus, the field of turbulence is isotropic, according to the usual definition of isotropic turbulence (e.g., see ref. 4). Moreover, equation (5-333) satisfies continuity, since $\kappa_i(\varphi_{ij})_0 = \kappa_j(\varphi_{ij})_0$ (see equation (5-304)).[10] Evaluation of f in equation (5-331) by substituting equation (5-333) at $t = t_0$ gives

$$f(\kappa_1, \kappa_2, \kappa_3) = \frac{J_0\kappa^4}{12\pi^2}\left(\kappa_1^2 + \kappa_3^2\right),$$

or

$$f\left[\kappa_1, \kappa_2 + a_{12}\kappa_1(t-t_0), \kappa_3\right] = \frac{J_0}{12\pi^2}\left\{\kappa_1^2 + \left[\kappa_2 + a_{12}\kappa_1(t-t_0)\right]^2 + \kappa_3^2\right\}^2\left(\kappa_1^2 + \kappa_3^2\right).$$

Then

$$\varphi_{22} = \frac{J_0\left\{\kappa_1^2 + \left[\kappa_2 + a_{12}\kappa_1(t-t_0)\right]^2 + \kappa_3^2\right\}^2\left(\kappa_1^2 + \kappa_3^2\right)}{12\pi^2\kappa^4}\exp\left\{-2\nu(t-t_0)\left[\kappa^2 + \frac{1}{3}\kappa_1^2a^2(t-t_0)^2 + a_{12}\kappa_1\kappa_2(t-t_0)\right]\right\}. \tag{5-334}$$

Similarly the component φ_{12}, which is associated with the turbulent shear stress, is

$$\varphi_{12} = \frac{J_0\left\{\kappa_1^2 + \left[\kappa_2 + a_{12}\kappa_1(t-t_0)\right]^2 + \kappa_3^2\right\}^2}{12\pi^2\kappa^2}\exp\left\{-2\nu(t-t_0)\left[\kappa^2 + a_{12}\kappa_1\kappa_2(t-t_0) + \frac{1}{3}\kappa_1^2a_{12}^2(t-t_0)^2\right]\right\}$$

$$\times\left\{\frac{\kappa_3^2}{\kappa_1\left(\kappa_1^2+\kappa_3^2\right)^{\frac{1}{2}}}\left[\tan^{-1}\frac{\kappa_2}{\left(\kappa_1^2+\kappa_3^2\right)^{\frac{1}{2}}} - \tan^{-1}\frac{\kappa_2 + a_{12}\kappa_1(t-t_0)}{\left(\kappa_1^2+\kappa_3^2\right)^{\frac{1}{2}}}\right] - \frac{\kappa_1\kappa_2}{\kappa^2}\right\}, \tag{5-335}$$

where the function of integration was evaluated from equation (5-333), as in the case of equation (5-334). The same expression is obtained for φ_{21}; that is, $\varphi_{12} = \varphi_{21}$.

The contracted component φ_{ii}, which is associated with the turbulent energy, is obtained from equation (5-324) as

$$\varphi_{ii} = \frac{J_0\left\{\kappa_1^2 + \left[\kappa_2 + a_{12}\kappa_1(t-t_0)\right]^2 + \kappa_3^2\right\}^2}{12\pi^2\kappa^2}\exp\left\{-2\nu(t-t_0)\left[\kappa^2 + a_{12}\kappa_1\kappa_2(t-t_0) + \frac{1}{3}a_{12}\kappa_1^2(t-t_0)^2\right]\right\}$$

$$\times\left\{\frac{\kappa^2}{\kappa_1^2 + \left[\kappa_2 + a_{12}\kappa_1(t-t_0)\right]^2 + \kappa_3^2} + 1 + \frac{\kappa_3^2\kappa^2}{\kappa_1^2\left(\kappa_1^2+\kappa_3^2\right)}\left[\tan^{-1}\frac{\kappa_2}{\left(\kappa_1^2+\kappa_3^2\right)^{\frac{1}{2}}} - \tan^{-1}\frac{\kappa_2 + a_{12}\kappa_1(t-t_0)}{\left(\kappa_1^2+\kappa_3^2\right)^{\frac{1}{2}}}\right]^2\right\}, \tag{5-336}$$

---

[10] Note, however, that $(\varphi_{ij})_0$ is not an isotropic or numerical tensor according to the usual definition (see section 2.4.3), except for $\boldsymbol{\kappa} = 0$. That definition would require that the components of $(\varphi_{ij})_0$ have the same numerical values for arbitrary rotations of the coordinate axes, even when $\boldsymbol{\kappa}$ does not rotate. Thus, a field of isotropic turbulence is described by a nonisotropic tensor (eq. (5-333)), since the only second-order isotropic tensor (when defined in the usual way) is the product of a scalar and δ_{ij} (section 2.4.3).

where the function of integration was again evaluated by using equation (5-334) and a_{12} is given by (5-332). Other components of φ_{ij} can be obtained in a similar manner. For example it is shown in reference 80 that φ_{11} is given by

$$\varphi_{11} = \frac{J_0\left\{\kappa_1^2 + \left[\kappa_2 + a_{12}\kappa_1(t-t_0)\right]^2 + \kappa_3^2\right\}^2}{12\pi^2} \exp\left\{-2\nu(t-t_0)\left[\kappa^2 + \frac{1}{3}\kappa_1^2 a_{12}^2 (t-t_0)^2 + a_{12}\kappa_1\kappa_2(t-t_0)\right]\right\}$$

$$\times\left\{\frac{\kappa_1}{\left(\kappa_1^2+\kappa_3^2\right)}\left(\frac{\kappa_2^2}{\kappa^4} - \left\{\frac{\kappa_2 + a_{12}\kappa_1(t-t_0)}{\kappa_1^2 + \left[\kappa_2 + a_{12}\kappa_1(t-t_0)\right]^2 + \kappa_3^2}\right\}^2\right) + \frac{\left[\kappa_2 + a_{12}\kappa_1(t-t_0)\right]^2 + \kappa_3^2}{\left\{\kappa_1^2 + \left[\kappa_2 + a_{12}\kappa_1(t-t_0)\right]^2 + \kappa_3^2\right\}^2} - \frac{2\kappa_2\kappa_3^2}{\left(\kappa_1^2+\kappa_3^2\right)^{\frac{3}{2}}\kappa^2}\right.$$

$$\left.\times\left[\tan^{-1}\frac{\kappa_2}{\left(\kappa_1^2+\kappa_3^2\right)^{\frac{1}{2}}} - \tan^{-1}\frac{\kappa_2 + a_{12}\kappa_1(t-t_0)}{\left(\kappa_1^2+\kappa_3^2\right)^{\frac{1}{2}}}\right] + \frac{\kappa_3^4}{\left(\kappa_1^2+\kappa_3^2\right)^2\kappa_1^2}\left[\tan^{-1}\frac{\kappa_2}{\left(\kappa_1^2+\kappa_3^2\right)^{\frac{1}{2}}} - \tan^{-1}\frac{\kappa_2 + a_{12}\kappa_1(t-t_0)}{\left(\kappa_1^2+\kappa_3^2\right)^{\frac{1}{2}}}\right]^2\right\}. \quad (5-337)$$

Note the similarities (and differences) among equations (5-334) to (5-337).

The quantities φ_{22}, φ_{12}, φ_{ii}, and φ_{11} are of interest in themselves; however, it is somewhat easier to interpret quantities that have been averaged over all directions in κ space, as was done in equations (5-325) to (5-327). In order to do this, we write equations (5-334) to (5-337) in terms of spherical coordinates by setting $\kappa_1 = \kappa\cos\varphi\sin\theta$, $\kappa_2 = \kappa\sin\varphi\sin\theta$, $\kappa_3 = \kappa\cos\theta$. Then equation (5-325) becomes

$$\psi_{ij}(\kappa) = \int_0^{\pi}\int_0^{2\pi}\varphi_{ij}(\kappa,\varphi,\theta)\kappa^2\sin\theta\, d\varphi\, d\theta. \quad (5-338)$$

Each of the terms in equations (5-326) and (5-327) can be obtained in a similar manner. For instance, from equations (5-324) and (5-326),

$$T_{ij}(\kappa) = \int_0^{\pi}\int_0^{2\pi}\kappa\cos\varphi\sin\theta\frac{\partial\varphi_{ij}}{\partial\kappa_2}(\kappa,\varphi,\theta)\kappa^2\sin\theta\, d\varphi\, d\theta. \quad (5-339)$$

Discussion of computed spectra. Dimensionless spectra of $\frac{1}{2}\overline{u_2^2}$, $\frac{1}{2}\overline{u_1u_2}$, and $\frac{1}{2}\overline{u_iu_i}$ for various values of dimensionless velocity gradient are plotted in figures 5-54 to 5-56. When plotted in the form shown, the spectrum curve for zero velocity gradient does not change with time, so that the various curves indicate how the velocity gradient influences the spectrum. The increase in the heights of the spectra with $(t - t_0)\, dU_1/dx_2$ appears to be associated with the production of turbulence by the mean velocity gradient. The spectra move toward the left as velocity gradient increases, since most of the production takes place in the low wavenumber region (see. fig. 5-62). Actually the spectral equation corresponding to $\overline{u_2^2}$ does not contain a production term (see eq. (5-324)). However, energy produced in the $\overline{u_1^2}$ component can be fed into or out of $\overline{u_2^2}$ by the pressure-force terms that transfer energy between directional components. The magnitude of the effect of pressure forces is illustrated by the dot-dashed curve in figure 5-54, where the pressure-force term in the spectral equation (fourth term in eq. (5-324)) is neglected. When the pressure-force term is neglected, the portion of equation (5-334) in front of the exponential becomes $J_0\left(\kappa_1^2+\kappa_3^2\right)/\left(12\pi^2\right)$, but the exponential is unchanged. Comparison of the dot-dashed curve with the solid curve for the same velocity gradient shows the considerable effects of pressure forces. That curve differs from the curve for zero velocity gradient because of the effect of the transfer term (third term in eq. (5-324)).

The spectrum of $\overline{u_2^2}$ moves to the left much more rapidly than does that of $\overline{u_iu_i}$, because of the action of pressure forces. The pressure-force term Q_{22} from the spectral equation (5-326) is plotted in figure 5-57. For all values of dimensionless velocity

gradient, Q_{22} is negative at the higher wavenumbers. This indicates that energy is transferred out of the spectrum of $\overline{u_2^2}$ at the higher wavenumbers and into the sum of the spectra of $\overline{u_1^2}$ and $\overline{u_3^2}$. Thus, the spectrum of $\overline{u_2^2}$ moves to the left faster with increasing velocity gradient than does that of $\overline{u_i u_i}$, the latter representing the average of the three components of the energy. This means that a typical eddy will be elongated in the transverse direction x_2 by the action of the pressure forces.[11]

The net areas under the curves of Q_{22} are positive for small velocity gradients and negative for large ones. Thus, the pressure forces transfer energy into the $\overline{u_2^2}$ component at low velocity gradients, whereas at high velocity gradients they transfer energy out of the $\overline{u_2^2}$ component into the sum of the $\overline{u_1^2}$ and $\overline{u_3^2}$ components. The resulting effect of this transfer on the components is shown in figure 5-58, where $\overline{u_2^2}\Big/\left(\frac{1}{3}\overline{u_i u_i}\right)$ is plotted against dimensionless velocity gradient. The values of $\overline{u_2^2}$ and $\frac{1}{3}\overline{u_i u_i}$ were obtained by integrating under the spectrum curves in figures 5-54 and 5-56. For isotropic turbulence (zero velocity gradient in the present case), $\overline{u_2^2}\Big/\left(\frac{1}{3}\overline{u_i u_i}\right)$ has the value 1. As the velocity gradient increases, $\overline{u_2^2}\Big/\left(\frac{1}{3}\overline{u_i u_i}\right)$ first increases very slightly and then decreases considerably because of the transfer of energy between directional components by the pressure forces. The quantities $\overline{u_1^2}\Big/\left(\overline{u_i u_i}/3\right)$ and $\overline{u_3^2}\Big/\left(\overline{u_i u_i}/3\right)$ are calculated in reference 80 and are plotted in figure 4 of that reference. The calculated ordering of the three components of $\overline{u_i u_i}$ is $\overline{u_1^2} > \overline{u_3^2} > \overline{u_2^2}$, in agreement with experiment (see, e.g., ref. 11 of chapter 4 and ref. 85 of this chapter).

Also plotted in figure 5-58 is the ratio $\overline{u_1 u_2}\Big/\left(\frac{1}{3}\overline{u_i u_i}\right)$, where $\overline{u_1 u_2}$ was obtained from the shear-stress spectra in figure 5-55. As would be expected, the shear stress is zero for zero velocity gradient. In other respects the curve is similar to that for $\overline{u_2^2}\Big/\left(\frac{1}{3}\overline{u_i u_i}\right)$, with the exception that it decreases more gradually as velocity gradient increases.

A quantity closely related to the shear stress is the eddy diffusivity ε, defined by

$$\varepsilon \equiv -\frac{\overline{u_1 u_2}}{dU_1/dx_2}. \qquad (5-340)$$

A plot of dimensionless eddy diffusivity against dimensionless velocity gradient is given in figure 5-58. Of some interest is the observation that the eddy diffusivity does not go to zero for zero velocity gradient. In this respect the eddy diffusivity (or eddy viscosity) is like the molecular viscosity. The result is reasonable, inasmuch as one would expect the turbulence to be diffusive even in the absence of a velocity gradient. It is, however, in disagreement with the usual mixing length theories, which predict zero eddy diffusivity for zero velocity gradient (see e.g., the relation for ε given by eqs. (4-125) and (5-340)). This does not imply that the usual mixing length theories are not useful for predicting mean velocity distributions in boundary layers, etc., inasmuch as the velocity profile is insensitive to the value of eddy diffusivity in the region where dU_1/dx_2 is small.[12] Figure 5-58 indicates that the value of dimensionless eddy diffusivity does not vary more than ±10% from a mean value, except at very high velocity gradients.

Local isotropy. The discussion in the preceding section concerning the transfer of energy between directional components by pressure forces is pertinent to the theory of local isotropy (ref. 42). According to that theory the high wavenumber (small-scale) components of the turbulence should be isotropic regardless of the directional orientation of the large-scale components. This tendency to isotropy of the small eddies is generally ascribed to the action of pressure forces. However, the present calculations indicate that in the presence of a mean velocity gradient the pressure forces can act to increase rather than decrease the anisotropy of the turbulence (fig. 5-58). The effect of this orientation on the small-scale components is clearly shown in

---

[11] In contrast to the behavior of Q_{22}, note that Q_{11} is always negative and Q_{33} is always positive, regardless of wave number (see ref. 80). Thus pressure forces transfer energy out of the spectrum of $\overline{u_1^2}$ and into the spectrum of $\overline{u_3}$ at all wave numbers. Most of the directional energy transfer at high velocity gradients is from $\overline{u_1^2}$ to $\overline{u_3^2}$; smaller transfer is effected by Q_{22}. At smaller velocity gradients the energy transfers in the three directions are of the same order (ref. 80).

[12] Moreover, according to equation (4-38), which is a more general mixing-length expression than that obtained from equations (4-125) and (5-340), ε does not necessarily go to zero for a velocity gradient of zero.

figure 5-59, where $\psi_{22}/(\frac{1}{3}\psi_{ii})$ is plotted against dimensionless wavenumber. For isotropic turbulence that ratio would be 1, but the curves indicate that it is far from 1 in the high wavenumber region, especially for high velocity gradients. These findings concerning the lack of local isotropy are in qualitative agreement with experimental results in reference 81, where turbulent spectra were measured in a low-speed boundary layer.

It should be pointed out that the action of the pressure forces in working against isotropy in the present analysis is due to the presence of the velocity gradient (eq. 5-326). Triple correlations, which are neglected here, can also affect the pressure forces at high turbulence Reynolds numbers (see eq. (4-149)) and may tend to increase the isotropy. However, it appears that one should be extremely cautious in assuming local isotropy in a boundary layer or pipe flow, inasmuch as high turbulence Reynolds numbers in those cases generally correspond to high velocity gradients, except possibly at a large distance from the wall. Reference 82, where the effects of anisotropy due to pressure forces were apparently not considered, indicates that local isotropy in a channel might conceivably occur, but only at extremely high Reynolds numbers. Local isotropy may be a better assumption for the turbulent wake of a cylinder (ref. 83).

Another quantity of interest in connection with local isotropy is the spectrum of the shear stress ψ_{12} (fig. 5-55.). For local isotropy to exist, that quantity should go to zero faster with increasing wavenumber than does the average intensity component $\frac{1}{3}\psi_{ii}$. However, as pointed out in reference 81, that is a necessary condition for local isotropy, but not a sufficient condition.

Values of $\psi_{12}/(\frac{1}{3}\psi_{ii})$ are plotted against dimensionless wavenumber in figure 5-60. The curves indicate that this function, in general, decreases with increasing wavenumber in agreement with the experimental findings of references 81, 84, and 85.

Energy transfer between wavenumbers. As discussed previously in connection with equation (5-327), the term $T_{ii}\,dU_1/dx_2$ makes no contribution to the change of total energy, but it can transfer energy between wavenumbers or eddies of various sizes. Spectra of T_{ii} for various values of dimensionless velocity gradient are plotted in figure 5-61. The curves are predominately negative for small wavenumbers and positive for large ones, so that, in general, energy is transferred from small wavenumbers to large ones. Thus, the effect here is similar to that of the transfer term due to triple correlations. The transfer apparently affects the shape of the spectra in figures 5-54 to 5-56 by exciting the higher wavenumber regions of those spectra, as in the case of the transfer due to triple correlations (see, e.g., section 5.3.2.2). This is shown by the dashed curves for zero velocity gradient normalized to the peaks of the curves for $(t - t_0)\,dU_1/dx_2 = 20$ in figures 5-54 to 5-56.

A natural explanation of the transfer of energy to the high wavenumber regions by the mean velocity gradient would be that the velocity gradient stretches the vortex lines associated with the turbulence. Some related problems in this connection are considered in reference 86. This picture might also explain the small amount of reverse transfer shown in figure 5-61 for low wavenumbers at small velocity gradients, since the velocity gradient should be able to compress, as well as stretch, the vortex lines if they are properly oriented. This reverse transfer was found to be more pronounced in the transfer term associated with $\overline{u_2^2}$ (not shown).

Production, energy-containing, and dissipation regions. Production, energy, and dissipation spectra, normalized to the same ordinate for comparison, are plotted in figure 5-62. The production and dissipation spectra correspond to the production and dissipation terms in equation (5-327). Curves are shown for a negligibly small and for a comparatively large dimensionless velocity gradient. For the small velocity gradient the production, energy-containing, and dissipation regions are only slightly separated; whereas at the higher velocity gradient they are more widely separated. The turbulent production by the mean velocity gradient occurs mostly in the low wavenumber or large eddy region; the dissipation occurs in the higher wavenumber region. Although the three regions separate as velocity gradient increases, there is still considerable overlap at a value of $(t - t_0)\,dU_1/dx_2$ of 50. Energy from the mean velocity gradient feeds into the turbulence over a considerable range of wavenumbers. The energy goes into the turbulence through the $\overline{u_1^2}$ component, inasmuch as the production terms are absent from the spectral equations for $\overline{u_2^2}$ and $\overline{u_3^2}$ (see eq. (5-324)). However, the energy can be transferred between the various directional components by the pressure forces as discussed previously.

The separation of the energy-containing and dissipation regions at high velocity gradients is similar to the separation of those regions at high turbulence Reynolds numbers without a velocity gradient (section 5.3.2.2). In both cases the separation appears to be a consequence of the change in shape of the energy spectrum produced by the transfer of energy to high wavenumbers (figs. 5-54 to 5-56).

A summary of turbulent energy processes. The sequence of turbulent energy processes in a flow with strong shear and/or weak turbulence might be summarized as follows. The turbulent energy is produced by the mean velocity gradient. This production occurs in the $\overline{u_1^2}$ component of the energy and predominately in the large eddy region. The pressure forces, which depend here on the velocity gradient, transfer the energy between various directional components. In doing this, they may increase the anisotropy of the turbulence, and, in particular, they oppose local isotropy in the high wavenumber region. In cases where the effect of the triple correlations on the pressure forces is not small, the turbulence might be somewhat more locally isotropic. The mean

velocity gradient, like the triple correlations, transfers energy from the large eddies to the small ones. This transfer can be interpreted as a stretching of the vortex lines by the mean velocity gradient. Finally, the energy is dissipated by viscous action in the small-eddy region.

Decay of the total turbulent energy. A dimensionless plot of the decay of turbulent energy for various velocity gradients is presented in figure 5-63. As velocity gradient increases, the rate of decrease of the turbulent energy with time decreases because of energy fed into the turbulent field by the mean velocity gradient. Although the changes produced by the velocity gradient are considerable (note that the vertical scale is logarithmic), the turbulence at all times decays.

The curves in figure (5-63) are plotted with three dimensionless groups in order to show the effects of time and mean velocity gradient separately. The curves are, however, similar and can be compressed into one by using the proper similarity parameters. The result is shown in figure 5-64, where $\nu^{5/2}(t-t_0)^{5/2}\overline{u_i u_i}/J_0$ is plotted against $(t-t_0)\,dU_1/dx_2$.

The ultimate decay of turbulent energy in all parts of wavenumber space can be seen from the structure of equation (5-336). At large times the argument of the exponential in that equation is negative for all values of κ_i and a_{12}.

Further understanding of the dynamics of shear-flow turbulence can be obtained by studying the random vorticity in sheared turbulence. One aspect of the interaction of turbulent vorticity with a mean shear will be considered in the next section.

Direction of maximum turbulent vorticity in a shear flow. The vorticity in a turbulent shear flow has been mentioned briefly in connection with the energy transfer between wavenumbers. Here we further discuss turbulent vorticity—in particular, the alignment of vorticity by a mean velocity gradient and the direction of maximum vorticity.[13]

Intuitively, one might expect the random vortices to tend to become aligned in the direction of maximum mean strain rate; that is, at 45° to the flow direction. Taylor (ref. 88) was evidently the first one to emphasize the stretching of turbulent vortex filaments as a mechanism for the production of turbulence. Theodorsen, (ref. 89) using a possibly overmechanized model, has attributed the maintenance of turbulence in a shear flow to the stretching of "horseshoe vortices" that are inclined to the direction of mean flow at an average angle of 45°. Weske and Plantholt (ref. 90) have discussed that concept further and have been able to generate such vortices artificially in a pipe flow.

Although it seems reasonable that the maximum turbulent vorticity should occur at 45° to the flow direction, further analysis (given below) indicates that it could occur at that angle only if the transverse component of vorticity equals the longitudinal component; that, of course, is not the case in an anisotropic shear flow. However, there may be a range of velocity gradients where the maximum vorticity could occur at angles reasonably close to 45°.

Since the turbulent vorticity $\overline{\omega_i\omega_j}$ is a second-order tensor, its components relative to a rotated coordinate system are given by (see eq. (2-12))

$$\overline{\omega_i^*\omega_j^*} = b_{ik}b_{j\ell}\overline{\omega_k\omega_\ell}, \tag{5-341}$$

where ω_i is an instantaneous vorticity component, and the overbars indicate averaged values. Unstarred quantities give components relative to coordinates x_i, and starred quantities are relative to coordinates x_i^*.[14] The quantity b_{ik} is the cosine of the angle between x_i^* and x_k. The summation convention is operative in equation (5-341). If we consider a counterclockwise rotation about x_3 so that x_1^* makes an angle α with x_1, equation (5-341) reduces to (by setting $i = j = 1$)

$$\overline{\omega_1^{*2}} = \frac{1}{2}\overline{\omega_1^2}(1+\cos 2\alpha) + \overline{\omega_1\omega_2}\sin 2\alpha + \frac{1}{2}\overline{\omega_2^2}(1-\cos 2\alpha). \tag{5-342}$$

The component $\overline{\omega_2^{*2}}$ is then obtained by substituting $\alpha + 90°$ for α in equation (5-342). The angle for which $\overline{\omega_1^{*2}}$ is a maximum is obtained from equation (5-342) by setting $\partial\overline{\omega_1^{*2}}/\partial\alpha = 0$. This gives

$$\alpha_{\omega_{max}} = \frac{1}{2}\tan^{-1}\frac{2\overline{\omega_1\omega_2}}{\overline{\omega_1^2} - \overline{\omega_2^2}}. \tag{5-343}$$

---

[13]The direction of maximum turbulent *stress* or *intensity* is, of course, also of interest (see, e.g., ref. 87), but the discussion here will be confined to vorticity.

[14]The use of stars here on rotated coordinates and on quantities measured relative to rotated coordinates is consistent with the usage in chapter 2. But note that stars are sometimes also used to designate dimensionless quantities and complex conjugates.

Equation (5-343) shows (as mentioned above) that for a finite $\overline{\omega_1\omega_2}$, $\alpha_{\omega_{max}}$ can be equal to 45° only for $\overline{\omega_1^2} = \overline{\omega_2^2}$, or for isotropic turbulence. (A similar result is obtained for velocity fluctuations by replacing the ω's in equations (5-341) to (5-343) by u's, since both $\overline{\omega_i\omega_j}$ and $\overline{u_iu_j}$ are second-order tensors.)

In order to calculate the angle $\alpha_{\omega_{max}}$ from equation (5-343), components of $\overline{\omega_i\omega_j}$ in the unrotated coordinate system must be known. To that end, the two-point tensor $\overline{\omega_i\omega_j'}(\mathbf{r})$ can be related to $\overline{u_iu_j'}(\mathbf{r})$ by writing equation (2-24) at points P and P'. Then

$$\overline{\omega_i\omega_j'} = \varepsilon_{i\ell m}\varepsilon_{jpq}\overline{\frac{\partial u_m}{\partial x_\ell}\frac{\partial u_q'}{\partial x_p'}} = -\varepsilon_{i\ell m}\varepsilon_{jpq}\overline{\frac{\partial^2 u_m u_q'}{\partial r_\ell \partial r_p}}, \tag{5-344}$$

where the relations $\partial/\partial x_i' = \partial/\partial r_i$ and $\partial/\partial x_i = \partial/\partial r_i$ were used and $\mathbf{r}$ is the vector extending from point P to point P'. Then defining the spectral tensor of $\overline{\omega_i\omega_j'}$ by

$$\overline{\omega_i\omega_j'}(\mathbf{r}) = \int_{-\infty}^{\infty}\Omega_{ij}(\boldsymbol{\kappa})e^{i\boldsymbol{\kappa}\cdot\mathbf{r}}d\boldsymbol{\kappa}, \tag{5-345}$$

and using

$$\overline{u_iu_j'}(\mathbf{r}) = \int_{-\infty}^{\infty}\varphi_{ij}(\boldsymbol{\kappa})e^{i\boldsymbol{\kappa}\cdot\mathbf{r}}d\boldsymbol{\kappa}, \tag{5-304}$$

we get

$$\Omega_{ij} = \varepsilon_{i\ell m}\varepsilon_{jpq}\kappa_\ell\kappa_p\varphi_{mq}. \tag{5-346}$$

But

$$\varepsilon_{i\ell m}\varepsilon_{jpq} = \delta_{ij}\delta_{\ell p}\delta_{mq} + \delta_{ip}\delta_{\ell q}\delta_{mj} + \delta_{iq}\delta_{\ell j}\delta_{mp} - \delta_{ij}\delta_{\ell q}\delta_{mp} - \delta_{ip}\delta_{\ell j}\delta_{mq} - \delta_{iq}\delta_{\ell p}\delta_{mj}, \tag{5-347}$$

as can be seen by substituting numerical values for the subscripts and using equations (2-23) or (2-23a) and (2-3). Then equation (5-346) becomes

$$\Omega_{ij} = \left(\delta_{ij}\kappa^2 - \kappa_i\kappa_j\right)\varphi_{\ell\ell} - \kappa^2\varphi_{ji}, \tag{5-348}$$

which is the same as equation (3.2.3) of reference 4. Finally, $\overline{\omega_i\omega_j'}(0) = \overline{\omega_i\omega_j}$ is obtained from equation (5-345).

Figure 5-65 shows the variation of $\alpha_{\omega_{max}}$ with dimensionless velocity gradient. The quantity t in the dimensionless velocity gradient is the time of decay, and t_0 is an initial time when the turbulence is isotropic. U_1 is the mean velocity, and x_2 is a transverse coordinate. As expected from the form of equation (5-343), the angle for which the turbulent vorticity is a maximum is 45° only when the dimensionless velocity gradient is zero (isotropic turbulence). However, it remains at values slightly greater than 45° (between 48° and 53°) for a considerable range of dimensionless velocity gradients. It is of interest that the experimental vortices of reference 90 appeared to be inclined to the mean flow at similar angles.

Figure 5-66 shows the degree of alignment of the turbulent vortices in the direction of maximum vorticity. For no alignment of the vortices, the ratio $\overline{\omega_{max}^2}/\overline{\omega_{min}^2}$ is, of course, one. On the other hand, if the vortices were all aligned at the angle $\alpha_{\omega_{max}}$, the ratio $\overline{\omega_{max}^2}/\overline{\omega_{min}^2}$ would be infinite. The figure shows that the ratio actually varies between 1 and about 12 for values of dimensionless velocity gradient shown. The decrease in degree of vortex alignment as dimensionless velocity gradient increases beyond 3 may be an effect of pressure fluctuations.

An effect of initial condition. For the results given in section 5.4.2.1 thus far, the turbulent energy always decayed with time (see fig. 63). Although energy was fed into the turbulence by the mean velocity gradient, so that the turbulence decayed at a

slower rate than it would have with no shear, the turbulent energy produced by the shear was less than that dissipated by viscous action. For the initial condition on the spectrum of the turbulence it was assumed that equation (5-333) holds at $t = t_0$. Equation (5-333) is for an initially isotropic turbulence and gives infinite initial total turbulent energy (per unit mass), although the energy at any finite wavenumber is finite. (At any time greater than t_0 the *total* turbulent energy is also finite.)

Recently, Hasen (ref. 91) used an expression for $(\varphi_{ij})_0$ equivalent to that in equation (5-333) multiplied by a negative exponential in κ^2. In that case the total initial energy was finite. Her results, which were limited to two-dimensional initial disturbances, showed that the turbulent energy can increase for a finite range of times. It is of interest to determine whether the same effect occurs for an initial three-dimensional isotropic turbulence (ref. 92). In order to do that we modify equation (5-333) to give

$$\left(\varphi_{ij}\right)_0 = \frac{J_0}{12\pi^2}\left(\delta_{ij}\kappa^2 - \kappa_i\kappa_j\right)e^{-\kappa^2/\kappa_0^2}, \qquad (5-349)$$

where $1/\kappa_0$ can be considered as an initial scale for the turbulence.

The equations for φ_{ij} given thus far in section 5.4.2.1 were derived for the initial condition given in equation (5-333). Those equations (eqs. (5-334) to (5-337)) can be modified so that the initial condition for φ_{ij} is given by equation (5-349) by multiplying their right sides by the exponential

$$\exp\left\{-\frac{1}{\kappa_0^2}\left[\kappa_1^2 + \left(\kappa_2 + \frac{dU_1}{dx_2}\kappa_1\left(t - t_0\right)\right)^2 + \kappa_3^2\right]\right\}.$$

Integration of φ_{ij} over all wavenumber space then gives the turbulent energy tensor $\overline{u_i u_j}$, where u_i and u_j are velocity components and the overbar indicates an averaged value.

Figure (5-67) shows a dimensionless plot of turbulent energy against time for various values of a Reynolds number R. The quantity $\frac{1}{2}\overline{u_i u_i} = \frac{1}{2}\left(\overline{u_1^2} + \overline{u_2^2} + \overline{u_3^2}\right)$ is the turbulent energy, and $\left(\overline{u_i u_i}\right)_0$ is the value of $\overline{u_i u_i}$ at the initial time t_0. The Reynolds number is based on mean velocity gradient dU_1/dx_2 and initial turbulence scale $1/\kappa_0$. The quantity U_1 is the mean velocity, x_2 is distance in the direction of the mean velocity gradient, and ν is the kinematic viscosity. The curves for the plot were obtained by using the modified equation (5-336) and equation (5-304) (with $r = 0$).

For small values of R the energy decreases monotonically with time, as in figure 5-63 where equation (5-333) rather than equation (5-349) was used for the initial condition. (Note that eq. (5-333) is obtained from eq. (5-349) by letting $R = 0$, or $\kappa_0 = \infty$.) For larger values of R, however, the energy increases during finite time intervals. Thus, for the larger Reynolds numbers there are time regions for which the energy fed into the turbulent field by the mean shear exceeds that dissipated by viscous action. For large times the energy again decays, and it appears that a steady state turbulence is not attained.

The ultimate decay of turbulent energy in all parts of wavenumber space, according to the analysis in the present section, can be seen from the structure of equation (5-336) and of the above exponential (by which equation (5-336) is multiplied here). At large times the argument of the exponential in equation (5-336), as well as that in the above exponential, is negative for all values of κ_i and dU_1/dx_2.

Some comments on the maintenance of turbulence. Since the turbulent energy can increase for finite time intervals, one might ask what happens physically at large times to cause the energy to again decrease. In order to answer that question, we look at the $\overline{u_2^2}$ component of the energy. Figure 5-68 shows a dimensionless plot of $\overline{u_2^2}$, the component of turbulent energy in the direction of mean velocity gradient. It is seen that regardless of the value of R, there are no time regions during which $\overline{u_2^2}$ increases, and for large times $\overline{u_2^2}$ becomes a small fraction of the total energy. This is evidently because there is no turbulence production term in the spectral equation for $\overline{u_2^2}$; so that the only way energy can be fed into the $\overline{u_2^2}$ component is by means of the pressure-velocity correlation terms, which can transfer energy between directional components. However, as shown in figure 5-57, the pressure-velocity terms tend to extract energy from the $\overline{u_2^2}$ component, rather than to deposit it there (except at small velocity gradients or times). Thus, the reason that all of the components of the turbulence decay for large times is evidently that the energy is drained out of the u_2 component of the velocity with the result that the turbulent shear $\overline{u_1 u_2}$ goes to zero. There is then no mechanism for maintaining the turbulence, since the turbulent energy is produced by the work done on the Reynolds stress $\overline{u_1 u_2}$ by the velocity gradient.

On the other hand, consider a somewhat stronger turbulence or small mean shear, where the triple-correlation terms in the equations for the pressure-velocity correlations are not negligible. Equation (5-301) becomes (neglecting buoyancy),

$$\frac{1}{\rho}\frac{\partial^2\overline{\sigma u_j'}}{\partial r_\ell \partial r_\ell} = 2\frac{\partial U_1}{\partial x_2}\frac{\overline{\partial u_2 u_j'}}{\partial r_1} - \frac{\partial^2\overline{u_\ell u_k u_j'}}{\partial r_\ell \partial r_\kappa}, \tag{5-350}$$

where unprimed and primed quantities refer, respectively, to values at points P and P′ separated by the vector r, σ is the pressure, and ρ is the density. A repeated subscript in a term indicates a summation. In this case it seems likely that the pressure-force terms will transfer energy into the $\overline{u_2^2}$ components, since their probable effect, when triple correlations are present, is to make the turbulence more isotropic (ref. 4, p. 88). The result may be that a nondecaying solution can be obtained with a uniform velocity gradient in a homogeneous turbulence, as seemed to be the case in the experiments of Rose (ref. 93). This in no way conflicts with the results of section 4.3.4, since there, inhomogeneities in the turbulence may have an additional sustaining effect on the turbulent energy.

Thus, if the above speculation concerning the directional transfer of energy is correct, it may be that the triple correlations play a crucial, although indirect, role in maintaining the turbulence by transferring energy between directional components through the pressure-velocity correlations. This effect of the triple correlations may be more important in turbulent shear flow than the transfer of energy between wavenumbers by those correlations. The latter seems to be simulated reasonably well by the energy transfer between wavenumbers which is produced by the mean velocity gradient (fig. 5-61). We shall return to the problem of the maintenance (or growth) of shear-flow turbulence in later sections. First, however, we want to get an idea as to whether predictions from our linearized theory are realistic.

5.4.2.2 A comparison of theory with experiment for uniformly sheared turbulence.—Approximately uniformly sheared turbulence has been investigated experimentally in references 93 to 95. Comparison of those results with the somewhat idealized theory of section 5.4.2.1 indicates that the latter shows qualitative features which are very much like those observed.

In order to obtain a quantitative comparison between theory and experiment, more realistic initial conditions than those given by equation (5-333) or (5-349) should be used. Initially isotropic turbulence was assumed in the theory, whereas the initial turbulence in the experiments was not isotropic. Also, the shape of the assumed initial energy spectrum is probably not realistic. In the present section we use an initial anisotropic spectral tensor which appears to be general enough to represent the initial experimental turbulence realistically. The theoretical results for the evolution of the turbulence are compared with those obtained experimentally to see whether a reasonable quantitative correspondence exists.

The evolution of the spectrum tensor corresponding to $\overline{u_i u_j'}(\mathbf{r})$ is given by equation (5-324):

$$\frac{\partial\varphi_{ij}}{\partial t} = -\left(\delta_{il}\varphi_{2j} + \delta_{jl}\varphi_{i2}\right)\frac{dU_1}{dx_2} + \kappa_1\frac{\partial\varphi_{ij}}{\partial\kappa_2}\frac{dU_1}{dx_2} + \left(2\frac{\kappa_1\kappa_i}{\kappa^2}\varphi_{2j} + 2\frac{\kappa_1\kappa_j}{\kappa^2}\varphi_{i2}\right)\frac{dU_1}{dx_2} - 2\nu\kappa^2\varphi_{ij}. \tag{5-324}$$

where the spectrum tensor φ_{ij} is defined by

$$\overline{u_i u_j'}(\mathbf{r}) = \int_{-\infty}^{\infty}\varphi_{ij}(\boldsymbol{\kappa})e^{i\boldsymbol{\kappa}\cdot\mathbf{r}}d\boldsymbol{\kappa}, \tag{5-304}$$

and $\boldsymbol{\kappa}$ is the wavenumber vector. The quantity φ_{ij} is the spectral component of $\overline{u_i u_j}$ at $\boldsymbol{\kappa}$. In order to interpret the terms in equation (5-324), we first multiply the equation through by $d\boldsymbol{\kappa}$. Then, the first term on the right side gives the rate of production of φ_{ij} in $d\boldsymbol{\kappa}$ by work done on φ_{ij} by the mean velocity gradient. The second term gives the net rate of transfer of φ_{ij} into $d\boldsymbol{\kappa}$ from other wavenumber regions by $\partial U_1/\partial x_2$. When this term is integrated over all $\boldsymbol{\kappa}$, the result is zero. The third term gives the rate of transfer of φ_{ij} between its directional components by pressure forces associated with $\partial U_1/\partial x_2$. This term drops out for i = j. Finally, the last term gives the rate of dissipation of φ_{ij} in $d\boldsymbol{\kappa}$.

In section 5.4.2.1 it is assumed that the initial turbulence is isotropic and is given by equation (5-333) or (5-349). The former equation is a special case of the latter, which is

$$\left(\varphi_{ij}\right)_0 = \frac{J_0}{12\pi^2}\left(\delta_{ij}\kappa^2 - \kappa_i\kappa_j\right)e^{-\ell^2\kappa^2}, \tag{5-351}$$

J_0 and ℓ are constants of the initial conditions, and the subscript 0 designates values at the initial time.

However, equation (5-349) is not general enough to represent the initial experimental turbulence in references 93 to 95. That turbulence is anisotropic and may have a spectrum whose shape is not given by equation (5-349). An expression for $(\varphi_{ij})_0$ which may be sufficiently general to represent the initial experimental turbulence is

$$\left(\varphi_{ij}\right)_0 = \frac{c_{\ell m}\kappa^2}{4\pi}\left(\delta_{i\ell} - \frac{\kappa_i\kappa_\ell}{\kappa^2}\right)\left(\delta_{jm} - \frac{\kappa_j\kappa_m}{\kappa^2}\right)\exp\left[-\left(\kappa\ell_{(\ell m)}\right)^{n_{(\ell m)}}\right], \tag{5-352}$$

where, for φ_{11}, φ_{22}, φ_{33}, and φ_{12} (the only components of φ_{ij} of interest here),

$$c_{\ell m} = \frac{3}{14}\frac{n_{(\ell m)}\ell^5_{(\ell m)}}{\Gamma\left(5/n_{(\ell m)}\right)}\left[10\overline{(u_\ell u_m)}_0 - \delta_{\ell m}\overline{(u_k u_k)}_0\right], \tag{5-353}$$

and where the $\ell_{\ell m}$ and $n_{\ell m}$ are constants of the initial conditions, and Γ is the gamma function. Parentheses are placed on some of the subscripts to indicate that there is no sum on those subscripts. Equations (5-352) and (5-353) are consistent with equation (5-304) for r = 0. As an aid to obtaining the initial constants $\ell_{\ell m}$, they can be related to the initial derivatives $(\partial\overline{u_i u_j}/\partial t)_0$ by substituting equations (5-352) and (5-353) in (5-324), multiplying (5-324) by $d\kappa$, integrating, and using equation (5-304) (with r = 0). This gives

$$\ell_{\ell m} = \left(\frac{\Gamma\left(7/n_{(\ell m)}\right)}{\Gamma\left(5/n_{\ell m}\right)}\frac{\left[10\overline{(u_\ell u_m)}_0 - \delta_{\ell m}\overline{(u_k u_k)}_0\right]}{10I_{\ell m} - \delta_{\ell m}I_{kk}}\right)^{1/2}, \tag{5-354}$$

where

$$I_{ij} = -\frac{1}{2\nu}\left(\frac{\partial\overline{u_i u_j}}{\partial t}\right)_0 - B_{ijk\ell}\frac{\overline{(u_k u_\ell)}_0}{\nu}\frac{dU_1}{dx_2}, \tag{5-355}$$

and where the nonzero components of $B_{ij\ell}$ are $B_{1112} = 23/49$, $B_{2212} = 16/49$, $B_{3312} = 10/49$, $B_{1211} = 29/490$, $B_{1222} = 68/490$, and $B_{1233} = -1/490$.

The values of the remaining constants of the initial conditions, the $n_{\ell m}$, depend on the shapes of the initial spectra. Since the initial spectra were not measured in the experiments, we determined the $n_{\ell m}$ from the evolution of the $\overline{u_i u_j}$. For the data of references 93 to 95, values for the nonzero $n_{\ell m}$ were obtained as $n_{11} = 3/4$, $n_{22} = 1/2$, $n_{33} = 3/4$, and $n_{12} = 4$.

Equation (5-324) is solved in section 5.4.2.1 for the special initial condition given by equation (5-351). For general initial conditions we obtain, for φ_{11}, φ_{22}, φ_{33} and φ_{12},

$$\varphi_{ij} = H_{ij}\exp\left[-2\nu\kappa^2(t-t_0)\left(1 + a^*_{12}\left(\kappa_1\kappa_2/\kappa^2\right) + \frac{1}{3}a^{*2}_{12}\kappa_1^2/\kappa^2\right)\right], \tag{5-356}$$

where

$$a^*_{12} = (dU_1/dx_2)(t-t_0), \tag{5-357}$$

$$H_{22} = (\varphi_{22})_0 D^2, \tag{5-358}$$

$$H_{12} = D\left[(\varphi_{12})_0 + (\varphi_{22})_0 R\right], \tag{5-359}$$

$$H_{11} = (\varphi_{11})_0 + 2(\varphi_{12})_0 R + (\varphi_{22})_0 R^2, \tag{5-360}$$

$$H_{ii} = (\varphi_{ii})_0 + \frac{2}{\kappa_1/\kappa}\left[(\varphi_{12})_0 E + (\varphi_{22})_0 I\right], \tag{5-361}$$

$$H_{33} = H_{ii} - H_{11} - H_{22}, \tag{5-362}$$

$$D = 1 + 2a_{12}^{*}\kappa_1\kappa_2/\kappa^2 + a_{12}^{*2}\kappa_1^2/\kappa^2, \tag{5-363}$$

$$R = \frac{E}{\kappa_1/\kappa} - \frac{2\kappa_1/\kappa}{D}F, \tag{5-364}$$

$$I = \frac{1}{2}\left[\left(D^2-1\right)\frac{\kappa_1}{\kappa} + \frac{E^2}{\kappa_1/\kappa}\right] - \frac{\kappa_1}{\kappa}\frac{F}{D}\left[E - (D+1)\frac{\kappa_2}{\kappa} - a_{12}^{*}\frac{\kappa_1}{\kappa}\right], \tag{5-365}$$

$$E = -\frac{D}{\left(1-\kappa_2^2/\kappa^2\right)^{1/2}}\tan^{-1}\left(\frac{a_{12}^{*}(\kappa_1/\kappa)\left(1-\kappa_2^2/\kappa^2\right)^{1/2}}{1+a_{12}^{*}\kappa_1\kappa_2/\kappa^2}\right), \tag{5-366}$$

and

$$F = \frac{D}{2\left(1-\kappa_2^2/\kappa^2\right)}\left[\frac{\kappa_2}{\kappa}(D-1) - a_{12}^{*}\frac{\kappa_1}{\kappa} + E\right]. \tag{5-367}$$

The quantity $(\varphi_{ij})_0$ is the value of φ_{ij} at the initial time t_0. In the present study it is obtained from equation (5-352). The correlations $\overline{u_i u_j}$ and $\overline{u_i u_j'}$ are calculated from equation (5-304).

Plots for the evolution of components of $\overline{u_i u_j}$ are shown in figure 5-69. Those evolutions were used to determine the constants in the initial-condition equation (5-352). Values of t for the experiments were calculated as the longitudinal distance divided by the centerline velocity. The agreement of the calculated curves with experiment indicates that the initial condition given by equation (5-352) is evidently general enough for our purposes. Note that the total strain in the experiments of reference 95 is appreciably greater than that in the other experiments. The results near the end of the curve for $\overline{u_2^2}^{1/2}$ in figure 5-69(c) indicate that those results may be partially outside the range of applicability of the analysis, although the accuracy of the experimental results in that region is uncertain.

Once the initial conditions have been determined from equation (5-352) and figure 5-69, one can make a comparison of theory with experiment for several turbulence quantities (figs. 5-70 to 5-72). Evolutions of turbulence macroscales L_i and Taylor microscales λ_i are plotted in figure 5-70. The scales are defined in the usual way as

$$L_i = \int_0^{\infty} \overline{u_1 u_1'}(r_i, 0, 0)\,dr_i / \overline{u_1^2} \tag{5-368}$$

and

$$\lambda_1^2 = -\frac{2\overline{u_1^2}}{\left(\partial^2 \overline{u_1 u_1'}/\partial r_i^2\right)_{r=0}}. \tag{5-369}$$

In figure 5-70 both theory and experiment indicate that the microscale λ_1 increases with time. Similar results were obtained for the other scales. The experimental scale ratios L_2/L_1 and λ_2/λ_1 are close to the values for isotropic turbulence (1/2 and $1/\sqrt{2}$). The theoretical values of L_2/L_1 and λ_2/λ_1 are close to the isotropic values at early times and tend to be, respectively, somewhat higher and lower than those values at later times.

This growth of the turbulence scales with time appears to be a characteristic of unbounded fields of turbulence with or without mean velocity gradients. An exception occurs at short times, when the spectral transfer of energy to larger wavenumbers

causes a decrease of scale (fig. 5-50). The growth of scales, which eventually wins out, is mainly due to the selective annihilation of eddies by viscous action, the smaller eddies being the first to go because of the larger shear stresses between them. If all eddy sizes are present at some time, as they are in equation (5-352), growth will continue indefinitely, so that a steady-state situation for uniform shear flow in which all turbulence quantities are constant with time appears unlikely.

Even if there is an upper limit on the initial eddy size, say the grid spacing, larger eddies may be generated by inertial transfer. Figure 5-73 shows that for the range of values of $(t - t_0)dU_1/dx_2$ of interest here (from 0 to about 2) there is considerable reverse energy transfer to lower wavenumbers (larger eddies) produced by the shear. This is indicated by the positive areas at low wavenumbers in figure 5-73 and may be a reason the experiment in reference 93 sometimes shows scales larger than the turbulence-generator spacing at large distances downstream. Of course, eventually the scale size will be limited by the size of the test section, but when that occurs, the turbulence will no longer be nearly homogeneous.

Two-point correlations. Of particular interest are the two-point velocity correlations in figures 5-71 and 5-72. They indicate that the negative region observed experimentally in the $\overline{u_1 u_1'}(0, 0, r_3)$ correlation, and the absence of such a region in the other correlations, are predicted by the theory. In isotropic turbulence negative values occur, of course, in both the $\overline{u_1 u_1'}(0, r_2, 0)$ and $\overline{u_1 u_1'}(0, 0, r_3)$ correlations as a result of the continuity equation (ref. 4). The confinement of such regions to the $\overline{u_1 u_1'}(0, 0, r_3)$ correlations in figures 5-71 and 5-72 seems to be associated with the turbulent shear flow. This was observed both in the experiments of Champagne et al. (ref. 94) and of Rose (ref. 93). The successful prediction of the two-point velocity correlations, particularly the correct negative and positive regions is somewhat of a triumph of the linearized theory. This, of course, does not mean that the turbulence is linear, but only that the nonlinear effects seem to be overshadowed in the present cases.

Comparison of the curves for $\overline{u_1 u_1'}(0, r_2, 0)$ in figures 5-71 and 5-72 indicates that the shape is nearly the same for the two times shown. Similarly, figure 5-74 shows that the shape of the $\overline{u_1 u_1'}(r_1, 0, 0)$ curve is nearly preserved over a considerable time span. Thus, although the turbulence scales grow with time, the distribution of eddy sizes seems to remain similar as the scales grow. This is somewhat like the final period of decay without shear, where the correlations and spectra remain similar as the turbulence decays and the scales grow (ref. 4, p. 96).

In view of the complexity of the over-all turbulence process, with contributions to the change in turbulence components being produced by turbulence production, by transfer between wavenumbers and directional components, and by dissipation (eq. 5-324), it seems remarkable that the combined effect is to change the turbulence in such a way that the eddy-size distribution remains nearly similar. Of course, one could not expect that this similarity would be preserved indefinitely. The spectra in reference 7 show that for large $(t - t_0)dU_1/dx_2$ the shapes of the spectra change. However, for the values of $(t - t_0)dU_1/dx_2$ in the experiments considered here, while the effects of the shear were great enough to produce a large influence on the turbulence levels (in the absence of shear all components of the turbulence would decrease monotonically, in fig. 5-69), they were not large enough to alter the shapes of the correlation curves appreciably.

Although the results indicate that in most cases a good correspondence exists between theory and experiment, a higher-order theory which retains turbulence self-interaction terms in the equations might give some improvement. However, the small inhomogeneities which, to some extent occur in all of the experiments may have as important an effect as the self-interaction.

5.4.2.3 Heat transfer and temperature fluctuations in a uniformly sheared turbulence.—Turbulent heat transfer and flow in passages and boundary layers are usually analyzed by using a phenomenological approach. That is, assumptions are introduced into the analysis to relate the turbulent shear stress and turbulent heat transfer to the mean flow. Examples of these analyses are given e.g., in sections 4.3.2.6 to 4.3.2.13 and in references 96 to 105. This approach is very useful and makes it possible to generalize large quantities of experimental data. In fact, it appears to be the only feasible way, at present, of analyzing the complex high Reynolds-number flows occurring in boundary layers and passages.

Although the phenomenological analyses are very useful, we can obtain a great deal more insight into the turbulent processes by using a statistical approach based on the equations of motion and energy. This of course, is the approach generally followed in this chapter. These studies should help to put the phenomenological analyses on a sounder basis. Because of the complexity of turbulence it is necessary to limit one's self at least at the beginning, to simple models, when studying it from a fundamental standpoint. Thus, Corrsin (ref. 106) and Dunn and Reid (ref. 107) studied heat transfer in isotropic turbulence with a uniform mean temperature gradient. (The term "isotropic," as usual indicates that the statistical properties of the turbulence are independent of direction.)

Here we extend the analysis of section 5.4.2.1 to include uniform heat transfer and temperature fluctuations (ref. 108). The mean temperature gradient, as well as the shear, is uniform. Locally, the heat transfer and flow in this case are somewhat similar to those in passages and boundary layers if the scales of the turbulence in the flows are reasonably small compared with the scales of the inhomeneities.

The fluid properties are assumed constant, so that the turbulent velocity field is independent of the temperature field. Thus the results for turbulence with a uniform velocity gradient from section 5.4.2.1 can be used for obtaining the turbulent heat transfer and temperature fluctuations. It was shown in section 5.4.2.1 that a homogeneous turbulent field with a uniform velocity gradient

decays with time. Although energy is fed into the turbulence from the mean velocity gradient, the production of turbulence is never great enough to offset the dissipation. The fluctuating temperature field and the turbulent heat transfer will also change with time.

Because of the decay of the turbulence with time it will be necessary to produce it initially by some means, for instance, by passing a stream through a grid. Then various distances downstream from the grid will correspond to various times of decay. Approximately uniform transverse velocity and temperature gradients in the stream could be produced by passing the flow through parallel channels before passing it through the grid. The temperature and velocity of the fluid in each channel would be adjusted to produce the desired velocity and temperature gradients across the stream emerging from the channels. Because of the higher velocities through some parts of the grid it might be necessary to vary the thickness of the wires in the grid to produce an approximately homogeneous turbulence. Heating of the grid would not be necessary because, as will be seen, temperature fluctuations can arise from the interaction of the turbulence and the mean temperature gradient.

As in section 5.4.2.1 the mean gradients are assumed to be large enough, or the turbulence weak enough, for the triple-correlation terms occurring in the analysis to be neglected or at least for those terms to be small enough compared with other terms to give a sensible solution. Thus equations (5-313) to (5-320), with $g_i = 0$ (buoyancy neglected), apply here. As in section 5.4.2.1 the mean velocity is in the x_1-direction, and the mean-velocity gradient is in the x_2-direction. The mean-temperature gradient is also taken to be in the x_2-direction. Then equations (5-313) to (5-320) become

$$\frac{\partial}{\partial t}\varphi_{ij} + \delta_{i1}\varphi_{2j}\frac{dU_1}{dx_2} + \delta_{j1}\varphi_{i2}\frac{dU_1}{dx_2} - \kappa_1\frac{\partial\varphi_{ij}}{\partial\kappa_2}\frac{dU_1}{dx_2} = -\frac{1}{\rho}\left(-i\kappa_i\lambda_j + i\kappa_j\lambda_i'\right) - 2\nu\kappa^2\varphi_{ij}, \tag{5-370}$$

$$\frac{\partial\delta}{\partial t} - \frac{dU_1}{dx_2}\kappa_1\frac{\partial\delta}{\partial\kappa_2} + \frac{dT}{dx_2}\left(\gamma_2 + \gamma_2'\right) = -2\alpha\kappa^2\delta \tag{5-371}$$

$$\frac{\partial\gamma_j}{\partial t} - \frac{dU_1}{dx_2}\kappa_1\frac{\partial\gamma_j}{\partial\kappa_2} + \varphi_{2j}\frac{dT}{dx_2} + \delta_{1j}\gamma_2\frac{dU_1}{dx_2} = -\frac{1}{\rho}i\kappa_j\zeta' - (\alpha+\nu)\kappa^2\gamma_j \tag{5-372}$$

$$\frac{\partial\gamma_i'}{\partial t} - \frac{dU_1}{dx_2}\kappa_1\frac{\partial\gamma_i'}{\partial\kappa_2} + \delta_{i1}\gamma_2'\frac{dU_1}{dx_2} + \varphi_{i2}\frac{dT}{dx_2} = \frac{1}{\rho}i\kappa_i\zeta - (\alpha+\nu)\kappa^2\gamma_i'. \tag{5-373}$$

$$-\frac{1}{\rho}i\kappa_j\lambda_i' = 2\frac{\kappa_1\kappa_j}{\kappa^2}\varphi_{i2}\frac{dU_1}{dx_2}, \tag{5-374}$$

$$\frac{1}{\rho}i\kappa_i\lambda_j = 2\frac{\kappa_1\kappa_i}{\kappa^2}\varphi_{2j}\frac{dU_1}{dx_2}, \tag{5-375}$$

$$\frac{1}{\rho}i\kappa_i\zeta = 2\frac{\kappa_1\kappa_i}{\kappa^2}\gamma_2'\frac{dU_1}{dx_2}, \tag{5-376}$$

and

$$-\frac{1}{\rho}i\kappa_j\zeta' = 2\frac{\kappa_1\kappa_j}{\kappa^2}\gamma_2\frac{dU_1}{dx_2}. \tag{5-377}$$

Substituting equations (5-376) and (5-377) into the right-hand sides of equation (5-373) and (5-372), letting $i = j = 2$, and comparing the resulting equations shows that $\gamma_2 = \gamma_2'$ for all times if they are equal at an initial time. Here it will be assumed that the temperature fluctuations are initially zero, so that the above relation will hold. If

$$\frac{dU_1}{dx_2} \equiv a_{12} \tag{5-378}$$

and

$$\frac{dT}{dx_2} \equiv b_2 \tag{5-379}$$

we finally obtain

$$\frac{\partial \gamma_2}{\partial t} - a_{12}\kappa_1 \frac{\partial \gamma_2}{\partial \kappa_2} = -b_2\varphi_{22} + \left[2a_{12}\frac{\kappa_1\kappa_2}{\kappa^2} - \left(\frac{1}{Pr}+1\right)\nu\kappa^2\right]\gamma_2 \tag{5-380}$$

and

$$\frac{\partial \delta}{\partial t} - a_{12}\kappa_1 \frac{\partial \delta}{\partial \kappa_2} = -2b_2\gamma_2 - 2a\kappa^2\delta, \tag{5-381}$$

where the Prandtl number $Pr = \nu/\alpha$.

In order to obtain solutions of equations (5-380) and (5-381) it will be assumed, as in section 5.4.2.1, that the turbulence is initially isotropic, so that we can use equation (5-333) for the initial φ_{ij}. The turbulence is not, of course, isotropic at later times.

Note that φ_{ij}, according to equations (5-370) and (5-333), is not a function of temperature (those equations do not contain T, δ, γ, or γ_i'). Thus the solution already obtained in section 5.4.2.1 can be used to obtain φ_{22} in equation (5-380):

$$\varphi_{22} = \frac{J_0\left\{\kappa_1^2 + \left[\kappa_2 + a_{12}\kappa_1(t-t_0)\right]^2 + \kappa_3^2\right\}^2\left(\kappa_1^2+\kappa_3^2\right)}{12\pi^2\kappa^4} \exp\left\{-2\nu(t-t_0)\left[\kappa^2 + \frac{1}{3}\kappa_1^2a^2(t-t_0)^2 + a_{12}\kappa_1\kappa_2(t-t_0)\right]\right\}. \tag{5-334}$$

where J_0 and t_0 are constants that depend on initial conditions. For a Prandtl number Pr of 1 the solution of (5-380) is

$$\kappa^2 \exp\left\{2\nu(t-t_0)\left[\kappa^2 + a_{12}\kappa_1\kappa_2(t-t_0) + \frac{1}{3}a_{12}^2\kappa_1^2(t-t_0)^2\right]\right\}\gamma_2 = \frac{J_0\left\{\kappa_1^2 + \left[\kappa_2 + a_{12}(t-t_0)\right]^2 + \kappa_3^2\right\}^2\left(\kappa_1^2+\kappa_3^2\right)^{1/2}}{12\pi^2 a_{12}\kappa_1} \tag{5-382}$$

$$\times\, b_2 \tan^{-1}\frac{\kappa_2}{\left(\kappa_1^2+\kappa_3^2\right)^{1/2}} + f\left[\kappa_1, \kappa_2 + a_{12}\kappa_1(t-t_0), \kappa_3\right]$$

where f is a function of integration. The method of solution is given in reference 79. In order to evaluate f, it is assumed that the temperature fluctuations are zero for $t = t_0$. Thus substituting $\gamma_2 = 0$ for $t = t_0$ in equation (5-382),

$$f(\kappa_1\kappa_2, \kappa_3) = -\frac{J_0\left(\kappa_1^2+\kappa_2^2+\kappa_3^2\right)^2\left(\kappa_1^2+\kappa_3^2\right)^{1/2}}{12\pi^2 a_{12}\kappa_1} b_2 \tan^{-1}\frac{\kappa_2}{\left(\kappa_1^2+\kappa_3^2\right)^{1/2}} \tag{5-383}$$

or

$$f\left[\kappa_1\kappa_2 + a_{12}\kappa_1(t-t_0), \kappa_3\right] = -\frac{J_0\left\{\kappa_1^2 + \left[\kappa_2 + a_{12}\kappa_1(t-t_0)\right]^2 + \kappa_3^2\right\}^2\left(\kappa_1^2+\kappa_3^2\right)^{1/2}}{12\pi^2 a_{12}\kappa_1} b_2 \tan^{-1}\frac{\kappa_2 + a_{12}\kappa_1(t-t_0)}{\left(\kappa_1^2+\kappa_3^2\right)^{1/2}}. \tag{5-384}$$

Substitution of equation (5-384) in (5-382) gives, for the Fourier transform of $\overline{\tau u_2'}$ for a Prandtl number of 1,

$$\gamma_2 = \frac{J_0\left\{\kappa_1^2+\left[\kappa_2+a_{12}\kappa_1(t-t_0)\right]^2+\kappa_3^2\right\}^2\left(\kappa_1^2+\kappa_3^2\right)^{1/2}}{12\pi^2 a_{12}\kappa_1\kappa^2} b_2 \exp\left\{-2\nu(t-t_0)\left[\kappa^2+a_{12}\kappa_1\kappa_2(t-t_0)+\frac{1}{3}a_{12}^2\kappa_1^2(t-t_0)^2\right]\right\} \tag{5-385}$$

$$\times\left[\tan^{-1}\frac{\kappa_2}{\left(\kappa_1^2+\kappa_3^2\right)^{1/2}}-\tan^{-1}\frac{\kappa_2+a_{12}\kappa_1(t-t_0)}{\left(\kappa_1^2+\kappa_3^2\right)^{1/2}}\right]$$

For $Pr \neq 1$, the solution for γ_2 can be written as

$$\gamma_2 = \frac{b_2 J_0\left(\kappa_1^2+\kappa_3^2\right)}{a_{12}\kappa_1\kappa^2\ 12\pi^2}\left\{\kappa_1^2+\left[\kappa_2+a_{12}\kappa_1(t-t_0)\right]^2+\kappa_3^2\right\}^2 \exp\left\{\frac{\left[(1/Pr)-1\right]\nu\kappa_2}{a_{12}\kappa_1}\left(\kappa_1^2+\frac{\kappa_2^2}{3}+\kappa_3^2\right)\right. \tag{5-385a}$$

$$\left.-2\nu(t-t_0)\left[\kappa^2+a_{12}\kappa_1\kappa_2(t-t_0)+\frac{1}{3}a_{12}^2\kappa_1^2(t-t_0)^2\right]\right\}\int_{\kappa_2}^{\kappa_2+a_{12}\kappa_1(t-t_0)}\frac{1}{\kappa_1^2+\xi^2+\kappa_3^2}$$

$$\times\exp\left\{-\left[\frac{\left[(1/Pr)-1\right]\nu}{a_{12}\kappa_1}\xi\left(\kappa_1^2+\frac{\xi^2}{3}+\kappa_3^2\right)\right]\right\}d\xi.$$

The expression for the Fourier transform of $\overline{\tau\tau'}$ for a Prandtl number of 1 is obtained by solution of equation (5-381):

$$\delta = \frac{J_0\left\{\kappa_1^2+\left[\kappa_2+a_{12}\kappa_1(t-t_0)\right]^2+\kappa_3^2\right\}^2 b^2}{12\pi^2 a_{12}^2\kappa_1^2}\exp\left\{-2\nu(t-t_0)\left[\kappa^2+a_{12}\kappa_1\kappa_2(t-t_0)+\frac{1}{3}a_{12}^2\kappa_1^2(t-t_0)^2\right]\right\} \tag{5-386}$$

$$\times\left[\tan^{-1}\frac{\kappa_2}{\left(\kappa_1^2+\kappa_3^2\right)^{1/2}}-\tan^{-1}\frac{\kappa_2+a_{12}\kappa_1(t-t_0)}{\left(\kappa_1^2+\kappa_3^2\right)^{1/2}}\right]^2$$

where δ was set equal to zero for $t = t_0$.

The spectral quantities γ_2 and δ are functions of the components of the wavevector $\boldsymbol{\kappa}$ as well as of its magnitude. It is somewhat easier to interpret quantities that are functions only of the magnitude κ. We can obtain such quantities in the usual way by integrating γ_2 and δ over all directions in wavenumber space. Thus, define a quantity Γ_2 by the equation

$$\Gamma_2(\kappa) = \int_0^A \gamma_2(\boldsymbol{\kappa})\, dA\,(\boldsymbol{\kappa}) \tag{5-387}$$

where A is the area of the surface of a sphere of radius κ. Then, since

$$\overline{\tau u_2} = \int_0^\infty \Gamma_2 d\kappa \tag{5-388}$$

(let $r = 0$ in equation (5-309)), $\Gamma_2\, d\kappa$ gives the contribution from wavenumber band $d\kappa$ to $\overline{\tau u_2}$. Thus a plot of Γ_2 against κ shows how contributions to $\overline{\tau u_2}$ are distributed among the various wavenumbers or eddy sizes.

Equations (5-385) and (5-386) can be written in terms of spherical coordinates by setting

$$\kappa_1 = \kappa \cos\varphi \sin\theta, \qquad \kappa_2 = \kappa \sin\varphi \sin\theta,$$
$$\kappa_3 = \kappa \cos\theta. \tag{5-389}$$

Then equation (5-387) becomes

$$\Gamma_2(\kappa) = \int_0^\pi \int_0^{2\pi} \gamma_2(\kappa, \varphi, \theta) \kappa^2 \sin\theta \, d\varphi \, d\theta. \tag{5-390}$$

A similar equation for δ integrated over all directions in wavenumber space is

$$\Delta(\kappa) = \int_0^\pi \int_0^{2\pi} \delta(\kappa, \varphi, \theta) \kappa^2 \sin\theta \, d\varphi \, d\theta. \tag{5-391}$$

Letting $r = 0$ in equation (5-311)

$$\overline{\tau^2} = \int_0^\infty \Delta \, d\kappa \tag{5-392}$$

so that, as in the case of Γ_2, $\Delta\, d\kappa$ gives contributions from the wavenumber band $d\kappa$ to $\overline{\tau^2}$.

Computed spectra. Spectra of $\overline{\tau u_2}$ and $\overline{\tau^2}$ for various values of dimensionless velocity gradient are plotted in figures 5-75 and 5-76. The integrations in equations (5-390), (5-391), (5-385), and (5-385a) were carried out numerically.

When plotted using the similarity variables shown, the curves for zero velocity gradient do not change with time, so that comparison of the various curves indicates how the velocity gradient will alter the spectrum. Thus the curves in figures 5-75 and 5-76 that lie above those for $a_{12}^* = 0$ indicate that for those cases $\overline{\tau u_2}$ or $\overline{\tau^2}$ at a particular time is greater than it would be for no velocity gradient. The turbulence itself is, of course, decaying with time. Figure 5-75 shows the effect of Prandtl number on the spectrum of $\overline{\tau u_2}$. As Prandtl number increases, the peaks of the spectra move toward the higher wavenumber region, the change being greater at the lower values of a_{12}^*. High wavenumbers correspond to small eddies, inasmuch as the wavenumber represents the reciprocal of an eddy size (or wave length).

For zero velocity gradient the results are the same as those obtained by Dunn and Reid (ref. 107). As the velocity gradient increases, the peaks of the spectra of $\overline{\tau u_2}$ move to lower wavenumbers because the spectrum of the production term $b_2\varphi_{22}$ in equation (5-380) moves to the left (see fig. 5-54). Since the production term in the equation for the spectrum of $\overline{\tau^2}$, equation (5-381), is proportional to γ_2, the peaks of the spectra of $\overline{\tau^2}$ also move to lower wavenumbers.

The spectra change from approximately symmetric curves to curves having more gradual slopes on the high wavenumber sides as a_{12}^* increases. The changes in shape of the spectra are apparently caused by a transfer of activity from low wavenumbers to high wavenumbers or from big eddies to small ones. This transfer is generally associated with triple correlations (ref. 31), but in the present case, where triple correlations are neglected, it is associated with the velocity gradient. Thus we can interpret the second terms in equations (5-380) and (5-381) as transfer terms. In order to do that, note that for our case $r_\ell \partial \overline{u_j'} / \partial r_k$ in equation (5-298) becomes $r_2 \partial \overline{\tau u_2'} / \partial r_1$, which is related to $\kappa_1 \partial \gamma_2 / \partial \kappa_2$ in equation (5-380) by

$$r_2 \frac{\partial \overline{\tau u_2'}}{\partial r_1} = -\int_{-\infty}^{\infty} \kappa_1 \frac{\partial \gamma_2}{\partial \kappa_2} e^{i\boldsymbol{\kappa}\cdot\mathbf{r}} d\boldsymbol{\kappa}. \qquad (5-393)$$

For $r = 0$, this becomes

$$\int_{-\infty}^{\infty} \kappa_1 \frac{\partial \gamma_2}{\partial \kappa_2} d\boldsymbol{\kappa} = 0. \qquad (5-394)$$

Similarly, in equation (5-381)

$$\int_{-\infty}^{\infty} \kappa_1 \frac{\partial \delta}{\partial \kappa_2} d\boldsymbol{\kappa} = 0. \qquad (5-395)$$

So these terms give zero total contribution to $\partial \overline{\tau u_2} / \partial t$ or $\tau_0 \partial \overline{\tau^2} / \partial t$. However, they can alter the distribution in wavenumber space of contributions to $\partial \overline{\tau u_2} / \partial t$ or $\partial \overline{\tau^2} / \partial t$, and thus can be interpreted as transfer terms. A similar term in the equation for $\overline{u_i u_j'}$ was obtained in section 5.4.2.1.

The expressions for the transfer terms in equations (5-380) and (5-381) can be integrated over all directions in wavenumber space by using equations similar to equations (5-390) and (5-391) in order to obtain quantities that are functions only of κ and dU_1/dx_2. A plot of the integrated transfer term corresponding to $\overline{\tau^2}$ is given in dimensionless form for a Prandtl number of 1 in figure 5-77. This term corresponds to the second term in equation (5-381) with the exception that it has not been multiplied by a_{12}. The total area enclosed by each curve is zero, in agreement with equation (5-395). The curves are predominately negative at low wavenumbers and positive at higher ones, so that, in general, contributions to $\overline{\tau^2}$ are transferred from low wavenumbers to high ones. In this way the higher wavenumber portions of the spectra of $\overline{\tau^2}$ in figure 5-76 are excited by the transfer of activity into those regions, so that the shapes of the spectra are altered. This effect is similar to that due to triple correlations (ref. 31). In the present case a natural explanation of the effect is that the transfer to higher wavenumbers is due to the stretching of the vortex lines in the turbulence by the velocity gradient. The velocity gradient should also be able to compress some of the vortex lines, particularly at low velocity gradients where the orientation of the vortex lines would tend to be random. This might explain the small amount of reverse transfer at low wavenumbers and low velocity gradients in figure 5-77.

Production, temperature-fluctuation, and conduction regions. By analogy with the interpretation of the equation for turbulent energy in section 5.4.2.1, one can say that the third term in equation (5-381) produces temperature fluctuations by the action of the mean temperature gradient on the turbulent heat transfer $\overline{\tau u_2}$. In the corresponding production term in the turbulent energy equation the mean velocity gradient does work on the turbulent shear stress. The last term in equation (5-381) is the conduction or dissipation term and tends to destroy the temperature fluctuations by conducting heat away from regions of high local temperature. This action is similar to the action of viscosity on the velocity fluctuations.

The production and conduction terms in equation (5-381) can be integrated over all directions in wavenumber space by substituting Γ_2 and Δ for γ_2 and δ respectively in those terms. These terms, together with the spectrum of $\overline{\tau^2}$ are plotted in normalized form in figures 5-78(a) and (b) for two values of a_{12}^* and a Prandtl number of 1. For the low dimensionless velocity gradient the production, temperature fluctuation, and conduction regions are but slightly separated. On the other hand, for the high velocity gradient ($a_{12}^* = 50$), the production takes place mostly in the low wavenumber or big eddy region and the conductive attenuation occurs in the high wavenumber region. The conductive attenuation occurs mostly in the high wavenumber region because conduction effects tend to "smear out" the small-scale temperature fluctuations more readily than the large ones. Note that the appearance of the curves in figure 5-78 is similar to that of the curves for the turbulent energy in figure 5-62.

One might summarize the history of the temperature fluctuations at high velocity gradients as follows: the temperature fluctuations are produced by the mean temperature gradient mainly in the big eddy region. This temperature-fluctuation activity or "energy" is transferred from the big temperature eddies to smaller ones by the action of the velocity gradient. Finally the temperature "energy" is dissipated by conduction effects in the small eddy region. The separation at high velocity gradients of the three regions shown in figure 5-78(b) is analogous to the separation of the production, energy-containing, and dissipation regions associated with the turbulent energy $\overline{u_i u_i}/2$ (fig. 5-62(b)).

Temperature-velocity correlation coefficient. The temperature-velocity correlation coefficient as introduced by Corrsin (ref. 106), is defined as $\overline{\tau u_2} \Big/ \left(\overline{\tau^2}\,\overline{u_2^2}\right)^{1/2}$. For perfect correlation between τ and u_2, this coefficient will have a value of 1. The

coefficient can be calculated by measuring the areas under the spectrum curves in figures 5-75 and 5-76 and in figure 5-54. A plot of the temperature-velocity correlation coefficient against dimensionless velocity gradient is given for a Prandtl number of 1 in figure 5-79. For zero velocity gradient, perfect correlation between the temperature and velocity fluctuations is indicated. It should be mentioned that this result applies only to a Prandtl number of 1. The Prandtl-number dependence of the coefficient for zero velocity gradient is given by equation (78) of reference 107. As the velocity gradient increases, figure 5-79 indicates that the correlation between the temperature and velocity is partially destroyed. At a value of a_{12}^* of 50 the correlation coefficient has decreased to about 0.5.

Ratio of eddy diffusivities for heat transfer to momentum transfer. The eddy diffusivities for heat transfer and for momentum transfer are defined as

$$\varepsilon_h = -\frac{\overline{\tau u_2}}{dT/dx_2} \tag{5-396}$$

and

$$\varepsilon = -\frac{\overline{u_1 u_2}}{dU_1/dx_2}. \tag{5-397}$$

The eddy diffusivity ratio $\varepsilon_h/\varepsilon$ is of considerable importance in the phenomenological theories of turbulent heat transfer and is usually assumed to be one. In fact that assumption gives the best agreement between analysis and experiment (fig. 4-4), except, possibly at very low Prandtl or Peclet numbers (refs. 109 and 110). A dimensionless eddy diffusivity for heat transfer $\nu^{5/2}(t-t_0)^{3/2}\varepsilon_h/J_0$ can be obtained from the areas under the curves in figure 5-75. A similar dimensionless eddy diffusivity for momentum transfer is given in figure 5-58. The ratio $\varepsilon_h/\varepsilon$ is plotted in figures 5-80 and 5-81. Figure 5-81 is included inasmuch as the eddy diffusivity ratio for $a_{12}^* = 0$ is not given in figure 5-80. This case corresponds to isotropic turbulence and can be calculated from the results in figure 5-58 and reference 107. For small velocity gradients $\varepsilon_h/\varepsilon$ is greater than 1 except for the low Prandtl number. However, as the velocity gradient increases, $\varepsilon_h/\varepsilon$ ultimately decreases and approaches 1 at large velocity gradients. This is shown on a spectral basis in figure 5-82, where the dimensionless spectra of ε_h and ε for a Prandtl number of 1 are compared. As the velocity gradient increases, the spectrum curves of ε_h and ε approach each other rapidly in the high wavenumber or small eddy region and somewhat more slowly in the low wavenumber region.

The approach to 1 of $\varepsilon_h/\varepsilon$ as the velocity gradient increases, occurs at all Prandtl numbers. This can be seen by inspection of equation 5-385a which indicates that for large values of the velocity gradient a_{12}, the effect of Prandtl number on γ_2 and thus on ε_h is negligible. However, the effect of Prandtl number is much greater at low values of Pr than at higher ones. This is because the terms in equation 5-385a which contain Prandtl number vary much more rapidly with low values of that quantity than with high ones.

Figure 5-80 indicates that as the velocity gradient increases, the approach of $\varepsilon_h/\varepsilon$ to 1 is most rapid for Prandtl numbers on the order of one and least rapid for very low Prandtl numbers.

It is of interest to compare the various terms in the differential equations for γ_2/b_2 and φ_{12}/a_{12} at high values of a_{12}. The quantities γ_2/b_2 and φ_{12}/a_{12} will, when integrated over wavenumber space, give ε_h and ε. Equation (5-380) can be written in terms of γ_2/b_2 as

$$\frac{\partial(\gamma_2/b_2)}{\partial t} - a_{12}\kappa_1\frac{\partial(\gamma_2/b_2)}{\partial\kappa_2} = -\varphi_{22} + 2a_{12}\frac{\kappa_1\kappa_2}{\kappa^2}\left(\frac{\gamma_2}{b_2}\right) - \left(\frac{1}{Pr}+1\right)\nu\kappa^2\left(\frac{\gamma_2}{b_2}\right). \tag{5-398}$$

From equation (5-324),

$$\frac{\partial(\varphi_{12}/a_{12})}{\partial t} - a_{12}\kappa_1\frac{\partial(\varphi_{12}/a_{12})}{\partial\kappa_2} = -\varphi_{22} + 2\frac{a_{12}\kappa_1\kappa_2}{\kappa^2}\left(\frac{\varphi_{12}}{a_{12}}\right) + 2\frac{\kappa_1^2}{\kappa^2}\varphi_{22} - 2\nu\kappa^2\left(\frac{\varphi_{12}}{a_{12}}\right). \tag{5-399}$$

These equations for γ_2/b_2 and for φ_{12}/a_{12} are the same except for the last term in equation (5-398) and the last two terms in equation (5-399). It appears, however, from the forms of the equations that these terms should not be important for high values of a_{12}. The next to the last term in equation (5-399) arises from the pressure fluctuations.

Although equations (5-398) and (5-399) are similar for large values of a_{12} the initial conditions for γ_2/b_2 and φ_{12}/a_{12} are different, the initial form for φ_{12} being given by equation (5-333) whereas γ_2 is initially zero. However, a numerical check indicates that γ_2/b_2 and φ_{12}/a_{12} as well as the integrated values ε_h and ε, are essentially equal for large values of a_{12}^*. This suggests that the initial conditions have a negligible effect on the results for large times or velocity gradients.

The calculations in this section are for the case where both the velocity and temperature gradients are in the x_2-direction. Fox (ref. 111) has considered a temperature gradient in an arbitrary direction on a plane normal to the flow direction. He showed that for large values of $(t-t_0)\, dU_1/dx_2$, the thermal eddy diffusivity corresponding to the temperature gradient normal to the velocity gradient can be much larger than that for the temperature gradient in the direction of the velocity gradient. That seems reasonable since $\overline{\tau u_2}$ should be smaller than $\overline{\tau u_3}$ because of the smaller velocity fluctuations in the x_2-direction (see section 5.4.2.1). The results do not support an assumption sometimes made that the radial and circumferential thermal eddy diffusivities in a turbulent tube flow are equal.

It is hard to make comparisons between the present results and a steady-state pipe flow or boundary layer inasmuch as a_{12}^* contains time. However, we can make a rough estimate of the order of magnitude of a_{12}^* for a steady state case as follows. From the turbulent energy spectra in figure 5-56, $\kappa^*_{average} \sim 1$. Then an average length, $1/\kappa_{average} = L$, associated with the turbulence is $[\nu(t-t_0)]^{1/2}$. Let δ be the radius of the pipe or the thickness of the boundary layer and U be a characteristic mean velocity. Letting $t-t_0 \sim L^2/\nu$ (see above), $dU_1/dx_2 \sim U/\delta$, and $L \sim 0.3\delta$, a_{12}^* will be on the order of $0.1\, U\delta/\nu$. Thus for values of mean flow Reynolds numbers usually obtained in the turbulent flows, $\varepsilon_h/\varepsilon$, according to figure 5-80, will probably be close to 1 for gases and liquids. For liquid metals $\varepsilon_h/\varepsilon$ may be less than 1, in qualitative agreement with those analyses which use a modified mixing-length theory to account for heat conduction to or from an eddy as it moves transversely in a mean temperature gradient (refs. 109 and 110). In making the above comparisons, it should of course, be remembered that the present calculations are for an idealized case which has only a partial correspondence to a passage or boundary layer. A discussion of possible differences between the two cases is given in reference 87.

Except for some qualitative discussion in chapter 1 we have not yet considered the effect of buoyancy on turbulence. To do that we will first study a simple (at least conceptually simple) case in which buoyancy effects are present, but mean velocity gradients are absent.

5.4.2.4 Turbulence in the presence of a vertical body force and temperature gradient.—The analysis described here is concerned with the effect of buoyancy forces on a homogeneous turbulent field (ref. 112). The buoyancy effects are produced by a uniform vertical temperature gradient and body force. Equations (5-314) to (5-320) become, for $\partial U_i/\partial x_j = 0$,

$$\frac{\partial \varphi_{ij}}{\partial t} = -\frac{1}{\rho}\left(i\kappa_j\lambda_i' - i\kappa_i\lambda_j\right) - 2\nu\kappa^2\varphi_{ij} - \beta g_j\gamma_j - \beta g_i\gamma_i', \tag{5-400}$$

$$-\frac{1}{\rho}\kappa^2\lambda_j = \beta g_k i\kappa_k\gamma_j, \tag{5-401}$$

$$-\frac{1}{\rho}\kappa^2\lambda_i' = -\beta g_k i\kappa_k\gamma_i', \tag{5-402}$$

$$\frac{\partial \gamma_j}{\partial t} = -\varphi_{kj}\frac{\partial T}{\partial x_k} - \frac{1}{\rho}i\kappa_j\zeta' - (\alpha+\nu)\kappa^2\gamma_j - \beta g_j\,\delta, \tag{5-403}$$

$$\frac{\partial \gamma_i'}{\partial t} = -\varphi_{ik}\frac{\partial T}{\partial x_k} + \frac{1}{\rho}\kappa_i\zeta - (\alpha+\nu)\kappa^2\gamma_i' - \beta g_i\,\delta, \tag{5-404}$$

$$-\frac{1}{\rho}\kappa^2\zeta = \beta g_k i\kappa_k\,\delta, \tag{5-405}$$

$$-\frac{1}{\rho}\kappa^2\zeta' = -\beta g_k i\kappa_k\ \delta, \tag{5-406}$$

and

$$\frac{\partial\delta}{\partial t} = -(\gamma_k' + \gamma_k)\frac{\partial T}{\partial x_k} - 2\alpha\kappa^2\ \delta. \tag{5-407}$$

Equations (5-400) to (5-407) should apply when the terms responsible for buoyancy effects are large enough, or the turbulence weak enough, for the triple correlation terms to be reasonably small compared with other terms in the correlation equations. Substitution of equations (5-401) and (5-402) into (5-400) and equations (5-405) and (5-406) into (5-404) and (5-403) shows that $\varphi_{ij} = \varphi_{ji}$ and $\gamma_i = \gamma_i'$ for all times if they are equal at an initial time. Here it will be assumed that the turbulence is initially isotropic and that the temperature fluctuations are initially zero, so that the above relations will hold. Thus the set of equations (5-400) to (5-407) becomes

$$\frac{\partial\varphi_{ij}}{\partial t} = \beta g_k\frac{\kappa_k\kappa_j}{\kappa^2}\gamma_i + \beta g_k\frac{\kappa_k\kappa_i}{\kappa^2}\gamma_j - 2\nu\kappa^2\varphi_{ij} - \beta g_i\gamma_j - \beta g_i\gamma_i, \tag{5-408}$$

$$\frac{\partial\gamma_j}{\partial t} = -\varphi_{kj}\frac{\partial T}{\partial x_k} + \beta g_k\frac{\kappa_k\kappa_j}{\kappa^2}\delta - (\alpha+\nu)\kappa^2\gamma_j - \beta g_j\ \delta, \tag{5-409}$$

and

$$\frac{\partial\delta}{\partial t} = -2\gamma_k\frac{\partial T}{\partial x_k} - 2\alpha\kappa^2\ \delta. \tag{5-410}$$

Assume that the only nonzero component of $\mathbf{g}$ is in the negative vertical direction, and let

$$g \equiv -g_3. \tag{5-411}$$

Also, assume that the uniform temperature gradient is in the vertical direction, and let

$$b_3 \equiv \partial T / \partial x_3. \tag{5-412}$$

Letting $i = j = 3$ in equations (5-408) to (5-410),

$$\frac{d\varphi_{33}}{dt} = -2\beta g\frac{\kappa_3^2}{\kappa^2}\gamma_3 - 2\nu\kappa^2\varphi_{33} + 2\beta g\gamma_3, \tag{5-413}$$

$$\frac{d\gamma_3}{dt} = -b_3\varphi_{33} - \beta g\frac{\kappa_3^2}{\kappa^2}\delta - (\alpha+\nu)\kappa^2\gamma_3 + \beta g\ \delta, \tag{5-414}$$

and

$$\frac{d\delta}{dt} = -2b_3\gamma_3 - 2\alpha\kappa^2\ \delta. \tag{5-415}$$

Contracting i and j in equation (5-408) gives

$$\frac{d\varphi_{ii}}{dt} = -2\nu\kappa^2\varphi_{ii} + 2\beta g\gamma_3. \tag{5-416}$$

The pressure term (second term in equation (5-413) drops out of equation (5-416) as can be seen from equation (5-296) and the relations $\partial/\partial r_j = -\partial/\partial x_j$ and $\partial/\partial r_i = \partial/\partial x_i'$. Thus, as in the case of homogeneous turbulence without buoyancy effects, the pressure term transfers energy between the directional components of the energy but gives no contribution to the change of energy at a particular wavenumber.

Solution of spectral equations. A general solution of the simultaneous equations (5-413) to (5-415) is

$$\varphi_{33} = C_1 \exp\left[-(\alpha+\nu)\kappa^2(t-t_0)\right] + C_2 \exp\left\{-\left[(\alpha+\nu)\kappa^2 - s\right](t-t_0)\right\}$$
$$+C_3 \exp\left\{-\left[(\alpha+\nu)\kappa^2 + s\right](t-t_0)\right\}, \tag{5-417}$$

$$\gamma_3 = -\Big(C_1(\alpha-\nu)\kappa^2 \exp\left[-(\alpha+\nu)\kappa^2(t-t_0)\right] + C_2\left[(\alpha-\nu)\kappa^2 - s\right]\exp\left\{-\left[(\alpha+\nu)\kappa^2 - s\right](t-t_0)\right\} + C_3\left[(\alpha-\nu)\kappa^2 + s\right]$$
$$\times \exp\left\{-\left[(\alpha+\nu)\kappa^2 + s\right](t-t_0)\right\}\Big) \Big/ \left[2\beta g\left(1-\frac{\kappa_3^2}{\kappa^2}\right)\right], \tag{5-418}$$

and

$$\delta = \left(2C_1 b_3 \beta g\left(1-\frac{\kappa_3^2}{\kappa^2}\right)\exp\left[-(\alpha+\nu)\kappa^2(t-t_0)\right] + C_2\left[(\alpha-\nu)^2\kappa^4 - (\alpha-\nu)\kappa^2 s - 2b_3\beta g\left(1-\frac{\kappa_3^2}{\kappa^2}\right)\right]\right.$$
$$\times \exp\left\{-\left[(\alpha+\nu)\kappa^2 - s\right](t-t_0)\right\} + C_3\left[(\alpha-\nu)^2\kappa^4 + (\alpha-\nu)\kappa^2 s - 2b_3\beta g\left(1-\frac{\kappa_3^2}{\kappa^2}\right)\right] \tag{5-419}$$
$$\left.\times \exp\left\{-\left[(\alpha+\nu)\kappa^2 + s\right](t-t_0)\right\}\right) \Big/ \left[2\beta^2 g^2\left(1-\frac{\kappa_3^2}{\kappa^2}\right)^2\right],$$

where

$$s \equiv \sqrt{(\alpha-\nu)^2\kappa^4 - 4b_3\beta g\left(1-\kappa_3^2/\kappa^2\right)} \tag{5-420}$$

and C_1, C_2, and C_3 are constants of integration.

For determining the constants of integration, we use the initial conditions that, for $t = t_0$, the turbulence is isotropic, and $\gamma_3 = \delta = 0$. The last two conditions correspond to the assumption that the temperature fluctuations are zero at $t = t_0$. This would be true, for instance, if the turbulence were produced by an unheated grid. The mean temperature gradient would then cause temperature fluctuations to arise at subsequent times. The assumption that the turbulence is isotropic at $t = t_0$ implies that for our case

$$\left(\varphi_{ij}\right)_0 = \frac{J_0}{12\pi^2}\left(\kappa^2\delta_{ij} - \kappa_i\kappa_j\right), \tag{5-333}$$

as given in section 5.4.2.1. The turbulence is not, of course, isotropic at subsequent times, as will be seen. By using these initial conditions, the constants of integration are found to be

$$C_1 = -\frac{J_0\kappa^2 b_3\beta g\left(1-\kappa_3^2/\kappa^2\right)^2}{6\pi^2 s^2}, \tag{5-421}$$

$$C_2 = \left(J_0\kappa^2\left(1-\frac{\kappa_3^2}{\kappa^2}\right)\right)\left[(\alpha-\nu)^3\kappa^6+(\alpha-\nu)^2\kappa^4 s-4(\alpha-\nu)\kappa^2 b_3\beta g\left(1-\frac{\kappa_3^2}{\kappa^2}\right)-2b_3\beta g\left(1-\frac{\kappa_3^2}{\kappa^2}\right)s\right]\Big/\left(24\pi^2 s^3\right), \qquad (5-422)$$

and

$$C_3 = -\left(J_0\kappa^2\left(1-\frac{\kappa_3^2}{\kappa^2}\right)\right)\left[(\alpha-\nu)^3\kappa^6-(\alpha-\nu)^2\kappa^4 s-4(\alpha-\nu)\kappa^2 b_3\beta g\left(1-\frac{\kappa_3^2}{\kappa^2}\right)+2b_3\beta g\left(1-\frac{\kappa_3^2}{\kappa^2}\right)s\right]\Big/\left(24\pi^2 s^3\right). \qquad (5-423)$$

For small values of κ, the quantity s, as given by equation (5-420) becomes imaginary. In that case the following solution can be used:

$$\varphi_{33} = \exp\left[-(\alpha+\nu)\kappa^2(t-t_0)\right]\left\{C_1' + C_2'\cos\left[s'(t-t_0)\right] + C_3'\sin\left[s'(t-t_0)\right]\right\}, \qquad (5-424)$$

$$\gamma_3 = -\Big(\exp\left[-(\alpha+\nu)\kappa^2(t-t_0)\right]\Big\{C_1'(\alpha-\nu)\kappa^2 + \left[C_2'(\alpha-\nu)\kappa^2 - C_3's'\right]\cos\left[s'(t-t_0)\right] + \left[C_3'(\alpha-\nu)\kappa^2 + C_2's'\right]\sin\left[s'(t-t_0)\right]\Big\}\Big)\Big/\left[2\beta g\left(1-\frac{\kappa_3^2}{\kappa^2}\right)\right], \qquad (5-425)$$

$$\delta = \Bigg(\exp-\left[(\alpha+\nu)\kappa^2(t-t_0)\right]\Bigg\{2C_1'b_3\beta g\left(1-\frac{\kappa_3^2}{\kappa^2}\right)+\left[C_2'(\alpha-\nu)^2\kappa^4 - C_3's'(\alpha-\nu)\kappa^2 - 2C_2'b_3\beta g\left(1-\frac{\kappa_3^2}{\kappa^2}\right)\right]\cos\left[s'(t-t_0)\right] + \left[C_3'(\alpha-\nu)^2\kappa^4 + C_2's'(\alpha-\nu)\kappa^2 - 2C_3'b_3\beta g\left(1-\frac{\kappa_3^2}{\kappa^2}\right)\right]\sin\left[s'(t-t_0)\right]\Bigg\}\Bigg)\Big/\left[2\beta^2 g^2\left(1-\frac{\kappa_3^2}{\kappa^2}\right)^2\right], \qquad (5-426)$$

where

$$s' \equiv \sqrt{4b_3\beta g\left(1-\frac{\kappa_3^2}{\kappa^2}\right)-(\alpha-\nu)^2\kappa^4}, \qquad (5-427$$

$$C_1' = \left[J_0\kappa^2 b_3\beta g\left(1-\frac{\kappa_3^2}{\kappa^2}\right)^2\right]\Big/\left(6\pi^2 s'^2\right), \qquad (5-428)$$

$$C_2' = J_0\kappa^2\left(1-\frac{\kappa_3^2}{\kappa^2}\right)\left[2b_3\beta g\left(1-\frac{\kappa_3^2}{\kappa^2}\right)-(\alpha-\nu)^2\kappa^4\right]\Big/\left(12\pi s'^2\right), \qquad (5-429)$$

and

$$C_3' = \left[J_0\kappa^4\left(1-\frac{\kappa_3^2}{\kappa^2}\right)(\alpha-\nu)\right]\Big/\left(12\pi^2 s'\right).^{15} \qquad (5-430)$$

[15]We have also analyzed magneto-fluid dynamic turbulence with a uniform imposed magnetic field (Phys. Fluids, vol. 6, no. 9, 1963, pp. 1250–1259). The solutions there are the same as those obtained here if some of the variables represent different quantities.

Finally, solution of equation (5-416) gives

$$\varphi_{ii} = \left[\frac{\varphi_{33}}{1-\left(\frac{\kappa_3^2}{\kappa^2}\right)}\right] + \left(\frac{J_0\kappa^2}{12\pi^2}\right) e^{-2\nu\kappa^2(t-t_0)}. \tag{5-431}$$

Although the quantities φ_{ij}, γ_i, and δ are of interest in themselves, it is somewhat easier to interpret quantities that have been integrated over all directions in wavenumber space as suggested by Batchelor (ref. 4). Thus, a quantity ψ_{ij} can be defined by the equation

$$\psi_{ij}(\kappa) = \int_0^A \varphi_{ij}\, dA, \tag{5-432}$$

where A is the area of a sphere of radius κ. Then, since

$$\overline{u_i u_j} = \int_0^\infty \psi_{ij}\, d\kappa \tag{5-433}$$

(let r = 0 in equation (5-304)), $\psi_{ij}\, d\kappa$ gives the contribution from the wavenumber band $d\kappa$ to $\overline{u_i u_j}$.

The equations for φ_{33}, φ_{ii}, γ_3, and δ can be written in spherical coordinates by using the transformations

$$\kappa_1 = \kappa \cos\varphi \sin\theta,$$
$$\kappa_2 = \kappa \sin\varphi \sin\theta,$$

and

$$\kappa_3 = \kappa \cos\theta.$$

Then, since φ_{33} (as well as φ_{ii}, γ_3, and δ) is not a function of the angle φ, the expression for ψ_{33} from equation (5-432) can be written as

$$\psi_{33} = 4\pi\kappa^2 \int_0^1 \varphi_{33}\, d(\cos\theta). \tag{5-434}$$

We can write similar expressions for φ_{ii}, γ_3, and δ integrated over all directions in wavenumber space:

$$\psi_{ii} = 4\pi\kappa^2 \int_0^1 \varphi_{ii}\, d(\cos\theta), \tag{5-435}$$

$$\Gamma_3 = 4\pi\kappa^2 \int_0^1 \gamma_3\, d(\cos\theta), \tag{5-436}$$

and

$$\Delta = 4\pi\kappa^2 \int_0^1 \delta\, d(\cos\theta). \tag{5-437}$$

Letting r = 0 in equations (5-309) and (5-311),

$$\overline{\tau u_j} = \int_0^\infty \Gamma_j\, d\kappa \tag{5-438}$$

and

$$\overline{\tau^2} = \int_0^\infty \Delta \, d\kappa, \tag{5-439}$$

so that, as in the case of ψ_{ij}, $\Gamma_j \, d\kappa$, and $\Delta \, d\kappa$ give, respectively, contributions from the wavenumber band $d\kappa$ to $\overline{\tau u_j}$ and $\overline{\tau^2}$. Computed spectra of the various turbulent quantities will be considered in the next section.

Effect of buoyancy on the turbulence. Before we consider in detail the spectra computed from the foregoing analysis, it may be worthwhile to indicate physically how the buoyancy forces would be expected to alter the turbulence. Figure 5-83 shows the effects of a negative and a positive vertical temperature gradient with the body force directed downward. For a negative temperature gradient, a turbulent eddy moving upward, for instance, will usually be hotter than the surrounding fluid. If the fluid has a positive temperature-expansion coefficient, the eddy will also be less dense than the surrounding fluid, so that buoyancy forces will tend to accelerate it upward. Similarly, an eddy moving downward will usually be accelerated downward. Thus, the negative temperature gradient tends to feed energy into the turbulent field, so that its effect is destabilizing. For a positive temperature gradient, it can be seen that the effect will be opposite to that just described; that is, the buoyancy forces will tend to stabilize the fluid.

Consider now whether it is possible, according to our analysis, for buoyancy to cause a growth of turbulence at large times. We recall that in section 5.4.2.1 a uniformly sheared turbulence ultimately decays. The energy fed into the turbulence by the mean gradient is less than that dissipated. However, the effect of buoyancy, as analyzed in the present section, is different. Consider equations (5-417) and (5-420). For $(\alpha - \nu)^2 \kappa^4 > 4b_3 \beta g (1 - \kappa_3^2/\kappa^2)$ and $s > (\alpha + \nu)\kappa^2$ the argument of the second exponential in equation (5-417) is positive and increases without limit for large times, and so does φ_{33}. So at least for some regions of wavenumber space, more energy can be fed into the turbulence than is dissipated, and the turbulent energy ultimately grows.

A dimensionless plot of the evolution of the turbulence, as calculated by integrating φ_{ii} over wavenumber space, is presented in figure 5-84. The turbulent energy does indeed grow at large times, for a destabilizing temperature (density) gradient, as predicted in the last paragraph.

Loeffler (ref. 113) has considered the effect of a gradient in electrical charge and an applied electric field on homogeneous turbulence. That problem is analogous to the present one for an infinite Prandtl number. It was determined that the turbulent energy increases without limit as time increases, when the electric field is in the direction of increasing charge density. For large times the turbulent energy was proportional to $(\exp t^{(b)})/(t^{(b)})^3$.[16]

Dimensionless energy spectra (spectra of $\overline{u_i u_i}$) are plotted in figure 5-85. For making the calculations, the indicated integration in equation (5-235) was carried out numerically. When plotted using the similarity variables shown, the spectrum for no buoyancy forces ($g^* = 0$) does not change with time, so that comparison of the various curves indicates how buoyancy effects will alter the spectrum. Thus, if a dimensionless spectrum curve lies above the curve for $g^* = 0$, the turbulent energy for that case is greater than it would be for no buoyancy forces. Curves are shown for Prandtl numbers ν/α of 0.7, 10, and 0.01. These Prandtl numbers correspond, respectively, as far as order of magnitude is concerned, to a gas, a liquid like water, and a liquid metal.

Negative values of the buoyancy parameter g^*, defined as $b_3\beta(t - t_0)^2 g$, correspond to negative temperature gradients, and positive values correspond to positive temperature gradients. (The quantity, b_3 in the definition of g^* is the temperature gradient.) In agreement with the discussion in connection with figure 5-83, the areas under the spectrum curves increase for negative temperature gradients and, in general, decrease for positive ones. A reversal of the expected trend is shown by the curve for a Prandtl number of 10 and a g^* of 4. The action of the buoyancy forces in producing turbulent energy is particularly evident for a Prandtl number of 0.01 and negative values of g^*. There, the buoyancy forces tend to produce an extra peak in the spectra in the low-wavenumber or large-eddy region.

Terms in the spectral energy equation, as well as energy spectra, are plotted in figure 5-86 for cases in which the buoyancy forces augment the turbulence. The curves are normalized to the same height for comparison. The terms for the energy equation were obtained by integrating the terms in equation (5-416) over all directions in wavenumber space by using equations (5-435) and (5-436). The second term in equation (5-416) gives the turbulent dissipation, and the last term gives the effect of buoyancy forces on the turbulence.

Consider first the curves in figure 5-86 for Prandtl numbers less than 1. Those curves indicate that the spectrum of the buoyancy term tends to coincide with the energy spectrum for Prandtl numbers less than 1. That is, the energy from the buoyancy forces feeds into most of the parts of the energy spectrum. On the other hand, the dissipation regions are considerably separated from the energy-containing regions, the separation being greater for the lower Prandtl number. The dissipation regions for the two Prandtl

[16] Loeffler also pointed out that according to the present analysis the turbulence need not decay at large times for destabilizing temperature gradients. The implication in our reference 112 that according to our analysis the turbulence always decays at large times should therefore be disregarded.

numbers are close together, thus indicating that buoyancy forces, which are influenced by Prandtl number, do not greatly influence the dissipation for Prandtl numbers less than 1. The dissipation occurs mostly at high wavenumbers, where the effect of buoyancy forces is not important. The low-wavenumber parts of the energy spectrum, by contrast, are much more affected by buoyancy forces at low Prandtl numbers than at higher ones, because the eddies associated with the temperature-velocity correlations (see equation (5-296)) are much larger at low Prandtl numbers. The spectra of the temperature-velocity correlations will be considered later (see fig. 5-90).

The curves in figure 5-86 for a Prandtl number of 10 indicate that for high Prandtl numbers, in contrast to the case of Prandtl numbers less than 1, the buoyancy forces can act on the small eddies. As a result of this effect, the buoyancy forces alter the dissipation spectrum for high Prandtl-number fluids.

Dimensionless spectra of $\overline{u_3^2}$, which is the component of the turbulent energy in the direction of the temperature gradient and body force, are presented in figure 5-87. The curves are somewhat similar to those for the spectra of $\overline{u_i u_i}$ and exhibit double peaks at the low Prandtl number. However, some of the spectra for $\overline{u_3^2}$ also have double peaks for a Prandtl number of 10. These are apparently caused by the action of the buoyancy forces on the small eddies. Another unexpected result is that the curve for a Prandtl number of 10 and a g^* of 4, although for a case where the buoyancy forces would be expected to be stabilizing, lies above the curve for no buoyancy effects. The physical reason for this result is not clear. It may be that some of the eddies, in this case, oscillate several times before being damped out.

In general, the turbulence is anisotropic. The anisotropy of the turbulence is clearly seen in figure 5-88, where the spectrum curves for $\overline{u_3^2}$ divided by those for $\overline{u_i u_i}/3$ are plotted. For isotropic turbulence all values of $\psi_{33}/(\psi_{ii}/3)$ would be 1, inasmuch as $\psi_{ii}/3$ represents the average spectrum of the components of the energy. For destabilizing conditions $\overline{u_3^2}$ is higher than the average component, whereas for stabilizing conditions it is lower. This is physically reasonable, inasmuch as the buoyancy forces would be expected to act mainly on the vertical components of the velocities of the eddies. In fact, equation (5-408) indicates that the buoyancy terms (last two terms) occur only in the equation for φ_{33} for a vertical body force.

For Prandtl numbers less than 1 the anisotropy is most pronounced in the large-eddy region, so that apparently the buoyancy forces act mostly on the large eddies. In the small-eddy region the curves for Prandtl numbers less than 1 approach 1, so that the turbulence is isotropic in the smallest eddies. Thus, the theory of local isotropy seems to apply here. This observation is in opposition to that for turbulence which is weak and/or for which a uniform mean velocity gradient is large, where local isotropy was absent (section 5.4.2.1). Also, the curves in figure 5-88 for a Prandtl number greater than 1 do not show local isotropy. Thus, local isotropy seems to be obtained only for Prandtl numbers less than 1 in the present analysis. The situation may be different for high turbulence Reynolds numbers and small mean gradients.

It was originally thought that the difference between the results for Prandtl numbers less than and greater than 1 was caused by a difference in the effect of pressure forces in the two cases. A calculation with the pressure-force terms absent, however, indicated that those terms have but a minor effect on the results. It appears that the effect is due to the way the buoyancy forces act in the two cases and that the buoyancy forces can act even on the smaller eddies at high Prandtl numbers. This is in agreement with the curves in figure 5-86.

Spectra of the temperature variance $\overline{\tau^2}$ are plotted in figure 5-89. For $g^* = 0$, the results reduce to those of Dunn and Reid (ref. 107). The trends with g^* are similar to those for the spectra of $\overline{u_i u_i}$; that is, the areas under the curves are larger for negative than for positive temperature gradients. However, the areas under the curves for low Prandtl numbers are much smaller than for the higher ones because, for the same viscosity, the high thermal conductivities associated with lower Prandtl-number fluids tend to smear out the temperature fluctuations. As Prandtl number decreases, the spectra move into the lower wavenumber regions because the conduction effects tend to destroy the small temperature eddies more readily than larger ones.

The last spectra to be considered are those of the temperature-velocity correlations $\overline{\tau u_3}$. These are plotted in dimensionless form in figure 5-90. The quantity $\overline{\tau u_3}$ is proportional to the turbulent heat transfer. The total heat transfer q_3 is the sum of the laminar and turbulent heat transfer; it is given by

$$q_3 = -k\left(\frac{dT}{dx_3}\right) + \rho c_p \overline{\tau u_3},$$

where k is the thermal conductivity and c_p is the specific heat at constant pressure. Inasmuch as the temperature gradient b_3 occurs in the denominator of the dimensionless spectrum function in figure 5-90, those curves can also be considered as the spectra of the eddy diffusivity for heat transfer. The eddy diffusivity for heat transfer ε_h is defined by

$$\varepsilon_h \equiv -\frac{\overline{\tau u_3}}{dT/dx_3}.$$

The spectra indicate that, when the buoyancy forces are destabilizing, the turbulent heat transfer is greater than it would be without buoyancy effects. This is congruous with the effect of buoyancy forces on the turbulent intensity shown in figure 5-85. Similarly, for positive values of g^*, the turbulent heat transfer is less than it would be for no buoyancy forces. However, as g^* continues to increase, the turbulent heat transfer goes to zero and then changes sign. That is, the turbulence begins to transfer heat against the temperature gradient. This is shown somewhat more clearly in figure 5-91, where the temperature-velocity correlation coefficient $\overline{\tau u_3}/[(\overline{\tau^2})^{1/2}(\overline{u_3^2})^{1/2}]$ is plotted against g^*. As g^* increases, the sign of the turbulent heat transfer oscillates. Although these are rather surprising results, turbulence has on occasion been observed to pump heat against a temperature gradient. This occurs, for instance, in a Ranque-Hilsch vortex tube, where expansion and contraction of eddies in a pressure gradient can cause heat to flow against a temperature gradient. The effect observed here, however, appears to be caused by the action of the buoyancy forces on the eddies. In the stabilizing case, the buoyancy forces ordinarily act in the direction opposite to that in which an eddy starts to move (see fig. 5-83), and so the sign of the velocity fluctuation might be changed without necessarily changing the sign of the corresponding temperature fluctuation. Thus, it appears possible that the direction of the turbulent heat transfer could be reversed.

For negative values of g^*, figure 5-91 indicates that nearly perfect correlation between the temperature and velocity fluctuations is approached. This, again, can be explained by the action of the buoyancy forces. Thus, as was mentioned previously, an eddy moving upward in a negative temperature gradient will usually be hotter than the surrounding fluid and so will be pushed upward still more by the buoyancy forces. If an eddy moving upward happens to be cooler than the surrounding fluid, it will be pushed downward. Therefore, positive contributions to $\overline{\tau u_3'}$ are amplified, whereas negative contributions are damped out by the buoyancy forces, so that the net effect is to increase the value of $\overline{\tau u_3'}$ toward 1.

It appears that by using the present method of analysis we can profitably study many of the turbulent processes. It is true that because we neglected triple-correlation terms we were not able to study the transfer of energy between eddies of various sizes, but that is only one of the important processes occurring in turbulence and can be studied separately. For instance, we could, as in section 5.3.2.2, consider three-point correlation equations and neglect fourth-order correlation terms. However, if that were done in the present case, where buoyancy effects are considered, the problem might tend to get out of hand. Alternatively, if a mean velocity gradient as well as a temperature gradient were included, we would obtain a transfer of energy from large to small eddies as in section 5.4.2.1, even though triple correlations were neglected. That will be done in the next section. It appears that the method of analysis followed here gives information about other turbulent processes such as the dissipation and the production or extraction of energy by buoyancy forces. Note, in particular, the solutions obtained for destabilizing buoyancy in which the turbulence does not die out at large times (fig. 5-84).

5.4.2.5 Effects of combined buoyancy and shear on turbulence.—The effects of shear and of buoyancy are considered separately in sections 5.4.2.1 and 5.4.2.4. In real situations, for instance in the atmosphere, the two effects occur simultaneously. The speculative theory given in reference 114 considers that case.

Herein, the methods used in sections 5.4.2.1 and 5.4.2.4 are extended to analyze the combined effects of buoyancy and shear on homogeneous turbulence (ref. 115).[17] We consider the case where the velocity and temperature gradients are in the x_3-direction (vertical) and the body force (gravity) is in the $-x_3$-direction. Then equations (5-313) to (5-320) become

$$\frac{\partial \varphi_{ij}}{\partial t} + \delta_{i1}a_{13}\varphi_{3j} + \delta_{j1}a_{13}\varphi_{i3} - a_{13}\kappa_1\frac{\partial \varphi_{ij}}{\partial \kappa_3} = -\frac{1}{\rho}\left(i\kappa_j\lambda_i' - i\kappa_i\lambda_j\right) - 2\nu\kappa^2\varphi_{ij} + \beta\delta_{i3}g\gamma_j + \beta\delta_{j3}g\gamma_i', \qquad (5-440)$$

$$\frac{\partial \delta}{\partial t} + b_3\gamma_3' + b_3\gamma_3 - a_{13}\kappa_1\frac{\partial \delta}{\partial \kappa_3} = -2\alpha\kappa^2\delta, \qquad (5-441)$$

$$\frac{\partial \gamma_j}{\partial t} + b_3\varphi_{3j} + a_{13}\delta_{1j}\gamma_3 - a_{13}\kappa_1\frac{\partial \gamma_j}{\partial \kappa_3} = -\frac{1}{\rho}i\kappa_j\zeta' - (\alpha+\nu)\kappa^2\gamma_j + \beta g\delta_{j3}\delta, \qquad (5-442)$$

[17] We have applied this analysis to the growth of random vortices to form tornadoes in an unstable atmosphere with vertical shear (see J. Atmos. Sciences, vol. 34, 1977, pp. 1502-1517).

$$\frac{\partial \gamma_i'}{\partial t} + b_3\varphi_{i3} + a_{13}\delta_{i1}\gamma_3' - a_{13}\kappa_1\frac{\partial \gamma_i'}{\partial \kappa_3} = -(\alpha+\nu)\kappa^2\gamma_i' + \frac{1}{\rho}i\kappa_i\zeta + \beta g\delta_{i3}\delta, \tag{5-443}$$

$$-\frac{1}{\rho}\kappa^2\lambda_i' = -2a_{13}i\kappa_1\varphi_{i3} + \beta g i\kappa_3\gamma_i', \tag{5-444}$$

$$-\frac{1}{\rho}\kappa^2\lambda_j = 2a_{13}i\kappa_1\varphi_{3j} - \beta g i\kappa_3\gamma_j, \tag{5-445}$$

$$-\frac{1}{\rho}\kappa^2\zeta = 2a_{13}i\kappa_1\gamma_3' - \beta g i\kappa_3\delta, \tag{5-446}$$

and

$$-\frac{1}{\rho}\kappa^2\zeta' = -2a_{13}i\kappa_1\gamma_3 + \beta g i\kappa_3\delta, \tag{5-447}$$

where, as in earlier sections, $g = -g_3$, $a_{13} = dU_1/dx_3$, b_3 - dT/dx_3, and the spectral quantities are defined by equations (5-304) to (5-311). Substitution of equations (5-444) to (5-447) into equations (5-440) to (5-443) shows that $\varphi_{ij} = \varphi_{ji}$ and $\gamma_i = \gamma_i'$ for all times if they are equal at an initial time. It will be assumed herein that the turbulence is initially isotropic and that the temperature fluctuations are initially isotropic and that the temperature fluctuations are initially zero, so that the above relations will hold. Thus, the set of equations (5-440) to (5-447) becomes

$$\frac{\partial \varphi_{ij}}{\partial t} = a_{13}\kappa_1\frac{\partial \varphi_{ij}}{\partial \kappa_3} - a_{13}\left(\delta_{i1}\varphi_{j3} + \delta_{1j}\varphi_{i3}\right) + 2a_{13}\left(\frac{\kappa_1\kappa_j}{\kappa^2}\varphi_{i3} + \frac{\kappa_i\kappa_1}{\kappa^2}\varphi_{j3}\right)$$

$$+\beta g\gamma_i\left(\delta_{j3} - \frac{\kappa_3\kappa_j}{\kappa^2}\right) + \beta g\gamma_j\left(\delta_{i3} - \frac{\kappa_i\kappa_3}{\kappa^2}\right) - 2\nu\kappa^2\varphi_{ij}, \tag{5-448}$$

$$\frac{\partial \gamma_i}{\partial t} = a_{13}\kappa_1\frac{\partial \gamma_i}{\partial \kappa_3} - b_3\varphi_{i3} + a_{13}\gamma_3\left(2\frac{\kappa_i\kappa_1}{\kappa^2} - \delta_{i1}\right) + \beta g\delta\left(\delta_{i3} - \frac{\kappa_i\kappa_3}{\kappa^2}\right) - (\alpha+\nu)\kappa^2\gamma_i, \tag{5-449}$$

and

$$\frac{\partial \delta}{\partial t} = a_{13}\kappa_1\frac{\partial \delta}{\partial \kappa_3} - 2b_3\gamma_3 - 2\alpha\kappa^2\delta. \tag{5-450}$$

Equations (5-448) to (5-450) give contributions of various processes to the rates of change of spectral components of $\overline{u_iu_j}$, $\overline{\tau u_i}$, and $\overline{\tau^2}$, respectively. The second term in each equation is a transfer term which transfers activity into or out of a spectral component by the stretching or compressing of turbulent vortex filaments by the mean velocity gradient, as discussed in sections 5.1.2.1, 5.4.2.1, and 5.4.2.3. The terms with κ^2 in the denominator are spectral components of pressure-velocity or pressure-temperature correlations and transfer activity between directional components (sections 5.4.2.1 and 5.4.2.3). The terms proportional to βg and δ_{i3} (or δ_{j3}) are buoyancy terms which augment or diminish the activity in a spectral component by buoyant action. The last terms in the equations are dissipation terms, which dissipate activity by viscous effects (eq. 5-448) or by conduction effects (eq. 5-450). The dissipation term in equation (5-449) contains both viscous and conduction effects, inasmuch as it dissipates spectral components of velocity-temperature correlations. The remaining terms in the equations produce activity by velocity or temperature-gradient effects. Although a buoyancy term does not appear in equation (5-450), buoyancy affects δ (or $\overline{\tau^2}$) indirectly through the temperature gradient and γ_3 (or $\overline{\tau u_3}$).

For solving equations (5-448) to (5-450), the turbulence is assumed to be initially isotropic at $t = t_0$. That condition is again given by equation (5-333):

$$\left(\varphi_{ij}\right)_0 = \frac{J_0}{12\pi^2}\left(\kappa^2\delta_{ij} - \kappa_i\kappa_j\right). \tag{5-333}$$

where J_0 is a constant that depends on initial conditions. For the initial conditions of δ and γ_i (at $t = t_0$), it is again assumed that

$$\delta_0 = \left(\gamma_i\right)_0 = 0. \tag{5-451}$$

That is, the turbulence-producing grid is assumed to be unheated, so that the temperature fluctuations are produced by the interactions of the mean temperature gradient with the turbulence.

Solution of spectral equations. In order to reduce the set of partial differential equations, equations (5-448) to (5-450), to ordinary differential equations, the running variables ξ and η are considered, of which at κ_3 and t are particular values such that $\xi = \kappa_3$ when $\eta = t$. If ξ and η are introduced into the set of equations in place of κ_3 and t, the resulting equations will, of course, automatically satisfy the original set. In addition,

$$\xi + a_{13}\kappa_1\left(\eta - \eta_0\right) = \text{constant} \tag{5-452}$$

during integration. Then

$$\left(\frac{\partial}{\partial\xi}\right)_\eta - \frac{1}{a_{13}\kappa_1}\left(\frac{\partial}{\partial\eta}\right)_\xi = \left(\frac{d}{d\xi}\right)_{\xi + a_{13}\kappa_1\eta} \tag{5-453}$$

where the subscripts outside the parentheses signify quantities which are held constant. Then equations (5-448) to (5-450) become

$$\frac{d\varphi_{33}(\xi)}{d\xi} = -4\frac{\xi\varphi_{33}}{\kappa_1^2 + \kappa_2^2 + \xi^2} - 2\frac{\beta g}{a_{13}\kappa_1}\left(1 - \frac{\xi^2}{\kappa_1^2 + \kappa_2^2 + \xi^2}\right)\gamma_3 + 2\nu\frac{\kappa_1^2 + \kappa_2^2 + \xi^2}{a_{13}\kappa_1}\varphi_{33}, \tag{5-454}$$

$$\frac{d\gamma_3(\xi)}{d\xi} = \frac{b_3}{a_{13}\kappa_1}\varphi_{33} - 2\frac{\xi\gamma_3}{\kappa_1^2 + \kappa_2^2 + \xi^2} - \frac{\beta g}{a_{13}\kappa_1}\left(1 - \frac{\xi^2}{\kappa_1^2 + \kappa_2^2 + \xi^2}\right)\delta + \left(\frac{\alpha}{\nu} + 1\right)\nu\frac{\kappa_1^2 + \kappa_2^2 + \xi^2}{a_{13}\kappa_1}\gamma_3, \tag{5-455}$$

$$\frac{d\delta(\xi)}{d\xi} = \frac{2b_3}{a_{13}\kappa_1}\gamma_3 + 2\alpha\frac{\kappa_1^2 + \kappa_2^2 + \xi^2}{a_{13}\kappa_1}\delta, \tag{5-456}$$

$$\frac{d\varphi_{13}(\xi)}{d\xi} = \frac{\varphi_{33}}{\kappa_1} - 2\frac{\left(\xi\varphi_{13} + \kappa_1\varphi_{33}\right)}{\kappa_1^2 + \kappa_2^2 + \xi^2} - \frac{\beta g}{a_{13}\kappa_1}\left(1 - \frac{\xi^2}{\kappa_1^2 + \kappa_2^2 + \xi^2}\right)\gamma_1 + \frac{\beta g}{a_{13}}\frac{\xi\gamma_3}{\kappa_1^2 + \kappa_2^2 + \xi^2} + 2\nu\frac{\kappa_1^2 + \kappa_2^2 + \xi^2}{a_{13}\kappa_1}\varphi_{13}, \tag{5-457}$$

$$\frac{d\varphi_{11}(\xi)}{d\xi} = \frac{2}{\kappa_1}\varphi_{13} - 4\frac{\kappa_1\varphi_{13}}{\kappa_1^2 + \kappa_2^2 + \xi^2} + \frac{2\beta g\xi\gamma_1}{a_{13}\left(\kappa_1^2 + \kappa_2^2 + \xi^2\right)} + 2\nu\frac{\kappa_1^2 + \kappa_2^2 + \xi^2}{a_{13}\kappa_1}\varphi_{11}, \tag{5-458}$$

$$\frac{d\varphi_{ii}(\xi)}{d\xi} = \frac{2}{\kappa_1}\varphi_{13} - \frac{2\beta g\gamma_3}{a_{13}\kappa_1} + 2\nu\frac{\kappa_1^2 + \kappa_2^2 + \xi^2}{a_{13}\kappa_1}\varphi_{ii}, \tag{5-459}$$

and

$$\frac{d\gamma_1(\xi)}{d\xi} = \frac{b_3\varphi_{13}}{a_{13}\kappa_1} - \left(2\frac{\kappa_1}{\kappa_1^2 + \kappa_2^2 + \xi^2} - \frac{1}{\kappa_1}\right)\gamma_3 + \frac{\beta g\xi\delta}{a_{13}\left(\kappa_1^2 + \kappa_2^2 + \xi^2\right)} + \left(\frac{\alpha}{\nu} + 1\right)\nu\frac{\kappa_1^2 + \kappa_2^2 + \xi^2}{a_{13}\kappa_1}\gamma_1. \tag{5-460}$$

Note that the first three of these equations are independent of the remaining ones.

The constant in equation (5-451) subject to initial conditions given by equations (5-333) and (5-451), may be determined by letting $\xi = \xi_0$ when $\eta = \eta_0$, or $\xi_0 = \xi + a_{13}\kappa_1(\eta - \eta_0)$. This equation applies for any value of ξ, and thus

$$\xi_0 = \kappa_3 + a_{13}\kappa_1(t - t_0). \tag{5-461}$$

Equation (5-461) gives the value of ξ at which to start the integration for given values of κ_3, κ_1, a_{13}, and $t - t_0$. The initial conditions, equations (5-333) and (5-451), may be satisfied by letting

$$\left.\begin{aligned}
\varphi_{33}(\xi) &= \frac{J_0}{12\pi^2}\left(\kappa_1^2 + \kappa_2^2\right), \\
\varphi_{13}(\xi) &= -\frac{J_0}{12\pi^2}\kappa_1\xi_0, \\
\varphi_{11}(\xi) &- \frac{J_0}{12\pi^2}\left(\kappa_2^2 + \xi_0^2\right), \\
\varphi_{ii} &= \frac{J_0}{6\pi^2}\left(\kappa_1^2 + \kappa_2^2 + \xi_0^2\right), \\
\text{and} \quad \gamma_i(\xi) &= \delta(\xi) = 0
\end{aligned}\right\} \text{when } \xi = \xi_0.$$

The integration of equations (5-454) to (5-460) then goes from ξ_0 to $\xi = \kappa_3$. Final values of φ_{ij}, γ_i, and δ, for which $\xi = \kappa_3$ and $\eta = t$ are of most interest. The quantity ξ can be considered as a dummy variable of integration.

The following relations are introduced in order to rescale equations (5-454) to (5-460) and convert them to dimensionless form:

$$\nu^{1/2}(t - t_0)^{1/2}\kappa_i \to \kappa_i, \tag{5-462}$$

$$\nu^{1/2}(t - t_0)^{1/2}\xi \to \xi, \tag{5-463}$$

$$\frac{\nu(t - t_0)}{J_0}\varphi_{ij} \to \varphi_{ij}, \tag{5-464}$$

$$\frac{\nu}{J_0 b_3}\gamma_i \to \gamma_i, \tag{5-465}$$

$$\frac{\nu\delta}{J_0 b_3^2(t - t_0)} \to \delta, \tag{5-466}$$

$$(t - t_0)a_{13} \to a_{13}, \tag{5-467}$$

$$\frac{\beta g b_3}{a_{13}^2} \to \mathrm{Ri}, \tag{5-468}$$

and

$$\frac{\nu}{\alpha} \rightarrow \mathrm{Pr}, \tag{5-469}$$

where the arrow $\rightarrow$ means "becomes". In addition, spherical coordinates are introduced into the equations by using the transformations

$$\left.\begin{aligned} \kappa_1 &= \kappa\cos\varphi\sin\theta, \\ \kappa_2 &= \kappa\sin\varphi\sin\theta, \\ \kappa_3 &= \kappa\cos\theta. \end{aligned}\right\} \tag{5-470}$$

Equations (5-454) to (5-460) then become

$$\frac{d\varphi_{33}(\xi)}{d\xi} = -4\frac{\xi\varphi_{33}}{\kappa^2\sin^2\theta+\xi^2} - 2\frac{a_{13}\mathrm{Ri}}{\kappa\cos\varphi\sin\theta}\left(1-\frac{\xi^2}{\kappa^2\sin^2\theta+\xi^2}\right)\gamma_3 + 2\frac{\kappa^2\sin^2\theta+\xi^2}{a_{13}\kappa\cos\varphi\sin\theta}\varphi_{33}, \tag{5-471}$$

$$\frac{d\gamma_3(\xi)}{d\xi} = 4\frac{\varphi_{33}}{a_{13}\kappa\cos\varphi\sin\theta} - \frac{2\xi\gamma_3}{\kappa^2\sin^2\theta+\xi^2} - \frac{a_{13}\mathrm{Ri}\delta}{\kappa\cos\varphi\sin\theta}\left(1-\frac{\xi^2}{\kappa^2\sin^2\theta+\xi^2}\right) + \left(\frac{1}{\mathrm{Pr}}+1\right)\frac{\kappa^2\sin^2\theta+\xi^2}{a_{13}\kappa\cos\varphi\sin\theta}\gamma_3, \tag{5-472}$$

$$\frac{d\delta(\xi)}{d\xi} = \frac{2\gamma_3}{a_{13}\kappa\cos\varphi\sin\theta} + \frac{2}{\mathrm{Pr}}\frac{\kappa^2\sin^2\theta+\xi^2}{a_{13}\kappa\cos\varphi\sin\theta}\delta, \tag{5-473}$$

$$\frac{d\varphi_{13}(\xi)}{d\xi} = \frac{\varphi_{33}}{\kappa\cos\varphi\sin\theta} - 2\frac{\xi\varphi_{13}+\kappa(\cos\varphi\sin\theta)\varphi_{33}}{\kappa^2\sin^2\theta+\xi^2} - \frac{a_{13}\mathrm{Ri}\gamma_1}{\kappa\cos\varphi\sin\theta}\left(1-\frac{\xi^2}{\kappa^2\sin^2\theta+\xi^2}\right)$$

$$+\frac{a_{13}\mathrm{Ri}\xi\gamma_3}{\kappa^2\sin^2\theta+\xi^2} + 2\frac{\kappa^2\sin^2\theta+\xi^2}{a_{13}\kappa\cos\varphi\sin\theta}\varphi_{13}, \tag{5-474}$$

$$\frac{d\varphi_{ii}(\xi)}{d\xi} = \frac{2\varphi_{13}}{\kappa\cos\varphi\sin\theta} - \frac{4\kappa(\cos\varphi\sin\theta)\varphi_{13}}{\kappa^2\sin^2\theta+\xi^2} + \frac{2a_{13}\mathrm{Ri}\xi\gamma_1}{\kappa^2\sin^2\theta+\xi^2} + 2\frac{\kappa^2\sin^2\theta+\xi^2}{a_{13}\kappa\cos\varphi\sin\theta}\varphi_{11}, \tag{5-475}$$

$$\frac{d\varphi_{11}(\xi)}{d\xi} = \frac{2\varphi_{13}}{\kappa\cos\varphi\sin\theta} - \frac{2a_{13}\mathrm{Ri}\gamma_3}{\kappa\cos\varphi\sin\theta} + 2\frac{\kappa^2\sin^2\theta+\xi^2}{a_{13}\kappa\cos\varphi\sin\theta}\varphi_{ii}, \tag{5-476}$$

$$\frac{d\gamma_1(\xi)}{d\xi} = \frac{\varphi_{13}}{a_{13}\kappa\cos\varphi\sin\theta} + \frac{a_{13}\mathrm{Ri}\xi\delta}{\kappa^2\sin^2\theta+\xi^2} - \left(\frac{2\kappa\cos\varphi\sin\theta}{\kappa^2\sin^2\theta+\xi^2} - \frac{1}{\kappa\cos\varphi\sin\theta}\right)\gamma_3 + \left(\frac{1}{\mathrm{Pr}}+1\right)\frac{\kappa^2\sin^2\theta+\xi^2}{a_{13}\kappa\cos\varphi\sin\theta}\gamma_1, \tag{5-477}$$

For integrating these equations, ξ starts at

$$\xi_0 = \kappa\cos\theta + a_{13}\kappa\cos\varphi\sin\theta,$$

where

$$\varphi_{33}(\xi) = \left(\frac{1}{12\pi^2}\right)\kappa^2 \sin^2\theta,$$

$$\varphi_{13}(\xi) = -\left(\frac{1}{12\pi^2}\right)\kappa(\cos\varphi \sin\theta)\xi_0,$$

$$\varphi_{11}(\xi) = \frac{1}{12\pi^2}\left(\kappa^2 \sin^2\varphi \sin^2\theta + \xi_0^2\right),$$

$$\varphi_{ii}(\xi) = \frac{1}{6\pi^2}\left(\kappa^2 \sin^2\theta + \xi_0^2\right),$$

and

$$\gamma_i(\xi) = \delta(\xi) = 0,$$

and goes to $\kappa\cos\theta$, where

$$\varphi_{ij}(\xi) = \varphi_{ij}(\kappa\cos\theta),$$

$$\gamma_i(\xi) = \gamma_i(\kappa\cos\theta),$$

and

$$\delta(\xi) = \delta(\kappa\cos\theta).$$

The integrations were carried out numerically for various fixed values of κ, θ, φa_{13}, Ri, and Pr. Directionally integrated spectrum functions can be obtained from

$$\begin{bmatrix} \Psi_{ij} \\ \Gamma_i \\ \Delta \\ \Lambda_{ij} \\ \Psi_{ij}^* \\ \Lambda_{ij}^* \end{bmatrix} = \int_0^{\pi}\int_0^{2\pi} \begin{bmatrix} \varphi_{ij} \\ \gamma_i \\ \delta \\ \Omega_{ij} \\ \varphi_{ij}^* \\ \Omega_{ij}^* \end{bmatrix} \kappa^2 \sin\theta \, d\varphi \, d\theta \qquad (5-478)$$

In this equation, Ω_{ij} is the vorticity spectrum tensor given by equation (5-345) and is related to φ_{ij} by equation (5-348):

$$\Omega_{ij} = \left(\delta_{ij}\kappa^2 - \kappa_i\kappa_j\right)\varphi_{\ell\ell} - \kappa^2\varphi_{ij}. \qquad (5-348)$$

The starred quantites φ_{ij}^* and Ω_{ij}^* give, respectively, components of φ_{ij} and Ω_{ij} in a coordinate system rotated 45° about the x_2-axis from the x_1-axis toward the x_3-axis. Since φ_{ij} and Ω_{ij} are second-order tensors, components in the rotated system are (see eqs. (2-12) and (5-342), and footnote 14).

$$\begin{bmatrix}\varphi_{11}^{*}\\ \Omega_{11}^{*}\end{bmatrix}=\frac{1}{2}\begin{bmatrix}\varphi_{11}\\ \Omega_{11}\end{bmatrix}+\begin{bmatrix}\varphi_{13}\\ \Omega_{13}\end{bmatrix}+\frac{1}{2}\begin{bmatrix}\varphi_{33}\\ \Omega_{33}\end{bmatrix} \tag{5-479}$$

and

$$\begin{bmatrix}\varphi_{33}^{*}\\ \Omega_{33}^{*}\end{bmatrix}=\frac{1}{2}\begin{bmatrix}\varphi_{11}\\ \Omega_{11}\end{bmatrix}-\begin{bmatrix}\varphi_{13}\\ \Omega_{13}\end{bmatrix}+\frac{1}{2}\begin{bmatrix}\varphi_{33}\\ \Omega_{33}\end{bmatrix}. \tag{5-480}$$

The spectrum functions given by equation (5-478) can be integrated over all wavenumbers to give

$$\begin{bmatrix}\overline{u_iu_j}\\ \overline{\tau u_i}\\ \overline{\tau^2}\\ \overline{\omega_i\omega_j}\\ \overline{(u_iu_j)^*}\\ \overline{(\omega_i\omega_j)^*}\end{bmatrix}=\int_0^\infty\begin{bmatrix}\Psi_{ij}\\ \Gamma_i\\ \Delta\\ \Lambda_{ij}\\ \Psi_{ij}^{*}\\ \Lambda_{ij}^{*}\end{bmatrix}d\kappa, \tag{5-481}$$

where the stars again refer to components in a coordinate system rotated 45°.

All the calculated results given here are for a gas with a Prandtl number of 0.7. Dimensionless energy spectra (spectra of $\overline{u_iu_i}$) and spectra of $\overline{\tau^2}$ are plotted in figures 5-92 and 5-93. The spectra are plotted for several values of $(t-t_0)dU_1/dx_3$ and of $\beta g(t-t_0)^2\,dT/dx_3$. The parameter $\beta g(t-t_0)^2\,dT/dx_3$ rather than the Richardson number $Ri=\beta g(t-t_0)^2\,dT/dx_3/(dU_1/dx_3)^2$ is used here since the use of $\beta g(t-t_0)^2\,dT/dx_3$ and $(t-t_0)dU_1/dx_3$ enables us to consider buoyancy and shear effects separately. (The Richardson number contains both buoyancy and shear effects.) The quantity $\beta g(t-t_0)^2\,dT/dx_3$ is related to Ri and the shear parameter by the equation

$$\beta g(t-t_0)^2\frac{dT}{dx_3}=(t-t_0)\frac{dU_1}{dx_3}Ri \tag{5-482}$$

When plotted by using the similarity variables shown in figures 5-92 and 5-93, the dimensionless spectra for buoyancy and shear parameters of zero do not change with time, and thus comparison of the various curves indicates how buoyancy and shear effects will alter the spectra. Thus, if a dimensionless-spectrum curve lies above the curve for buoyancy and shear parameters of zero, the turbulent activity for that case is greater than it would be for no buoyancy and shear effects.

Positive values of the buoyancy parameter correspond to stabilizing conditions, and negative values correspond to destabilizing conditions. Figures 5-92 and 5-93 show that the trends with buoyancy parameter for a shear parameter of 2 ($a_{13}^{*}=2$) are similar to those in figure 5-85 for no shear. That is, in the destabilizing case, buoyancy forces tend to feed energy or activity into the turbulent field, whereas in the stabilizing case they tend to extract it. Comparison of the curves with shear (solid curves) with those without shear (dashed curves) for values of buoyancy parameter of –4, 0, and 4 indicates that for all three cases the effect of the shear is to feed energy or activity into the turbulent field. Thus for the destabilizing case, the buoyancy and shear have similar effects; but for the stabilizing case, they have opposite effects. Comparison of the curve in figure 5-92 for a dimensionless g of 4 and a shear parameter of 2 with that for those parameters = 0 indicates that for the former curve the energy added by the shear effects approximately balances that extracted by buoyancy but that the wavenumber distributions for the two processes are slightly different.

As the shear parameter increases, the spectra become asymmetric, the slopes on the high-wavenumber sides of the curves becoming more gradual. The dot-dashed curves for a shear parameter of 4 and a buoyancy parameter of 1.6 are plotted to show this effect. As in figures 5-56 and 5-76 the effect is due to the transfer of energy or activity into the high-wavenumber regions by the transfer term associated with the mean velocity gradient (see the discussion in the paragraph following eq. (5-450)).

The buoyancy forces might be expected to act more strongly on the turbulent-velocity components lying in the direction of those forces than on the other components. This expectation is confirmed in the plot of $\overline{u_3^2}/\overline{u_1^2}$ for no shear in figure 5-94. The

ratio $\overline{u_2^2}/\overline{u_1^2}$ is greater than 1 in the destabilizing case and less than 1 in the stabilizing case. However, although $\overline{u_3^2}/\overline{u_1^2}$ becomes small, it does not approach zero for highly stable conditions. Apparently $\overline{u_1^2}$ begins to decrease as rapidly as, or more rapidly than $\overline{u_3^2}$, as the buoyancy becomes large.

The vorticity component ratio $\overline{\omega_3^2}/\overline{\omega_1^2}$ is also plotted in figure 5-94. The trends for $\overline{\omega_3^2}/\overline{\omega_1^2}$ are opposite to those for $\overline{u_3^2}/\overline{u_1^2}$. For the stabilizing case, the vorticity tends to be aligned in the direction of the buoyancy forces. The turbulent velocities associated with that vorticity will then tend to be normal to the buoyancy forces, in agreement with the curve for $\overline{u_3^2}/\overline{u_1^2}$. For the destabilizing case, the vorticity tends to lie in directions normal to the buoyancy forces. That will tend to increase $\overline{u_3^2}/\overline{u_1^2}$ as shown in figure 5-94, although the ratio will not approach infinity, because even if all the vorticity lies in directions normal to the buoyancy forces, $\overline{u_1^2}$ or $\overline{u_2^2}$ will not be zero.

In the preceding discussion, the effects of buoyancy forces on the turbulence components without mean shear were considered. Next, consider the case of shear with no buoyancy effects. In that case, the turbulent vorticity (or vortex filaments) would be expected to tend to align in the direction of maximum strain, which is at 45° to the mean velocity. Figure 5-95 shows turbulent vorticity and velocity components ratios in a coordinate system rotated 45° counter clockwise about the x_2-axis. If the vorticity were all aligned in the direction of maximum strain, $\overline{\omega_3^{2*}}/\overline{\omega_1^{2*}}$ would be zero. The curve shows that there is a strong tendency for that alignment to occur at moderate values of shear parameter, but the degree of alignment does not continue to improve as the shear becomes large. The tendency for the vortex filaments to align in the direction of maximum strain is reflected in the trend for the turbulent velocity components to become maximum in a direction normal to the maximum strain, as shown in the curve for $\overline{u_3^{2*}}/\overline{u_1^{2*}}$. The degree of alignment, however, does not continue to improve as the shear becomes large.

Combined effects of buoyancy and shear on $\overline{u_3^2}/\overline{u_1^2}$ are shown in figure 5-96. The curves show that for no buoyancy effects the turbulence component $\overline{u_3^2}$, which is in the direction of the mean velocity gradient, is reduced in comparison with $\overline{u_1^2}$ by the shear. This trend also occurs for negative (destabilizing) values of dimensionless g and for small positive (stabilizing) values of dimensionless g. For more strongly stabilizing conditions, the trends become more complex, and the curves cross over one another.

The effects of buoyancy and shear are considered separately in figure 5-96, which utilizes dimensionless g and the shear parameter. Since the Richardson number contains both buoyancy and shear effects, one might suppose that its use would reduce or eliminate the need for another parameter. Figure 5-97 shows that is not the case, since $\overline{u_3^2}/\overline{u_1^2}$ is a strong function of both Richardson number and shear parameter.

The ratio of two turbulence components which are normal to the body forces and mean velocity gradient plotted as a function of dimensionless g and the shear parameter are shown in figure 5-98. For no shear $\overline{u_2^2}/\overline{u_1^2}$ is 1 since the turbulence is axially symmetric. For a shear parameter ≠0, the shear tends to destroy the axial symmetry and to reduce $\overline{u_2^2}/\overline{u_1^2}$ below 1.

Consider next the turbulent heat transfer and the turbulent shear stress. Temperature-velocity correlation coefficients $-\overline{\tau u_3}\Big/\left[\left(\overline{\tau^2}\right)^{1/2}\left(\overline{u_3^2}\right)^{1/2}\right]$ are plotted in figure 5-99. The correlation $\overline{\tau u_3}$ is proportional to the turbulent heat transfer in the direction of the temperature gradient. The unusual feature of these results is that $\overline{\tau u_3}$ changes sign as dimensionless g becomes large. That is, for very stable conditions, the turbulence begins to pump heat against the temperature gradient. This phenomenon was also observed in the results in figure 5-91 for a shear parameter of zero. As the shear increases, the value of dimensionless g at which $\overline{\tau u_3}$ changes sign increases.

Velocity-velocity correlation coefficients for shear are plotted in figure 5-100. At small values of dimensionless g, the trends with shear parameter are opposite to those for figure 5-99; the values of $\overline{u_1 u_3}\Big/\left[\left(\overline{u_1^2}\right)^{1/2}\left(\overline{u_3^2}\right)^{1/2}\right]$ are zero for a shear parameter of 0, while the values of $-\overline{\tau u_3}\Big/\left[\left(\overline{\tau^2}\right)^{1/2}\left(\overline{u_3^2}\right)^{1/2}\right]$ are close to 1 for small shear parameter and dimensionless g. As was the case for $\overline{\tau u_3}$, $\overline{u_1 u_3}$ changes sign as g* becomes large. As conditions become strongly stabilizing, the turbulence begins to pump the fluid in such a way as to tend to increase the velocity gradient. Thus, there occurs, for sufficiently large values of dimensionless g, a negative eddy viscosity as well as a negative eddy conductivity. Although a negative eddy conductivity can occur with only buoyancy effects present, the occurrence of a negative eddy viscosity requires combined buoyancy and shear.

A possible explanation for the theoretically observed negative eddy viscosity and conductivity can be given in terms of a modified mixing length theory as illustrated in figure 5-101. Normal turbulent heat transfer or shear stress is shown in the left

portion of the figure. An eddy originating at the mean velocity and temperature of the fluid at a point may move either upward or downward. By conduction and viscous effects, it will tend to acquire the local mean temperature and velocity of the fluid as it moves, and thus its path will curve toward the mean velocity or temperature line. When the eddy mixes with the fluid, it will tend to decrease the mean temperature and velocity gradients. The effective eddy conductivity and viscosity will be positive since they act in the same direction as the molecular conductivity and viscosity.

By contrast, for the abnormal case where the buoyancy forces are strongly stabilizing, the original direction of motion of an eddy may be reversed. This reversal might happen because the buoyancy force, in the stabilizing case, acts in the direction opposite to that in which the eddy starts to move. Possible paths for the eddy on the distance-temperature or distance-velocity plane under these conditions are sketched on the right side of figure 5-101. As shown, the eddy path can cross the mean temperature or velocity line. As the eddy mixes with the fluid, it will then tend to increase the mean temperature and velocity gradients, and thus the effective eddy conductivity and viscosity will be negative. The actual mechanism may be more complicated than that considered here. The preceding explanation is given only to show that negative eddy conductivities and viscosities are physically reasonable. The turbulent heat transfer and shear stress do not necessarily change sign at the same value of dimensionless g, since the eddy paths on the distance-temperature plane and on the distance-velocity plane may be different because of differences between the conduction and viscous effects on the eddy as it moves. Comparison of figures 5-99 and 5-100 shows that the turbulent shear stress changes sign first as dimensionless g increases.

The ratio of eddy conductivity to eddy viscosity plotted against dimensionless g is shown in figure 5-102. The eddy conductivity and eddy viscosity are defined by the relations

$$\varepsilon_h = -\frac{\overline{\tau u_3}}{dT/dx_3}$$

$$\varepsilon = -\frac{\overline{u_1 u_3}}{dU_1/dx_3}$$

For small values of shear parameter, $\varepsilon_h/\varepsilon$ decreases with increasing buoyancy parameter except for large buoyancy. For a shear parameter of 4, $\varepsilon_h/\varepsilon$ increases with increasing dimensionless g. The sharp increases in $\varepsilon_h/\varepsilon$ near the ends of the curves occur because the eddy viscosity approaches zero and changes sign near those points.

Values of the correlation coefficient $\overline{\tau u_1}\Big/\left[\left(\overline{\tau^2}\right)^{1/2}\left(\overline{u_1^2}\right)^{1/2}\right]$ are presented in figure 5-103. The correlation $\overline{\tau u_1}$ is proportional to turbulent heat transfer in the x_1-direction. The fact that there should be heat transfer in the x_1-direction is surprising since there is a temperature gradient only in the x_3-direction. It appears, however, that $\overline{\tau u_1}$ can be nonzero because of the nonzero values of $\overline{\tau u_3}$ and $\overline{u_1 u_3}$. Since there is a correlation between τ and u_3 and between u_3 and u_1, the fact that a correlation should occur between τ and u_1 seems reasonable. It must be admitted, though, that heat transfer in a direction of zero temperature gradient runs contrary to normal intuition. It should be noted that the effect is not dependent on the presence of buoyancy forces (i.e., dimensionless g can be zero). The turbulent heat transfer in the x_1-direction is not necessarily small compared with that in the x_3-direction. Figure 5-104, which shows plotted values of $-\overline{\tau u_3}/\overline{\tau u_1}$, indicates that the turbulent heat transfer in the two directions can be of the same order of magnitude, even though the temperature gradient in the x_1-direction is zero.

Comparison of the present analytical results with available experimental data is of interest in order to see if there is a correspondence. Experimental data for grid-generated turbulence in the presence of combined buoyancy and shear are given in reference 116. Unfortunately, it is hard to estimate the values of the shear parameter $(t - t_0)\, dU_1/dx_3$ in the experiments because of uncertainties in the initial and other conditions. A comparison between analysis and data for $\overline{u_3^2}/\overline{u_1^2}$ at station 5 in reference 116 is plotted in figure 5-105. For a shear parameter of 2 the trend with Richardson number for the data appears to correspond with that for the analysis.

Growth due to buoyancy of turbulence with shear. So far we have not considered the question of whether or not, according to our analysis, turbulence with combined buoyancy and shear ultimately decays with time; the dimensionless parameters plotted in figures 5-92 to 5-105 do not provide that information.

Studies of homogeneous turbulence with uniform mean shear for which mean gradients are large enough, or the turbulence weak enough, to neglect terms containing triple correlations are described in section 5.4.2.1 (see figs. 5-54 to 5-68). In the results

obtained there, the turbulent energy ultimately decayed with time. The energy produced by the mean velocity gradient was less than that dissipated. In figures 5-67 and 5-68 where the initial condition was modified to give a finite initial turbulent energy, the energy sometimes increased for a while, but it still ultimately decayed. This behavior was attributed to the fact that while the total energy was increasing, energy was being drained out of the component of the turbulence in the direction of the velocity gradient by the pressure-velocity correlation terms associated with the mean shear. Since there was no turbulence production in that component, it quickly decayed, with the result that the turbulent shear stress, and consequently the turbulence production in all the components, ultimately decreased.

Thus the key to obtaining a nondecaying turbulent shear stress flow appears to lie in keeping the energy from being drained out of the turbulence component in the direction of the mean velocity gradient. In turbulence where the nonlinear terms are important, the distribution of energy among the directional components is evidently accomplished by the pressure-velocity correlations, but in our case those correlations generally tend to make the turbulence more anisotropic. If, however, we superimpose on the shear flow destabilizing buoyancy forces in the direction of the mean velocity gradient, it may be possible to obtain a nondecaying solution for our turbulence. Those buoyancy forces should tend to prevent the turbulence component in the direction of the mean velocity gradient from decaying, as in figure 5-84 where mean shear was absent. It will be shown that although our turbulence with mean shear ultimately decays when buoyancy is absent, the presence of destabilizing buoyancy counteracts the decay, and the turbulence grows at large times (ref. 117).

In this section we use for the initial φ_{ij}, the relation for isotropic turbulence given by equation (5-349):

$$\left(\varphi_{ij}\right)_0 = \frac{J_0}{12\pi^2}\left(\delta_{ij}\kappa^2 - \kappa_i\kappa_j\right)e^{-\kappa^2/\kappa_0^2}, \qquad (5-349)$$

where J_0 is again a constant that depends on initial conditions, and κ_0 is an initial wavenumber that is characteristic of the turbulence. Except for the use of equation (5-349) for $(\varphi_{ij})_0$ in place of equation (5-333), the calculations in this section are done in the same way as those already given for combined shear and buoyancy. The two expressions for $(\varphi_{ij})_0$ differ only by an exponential, and are identical for $\kappa_0 = \infty$. It is, of course, again assumed that δ_0 and $(\gamma_i)_0$ are zero. That is, as before, the turbulence producer (grid) is assumed to be unheated, so that the temperature fluctuations at later times are produced entirely by the interactions of the mean temperature gradient with the turbulence.

The effect of destabilizing buoyancy forces (vertical temperature gradient, negative) on weak homogeneous shear-flow turbulence in a gas is illustrated in figure 5-106. The superscript (a) on $\overline{u_i u_j}^{(a)}$ and $\kappa_0^{(a)}$ indicates that those parameters have been made dimensionless by using quantities related to the shear (in contrast to those related to the buoyancy, which will be used later). Curves are shown for two values of Richardson number Ri and of the initial wavenumber parameter.

The curves indicate that for a Richardson number of 0 (no buoyancy effects) all components of the turbulent energy decrease with time. The turbulent shear stress $-\overline{u_1 u_3}$ also decreases with time, except near the initial time. (At $t^{(a)} = 0$ the turbulence is isotropic and $\overline{u_1 u_3}$ is 0.)

The decay of the components of turbulent energy for no buoyancy effects evidently occurs mainly because there is no production term in the equation for $\overline{u_3 u_3}$ (component in the direction of the mean velocity gradient). This can be seen by letting $i = j = 3$ in equation (5-448), in which case the production term (second term on the right side) drops out. In addition, the pressure-velocity correlation term in equation (5-448) (third term on the right side) tends to drain energy out of the $\overline{u_3^2}$-component, as discussed in section 5.4.2.1. As a result the $\overline{u_3^2}$-component decays rapidly compared with the other components, which have energy fed into them by the mean velocity gradient or by the pressure-velocity correlations (see fig. 5-106). When $\overline{u_3^2}$ decays, the shear component $\overline{u_3 u_1}$ must also decay. There is then no mechanism for maintaining the turbulence since that maintenance apparently takes place as a result of work done on the turbulent shear stress by the velocity gradient (see second term on right side of equation (5-448)). All of the turbulence components must then decay.

By contrast, for $Ri = -1$ (buoyancy forces destabilizing), all components of the turbulent energy decay for a while and then begin to increase without limit as time becomes large. This increase evidently occurs because the vertical buoyancy forces excite the $\overline{u_3^2}$-component of the turbulence and replenish the energy being drained out of it.

It might seem surprising that all components of the turbulence continue to increase with time rather than level off. There are no boundaries on the flow considered here, however, so that the effective Reynolds number and Rayleigh number of the mean flow are infinite. As the scale or mixing length of the turbulence continues to grow, the eddies encounter larger and larger velocity and temperature differences, so that the effective driving forces on the turbulence continue to grow.

Comparison of figures 5-106(a) and (b) shows, as expected that for $\kappa_0^{(a)} = \infty$ (all wavenumbers present), the components of the initial energy are infinite, whereas for $\kappa_0^{(a)} = 1$ they have a finite value. The turbulent shear stress $-\overline{u_3 u_1}$ starts at zero on both plots since the turbulent shear stress for isotropic turbulence is zero. For the case of $\kappa_0^{(a)} = \infty$, however, the value of $-\overline{u_3 u_1}$ jumps to infinity in an infinitely short time and then decreases. For $\kappa_0^{(a)} = 1$, $-\overline{u_3 u_1}$ first increases steadily and then either decreases (Ri = 0) or continues to increase (Ri = −1).

To give an idea of the distribution of the turbulent energy with wavenumber, energy spectra (spectra of $\overline{u_i u_i}$) are plotted in figure 5-107 for $\kappa_0^{(a)} = \infty$ and Ri = 0 and 1. For $t^{(a)} = 0$, ψ_{ii} is proportional to κ^4 (equation (5-349)). As time increases, the spectra move to the small wavenumber regions; that is, the scale of the turbulence grows indefinitely large with time, since the fluid is unbounded.

Thus far we have been considering the effect of buoyancy on a shear-flow turbulence. Next we want to consider the related problem of the effect of imposing a mean shear on turbulence that is buoyancy-controlled. For doing this it is convenient to use the parameters $\overline{u_i^2}^{(b)}$, $t^{(b)}$, $\kappa_0^{(b)}$, $\overline{\tau^2}^{(b)}$, $\overline{\tau u_3}^{(b)}$, which have been made dimensionless by using quantities related to the buoyancy (see fig. 5-108 and 5-109). The parameters used in figures 5-106 and 5-107 were, on the other hand, nondimensionalized by using quantities related to the shear.

The effects of shear on buoyancy-controlled turbulence are illustrated in figures 5-108 and 5-109, where $\overline{u_i^2}^{(b)}$, $\overline{\tau^2}^{(b)}$, and $\overline{\tau u_3}^{(b)}$ are plotted against $t^{(b)}$ for several values of Richardson number and $\kappa_0^{(b)}$. For the case of no shear (Ri = −∞) the results were obtained from the integrated equations in section 5.4.2.4. All components of the turbulent energy, as well as the temperature fluctuations and the temperature-velocity correlations, increase as $t^{(b)}$ becomes large. This occurs even when shear is absent and the turbulence is completely controlled by the destabilizing buoyancy forces (Ri = −∞). Although all turbulent energy components can increase with time when shear is absent, the component in the direction of the buoyancy forces is, in that case, at least an order of magnitude greater than the other components. On the other hand when both buoyancy and shear are present, all components can be of the same order of magnitude.

As the shear increases (as Ri goes from −∞ to −2), the turbulent activity in general increases, at least at the earlier times. The shear does not seem to affect $\overline{\tau^2}^{(b)}$ or $\overline{\tau u_3}^{(b)}$ at the smaller times when $\kappa_0^{(b)} = 1$, however. At larger times, although $\overline{u_1^2}$ and $\overline{u_2^2}$ increase with increasing shear, $\overline{u_3^2}$, $\overline{\tau^2}$, and $\overline{\tau u_3}$ all decrease with increasing shear. These decreases appear to be related to the fact that at large times the presence of the shear causes energy to be drained out of the $\overline{u_3^2}$ component (as discussed earlier), and thus out of $\overline{\tau u_3}$ and $\overline{\tau^2}$ (see eqs. (5-449) and (5-450)).

Summary of results for combined buoyancy and shear. The results for combined effects of vertical buoyancy forces and vertical velocity gradients indicate that, as in the case of no shear, destabilizing buoyancy forces can feed energy or activity into a turbulent field whereas stabilizing buoyancy forces can extract it. The effect of the shear is to feed energy or activity into the turbulent field. Thus for the destabilizing case, the buoyancy and shear have similar effects; but for the stabilizing case, they work in opposite directions.

Energy or activity transfer between wavenumbers by the stretching of turbulent vortex filaments by the mean velocity gradient causes the spectra to become asymmetric; the slopes on the high-wavenumber sides of the spectra become more gradual.

For the destabilizing case, buoyancy forces tend to increase the vertical turbulence component in comparison to the horizontal component in the flow direction while the shear tends to decrease it. For weakly stabilizing conditions both the buoyancy and shear tend to decrease the ratio of vertical to horizontal turbulence components. For more strongly stabilizing conditions, the trends become less well defined.

The shear tends to align the turbulent vorticity in the direction of maximum mean strain, which is 45° from the flow direction. Destabilizing buoyancy forces tend to align the vorticity in horizontal directions whereas stabilizing forces tend to align it vertically.

Some deductions from our analysis appear at first sight to be counter-intuitive. When buoyancy forces are strongly stabilizing, the eddy conductivity and viscosity can be negative. This result appears reasonable when considered from the standpoint of a modified mixing length theory. Also, turbulent heat transfer can occur in a horizontal as well as a vertical direction, even though the velocity and temperature gradients are both vertical. This latter effect is not dependent on the presence of buoyancy forces.

Uniformly sheared turbulence which is weak, or for which the mean velocity gradient is large, ultimately decays with time (see section 5.4.2.1). However, the presence of destabilizing buoyancy forces in the direction of the mean velocity gradient can

prevent that decay. In that case the buoyancy forces replenish the energy being drained out of the component of the turbulence in the direction of the mean velocity gradient by the shearing deformation, and the turbulent energy increases without limit as time increases. Apparently the energy can increase without limit because the effective Reynolds and Rayleigh numbers are infinite in an unbounded fluid. As the scale or mixing length of the turbulence continues to grow, the eddies encounter larger and larger velocity and temperature differences, so that the effective driving forces acting on the turbulence continue to grow.

So far we have not considered the effects of normal strain on turbulence. That will be done in the next sections.

5.4.2.6 Turbulence in an idealized flow through a cone.—When fluid flows axially through a section of a cone, the fluid elements are distorted because of the changing cross sectional area of the flow. If turbulence is initially present, it is modified by this distortion of the fluid. The interaction between turbulence and an idealized distorting mean flow in a cone is studied in this section. Flow in a cone is of particular interest because wind tunnels and rocket nozzles frequently contain conical sections.

The effect of an irrotational distortion (no shear) on turbulence has been studied in references 118 to 121. In those studies the effects of viscosity were neglected and the distortion was assumed to occur so rapidly that the turbulent velocities have a negligible effect on the motion during distortion. The present work is more closely related to that of Pearson (ref. 78). In his work the effects of viscosity are included and the requirement that the distortion be rapid is not imposed. If the distortion is not rapid, however, the turbulence must be weak enough to neglect terms containing triple correlations in comparison to other terms in the equations. Pearson's analysis assumes that the normal velocity gradients are uniform and that the turbulence is homogeneous.

The present analysis of turbulence in incompressible idealized flow through a cone (ref. 122) uses generalized two-point correlation equations that are based on the Navier-Stokes and continuity equations (see equations (4-145) to (4-150)). The normal velocity gradients $\partial U_1/\partial x_1$, $\partial U_2/\partial x_2$, and $\partial U_3/\partial x_3$ are allowed to vary axially but not transversely. The turbulence is assumed to be homogeneous in the transverse direction but only locally homogeneous in the axial direction. That is, the variation in intensity of the turbulence over a correlation (or mixing) length in the axial direction is assumed to be small. The mean axial velocity is assumed uniform over a cross section, and mean shear stresses are assumed absent. The turbulence is initially isotropic but is allowed to become anisotropic under the distorting influence of the mean flow. Components of the turbulent velocity and vorticity variances are calculated, as well as components of the spectra of those quantities. A mean-strain energy-transfer term in the spectral equation which transfers energy components between wavenumbers is also considered. By using the momentum-heat-transfer analogy, the results are related to heat transfer between the fluid and the cone wall.

General two-point correlation equations for turbulence in an incompressible fluid with mean velocity gradients are obtained in section 4.3.4 from the Navier-Stokes and continuity equations as follows:

$$\frac{\partial}{\partial t}\overline{u_i u_j'} + \overline{u_k u_j'}\frac{\partial U_i}{\partial x_k} + \overline{u_i u_k'}\frac{\partial U_j'}{\partial x_k'} + (U_k' - U_k)\frac{\partial}{\partial r_k}\overline{u_i u_j'} + \frac{1}{2}(U_k + U_k')\frac{\partial}{\partial (x_k)_m}\overline{u_i u_j'} + \frac{1}{2}\frac{\partial}{\partial (x_k)_m}\left(\overline{u_i u_j' u_k'} + \overline{u_i u_k u_j'}\right)$$

$$+\frac{\partial}{\partial r_k}\left(\overline{u_i u_j' u_k'} - \overline{u_i u_k u_j'}\right) = -\frac{1}{\rho}\left\{\frac{1}{2}\left[\frac{\partial}{\partial (x_i)_m}\overline{\sigma u_j'} + \frac{\partial}{\partial (x_j)_m}\overline{u_i \sigma'}\right] + \frac{\partial}{\partial r_j}\overline{u_i \sigma'} - \frac{\partial}{\partial r_i}\overline{\sigma u_j'}\right\} + \frac{1}{2}\nu\frac{\partial^2 \overline{u_i u_j'}}{\partial (x_k)_m \partial (x_k)_m} + 2\nu\frac{\partial^2 \overline{u_i u_j'}}{\partial r_k \partial r_k},$$

(5 – 483)

$$\frac{1}{\rho}\left[\frac{1}{4}\frac{\partial^2 \overline{u_i \sigma'}}{\partial (x_j)_m \partial (x_j)_m} + \frac{\partial^2 \overline{u_i \sigma'}}{\partial (x_j)_m \partial r_j} + \frac{\partial^2 \overline{u_i \sigma'}}{\partial r_j \partial r_j}\right] = -2\frac{\partial U_j'}{\partial x_k'}\left[\frac{1}{2}\frac{\partial \overline{u_i u_k'}}{\partial (x_j)_m} + \frac{\partial \overline{u_i u_k'}}{\partial r_j}\right] - \frac{1}{4}\frac{\partial^2 \overline{u_i u_j' u_k'}}{\partial (x_j)_m \partial (x_k)_m} - \frac{1}{2}\frac{\partial^2 \overline{u_i u_j' u_k'}}{\partial (x_j)_m \partial r_k}$$

$$-\frac{1}{2}\frac{\partial^2 \overline{u_i u_j' u_k'}}{\partial (x_k)_m \partial r_j} - \frac{\partial^2 \overline{u_i u_j' u_k'}}{\partial r_j \partial r_k}, \qquad (5-484)$$

and

$$\frac{1}{\rho}\left[\frac{1}{4}\frac{\partial^2\overline{\sigma u_j'}}{\partial(x_i)_m\partial(x_i)_m}-\frac{\partial^2\overline{\sigma u_j'}}{\partial(x_i)_m\partial r_i}+\frac{\partial^2\overline{\sigma u_j'}}{\partial r_i\partial r_i}\right]=-2\frac{\partial U_i}{\partial x_k}\left[\frac{1}{2}\frac{\partial\overline{u_k u_j'}}{\partial(x_i)_m}-\frac{\partial\overline{u_k u_j'}}{\partial r_i}\right]-\frac{1}{4}\frac{\partial^2\overline{u_i u_k u_j'}}{\partial(x_i)_m\partial(x_k)_m}+\frac{1}{2}\frac{\partial^2\overline{u_i u_k u_j'}}{\partial(x_i)_m\partial r_k}$$

$$+\frac{1}{2}\frac{\partial^2\overline{u_i u_k u_j'}}{\partial(x_k)_m\partial r_i}-\frac{\partial^2\overline{u_i u_k u_j'}}{\partial r_i\partial r_k}. \qquad (5-485)$$

The above equations are obtained from those in section 4.3.4, where $0 \le n \le 1$, by setting the constant n equal to 1/2 and replacing the subscript n by m. Then the vector configuration in figure 4-17 becomes that in figure 5-110. The quantities u_i and u_j' are fluctuating velocity components at P and P', U_i and U_j' are mean velocity components, x_i is a space coordinate, t is the time, ρ is the density, v is the kinematic viscosity, and σ is the instantaneous (mechanical) pressure. Bars over terms designate correlations or averaged quantities. The subscripts can take on the values 1, 2, or 3, and a repeated subscript in a term indicates a summation.

For locally homogeneous turbulence the turbulence is considered homogeneous over a correlation length, or the scale of the inhomogeneity is much greater than the scale of the turbulence. Thus, a quantity such as $\partial^2\overline{u_i u_j'}/\partial(x_k)_m\,\partial(x_k)_m$ in equation (5-483) will be negligible compared with $\partial^2\overline{u_i u_j'}/\partial r_k\,\partial r_k$. (A calculation for axially decaying turbulence without mean velocity gradients (ref. 7, fig. 3) shows that this is a good approximation except very close to the virtual origin of the turbulence.) In general, for locally homogenous turbulence,

$$\frac{\partial}{\partial(x_i)_m} \ll \frac{\partial}{\partial r_i}.$$

Also, for that type of turbulence the mean velocity will vary linearly over distances for which correlations are appreciable so that

$$\frac{\partial U_j'}{\partial x_k'}=\frac{\partial U_j}{\partial x_k}=\frac{\partial(U_j)_m}{\partial(x_k)_m},\quad U_k'-U_k=\frac{r_\ell\,\partial(U_k)_m}{\partial(x_\ell)_m},\quad \frac{(U_k+U_k')}{2}=(U_k)_m.$$

Finally, in order to make the set of equations determinate, the turbulence is assumed weak enough to neglect terms containing triple correlations. It should again be noted that, as the turbulence in a flow with large velocity gradients may not have to be as weak as that in a flow without velocity gradients. The terms containing those gradients may be large compared with triple correlation terms, even if the turbulence is moderately strong. Equations (5-483) to (5-485) become, for the steady state at a fixed point,

$$\overline{u_k u_j'}\frac{\partial(U_i)_m}{\partial(x_k)_m}+\overline{u_i u_k'}\frac{\partial(U_j)_m}{\partial(x_k)_m}+\frac{\partial(U_k)_m}{\partial(x_\ell)_m}r_\ell\frac{\partial}{\partial r_k}\overline{u_i u_j'}+(U_k)_m\frac{\partial}{\partial(x_k)_m}\overline{u_i u_j'}=-\frac{1}{\rho}\left(\frac{\partial}{\partial r_j}\overline{u_i\sigma'}-\frac{\partial}{\partial r_i}\overline{\sigma u_j'}\right)+2\nu\frac{\partial^2\overline{u_i u_j'}}{\partial r_k\partial r_k}, \qquad (5-486)$$

$$\frac{1}{\rho}\frac{\partial^2\overline{u_i\sigma'}}{\partial r_j\partial r_j}=-2\frac{\partial(U_j)_m}{\partial(x_k)_m}\frac{\partial\overline{u_i u_k'}}{\partial r_j}, \qquad (5-487)$$

and

$$\frac{1}{\rho}\frac{\partial^2\overline{\sigma u_j'}}{\partial r_i\partial r_i}=2\frac{\partial(U_i)_m}{\partial(x_k)_m}\frac{\partial\overline{u_k u_j'}}{\partial r_i}. \qquad (5-488)$$

Equations (5-486) to (5-488) are the correlation equations for steady-state locally homogeneous turbulence with mean velocity gradients. The equations can be converted to spectral form by using the usual three-dimensional Fourier transforms already defined in equations (5-304) to (5-306):

$$\overline{u_i u_j'}(\mathbf{r}) = \int_{-\infty}^{\infty} \varphi_{ij}(\boldsymbol{\kappa}) e^{i\boldsymbol{\kappa}\cdot\mathbf{r}} d\boldsymbol{\kappa}, \tag{5-304}$$

$$\overline{\sigma u_j'} = \int_{-\infty}^{\infty} \lambda_j e^{i\boldsymbol{\kappa}\cdot\mathbf{r}} d\boldsymbol{\kappa}, \tag{5-305}$$

$$\overline{u_i \sigma'} = \int_{-\infty}^{\infty} \lambda_i' e^{i\boldsymbol{\kappa}\cdot\mathbf{r}} d\boldsymbol{\kappa}, \tag{5-306}$$

where $d\boldsymbol{\kappa} = d\kappa_1\, d\kappa_2\, d\kappa_3$. Then,

$$r_\ell \frac{\partial \overline{u_i u_j'}}{\partial r_k} = \int_{-\infty}^{\infty} -\left(\kappa_k \frac{\partial \varphi_{ij}}{\partial \kappa_\ell} + \delta_{\ell k}\varphi_{ij}\right) e^{i\boldsymbol{\kappa}\cdot\mathbf{r}} d\boldsymbol{\kappa}, \tag{5-489}$$

where $\delta_{\ell k}$ is the Kronecker delta. Equation (5-489) can be obtained by differentiating equation (5-304) with respect to r_k, writing the inverse transform, and then differentiating with respect to κ_ℓ. Taking the Fourier transforms of equations (5-486) to (5-488) results in

$$\varphi_{kj}\frac{\partial (U_i)_m}{\partial (x_k)_m} + \varphi_{ik}\frac{\partial (U_j)_m}{\partial (x_k)_m} - \frac{\partial (U_k)_m}{\partial (x_\ell)_m}\left(\kappa_k \frac{\partial \varphi_{ij}}{\partial \kappa_\ell} + \delta_{\ell k}\varphi_{ij}\right) + (U_k)_m \frac{\partial}{\partial (x_k)_m}\varphi_{ij} = \frac{1}{\rho}\left(i\kappa_j\lambda_i' - i\kappa_i\lambda_j\right) - 2\nu\kappa^2\varphi_{ij}, \tag{5-490}$$

$$-\frac{1}{\rho} i\kappa_j \lambda_i' = 2\frac{\partial (U_\ell)_m}{\partial (x_k)_m}\frac{\kappa_\ell \kappa_j}{\kappa^2}\varphi_{ik}, \tag{5-491}$$

$$\frac{1}{\rho} i\kappa_i \lambda_j = 2\frac{\partial (U_\ell)_m}{\partial (x_k)_m}\frac{\kappa_\ell \kappa_i}{\kappa^2}\varphi_{jk}. \tag{5-492}$$

Combining equations (5-490) to (5-492) and noting that $\delta_{\ell k}\,\partial U_\ell/\partial x_k = \partial U_\ell/\partial x_\ell = 0$ by continuity result in

$$(U_k)_m \frac{\partial}{\partial (x_k)_m}\varphi_{ij} = \frac{\partial (U_\ell)_m}{\partial (x_k)_m}\left[\left(2\frac{\kappa_\ell \kappa_j}{\kappa^2} - \delta_{j\ell}\right)\varphi_{ik} + \left(2\frac{\kappa_\ell \kappa_i}{\kappa^2} - \delta_{i\ell}\right)\varphi_{kj} + \kappa_\ell \frac{\partial \varphi_{ij}}{\partial \kappa_k}\right] - 2\nu\kappa^2\varphi_{ij}. \tag{5-493}$$

Equation (5-493) is the spectral equation for steady-state locally homogeneous turbulence which is weak or for which mean velocity gradients are large.

Consider next the case where the mean strain is irrotational, that is, where the shearing components of the mean velocity gradient are zero. If we let

$$a_{11} \equiv \frac{\partial (U_1)_m}{\partial (x_1)_m}, a_{22} \equiv \frac{\partial (U_2)_m}{\partial (x_2)_m}, a_{33} \equiv \frac{\partial (U_3)_m}{\partial (x_3)_m},$$

Equation (5-493) becomes, for irrotational strain,

$$(U_k)_m \frac{\partial}{\partial(x_k)_m}\varphi_{ij} = a_{(\ell\ell)}\left[\left(2\frac{\kappa_\ell\kappa_j}{\kappa^2}-\delta_{i\ell}\right)\varphi_{j\ell}+\left(2\frac{\kappa_\ell\kappa_j}{\kappa^2}-\delta_{j\ell}\right)\varphi_{\ell i}+\kappa_\ell\frac{\partial\varphi_{ij}}{\partial\kappa_\ell}\right]-2\nu\kappa^2\varphi_{ij}, \qquad (5-494)$$

where $(\ell\ell)$ is not strictly a tensor subscript. For axisymmetric strain at each point in a cross section, as occurs in uniform flow through a cone, $a_{22} = a_{33}$, and by continuity of the mean flow,

$$a_{22} = a_{33} = -\frac{1}{2}a_{11}. \qquad (5-495)$$

The subscript 1 refers to the direction of an axis of symmetry for the turbulence. Since $a_{11} = f(x_1)$, integration of equation (5-495) gives $U_2 = -(1/2)\,a_{11}\,x_2$ and $U_3 = -(1/2)\,a_{11}\,x_3$ or for circular cross section, the radial velocity $U_r = (1/2)\,a_{11}\,r$. In addition, it is assumed that the turbulence is homogeneous over a cross section of the flow and that the turbulence changes only in the axial or x_1 direction, so that

$$(U_k)_m \frac{\partial\varphi_{ij}}{\partial(x_k)_m} = (U_1)_m \frac{\partial\varphi_{ij}}{\partial(x_1)_m}. \qquad (5-496)$$

To simplify the notation, let $(U_1)_m \equiv U$, $(x_1)_m \equiv x$, and $a_{11} \equiv a$ in the remainder of this section. Then for φ_{11} equation (5-494) becomes

$$\frac{U}{a}\frac{\partial\varphi_{11}}{\partial x}-\kappa_1\frac{\partial\varphi_{11}}{\partial\kappa_1}+\frac{1}{2}\kappa_2\frac{\partial\varphi_{11}}{\partial\kappa_2}+\frac{1}{2}\kappa_3\frac{\partial\varphi_{11}}{\partial\kappa_3}=\varphi_{11}\left(6\frac{\kappa_1^2}{\kappa^2}-2-\frac{2\nu}{a}\kappa^2\right), \qquad (5-497)$$

where use was made of the continuity relation in the form $\kappa_2\,\varphi_{12} + \kappa_3\,\varphi_{13} = -\kappa_1\,\varphi_{11}$. Similarly, for φ_{ii},

$$\frac{U}{a}\frac{\partial\varphi_{ii}}{\partial x}-\kappa_1\frac{\partial\varphi_{ii}}{\partial\kappa_1}+\frac{1}{2}\kappa_2\frac{\partial\varphi_{ii}}{\partial\kappa_2}+\frac{1}{2}\kappa_3\frac{\partial\varphi_{ii}}{\partial\kappa_3}=-3\varphi_{11}+\varphi_{ii}-2\frac{\nu}{a}\kappa^2\varphi_{ii}, \qquad (5-498)$$

Next we determine U and a as functions of x for flow through a cone of arbitrary cross section. With the aid of the diagram in figure 5-111 these are obtained as

$$U = U_0\left(1+\frac{x-x_0}{r_0}\tan\alpha\right)^{-2} = \frac{U_0 r_0^2}{X^2\tan^2\alpha}, \qquad (5-499)$$

$$a = -\frac{2U_0\tan\alpha}{r_0}\left(1+\frac{x-x_0}{r_0}\tan\alpha\right)^{-3} = -\frac{2U_0 r_0^2}{X^3\tan^2\alpha}, \qquad (5-500)$$

where

$$X \equiv x - x_0 + \frac{r_0}{\tan\alpha} = -2\frac{U}{a}. \qquad (5-501)$$

Then equations (5-497) and (5-498) become

$$X\frac{\partial\varphi_{11}}{\partial X}+2\kappa_1\frac{\partial\varphi_{11}}{\partial\kappa_1}-\kappa_2\frac{\partial\varphi_{11}}{\partial\kappa_2}-\kappa_3\frac{\partial\varphi_{11}}{\partial\kappa_3}=\left(-12\frac{\kappa_1^2}{\kappa^2}+4-\frac{2\nu\tan^2\alpha}{U_0 r_0^2}X^3\kappa^2\right)\varphi_{11} \qquad (5-502)$$

and

$$X\frac{\partial\varphi_{ii}}{\partial X}+2\kappa_1\frac{\partial\varphi_{ii}}{\partial\kappa_1}-\kappa_2\frac{\partial\varphi_{ii}}{\partial\kappa_2}-\kappa_3\frac{\partial\varphi_{ii}}{\partial\kappa_3}=-2\left(1+\frac{\nu\tan^2\alpha}{U_0r_0^2}X^3\kappa^2\right)\varphi_{ii}+6\varphi_{11}. \tag{5-503}$$

Equations (5-502) and (5-503) apply to either diverging or converging flow through a cone, depending on whether α is positive or negative.

Before equations (5-502) and (5-503) can be solved in an initial value problem, the turbulence must, of course, be specified at an initial position. It is assumed that the turbulence is isotropic at $x = x_0$, the virtual origin of the turbulence (or at $X = X_0 = r_0/\tan\alpha$, by equation (5-501), and that , as in previous sections, $(\varphi_{ij})_0$ is given by equation (5-333):

$$\left(\varphi_{ij}\right)_0=\frac{J_0}{12\pi^2}\left(\kappa^2\delta_{ij}-\kappa_i\kappa_j\right), \tag{5-333}$$

where J_0 is a constant. Equation (5-333) gives results that, at all values of x, reduce to those for isotropic turbulence as the mean strain goes to zero. The use of that initial condition implies that Pearson's parameter $\tau=\nu\kappa_0^2/a$ approaches ∞, where κ_0 is a characteristic initial wavenumber of the turbulence (ref. 78). Thus, the present results should be applicable for large kinematic viscosity, small initial turbulence scale, or small strain rate. The case $\tau\to\infty$ was not considered by Pearson.

Equations (5-502) and (5-503) are first-order partial differential equations in four independent variables and can be solved by methods similar to those given in reference 79. Solutions of these equations in rescaled (dimensionless) form, subject to the initial condition given in equation (5-333), are

$$\varphi_{11}=\frac{1}{12\pi^2}X^6\left(\kappa_2^2+\kappa_3^2\right)\frac{1}{\kappa^4}\left(X^{-6}\kappa_1^2+\kappa_2^2+\kappa_3^2\right)^2e^z \tag{5-504}$$

and

$$\varphi_{ii}=-\frac{\kappa^2}{\kappa_1^2}\varphi_{11}+\frac{1}{12\pi^2}\frac{X^6}{\kappa_1^2}\left(2X^{-6}\kappa_1^2+\kappa_2^2+\kappa_3^2\right)\left(X^{-6}+\kappa_1^2+\kappa_2^2+\kappa_3^2\right)e^z, \tag{5-505}$$

where

$$-2X^2\left[\frac{1}{7}\kappa_1^2\frac{X^7-1}{X^6(X-1)}+\kappa_2^2+\kappa_3^2\right]\to z, \tag{5-506}$$

$$\frac{X}{X_0}=1+\left(x-x_0\right)\frac{\tan\alpha}{r_0}\to X, \tag{5-507}$$

$$\left[\frac{\nu\left(x-x_0\right)}{U_0}\right]^{1/2}\kappa_i\to\kappa_i, \tag{5-508}$$

$$\frac{\left(x-x_0\right)\nu}{J_0U_0}\varphi_{ij}\to\varphi_{ij}, \tag{5-509}$$

and the arrows $\to$ are read "has been replaced by." It is of interest that φ_{11} and φ_{ii} are functions only of $(x-x_0)\tan\alpha/r_0$ and κ_i. Because of axial symmetry it is not necessary to obtain equations for φ_{22} and φ_{33}.

In order to integrate over wavenumber space, it is convenient to introduce spherical coordinates as follows:

$$\kappa_1=\kappa\cos\theta,\quad \kappa_2=\kappa\cos\varphi\sin\theta,\quad \kappa_3=\kappa\sin\varphi\sin\theta. \tag{5-510}$$

Equation (5-304) then becomes, for $r = 0$

$$\overline{u_i u_j} = \int_0^\infty \psi_{ij}\, d\kappa, \tag{5-511}$$

where

$$\psi_{ij} = \int_0^\pi \int_0^{2\pi} \varphi_{ij}\, \kappa^2 \sin\theta\, d\varphi\, d\theta. \tag{5-512}$$

The quantity ψ_{ij} is a function only of the magnitude of the wavenumber κ and represents an energy-spectrum tensor which has been integrated over all directions in wavenumber space.

The velocity variances $\overline{u_1^2}$, $\overline{u_i u_i}$, $\overline{u_2^2}$, and $\overline{u_3^2}$ are calculated from equations (5-504) to (5-512) as

$$\overline{u_1^2} = \frac{1}{24\sqrt{\pi}X^6}\left\{\frac{1}{2^{3/2}X^5\hbar g^{1/2}}\left(\frac{1+X^6-2X^{12}}{\hbar}+\frac{X^{12}}{2f}\right)+\frac{1}{2^{5/2}X^5(1+\hbar)^{1/2}}\left[\frac{2X^6-3X^{12}}{\hbar}+\frac{X^{12}(3+2\hbar)}{1+\hbar}\right]\right.$$

$$\left.+\frac{3\left(1-4X^6+3X^{12}\right)}{4X^4\hbar^2}H+\frac{15\left(1-2X^6+X^{12}\right)}{8X^6\hbar^3}\left(-\sqrt{2}X f^{1/2}+B\right)\right\}, \tag{5-513}$$

$$\overline{u_i u_i} = -\frac{7^{3/2}}{96\sqrt{2\pi}X^2\hbar}(X-1)\left(\frac{X-1}{X^7-1}\right)^{1/2}\left[\frac{2-X^6-X^{12}}{X^7-1}+\frac{3\left(1-X^6\right)^2}{7\hbar X^6(X-1)}\right]+\frac{1}{24\sqrt{\pi}X^6}$$

$$\times\left[\frac{X\left(1+X^6\right)(3+2\hbar)}{2^{5/2}(1+\hbar)^{3/2}}+\frac{1+X^6-2X^{12}}{2^{5/2}X^5\hbar(1+\hbar)^{1/2}}+\frac{3\left(1-X^6\right)^2}{4X^4\hbar^2}H\right], \tag{5-514}$$

$$\overline{u_2^2} = \overline{u_3^2} = \frac{1}{2}\left(\overline{u_i u_i} - \overline{u_1^2}\right), \tag{5-515}$$

where

$$\frac{(x-x_0)^{5/2}\nu^{5/2}}{J_0 U_0^{5/2}}\overline{u_i u_j} \tag{5-516}$$

$$\hbar = \frac{-6X^7+7X^6-1}{7X^6(X-1)}, \tag{5-517}$$

$$f = \frac{X^7-1}{7X^6(X-1)}, \tag{5-518}$$

$$\left.\begin{aligned} H &= \frac{1}{X\sqrt{2\hbar}}\ln\left(\sqrt{\hbar}+\sqrt{\hbar+1}\right) \quad \text{for } \hbar > 0, \\ H &= \frac{1}{X\sqrt{-2\hbar}}\sin^{-1}\sqrt{-\hbar} \qquad \text{for } \hbar < 0, \end{aligned}\right\} \tag{5-519}$$

$$\left.\begin{aligned} B &= \frac{1}{\sqrt{2}}X\sqrt{\hbar+1}+\frac{X}{\sqrt{2\hbar}}\ln\left(\sqrt{\hbar}+\sqrt{\hbar+1}\right) \qquad \text{for } \hbar > 0, \\ B &= \frac{1}{\sqrt{2}}X\sqrt{\hbar+1}+\frac{X}{\sqrt{-2\hbar}}\sin^{-1}\sqrt{-\hbar} \qquad \text{for } \hbar > 0, \end{aligned}\right\} \tag{5-520}$$

where X has been rescaled by using equation (5-507).

An important physical quantity related to the turbulence is the vorticity tensor $\overline{\omega_i\omega_j}$. The vorticity spectrum tensor is given by equation (5-348):

$$\Omega_{ij} = \left(\delta_{ij}\kappa^2 - \kappa_i\kappa_j\right)\varphi_{\ell\ell} - \kappa^2\varphi_{ij}. \tag{5-348}$$

By analogy with equation (5-512) a directionally integrated vorticity spectrum tensor can be defined as

$$\Lambda_{ij} = \int_0^{\pi}\int_0^{2\pi} \Omega_{ij}\kappa^2 \sin\theta \, d\varphi \, d\theta. \tag{5-521}$$

Then the vorticity tensor is given by

$$\overline{\omega_i\omega_j} = \int_0^{\infty} \Lambda_{ij} \, d\kappa. \tag{5-522}$$

One other quantity of considerable interest is the transfer term in equation (5-490),

$$\frac{\partial(U_k)_m}{\partial(x_\ell)_m}\left(\kappa_k\frac{\partial\varphi_{ij}}{\partial\kappa_\ell} + \delta_{\ell k}\varphi_{ij}\right) = \beta_{ij}. \tag{5-523}$$

This term is, of course, nonzero only in the presence of mean strain. The term was previously discussed in section 5.4.2.1 for the case of a shear flow. That it can be interpreted as a transfer term can be seen from equation (5-489), where, if we let $\mathbf{r} = 0$, we get

$$\int_{-\infty}^{\infty}\left(\kappa_k\frac{\partial\varphi_{ij}}{\partial\kappa_\ell} + \delta_{\ell k}\varphi_{ij}\right) d\kappa = 0. \tag{5-524}$$

That is, when the term is integrated over all-wavenumber space it gives zero contribution to the rate of change of $\overline{u_iu_j}$. (The quantity $(U_k)_m\partial\,\overline{u_iu_j}/\partial(x_k)_m$ in equation (5-486) can be interpreted as a rate of change.) The term β_{ij} can, however, transfer energy between wavenumbers. Evidently the transfer takes place by the stretching or compressing of the vortex lines associated with the turbulence

by the mean strain. This transfer is similar to that produced by triple correlations, except that in that case the stretching or compressing of the vortex lines is accomplished by the action of the turbulence on itself, rather than by a mean strain. For the present case of axially symmetric irrotational strain, equation (5-523) becomes, for $i = j = 1$,

$$\beta_{11} = a\left(\kappa_1 \frac{\partial \varphi_{11}}{\partial \kappa_1} - \frac{1}{2}\kappa_2 \frac{\partial \varphi_{11}}{\partial \kappa_2} - \frac{1}{2}\kappa_3 \frac{\partial \varphi_{11}}{\partial \kappa_3}\right), \tag{5-525}$$

where φ_{11} is obtained from equation (5-504). As in the case of φ_{ij} (eq. (5-512)), β_{ij} can be integrated over all directions in wavenumber space to give

$$T_{ij} = \int_0^{\pi} \int_0^{2\pi} \beta_{ij} \kappa^2 \sin\theta \, d\varphi \, d\theta. \tag{5-526}$$

Computed velocity variances, vorticities, and spectra will be discussed next.

Turbulent velocity variances $\overline{u_1^2}$, $\overline{u_2^2}$, and $\overline{u_3^2}$, calculated using equations (5-513) to (5-515), are plotted in dimensionless form in figure 5-112. Also included is the curve obtained by solving equation (5-502) as though the effects of strain were absent by omitting the transfer, pressure and production terms (terms 2 to 6). The resulting equation is

$$\left|\frac{v r_0}{U_0 \tan\alpha}\right|^{5/2} \frac{\overline{u_1^2}}{J_0} = \frac{3}{16\sqrt{2\pi/3}} \left|X^3 - 1\right|^{-5/2}, \tag{5-527}$$

where equation (5-507) is again used to rescale X. Negative values of x', the abscissa, correspond to a converging flow and positive values to a diverging flow. The virtual origin of the turbulence ($x' = 0$) is the point at which the energy of the turbulence would be infinite.

In a converging flow, velocity fluctuations first decrease as one moves from the virtual origin toward the apex of the cone because of viscous dissipation. The distorting influence of the cone causes the longitudinal components to decrease more rapidly and the transverse components to decrease less rapidly than they would without the effects of strain. As the apex of the cone is approached, the longitudinal component continues to decrease rapidly toward zero. The transverse components, on the other hand, begin to increase as the effects of strain become greater than the effects of viscous dissipation. From equation (5-500) it can be seen that the strain rate increases rapidly as the apex is approached. At the apex, where the mean velocity and strain rate approach infinity, the transverse velocity fluctuations would also become infinite. In practice, of course, the tip of the cone must be removed in order to allow flow. It is of interest that this increase in transverse turbulent velocity component with mean velocity or contraction ratio at large velocity ratios was not observed in reference 78, where the velocity gradients were uniform.

For a diverging flow in a cone (positive x') the effects of strain are opposite to those for a converging flow. The longitudinal component decreases less rapidly than it would for no strain. Although the effect of strain is to increase the longitudinal component, that component continues to decrease as x' increases because, as shown in equation (5-500), the strain rate decreases with x'. That is, the effect of viscous decay in this case is greater than the effect of strain.

Trends similar to those shown in figure 5-512 for converging flow have been observed experimentally in references 123 and 124. A comparison between the present analysis and experimental results from reference 123 for a 4-to-1 contraction is given in figure 5-113. The subscript a refers to conditions upstream of the contraction at the point where the mean velocity begins to vary. (It should be noted that the contraction in the experiment was evidently not a true cone). Values of U/U_a at the minimum point for the analytical curves were obtained by assuming that the value of U/U_a at the minimum point in the analytical curve for the transverse component ($i = 2$) corresponds to the value of U/U_a at the minimum point in the experimental curve for the same component. The overall change in the turbulent components produced by the contraction appears to be given reasonably well by the analysis, but the minimum in the experiment for $i = 2$ is sharper than that in the corresponding analytical curve.

To explain the trends shown in figure 5-112, turbulent vorticity variances are plotted in figure 5-114. The dashed curves in the figure, for no effects of strain, were obtained from the equation

$$\left|\frac{v r_0}{U_0 \tan\alpha}\right|^{7/2} \frac{\overline{\omega_1^2}}{J_0} = \frac{45}{64\sqrt{2\pi/3}} \left|X^3 - 1\right|^{-7/2}, \tag{5-528}$$

where, as before, equation (5-507) is used to rescale X. In general, the trends for the vorticity components are opposite to those for the velocities. For a converging flow, the longitudinal vortices are stretched and thus strengthened by the accelerating flow and the transverse vortices are shortened along their axes and are thus weakened. The straining action also tends to turn the axes of the oblique vortices and to align them in the direction of the cone axis. Both of these effects tend to increase the longitudinal vorticity component and decrease the transverse components, as shown in figure 5-114. The opposite trends occur for a diverging flow; the strain in that case tends to decrease the longitudinal vorticity component and to increase the transverse components.

The relation of the vorticity to the fluctuating velocity components for a contracting flow has been pointed out by Prandtl (ref. 118) and Taylor (ref. 119). When the vortex axes lie predominately in the direction of the mean flow, the longitudinal velocity fluctuations are small, whereas the transverse velocity fluctuations can be large. The opposite effects occur for a diverging flow. There is, however, an important difference between the two cases. This is illustrated in figure 5-115, where $\overline{u_1^2}/\overline{u_2^2}$ and $\overline{\omega_1^2}/\overline{\omega_2^2}$ are plotted against U/U_0. (The relation between this abscissa and the one in the preceding plots is given by equation (5-499). Although $\overline{u_1^2}/\overline{u_2^2}$ goes to zero as $\overline{\omega_1^2}/\overline{\omega_2^2}$ goes to infinity for a converging flow, the opposite limits are not approached for a diverging flow; that is, $\overline{u_1^2}/\overline{u_2^2}$ does not go to infinity as $\overline{\omega_1^2}/\overline{\omega_2^2}$ goes to zero but approaches a limiting value of 5. This occurs in the diverging flow because transverse as well as longitudinal velocity fluctuations are present when the vortex axes are aligned transversely, while in converging flow, the longitudinal velocity fluctuations approach zero as the vortex axes become aligned longitudinally. Included in the plot (fig. 5-115) for comparison is the curve for $\overline{u_1^2}/\overline{u_2^2}$ for a sudden contraction without viscosity as obtained from reference 121.

Relative intensity ratios for turbulent components corrected to eliminate decay are plotted in figure 5-116. To obtain the ordinates in this figure, the ordinates for the solid curves in figure 5-112 were corrected for decay (as indicated by the subscript c) by dividing them by the ordinates for the dashed curves, which are for a pure viscous decay. (The subscript w means without the effects of strain.) The result, after the square root has been extracted, is divided by U/U_0 to give intensity ratios relative to the local mean velocity. Curves obtained from reference 121 for a sudden contraction and no viscosity are included in the plot in figure 5-116 and are similar to those for analysis.

The curve in figure 5-116 for $\left\{\left(\overline{u_2^2}^{1/2}/U\right)\Big/\left[\left(\overline{u_2^2}^{1/2}\right)_0/U_0\right]\right\}_c$ can be related approximately to the heat transfer between a cone wall and a fluid, which occurs, for instance, in a cooled rocket nozzle. The comparison is made by using the following argument, which is based on the momentum-heat transfer analogy: Except very close to the wall, the turbulent heat transfer is large compared with the molecular heat transfer, so that the total radial heat flow per unit area q is approximately $\rho c_p \varepsilon\, dT/dr$. The radial temperature gradient dT/dr at a particular radius is assumed proportional to $\Delta T/\delta$, where δ is the boundary layer thickness. The eddy diffusivity ε is replaced by the product of a transverse velocity fluctuation and a mixing length which is assumed proportional to δ, so that $\varepsilon \sim \overline{u_2^2}^{1/2}\,\delta$. Then the heat-transfer coefficient $h = q/\Delta T \sim \rho c_p \overline{u_2^2}^{1/2}$, or the Stanton number $St = h/(\rho U c_p) \sim \overline{u_2^2}^{1/2}/U$.

We assume that the change in turbulent intensity along the cone in the boundary layer is determined primarily by the normal strain rather than by the shear, as it might be when the strain is very rapid. (The initial turbulent intensity in the boundary layer at the entrance of the cone would, of course, be determined by the shear in the upstream boundary layer.) By using the preceding relation for Stanton number, we can then replace the ordinate of the curve for i = 2 in figure 5-116 by St/St_0. That curve, which has been corrected to eliminate viscous decay, is used because the inhomogeneous shear that occurs in a boundary layer will normally offset the viscous decay. The curve, replotted in figure 5-117, shows that Stanton number decreases rapidly along a converging cone. If, by contrast, the Stanton number is calculated from local conditions in a boundary layer without considering normal strain, the decrease is much more gradual. In that case the Stanton number is roughly proportional to $(\rho U D)^{-0.2}$ (assuming that $\delta \sim D$), and

$$\frac{St}{St_0} = (1 + x')^{0.2}. \qquad (5-529)$$

The curve for equation (5-529) is the dashed curve in figure 5-117.

The heat transfer in the boundary layer of a rocket nozzle may, of course be more complicated than the case considered herein, where changes are assumed governed by the normal strain. The effects of shear and variable properties, as well as of normal strain, may not be negligible. However, experimental data for heat transfer in cooled conical nozzles (refs. 125 to 127) indicate trends very similar to those obtained herein. Data from references 125 and 126 for $M < 0.2$ in the conical portions of two nozzles are plotted in figure 5-117. Comparison of the data with the solid and dashed curves seems to indicate that changes in the Stanton numbers along the cone are more dependent on the normal strain than on the shear in the boundary layer. For plotting the data, it was assumed that the entrance of the cone corresponds to $x' = 0$. Although there is some uncertainty as to the point in the analysis which corresponds

to the entrance of the cone in the experiment, it turns out that the results are insensitive to the point chosen. If, for instance, we chose $x' = -0.5$ instead of $x' = 0$ as the starting point, the results would be nearly identical.

Spectra of $\overline{u_1^2}$ and $\overline{u_2^2}$ are plotted in figures 5-118 and 5-119 and show how contributions to $\overline{u_1^2}$ and $\overline{u_2^2}$ are distributed among dimensionless wavenumbers (or reciprocal eddy sizes). Plotted in this way the curve for no convergence or divergence ($x' = 0$) does not change with x. Thus, comparison of the curves for various values of x' with the curve for $x' = 0$ shows how convergence or divergence affects the spectrum at a given position in comparison with the spectrum at the same position with no strain. For converging flow (negative x') the contributions to $\overline{u_1^2}$ occur at smaller wavenumbers (larger eddies) than they would for no convergence, whereas contributions to $\overline{u_2^2}$ move to higher wavenumbers. For diverging flow, by contrast, both ψ_{11} and ψ_{22} move to lower wavenumbers than they would for no divergence.

Of some theoretical interest is the extreme asymmetry of the spectrum of $\overline{u_1^2}$ for negatively large x'. This effect has been observed previously (section 5.4.2.1), but it is much more pronounced here, possibly because the strain rate increases sharply as x' becomes more negative. As in the previous cases the asymmetry is associated with a spectral transfer term that depends on the mean strain rate. That the effect is associated with a transfer term (eq. (5-526)) was verified by solving the spectral equation with the transfer term omitted. The spectrum obtained was found to be nearly symmetrical.

A plot of the dimensionless transfer term associated with the mean strain is given in figure 5-120. The net area under each curve is zero, in agreement with equation (5-524). The curve for negative x' is predominately negative at low wavenumbers and positive at higher ones, so that energy is in general transferred from low wavenumbers to higher ones. The curve also indicates that a small amount of reverse transfer to low wavenumbers takes place in the very low wavenumber region.

The fact that the energy transfer in the longitudinal component of the turbulence is primarily from low to high wavenumbers is possibly surprising, since according to a simplified theory one might assume that the $\overline{u_1^2}$ component is produced by vortices that are aligned transversely. The axes of those vortices would tend to be shortened in a converging flow. However, the proportion of vortices aligned in the transverse direction is small in a converging flow. Most of the contribution to $\overline{u_1^2}$ probably comes from oblique vortices, and in those vortices the energy transfer can be in the direction indicated in figure 5-120. For diverging flow (positive x') the energy transfer is in the opposite direction, that is, from high to low wavenumbers. In that case the effect of the energy transfer on the shape of the $\overline{u_1^2}$ spectrum seems to be small.

For the converging case, figure 5-120 shows that the positive area in the high wavenumber region is spread out over a wide range of wavenumbers. As x' becomes more negative this range widens still more. This elongated positive area of energy transfer is responsible for the long tail on the spectrum of $\overline{u_1^2}$. To carry the effect to the extreme, the energy spectrum of dimensinless $\overline{u_1^2}$ for $x' = -0.99$ is plotted semilogarithmically in figure 5-121. Included also in the plot is the dissipation spectrum, which is proportional for $\kappa^2 \psi_{11}$. The energy and dissipation regions in this case show essentially complete separation and are separated by a pseudo-inertial subrange in which energy transfer is the dominating process. This inertial subrange is termed pseudo because it occurs only in one component of the turbulence and because it is produced by inertial effects associated with the mean strain rather than with the triple correlations that are usually considered to be responsible for an inertial subrange (ref. 4). Figure 5-121 is, however, a good illustration of a calculated case in which essentially complete separation of energy and dissipation regions occurs.

Figure 5-122 shows a log-log plot of the spectrum of dimensionless $\overline{u_1^2}$ for $x' = -0.99$. In this plot ψ_{11} is proportional to κ^{-1} over about four decades of κ. The region in which the curve begins to fall off more rapidly than κ^{-1} is roughly the region in which dissipation effects become important. For $x' = -1$, the dissipation region would be moved to infinity and ψ would vary as κ^{-1} over the entire range of wavenumbers. The present results for a turbulence with large mean strain rates differ from the usual Kolmogorof $-5/3$ power spectrum that appears to apply at very high Reynolds numbers (ref. 128). As shown by the present results, however, a $-5/3$ power region in an energy spectrum is not necessary for complete separation of the energy and dissipation regions. In fact, any power between 0 and -2 will do as well, since the dissipation spectrum is obtained by multiplying the energy spectrum by κ^2.

Vorticity spectra were also calculated, and representative results for spectra of dimensionless $\overline{\omega_2^2}$ plotted in figure 5-123. As x' becomes more negative, the spectra move to higher dimensionless wavenumbers. Contributions to $\overline{\omega_2^2}$ also become spread out over a much wider range of wavenumbers or vortex sizes. As x' increases positively, the spectra move to lower dimensionless wavenumbers. The trends for the spectra of $\overline{\omega_1^2}$ (not shown) are similar to those shown in figure 5-123 with the exception that the shapes of the spectra do not change appreciably with strain. Thus, the vortices in converging flow tend to be smaller at a given x than they would be for no convergence, whereas they tend to be comparatively large for diverging flow.

To summarize the results in this section, note that near the virtual origin of the turbulence, for both converging and diverging flow through a cone, all turbulence components decreased along the flow because of viscous dissipation. For a converging flow the effect of the distortion was to tend to align the turbulent vorticity in the direction of mean flow. This caused the longitudinal component of the velocity variance to decrease toward zero and the lateral component to increase. For a diverging flow the vorticity tended to be alined in the transverse direction. In that case the ratio of longitudinal to transverse velocity variance ultimately

approached a limit of 5. When the results for turbulent intensity were corrected to eliminate viscous decay and divided by local mean velocity, both longitudinal and transverse components decreased along a converging flow and increased along a diverging flow. The results were related approximately to heat transfer between a cone wall and a fluid and gave trends very similar to those observed experimentally.

Turbulent vorticity spectra showed that the turbulent vortices in a converging flow tend to be smaller at a given location than they would be for no convergence, whereas those in a diverging flow tend to be relatively large. A mean-strain transfer term in the spectral equation for the longitudinal component of the turbulence transferred energy in the high wavenumber direction for a converging flow. This transfer caused the spectrum for the longitudinal component of the energy to become strongly asymmetric. Near the cone apex essentially complete separation of the longitudinal energy and dissipation spectra was obtained. A – 1 rather than a – 5/3 power specrum that extended over a considerable range of wavenumbers was noted for the longitudinal energy component. Thus, a – 5/3 power spectrum is not a necessary consequence of the separation of the energy and dissipation regions.

5.4.2.7 Turbulence and heat transfer with uniform normal strain.—The analysis in the last section was limited to turbulent flow through a cone. Here the study is extended to include turbulence and heat transfer with uniform normal strain (ref. 129). That case has application, for example, to the heat transfer at a stagnation point.

We consider the effect of uniform mean velocity gradients $dU_1/dx_1, dU_2/dx_2, dU_3/dx_3$ on locally homogeneous turbulence and on longitudinal turbulent heat transfer. Locally homogeneous, as in the last section means that the intensity of the turbulence does not vary appreciably over a correlation or mixing length. Shear stresses are assumed to be absent, and the flow is considered incompressible and axsisymmetric. The turbulence portion of this work (no heat transfer) has been considered by Pearson (ref. 78). Additional results for the turbulence are given herein, inasmuch as Pearson gave results only for the accelerating case and did not include turbulent vorticities or spectra. Instead of a steady-state locally homogeneous but longitudinally varying turbulence, as considered herein, Pearson considered a homogeneous time-varying turbulence. The two treatments, however, give the same results.

The turbulence and turbulent heat transfer are assumed to be homogeneous in the transverse direction but only locally homogeneous in the longitudinal direction. The mean axial velocity is taken as uniform over a cross section. The turbulence is initially isotropic but is allowed to become anisotropic under the distorting influence of the mean flow.

The equations for locally homogeneous turbulent heat transfer will be considered first; the equations for the turbulence itself are obtained from section 3.4.2.7. By writing the incompressible Navier-Stokes and energy equations at two points P and P′ in the turbulent fluid, we get

$$\frac{\partial\overline{\tau u_j'}}{\partial t}+U_k\frac{\partial\overline{\tau u_j'}}{\partial x_k}+\overline{u_k u_j'}\frac{\partial T}{\partial x_k}+\frac{\partial}{\partial x_k}\overline{\tau u_k u_j'}+\overline{\tau u_k'}\frac{\partial U_j'}{\partial x_k'}+U_k'\frac{\partial\overline{\tau u_j'}}{\partial x_k'}+\frac{\partial}{\partial x_k'}\overline{\tau u_j' u_k'}=-\frac{1}{\rho}\frac{\partial\overline{\tau\sigma'}}{\partial x_j'}+\nu\frac{\partial^2\overline{\tau u_j'}}{\partial x_k'\partial x_k'}+\alpha\frac{\partial^2\overline{\tau u_j'}}{\partial x_k\partial x_k}. \quad (5-530)$$

Equation (5-530) is the same as equation (11) in reference 108, where the derivation is carried out in detail. The vector configuration for correlations between fluctuating quantities at points P and P′ is shown in figure 5-110. The quantity τ is the fluctuating component of the temperature at P, u_k, and u_j' are fluctuating velocity components at P and P′, U_k and U_j' are mean velocity components, T is the mean temperature at P, x_k, and x_k' are space coordinates, t is the time, ρ is the density, ν is the kinematic viscosity, α is the thermal diffusivity, and σ is the instantaneous (mechanical) pressure. The overbars designate correlations or averaged quantities. The subscripts can take on the values 1, 2, or 3, and a repeated subscript in a term indicates a summation. From equation (4-148) we get,

$$\frac{1}{\rho}\frac{\partial^2\overline{\tau\sigma'}}{\partial x_j'\partial x_j'}=-2\frac{\partial U_j'}{\partial x_k'}\frac{\partial\overline{\tau u_k'}}{\partial x_j'}-\frac{\partial\overline{\tau u_j' u_k'}}{\partial x_j'\partial x_k'} \quad (5-531)$$

Introducing the new independent variables $r_k \equiv x_k' - x_k$ and $(x_k)_m \equiv \frac{1}{2}(x_k + x_k')$ in equations (5-530) and (5-531) results in (fig. 5-110)

$$\frac{\partial}{\partial t}\overline{\tau u_j'}+\frac{1}{2}(U_k+U_k')\frac{\partial}{\partial(x_k)_m}\overline{\tau u_j'}+(U_k'-U_k)\frac{\partial}{\partial r_k}\overline{\tau u_j'}+\overline{u_k u_j'}\frac{\partial T}{\partial x_k}+\overline{\tau u_k'}\frac{\partial U_j'}{\partial x_k'}+\frac{1}{2}\frac{\partial}{\partial(x_k)_m}\left(\overline{\tau u_k u_j'}+\overline{\tau u_j' u_k'}\right)$$

$$+\frac{\partial}{\partial r_k}\left(\overline{\tau u_j' u_k'}-\overline{\tau u_k u_j'}\right)=-\frac{1}{2\rho}\frac{\partial\overline{\tau\sigma'}}{\partial(x_j)_m}-\frac{1}{\rho}\frac{\partial}{\partial r_j}\overline{\tau\sigma'}+\frac{1}{4}(\nu+\alpha)\frac{\partial^2\overline{\tau u_j'}}{\partial(x_k)_m\partial(x_k)_m}+(\nu-\alpha)\frac{\partial^2\overline{\tau u_j'}}{\partial(x_k)_m\partial r_k}+(\nu+\alpha)\frac{\partial^2\overline{\tau u_j'}}{\partial r_k\partial r_k} \quad (5-532)$$

and

$$\frac{1}{\rho}\left[\frac{1}{4}\frac{\partial^2\overline{\tau\sigma'}}{\partial(x_j)_m\partial(x_j)_m}+\frac{\partial^2\overline{\tau\sigma'}}{\partial(x_j)_m\partial r_j}+\frac{\partial^2\overline{\tau\sigma'}}{\partial r_j\partial r_j}\right]=-2\frac{\partial U_j'}{\partial x_k'}\left[\frac{1}{2}\frac{\partial\overline{\tau u_k'}}{\partial(x_j)_m}+\frac{\partial\overline{\tau u_k'}}{\partial r_j}\right]$$

$$-\frac{1}{4}\frac{\partial^2\overline{\tau u_j'u_k'}}{\partial(x_j)_m\partial(x_k)_m}-\frac{1}{2}\frac{\partial^2\overline{\tau u_j'u_k'}}{\partial(x_j)_m\partial r_k}-\frac{1}{2}\frac{\partial^2\overline{\tau u_j'u_k'}}{\partial(x_k)_m\partial r_j}-\frac{\partial^2\overline{\tau u_j'u_k'}}{\partial r_j\partial r_k}. \qquad (5-533)$$

For locally homogeneous turbulence and turbulent heat transfer, the turbulence is considered homogeneous over a correlation length, or the scale of the inhomogeniety is much greater than the scale of the turbulence. Thus, a quantity such as $\partial^2\overline{\tau u_j'}/\partial(x_k)_m\,\partial(x_k)_m$ in equation (5-532) will be negligible compared with $\partial^2\overline{\tau u_j'}/\partial r_k\,\partial r_k$. (A calculation for axially decaying turbulence without mean velocity gradients, reference 7, figure 3, implies that this is a good approximation except very close to the virtual origin of the turbulence.) In general, for locally homogeneous turbulence, $\partial/\partial(x_i)_m \ll \partial/\partial r_i$. Also, for that type of turbulence, the mean velocity and mean temperature will vary linearly over distances for which correlations are appreciable so that $\partial U_j'/\partial x_k' = \partial U_j/\partial x_k = \partial(U_j)_m/\partial(x_k)_m$, $U_k' - U_k = r_\ell\,\partial(U_k)_m/\partial(x_\ell)_m$, $(U_k + U_k')/2 = (U_k)_m$, and $\partial T/\partial x_k = \partial T_m/\partial(x_k)_m$. Finally, in order to make the set of equations determinate, the turbulence is assumed to be weak enough and/or the mean gradients large enough to neglect terms containing triple correlations. The turbulence in a flow with large velocity or temperature gradients may not have to be as weak as that in a flow without mean gradients. The terms containing those gradients may be large compared with triple correlation terms, even if the turbulence is mdoerately strong. Equations (5-532) and (5-333) become, for steady state at a fixed point,

$$\overline{\tau u_k'}\frac{\partial(U_j)_m}{\partial(x_k)_m}+(U_k)_m\frac{\partial}{\partial(x_k)_m}\overline{\tau u_j'}+r_\ell\frac{\partial(U_k)_m}{\partial(x_\ell)_m}\frac{\partial}{\partial r_k}\overline{\tau u_j'}+\overline{u_k u_j'}\frac{\partial T_m}{\partial(x_k)_m}=-\frac{1}{\rho}\frac{\partial}{\partial r_j}\overline{\tau\sigma'}+(\nu+\alpha)\frac{\partial^2\overline{\tau u_j'}}{\partial r_k\partial r_k} \qquad (5-534)$$

and

$$\frac{1}{\rho}\frac{\partial^2\overline{\tau\sigma'}}{\partial r_j\partial r_j}=-2\frac{\partial(U_j)_m}{\partial(x_k)_m}\frac{\partial\overline{\tau u_k'}}{\partial rj}. \qquad (5-535)$$

The case of uniform axisymmetric strain with no shear and with mean temperature gradient in the longitudinal direction is considered herein. Equation (5-534) for $j = 1$ and equation (5-535) then become

$$(U_k)_m\frac{\partial}{\partial(x_k)_m}\overline{\tau u_1'}+a_{(\ell\ell)}r_\ell\frac{\partial}{\partial r_\ell}\overline{\tau u_1'}+b_{(1)}\overline{u_1u_1'}+a_{(11)}\overline{\tau u_1'}=-\frac{1}{\rho}\frac{\partial}{\partial r_1}\overline{\tau\sigma'}+(\nu+\alpha)\frac{\partial^2\overline{\tau u_1'}}{\partial r_k\partial r_k} \qquad (5-536)$$

and

$$\frac{1}{\rho}\frac{\partial^2\overline{\tau\sigma'}}{\partial r_j\partial r_j}=-2a_{(\ell\ell)}\frac{\partial\overline{\tau u_\ell'}}{\partial r_\ell}. \qquad (5-537)$$

where subscripts in paretheses are not strictly tensor subscripts. Equations (5-536) and (5-537) can be converted to spectral form by introducing the usual three-dimensional Fourier transforms defined as follows:

$$\overline{u_iu_j'}=\int_{-\infty}^{\infty}\varphi_{ij}e^{i\kappa\cdot r}d\kappa, \qquad (5-538)$$

$$\overline{\tau u_j'}=\int_{-\infty}^{\infty}\gamma_j e^{i\kappa\cdot r}d\kappa, \qquad (5-539)$$

and

$$\overline{\tau\sigma'} = \int_{-\infty}^{\infty} \zeta' e^{i\kappa\cdot r} d\kappa. \tag{5-540}$$

Then, using continuity and the inverse transform of equation (5-539) gives

$$a_{(\ell\ell)} r_\ell \frac{\partial}{\partial r_\ell} \overline{\tau u_j'} = -\int_{-\infty}^{\infty} a_{(\ell\ell)} \kappa_\ell \frac{\partial \gamma_j}{\partial \kappa_\ell} e^{i\kappa\cdot r} d\kappa. \tag{5-541}$$

where κ is a wavevector having the dimension 1/length and $d\kappa = d\kappa_1\, d\kappa_2\, d\kappa_3$. Taking the Fourier transforms of equations (5-536) and (5-537) results in

$$(U_k)_m \frac{\partial \gamma_1}{\partial (x_k)_m} - a_{(\ell\ell)} \kappa_\ell \frac{\partial \gamma_1}{\partial \kappa_\ell} + b_1 \varphi_{11} + a_{(11)} \gamma_1 = 2a_{(\ell\ell)} \frac{\kappa_1 \kappa_\ell}{\kappa^2} \gamma_1 - (\alpha + \nu)\kappa^2 \gamma_1, \tag{5-542}$$

where two equations have been combined into one by eliminating ζ'.

For axisymmetric strain $a_{22} = a_{33}$; and by continuity of the mean flow,

$$a_{22} = a_{33} = -\left(\frac{1}{2}\right) a_{11} \tag{5-543}$$

The turbulence is also assumed to be homogeneous in the transverse direction and changes only in the longitudinal or x_1 -direction, so that

$$(U_k)_m \frac{\partial \gamma_1}{\partial (x_k)_m} = (U_1)_m \frac{\partial \gamma_1}{\partial (x_1)_m}. \tag{5-544}$$

To simplify the notation, let $(U_1)_m \equiv U$, $(x_1)_m \equiv x$, $a_{11} \equiv a$, and $b_1 \equiv b$ in the remainder of this section. Then equation (5-542) becomes

$$U \frac{\partial \gamma_1}{\partial x} - a\kappa_1 \frac{\partial \gamma_1}{\partial \kappa_1} + \frac{1}{2} a\kappa_2 \frac{\partial \gamma_1}{\partial \kappa_2} + \frac{1}{2} a\kappa_3 \frac{\partial \gamma_1}{\partial \kappa_3} = -b\varphi_{11} - a\gamma_1 + 3a \frac{\kappa_1^2}{\kappa^2} \gamma_1 - (\alpha + \nu)\kappa^2 \gamma_1, \tag{5-545}$$

where use was made of the continuity relation in the form $\kappa_2\gamma_2 + \kappa_3\gamma_3 = -\kappa_1\gamma_1$. Corresponding expressions for φ_{11} and φ_{ii} are given as equations (5-497) and (5-498):

$$\frac{U}{a} \frac{\partial \varphi_{11}}{\partial x} - \kappa_1 \frac{\partial \varphi_{11}}{\partial \kappa_1} + \frac{1}{2} \kappa_2 \frac{\partial \varphi_{11}}{\partial \kappa_2} + \frac{1}{2} \kappa_3 \frac{\partial \varphi_{11}}{\partial \kappa_3} = \varphi_{11} \left(6 \frac{\kappa_1^2}{\kappa^2} - 2 - \frac{2\nu}{a} \kappa^2 \right), \tag{5-497}$$

and

$$\frac{U}{a} \frac{\partial \varphi_{ii}}{\partial x} - \kappa_1 \frac{\partial \varphi_{ii}}{\partial \kappa_1} + \frac{1}{2} \kappa_2 \frac{\partial \varphi_{ii}}{\partial \kappa_2} + \frac{1}{2} \kappa_3 \frac{\partial \varphi_{ii}}{\partial \kappa_3} = -3\varphi_{11} + \varphi_{ii} - 2\frac{\nu}{a} \kappa^2 \varphi_{ii}, \tag{5-498}$$

For uniform $a = dU/dx$,

$$c \equiv \frac{U}{U_0} = 1 + \frac{a(x - x_0)}{U_0} \tag{5-546}$$

Equations (5-545), (5-497), and (5-498) can be written in terms of c as

$$c\frac{\partial\gamma_1}{\partial c}-\kappa_1\frac{\partial\gamma_1}{\partial\kappa_1}+\frac{1}{2}\kappa_2\frac{\partial\gamma_1}{\partial\kappa_2}+\frac{1}{2}\kappa_3\frac{\partial\gamma_1}{\partial\kappa_3}=-\frac{b}{a}\varphi_{11}+\gamma_1\left[3\frac{\kappa_1^2}{\kappa^2}-1-\frac{(\alpha+\nu)}{a}\kappa^2\right], \tag{5-547}$$

$$c\frac{\partial\varphi_{11}}{\partial c}-\kappa_1\frac{\partial\varphi_{11}}{\partial\kappa_1}+\frac{1}{2}\kappa_2\frac{\partial\varphi_{11}}{\partial\kappa_2}+\frac{1}{2}\kappa_3\frac{\partial\varphi_{11}}{\partial\kappa_3}=\varphi_{11}\left(6\frac{\kappa_1^2}{\kappa^2}-2-\frac{2\nu}{a}\kappa^2\right), \tag{5-548}$$

and

$$c\frac{\partial\varphi_{ii}}{\partial c}-\kappa_1\frac{\partial\varphi_{ii}}{\partial\kappa_1}+\frac{1}{2}\kappa_2\frac{\partial\varphi_{ii}}{\partial\kappa_2}+\frac{1}{2}\kappa_3\frac{\partial\varphi_{ii}}{\partial\kappa_3}=-3\varphi_{11}+\varphi_{ii}\left(1-2\frac{\nu}{a}\kappa^2\right). \tag{5-549}$$

For solving equations (5-500) to (5-502), the turbulence is assumed to be initially isotropic (at c =1), and, as usual, equation (5-333) is used:

$$\left(\varphi_{ij}\right)_0=\frac{J_0}{12\pi^2}\left(\kappa^2\delta_{ij}-\kappa_i\kappa_j\right), \tag{5-333}$$

where J_0 is a constant that depends on initial conditions. For the initial condition on γ_1 (at c = 1), it is again assumed that

$$\left(\gamma_1\right)_0=0. \tag{5-550}$$

That is, the turbulence-producing grid is assumed to be unheated, so that the temperature fluctuations are produced by the interaction of the mean longitudinal temperature gradient with the turbulence. Equation (5-333) appears to be the simplest condition that gives results that, at all values of x, reduce to those for isotropic turbulence as the mean strain goes to zero. The use of that initial condition for φ_{ij} implies that Pearson's parameter $\nu\kappa_0^2/a$ approaches ∞, where κ_0 is a characteristic initial wavenumber of the turbulence (ref. 78). Thus, the present results should be applicable for large kinematic viscosity, small initial turbulence scale, or small strain rate. The case $\nu\kappa_0^2/a\rightarrow\infty$ was not considered by Pearson.

Equations (5-547) to (5-549) can be solved by methods similar to those given in reference 79. Solutions of these equations subject to the initial condiitons given in equations (5-333) and (5-550) are, in dimensionless form,

$$\gamma_1=-\frac{1}{12\pi^2}\frac{c^{-5}}{(c-1)}\frac{\kappa_2^2+\kappa_3^2}{\kappa^2}\left(c^3\kappa_1^2+\kappa_2^2+\kappa_3^2\right)^2\exp\left\{-\left(\frac{1}{Pr}+1\right)\left[\frac{1}{2}(c+1)\kappa_1^2+c^{-1}\left(\kappa_2^2+\kappa_3^2\right)\right]\right\}\int_1^c\frac{\xi}{\kappa_1^2+c^{-3}\xi^3\left(\kappa_2^2+\kappa_3^2\right)}$$

$$\times\exp\left\{\left(\frac{1}{Pr}-1\right)(c-1)^{-1}\left[\frac{1}{2}\kappa_1^2\left(\frac{c}{\xi}\right)^2\left(\xi^2-1\right)+\left(\kappa_2^2+\kappa_3^2\right)c^{-1}(\xi-1)\right]\right\}d\xi, \tag{5-551}$$

$$\varphi_{11}=\frac{1}{12\pi^2}\left(\kappa_2^2+\kappa_3^2\right)\frac{c^{-3}}{\kappa^4}\left(c^3\kappa_1^2+\kappa_2^2+\kappa_3^2\right)^2\exp\left\{-2\left[\frac{1}{2}(1+c)\kappa_1^2+c^{-1}\left(\kappa_2^2+\kappa_3^2\right)\right]\right\}, \tag{5-552}$$

and

$$\varphi_{ii}=\frac{1}{12\pi^2}\left[\frac{c^{-3}}{\kappa^2}\left(c^3\kappa_1^2+\kappa_2^2+\kappa_3^2\right)^2+c^3\kappa_1^2+\kappa_2^2+\kappa_3^2\right]\exp\left\{-2\left[\frac{1}{2}(1+c)\kappa_1^2+c^{-1}\left(\kappa_2^2+\kappa_3^2\right)\right]\right\}, \tag{5-553}$$

where

$$\left[\frac{\nu(x-x_0)}{U_0}\right]^{1/2}\kappa_i \rightarrow \kappa_i, \tag{5-554}$$

$$\frac{(x-x_0)\nu}{J_0U_0}\varphi_{ij} \rightarrow \varphi_{ij}, \tag{5-555}$$

$$\frac{\nu}{J_0 b}\gamma_1 \rightarrow \gamma_1, \tag{5-556}$$

and

$$\frac{\nu}{\alpha} \rightarrow \mathrm{Pr}. \tag{5-557}$$

The arrows $\rightarrow$ indicate "has been replaced by." It can be seen that γ_1, φ_{11}, and φ_{ii} are functions only of c, κ_i, and Prandtl number. For Pr = 1, equation (5-551) can be integrated to give

$$\gamma_1 = \frac{1}{12\pi^2}(c-1)^{-1}c^{-3}\left(\frac{\kappa_2^2+\kappa_3^2}{\kappa_1^2}\right)^{1/3}\kappa^{-2}\left(c^3\kappa_1^2+\kappa_2^2+\kappa_3^2\right)^2$$

$$\times\left\{\frac{1}{6}\ln\frac{\left[\left(\kappa_2^2+\kappa_3^2\right)^{2/3}-\kappa_1^{2/3}\left(\kappa_2^2+\kappa_3^2\right)^{1/3}+\kappa_1^{4/3}\right]\left[\left(\kappa_2^2+\kappa_3^2\right)^{1/3}-c^{-1}+\kappa_1^{2/3}\right]^2}{\left[\left(\kappa_2^2+\kappa_3^2\right)^{2/3}c^{-2}-\kappa_1^{2/3}\left(\kappa_2^2+\kappa_3^2\right)^{1/3}c^{-1}+\kappa_1^{4/3}\right]\left[\left(\kappa_2^2+\kappa_3^2\right)^{1/3}-c^{-1}+\kappa_1^{2/3}\right]^2}\right.$$

$$\left.+\frac{1}{\sqrt{3}}\tan^{-1}\left[\frac{2\left(\kappa_2^2+\kappa_3^2\right)^{1/3}-\kappa_1^{2/3}}{\sqrt{3}\kappa_1^{2/3}}\right]-\frac{1}{\sqrt{3}}\tan^{-1}\left[\frac{2\left(\kappa_2^2+\kappa_3^2\right)^{1/3}c^{-1}-\kappa_1^{2/3}}{\sqrt{3}\kappa_1^{2/3}}\right]\right\}$$

$$\times\exp\left\{-2\left[\frac{1}{2}(1+c)\kappa_1^2+c^{-1}\left(\kappa_2^2+\kappa_3^2\right)\right]\right\} \tag{5-558}$$

In order to integrate over wavenumber space, spherical coordinates are introduced as follows:

$$\kappa_1 = \kappa\cos\theta, \tag{5-559a}$$

$$\kappa_2 = \kappa\cos\varphi\sin\theta, \tag{5-559b}$$

and

$$\kappa_3 = \kappa\sin\varphi\sin\theta. \tag{5-559c}$$

For r = 0, equations (5-538) and (5-539) then become

$$\overline{u_i u_j} = \int_0^\infty \psi_{ij}\,d\kappa \tag{5-560}$$

and

$$\overline{\tau u_j} = \int_0^\infty \Gamma_j d\kappa, \tag{5-561}$$

where

$$\psi_{ij} = \int_0^\pi \int_0^{2\pi} \varphi_{ij} \kappa^2 \sin\theta \, d\varphi \, d\theta \tag{5-562}$$

and

$$\Gamma_j = \int_0^\pi \int_0^{2\pi} \gamma_j \kappa^2 \sin\theta \, d\varphi \, d\theta. \tag{5-563}$$

The quantities φ_{ij} and Γ_j are functions only of the magnitude of the wavenumber and represent spectrum functions that have been integrated over all directions in wavenumber space.

The expressions for the velocity variances $\overline{u_1^2}$, $\overline{u_i u_i}$, $\overline{u_2^2}$, and $\overline{u_3^2}$ can be integrated as follows:

$$\overline{u_1^2} = \frac{1}{12\sqrt{\pi}c^3(c+1)^{1/2}}\left[\frac{3}{2(c+1)^2} + \frac{c(c^3-1)}{(c+1)(c^2+c-2)} + \frac{5}{2}\frac{c^2(c^3-1)^2}{(c^2+c-2)^2} + \frac{3}{4}\frac{(c^2+c-2)}{c+1} + \frac{1}{4}\frac{c}{c+1}(2c^3+c^2+c-5)\right.$$

$$\left. - \frac{3}{2}\frac{c^2(c^3-1)(c^3-3)}{(c^2+c-2)^2}\right] + \frac{1}{6\sqrt{\pi}c^3}\left\{\frac{3}{4}\frac{c^2(c^3-1)(c^3-3)}{(c^2+c-2)^2}H - \frac{15}{4}\frac{c^2(c^3-1)^2}{(c^2+c-2)^3}\left[\frac{c(c+1)^{1/2}}{2} - H\right]\right\}, \tag{5-564}$$

$$\overline{u_i u_i} = \frac{1}{6\sqrt{\pi}c^3(c+1)^{1/2}}\left[-\frac{c(2c^6-c^3-1)}{4(c+1)(c^2+c-2)} - \frac{3}{4}\frac{c^2(c^3-1)^2}{(c^2+c-2)^2} + \frac{c(c^3+1)(c^2+c+1)}{8(c+1)} + \frac{c^2(c^3-1)(c^3+2)}{8(c^2+c-2)}\right.$$

$$\left. + \frac{3}{4}\frac{c^2(c^3-1)^2(c+1)^{1/2}}{(c^2+c-2)^2}H\right], \tag{5-565}$$

and

$$\overline{u_2^2} = \overline{u_3^2} = \frac{1}{2}\left(\overline{u_i u_i} - \overline{u_1^2}\right), \tag{5-566}$$

where

$$\frac{(x-x_0)^{5/2}\nu^{5/2}}{J_0 U_0^{5/2}}\overline{u_i u_j} \to \overline{u_i u_j}, \tag{5-567}$$

$$H = \left(\frac{c}{c^2+c-2}\right)^{1/2} \ln\left\{\left(\frac{c^2+c-2}{2}\right)^{1/2} + \left[\frac{c(c+1)}{2}\right]^{1/2}\right\} \qquad \text{for } c > 1, \tag{5-568a}$$

$$H = \left(\frac{-c}{c^2+c-2}\right)^{1/2} \sin^{-1}\left(\frac{c^2+c-2}{-2}\right)^{1/2} \qquad \text{for } c < 1, \tag{5-568b}$$

and $c = U/U_0$.

Another quantity of importance is the turbulent vorticity tensor $\overline{\omega_i\omega_j}$. The vorticity spectrum tensor is given by equation (5-348), which we write as

$$\Omega_{ij} = \left(\delta_{ij}\kappa^2 - \kappa_i\kappa_j\right)\varphi_{\ell\ell} - \kappa^2\varphi_{ij}. \tag{5-569}$$

As was the case for φ_{ij}, equation (5-348) can be integrated over all directions in wavenumber space to give

$$\Lambda_{ij} = \int_0^{\pi}\int_0^{2\pi}\Omega_{ij}\kappa^2 \sin\theta \, d\varphi \, d\theta. \tag{5-570}$$

The vorticity tensor is then given by

$$\overline{\omega_i\omega_j} = \int_0^{\infty}\Lambda_{ij} \, d\kappa. \tag{5-571}$$

Calculated turbulent velocities, vorticities, temperature-velocity correlations, and spectra will be considered next.

Figure 5-124 shows turbulent velocity variances $\overline{u_1^2}$, $\overline{u_2^2}$, and $\overline{u_3^2}$ plotted logarithmically in dimensionless form. Included in the plot is the curve obtained by solving equation (5-548) as though the effects of strain were absent by omitting the second to sixth terms. This solution gives

$$\left|\frac{\nu}{a}\right|^{5/2}\frac{\overline{u_1^2}}{J_0} = \frac{\ln^{-5/2} c}{48\sqrt{2\pi}}. \tag{5-572}$$

For an accelerating flow with uniform strain, the longitudinal component $\overline{u_1^2}$ decreases more rapidly and the lateral components decrease less rapidly than they would if the effects of strain were absent. For large values of U/U_0, the lateral components reach a steady-state value as observed in Pearson's results (ref. 78). This result differs from flow through a converging cone (see the last section) where the increasing strain rate with distance caused the lateral components to increase without limit as the apex of the cone was approached. The asymptotic equilibrium solution shown in figure 5-125 is given by

$$\overline{u_2^2} = \overline{u_3^2} = \frac{J_0}{96\sqrt{\pi}}\left(\frac{a}{\nu}\right)^{5/2}. \tag{5-573}$$

Thus, the solution represents a case in which the energy fed into the lateral components by straining action balances the energy dissipated by viscous forces. For decelerating flow near the virtual origin, both the longitudinal and the lateral components of the velocity fluctuations decrease in the direction of flow. For lower values of U/U_0, all components begin to increase as the effect of normal strain becomes greater than the effect of viscous dissipation. The region of increasing turbulent intensity in the decelerating case was not observed for the cone in the last section, where the strain rate a decreased sufficiently with distance to allow the turbulence to decay. As U approaches zero in the present case, the turbulence components will tend to increase without limit. The assumption of local homogeneity will, however, tend to break down in that region, and the turbulence components will remain finite in a real situation. An increase in turbulent fluctuation in the decelerating flow near a stagnation point (in comparison with the free-stream fluctuation) has been observed experimentally in reference 130.

The reasons for the trends observed in the turbulent velocity variances will become clearer if the vorticity variances $\overline{\omega_1^2}$ plotted in figure 5-125 are considered. The dashed curves for no effects of strain were obtained from the equation

$$\left|\frac{\nu}{a}\right|^{7/2}\frac{\overline{\omega_1^2}}{J_0} = \frac{5}{192\sqrt{2\pi}}\ln^{-7/2} c. \tag{5-574}$$

Consider first the accelerating case. Here the trends are opposite to those for the velocity variances in figure 5-124; that is, the longitudinal vorticity component decays less rapidly and the lateral components decay more rapidly, than they would if the effects of strain were absent. Thus, the

turbulent vorticity tends to become aligned in the flow direction. That alignment occurs first, because the longitudinal vortex filaments are strengthened by the stretching action of the mean flow, whereas the lateral filaments are shortened and thus weakened; and, second, because the mean strain rotates the vortex filaments which were originally oblique so that their axes tend to lie in the flow direction. The velocities associated with the turbulent vortex filaments will then tend to lie in the transverse directions, in agreement with the curves for velocity variances in figure 5-124. As for the lateral components of the velocity variance, the longitudinal component of the vorticity variance approaches an equilibrium solution for large values of U/U_0 in which the vorticity generated by the mean strain balances that dissipated by viscous action. This solution is given by

$$\overline{\omega_1^2} = \frac{J_0}{96\sqrt{\pi}}\left(\frac{a}{\nu}\right)^{7/2} . \qquad (5-575)$$

For decelerating flow at low values of U/U_0, the lateral components of the vorticity tend to increase, whereas the longitudinal component decreases more rapidly than it would if the effects of strain were absent. Thus, the vortex filaments tend to be aligned in the transverse directions. This alignment occurs because the lateral vortex filaments are strengthened by stretching, while the longitudinal components are weakened since they are shortened, and because the axes of vortex filaments which were originally oblique are rotated toward the transverse directions by the stretching action of the mean strain in the transverse directions. With the turbulent vortex filaments mostly aligned in the transverse directions, the velocities associated with them can be either in the longitudinal or the transverse directions. This explains why, for low values of U/U_0, the curves for both the longitudinal and the transverse components of the turbulent velocity variance in figure 5-124 increase in the flow direction, whereas in the curves for vorticity variance, only the lateral component can increase. The lateral stretching of the vortex filaments intensifies both the longitudinal and the transverse velocity fluctuations.

Relative intensity ratios for turbulence components corrected to eliminate viscous decay are plotted in figure 5-126. For obtaining the ordinates in this figure, values of turbulent velocity variance with the effects of strain included (solid curves in fig. 5-124) are corrected to eliminate the effects of decay by dividing them by corresponding values for pure viscous decay (dashed curves in fig. 5-124). The result (after taking the square root) is divided by U/U_0 to give intensity ratios that are relative to the local mean velocity. In addition to the present results for uniform strain in an incompressible flow, results from the preceding section for flow through a cone and for uniform longitudinal strain in a compressible flow (ref. 131) are shown in the figure for comparison. The curves for uniform longitudinal strain in a compressible flow were obtained from equations (31) and (32) in reference 131 by noting that $U_g = U_0 - ax_0$ and $U_g/\nu = U_0/\nu_0$ in those equations. The values for pure viscous decay were obtained by solving equation (23) in reference 133 with all but the first and last terms deleted, and again using $U_g/\nu = U_0/\nu_0$ and $U_g = U_0 - ax_0$. This solution gives $(U/U_0)^{-7/4}$ for the ordinate of the dot-dashed curve for $i = 1$ and $(1 + U/U_0)^{1/2} \times U/U_0)^{-3/4}/\sqrt{2}$ for the ordinate of the dot-dashed curve for $i = 2, 3$.

The curves for the lateral components ($i = 2, 3$) for accelerating flow are of particular interest because, as shown in the last section, the ordinates of those curves give approximately, for certain conditions, the Stanton number ratio St/St_0 for the heat transfer between the fluid and a wall. In obtaining that relation, the normal strain is assumed to be so large that changes in the Stanton number along the flow are governed by normal strain rather than by shear.

The curves for the lateral components (and thus for the Stanton number ratio) for accelerating flow in figure 5-126 indicate but a slight difference in the results for uniform incompressible strain and for flow in a cone. That is, when plotted in this way, the results at a given U/U_0 for accelerating flow seem to depend but slightly on how the strain dU/dx varies along the flow. On the other hand the results for uniform longitudinal strain in a compressible flow in a cone. That is, when plotted in this way, the results at a given U/U_0 for accelerating flow seem to depend but slightly on how the strain dU/dx varies along the flow. On the other hand the results for uniform longitudinal strain in a compressible flow lie significantly above the others. These results can evidently be explained by the fact that the stretching of the vortex filaments is more intense in that case, since the lateral compressive strain is absent because of the lack of a radial flow. The dot-dashed curve might be related to heat transfer in a highly heated constant-area tube with fluid density changes along the length, whereas the other two curves are more closely related to nozzle heat transfer in which the effects of compressibility are small (fig. 5-117).

Figure 5-127 shows the effect of uniform normal strain on dimensionless longitudinal turbulent heat transfer $\overline{\tau u_1}$. Since $\overline{\tau u_1}$ is divided by the temperature gradient b, the ordinates can be considered as representing the variation of longitudinal eddy conductivity with U/U_0. Results are given for Prandtl numbers of 0.01 (liquid metals), 1 and 0.7 (gases), and ∞. As Prandtl number decreases, the eddy conductivity decreases, apparently because a turbulent eddy in a high conductivity fluid, such as a liquid metal ($Pr \sim 0.01$) gains or loses heat by conduction as it moves longitudinally and thus transfers heat with relatively low effectiveness (fig. 5-80). At a given Prandtl number, the trends in the curves are generally similar to those observed for the longitudinal component of the velocity variance $\overline{u_1^2}$ in figure 5-124. A notable exception, however, is that $\overline{\tau u_1}$ reaches a maximum at low values of U and then approaches zero at $U = 0$, whereas $\overline{u_1^2}$ became indefinitely large as U approached zero. The ratio of maximum to minimum $\overline{\tau u_1}$ is greater at low Prandtl numbers.

The curves for decelerating flow in figure 5-127 illustrate the large increase that normal strain can produce in the longitudinal heat transfer between a body and a stream in the vicinity of a stagnation point when free-stream turbulence is present. The eddy conductivity would decay to very low values (dashed curves) if the effects of strain were absent. (The time available for decay is quite large, since the fluid velocity becomes very small as the stagnation point is approached.) This increase in heat transfer is in agreement with the experiments in reference 132

and the analysis of reference 133. The increase is evidently produced by the lateral stretching of vortex filaments as assumed in reference 133. Reference 133, however, considered only transverse vortices, whereas the present analysis considers random vorticity in all directions. The present analysis does not, however, consider the damping effect of the wall at the stagnation point (effect of viscous diffusion), so that the increase in turbulent heat transfer due to normal strain is probably exaggerated here. In fact, an attempt to calculate the heat transfer near a stagnation point by assuming that the maximum in the curve in figure 5-527 (Pr = 0.7 for gases) corresponds to the maximum eddy conductivity in the boundary layer, and that the minimum in the curve for i = 1 in figure 5-124 corresponds to the turbulence level in the undisturbed stream, gave (by dividing one ordinate by the other) increases in total heat transfer considerably higher than those observed experimentally. The results do indicate, however, that the combination of free-stream turbulence and normal strain (or lateral vortex stretching) can be an important factor in increasing the heat transfer in the vicinity of a stagnation point.

Dimensionless spectra of components of the velocity and vorticity variances are plotted in figures 5-128 to 5-130. The spectra show how contributions to the dimensionless mean velocity or vorticity fluctuations are distributed among dimensionless wavenumbers. Plotted in this way, the curves for no strain ($U/U_0 = 1$) reduce to a single curve that does not change with x. Thus, comparison of the curves for various values of U/U_0 shows how strain affects the spectrum at a given position in comparison with the spectrum at the same position with no strain. For instance, figure 5-130 shows that for decelerating flow ($U/U_0 < 1$) contributions to the transverse vorticity occur at smaller wavenumbers (larger vortices) than they would for no acceleration. This trend seems to be congruous with the observation in the analysis of reference 133 that only the larger transverse vortices are amplified by stretching in the neighborhood of a stagnation point. Figures 5-128 and 5-129 show that contributions to components of the velocity variance also move to lower dimensionless wavenumbers as velocity ratio decreases. For $U/U_0 > 1$, the trends are opposite to those for decelerating flow, or contributions to the mean fluctuations move to higher dimensionless wavenumbers.

Figure 5-131 shows spectra corresponding to the asymptotic equilibrium solutions given by equations (5-573) and (5-575) for $U/U_0 \rightarrow \infty$. Note that the dimensionless quantities used in these spectra have been changed from those used in the preceding spectra in order to obtain finite dimensionless quantities for $U \rightarrow \infty$. The spectra in figure 5-131 are of interest because they show how contributions to the velocity and vorticity variances are distributed among wavenumbers for a case in which the energy fed into the turbulence by the mean strain exactly balances that dissipated by viscous action. Although the curves are in equilibrium at each wavenumber, there is not necessarily an equilibrium between production and dissipation at each wavenumber because energy can be transferred between wavenumbers by the stretching of the vortex filaments by the mean velocity gradients as we discussed for example, in sections 5.4.2.1, 5.4.2.3, and 5.4.2.6.

Spectra of the dimensionless longitudinal eddy conductivity $\overline{\tau u_1}$ are plotted in figure 5-132 for Prandtl numbers of 0.7 and 0.01. The shifting of the curves to lower dimensionless wavenumbers as U/U_0 decreases is similar to that for the spectra of the longitudinal velocity fluctuations shown in figure 5-128.

To summarize the results in this section, we note that for an incompressible accelerating flow with uniform strain, the longitudinal velocity fluctuations decreased more rapidly, and the lateral fluctuations decreased less rapidly in the flow direction than they would if the effects of normal strain were absent. For large values of velocity ratio, the lateral components were found to reach a steady-state equilibrium value, as observed in Pearson's results. This result differs from flow through a converging cone, where the increasing strain rate with distance caused the lateral components to increase without limit as the apex of the cone was approached.

For decelerating flow at low values of velocity ratio both the longitudinal and transverse velocity fluctuations increased in the flow direction as the effect of normal strain becomes greater than the effect of viscous dissipation. A somewhat similar increase in velocity fluctuation in the decelerating flow near a stagnation point has been observed experimentally. This region of increasing turbulent intensity in the decelerating case was not observed in the analysis of flow through a diverging cone, where the strain rate decreased sufficiently with distance to allow the turbulence to decay.

Many of the trends observed for the velocity-fluctuation components could be explained by the analytical result that the vorticity became aligned in the longitudinal direction for accelerating flow and in the transverse directions for decelerating flow.

When the results for turbulent intensity were corrected for viscous decay and divided by local mean velocity, the transverse component for accelerating flow, which can be related to heat transfer between the fluid and a wall, was approximately the same for flow in a cone and for uniform incompressible strain. On the other hand the curve for uniform longitudinal compressible strain lay appreciably above the others, apparently because of the more intense vortex stretching for that case.

The results for longitudinal eddy conductivity in a decelerating flow showed that normal strain could increase that quantity to values considerably above those which it would have if the effects of strain were absent. Thus, free-stream turbulence with normal strain (or lateral vortex stretching) could be an important factor in increasing the heat transfer in the vicinity of a stagnation point.

Turbulent vorticity spectra showed that the turbulent vortexes in a decelerating flow tended to be larger at a given location than they would be for no deceleration. The eddies associated with the energy and with the longitudinal eddy conductivity also became comparatively larger. Spectra were also obtained for the energy and the vorticity for the asymptotic equilibrium solutions at large velocity ratios.

5.4.2.8 Turbulence and heat transfer with combined two-dimensional shear and normal strain.—The effects of uniform shear and of normal strain on turbulence have been analyzed separately, for example, in sections 5.4.2.1 and 5.4.2.7. There are important cases, however, where shear and normal strain act simultaneously, as in the boundary layer of a fluid flowing through a contraction. Effects which are absent when one or the other types of strain acts by itself may be present when they act simultaneously. For instance, an apparent laminarization seems to occur in the boundary layers of certain accelerating flows (refs. 134 to 136).

Also, recall that there is a strong tendency for the energy to be drained out of a transverse component of a shear-flow turbulence, with a consequent ultimate decay of the total turbulent energy (see section 5.4.2.1 and fig. 5-63). One way of maintaining the turbulence by preventing that drain, even in the absence of triple correlations, is to add a normal mean strain to the flow, as will be discussed in section 5.4.2.9 (Another way of doing that is to introduce a destabilizing buoyancy, as already discussed in section 5.4.2.5.)

In this section a simplified model is analyzed in an attempt to obtain some understanding of the effects of combined shear and normal strain on turbulence and turbulent heat transfer. Uniform shear and uniform normal velocity gradients, as well as a uniform transverse temperature gradient, are assumed to be acting on a field of initially isotropic turbulence. The turbulence quickly becomes anisotropic under the influence of the mean gradients. The turbulent field, although homogeneous in the transverse directions, is assumed to be only locally homogeneous in the longitudinal or flow direction; that is, the effects of changes in the intensity of the turbulence over a correlation or mixing length in the longitudinal direction are negligible. The normal strains in the present model correspond to a two-dimensional contraction with the transverse normal strains occurring in the same direction as the transverse shear and temperature gradients.

Two-point steady-state correlation equations for locally homogeneous turbulence have been obtained as equations (5-486) to (5-488) and (5-534) to (5-537). For uniform mean gradients one can write those equations as

$$\overline{u_k u_j'}\frac{\partial U_i}{\partial x_k}+\overline{u_i u_k'}\frac{\partial U_j}{\partial x_k}+\frac{\partial U_k}{\partial x_\ell}r_\ell\frac{\partial}{\partial r_k}\overline{u_i u_j'}+U_k\frac{\partial}{\partial x_k}\overline{u_i u_j'}=-\frac{1}{\rho}\left(\frac{\partial}{\partial r_j}\overline{u_i\sigma'}-\frac{\partial}{\partial r_i}\overline{\sigma u_j'}\right)+2\nu\frac{\partial^2\overline{u_i u_j'}}{\partial r_k\,\partial r_k}, \qquad (5-576)$$

$$\frac{1}{\rho}\frac{\partial^2\overline{u_i\sigma'}}{\partial r_j\,\partial r_j}=-2\frac{\partial U_j}{\partial x_j}\frac{\partial\overline{u_i u_k'}}{\partial r_j}, \qquad (5-577)$$

$$\frac{1}{\rho}\frac{\partial^2\overline{\sigma u_j'}}{\partial r_i\,\partial r_i}=2\frac{\partial U_i}{\partial x_k}\frac{\partial\overline{u_k u_j'}}{\partial r_i}, \qquad (5-578)$$

$$\overline{\tau u_k'}\frac{\partial U_j}{\partial x_k}+U_k\frac{\partial}{\partial x_k}\overline{\tau u_j'}+r_\ell\frac{\partial U_k}{\partial x_\ell}\frac{\partial}{\partial r_k}\overline{\tau u_j'}+\overline{u_k u_j'}\frac{\partial T}{\partial x_k}=-\frac{1}{\rho}\frac{\partial}{\partial r_j}\overline{\tau\sigma'}+(\nu+\alpha)\frac{\partial^2\overline{\tau u_j'}}{\partial r_k\,\partial r_k}, \qquad (5-579)$$

and

$$\frac{1}{\rho}\frac{\partial^2\overline{\tau\sigma'}}{\partial r_j\,\partial r_j}=-2\frac{\partial U_j}{\partial x_k}\frac{\partial\overline{\tau u_k'}}{\partial r_j}, \qquad (5-580)$$

where u_i and u_j' are fluctuating velocity components at the arbitrary points P and P′, U_i is a mean velocity component, x_i is a space coordinate, r_i is a component of the vector extending from a point P to P′, t is the time, ρ is the density, ν is the kinematic viscosity, σ is the instantaneous pressure, and τ is the temperature fluctuation. Bars over terms designate correlations or averaged quantities. The subscripts can take on the values 1, 2, or 3, and a repeated subscript in a term indicates a summation.

In obtaining equations (5-576) to (5-580), the instantaneous velocities and temperatures in the incompressible Navier-Stokes and energy equations were first broken into mean and fluctuating components. The resulting equations were then written at two points in the turbulent field, multiplied by appropriate temperatures or velocity components and averaged. The equations for correlations involving pressures were obtained by taking the divergence of the Navier-Stokes equation and applying continuity. In order to make the locally-homogeneous approximation, the turbulence was considered homogeneous over a correlation length, or the scale of the inhomogeneity was much greater than the scale of the turbulence. Thus, $\partial/\partial x_i \ll \partial/\partial r_i$, where the operators operate on two-point correlations. (A calculation for axially decaying turbulence without mean velocity gradients (ref. 7, fig. 3) implies that this is a good approximation except in the region very close to the virtual origin of the turbulence.) Note also that, for locally homogeneous turbulence, the mean velocity and temperature may be considered to vary linearly over the small distances for which the correlations are appreciable, as assumed here. Finally, in order to make the set of equations determinate, the turbulence was assumed to be weak enough, or the mean gradients large enough, to neglect terms containing triple correlations. The turbulence in a flow with large velocity or temperature gradients may not have to be as weak as that in a flow without mean gradients. The terms containing those gradients may be large compared with triple correlation terms, even if the turbulence is moderately strong.

Equations (5-576) to (5-580) can be converted to spectral form by introducing the usual three-dimensional Fourier transforms defined as follows:

$$\overline{u_i u_j'}=\int_{-\infty}^{\infty}\varphi_{ij}e^{i\kappa\cdot r}d\kappa, \qquad (5-581)$$

$$\overline{\sigma u_j'} = \int_{-\infty}^{\infty} \lambda_j e^{i\kappa\cdot r} d\kappa, \tag{5-582}$$

$$\overline{u_i \sigma'} = \int_{-\infty}^{\infty} \lambda_i' e^{i\kappa\cdot r} d\kappa, \tag{5-583}$$

$$\overline{\tau u_j'} = \int_{-\infty}^{\infty} \gamma_j e^{i\kappa\cdot r} d\kappa, \tag{5-584}$$

and

$$\overline{\tau\sigma'} = \int_{-\infty}^{\infty} \zeta' e^{i\kappa\cdot r} d\kappa, \tag{5-585}$$

where κ is a wavevector having the dimension 1/length and $d\kappa = d\kappa_1\, d\kappa_2\, d\kappa_3$. Taking the Fourier transforms of equations (5-576) to (5-580), eliminating the pressure-velocity and pressure-temperature terms, and using continuity result in

$$U_k \frac{\partial}{\partial x_k}\varphi_{ij} = \frac{\partial U_\ell}{\partial x_k}\left[\left(2\frac{\kappa_\ell\kappa_j}{\kappa^2} - \delta_{j\ell}\right)\varphi_{ik} + \left(2\frac{\kappa_\ell\kappa_i}{\kappa^2} - \delta_{i\ell}\right)\varphi_{kj} + \kappa_\ell \frac{\partial \varphi_{ij}}{\partial \kappa_k}\right] - 2\nu\kappa^2\varphi_{ij} \tag{5-586}$$

and

$$U_k \frac{\partial \gamma_j}{\partial x_k} = \frac{\partial U_\ell}{\partial x_k}\left[\left(2\frac{\kappa_\ell\kappa_j}{\kappa^2} - \delta_{j\ell}\right)\gamma_k + \kappa_\ell \frac{\partial \gamma_j}{\partial \kappa_k}\right] - \frac{\partial T}{\partial x_k}\varphi_{kj} - (\alpha+\nu)\kappa^2\gamma_j, \tag{5-587}$$

where δ_{ij} is the Kronecker delta.

Equations (5-586) and (5-587) give contributions of various processes to the rates of change (with x_k) of spectral components of the turbulent energy tensor $\overline{u_i u_j}$ and of the turbulent heat transfer vector $\overline{\tau u_j}$. The terms in the equations which are proportional to $\partial/\partial\kappa_k$ are transfer terms which transfer activity into or out of a spectral component by the stretching or compressing of turbulent vortex filaments by the mean velocity gradient, as discussed in sections 5.4.2.1, 5.4.2.6, and 5.4.2.7. The terms with κ^2 in the denominator are spectral components of pressure-velocity or pressure-temperature correlations and transfer activity between directional components (section 5.4.2.1). The last terms in the equations are dissipation terms, which dissipate activity by viscous or by conduction effects. The dissipation term in equation (5-587) contains both viscous and conduction effects because it dissipates spectral components of velocity-temperature correlations. The remaining terms in the equations produce energy or activity by mean velocity or temperature-gradient effects.

For the present model, a two-dimensional contraction with the through-flow in the x_1-direction and the contraction in the x_3-direction is considered. The shear and temperature gradients also occur in the x_3-direction. Thus, the mean gradients present in the flow are $\partial U_1/\partial x_1$, $\partial U_3/\partial x_3$, $\partial U_1/\partial x_3$, and $\partial T/\partial x_3$. These gradients are all taken to be independent of position. By continuity of the mean flow,

$$\frac{\partial U_1}{\partial x_1} = -\frac{\partial U_3}{\partial x_3} \equiv a_{11}. \tag{5-588}$$

Similarly, set

$$\frac{\partial U_1}{\partial x_3} \equiv a_{13} \tag{5-589}$$

and

$$\frac{\partial T}{\partial x_3} \equiv b_3. \tag{5-590}$$

In addition, it is assumed that the turbulence is homogeneous in the transverse directions and that it changes only in the longitudinal or x_1 direction, so that

$$U_k \frac{\partial}{\partial x_k} = U_1 \frac{\partial}{\partial x_1}, \tag{5-591}$$

where the operators operate on the correlations or their Fourier transforms. For the model considered, then, equations (5-586) and (5-587) can be written as

$$U_1 \frac{\partial \varphi_{ij}}{\partial x_1} = a_{13}\left[\left(2\frac{\kappa_1\kappa_j}{\kappa^2} - \delta_{j1}\right)\varphi_{i3} + \left(2\frac{\kappa_1\kappa_i}{\kappa^2} - \delta_{i1}\right)\varphi_{3j} + \kappa_1 \frac{\partial \varphi_{ij}}{\partial \kappa_3}\right] + a_{11}\left[\left(2\frac{\kappa_1\kappa_j}{\kappa^2} - \delta_{j1}\right)\varphi_{i1} + \left(2\frac{\kappa_1\kappa_i}{\kappa^2} - \delta_{i1}\right)\varphi_{1j}\right.$$

$$\left. -\left(2\frac{\kappa_3\kappa_j}{\kappa^2} - \delta_{j3}\right)\varphi_{i3} - \left(2\frac{\kappa_3\kappa_i}{\kappa^2} - \delta_{i3}\right)\varphi_{3j} + \kappa_1 \frac{\partial \varphi_{ij}}{\partial \kappa_1} - \kappa_3 \frac{\partial \varphi_{ij}}{\partial \kappa_3}\right] - 2\nu\kappa^2\varphi_{ij} \tag{5-592}$$

and

$$U_1 \frac{\partial \gamma_j}{\partial x_1} = a_{13}\left[\left(2\frac{\kappa_1\kappa_j}{\kappa^2} - \delta_{j1}\right)\gamma_3 + \kappa_1 \frac{\partial \gamma_j}{\partial \kappa_3}\right] + a_{11}\left[\left(2\frac{\kappa_1\kappa_j}{\kappa^2} - \delta_{j1}\right)\gamma_1 - \left(2\frac{\kappa_3\kappa_j}{\kappa^2} - \delta_{j3}\right)\gamma_3 + \kappa_1 \frac{\partial \gamma_j}{\partial \kappa_1} - \kappa_3 \frac{\partial \gamma_j}{\partial \kappa_3}\right]$$

$$- b_3\varphi_{3j} - (\alpha + \nu)\kappa^2\gamma_j. \tag{5-593}$$

In these equations the shear and normal strain terms are separated and written as the first and second bracketed terms on the right sides of the equations.

For solving equations (5-592) and (5-593) it is assumed that the turbulence is isotropic at $x_1 = (x_1)_0$. That condition is satisfied by the relation (5-333):

$$\left(\varphi_{ij}\right)_0 = \frac{J_0}{12\pi^2}\left(\kappa^2\delta_{ij} - \kappa_i\kappa_j\right), \tag{5-333}$$

where J_0, as before, is a constant that depends on initial conditions. For the initial condition on $\gamma_i\left(\text{at } x_1 = (x_1)_0\right)$ it is assumed that

$$\left(\gamma_i\right)_0 = 0. \tag{5-594}$$

Thus, if the initial turbulence is produced by flow through a grid, that grid is unheated, and the temperature fluctuations are produced by the interaction of the mean temperature gradient with the turbulence.

Equations (5-592) and (5-593) are first-order partial differential equations in the three independent variables x_1,κ_1, and κ_3. In solving the equations, it is convenient to introduce the velocity ratio c which, for a uniform normal strain, is

$$c \equiv \frac{U_1}{(U_1)_0} = 1 + \frac{x_1 - (x_1)_0}{(U_1)_0} a_{11}. \tag{5-595}$$

Then,

$$U_1 \frac{\partial}{\partial x_1} = a_{11} c \frac{\partial}{\partial c}. \tag{5-596}$$

In order to reduce equations (5-592) and (5-593) to ordinary differential equations, the running variables ξ_1, ξ_3, and η are considered, of which κ_1, κ_3, and c are particular values such that $\xi_1 = \kappa_1$ and $\xi_3 = \kappa_3$ when $\eta = c$. If ξ_1, ξ_3, and η are introduced into the set of equations in place of κ_1, κ_3, and c, the resulting equations will, of course, automatically satisfy the original set.

Equation (5-592) (and eq. (5-593) with φ_{ij} replaced by γ_j) will then be of the form

$$-\xi_1 \frac{\partial \varphi_{ij}}{\partial \xi_1} + \eta \frac{\partial \varphi_{ij}}{\partial \eta} + \left(\xi_3 - \frac{a_{13}}{a_{11}} \xi_1 \right) \frac{\partial \varphi_{ij}}{\partial \xi_3} = F\left(\xi_1, \xi_3, \varphi_{ij}, \kappa_2\right).$$

To determine under what conditions

$$-\xi_1 \frac{\partial \varphi_{ij}}{\partial \xi_1} + \eta \frac{\partial \varphi_{ij}}{\partial \eta} + \left(\xi_3 - \frac{a_{13}}{a_{11}} \xi_1 \right) \frac{\partial \varphi_{ij}}{\partial \xi_3} = -\xi_1 \frac{d\varphi_{ij}}{d\xi_1}, \tag{5-597}$$

note that φ_{ij} is a function of ξ_1, ξ_3, and η and κ_2, so that

$$-\xi_1 \frac{d\varphi_{ij}}{d\xi_1} = -\xi_1 \frac{\partial \varphi_{ij}}{\partial \xi_1} - \xi_1 \frac{\partial \varphi_{ij}}{\partial \xi_3} \frac{d\xi_3}{d\xi_1} - \xi_1 \frac{\partial \varphi_{ij}}{\partial \eta} \frac{d\eta}{d\xi_1}.$$

Comparison of this last equation with equation (5-597) shows that they are equivalent if

$$-\xi_1 \frac{d\xi_3}{d\xi_1} = \xi_3 - \frac{a_{13}}{a_{11}} \xi_1$$

and

$$-\xi_1 \frac{d\eta}{d\xi_1} = \eta,$$

or

$$\xi_1 \xi_3 - \frac{1}{2} \frac{a_{13}}{a_{11}} \xi_1^2 = (\text{constant})_1 = \kappa_1 \kappa_3 - \frac{1}{2} \frac{a_{13}}{a_{11}} \kappa_1^2 \tag{5-598}$$

and

$$\eta \xi_1 = (\text{constant})_2 = c\kappa_1. \tag{5-599}$$

Thus, equation (5-597) will hold if $\xi_1 \xi_3 - (1/2)(a_{13}/a_{11}) \xi_1^2$ and $\eta \xi_1^2$ are constant during integration. With the introduction of equations (5-595) to (5-599), equations (5-592) and (5-593) become ordinary differential equations, components of which are

$$\frac{d\varphi_{11}(\xi_1)}{d\xi_1} = -\frac{2}{\xi_1} \left(2\frac{\xi_1^2}{h^2} - 1 - \frac{vh^2}{a_{11}} \right) \varphi_{11} - \frac{2}{\xi_1} \left[\frac{a_{13}}{a_{11}} \left(2\frac{\xi_1^2}{h^2} - 1 \right) - 2\frac{\xi_1 f}{h^2} \right] \varphi_{13}, \tag{5-600}$$

$$\frac{d\varphi_{13}(\xi_1)}{d\xi_1} = -2\frac{f}{h^2} \varphi_{11} - \frac{2}{\xi_1} \left[\frac{\xi_1 f}{h^2} \left(\xi_1^2 - f^2 + \frac{a_{13}}{a_{11}} \xi_1 f \right) - \frac{vh^2}{a_{11}} \right] \varphi_{13} - \frac{1}{\xi_1} \left[-2\frac{\xi_1 f}{h^2} + \frac{a_{13}}{a_{11}} \left(2\frac{\xi_1^2}{h^2} - 1 \right) \right] \varphi_{33}, \tag{5-601}$$

$$\frac{d\varphi_{33}(\xi_1)}{d\xi_1} = -4\frac{f}{h^2} \varphi_{13} - \frac{2}{\xi_1} \left[-\left(2\frac{f^2}{h^2} - 1 \right) + 2\frac{a_{13}}{a_{11}} \frac{\xi_1 f}{h^2} - \frac{vh^2}{a_{11}} \right] \varphi_{33}, \tag{5-602}$$

$$\frac{d\varphi_{ii}(\xi_1)}{d\xi_1} = -\frac{2}{\xi_1} (\varphi_{33} - \varphi_{11}) + \frac{2}{\xi_1} \frac{a_{13}}{a_{11}} \varphi_{13} + \frac{2}{\xi_1} \frac{vh^2}{a_{11}} \varphi_{ii}, \tag{5-603}$$

$$\frac{d\gamma_1(\xi_1)}{d\xi_1}=\frac{b_3}{\xi_1 a_{11}}\varphi_{13}-\frac{1}{\xi_1}\left[2\frac{\xi_1^2}{h^2}-1-(\alpha+\nu)\frac{h^2}{a_{11}}\right]\gamma_1-\frac{1}{\xi_1}\left[\frac{a_{13}}{a_{11}}\left(2\frac{\xi_1^2}{h^2}-1\right)-2\frac{\xi_1 f}{h^2}\right]\gamma_3, \tag{5-604}$$

and

$$\frac{d\gamma_3(\xi_1)}{d\xi_1}=\frac{b_3}{\xi_1 a_{11}}\varphi_{33}-2\frac{f}{h^2}\gamma_1-\frac{1}{\xi_1}\left[1-2\frac{f^2}{h^2}+2\frac{a_{13}}{a_{11}}\frac{\xi_1 f}{h^2}-(\alpha+\nu)\frac{h^2}{a_{11}}\right]\gamma_3, \tag{5-605}$$

where

$$f\equiv\frac{1}{\xi_1}\left[\frac{1}{2}\frac{a_{13}}{a_{11}}\left(\xi_1^2-\kappa_1^2\right)+\kappa_1\kappa_3\right] \tag{5-606}$$

and

$$h^2\equiv\xi_1^2+\kappa_2^2+\frac{1}{\xi_1^2}\left[\frac{1}{2}\frac{a_{13}}{a_{11}}\left(\xi_1^2-\kappa_1^2\right)+\kappa_1\kappa_3\right]^2. \tag{5-607}$$

In these equations ξ_3 has been eliminated by equation (5-598). The first three equations are independent of the remaining ones, but the converse is not true.

In order to apply initial conditions to the set of equations (5-600) to (5-605), let $\varphi_{ij}(\xi_1)=\left[\varphi_{ij}(\xi_1)\right]_0$ and $\gamma_i(\xi_1)=\left[\gamma_i(\xi_1)\right]_0$ when $\eta = 1$. These conditions will then automatically satisfy the desired initial conditions that $\varphi_{ij}(\kappa_1)=\left[\varphi_{ij}(\kappa_1)\right]_0$ and $\gamma_i(\kappa_1)=\left[\gamma_i(\kappa_1)\right]_0$ when $c = 1$ $\left[\text{or } U_1=(U_1)_0\right]$ since, by definition, $\xi_1=\kappa_1$ when $\eta = c$. Equation (5-599) shows that

$$(\xi_1)_0=c\kappa_1. \tag{5-608}$$

Equation (5-608) gives the value of ξ_1 at which to start the integration for given values of κ_1 and c. In order to satisfy the initial conditions (5-333) and (5-594), let

$$\left.\begin{aligned}
\varphi_{11}(\xi_1)&=\frac{J_0}{12\pi^2}\left(h^2-\xi_1^2\right)\\
\varphi_{13}(\xi_1)&=-\frac{J_0}{12\pi^2}\xi_1 f\\
\varphi_{33}(\xi_1)&=\frac{J_0}{12\pi^2}\left(h^2-f^2\right)\\
\varphi_{ii}(\xi_1)&=\frac{J_0}{6\pi^2}h^2\\
\gamma_i&=0
\end{aligned}\right\}\text{when } \xi_1=(\xi_1)_0,$$

where f and h are again given by equations (5-606) and (5-607). The integration of equations (5-600) to (5-605) then goes from $(\xi_1)_0$ to $\xi_1=\kappa_1$. We are mainly interested in the final values of φ_{ij} and γ_i, for which $\xi_1=\kappa_1$ (and $\xi_2=\kappa_2$ and $\eta= c$). The quantity ξ_1 can be considered as a dummy variable of integration.

In order to solve equations (5-600) to (5-605) numerically, it is convenient to convert them to dimensionless form by introducing the following dimensionless quantities:

$$\left[\frac{\nu(x-x_0)}{U_0}\right]^{1/2}\kappa_i \rightarrow \kappa_i, \tag{5-609}$$

$$\left[\frac{\nu(x-x_0)}{U_0}\right]^{1/2}\xi_1 \rightarrow \xi_1, \tag{5-610}$$

$$\left[\frac{(x-x_0)\nu}{J_0U_0}\right]\varphi_{ij} \rightarrow \varphi_{ij}, \tag{5-611}$$

$$\left(\frac{\nu}{J_0b_3}\right)\gamma_i \rightarrow \gamma_i, \tag{5-612}$$

$$\left[\frac{(x-x_0)}{U_0}\right]a_{13} \rightarrow a_{13}, \tag{5-613}$$

and

$$\frac{\nu}{\alpha} \rightarrow \mathrm{Pr}. \tag{5-614}$$

In addition, spherical coordinates were introduced into the equations by using the transformations

$$\left.\begin{aligned}\kappa_1 &= \kappa\cos\varphi\sin\theta\\ \kappa_2 &= \kappa\sin\varphi\sin\theta\\ \kappa_3 &= \kappa\cos\theta\end{aligned}\right\}. \tag{5-615}$$

The integrations were carried out numerically on a high-speed computer for various fixed values of dimensionless κ, θ, φ, a_{13}, and c. Directionally integrated spectrum functions can be obtained from (see sections 5.4.2.1. and 5.4.2.3).

$$\begin{pmatrix}\Psi_{ij}\\ \Gamma_i\\ \Lambda_{ij}\end{pmatrix} = \int_0^{\pi}\int_0^{2\pi}\begin{pmatrix}\varphi_{ij}\\ \gamma_i\\ \Omega_{ij}\end{pmatrix}\kappa^2\sin\theta\,d\varphi\,d\theta. \tag{5-616}$$

In this equation , Ω_{ij} is the vorticity spectrum tensor given by equation (5-348):

$$\Omega_{ij} = \left(\delta_{ij}\kappa^2 - \kappa_i\kappa_j\right)\varphi_{\ell\ell} - \kappa^2\varphi_{ij}. \tag{5-348}$$

The spectrum functions given by equations (5-616) can be integrated over all wavenumbers to give

$$\begin{pmatrix} \overline{u_i u_j} \\ \overline{\tau u_i} \\ \overline{\omega_i \omega_j} \end{pmatrix} = \int_0^\infty \begin{pmatrix} \Psi_{ij} \\ \Gamma_i \\ \Lambda_{ij} \end{pmatrix} d\kappa \qquad (5-617)$$

Thus, Ψ_{ij}, Γ_i and Λ_{ij} show how contributions to $\overline{u_i u_j}$, $\overline{\tau u_i}$, and $\overline{\omega_i \omega_j}$ are distributed among various wavenumbers or eddy sizes. Computed spectra and correlations will be considered next. For the quantities which involve temperature gradients, the curves will be given for a gas with a Prandtl number Pr of 0.7.

Calculated dimensionless energy spectra (spectra of dimensionless $\overline{u_i u_i}$) and dimensionless $\overline{\tau u_3}$ spectra are plotted in figures 5-133 and 5-134. The spectra are plotted for several values of the shear parameter and the normal strain parameter which are, respectively, proportional to $\partial U_1/\partial x_3$ and $\partial U_1/\partial x_1$ (see fig. 5-133). Both parameters are, in addition, proportional to longitudinal distance, so that increasing longitudinal distance has an effect similar to that of increasing the velocity gradients.

When plotted by using the similarity variables shown in figures 5-133 and 5-134, the dimensionless spectra for no shear and normal strain effects ($a_{13} = a_{11} = 0$) are the same for all values of x_1, although the turbulence itself decays. Comparison of the various curves indicates how normal strain and shear effects will alter the spectra for a given position and initial mean velocity. If, for instance, a dimensionless spectrum lies above the curve for $a_{13} = a_{11} = 0$, the turbulent activity for that case is greater than it would be for no shear or normal strain effects.

The curves in figures 5-133 and 5-134 (as well as the succeeding ones) are all for positive values of a_{11} and correspond to an accelerating flow. The curves indicate that, in general, the effects of both shear and normal strain in an accelerating flow are to feed energy or activity into the turbulent field. The effect of shear on the spectra is greater at small values of a_{11} than at larger ones; that is, it is greater when the ratio a_{13}/a_{11} is large.

A turbulent velocity-component parameter $(\nu/a_{11})^{5/2}\,\overline{u_i^2}/J_0$, with i = 1, 2, and 3, is plotted against longitudinal velocity ratio in figure 5-135. This parameter, in contrast to the spectral parameters in figures 5-133 and 5-134, does not contain $x_1 - (x_1)_0$, and thus can be used to show how $\overline{u_i^2}$ changes with longitudinal position (or velocity ratio) as well as with shear. Included in the plot is the curve obtained by solving equation (5-592) with the effects of shear and normal strain absent. This solution gives

$$\left(\frac{\nu}{a_{11}}\right)^{5/2} \frac{\overline{u_i^2}}{J_0} = \frac{\ln^{-5/2} c}{48\sqrt{2\pi}} \qquad (5-618)$$

Although the turbulence was taken to be initially isotropic, the results here show the turbulence as already strongly anisotropic from the effects of shear and normal strain. As was the case for the spectra, these results show that $\overline{u_i^2}$ is increased by the shear and that the effect of shear is greatest at low values of velocity ratio or normal strain parameter. For low values of velocity ratio, all components decay because of the effects of viscosity. In that region the lateral components decrease less rapidly than they would if the effects of normal strain were neglected (compare with dashed curve) and, for $a_{13} = 0$, the longitudinal component decays more rapidly. At larger velocity ratios, the components in the x_2- and x_3-directions begin to increase as the effects of normal strain offset those of viscosity. The component in the x_1-direction continues to decrease, but at a slower rate than it would if the effects of normal strain were absent. In this way, the curves in figure 5-135, which are for a two-dimensional contraction, differ from those for the axially symmetric strains in reference 78 and sections 5.4.2.6 and 5.4.2.7. For the axially symmetric strains, the longitudinal component decays more rapidly than it would for no effects of strain, whereas, in the present two-dimensional contraction, it decays less rapidly, except at small velocity ratios. Thus, in this case energy is fed into each of the three components of the turbulent energy by normal strain.

In an attempt to understand the trends shown in figure 5-135, the three components of the dimensionless turbulent vorticity $(\nu/a_{11})^{7/2}\,\overline{\omega_i^2}/J_0$ are plotted against velocity ratio in figure 5-136 for $a_{13} = 0$. The dashed curve for no effects of strain was obtained from the equation

$$\left(\frac{\nu}{a_{11}}\right)^{7/2} \frac{\overline{\omega_i^2}}{J_0} = \frac{5}{192\sqrt{2\pi}} \ln^{-7/2} c$$

The plot shows that the vorticity components in both the x_1- and x_2-directions decay less rapidly than they would if the effects of strain were absent, while the x_3-component decays more rapidly. On the other hand, for the axially symmetric cases considered in sections 5.4.2.6 and 5.4.2.7, only the longitudinal component $\overline{\omega_1^2}$ decayed less rapidly. Thus, although in the axially symmetric case, the turbulent vortex filaments all tended to line up in the longitudinal direction, in the present two-dimensional contraction there is also a tendency (although less pronounced) for an alignment to occur in the x_2-direction (direction of no contraction). These trends are in agreement with the trends for velocity fluctuations shown in figure 5-135. The velocities associated with a vortex filament will, of course, lie in planes normal to the direction of the filament. Thus, the vortex filaments aligned in the longitudinal direction will tend to feed energy into the two lateral velocity components, while those aligned in the x_2-direction can give energy to the longitudinal velocity component, as well as to the x_3-component.

It may be of interest to compare the behavior of the components of turbulent energy at large velocity ratios for several types of mean strain. A qualitative comparison is given in the following table:

Type of mean normal strain	Behavior of turbulent energy components at large velocity ratios in accelerating flow
Incompressible axisymmetric strain for flow in a cone (section 5.4.2.6)	Lateral components increase with longitudinal distance. Longitudinal component decreases faster than it would without effect of strain.
Uniform incompressible axisymmetric strain (section 5.4.2.7)	Lateral components approach steady state. Longitudinal component decreases faster with distance than it would without effects of strain.
Uniform compressible longitudinal axisymmetric strain (no lateral strain) (ref. 131)	Lateral components decrease less rapidly with distance than they would without effects of strain. Longitudinal component decreases more rapidly.
Uniform incompressible two-dimensional strain (present analysis)	Lateral components increase with longitudinal distance. Longitudinal component decreases, but at a rate slower than it would without effect of strain.

Figure 5-137 shows the effect of uniform shear and normal strain (velocity ratio) on ratios of the turbulent energy components for accelerating flow. Both $\overline{u_3^2}/\overline{u_1^2}$ and $\overline{u_2^2}/\overline{u_1^2}$ tend to decrease with increasing shear parameter and to increase with increasing normal strain parameter; that is, the effect of shear is to make $\overline{u_3^2}$ and $\overline{u_2^2}$ less than $\overline{u_1^2}$, and normal strain tends to make those quantities greater than $\overline{u_1^2}$.

Dimensionless turbulent heat-transfer parameters $\left[\nu^{5/2}/\left(J_0 a_{11}{}^{3/2}\right)\right]\overline{\tau u_i}/b_3$ with i = 3 and 1 are plotted in figure 5-138 as functions of velocity ratio and shear parameter. The trends shown here are qualitatively similar to those for the dimensionless velocity parameter shown in figure 5-135. It might seem surprising that there should be turbulent heat transfer in the longitudinal direction x_1, as given by the temperature-velocity correlation $\overline{\tau u_1}$, since there is no temperature gradient in the x_1-direction. However, since there is a correlation between τ and u_3 (because of the temperature gradient dT/dx_3) and a correlation between u_1 and u_3 (because of the velocity gradient dU_1/dx_3), it seems reasonable that there should be a correlation between τ and u_1, and thus a heat transfer in the x_1-direction.

Shear correlation coefficient $-\overline{u_1 u_3}\Big/\left[\left(\overline{u_1^2}\right)^{1/2}\left(\overline{u_3^2}\right)^{1/2}\right]$ is plotted as a function of longitudinal velocity ratio and shear parameter in figure 5-139. The shear correlation is, of course, zero for zero shear and increases as dimensionless a_{13} increases. Except at small velocity ratios and large values of shear parameter, where some increase in correlation with increasing normal strain (velocity ratio) occurs, normal strain tends to destroy the shear correlation.

Figure 5-140 shows the ratio of eddy conductivity to eddy viscosity plotted as a function of velocity ratio and shear parameter. The eddy conductivity and eddy viscosity are defined by the relations

$$\varepsilon_h = -\frac{\overline{\tau u_3}}{dT/dx_3}$$

and

$$\varepsilon = -\frac{\overline{u_1 u_3}}{dU_1/dx_3}.$$

As the shear parameter, dimensionless a_{13} increases, the ratio $\varepsilon_h/\varepsilon$ increases, reaches a maximum, and then decreases, although the trend is confined to moderately low values of velocity ratio. Results from section 5.4.2.3 for no normal strain show that $\varepsilon_h/\varepsilon$ ultimately approaches 1 as dimensionless a_{13} continues to increase. The results in figure 5-140 indicate that $\varepsilon_h/\varepsilon$ reaches a maximum with increasing velocity ratio, as well as with increasing dimensionless a_{13}.

As mentioned at the beginning of this section an apparent laminarization sometimes occurs in the turbulent boundary layers of accelerating flows. Some observed low heat-transfer values for flow in nozzles can evidently be explained by the fact that the mean velocity increases with distance in an accelerating flow (section 5.4.2.6). Some of the visual observations, however, seem to indicate that the turbulent energy itself decreases (ref. 134). Back, Massier, and Gier (ref. 136) suggested that the effect may be caused by a normal strain term in the energy equation which acts like a sink for turbulent energy. The term $2a_{11}\left(\overline{u_3^2} - \overline{u_1^2}\right)$ corresponds to the second term in equation (5-603), if that term is multiplied by $-\xi_1$ and integrated over all wavenumbers. The term can act like a sink only if $\overline{u_1^2}$ is greater than $\overline{u_3^2}$; otherwise, it acts like a normal strain production term. The results in figure 5-137 for $\overline{u_3^2}/\overline{u_1^2}$ indicate that the normal-strain production term will be negative at low values of velocity ratio and high values of shear parameter. On the other hand, the shear production term $-2a_{13}\overline{u_1 u_3}$ (which corresponds to the third term in equation (5-603) multiplied by $-\xi_1$ and integrated over all wavenumbers) will always be positive.

The ratio of the two production terms is shown in figure 5-141 as a function of longitudinal velocity ratio and shear parameter. The curves show that the normal-strain production term can be negative and thus act like a sink term for turbulent energy at low velocity ratios and high shear. However, in order for that term to offset the effect of the shear production term, the ratio of the two terms would, of course, have to be less than –1, and that does not occur for results in figure 5-141. It is possible that the ratio could be less than –1 at sufficiently large values of shear parameter. There appears to be a problem in making the normal strain production term sufficiently negative to offset the effect of the shear production term. The shear must be large to make the normal strain production term negative (by making $\overline{u_1^2} > \overline{u_3^2}$). In that case, however, the shear production term will also be large. The curves in figure 5-141 show that as velocity ratio (or normal strain parameter) increases, the normal strain production term becomes strongly positive, since the effect of normal strain is to make $\overline{u_1^2} < \overline{u_3^2}$.

To summarize the results of this section, note that, in general, both shear and normal strain in an accelerating flow increase the energy in the turbulent field in comparison to that which would be present for no shear or normal strain. This increase occurs in spite of the normal-strain production term in the turbulent energy equation that can, under certain conditions of combined shear and normal strain, be negative and thus act as a turbulent energy sink. For the results computed, the shear production term more than offsets the effect of the sink term, and the net result is that the turbulent energy increases.

The present results for a two-dimensional contraction show that the lateral components of the turbulent energy increase with longitudinal distance at large mean velocity ratios. The longitudinal component decreases, but at a slower rate than it would if the effects of normal strain were absent. Thus, energy is fed into each of the three components of the turbulent energy by normal strain (and shear). This case differs from axially symmetric strain cases of accelerating flows, where the longitudinal turbulence component decays faster with distance than it would if the effects of normal strain were absent. For the two-dimensional contraction, although most of the vortex filaments tend to line up in the longitudinal direction, there is also some tendency for them to align in the transverse direction of no normal strain.

The normal strain and shear both tend to produce anisotropy in the turbulence, but they work in opposite directions. The normal strain increases the ratios of the lateral components to the longitudinal component of the turbulent energy, while shear decreases the ratio.

In general, the turbulent shear correlation tends to be destroyed by the normal strain. An exception occurs at small velocity ratios and large shear, where some increase in correlation with increasing normal strain (velocity ratio) occurs.

As either the shear or normal strain parameter increases, the ratio of eddy conductivity to eddy viscosity reaches a maximum and then decreases. In the presence of lateral mean-shear velocity gradients and lateral temperature gradients, turbulent heat transfer occurs in the longitudinal as well as in the lateral direction, even though there is no longitudinal temperature gradient.

5.4.2.9 Maintenance and growth of shear-flow turbulence.—It is well known experimentally that turbulence can be maintained or caused to grow by a mean shear (e.g., in a boundary layer). However, it is not easy to explain that observation theoretically. It is usually assumed that the turbulence in a shear flow is maintained against viscous dissipation by work done on the Reynolds shear stress by the velocity gradient. Although that is no doubt true, it appears that the actual mechanism is slightly more subtle. For instance, although the turbulent energy may be maintained by work done on the Reynolds shear stress by the velocity gradient, it is not clear that the Reynolds shear stress itself will not decay.

Our study of homogeneous turbulence with uniform shear, which includes the interaction of the turbulence with the shear but neglects the turbulence self-interaction, shows that the turbulence ultimately decays (see section 5.4.2.1 and figure 5-63). This is shown by the dashed curves in figure 5-142, where u_i is a velocity fluctuation component, ν is the kinematic viscosity, J_0 is a constant depending on initial conditions, U_1 is the mean velocity, x_2 is the coordinate in the direction of the velocity gradient dU_1/dx_2, t is the time, and the overbar indicates an averaged value. (This nomenclature differs slightly from that in the preceding section, where the velocity gradient was in the x_3-direction, but is the same as that in section 5.4.2.1.) The turbulence is assumed isotropic at its virtual origin t_0. The decay occurs in spite of the fact that the model includes work done on the Reynolds stress by the velocity gradient. In section 5.4.2.1 it is shown that for certain initial conditions, the total energy at a point can grow for awhile. The transverse component of the turbulence in the direction of the mean gradient always decays, however, and eventually all of the components decay. On the basis of these results one might even be tempted to suppose that the Navier-Stokes equations are inadequate for investigating the possibility of a nondecaying turbulence; however, that supposition would not seem to be justified (ref. 137).

The equation for the rate of change of the two-point correlations (eq. (4-147)) can for the present case, be written in abbreviated form as

$$\frac{\overline{\partial u_i u_j'}}{\partial t} = -\left(\delta_{i1}\overline{u_2 u_j'}\frac{dU_1}{dx_2} + \delta_{j1}\overline{u_i u_2'}\frac{dU_1'}{dx_2'}\right) + D_{ij} + P_{ij} + T_{ij} + G_{ij}, \qquad (5-619)$$

where the primed and unprimed quantities are measured at the points P′ and P, and i and j can take on the values 1, 2, or 3. The Kronecker delta δ_{ij} equals 1 for $i = j$ and 0 for $i \neq j$. The first term on the right-hand side of equation (5-619) is the production term, and D_{ij}, P_{ij}, T_{ij}, and G_{ij} represent, respectively, dissipation, pressure, transfer, and diffusion terms.

It is argued in section 5.4.2.1 that $\overline{u_2^2}$ (or $\overline{u_2 u_2'}$), the turbulence component in the direction of the mean gradient, decays because the equation for the rate of change of that component does not contain a production term, and, in addition, the pressure-velocity correlations, for the model used, extract energy from that component. The decay of $\overline{u_2^2}$ then causes the Reynolds shear stress $\overline{u_1 u_2}$ to decay, since the latter contains u_2. There is then no mechanism for maintaining the turbulence, and all of the components ultimately decay because of viscous dissipation (see eq. (5-619)).

If the decay in the foregoing model of shear turbulence is due to the draining of energy out of the transverse component $\overline{u_2^2}$, as discussed above, then if that drain were prevented or counteracted, the turbulence should grow or at least be maintained. In the subsection **growth due to buoyancy**, etc. of section 5.4.2.5 it is shown that this depletion can be counteracted by introducing destabilizing buoyancy forces in the direction of the mean velocity gradient, and that all of the turbulence components then ultimately grow. However, it is not clear from that result just how much of the growth is due to the shear, since the buoyancy by itself can cause all three of the directional components of the turbulence to grow, although in that case the component in the direction of the buoyancy forces grows much faster than the others.

In order to determine whether shear by itself can cause turbulence to grow, we have prevented the energy drain from $\overline{u_2^2}$ by setting $\varphi_{22} = 1/2\varphi_{11}$ in the analysis of section 5.4.2.1, where φ_{ij} is the Fourier transform of $\overline{u_i u_j'}$. Since the equation for φ_{33}, like that for φ_{22}, does not contain a production term, we also set $\varphi_{33} = 1/2\varphi_{11}$ in order to prevent energy depletion in that component. However, the last assumption is unnecessary if we are interested only in the φ_{11}, φ_{22}, and φ_{12} components, since φ_{33} does not occur in the equations for those components. If we set $\varphi_{22} = \varphi_{33} = 1/2\varphi_{11}$, then $\overline{u_2^2} = \overline{u_3^2} = 1/2\,\overline{u_1^2}$. In making the calculations, we use the spectral equations of motion from section 5.4.2.1 for φ_{11} and φ_{12}, both of which contain production terms (see eq. (5-619)).

The results are shown by the solid curves in figure 5-142. In contrast with the dashed curves, where the energy was allowed to drain out of the transverse components, and all of the components decayed, the components $\overline{u_1^2}$ and $\overline{u_1 u_2}$ (and thus $\overline{u_2^2}$ and $\overline{u_3^2}$, since $\overline{u_2^2} = \overline{u_3^2} = 1/2\,\overline{u_1^2}$) now grow at large times. That is, if we keep the energy from draining out of the transverse components (particularly $\overline{u_2^2}$), the mean shear can cause an ultimate growth of the turbulence. Although the assumption that $\overline{u_2^2} = \overline{u_3^2} = 1/2\,\overline{u_1^2}$ may be somewhat arbitrary, the calculation under that assumption is enlightening, in that before making it we had no assurance that turbulence could grow or be maintained by shear when the drain of energy out of the transverse components was prevented.

The next question is how a severe imbalance between the directional components is prevented in an actual turbulent flow (other than a weak homogeneous turbulent flow). As discussed in section 5.4.2.1, if the turbulence is nonweak and/or the shear is not large the interaction of triple correlations with the pressure-velocity correlations can cause the latter to have an equalizing effect on the directional components. Also, inhomogeneities in the turbulent field may have an effect (ref. 138). Rotta (ref. 139) has discussed the directional redistribution of energy by the one-point pressure velocity-gradient correlations.

Another flow which sheds some light on the turbulence-producing mechanism was analyzed in the last section. That is the case of combined two-dimensional shear and normal strain in locally homogeneous turbulence without turbulence self-interaction. Although that flow was analyzed in the last section, the results given there did not elucidate the turbulence-growth aspects of the flow. The results in figure 5-143, which show the evolution of the turbulence components for a given value of $(\partial U_1/\partial x_2)/(\partial U_1/\partial x_1)$ do, however, show those aspects. The time increment $t - t_0$ is the time which would elaspse for an observer traveling with the accelerating fluid from the virtual origin of the turbulence at t_0 to the position x_1. For the results given, the fluid is being stretched in the direction of flow.

The dashed curves in figure 5-143 show that when the shear is zero, the positive longitudinal strain can cause $\overline{u_2^2}$ and $\overline{u_3^2}$ to grow, but that $\overline{u_1^2}$, the component in the direction of flow, decays. The shear component $\overline{u_1 u_2}$ is, of course, zero in that case. When a mean shear is applied (solid curves), all of the components ultimately grow. Here, it is clearer that the shear is having an important effect on the maintenance of turbulence than in the buoyancy case analyzed in section 5.4.2.5, where all of the directional components were maintained by the buoyancy alone. In the present case, the acceleration alone does not maintain the $\overline{u_1^2}$ component. (If $\partial U_1/\partial x_1 = 0$ but $\partial U_1/\partial x_2 \neq 0$, all of the components would decay as in the dashed curves of fig. 5-142.) The growth of all of the components in the present case is again due to the equalization of the energy in the directional components. (See fig. 5-143). Here, the shear and the normal strain have opposite effects as far as the directional distribution of energy is concerned, so that their combined effect is to keep the energy directionally distributed so that all components can grow.

It might seem surprising that in all of the cases considered here, in which a severe imbalance of energy between the directional components was prevented, the turbulence continued to increase with time rather than level off. There are no boundaries on the flows considered here, however, so that the effective Reynolds number of the mean flow is infinite. As the scale of the turbulence continues to grow, the eddies encounter larger and larger velocity differences, so that the effective driving forces on the disturbances continue to grow. The turbulence only grows, of course, at least in the case of uniform shear without acceleration, if sufficient energy is transferred into the transverse components, particularly into $\overline{u_2^2}$, as already discussed. It is conceiveable that the transfer of energy into $\overline{u_2^2}$ might in some cases be sufficient to prevent the turbulence from decaying as it does in section 5.4.2.1, but insufficient to cause it to grow. That, in fact, seems to be the case in the experiments of Rose (ref. 93), and of Champagne et al. (ref. 94) where a leveling off of intensity appears to occur, although the scale continues to grow. On the other hand, the work of Mulhearn and Luxton (ref. 95), where the total strains were larger than those of references 93 and 94, indicates a growth of intensity at large times. In the present paper we are mainly interested in whether, from a theoretical standpoint, the effect of a mean shear can be great enough to offset the effects of viscosity and keep a turbulent field from decaying, regardless of whether the turbulence ultimately grows or reaches a steady state.

5.4.3 Uniformly and Steadily Sheared Homogeneous Turbulence When Triple Correlations May Be Important

Thus far in section 5.4 we have considered only cases where mean gradients are large and/or the turbulence is weak (see section 5.4.2). In those cases one can generally neglect triple-correlation terms in the correlation equations, those terms being small compared with other terms. For other cases those terms should be retained.

In this section we obtain a numerical solution of the unaveraged Navier-Stokes equations for a uniformly and steadily sheared turbulence, as in reference 140.[18] Conceptually, that is the simplest turbulent shear flow (although certainly not the simplest to produce experimentally (see, e.g., ref. 94)). A number of other significant numerical studies of that type of turbulence have also been made (see, e.g., ref. 141). In those studies random initial conditions with a range of eddy sizes were used. That is in contrast to the present study, where nonrandom initial conditions with a single length scale are used.

The numerical method used here is essentially the same as that in section 5.3.2.6; fourth-order finite-spatial-differencing and a predictor-corrector time-differencing are used (a second-order leapfrog predictor and a third-order Adams-Moulton corrector (ref. 65)).

We use the unaveraged Navier-Stokes equations because, as discussed in the last chapter, the closure problem arises when nonlinear equations are averaged to obtain correlation equations. The equations to be solved are the incompressible Navier-Stokes equations given by equation (5-130):

$$\frac{\partial \tilde{u}_i}{\partial t} + \frac{\partial (\tilde{u}_i \tilde{u}_k)}{\partial x_k} = -\frac{1}{\rho}\frac{\partial \tilde{\sigma}}{\partial x_i} + \nu \frac{\partial^2 \tilde{u}_i}{\partial x_k \partial x_k} \qquad (5-130)$$

[18]The results obtained here are qualitatively similar to those in reference 140, although some of the latter were numerically underresolved.

where the mechanical pressure (see eq. (3-14)) is given by the Poisson equation (eq. (5-150)):

$$\frac{1}{\rho}\frac{\partial^2\tilde{\sigma}}{\partial x_\ell\,\partial x_\ell}=-\frac{\partial^2(\tilde{u}_\ell\tilde{u}_m)}{\partial x_\ell\,\partial x_m}, \tag{5-150}$$

and where as usual, the subscripts can take on the values 1, 2, or 3, and a repeated subscript in a term indicates a summation. The quantities $\tilde{u}_i$ and $\tilde{u}_j'$ are instantaneous velocity components (which include the mean velocity components), x_i is a space coordinate, t is the time, ρ is the density, ν is the kinematic viscosity, and $\tilde{\sigma}$ is the instantaneous (mechanical) pressure. Equation (5-150) is obtained by taking the divergence of equation (5-130) and using continuity (eq. 3-4).

In the spirit of section 5.3.2.6, the present numerical study of uniformly sheared turbulence starts with simple determinate initial conditions which possess a single length scale. As in section 5.3.2.6, we can in this way study how the turbulence develops from nonturbulent initial conditions, as it does for experimental grid-generated turbulence. Again, much higher Reynolds-number flows can be calculated with a given numerical grid when a single length scale is initially present, at least for early and moderate times.

As will be seen, several interesting results which could not be obtained in the previous work on turbulent shear flow are obtained here. One of the significant findings is that the structure of the turbulence produced in the presence of shear is finer than that produced in its absence.

For the numerical solutions considered here, the initial velocity fluctuation is assumed to be given by

$$u_i=\sum_{n=1}^{3}a_i^n\cos\mathbf{q}^n\cdot\mathbf{x}\,. \tag{5-620}$$

Then, from equation (4-14),

$$\tilde{u}_i=\sum_{n=1}^{3}a_i^n\cos\mathbf{q}^n\cdot\mathbf{x}+U_i\,. \tag{5-621}$$

The quantity a_i^n is an initial velocity amplitude or Fourier coefficient of the velocity fluctuation, $\mathbf{q}^n$ is an initial wavevector, and U_i is an initial mean-velocity component. In order to satisfy the continuity conditions, equations (4-10) and (4-21), we set

$$a_i^n q_i^n=0. \tag{5-622}$$

For the present work let

$$\begin{gathered}a_i^1=k(2,\pm1,1),\quad a_i^2=k(1,\pm2,1),\quad a_i^3=k(1,\pm1,2),\\ q_i^1=(-1,\pm1,1)/x_0,\quad q_i^2=(1,\mp1,1)/x_0,\quad q_i^3=(1,\pm1,-1)/x_0,\end{gathered} \tag{5-623}$$

where k has the dimensions of a velocity and determines the intensity of the initial velocity fluctuation. The quantity x_0 is the length scale of the initial velocity fluctuation. The quantities k and x_0, together with the kinematic viscosity ν and equation (5-623), then determine the initial Reynolds number $\left(\overline{u_0^2}\right)^{1/2}x_0/\nu$, since the square of equation (5-620), averaged over a period, gives $\overline{u_0^2}$. In addition to satisfying the continuity equation (5-622), equations (5-620) and)5-623) give

$$\overline{u_1^2}=\overline{u_2^2}=\overline{u_3^2}=\overline{u_0^2} \tag{5-624}$$

at the initial time. (The first three terms of equation (5-624) apply at all times when there are no mean gradients in the flow.) Thus equations (5-620) or (5-621), and (5-623) give a particularly simple initial condition, in that we need specify only one component

of the mean-square velocity fluctuation. Moreover, for no mean shear, they give an isotropic turbulence at later times, as in section 5.3.2.6. Note that it is necessary to have at least three terms in the summation in equations (5-620) or (5-621) to satisfy equation (5-624). We do not specify an initial condition for the pressure because it is determined by the Poisson equation for the pressure (eq. (5-150)) and the initial velocities.

In order to carry out numerical solutions subject to the initial condition given by equations (5-620) or (5-621), and(5-623), we use a stationary cubical grid with a maximum of 128^3 points and with faces at $x_i^* = x_i / x_0 = 0$ and 2π. For boundary conditions we assume periodicity for the fluctuating quantities; we consider turbulence (or a turbulent like flow) in a box with periodic walls. That is, let

$$(u_i)_{x_j^*=2\pi+b_j^*} = (u_i)_{x_j^*=b_j^*} \tag{5-625}$$

and

$$\sigma_{x_j^*=2\pi+b_j^*} = \sigma_{x_j^*=b_j^*}, \tag{5-626}$$

where $b_j^* = b_j / x_0, x_j^* = x_j / x_0$, and b_j is a variable length.

Using equations (4-14) and (4-15) these become

$$(\tilde{u}_i)_{x_j^*=2\pi+b_j^*} = (\tilde{u}_i)_{x_j^*=b_j^*} + (U_i)_{x_j^*=2\pi+b_j^*} - (U_i)_{x_j^*=b_j^*} \tag{5-627}$$

and

$$\tilde{\sigma}_{x_j^*=2\pi+b_j^*} = \tilde{\sigma}_{x_j^*=b_j^*} + P_{x_j^*=2\pi+b_j^*} - P_{x_j^*=b_j^*}. \tag{5-628}$$

In the present work we assume also that P, given by equation (4-27) when buoyancy is absent, is periodic, so that

$$P_{x_j^*=2\pi+b_j^*} = P_{x_j^*=b_j^*}, \tag{5-629}$$

and equation (5-628) becomes

$$\tilde{\sigma}_{x_j^*=2\pi+b_j^*} = \tilde{\sigma}_{x_j^*=b_j^*}. \tag{5-630}$$

These equations are used to calculate numerical derivatives at the boundaries of the computational grid.

Since we are considering a uniform shear, we let

$$U_i = \delta_{i1} \frac{dU_1}{dx_2} x_2 \tag{5-631}$$

in the initial condition (5-621) and

$$(U_i)_{x_j^*=2\pi+b_j^*} - (U_i)_{x_j^*=b_j^*} = \delta_{i1}\delta_{j2} 2\pi \frac{dU_1}{dx_2} \tag{5-632}$$

in the boundary condition 5-627. Equation (5-631) applies, of course, at all times and all x_i. For the coefficients in equation (5-621) we use equation (5-623), where we choose the first set of signs. Equations (5-130) and (5-150) are written in terms of the total velocity $\tilde{u}_i$, but we can calculate the fluctuating component u_i from equation (4-14). It should be emphasized that we do not consider here a sawtooth type of mean velocity profile, but a continuous profile in which the mean-velocity gradient is uniform at all points. Even with a uniform mean-velocity gradient, some local inhomogeneity is introduced into the fluctuations by the periodic boundary conditions. We shall not concern ourselves with that inhomogeneity, however, since we can still calculate products involving velocities and/or pressures averaged over a three-dimensional period. Those values are independent of the position of the boundaries of the cycle (see the paragraph containing equation (4-4)).

There may be another (related) problem in using periodic boundary conditions (eqs. (5-625) to (5-630)) with a uniform mean velocity gradient and a stationary (nondeforming) grid. For that case there is a tendency for singularities (discontinuties) to form at the boundaries of the computational box. This can be seen from equation (4-22), which for our case, can be written as

$$\frac{\partial u_i}{\partial t} = -\delta_{i1}\frac{dU_1}{dx_2}u_2 - \frac{dU_1}{dx_2}x_2\frac{\partial u_i}{\partial x_1} - \frac{\partial}{\partial x_k}(u_i u_k) - \frac{1}{\rho}\frac{\partial \sigma}{\partial x_i} + \nu\frac{\partial^2 u_i}{\partial x_k}. \qquad (5-633)$$

As noted earlier, σ_e drops out of the equations of motion for $g_i = 0$ by virtue of the equation following (3-22). Equation (5-633) can also be obtained from (5-130) and (5-631) by using Reynolds decomposition (see section 4.2).

By inspection of equation (5-633) one sees that the term $(dU_1/dx_2)\, x_2\, \partial u_i/\partial x_1$, will cause the fluctuation u_i to grow on the boundary at $x_2 = 2\pi\, x_0$ but not on the boundary at $x_2 = 0$. So with periodic boundary conditions there will be a tendency for discontiuties, and thus numerical instabilities, to form on the boundaries for x_2. That tendency can be eliminated by using a deforming numerical grid, as in references 142 and 141. In that case, however, the grid is soon distorted out of shape, and in addition the physical significance of the term $(dU_1/dx_2)\, x_2\, \partial u_i/dx_1$ is lost because that term is eliminated from the evolution equation for u_i. Fortunately the viscous term in equation (5-633) tends to smooth out discontinuties, particularly if the Reynolds number is not high. Our results, which use a stationary grid, bear that out. However, before presenting results for the nonlinear case we will discuss the simplified linearized equations. By doing that we may gain some insight into uniformly sheared turbulence, both with periodic boundary conditions and with boundary conditions at infinity, and into the relation of that turbulence to the term $(dU_1/dx_2)\, x_2\, \partial u_i/\partial x_1$.

5.4.3.1 The linearized problem.—By using Reynolds decomposition, equation (5-150) becomes, for our case (uniform mean shear and uniform mean pressure),

$$\frac{\partial^2 \sigma}{\partial x_\ell\, \partial x_\ell} = -\frac{\partial^2 (u_k u_\ell)}{\partial x_k\, \partial x_\ell} - 2\frac{\partial u_2}{\partial x_1}\frac{\partial U_1}{\partial x_2}, \qquad (5-634)$$

where equations (4-14) and (4-15) are used. Equations (5-633) and (5-634) are linearized by neglecting the terms $-\partial(u_i u_k)/\partial x_k$ and $-\partial^2(u_k u_\ell)/\partial x_k \partial x_\ell$. The numerical solution, with initial and (periodic) boundary conditions given by equations (5-620), (5-623), (5-625), and (5-626), then proceeds as in the nonlinear case.

We first obtain an analytical solution for unbounded linearized fluctuations by using unbounded three-dimensional Fourier transforms. Instead of working with the averaged equations as in section 5.4.2.1, it is instructive to work with the unaveraged ones, and use the initial condition given by equation (5-620). In this case the Fourier transforms must be generalized functions (a series of δ functions) (section 5.2), but the method of solution is the same as that in the earlier work. Equation (5-633) for u_2 and equation (5-634), when linearized, are independent of u_1 and u_3.The solution obtained by using the initial condition (5-620) is

$$u_2 = \sum_{n=1}^{3} U_2^n \cos\left(\mathbf{q}^n \cdot \mathbf{x} - a_{12} q_1^n t x_2\right), \qquad (5-635)$$

$$\sigma = \sum_{n=1}^{3} P^n \sin\left(\mathbf{q}^n \cdot \mathbf{x} - a_{12} q_1^n t x_2\right), \qquad (5-636)$$

where

$$U_2^n = \frac{a_2^n q^{n^2}}{q^{n^2} - 2a_{12}q_1^n q_2^n t + a_{12}^2 q_1^{n^2} t^2} \exp\left[-\nu t\left(q^{n^2} - a_{12}q_1^n q_2^n t + \frac{1}{3}a_{12}^2 q_1^{n^2} t^2\right)\right], \qquad (5-637)$$

$$P^n = \frac{-2\rho a_{12} a_2^n q_1^n q^{n^2}}{\left(q^{n^2} - 2a_{12}q_1^n q_2^n t + a_{12}^2 q_1^{n^2} t^2\right)^2} \exp\left[-\nu t\left(q^{n^2} - a_{12}q_1^n q_2^n t + \frac{1}{3}a_{12}^2 q_1^{n^2} t^2\right)\right], \qquad (5-638)$$

$a_{12} = dU_1/dx_2$, $q^{n^2} = q_1^{n^2} + q_2^{n^2} + q_3^{n^2}$, and the a_i^n and q_i^n are given in the initial conditions (eqs. (5-620) and (5-623) (with the first set of signs). Mean values are obtained by integrating over all space. For instance,

$$\overline{\sigma u_2} = \sum_{n=1}^{3} \frac{1}{2} P^n U_2^n. \tag{5-639}$$

According to the linearized analytical solution given by equation (5-635), the manufacture of small-scale fluctuations takes place only in the x_2-direction. Because of the analytical character of equation (5-635) and the regularity of the initial condition, the fluctuation u_2 is nonrandom. Evidently, as in the case of no mean gradients, the only way one can have a linear turbulent solution is to put the turbulence in the initial conditions (section 5.4.2.1). The development of small-scale nonrandom structure is produced by the quantity $a_{12}\, q_1^n t x_2$ in the argument of the cosine in equation (5-635) ($a_{12} = dU_1/dx_2$). That quantity arises from the term $-a_{12}x_2\partial u_2/\partial x_1$ in equation (5-633). Thus the term $a_{12}x_2\partial u_2/\partial x_1$, or equivalently $a_{12}\, q_1^n t x_2$, acts like a chopper which breaks the flow into small-scale components.

For discussing the linearized case for constant periodic boundary conditions, it is convenient to convert equations (5-633) and (5-634) to a spectral form by taking their three-dimensional Fourier transforms (section 5.2). This gives for u_2, on neglecting nonlinear terms,

$$\frac{\partial \varphi_2^n}{\partial t} = a_{12} q_1^n \sum_{\kappa_2'} \frac{1}{\kappa_2'} \varphi_2^n(\kappa_1, \kappa_2 - \kappa_2', \kappa_3) - \nu\left(q_1^{n^2} + \kappa_2^2 + q_3^{n^2}\right)\varphi_2^n + \frac{2a_{12} q_1^n \kappa_2 \varphi_2^n}{q_1^{n^2} + \kappa_2^2 + q_3^{n^2}}, \tag{5-640}$$

where

$$\varphi_2^n(\kappa) = \frac{1}{8\pi^3} \int_{-\pi}^{\pi} dx_2 \int\int_{-\infty}^{\infty} u_2^n(x) e^{-i\kappa \cdot x} dx_1 dx_3, \tag{5-641}$$

$$u_2^n(x) = \sum_{\kappa_2 = -\infty}^{\infty} \int\int_{-\infty}^{\infty} \varphi_2^n(\kappa) e^{i\kappa \cdot x} d\kappa_1 d\kappa_3, \tag{5-642}$$

$$u_2 = \sum_{n=-3}^{3} u_2^n, \varphi_2 = \sum_{n=-3}^{3} \varphi_2^n, \tag{5-643}$$

κ is the wavevector, and φ_2 is the Fourier transform of u_2. Note that a finite transform is used in the x_2-direction in order to satisfy periodic boundary conditions at $x_2/x_0 = -\pi, \pi$.

Strictly speaking, equation (5-640) is for a sawtooth mean-velocity profile, whereas the numerical results are for a uniform mean-velocity gradient. Equation (5-640) should still apply, however, at least for the present discussion purposes to points inside but not outside the computational grid.

For constant periodic boundary conditions for u_i, small-scale structure in the fluctuations or the transfer of energy between wavenumbers is produced by the term containing the summation over κ_2' in equation (5-640). That term is the Fourier transform of $-a_{12}x_2\partial u_2/\partial x_1$ (eq. (5-633)). From its form we see that it can produce a complicated inter-wavenumber interaction. The quantity φ_2^n at each κ_2 interacts with φ_2^n at every other allowable κ_2. A difference between the solutions for unbounded conditions and those for constant periodic conditions is that only fluctuations at intergal κ_2 are possible when periodic conditions are imposed, whereas for unbounded conditions, fluctuations are possible at all values of κ_2. Thus spectra plotted against κ_2 are discrete for periodic boundary conditions, rather than continuous as they are for unbounded flows.

5.4.3.2 Nonlinear results.—Figure 5-144 shows a numerically calculated development of instantaneous velocity profiles for uniformly sheared turbulence. The profiles, which are initially regular and given by equation (5-621), soon take on a turbulent-like appearance. In particular, that is the case for profiles plotted in the x_2-direction. For the low initial Reynolds number shown, and 128^3 grid points, the profiles are well-resolved, even though steep gradients characteristic of turbulent flow often occur. Note, however, that we have to use a much finer computational gird with sheared turbulence than we did for the unsheared turbulence in section 5.3.2.6, apparently to resolve singularities which may tend to form in our sheared case. The viscous terms in the instantaneous equations appear to do a good job of smoothing out any singularities which may tend to form (see discussion following equation (5-633)). Calculated values at grid points are indicated by symbols.

As discussed in the last section, the linear term $(dU_1/dx_2)\, x_2\, \partial u_i/\partial x_2$ in equation (5-633) acts like a chopper which manufactures small-scale components, but cannot by itself produce radomization. Only the nonlinear term $\partial(u_i u_k)/\partial x_k$ can by itself, do that. But the linear term in combination with $\partial(u_i u_k)/\partial x_k$ can produce randomization by proliferation of harmonic components (one loses track of the individual components because of their sheer number) and by strange behavior (strange attractors in the nondecaying case), as will be discussed in the chapter on chaos and sensitive dependence on initial conditions (chapter VI).

The linear term $(dU_1/dx_2)x_2\, \partial u_i/\partial x_1$ in equation (5-633) apparently produces small-scale temporal as well as small-scale spatial fluctuations. That is illustrated in figure 5-145. When the mean shear is removed from the flow, the small-scale temporal fluctuations die out, leaving only larger ones. Figure 5-145 shows, in a particularly graphic manner, the effectiveness of the term $(dU_1/dx_2)x_2\, \partial u_i/\partial x_1$ in producing small-scale turbulent structure. Note the correspondence between that term and the mean-gradient transfer term $T_{ij}''(\kappa)$ in equations (5-326) and (5-330).

Finally, we present evolution curves for mean-square values of u_1, u_2, and u_3 in figure 5-146, where the overbars indicate space-averaged values (see paragraphs containing eqs. (4-4) and (4-3)). The longitudinal component $\overline{u_1^2}$ soon becomes much larger than the other directional components. That occurs because the turbulence-production terms (the second and third terms in equation (5-296)) are nonzero only in the evolution equation for $\overline{u_1^2}$. Whatever energy goes into $\overline{u_2^2}$ and $\overline{u_3^2}$ gets there through directional transfer by the pressure-velocity terms in equation (5-296). The smallest component of the sheared turbulence is $\overline{u_2^2}$, in agreement with the analytical results in section 5.4.2 and experiment. After the shear is removed, the three components ultimately tend toward equality; that is a necessary condition for the turbulence to approach the isotropic state. Again, *that* effect is produced by the pressure-velocity terms in equation (5-296). Note that $\overline{u_2^2}$ continues to increase for a short time after the shear is removed, probably because it receives energy from $\overline{u_1^2}$. It is not entirely clear why $\overline{u_3^2}$ does not also increase by receiving energy from $\overline{u_1^2}$. It seems likely that since energy has been drained out of the $\overline{u_2^2}$ – component by the shear to a greater extent than out of $\overline{u_3^2}$, it will tend to return more rapidly to $\overline{u_2^2}$ than to $\overline{u_3^2}$ when the shear is removed. That argument would make more sense if the shear were removed earlier, when $\overline{u_2^2}$ is still significantly less than $\overline{u_3^2}$. Perhaps the numerical method breaks down for the portions of the curves from say $t^* = 0.25$ to 0.325; the Reynolds number based on $\overline{u_1^2}^{1/2}$ may become too high in that region for accurate numerical results to be obtained.

5.5 CONCLUDING REMARKS

This long chapter begins with a discussion of Fourier analysis; it is pointed out that Fourier analysis is a convenient way of studying the distribution and transfer of turbulent activity among scales of motion. In addition it simplifies the basic equations by replacing spatial derivatives by algebraic expressions. A distinction has to be made between equations containing only averaged quantities and those containing, in addition, instantaneous (unaveraged) quantities. The latter require a consideration of generalized functions (functions which do not exist in the ordinary sense). Basic continuum equations for turbulence are obtained in physical and in spectral space; these include the averaged and unaveraged (instantaneous) forms. Spectral transfer of turbulent activity is studied for both homogeneous and inhomogeneous turbulence.

The remainder of the chapter consists mostly of illustrative solutions of the basic turbulence equations, those solutions being obtained to study various turbulence processes. The solutions are divided into those with and without uniform mean gradients. The latter consider mainly spectral transfer between wavenumbers produced by nonlinear turbulence self-interaction and its interaction with turbulence dissipation. The former consider, on the other hand, spectral transfer and production of turbulence by mean gradients. Linearized analytical solutions are obtained for weak turbulence without mean gradients and for stronger turbulence with large mean gradients; they are shown to agree quite well with available experimental data. Solutions for stronger turbulence without mean gradients in which the correlation equations are closed by specification of sufficient random initial conditions also give realistic results in agreement with experiment. Those solutions involve the "gap" problem—that is, the problem of bridging the gap between the infinite amount of data theoretically required to specify the initial condition of the turbulence and the limited data generally available. Our solutions appear to successfully bridge the gap, in that the evolution of all of the quantities used to specify the initial turbulence are calculated. Also, nonlinear turbulent solutions with and without uniform mean velocity gradients, and in which the initial conditions are nonrandom, are obtained numerically. The regular initial fluctuations quickly acquire a turbulent like appearance. Moreover, the insertion of mean shear into the flow produces small-scale temporal fluctuations.

REFERENCES

1. Orszag, S.A.: Numerical Simulation of Turbulent Flows; in Handbook of Turbulence, vol. 1, edited by W. Frost and T.H. Moulden, Plenum Press, New York, NY, 1977, pp. 281–313.
2. Farge, M.: Wavelet Transforms and their Applications to Turbulence; in Annu. Rev. Fluid Mech., vol. 24, edited by J.L. Lumley, M. Van Dyke, and H.L. Reed, Annual Reviews Inc., Palo Alto, CA, 1992, pp. 395–457.
3. Lumley, J.L.: Coherent Structures in Turbulence; in Transition and Turbulence, edited by R.E. Meyer, Academic Press, New York, NY, 1981, pp. 215–242.
4. Batchelor, G.K.: The Theory of Homogeneous Turbulence. Cambridge University Press, New York, NY, 1953.
5. Tolstov, G.P.: Fourier Series. Prentice-Hall, Inc., Englewood Cliffs, NJ, 1962.
6. Tranter, C.J.: Integral Transforms in Mathematical Physics. John Wiley and Sons, Inc., New York, NY, 1956.
7. Deissler, R.G.: Effects of Inhomgeneity and of Shear Flow in Weak Turbulent Fields. Phys. Fluids, vol. 4, no. 10, 1961, pp. 1187–1198.
8. Craya, A.: Contribution a l'Analyse de la Turbulence Associee a des Vitesses Moyennes. Publ. SCi. Tech. Minist. Air Fr. no. 345, 1958.
9. Richardson, L.F.: Weather Prediction by Numerical Process. Cambridge University Press, Cambridge, 1922.
10 Monin, A.S. and Yaglom, A.M.: Statistical Fluid Mechanics: Mechanics of Turbulence, vol. 2. MIT Press, Cambridge, MA, 1975.
11. Gel'fand, I.M. and Shilov, G.E.: Generalized Functions, vol. 1, Properties and Operations, Academic Press, New York, NY, 1964.
12. Lightlhill, M.J.: Introduction to Fourier Analysis and Generalized Functions, Cambridge University Press, New York, NY, 1970.
13. Lumley, J.L.: Stochastic Tools in Turbulence, Academic Press, New York, NY, 1970.
14. Gradshteyn, I.S. and Ryzhik, I.M.: Table of Integrals, Series, and Products, Academic Press, New York, NY, 1980, pp. 496, 1034, and 337.
15. Batchelor, G.K. and Proudman, I.: The Large-Scale Structure of Homogeneous Turbulence. Phil. Trans. Roy. Soc. A, vol. 248, no. 949, 1956, pp. 369-405.
16. Heisenberg, W.: Zur Statistischen Theorie der Turbulenz, Z. Phys., vol. 124, 1948, pp. 628-657.
17. Kovaznay, L.S.G.: Spectrum of Locally Isotropic Turbulence. J. Aeronaut. Sci. vol. 15, no. 12, 1948, pp. 745-753.
18. Kraichnan, R.H.: Lagrangian-History Closure Approximation for Turbulence. Phys. Fluids, vol. 8, 1965, pp. 575-598.
19. Herring, J.R.: Statistical Turbulence Theory and Turbulence Phenomenology; in Free Turbulent Shear Flows, vol. 1: Conference Proceedings. NASA SP-321, 1973, pp. 41-66.
20. Herring, J.R.: An Introduction and Overview of Various Theoretical Approaches to Turbulence; in Theoretical Approaches to Turbulence, edited by D.L. Dwoyer, M.Y. Hussaini, and R.G. Voigt, Springer-Verlag, New York, NY, 1985, pp. 73-90.
21. Deissler, R.G.: On the Decay of Homogeneous Turbulence before the Final Period. Phys. Fluids, vol. 1, no. 2, 1958, pp. 111-121.
22. Deissler, R.G.: A Theory of Decaying Homogeneous Turbulence. Phys. Fluids, vol. 3, no. 2, 1960, pp. 176-187.
23. Kraichnan, R.H.: Relationships among some Deductive Theories of Turbulence; in Mechanics of Turbulence, Gordon and Breach, New York, NY, 1964, pp. 99-106.
24. Orszag, S.A.: Lectures on the Statistical Theory of Turbulence; in Fluid Dynamics, edited by R. Balian and Peube, J.L., Gordon and Breach, New York, NY, 1985, pp. 235-374.
25. Leslie, D.C.: Developments in the Theory of Turbulence. Clarendon, Oxford, England, 1973.
26. Kraichnan, R.H.: Dynamics of Nonlinear Stochastic Systems. J. Math. Phys., vol. 2, 1961, pp. 124-148. Erratum: vol. 3, 1962, p. 205.
27. von Kármán, T. and Howarth, L.: On the Statistical Theory of Isotropic Turbulence. Proc. Roy. Soc. A. vol. 164, 1938, pp. 192-215.
28. Tatsumi, T.: The Theory of Decay Process of Incompressible Isotropic Turbulence. Proc. Roy. Soc. (London) A, vol. 230, 1957, pp. 16-145.
29. Saffman, P.G.: The Large-Scale Structure of Homogeneous Turbulence, J. Fluid Mech., vol. 27, part 3, 1967, pp. 581-593.
30. Miller, W.L. and Gordon, A.R.: Numerical Evaluation of Infinite Series and Integrals which arise in Certain Problems of Linear Heat Flow, Electrochemical Diffusion, etc. J. Phys. Chem., vol. 35, 1931, pp. 2785-2884.

31. Loeffler, A.L. and Deissler R.G.: Decay of Temperature Fluctuations in Homogeneous Turbulence Before the Final Period. Int. J. Heat Mass Transfer. vol. 1, no. 4, 1961, pp. 312-324.
32. Batchelor, G.K. and Townsend, A.A.: Decay of Turbulence in the Final Period. Proc. Roy. Soc. A, vol. 194, 1948, pp. 527-543.
33. Clark, R.A., Ferziger, J.H., and Reynolds, W.C.: Evaluation of Subgrid-Scale Models Using an Accurately Simulated Turbulent Flow. J. Fluid Mech. vol. 91, part 1, 1979, pp. 1-16.
34. Stewart, R.W. and Townsend, A.A.: Similarity and Self-Preservation in Isotropic Turbulence. Phil. Trans. Roy. Soc. A., vol. 243, no. 867, 1951, pp. 359-386.
35. Uberoi, M.S.: Energy Transfer in Isotropic Turbulence. Phys. Fluids, vol. 6, no. 8, 1963, pp. 1048-1056.
36. Van Atta, C.W. and Chen, W.Y.: Measurements of Spectral Energy transfer in Grid Turbulence. J. Fluid Mech., vol. 38, no. 4, 1969, pp. 743-763.
37. Ling, S.C. and Saad, A.: Experimental Study of the Structure of Isotropic Turbulence with Intermediate Range of Reynolds Number, vol. 20, no. 11, 1977, pp. 1796-1799.
38. Ling, S.C. and Huang, T.T.: Decay of Weak Turbulence. Phys. Fluids, vol. 13, no. 12, 1970, pp. 2912-2924.
39. Kolmogorov, A.N.: The Local Structure of Turbulence in Incompressible Viscous Fluid for very Large Reynolds Numbers. Proc. R. Soc. Lon. A, vol. 434, 1991; pp. 9-13. (First published in Russian in Dokl. Akad. Nauk SSSR, vol. 30, no. 4, 1941, pp. 299-303.)
40. Obukhov, A.M.: Spectral Energy Distribution in a Turbulent Flow. Dokl. Akad, Nauk SSSR, vol. 32, no. 1, 1941, pp. 22-24.
41. Obukhov, A.M.: Structure of the Temperature Field in a Turbulent Flow. Izv. Akad. Nauk SSSR, Ser. Geogr. i Geofiz., vol. 13, no. 1, 1949, pp. 58-69.
42. Hunt, J.C.R. and Vassilicos, J.C.: Kolmogorov's Contributions to the Physical and Geometrical Understanding of Small-Scale Turbulence and Recent Developments. Proc. R. Soc. Lond. A, vol. 434, 1991, pp. 183-210.
43. Landahl, M.T. and Mollo-Christensen, E.: Turbulence and Random Processes in Fluid Mechanics. Cambridge University PressNew York, NY, 1986, p. 63.
44. Betchov, R.: On the Non-Gausian Aspects of Turbulence. Archives of Mechanics; Archiwum Mechaniki Stosowanej· 28, 5-6, pp. 837-845, Warszawa 1976.
45. Kraichnan, R.H.: The Structure of Isotropic Turbulence at Very High Reynolds Numbers. J. Fluid Mech. vol. 5, 1959, pp. 497-543.
46. Kraichnan, R.H.: Inertial-Range Transfer in Two- and Three-Dimensional Turbulence, vol. 47, part 3, 1971, pp. 525-535.
47. Lii, K.S., Rosenblatt, M., and Van Atta, C.: Bispectral Measurements in Turbulence. J. Fluid Mech., vol. 77, part 1, 1976, pp. 45-62.
48. Yeung, P.K. and Brasseur, J.G.: The Response of Isotropic Turbulence to Isotropic and Anisotropic Forcing at the Large Scales. Phys. Fluids A, vol. 3, no. 5, May, 1991, pp. 884-987.
49. Domaradzki, J.A. and Rogallo, R.S.: Local Energy Transfer and Nonlocal Interactions in Homogeneous, Isotropic Turbulence. Phys. Fluids A, vol. 2, no. 3, March, 1990, pp. 413-426.
50. Deissler, R.G.: On the Localness of the Spectral Energy Transfer in Turbulence. Appl. Sci. Res., vol. 34, Winter 1978, pp. 379-392.
51. Deissler, R.G.: Comparison of a Correlation Term-Discard Closure for Decaying Homogeneous Turbulence with Experiment. Phys. Fluids, vol. 22, no. 1, Jan. 1979, pp. 185-186.
52. Deissler, R.G.: Remarks on the Decay of Homogeneous Turbulence from a Given State. Phys. Fluids, vol. 17, no. 3, Mar. 1974, pp. 652-653.
53. Deissler, R.G.: Some Remarks on the Approximations for Moderately Weak Turbulence. Phys. Fluids, vol. 8, no. 11, Nov. 1965, pp. 2106-2107.
54. Kraichnan, R.H.: Convergents to Turbulence Functions. J. Fluid Mech., vol. 41, pt. 1, Mar. 26, 1970, pp. 189-217.
55. Kraichnan, R.H.: Invariance Principles and Approximation in Turbulence Dynamics. Dynamics of Fluids and Plasmas. S.I. Pai, ed., Academic Press, 1966, pp. 239-255.
56. Erdélyi, A.: Asymptotic Expansions. Dover Pulications, 1956.
57. Deissler, R.G.: Nonlinear Decay of a Disturbance in an Unbounded Viscous Fluid. NASA TN D-4947, 1968. (Also in Appl. Sci. Res., vol. 21, no. 6, Jan. 1970, pp. 393–410.)
58. Deissler, R.G.: Decay of Homogeneous Turbulence from a Given Initial State. Phys. Fluids, vol. 14, no. 8, Aug. 1971, pp. 1629-1638. (Corrected and expanded version in NASA TN D-6728, 1972.)

59. Deissler, R.G.: Decay of Homogeneous Turbulence from a Given State at Higher Reynolds Number. Phys. Fluids, vol. 22, no. 10, Oct. 1979, pp. 1852-1856.
60. Hogge, H.D. and Meecham, W.C.: The Wiener-Hermite Expansion Applied to Decaying Isotropic Turbulence Using a Renormalized Time-Dependent Base. J. Fluid Mech., vol.. 85, part 2, 1978, pp. 325-347.
61. Graff, P.: An Exact Turbulence Theory for the Burgers Equation. Z. Angew. Math. Phys., vol. 20, 1969, pp. 461-478.
62. Taylor, G.I. and Green, A.E.: Mechanism of the Production of Small Eddies from Large Ones. Proc. Roy. Soc. (London), ser. A, vol. 158, no. 895, Feb. 3, 1937, pp. 499-521.
63. McCormick, J.M. and Salvadore, M.G.: Numerical Methods in Fortran. Prentice-Hall, Englewood Cliffs, NJ, 1964, p. 38.
64. Orszag, S.A. and Israeli, M.: Numerical Simulation of Viscous Incompressible Flows. In Annu. Rev. Fluid Mech. vol. 6, ed. by M. Van Dyke, W.G. Vincenti, and J.V. Wehausen, Annual Reviews Inc., Palo Alto, CA, 1974, pp. 281-318.
65 Ceschino, F. and Kuntzmann, J.: Numerical Solution of Initial Value Problems. Prentice-Hall, Englewood Cliffs, NJ, 1966, p. 141, example 2, and p. 143.
66. Deissler, R.G.: Turbulent Solutions of the Navier-Stokes Equations. Phys. Fluids, vol. 24, 1981, pp. 1595-1601.
67. Taylor, G.I.: Diffusion by Continuous Movements. Proc. London Math. Soc., vol. 20, 1922, pp. 196-212.
68. Frenkiel, F.N.: Turbulent Diffusion: Mean Concentration Distribution in a Flow Field of Homogeneous Turbulence. Vol. III of Advances in Appl. Mech., Richard von Mises and Theodore von Kármán, eds., Academic Press, Inc., 1953, pp. 61-107.
69. Batchelor, G.K. and Townsend. A.A.: Turbulent Diffusion. Surveys in Mechanics, G.K. Batchelor and R.M. Davies, eds., Cambridge Univ. Press, 1956.
70. Deissler, R.G.: Analysis of Multipoint-Multitime Correlations and Diffusion in Decaying Homogeneous Turbulence. NASA TR R-96, 1961.
71. Burgers, J.M.: On Turbulent Fluid Motion. Rep. E-34.1, Hydrodynamics Lab., C.I.T., July 1951.
72. Baldwin, L.V.: Turbulent Diffusion in the Case of Fully Developed Pipe Flow. Ph,. D. Thesis. Case Inst. Tech., 1959.
73. Bass, J.: Space and Time Correlations in a Turbulent Fluid, pts. I and II. Univ. Calif. Pub. in Statistics, Univ. Calif. Press, 1954.
74. Lin, C.C.: Remarks on the Spectrum of Turbulence. Proc. First Symposia of Appl. Math. vol. 1. Am. Math. Soc., 1949, pp. 81-86.
75. Uberoi, M.S. and Corrsin, S.: Diffusion of Heat from a Line Source in Isotropic Turbulence. NACA Rept. 1142, 1953. (Supersedes NACA TN-2710.)
76. Burgers, J.M. and Mitchner, M.: On Homogeneous Non-Isotropic Turbulence Connected with a Mean Motion having a Constant Velocity Gradient. I. Koninklijke Nederlandse Akademie van Wetenschappen, Proc. Ser. B., vol. 56, no. 3, 1953, pp. 228-235.
77. Burgers, J.M. and Mitchner, M.: On Homogeneous Non-Isotropic Turbulence Connected with a Mean Motion having a Constant Velocity Gradient II. Koninklijke Nederlandse Adaemie van Wetenschappen. Proc. Ser. B., vol. 56, no. 4, pp. 343-354.
78. Pearson, J.R.A.: The Effect of Uniform Distortion on Weak Homogeneous Turbulence. J. Fluid Mech., vol. 5, pt. 2, Feb. 1959, pp. 274-288.
79. Hildebrand, F.B.: Advanced Calculus for Engineers. Prentice-Hall, Inc., Englewood Cliffs, NJ, 1948, p. 374.
80. Fox, J.: Velocity Correlations in Weak Turbulent Shear Flow. Phys. Fluids, vol. 7, no. 4, Apr. 1964, pp. 562-564.
81. Sandborn, V.A. and Braun, W.H.: Turbulent Shear Spectra and Local Isotropy in the Low-Speed Boundary Layer. NACA TN-3761, 1956.
82. Corrsin, S.: Local Isotropy in Turbulent Shear Flow. NACA RM 58B11,1958.
83. Townsend, A.A.: Local Isotropy in the Turbulent Wake of a Cylinder. Australian J. Sci. Research, Ser. A, vol. 1, no. 2, 1948, pp. 161-174.
84. Corrsin, S., and Uberoi, M.S.: Spectra and Diffusion in a Round Turbulent Jet. NACA Rept. 1040, 1951 (Supersedes NASA TN-3761).
85. Laufer, J.: Some Recent Measurements in a Two-Dimensional Turbulent Channel. J. Aeronaut. Sci., vol. 17, May, 1950, pp. 277-287.
86. Townsend, A.A.: On the Fine Scale Structure of Turbulence. Proc. Roy. Soc. (London) Series A, vol. 208, no. 1095, 1951, pp. 534-542.
87. Corrsin, S.: Some Current Problems in Turbulent Shear Flows. Symposium on Naval Hydrodynamics, Academy of Sciences-National Research Council, Publication No. 515, Washington, DC, 1957, pp. 373-407.

88. Taylor, G.I.: Production and Dissipation of Vorticity in a Turbulent Fluid. Proc. Roy. Soc. (London) Series A, vol. 164, no. 918, 1938, pp. 15-23.
89. Theodorsen, T.: The Mechanism of Turbulence. Proceedings of the Second Midwestern Conference on Fluid Mechanics, Ohio State Univ., Columbus, OH, 1952, pp. 1-18.
90. Weske, J.R. and Plantholt, A.H.: Discrete Vortex Systems in the Transition Range of Fully Developed Flow in a Pipe. J. Aeronaut. Sci., vol. 20, 1953, pp. 717-718.
91. Hasen, E.M.: A Nonlinear Theory of Turbulence Onset in a Shear Flow. J. Fluid Mech., vol. 29, pt. 4, 1967, pp. 721-729.
92. Deissler, R.G.: Effect of Initial Condition on Weak Homogeneous Turbulence with Uniform Shear. Phys. Fluids, vol. 13, no. 7, July 1970, pp. 1868-1869.
93. Rose, W.G.: Results of an Attempt to Generate a Homogeneous Turbulent Shear Flow. J. Fluid Mech., vol. 25, pt. 1, 1966, pp. 97-120.
94. Champagne, F.H., Harris, V.G., and Corrsin, S.: Experiments on Nearly Homogeneous Turbulent Shear Flow. J. Fluid Mech., vol. 41, pt. 1, 1970, pp. 81-139.
95. Mulhearn, P.J. and Luxton, R.E.: The Development of Turbulence Structure in a Uniform Shear Flow. J. Fluid Mech., vol. 68, pt. 3, 1975, pp. 577-590.
96. Lin, C.C., ed.: Turbulent Flows and Heat Transfer. Princeton Univ. Press, Princeton, NJ, 1959.
97. Hinze, J.O.: Turbulence. McGraw-Hill, New York, 1959.
98. Knudsen, J.G. and Katz, D.L.: Fluid Dynamics and Heat Transfer. McGraw-Hill, New York, 1958.
99. Jakob, M.: Heat Transfer, vol. II. John Wiley and Sons, New York, 1957.
100. Eckert, E.R.G. and Drake, R.M., Jr.: Analysis of Heat and Mass Transfer. McGraw-Hill, New York, 1972.
101. Burmeister, L.C.: Convective Heat Transfer. John Wiley and Sons, New York, 1983.
102. Kays, W.M.: Convective Heat and Mass Transfer. McGraw-Hill, New York, 1966.
103. Rohsenow, W.M. and Choi, H.Y.: Heat, Mass, and Momentum Transfer. Prentice-Hall, Englewood Cliffs, NJ, 1961.
104. McAdams, W.H.: Heat Transmission. McGraw-Hill, New York, 1954.
105. Kreith, F.: Principles of Heat Transfer, 4th ed. Harper and Row, New York, 1986.
106. Corrsin, S.: Heat Transfer in Isotropic Turbulence. J. Appl. Phys., vol. 23, 1952, pp. 113-118.
107. Dunn, D.W. and Reid, W.H.: Heat Transfer in Isotropic Turbulence during the Final Period of Decay. NACA TN-4168, 1958.
108. Deissler, R.G.: Turbulent Heat Transfer and Temperature Fluctuations in a Field with Uniform Velocity and Temperature Gradients. Int. J. Heat Mass Transfer, vol. 6, 1963, pp. 257-270.
109. Deissler, R.G.: Analysis of Fully Developed Turbulent Heat Transfer at Low Peclet Numbers in Smooth Tubes with Application to Liquid Metals. NACA RME52F05, 1952.
110. Jenkins, R.: Variation of the Eddy Conductivity with Prandtl Modulus and its Use in Prediction of Turbulent Heat Transfer Coefficients. Preprints of Papers-Heat Transfer and Fluid Mechanics Institute. Stanford University Press, Stanford, CA, 1951, pp. 147-158.
111. Fox, J.: Turbulent Temperature Fluctuations and Two-Dimensional Heat Transfer in a Uniform Shear Flow. Int. J. Heat Mass Transfer, vol. 8, 1965, pp. 467-480.
112. Deissler, R.G.: Turbulence in the Presence of a Vertical Body Force and Temperature Gradient. J. Geophys. Res., vol. 67, no. 8, July 1962, pp. 3049.
113. Loeffler, A.L.: Electric Field Modification of Turbulence in a Fluid Containing Space Charge. Grumman Research Report, RE-384, July 1970. Grumman Aircraft Engineering Corp., Bethpage, NY.
114. Townsend, A.A.: Turbulent Flow in a Stably Stratified Atmosphere. J. Fluid Mech., vol. 3, p. 4, Jan. 1958, pp. 361-372.
115. Deissler, R.G.: Effects of Combined Buoyancy and Shear on Weak Homogeneous Turbulence. NASA TN D-3999, 1967.
116. Webster, C.A.G.: An Experimental Study of Turbulence in a Density-Stratified Shear Flow. J. Fluid Mech., vol. 19, p. 2, June 1964, pp. 221-245.
117. Deissler, R.G.: Growth due to Buoyancy of Weak Homogeneous Turbulence with Shear. Z. Angew. Math. Phys. vol. 22, 1971, pp. 267-274.
118. Prandtl, L.: Attaining a Steady Air Stream in Wind Tunnels. NACA TM–726, 1933.
119. Taylor, G.I.: Turbulence in Contracting Stream. Zeit. Angew. Math. Mech., vol. 15, no. 1/2, Feb. 1935, pp. 91-96.
120. Ribner, H.S. and Tucker, M.: Spectrum of Turbulence in a Contracting Stream. NACA TN-2606, 1952.
121. Batchelor, G.K. and Proudman, I.: The Effect of Rapid Distortion of a Fluid in Turbulent Motion. Quart. J. Mech. Appl. Math., vol. 7, 1954, pp. 83-103.

122. Deissler, R.G.: Weak Locally Homogeneous Turbulence in Idealized Flow through a Cone. J. Appl. Math. Phys. (ZAMP), vol. 18, Fasc. 2, 1967, pp. 165-183 (see also NASA TN D-3613, 1966).
123. Mills, R.R., Jr. and Corrisin, S.: Effect of Contraction on Turbulence and Temperature Fluctuations Generated by a Warm Grid. NASA Memo 5-5-59W, 1959.
124. Uberoi, S.: Effect of Wind-Tunnel Contraction on Free-Stream Turbulence. J. Aeron. Sci. 23, No. 8, pp. 754-764, 1956.
125. Boldman, D.R., Schmidt, J.F., and Fortini, A.: Turbulence, Heat-Transfer, and Boundary Layer Measurements in a Conical Nozzle with a Controlled Inlet Velocity Profile, NASA TN D-3221, 1966.
126. Boldman, D.R., Schmidt, J.F., and Ahlers, R.C.: Effect of Inlet Configuration on the Turbulent Boundary Layer and Heat Transfer in a Conical Nozzle Operating with Air, ASME Preprint, 1967.
127. Back, L.H., Massier, P.F., and Gier, H.L.: Convective Heat Transfer in a Convergent-Divergent Nozzle, Int. J. Heat Mass Transfer. 7, no. 5, pp. 549-568, 1964.
128. Grant, H.L., Stewrat, R.W., and Molliet, A.: Turbulence Spectra from a Tidal Channel. J. Fluid Mech., vol. 12, pt. 2, Feb. 1962, pp. 241-268.
129. Deissler, R.G.: Weak Locally Homogeneous Turbulence and Heat Transfer with Uniform Normal Strain. J. Appl. Math. Mech (ZAMM), vol. 48, Heft 2, 1968, pp. 87-98 (see also NASA TN D-3779, 1967).
130. Kuethe, A.M., Willmarth, W.W., and Crocker, G.H.: Stagnation Point Fluctuations on Bodies of Revolution with Hemispherical Noses. Rep. No. 02753-2-F (AFOSR TR 60-65), Michigan University, College of Eng., June 1960.
131. Deissler, R.G.: Effect of Uniform Longitudinal Strain Rate on Weak Homogeneous Turbulence in a Compressible Flow. NASA TN D-2800, 1965.
132. Kestin, J., Maeder, P.F., and Sogin, H.H.: The Influence of Turbulence on the Transfer of Heat to Cylinders near the Stagnation Point. Z. Angew. Math. Phys., vol. 12, no. 2, 1961, pp. 115-132.
133. Sutera, S.P.: Vorticity Amplification in Stagnation-Point Flow and its Effect on Heat Transfer. J. Fluid Mech., vol. 21 pt. 3, Mar. 1965, pp. 513-534.
134. Kline, S.J.: Observed Structure Features in Turbulent and Transitional Boundary Layers. Fluid Mechanics of Internal Flow. Gino Sovran, ed., Elsevier Publ. Co., 1967, p. 39.
135. Kays, W.M.: Convective Heat and Mass transfer. MCGraw-Hill Book Co., Inc., 1966, p. 96.
136. Back, L.H., Massier, P.F., and Gier, H.L.: Convective Heat Transfer in a Convergent-Divergent Nozzle. Int. J. Heat Mass Transfer, vol. 7, no. 5, 1964, pp. 549–568.
137. Deissler, R.G.: Growth of Turbulence in the Presence of Shear. Phys. Fluids, vol. 15, no. 11, Nov. 1972, pp. 1918-1920.
138. Deissler, R.G.: Problem of Steady-State Shear-Flow Turbulence. Phys. Fluids, vol. 8, no. 3, 1965, pp. 391-398.
139. Rotta, J.C.: Turbulent Boundary Layers in Incompressible Flow. In Prog. Aeronaut. Sci., vol. 2, ed., by A. Ferri, D. Kuchemann and L.H.G. Sterne. Pergamon Press, Oxford, New York, pp. 1-219.
140. Deissler, R.G.: Turbulent Solutions of the Equations of Fluid Motion. Rev. Mod. Phys., vol. 56, no. 2, part 1, April 1984, pp. 223-254.
141. Rogallo, R.S.: Numerical experiments in Homogeneous Turbulence. NASA TM-81315, 1981.
142. Deissler, R.G. and Rosenbaum,, B.M.: Nonlinear Evolution of a Disturbance in an Unbounded Viscous Fluid with Uniform Shear. NASA TN D-7284, 1973.

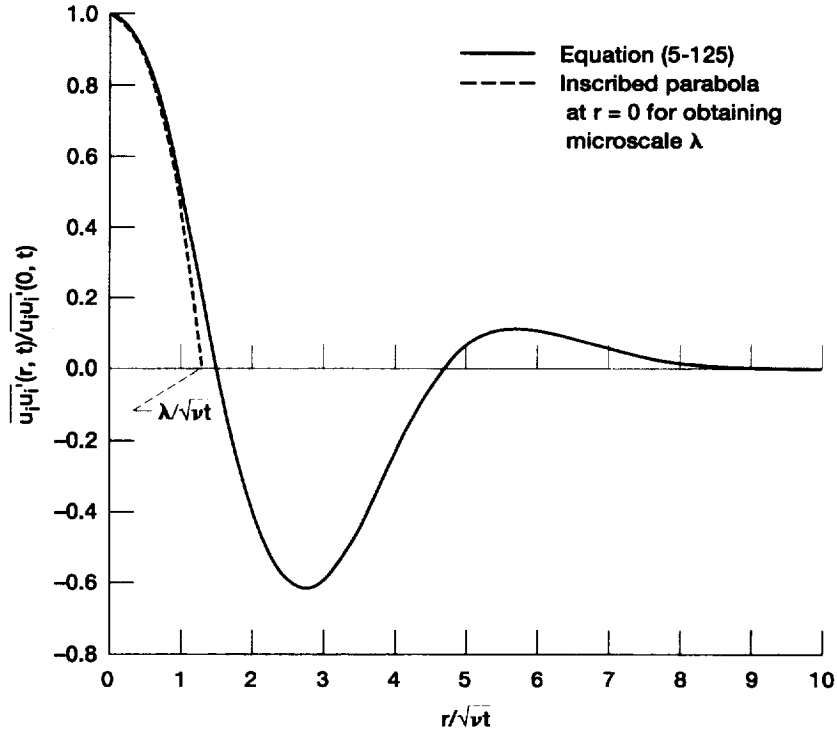

Figure 5-1.—Dimensionless plot of a two-point turbulent velocity correlation in the final period of decay.

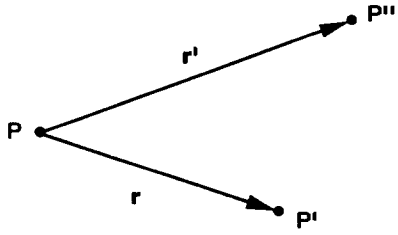

Figure 5-2.—Vector configuration for three-point correlation equations.

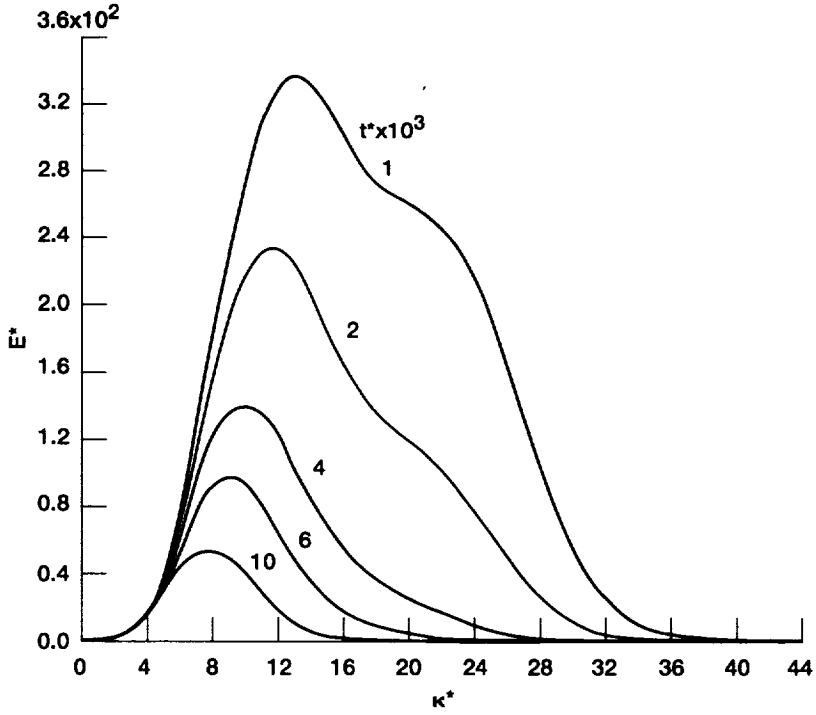

Figure 5-3.—Variation of theoretical energy spectrum with time for approach to final period. Reynolds number based on mesh size and mean velocity, 950. $\beta_0^* = 1.55x10^{-11}$, $t_0^* = -6.33x10^{-3}$.

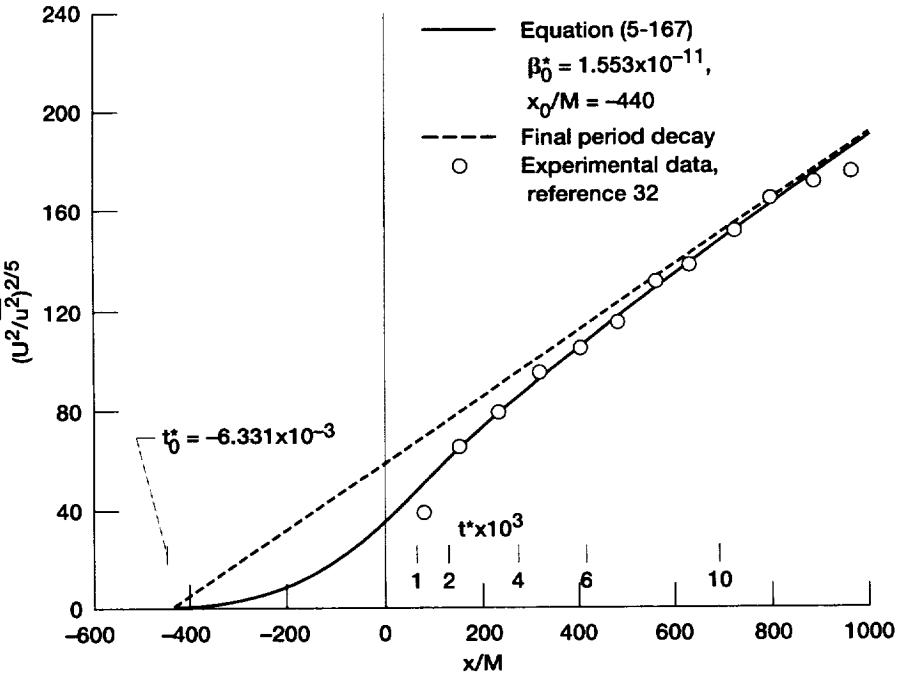

Figure 5-4.—Turbulence-decay plot for determining parameters in figure 5-3. $J_0^* = J_0 U^{1/2}/(\nu M)^{5/2} = 1.929 \times 10^4$, $\beta_0^* = \nu^5 \beta_0 / J_0^4 = 1.553 \times 10^{-11}$, $x_0/M = -440$, M = 0.159 cm, R = UM/ν = 950, $t^* = (x/M)/(J_0^* R)^{2/3}$.

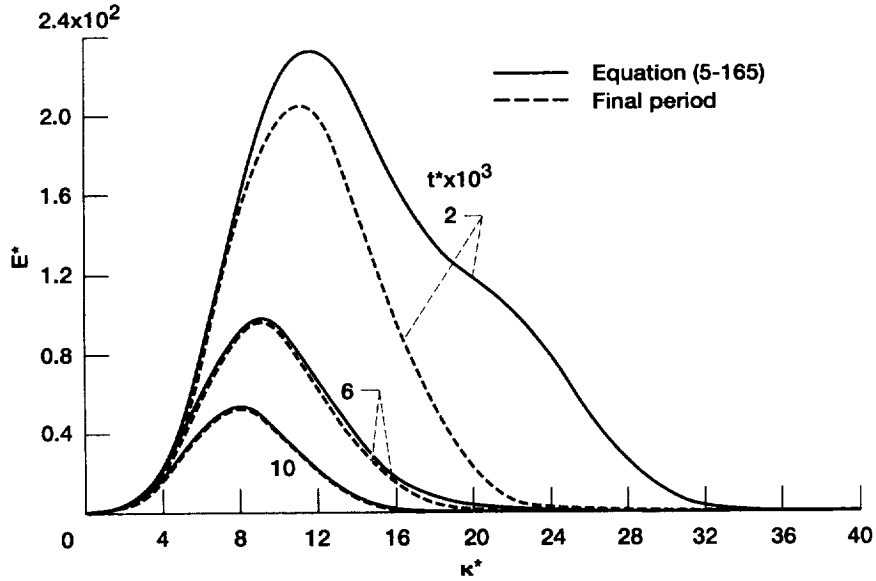

Figure 5-5.—Comparision of theoretical spectra with those for final period. R = 950, $\beta_0^* = 1.55 \times 10^{-11}$, $t_0^* = -6.33 \times 10^{-3}$, $5 < R_\lambda < 8$.

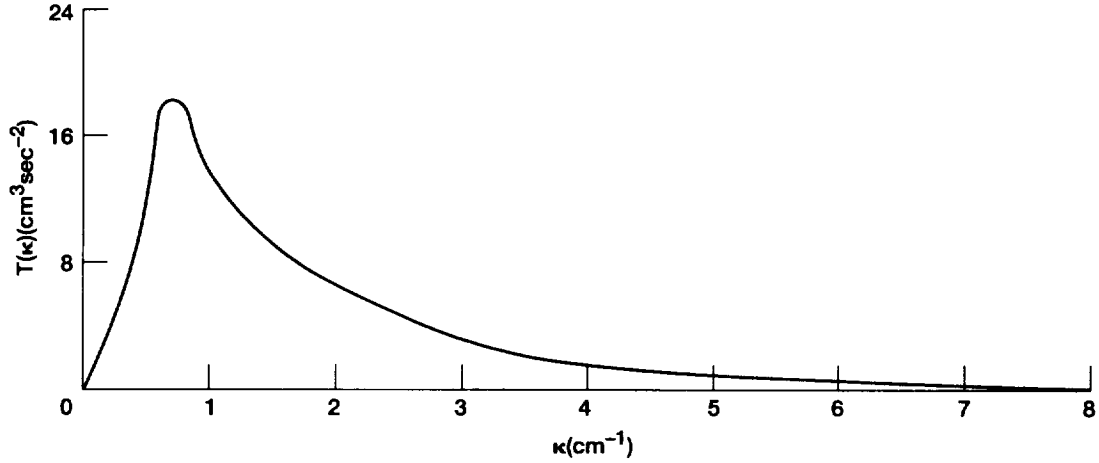

Figure 5-6.—Energy spectrum for homogeneous turbulence obtained from a numerical solution of the instantaneous Navier-Stokes equations by Clark, Ferziger and Reynolds (ref. 33). $R_\lambda = 36.6$.

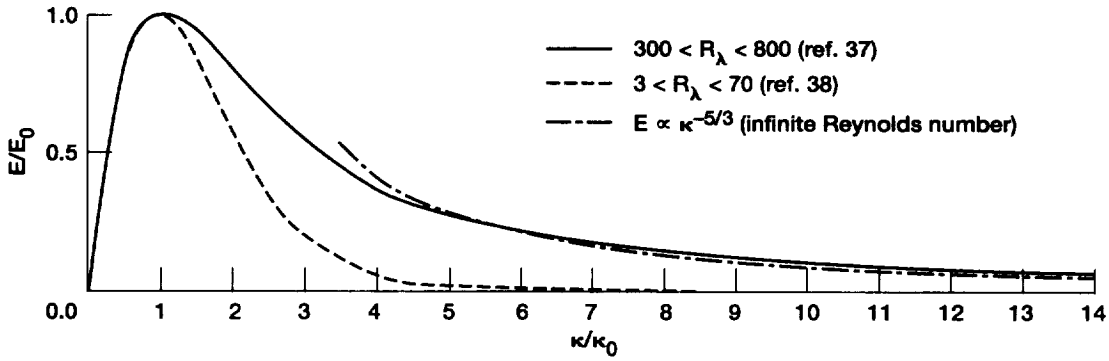

Figure 5-7.—Experimental and –5/3-power energy spectra. Subscript zeroes refer to values at peak.

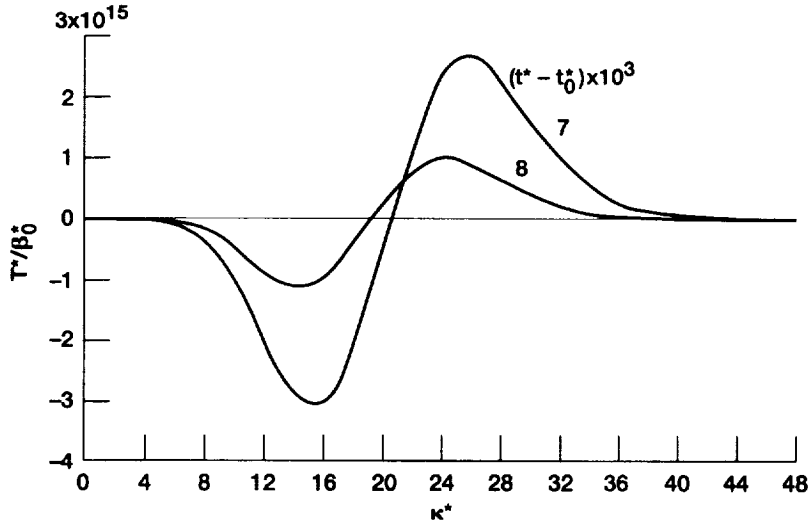

Figure 5-8.—Variation of dimensionless energy transfer term with κ^* and $t^* - t_0^*$.

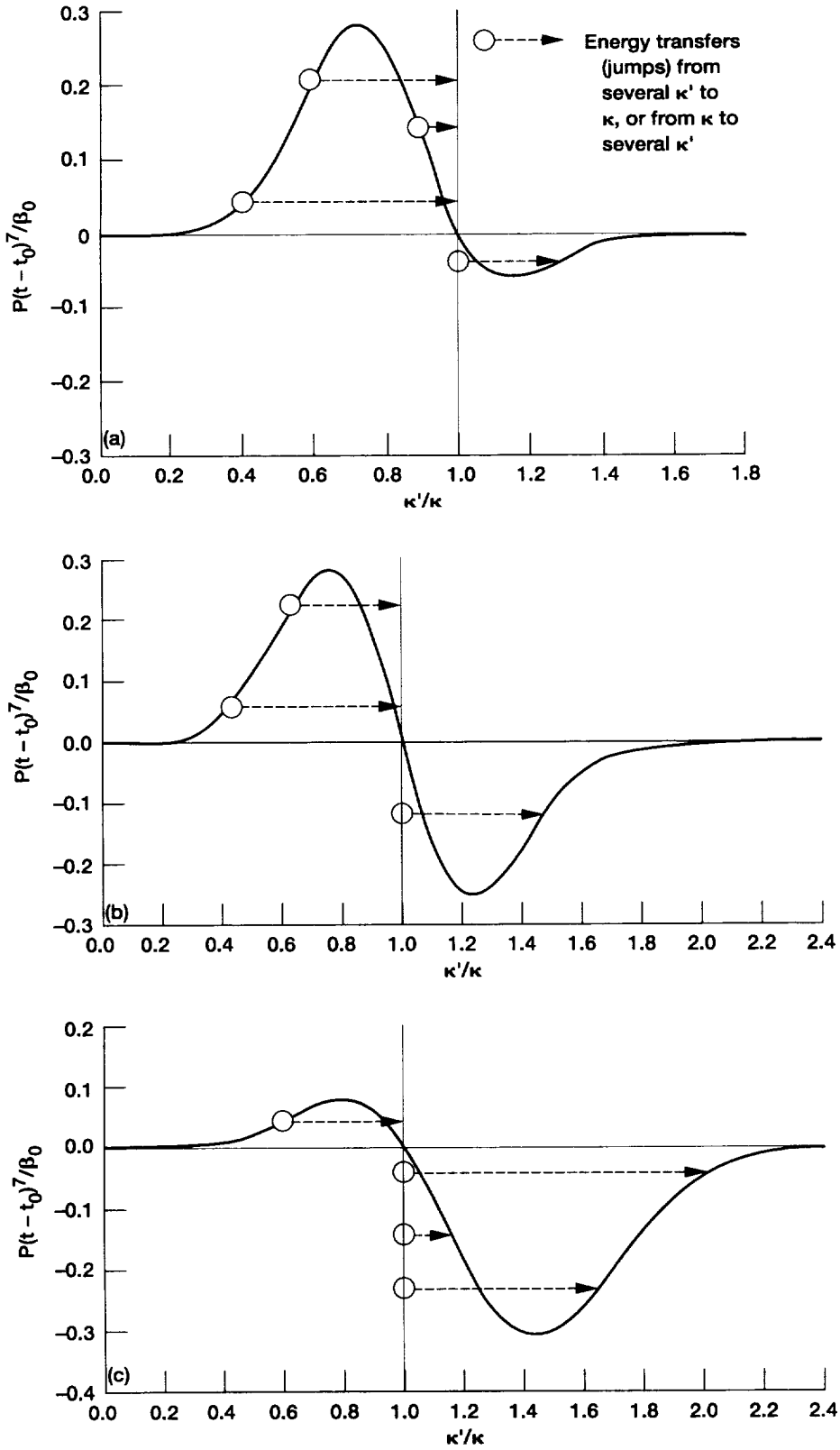

Figure 5-9.—Plot showing contributions to energy transfer at κ from various wave numbers κ'. (a) $\kappa[\nu(t - t_0)]^{1/2} = 2.15$, T a positive maximum. (b) $\kappa[\nu(t - t_0)]^{1/2} = 1.71$, T = 0. (c) $\kappa[\nu(t - t_0)]^{1/2} = 1.29$, T a negative maximum.

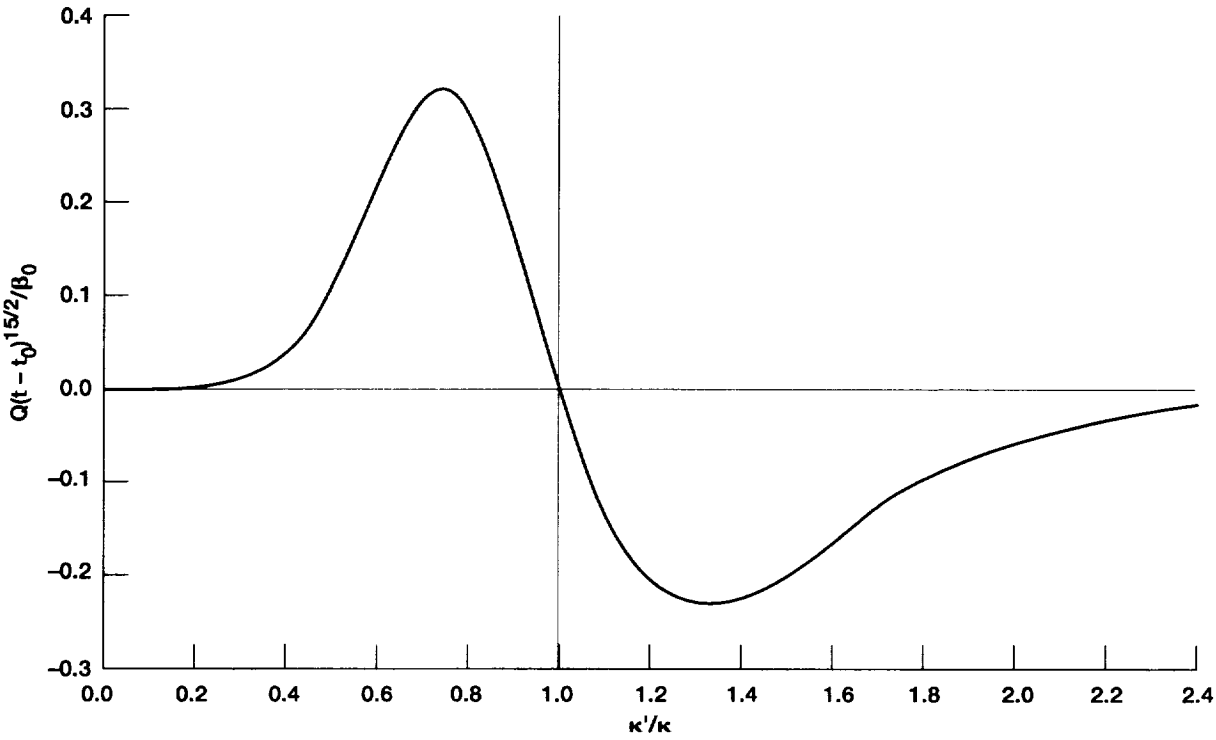

Figure 5-10.—Plot showing contributions to energy transfer from various wave numbers κ' at average κ according to equation (5-171) and figure 5-9.

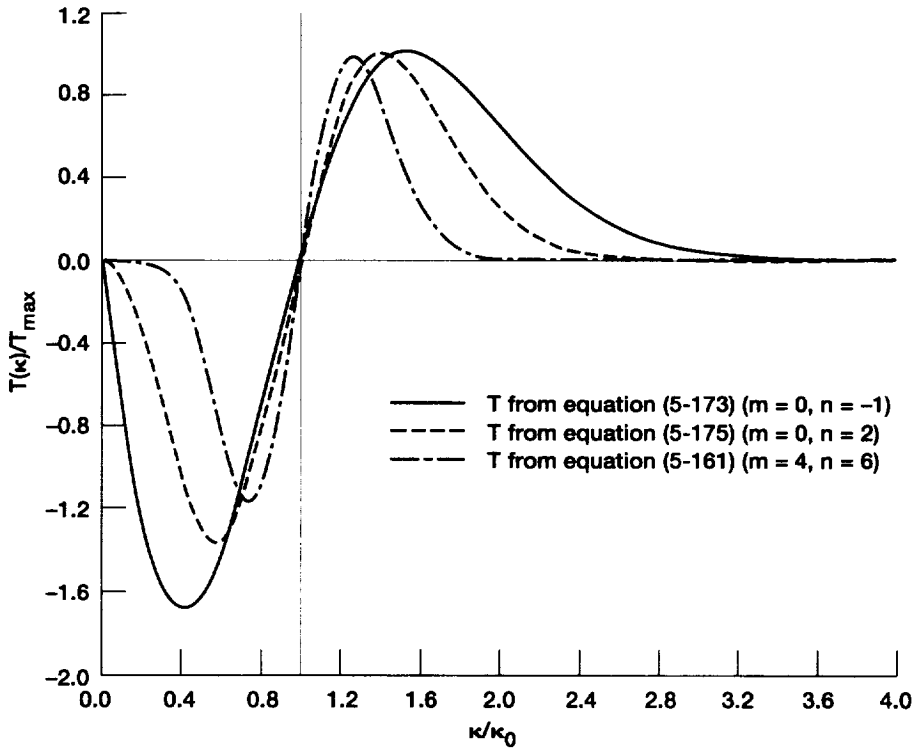

Figure 5–11.—Effect of m and n in the initial condition given by equation (5-156) on the calculated net energy-transfer term T(κ) (eq. (5-158)). κ_0 is the wavenumber where T(κ) = 0.

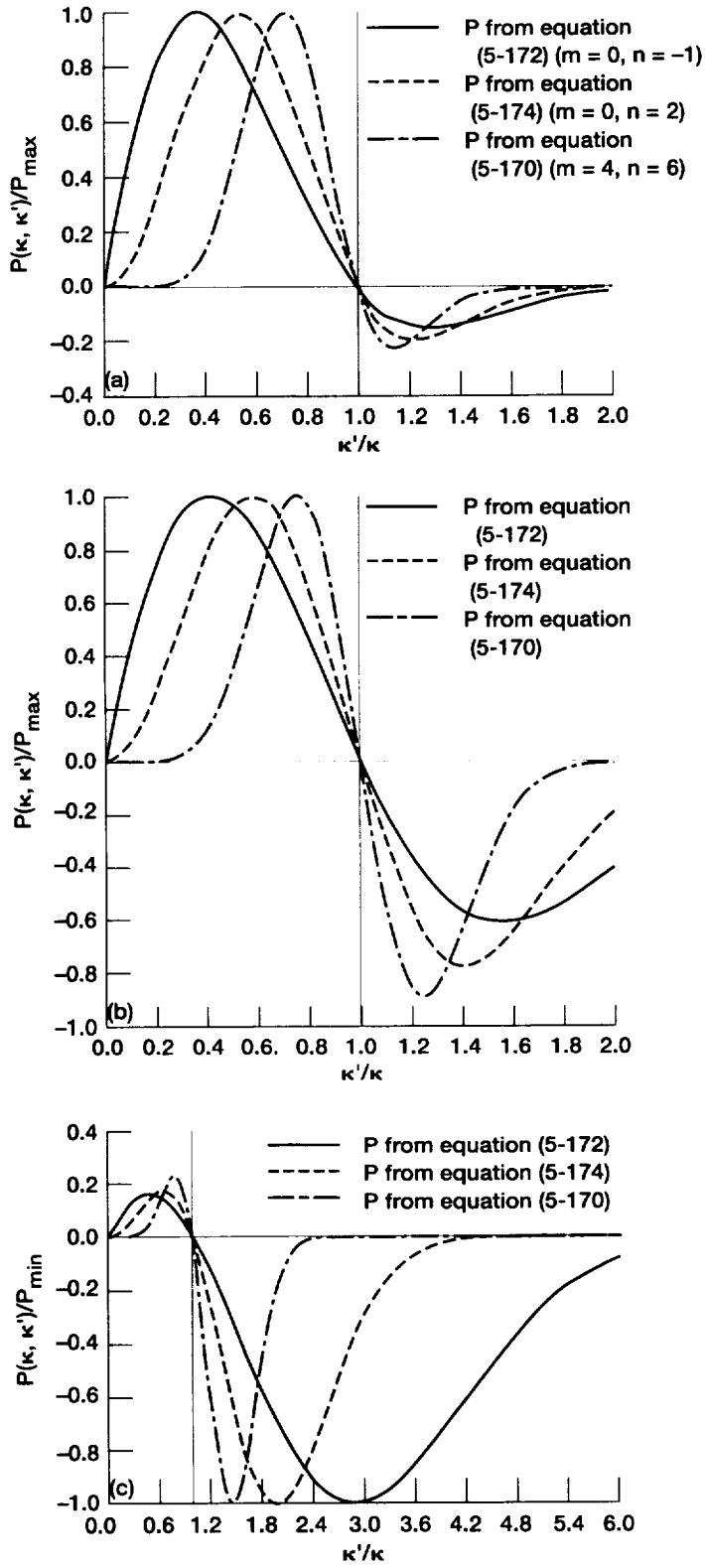

Figure 5-12.—Effect of m and n in equation (5-156) on calculated contributions $P(\kappa, \kappa')$ to net energy transfer $T(\kappa)$ (fig. 5-11) at wavenumber κ from wavenumbers κ'. (a) $T(\kappa)$ a maximum (from fig. 5-11). (b) $T(\kappa) = 0$ (from fig. 5-11). (c) $T(\kappa)$ a minimum (from fig. 5-11).

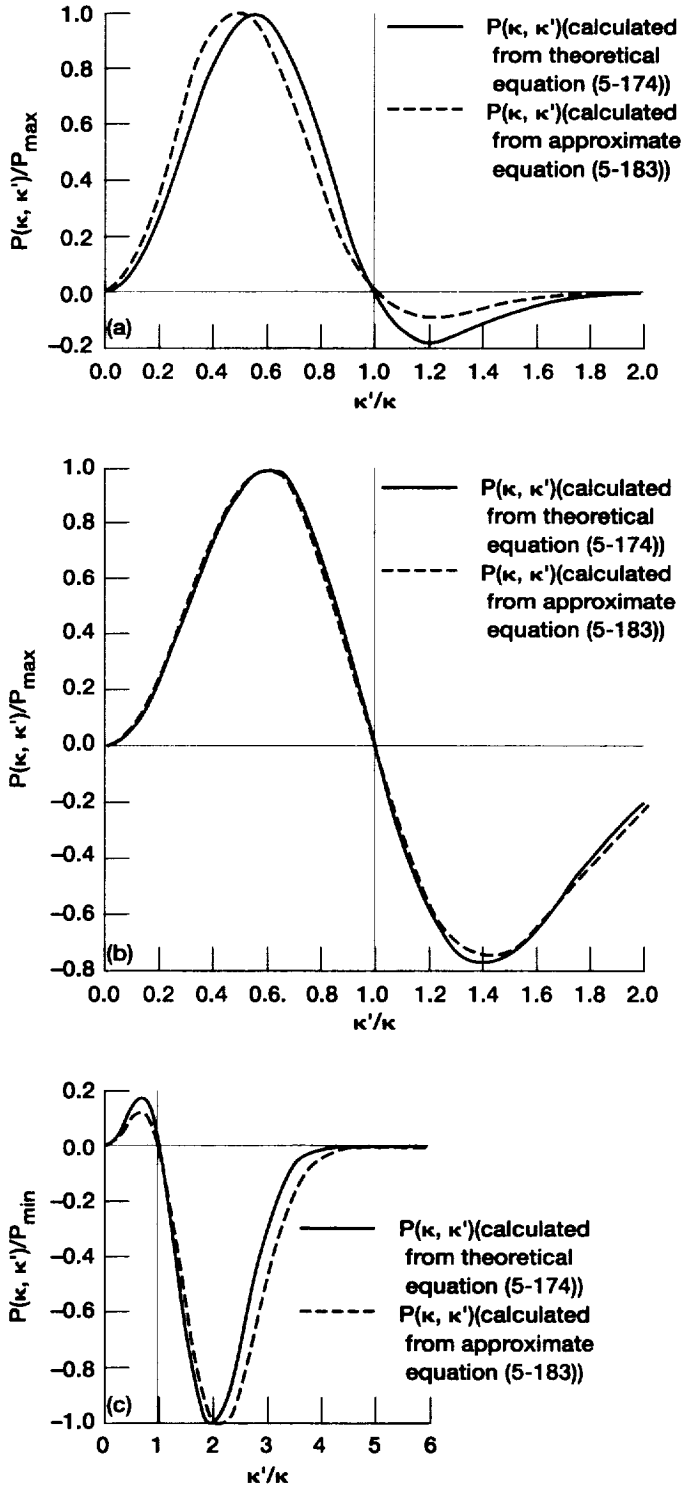

Figure 5-13.—Comparision of contributions P(κ, κ') to net energy transfer T(κ) as calculated from theoretical equation and by approximate method. T(κ) is obtained from equation (5-175)(dashed curve in figure 5-11). (a) T(κ) a maximum. (b) T(κ) = 0. (c) T(κ) a minimum.

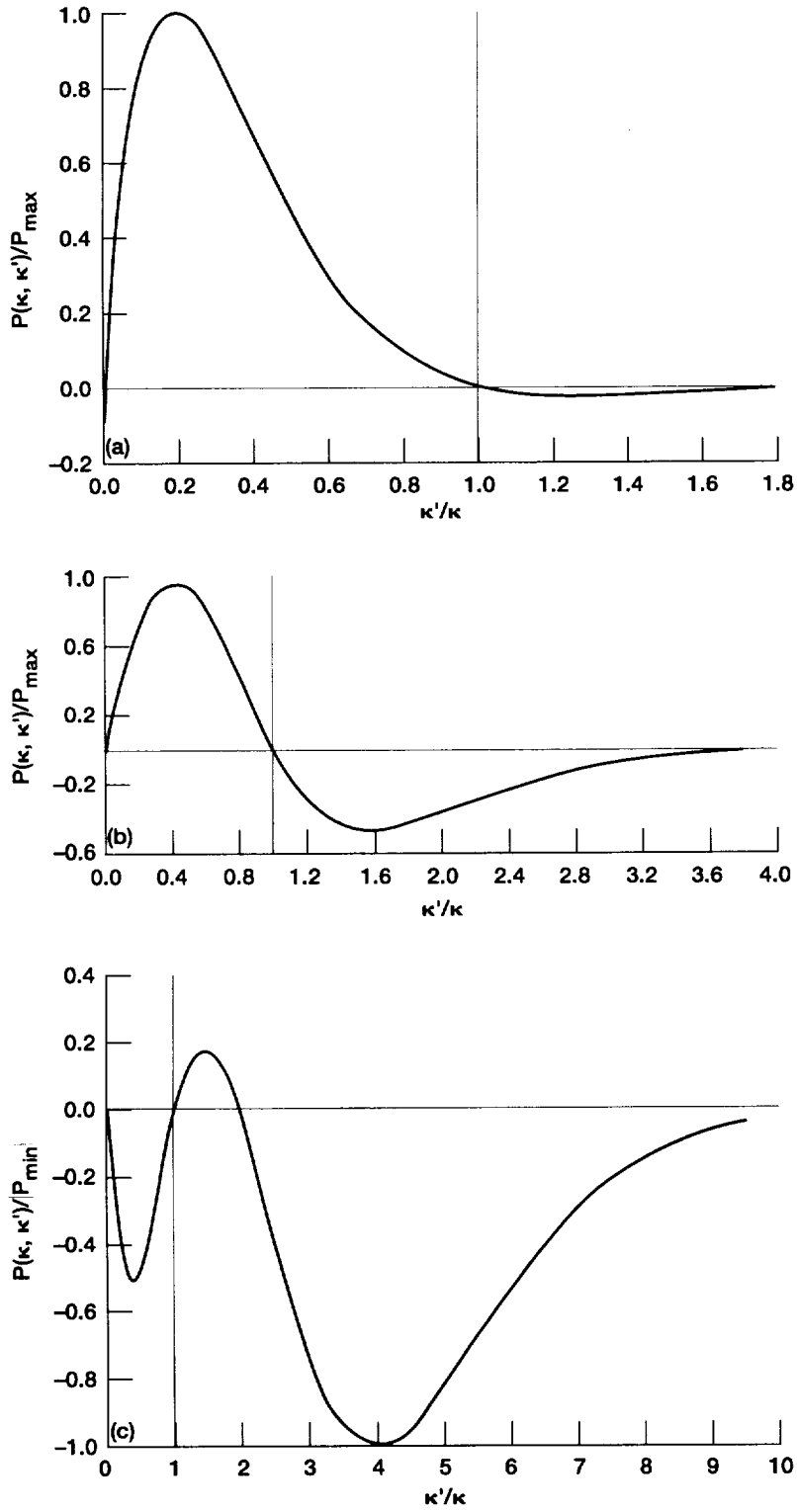

Figure 5-14.—Contributions $P(\kappa,\kappa')$ to experimental energy transfer $T(\kappa)$ (ref. 38) from wavenumbers κ'. $P(\kappa,\kappa')$ calculated from approximate equation (5-188). (a) $T(\kappa)$ a maximum (eq. (5-184)). (b) $T(\kappa) = 0$ (eq. (5-184)). (c) $T(\kappa)$ a minimum (eq. (5-184)).

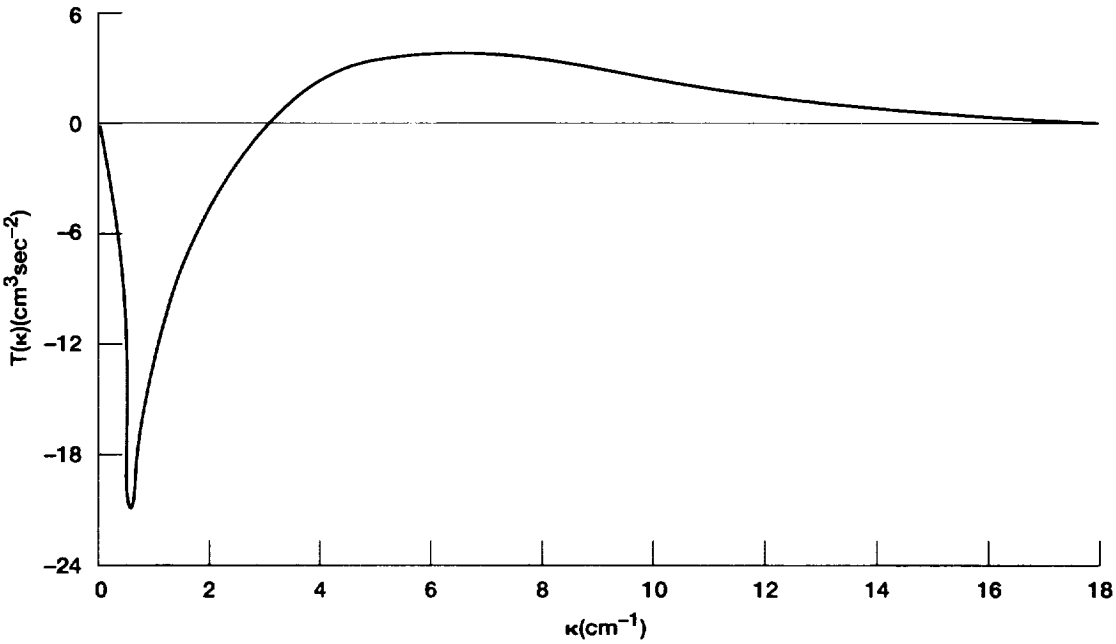

Figure 5-15.—Energy-transfer spectrum for homogeneous turbulence obtained from a numerical solution of the instantaneous Navier-Stokes equations by Clark, Ferziger and Reynolds (ref. 33). $R_\lambda = 36.6$.

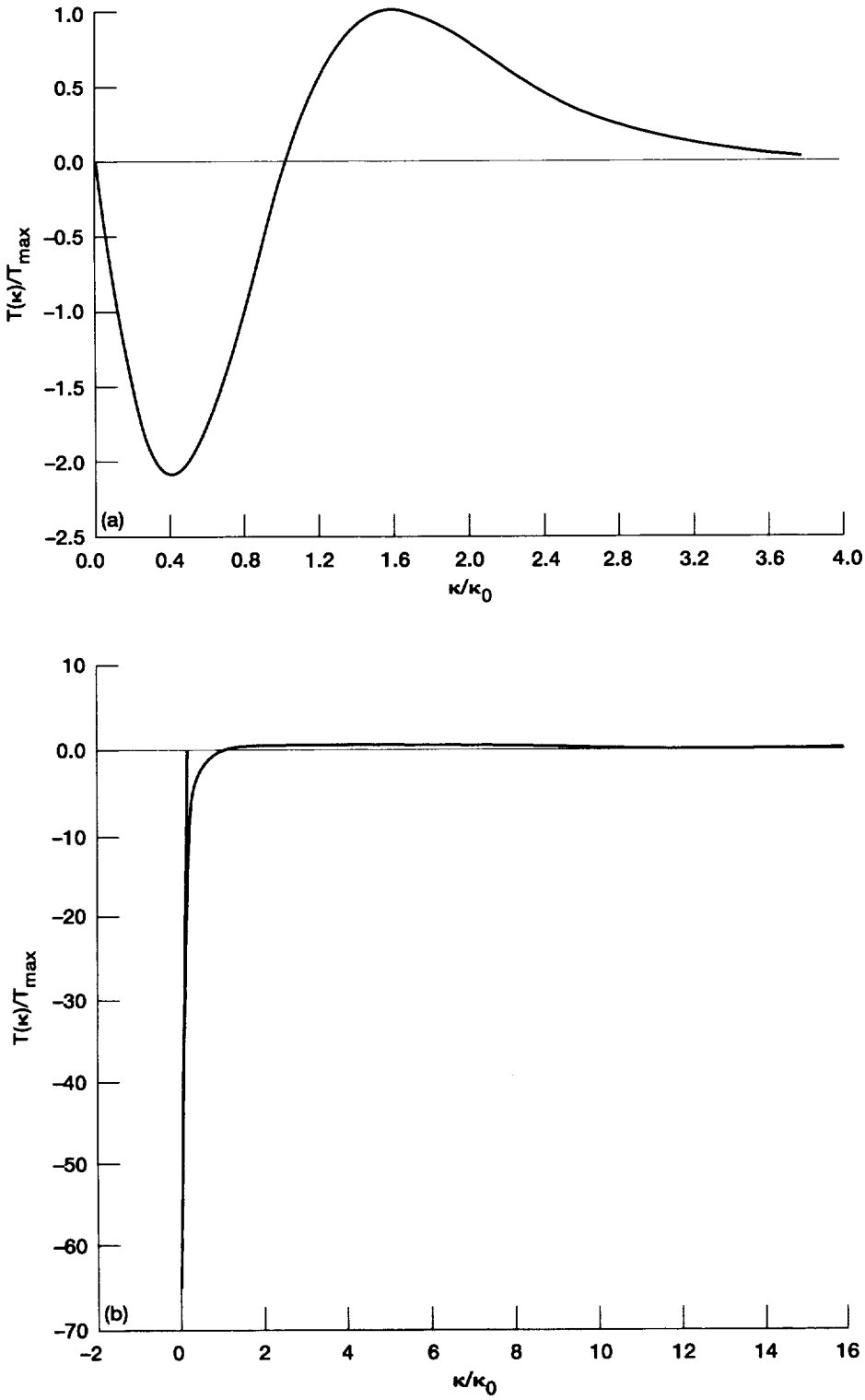

Figure 5–16.—Effect of Reynolds number on experimental energy-transfer spectra. κ_0 is the wavenumber where $T(\kappa) = 0$. (a) $3 < R_\lambda < 30$ (Ling and Huang, ref. 38). (b) $300 < R_\lambda < 800$ (Ling and Saad, ref. 37).

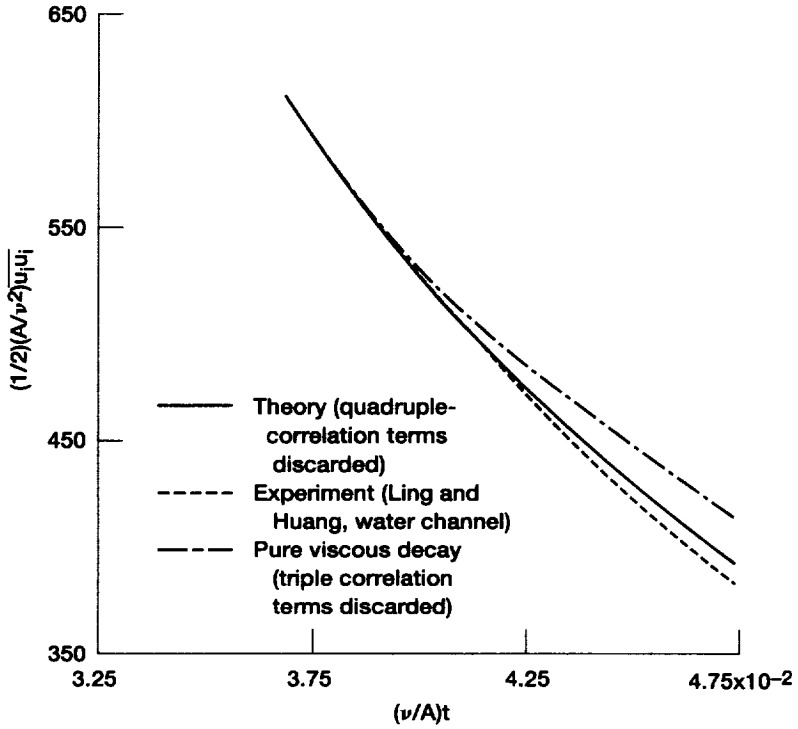

Figure 5-17.—Comparision of theory with the experiment of ref. 38 for decay of turbulent energy.

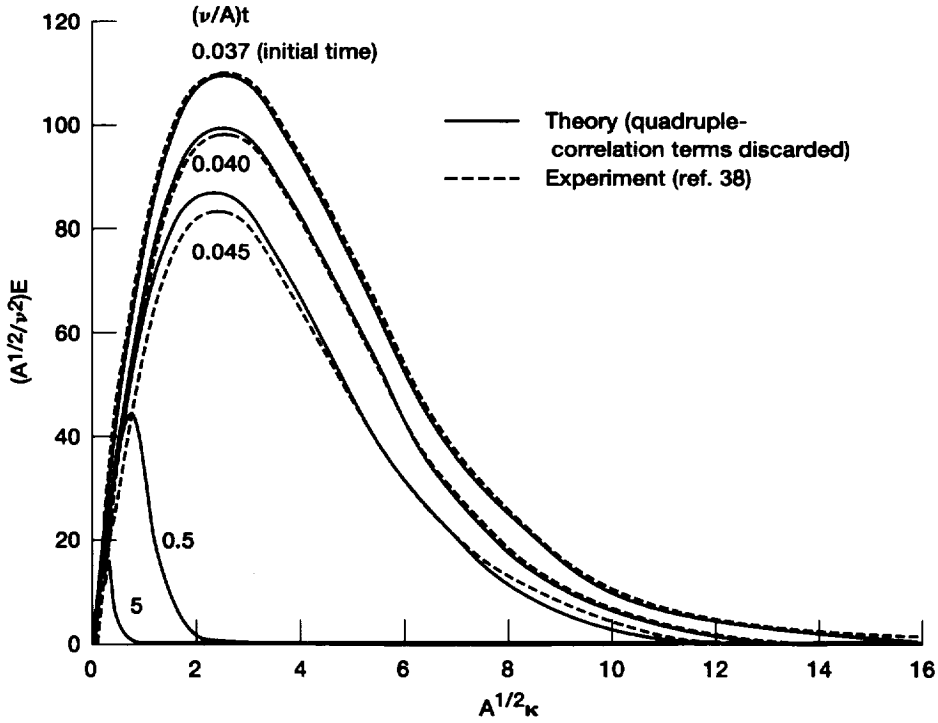

Figure 5-18.—Comparison of theory and experiment for decay of three-dimensional turbulent-energy spectra.

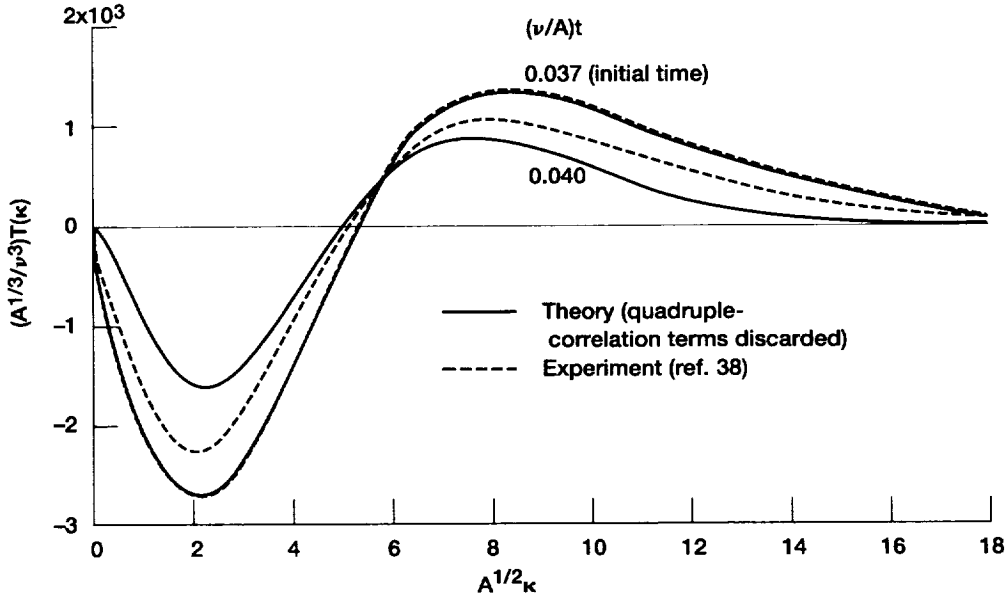

Figure 5-19.—Comparision of theory and experiment for decay of energy-transfer spectra.

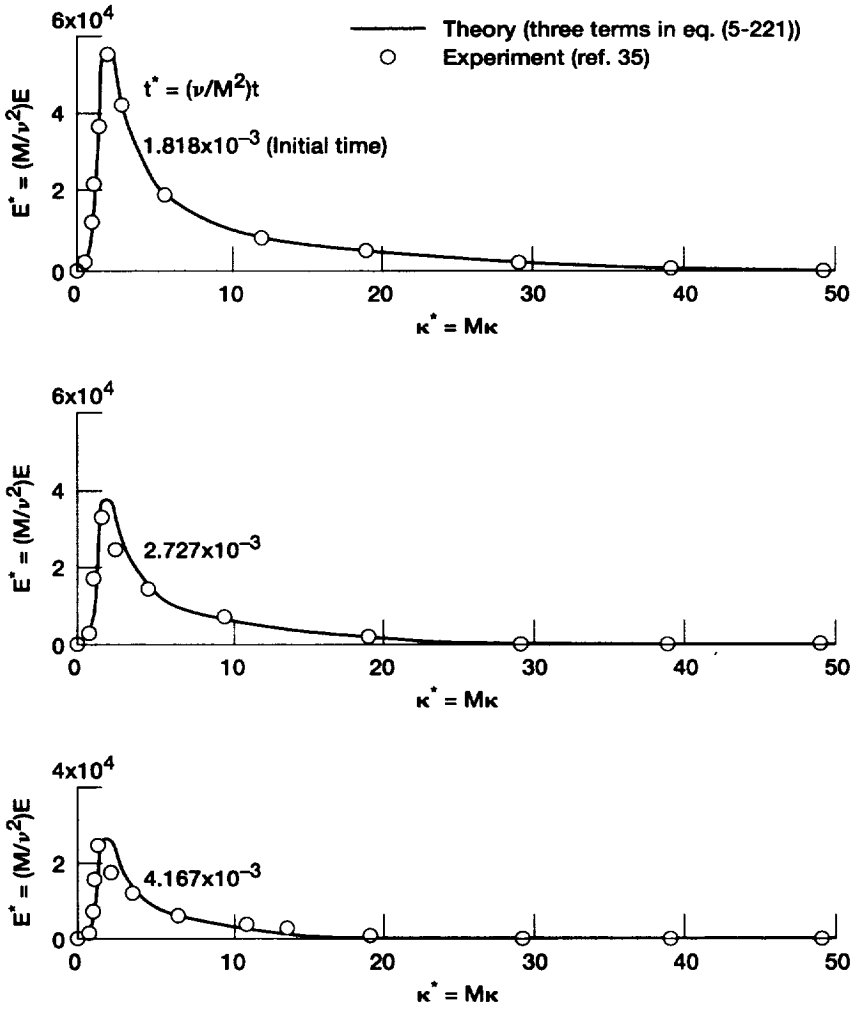

Figure 5-20.—Comparison of theory with experiment of reference 35 for decay of turbulent-energy spectra.

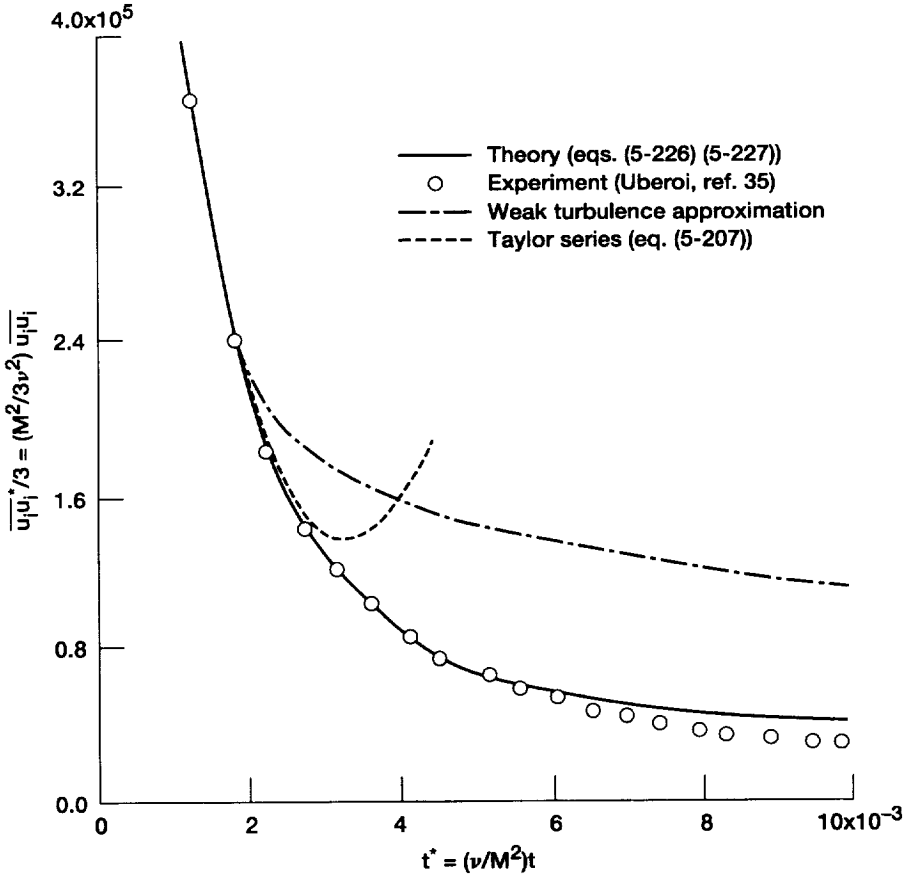

Figure 5-21.—Comparison of theory with experiment of reference 35 for decay of average component of velocity variance.

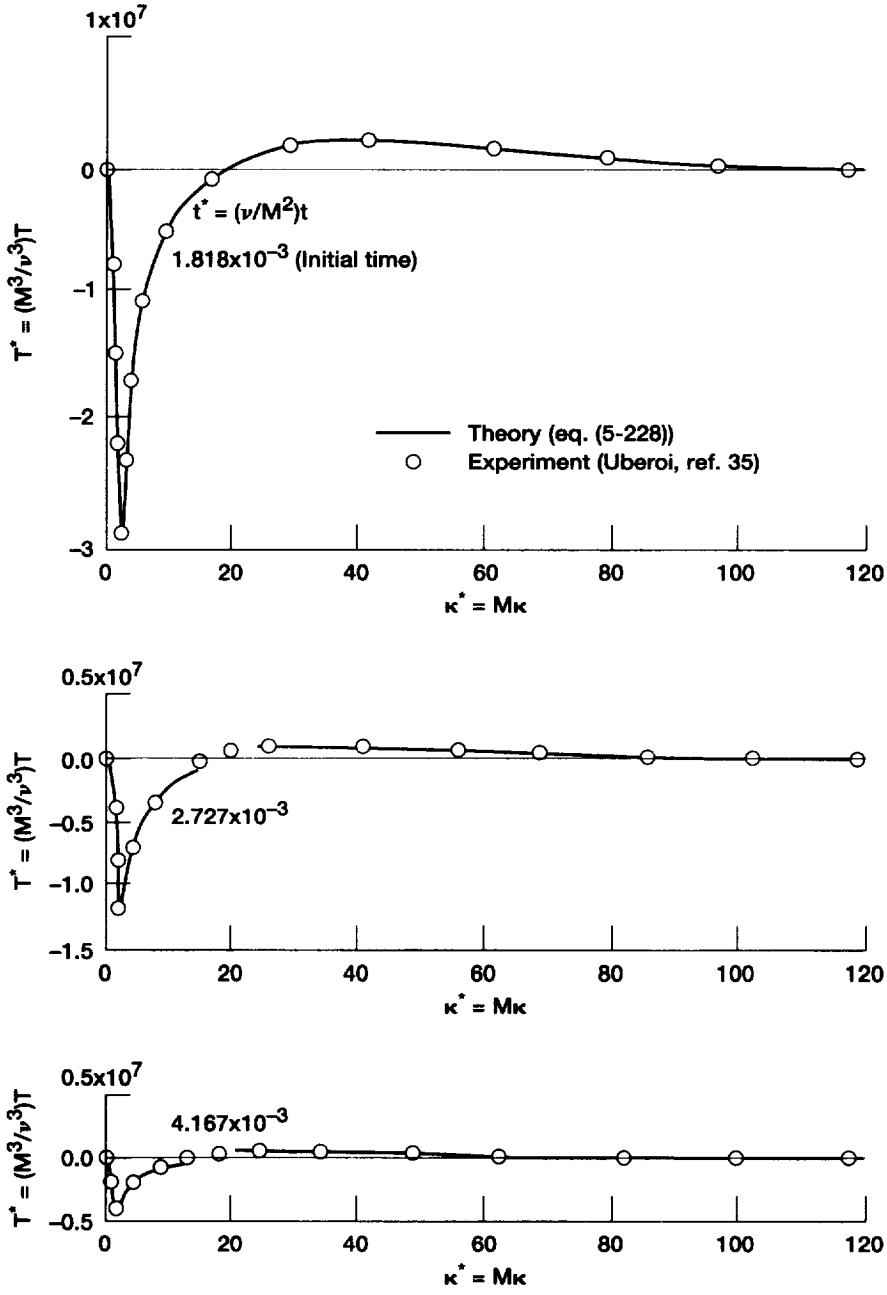

Figure 5-22.—Comparison of theory with experiment of reference 35 for decay of energy-transfer spectra.

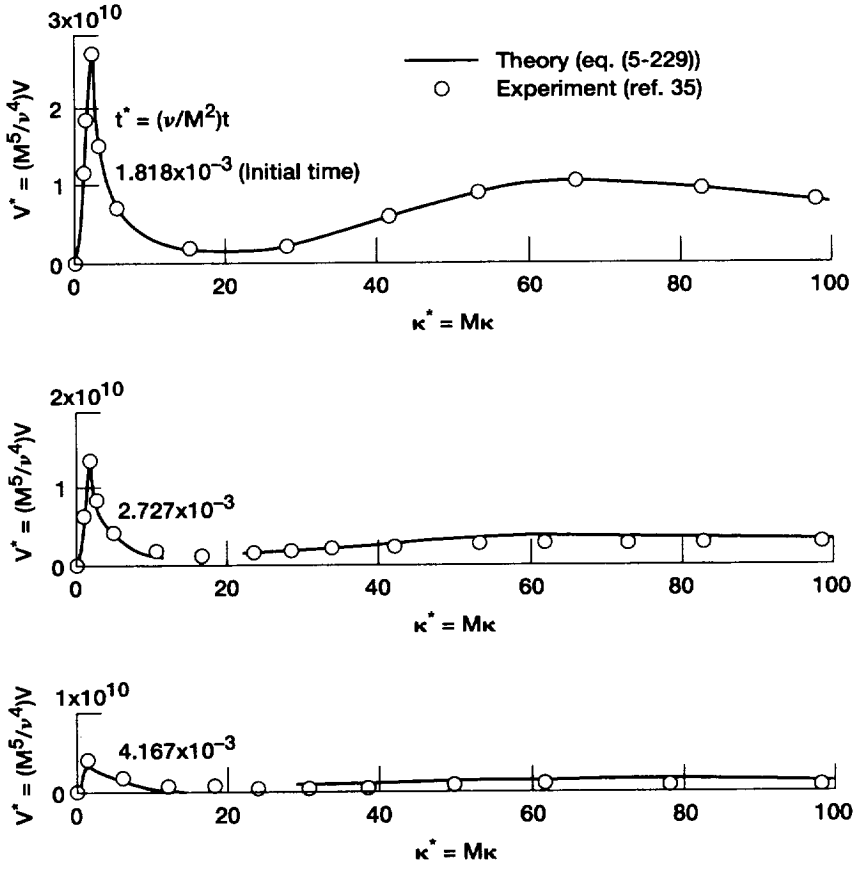

Figure 5-23.—Comparison of theory with experiment of reference 35 for decay of higher-order spectral quantity V (eq. (5-205)).

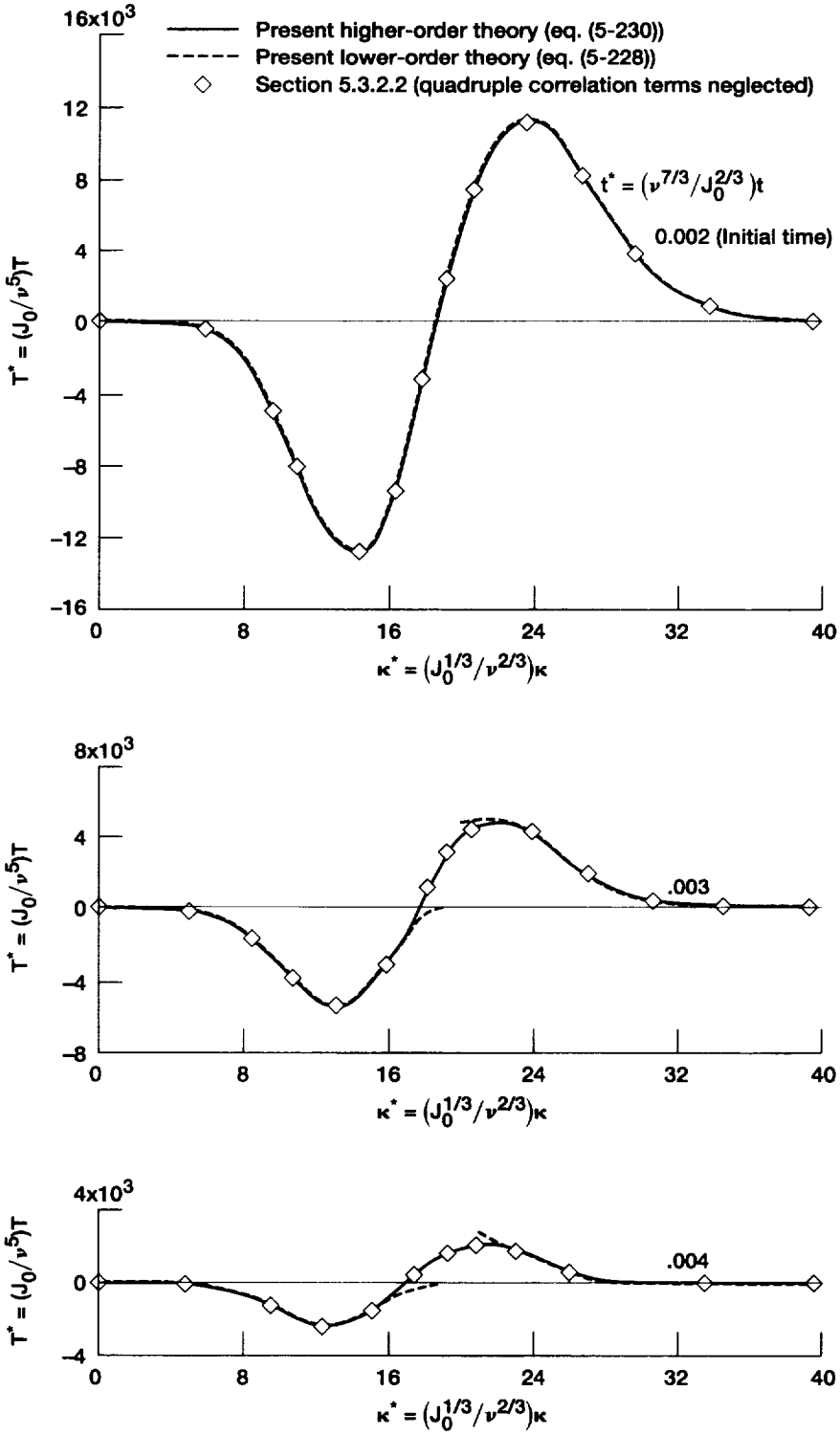

Figure 5-24.—Comparison of present theory with that of section 5.3.2.2 for decay of energy-transfer spectrum.

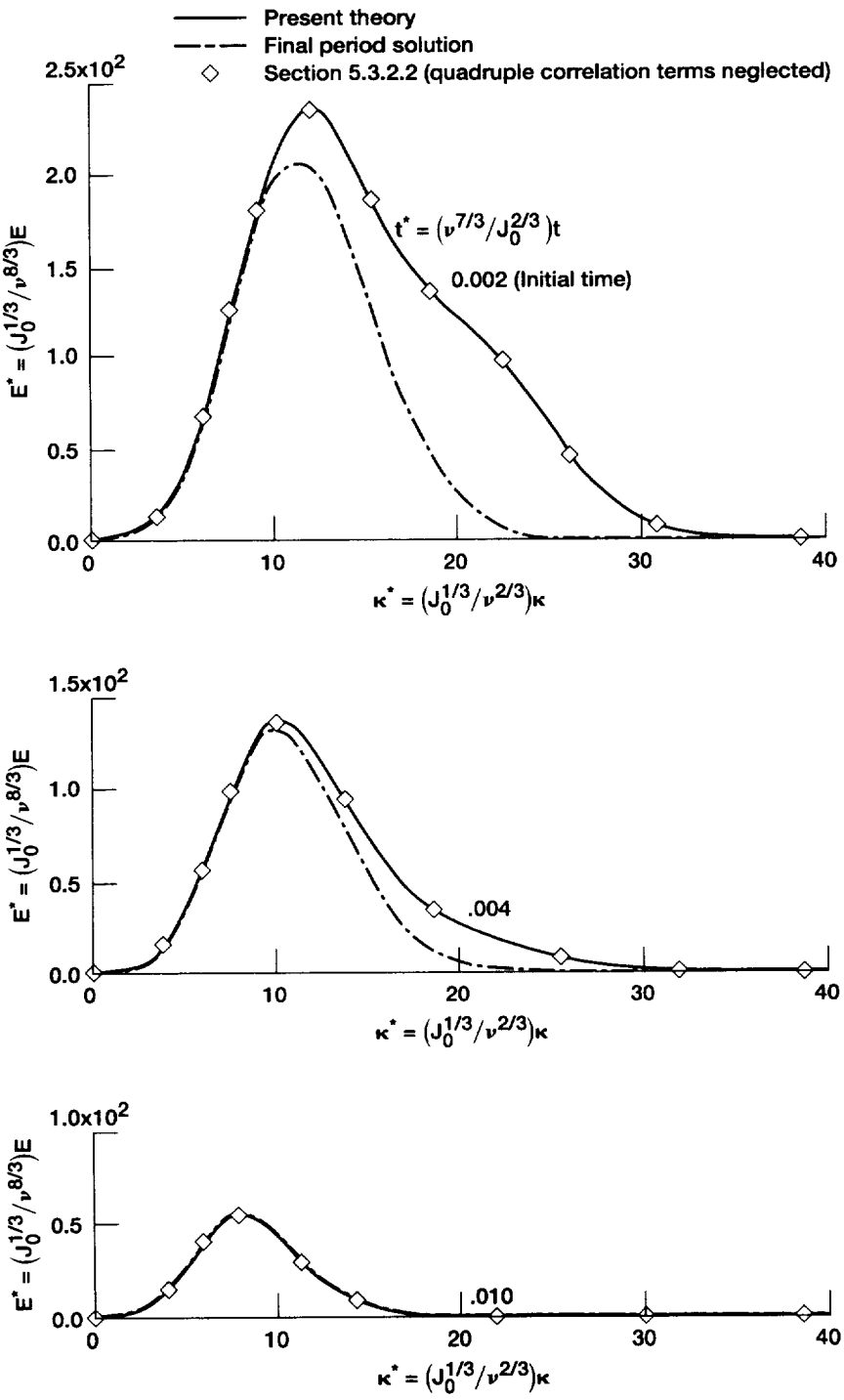

Figure 5-25.—Comparison of present (higher-order) theory with that of section 5.3.2.2 for decay of turbulent-energy spectrum.

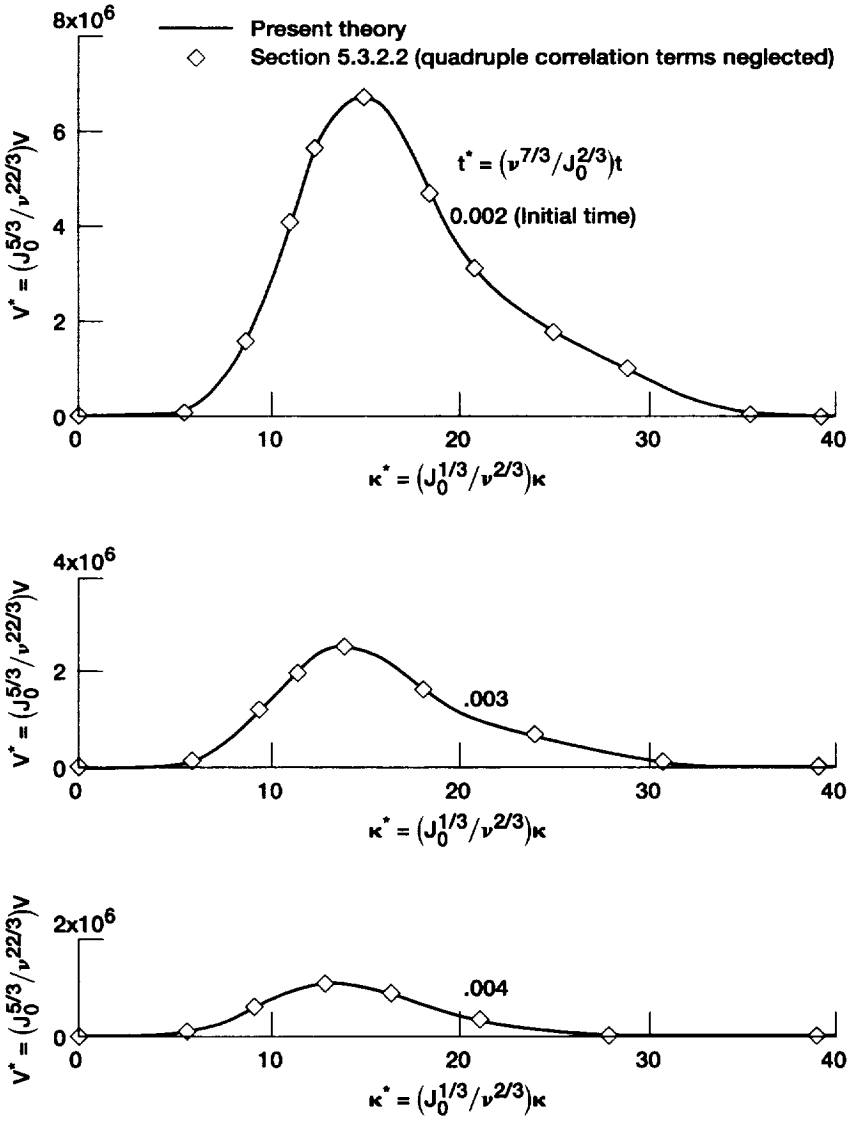

Figure 5-26.—Comparison of present (higher-order) theory with that of section 5.3.2.2 for decay of higher-order spectral quantity V (eq. (5-205)).

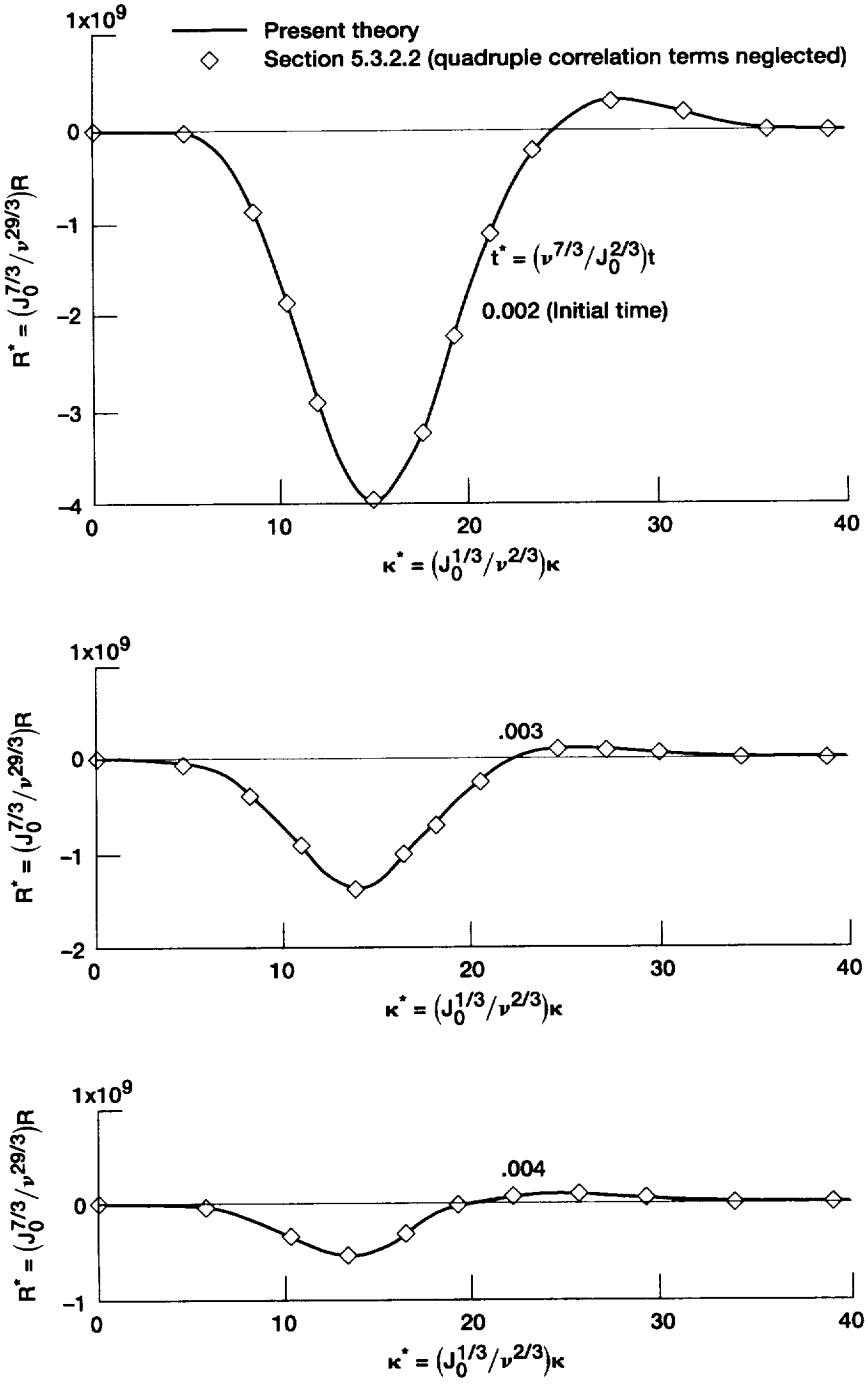

Figure 5-27.—Comparison of present (higher-order) theory with that of section 5.3.2.2 for decay of higher-order spectral quantity R (eq. (5-235)).

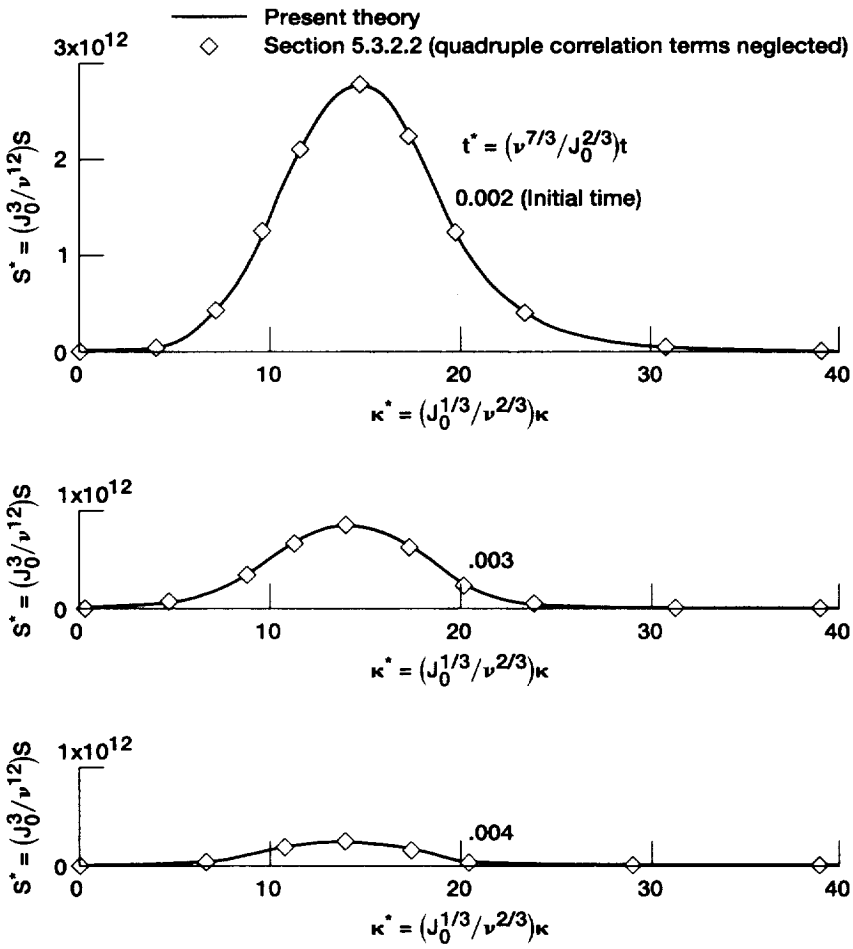

Figure 5-28.—Comparison of present (higher-order) theory with that of section 5.3.2.2 for decay of higher-order spectral quantity S (eq. (5-236)).

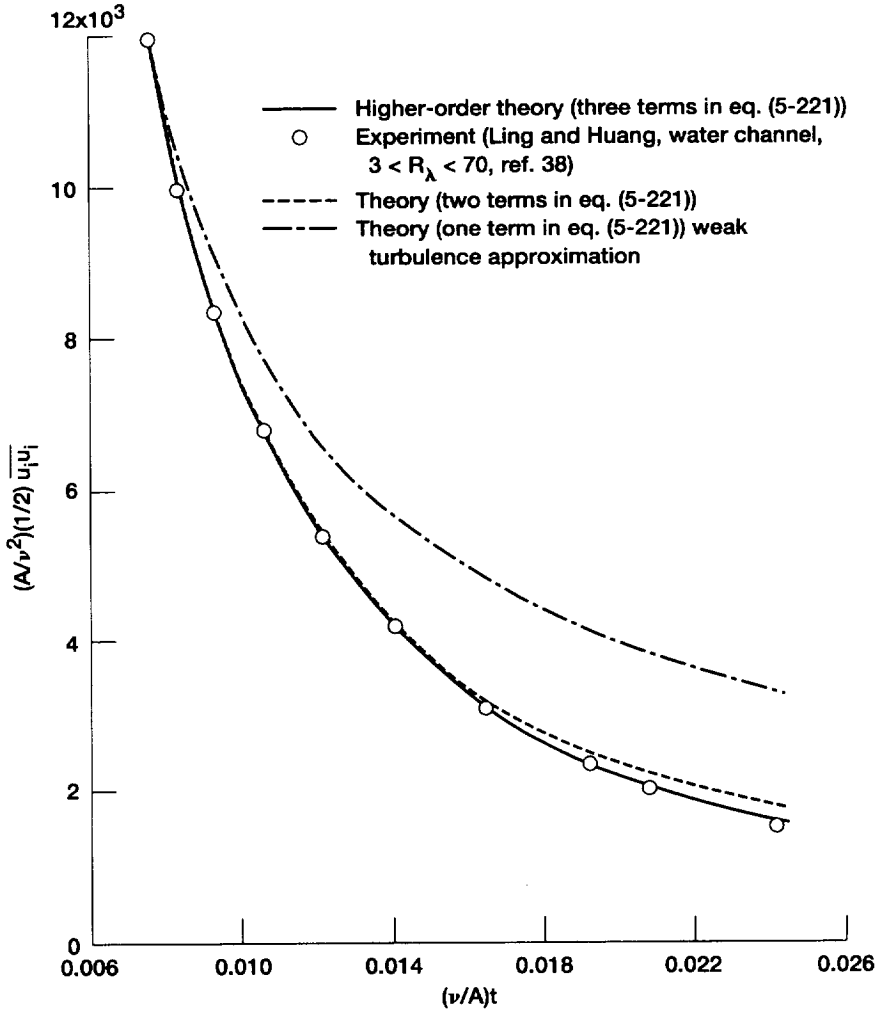

Figure 5-29.—Comparison of theory with experiment of reference 38 for decay of turbulent energy.

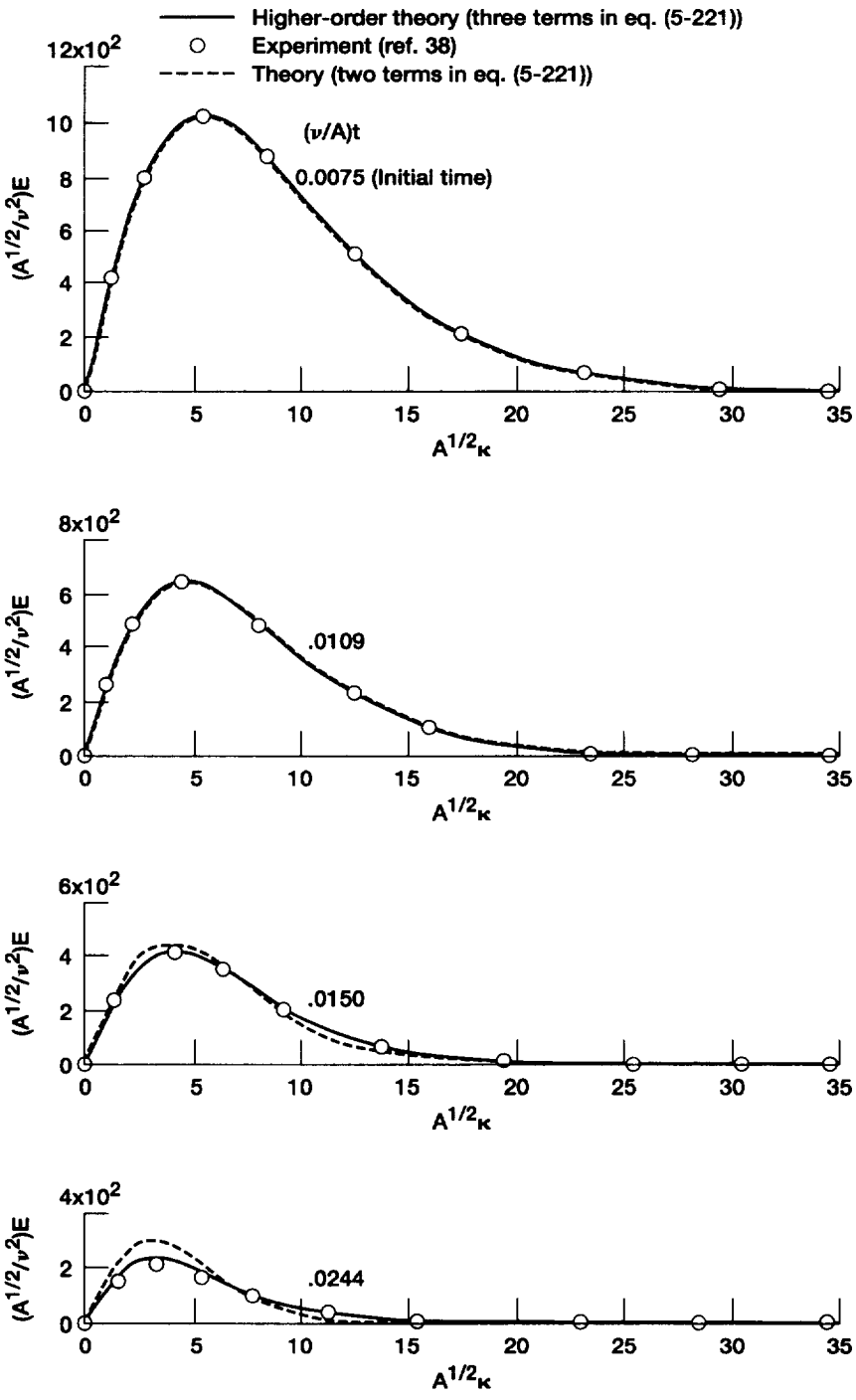

Figure 5-30.—Comparison of theory with experiment of reference 38 for decay of three-dimensional turbulent-energy spectra.

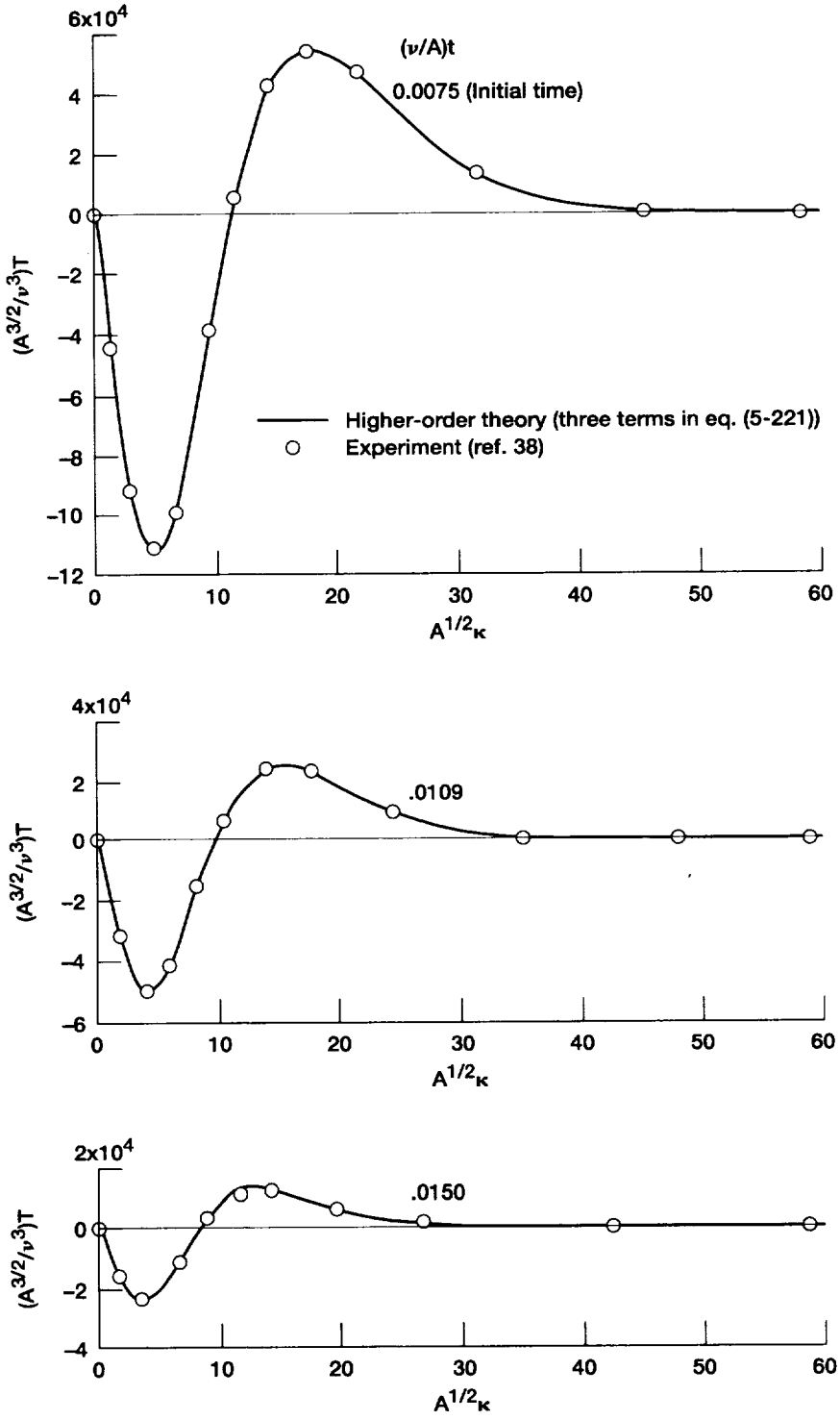

Figure 5-31.—Comparison of theory with experiment of reference 38 for decay of energy-transfer spectra.

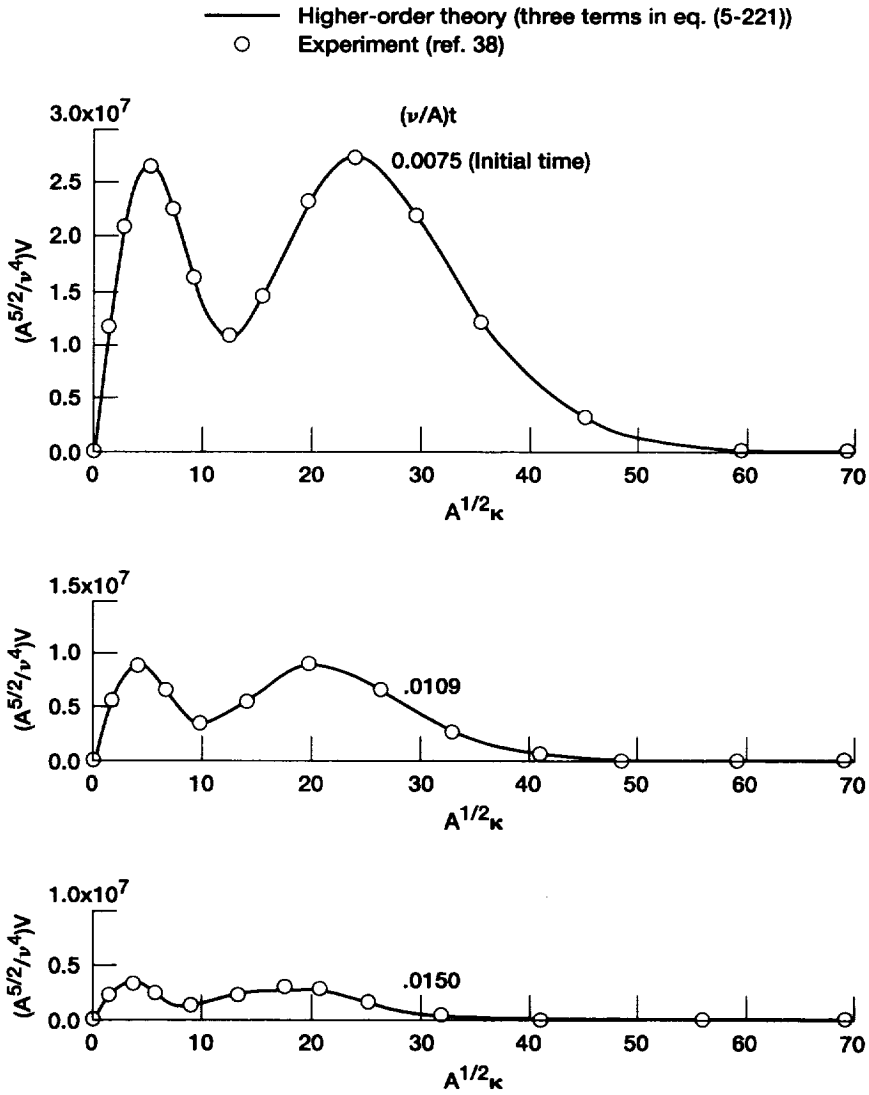

Figure 5-32.—Comparison of theory with experiment of reference 38 for decay of higher-order spectral quantity V (eq. (5-205)).

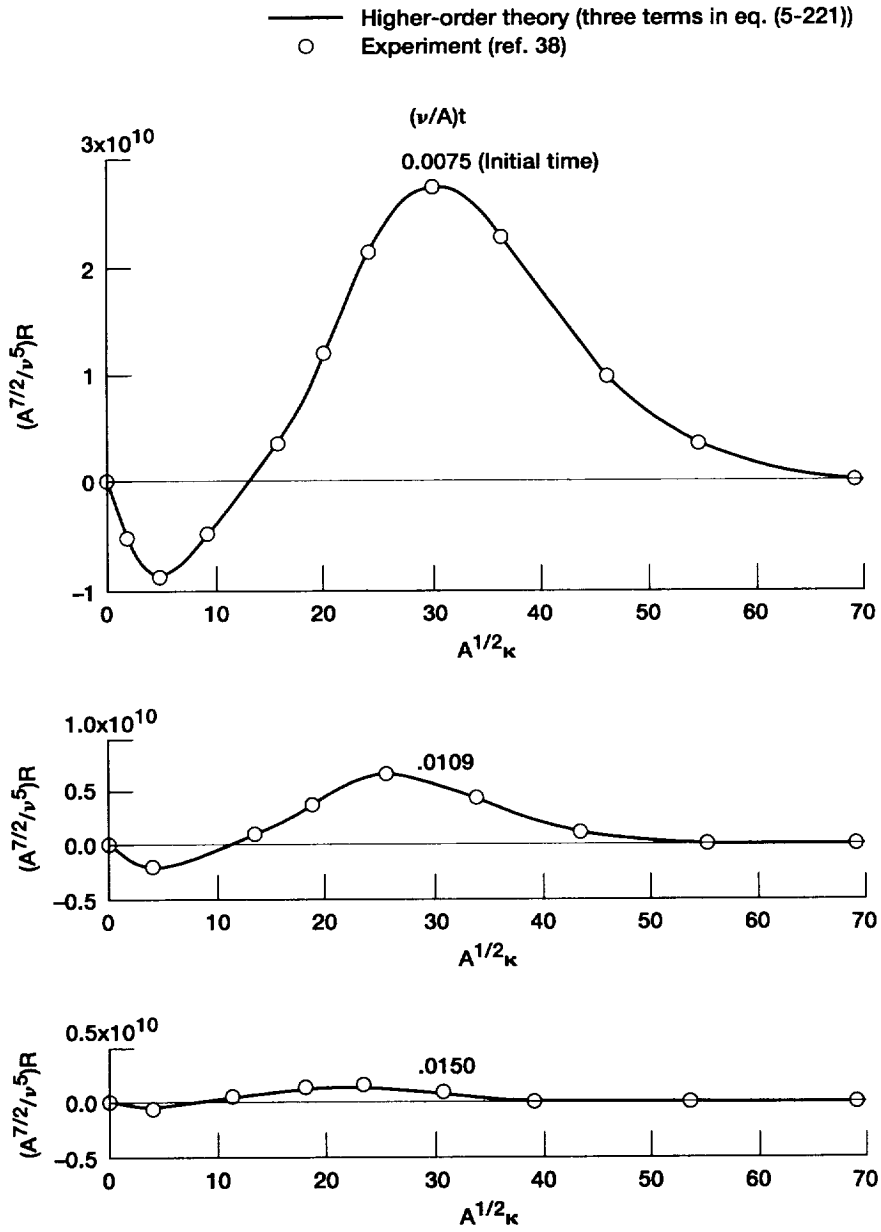

Figure 5-33.—Comparison of theory with experiment of reference 38 for decay of higher-order spectral quantity R (eq. (5-235)).

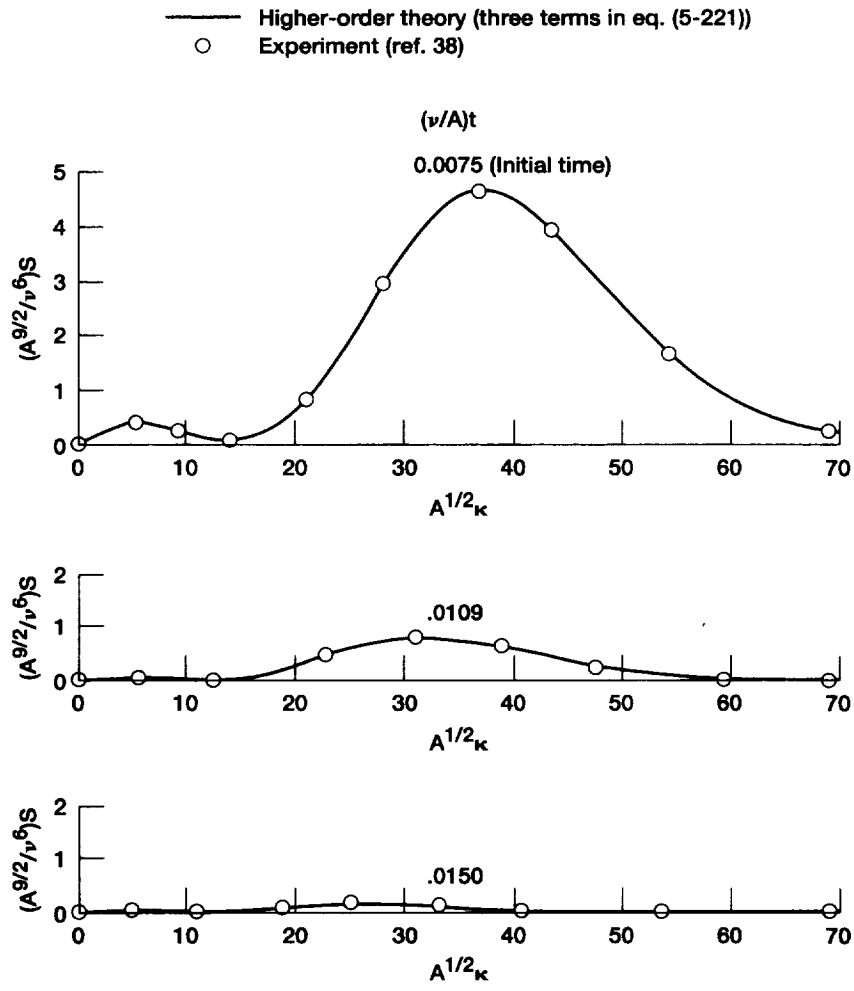

Figure 5-34.—Comparison of theory with experiment of reference 38 for decay of higher-order spectral quantity S (eq. (5-236)).

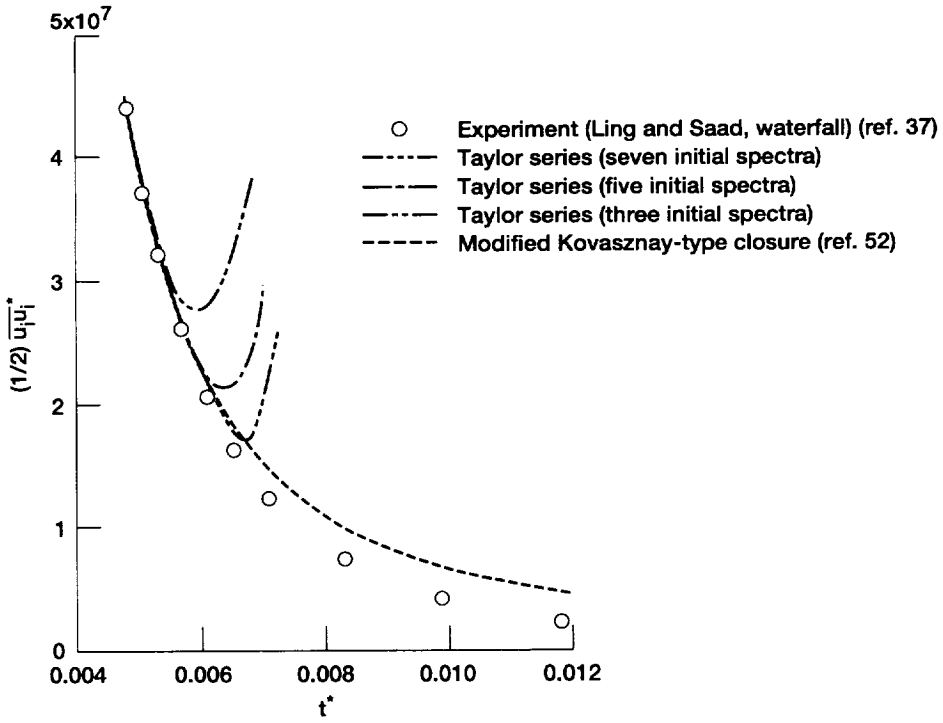

Figure 5-35.—Comparison of theories with the high Reynolds number experiment of reference 37 for decay of turbulent energy ($300 < R_\lambda < 800$). Turbulence equations closed by specification of initial conditions using a Taylor series and by a modified Kovasznay-type closure.

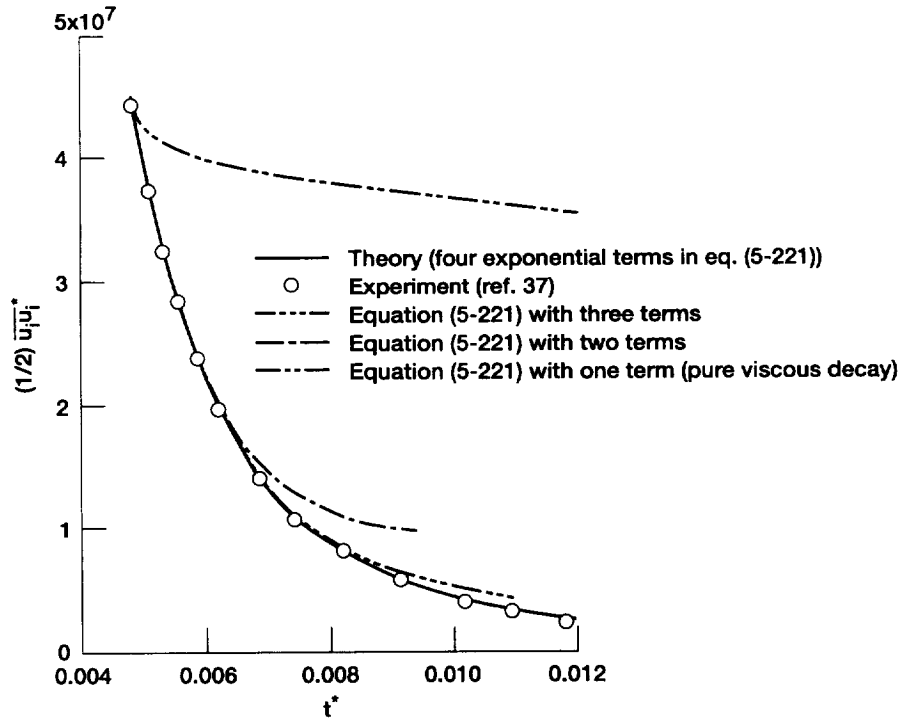

Figure 5-36.—Comparison of theory with the high Reynolds number experiment of reference 37 for decay of turbulent energy ($300 < R_\lambda < 800$). Turbulence equations closed by specification of sufficient initial conditions using an exponential series (eq. (5-221)).

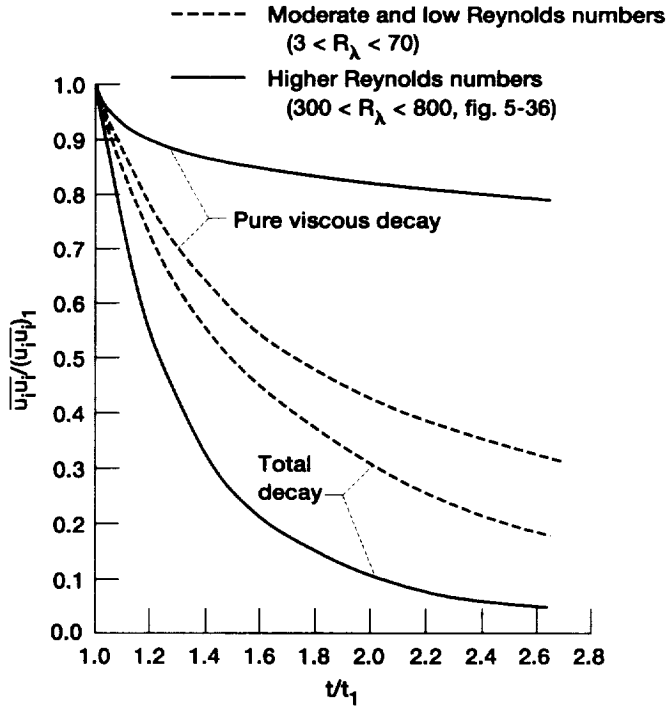

Figure 5-37.—Effect of Reynolds number on turbulence decay processes.

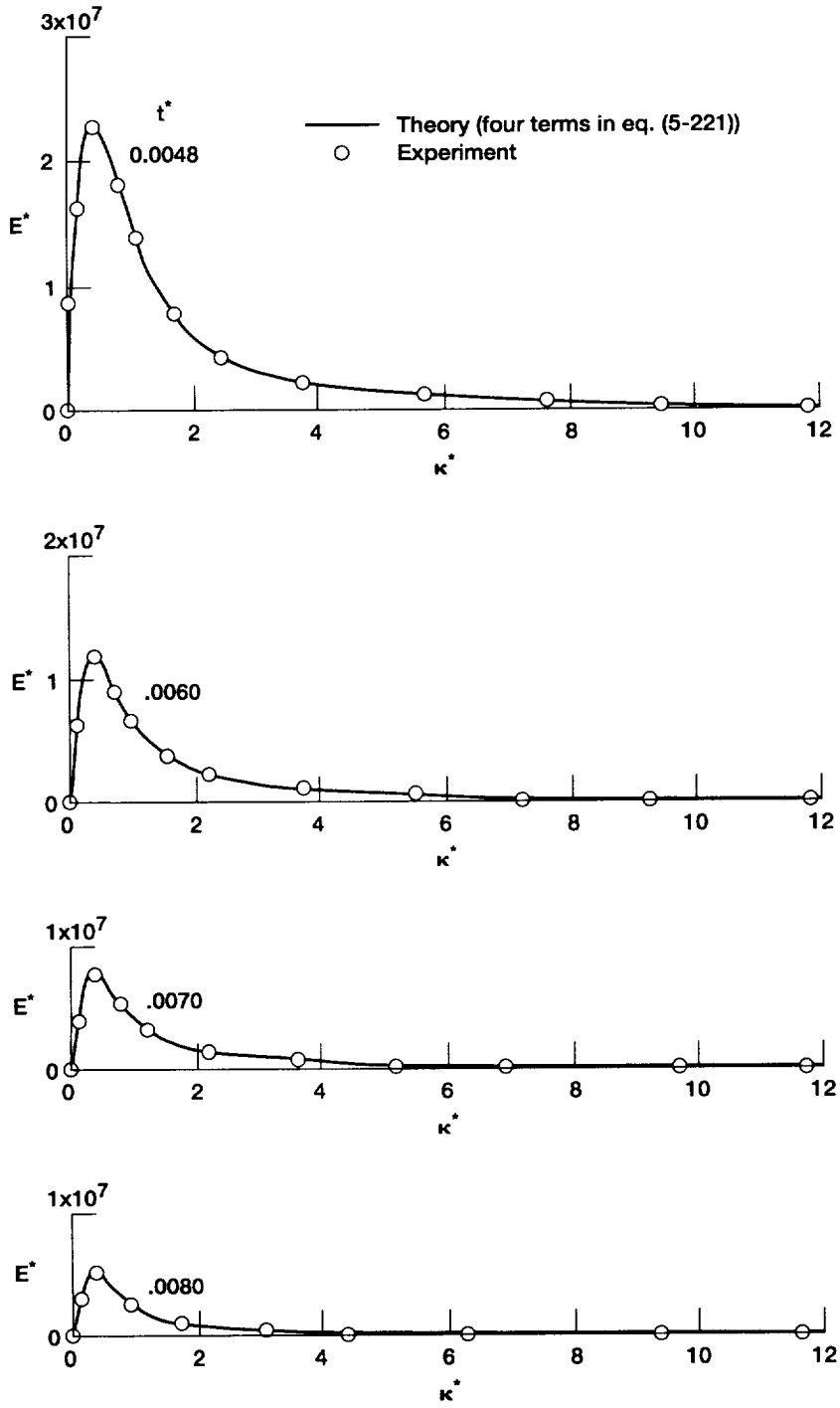

Figure 5-38.—Comparison of higher-order theory with the high Reynolds number experiment (ref. 37) for decay of three-dimensional energy spectra.

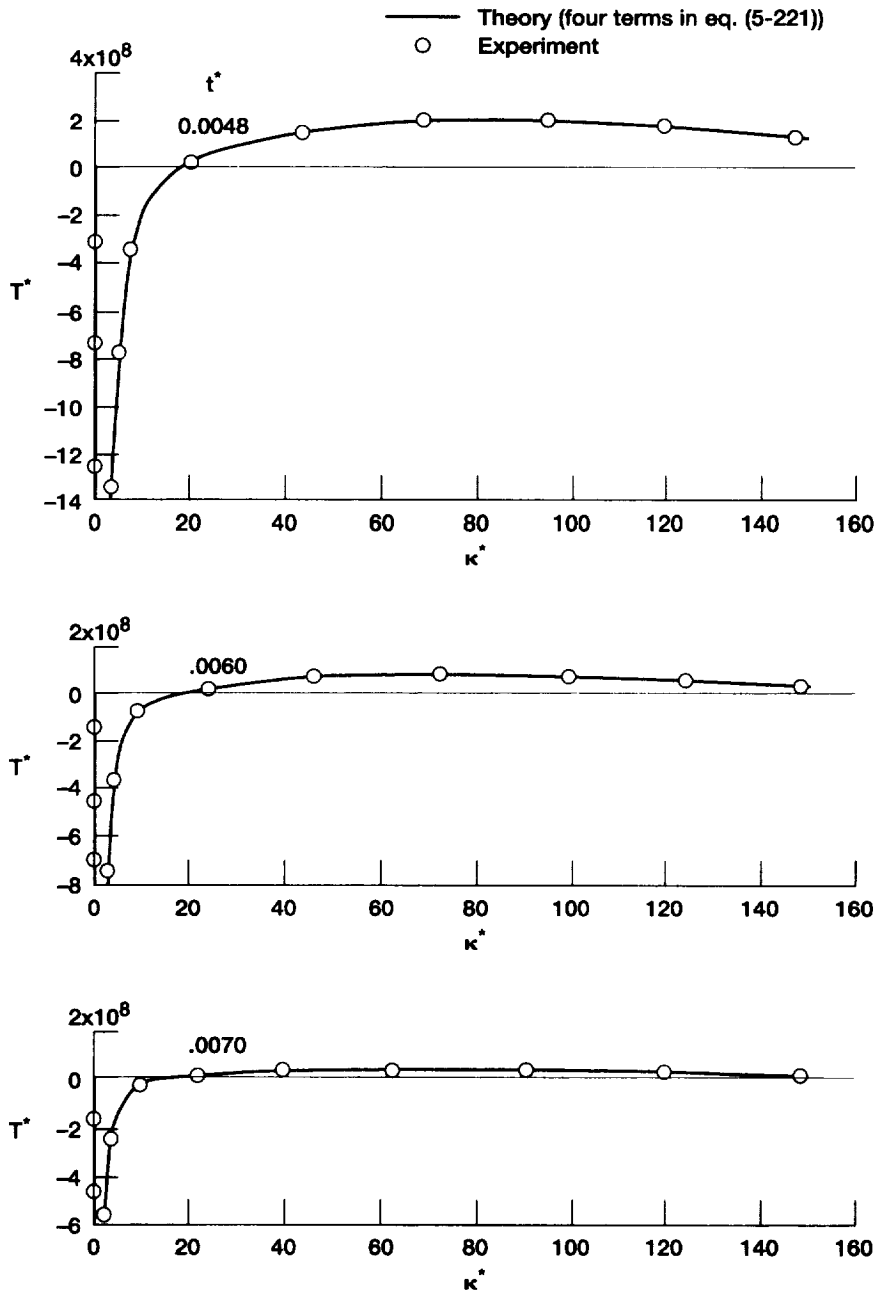

Figure 5-39.—Comparison of higher-order theory with the high Reynolds number experiment (ref. 37) for decay of energy transfer spectra.

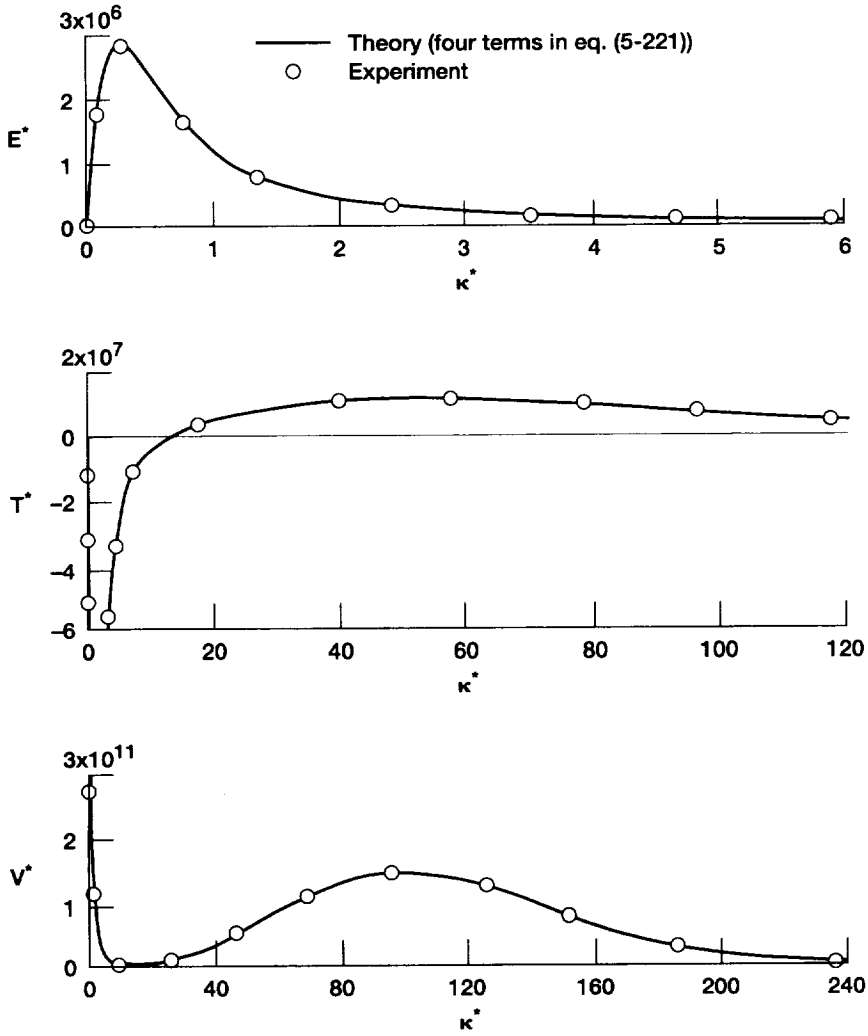

Figure 5-40.—Comparison of higher-order theory with the high Reynolds number experiment (ref. 37) at a late time ($t^* = 0.01$) for the lower-order spectral quantities used to specify the initial turbulence.

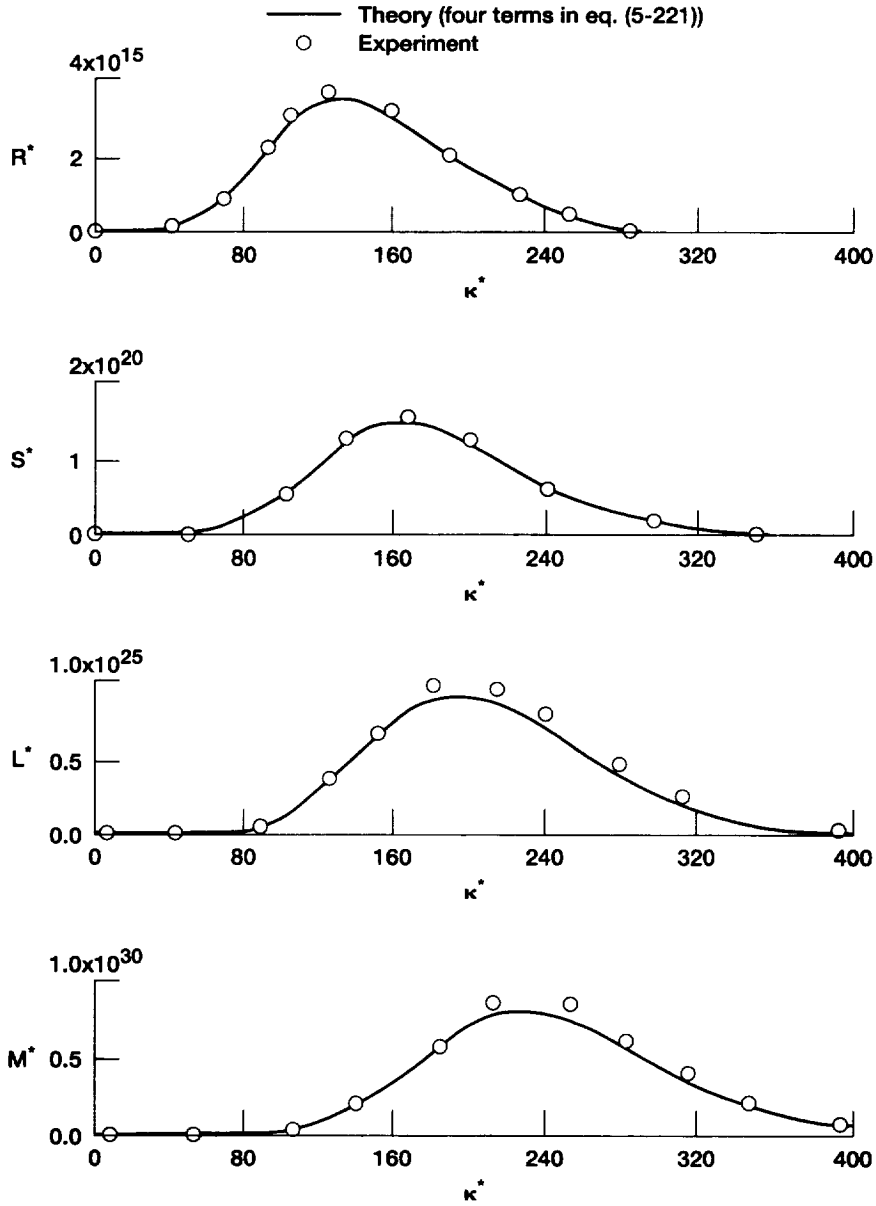

Figure 5-41.—Comparison of higher-order theory with high Reynolds number experiment (ref. 37) at a late time ($t^* = 0.01$) for the higher-order spectral quantities used to specify the initial turbulence.

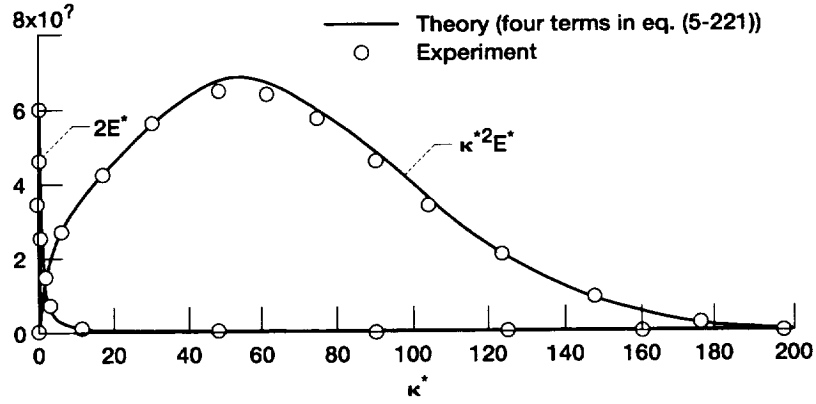

Figure 5-42.—Comparison of theoretical energy dissipation spectrum at a late time ($t^* = 0.01$) with high Reynolds number experiment (ref. 37) and with energy spectra.

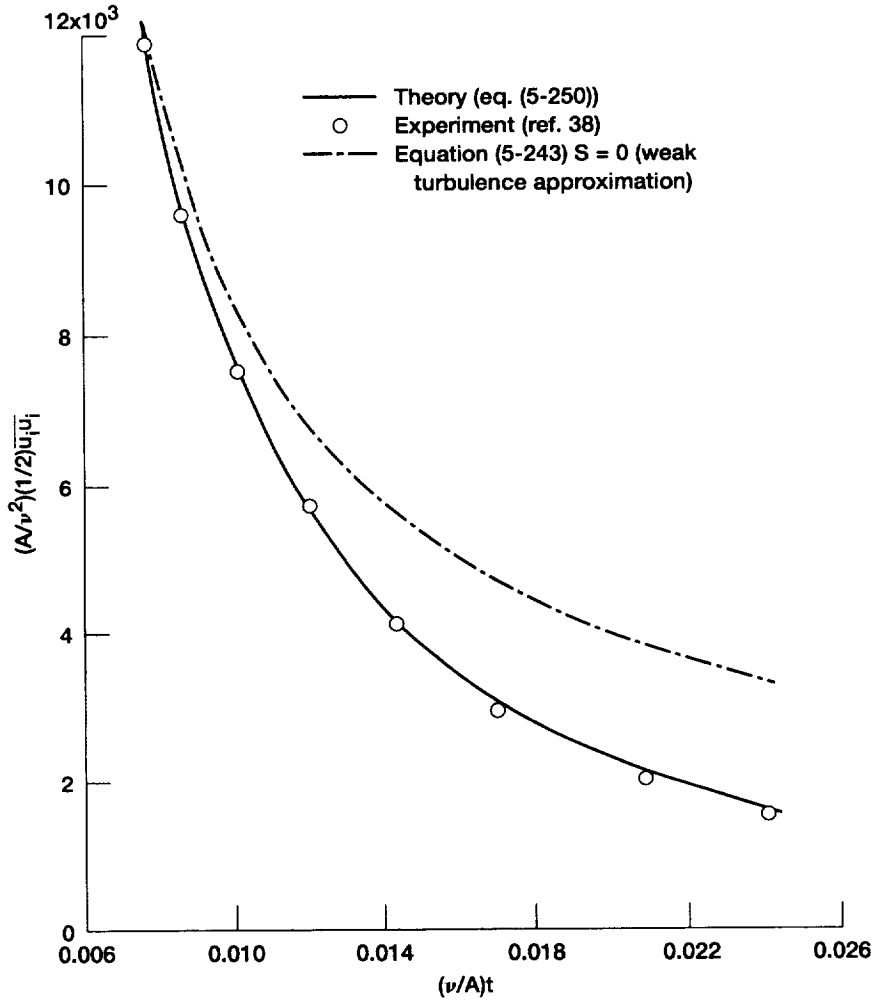

Figure 5-43.—Comparison of theory (eq. (5-250)) and experiment (ref. 38) for decay of turbulent energy.

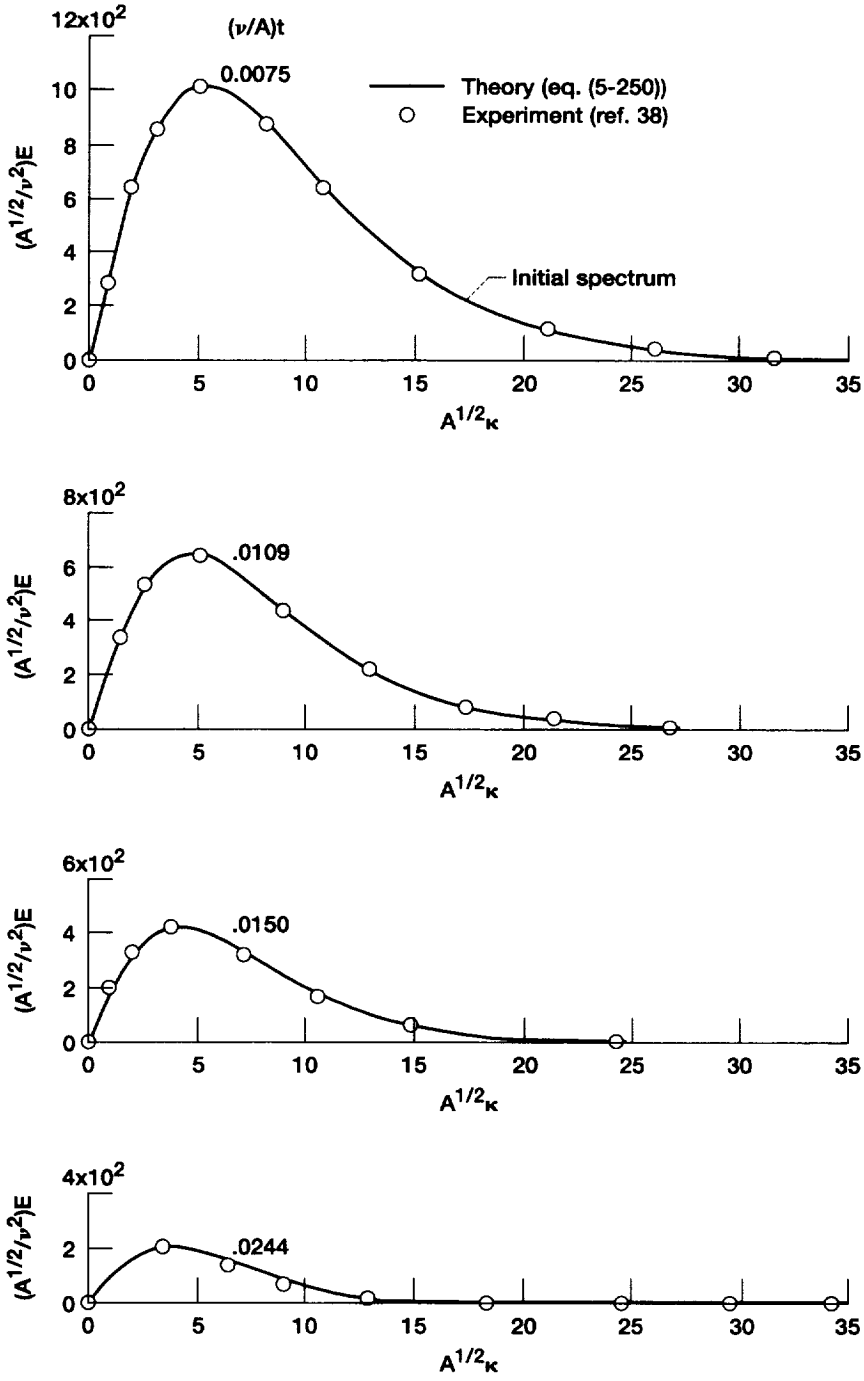

Figure 5-44.—Comparison of theory (eq. (5-250) and experiment (ref. 38) for decay of three-dimensional turbulent-energy spectra.

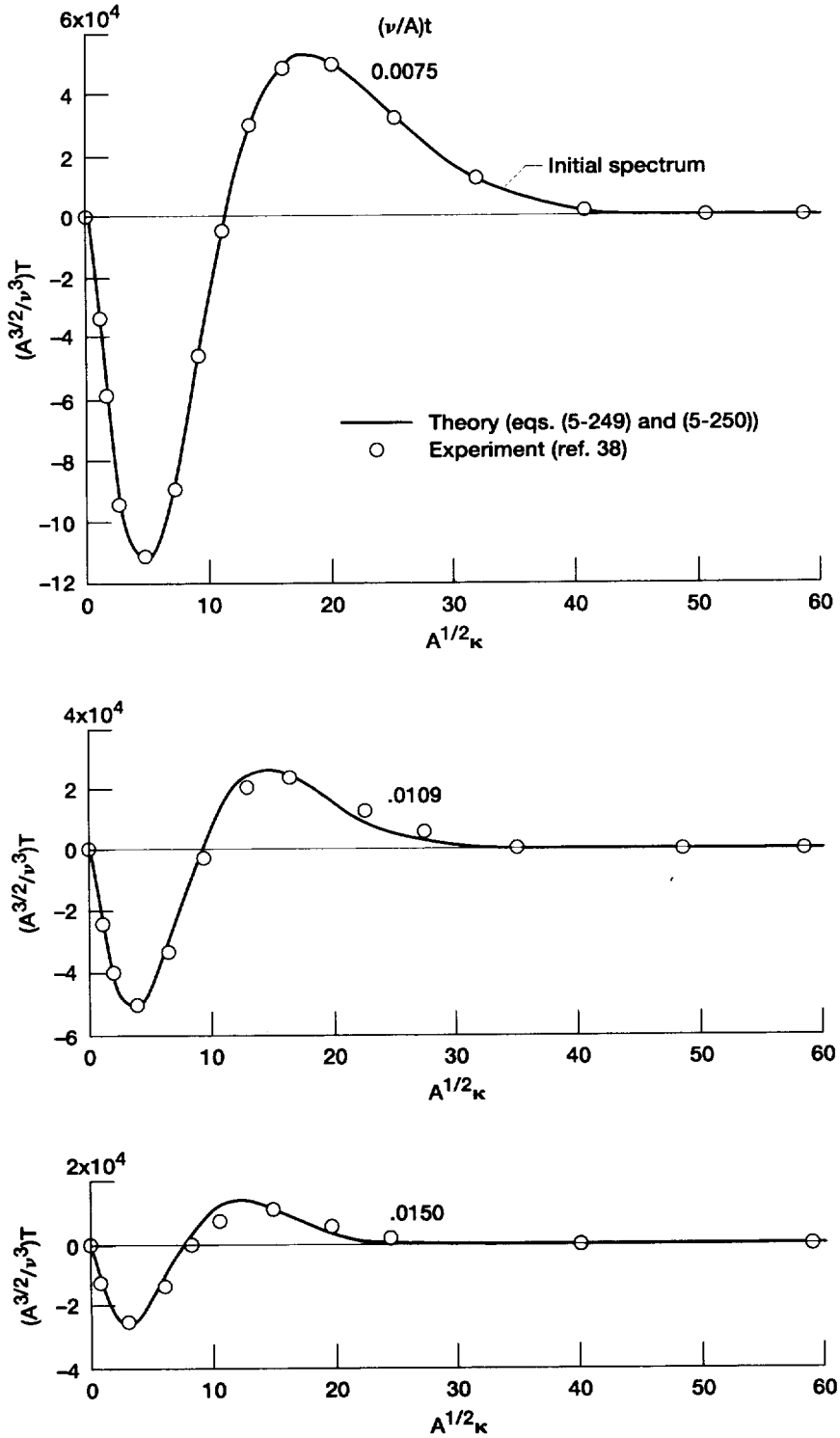

Figure 5-45.—Comparison of theory (eqs. (5-249) and (5-250)) and experiment (ref. 38) for decay of energy-transfer spectra.

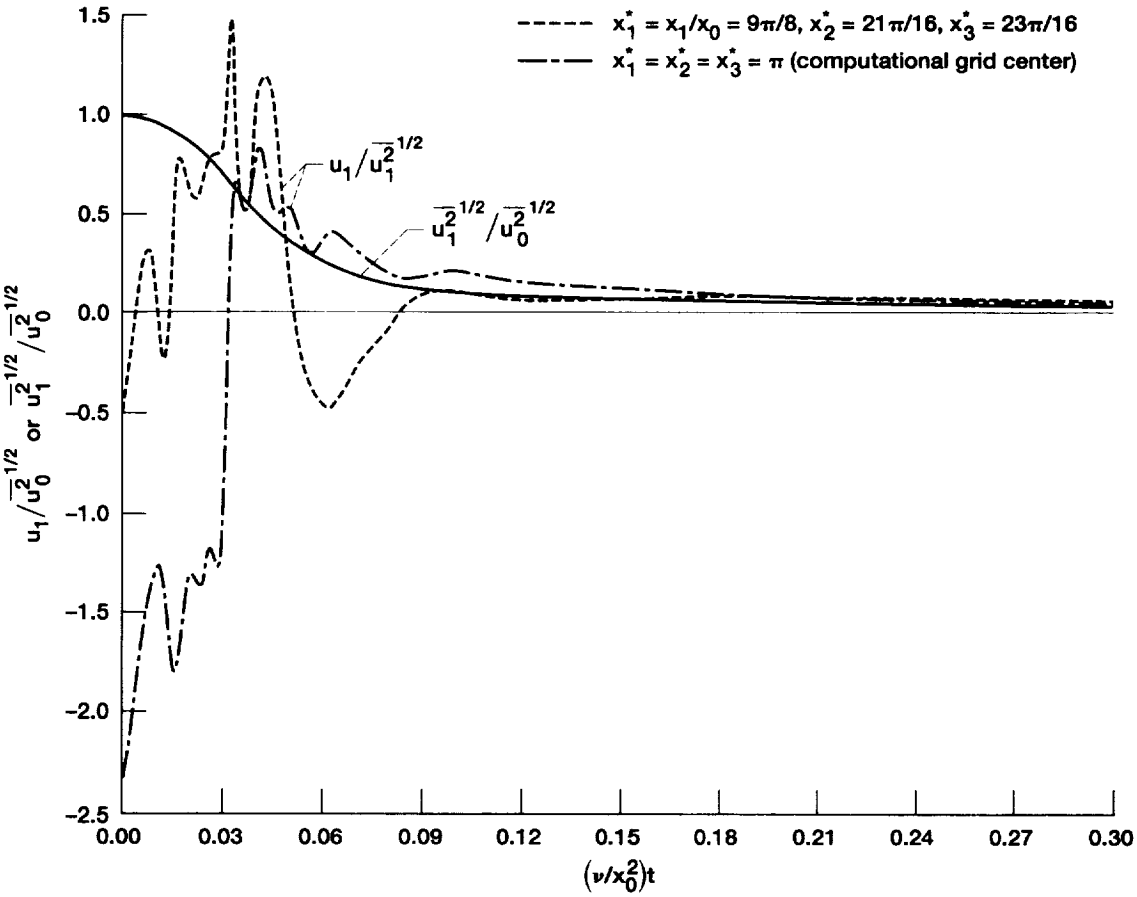

Figure 5-46.—Calculated time evolution of turbulent-like velocity fluctuations (normalized by initial condition) for an initial Reynolds number $R_0 = \overline{u_0^2}^{1/2} x_0/\nu = 138.6$. Root-mean-square fluctuations are spatially averaged. 32^3 grid points.

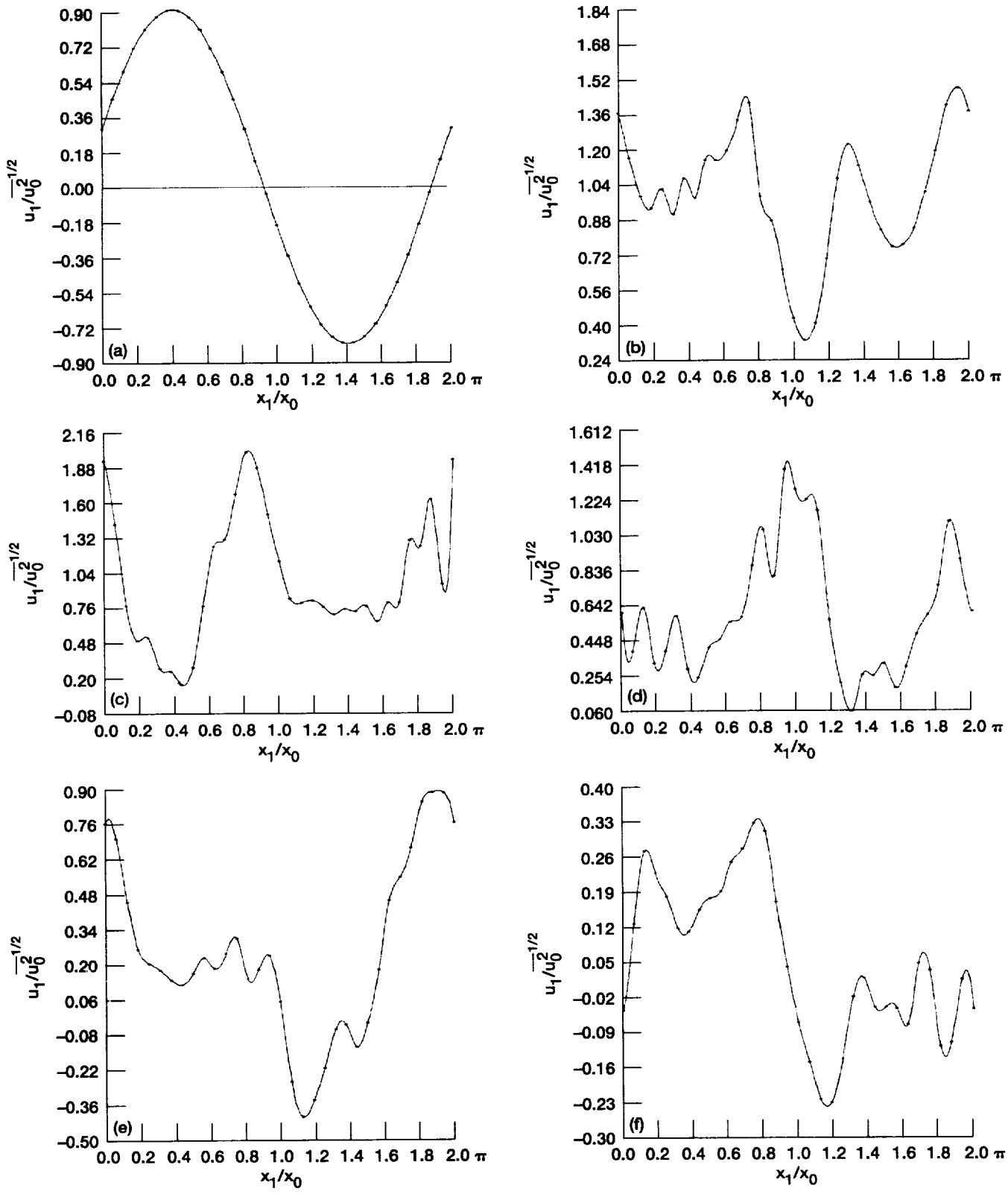

Figure 5-47.—Evolution of an instantaneous velocity profile on an off-center plane through the computational grid. $x_2^* = x_2/x_0 = 21\pi/16$, $x_3^* = 23\pi/16$, $R_0 = \overline{u_0^2}^{1/2} x_0/\nu = 138.6$. Symbols are at grid points. (a) $(\nu/x_0^2)\ t = 0$. (b) $(\nu/x_0^2)\ t = 0.01443$. (c) $(\nu/x_0^2)\ t = 0.02887$. (d) $(\nu/x_0^2)\ t = 0.04330$. (e) $(\nu/x_0^2)\ t = 0.05773$. (f) $(\nu/x_0^2)\ t = 0.07217$.

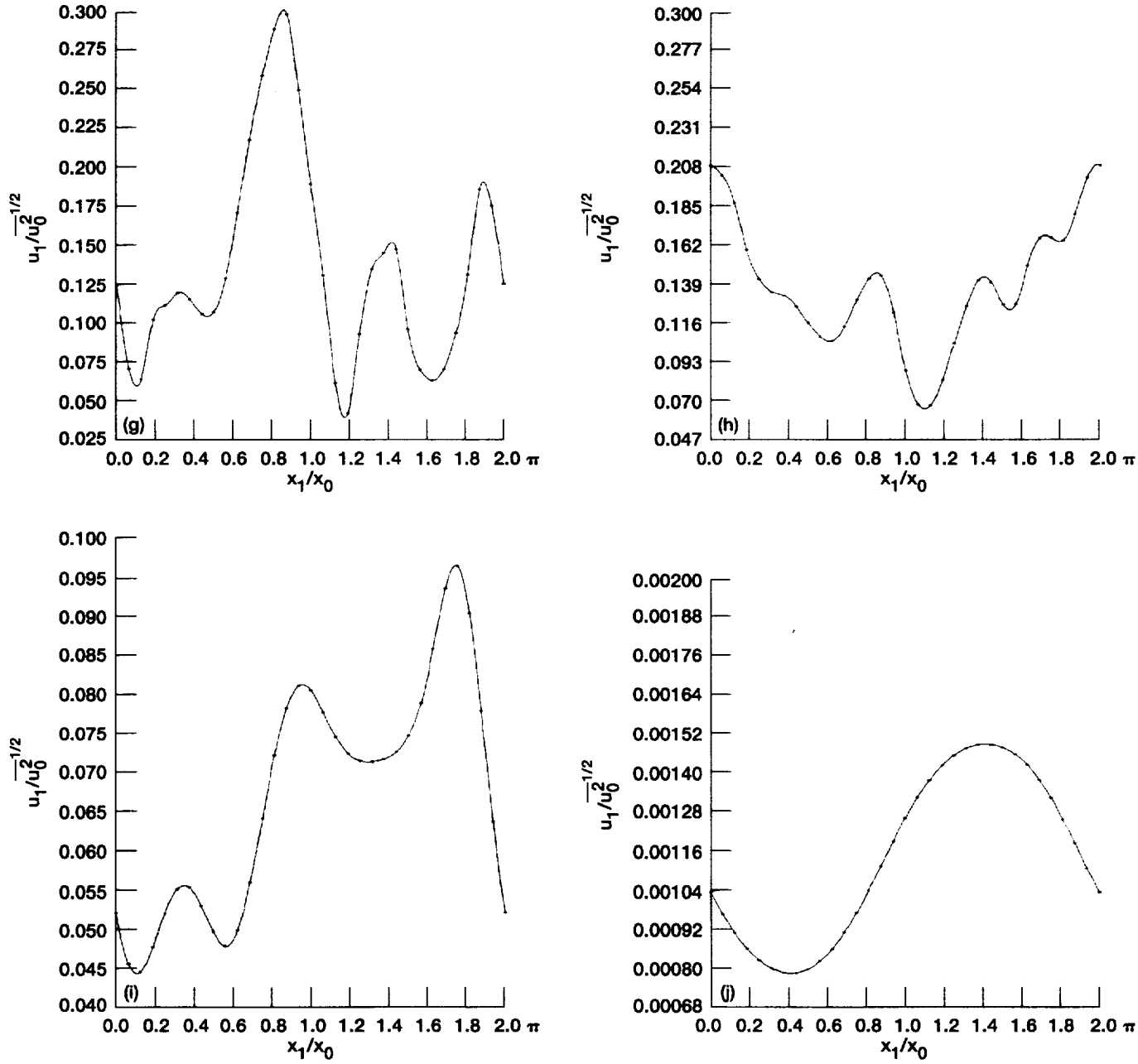

Figure 5-47.—Concluded. (g) (ν/x_0^2) t = 0.08660. (h) (ν/x_0^2) t = 0.1155. (i) (ν/x_0^2) t = 0.2454. (j) (ν/x_0^2) t = 1.097.

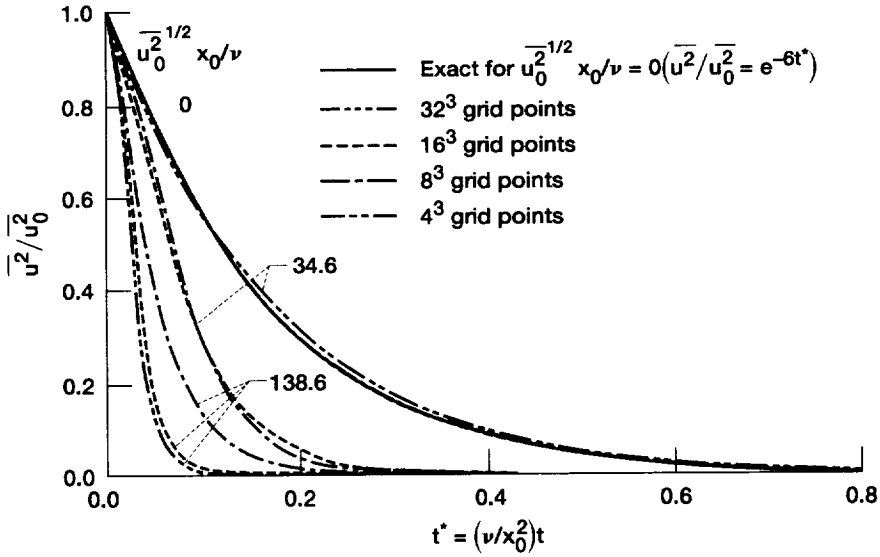

Figure 5-48.—Effect of numerical mesh size on evolution of $\overline{u^2}$ at low and moderate Reynolds numbers. $\overline{u^2} \equiv \overline{u_1^2} = \overline{u_2^2} = \overline{u_3^2}$.

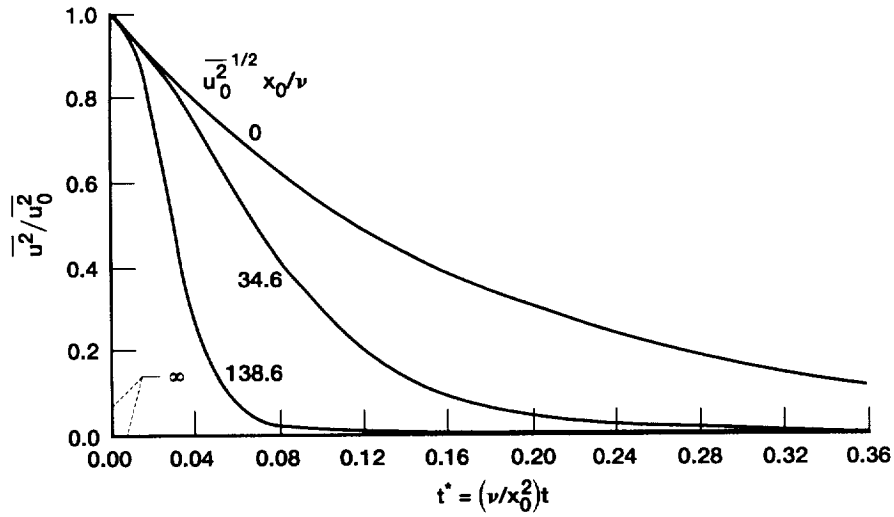

Figure 5-49.—Calculated evolution of mean-square velocity fluctuations (normalized by initial value) for various initial Reynolds numbers. No mean shear. $\overline{u^2} \equiv \overline{u_1^2} = \overline{u_2^2} = \overline{u_3^2}$.

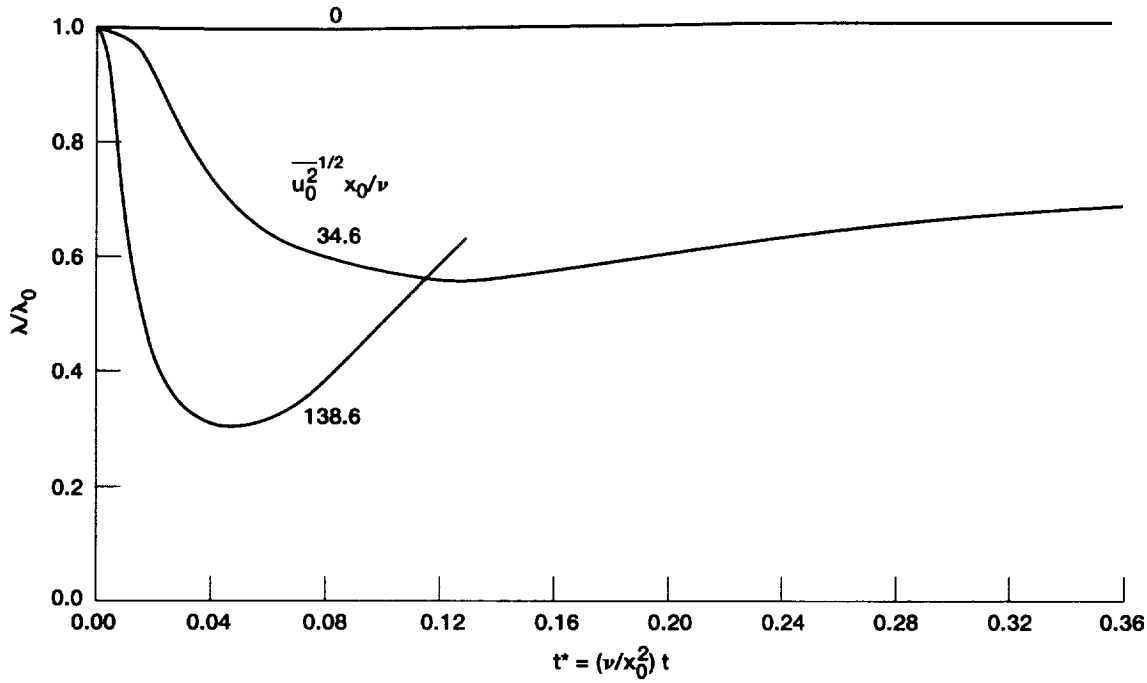

Figure 5-50.—Calculated evolution of microscale of velocity fluctuations (normalized by initial value) for various initial Reynolds numbers.

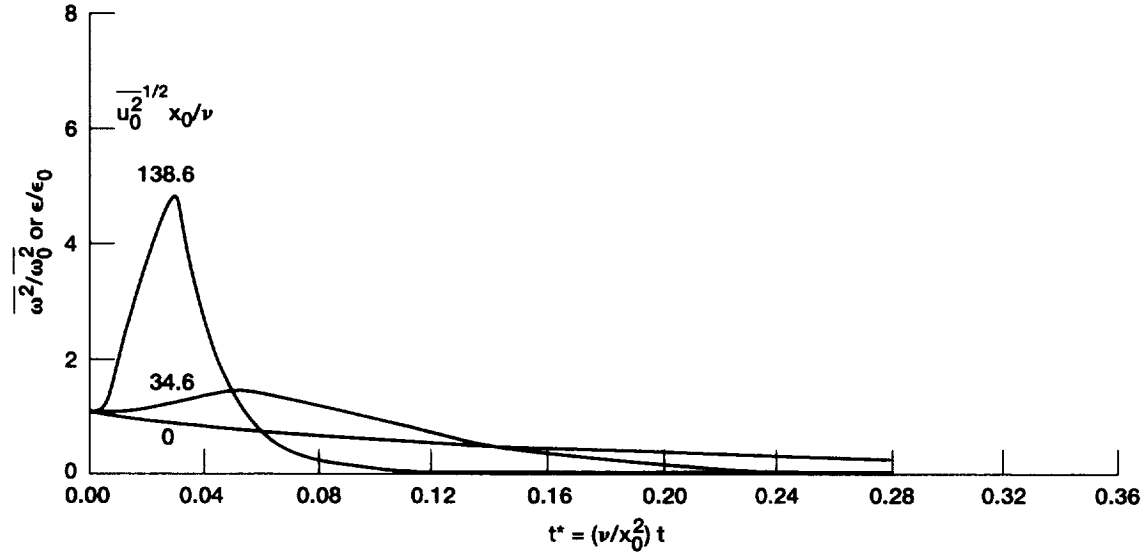

Figure 5-51.—Calculated development of mean-square vorticity fluctuations $\overline{\omega^2}$ or dissipation ϵ (normalized by initial value) for various initial Reynolds numbers.

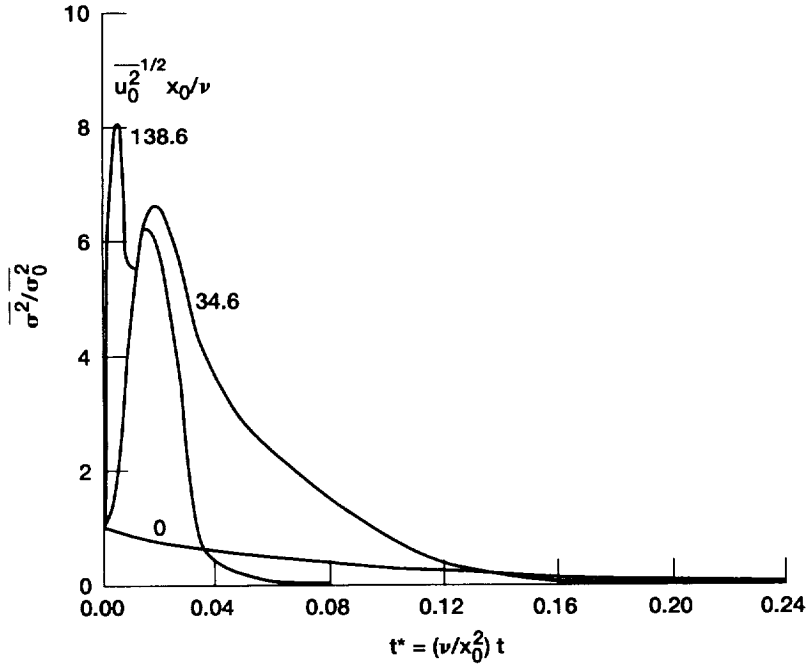

Figure 5-52.—Calculated evolution of mean-square pressure fluctuation (normalized by initial value) for various initial Reynolds numbers.

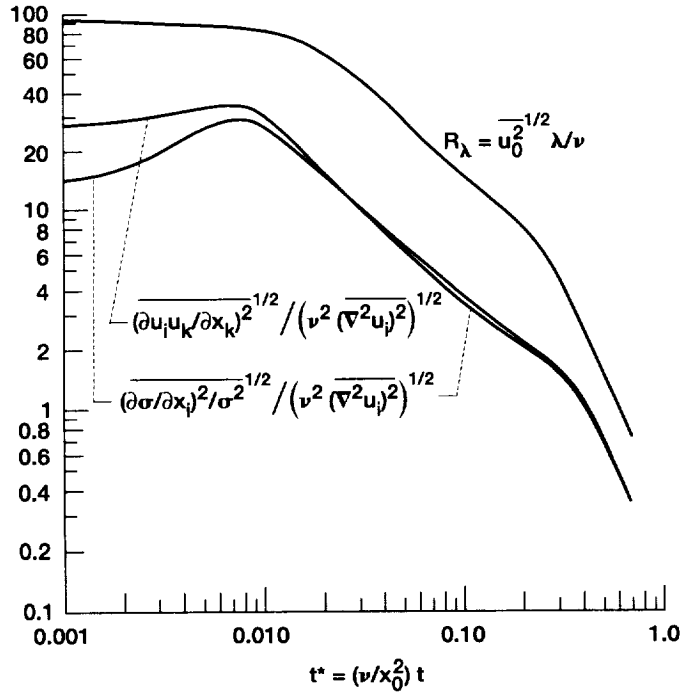

Figure 5-53.—Three measures of relative importance of inertial and viscous effects versus dimensionless time.
$\overline{u_0^2}^{1/2} x_0/\nu = 69.3$. i = 1, 2, or 3.

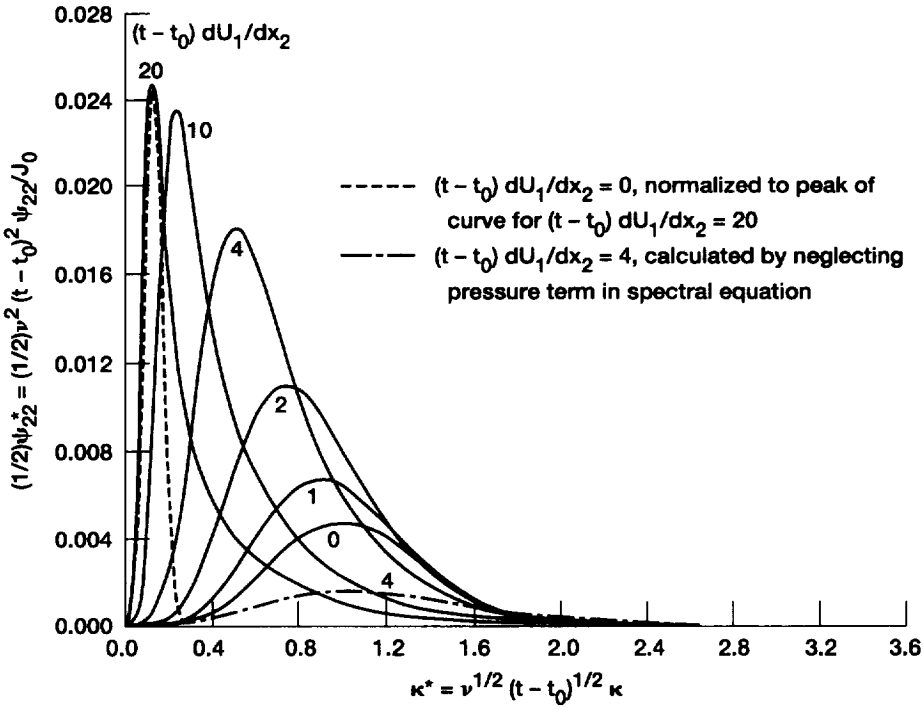

Figure 5-54.—Dimensionless spectra of $(1/2)\overline{u_2^2}$ for uniform transverse velocity gradient.

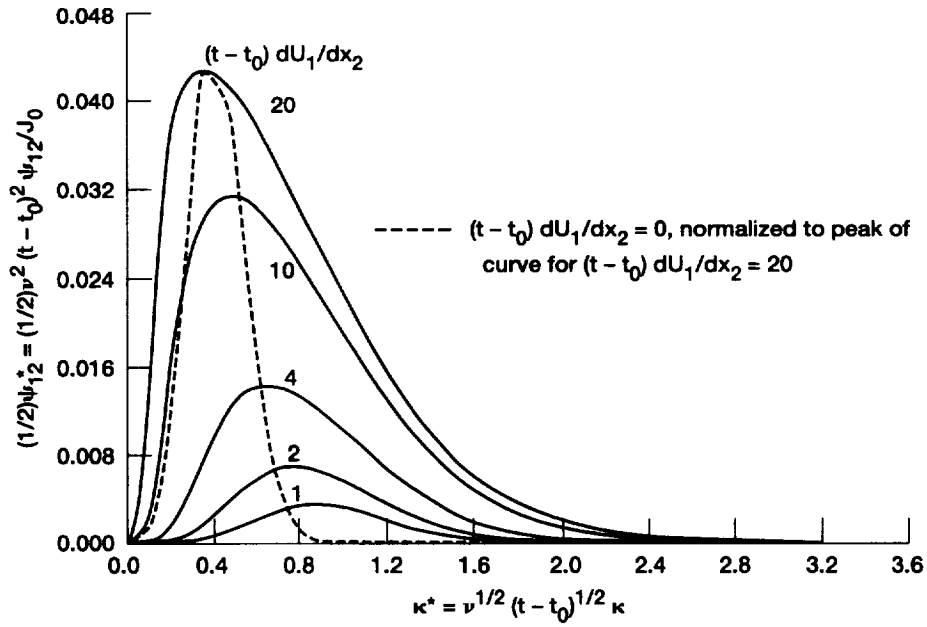

Figure 5-55.—Dimensionless spectra of $(1/2)\overline{u_1 u_2}$ for uniform transverse velocity gradient.

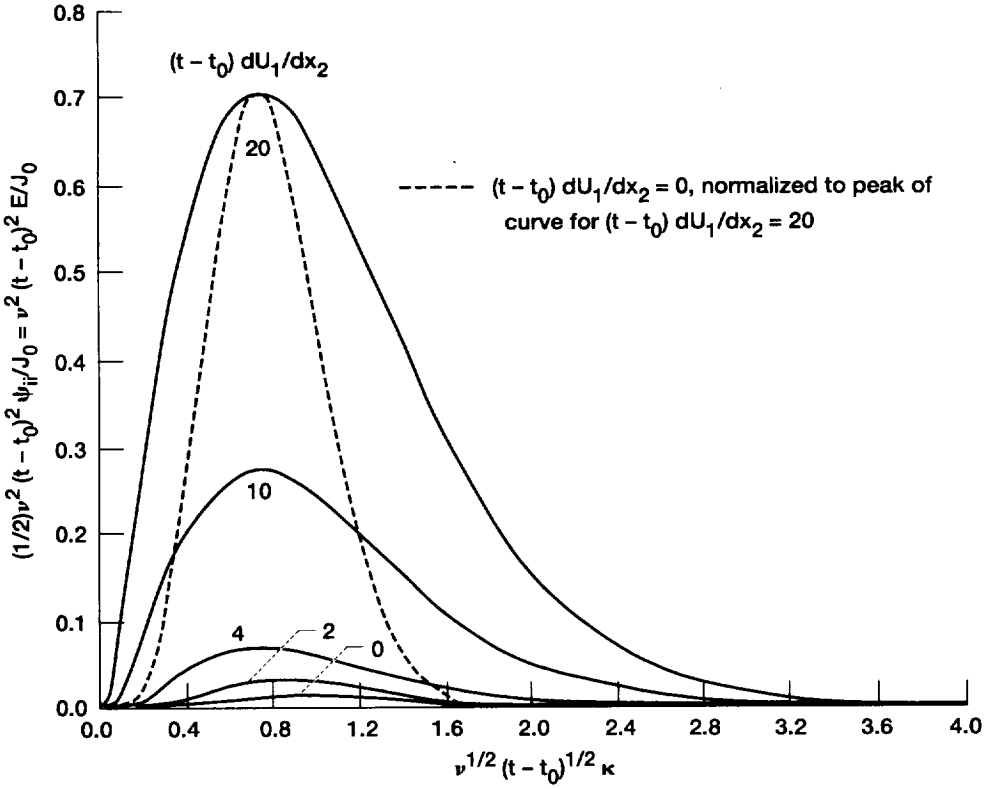

Figure 5-56.—Dimensionless spectra of turbulent energy $(1/2)\overline{u_i u_i}$ for uniform transverse velocity gradient.

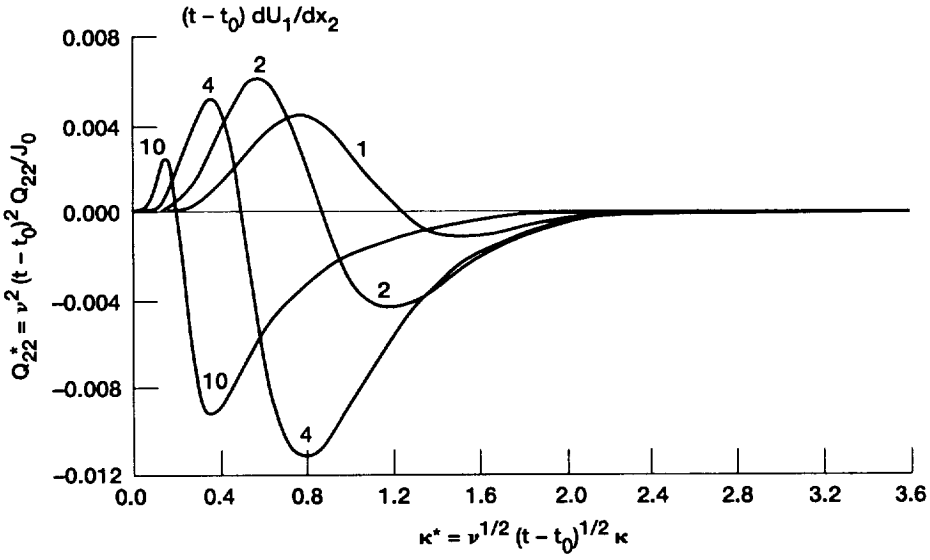

Figure 5-57.—Plot of dimensionless pressure term in spectral equation (eq. (5-326)) for i = j = 2.

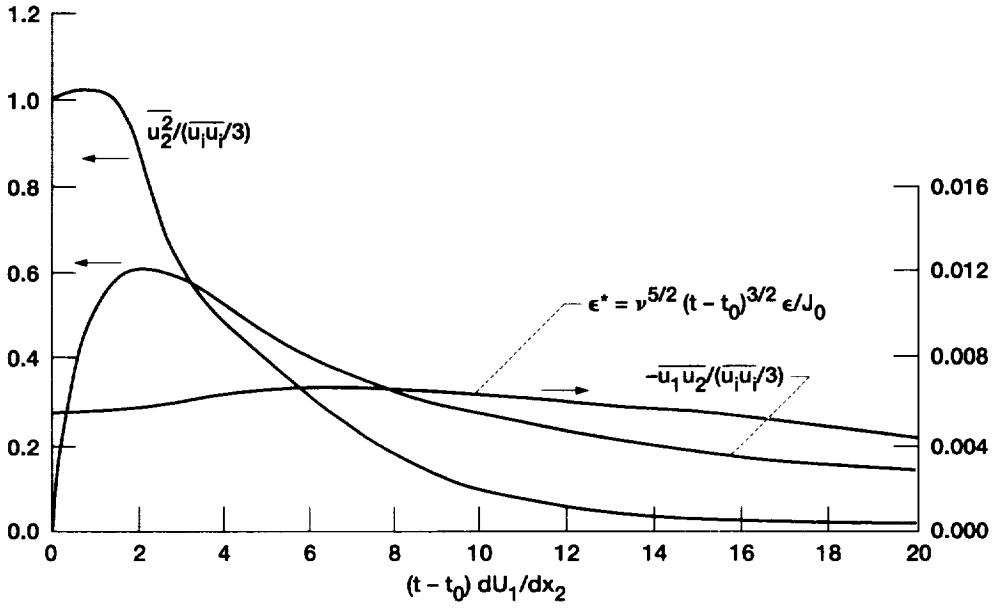

Figure 5-58.—Plot showing $\overline{u_2^2}/((1/3)\overline{u_i u_i})$, $-\overline{u_1 u_2}/((1/3)\overline{u_i u_i})$, and ϵ^* against dimensionless velocity gradient.

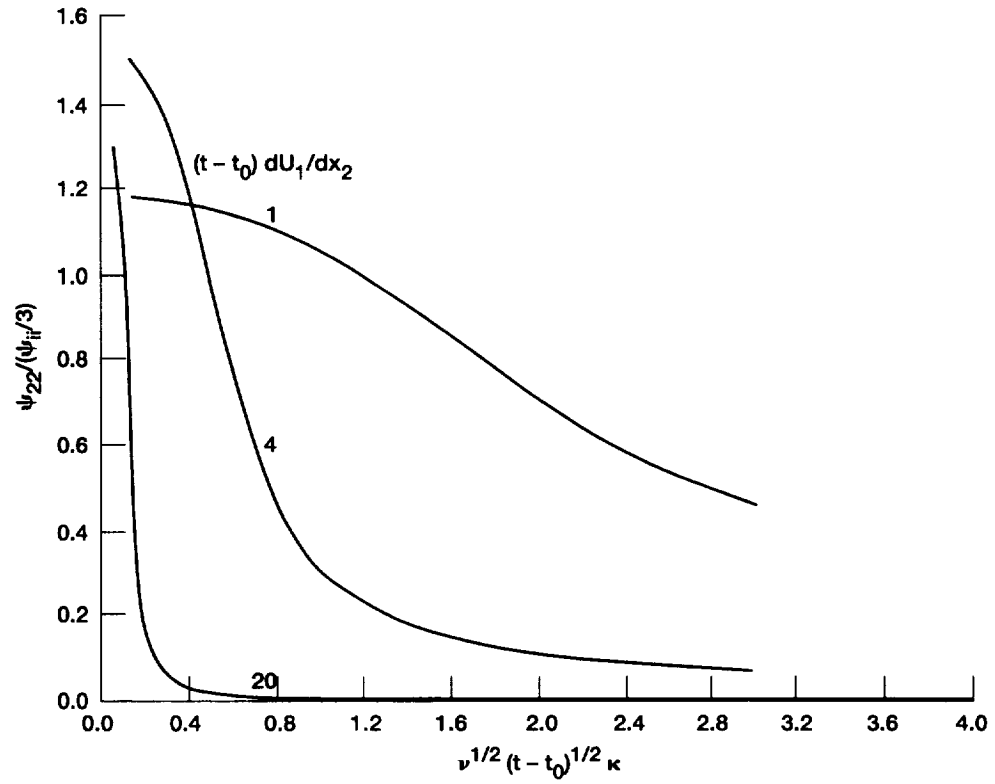

Figure 5-59.—Plot showing $\psi_{22}/((1/3)\psi_{ii})$ against dimensionless wavenumber.

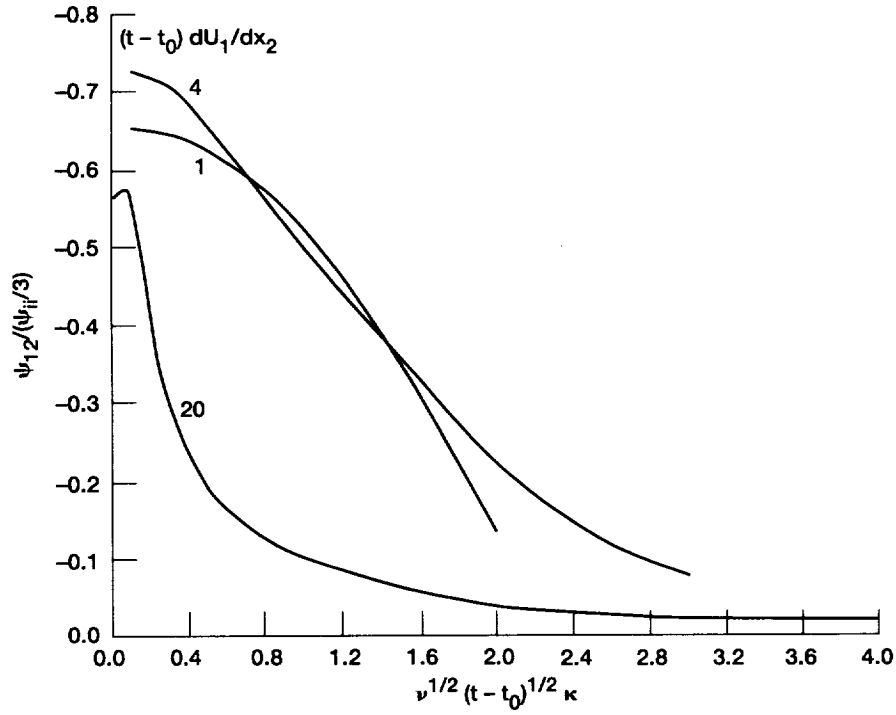

Figure 5-60.—Plot showing $\psi_{12}/((1/3)\psi_{ii})$ against dimensionless wavenumber.

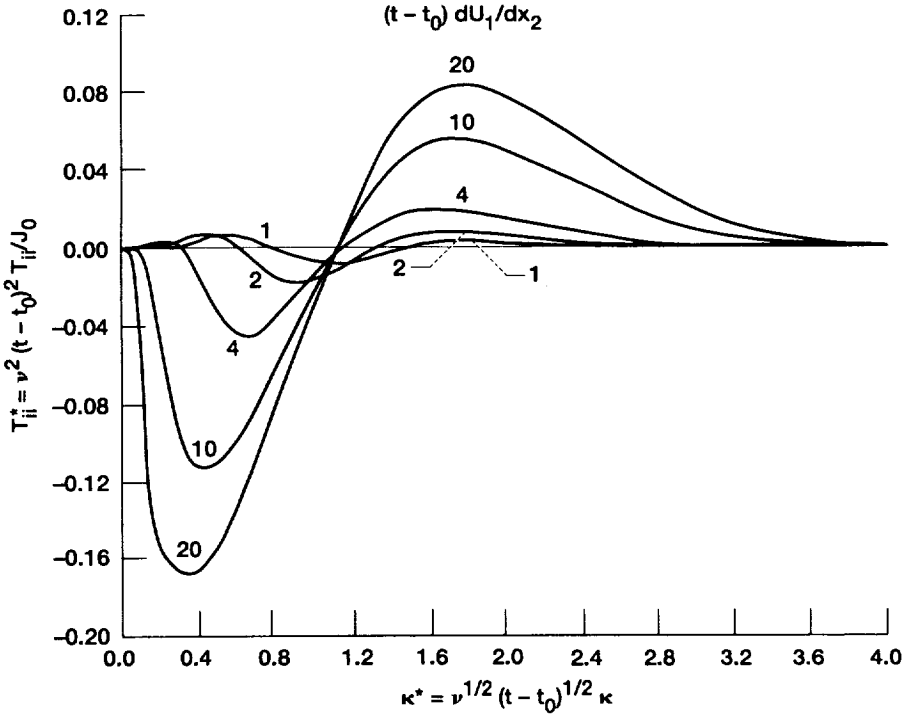

Figure 5-61.—Dimensionless spectra of transfer term due to mean velocity gradient in spectral equation for ψ_{ii} (eq. (5-327)).

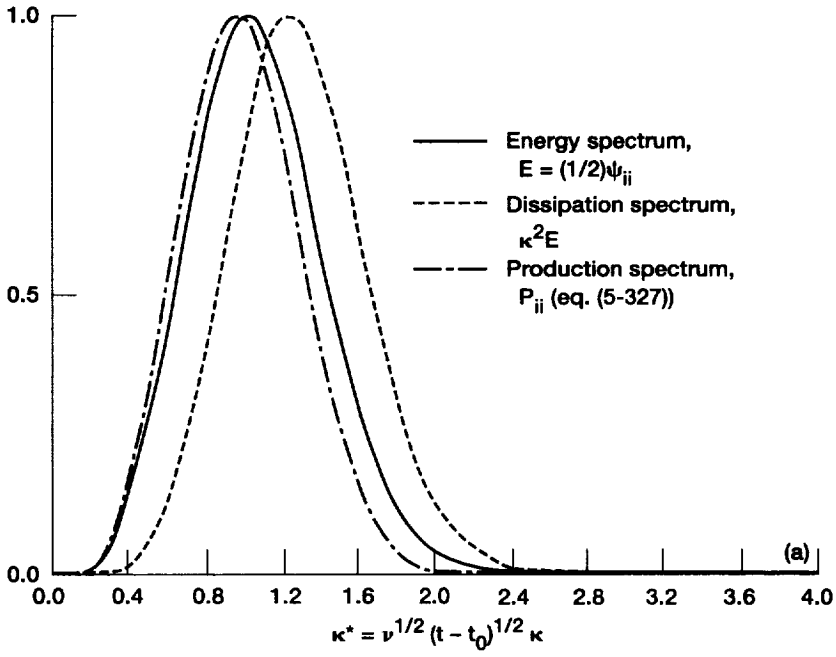

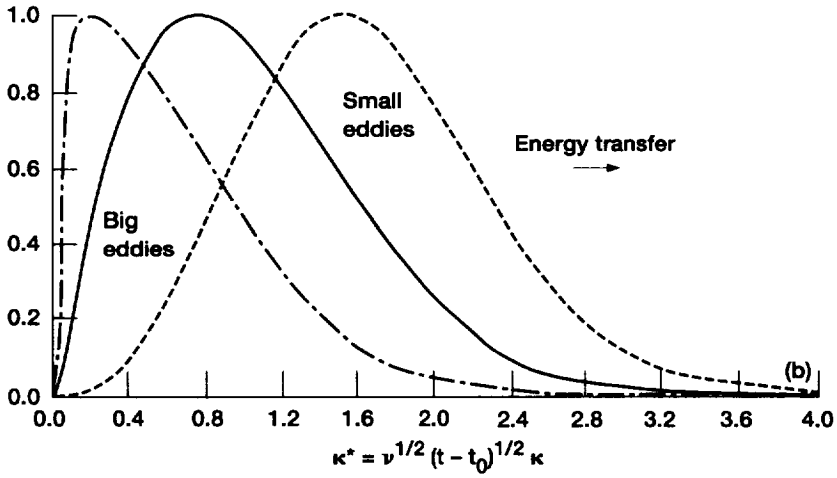

Figure 5-62.—Comparison of production, energy, and dissipation spectra. Curves in each plot are normalized to same height. (a) $(t - t_0)\, dU_1/dx_2 \to 0$. (b) $(t - t_0)\, dU_1/dx_2 = 50$.

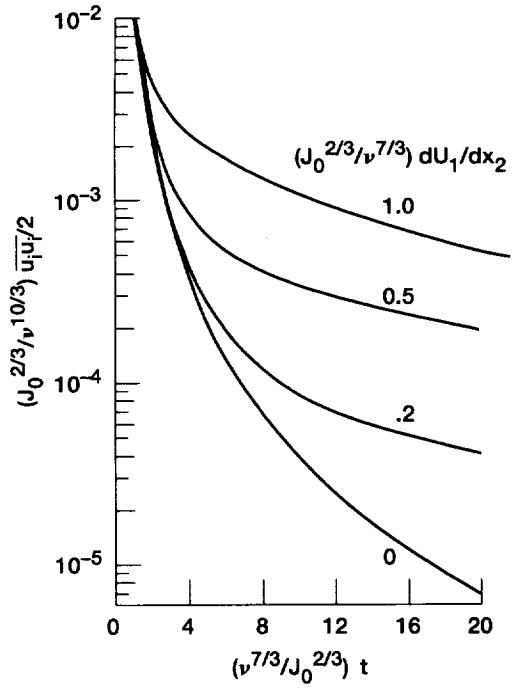

Figure 5-63.—Effect of uniform shear on decay of turbulent energy. In all cases the turbulence ultimately decays.

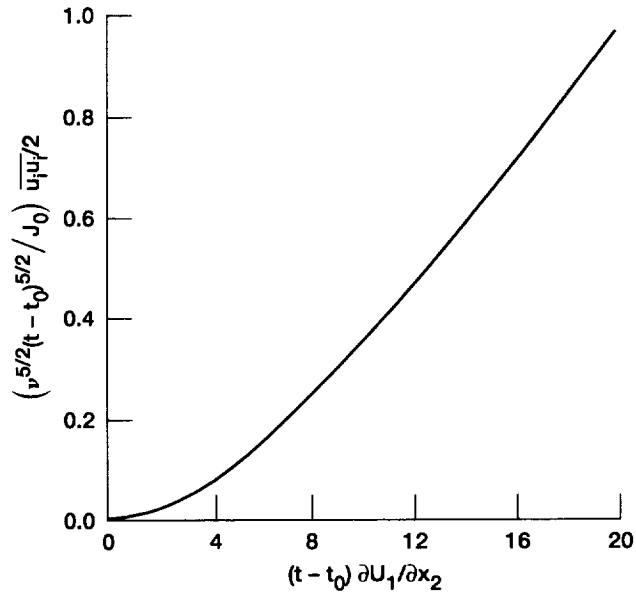

Figure 5-64.—Effect of uniform shear on turbulent energy. Curves from figure 5-63 collapsed into one.

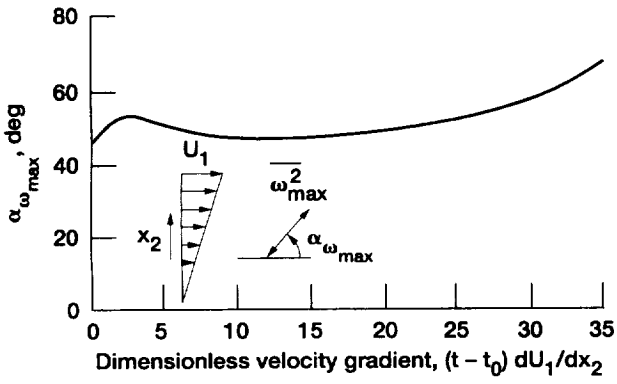

Figure 5-65.—Variation of angle of maximum turbulent vorticity with dimensionless velocity gradient.

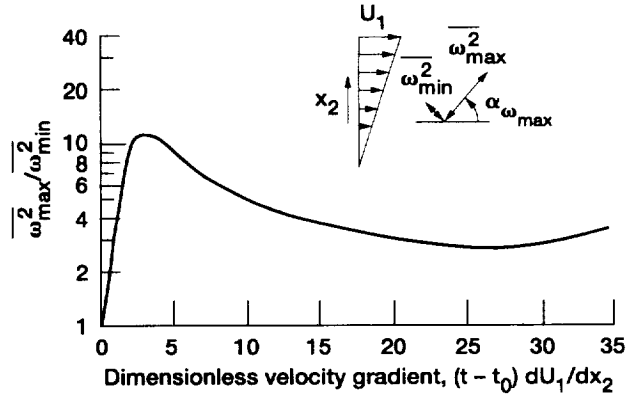

Figure 5-66.—Variation of ratio of maximum to minimum mean square turbulent vorticity with dimensionless velocity gradient.

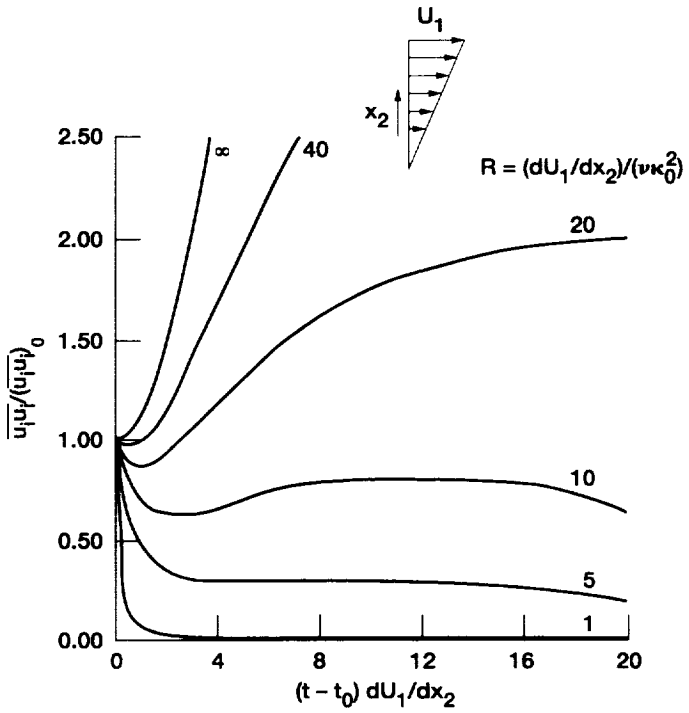

Figure 5-67.—Variation of total turbulent energy (per unit mass) with dimensionless time and Reynolds number R.

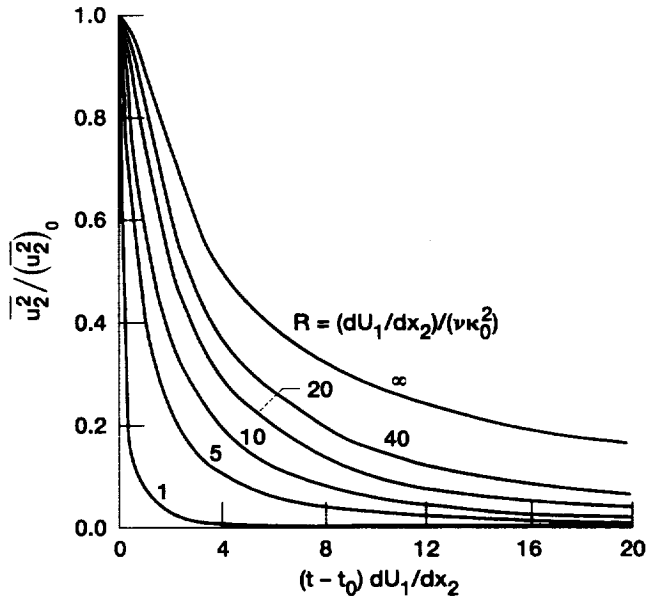

Figure 5-68.—Variation of component of turbulent energy in direction of mean velocity gradient with dimensionless time and Reynolds number R.

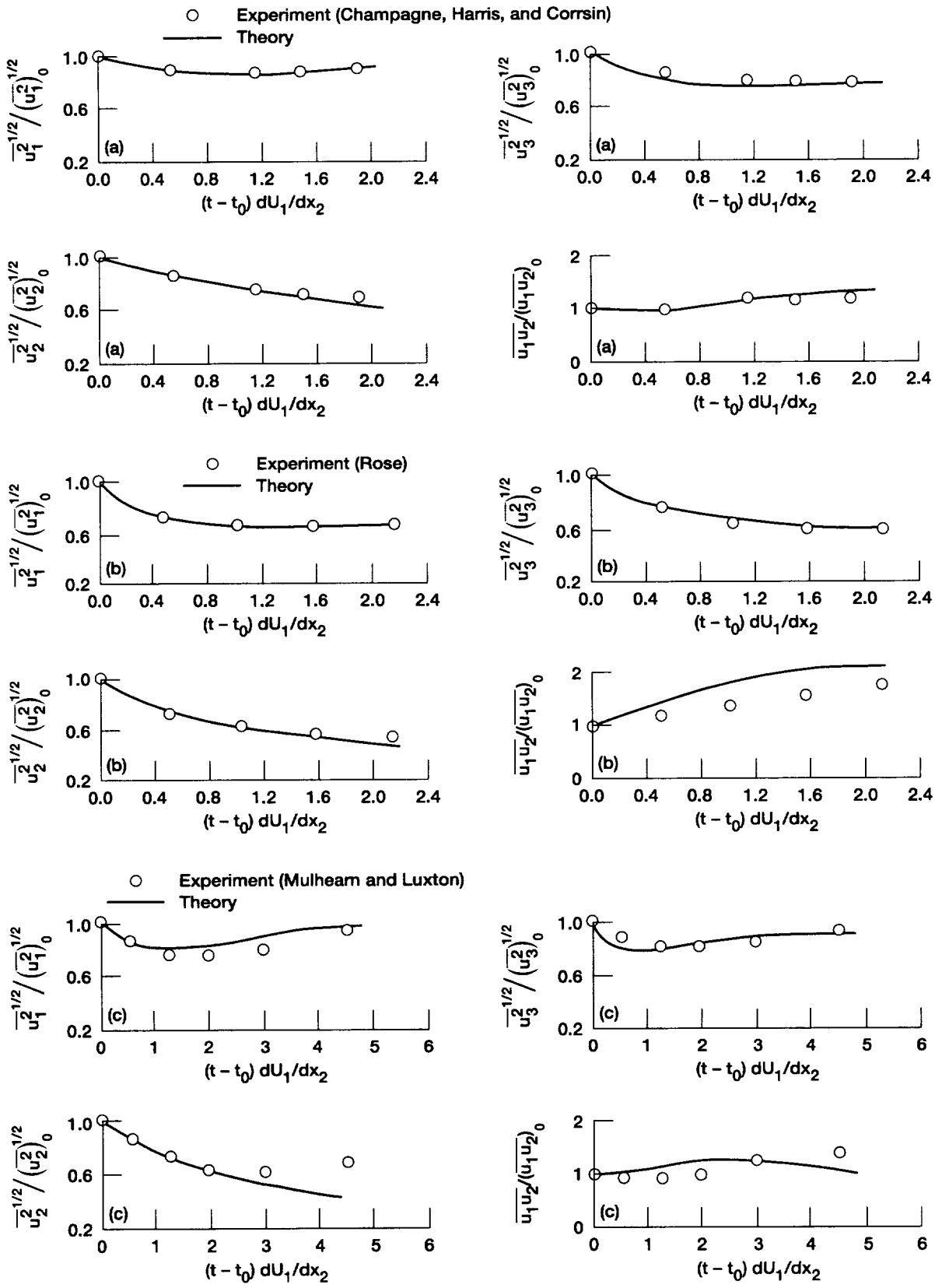

Figure 5-69.—Evolution of one-point turbulence components; plots for determining constants (eq. (5-352)) for initial conditions. (a) Data from reference 94. (b) Data from reference 93. (c) Data from reference 95.

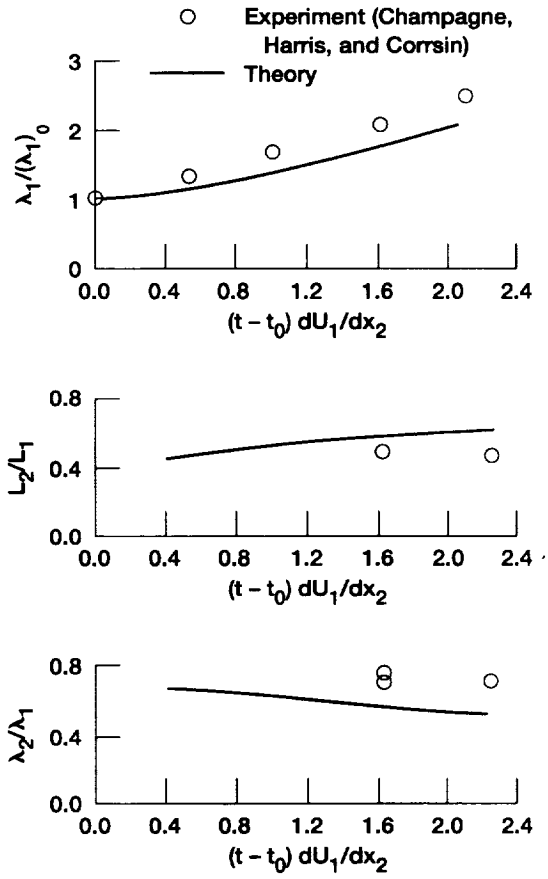

Figure 5-70.—Comparison of theory and experiment for evolution of scale ratios. Data from reference 94.

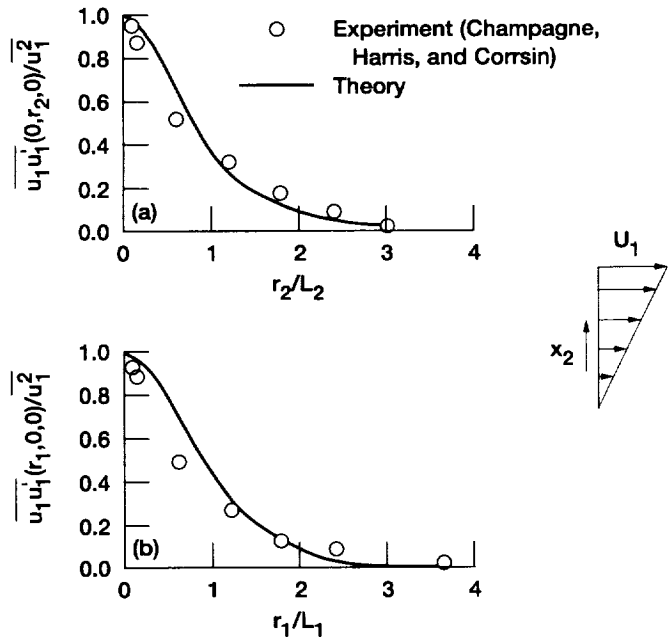

Figure 5-71.—Comparison of theory and experiment for two-point velocity correlations. $(dU_1/dx_2)(t - t_0) = 1.641$. Data from reference 94. (a) Two points separated along direction of velocity gradient. (b) Two points separated along flow direction.

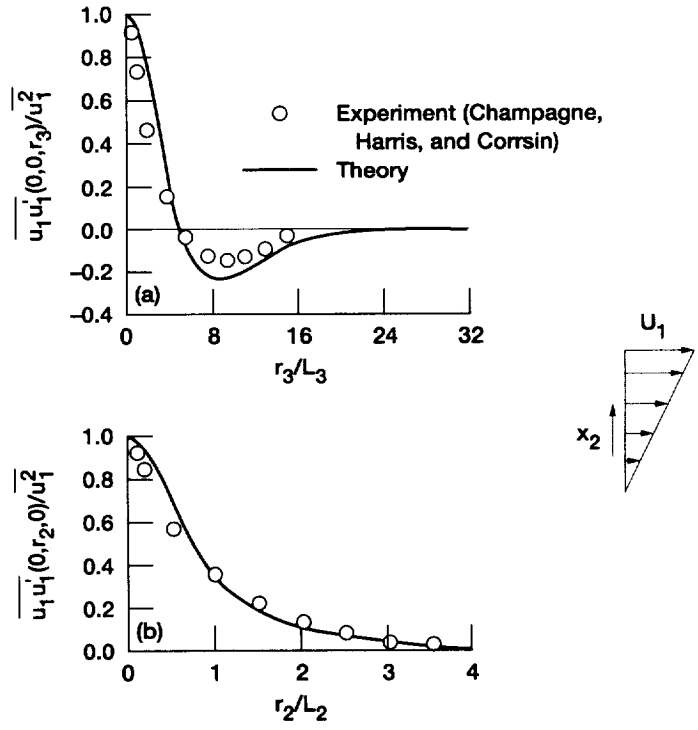

Figure 5-72.—Comparison of theory and experiment for two-point velocity correlations. $(dU_1/dx_2)(t - t_0) = 2.27$. Data from reference 94. (a) Two points separated along direction normal to both flow direction and direction of velocity gradient. (b) Two points separated along direction of velocity gradient.

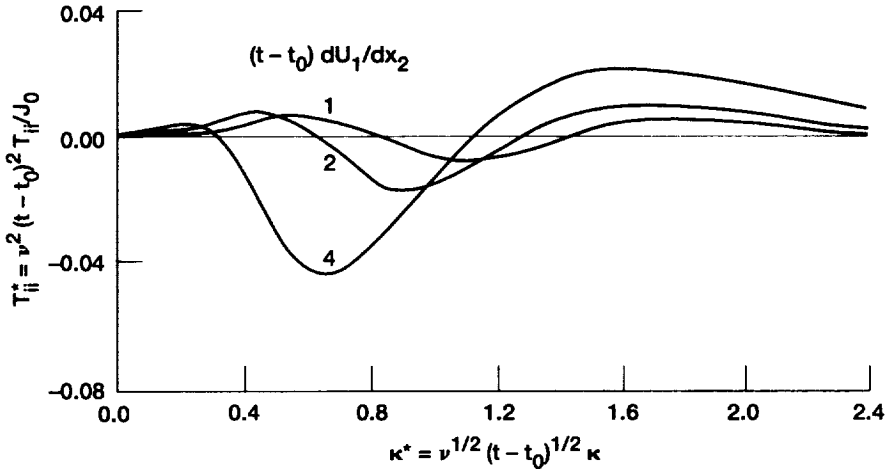

Figure 5-73.—Dimensionless spectra of energy transfer term due to mean velocity gradient (eq. (5-324)) (second term on right side) integrated over all directions in wavenumber space. Equation (5-351) with $\ell = 0$ was used for initial condition.

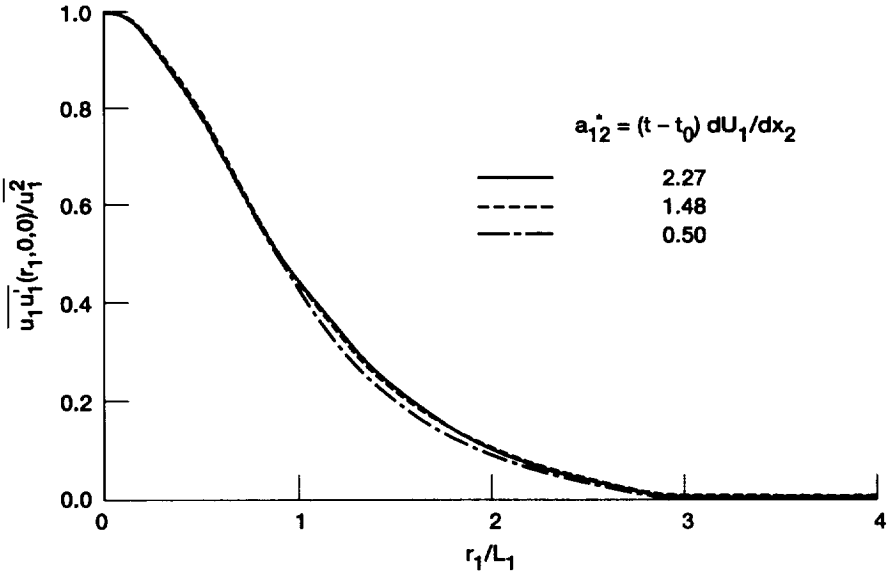

Figure 5-74.—Curves showing the similarity of the $\overline{u_1 u_1'}(r_1,0,0)$ correlations at various times.

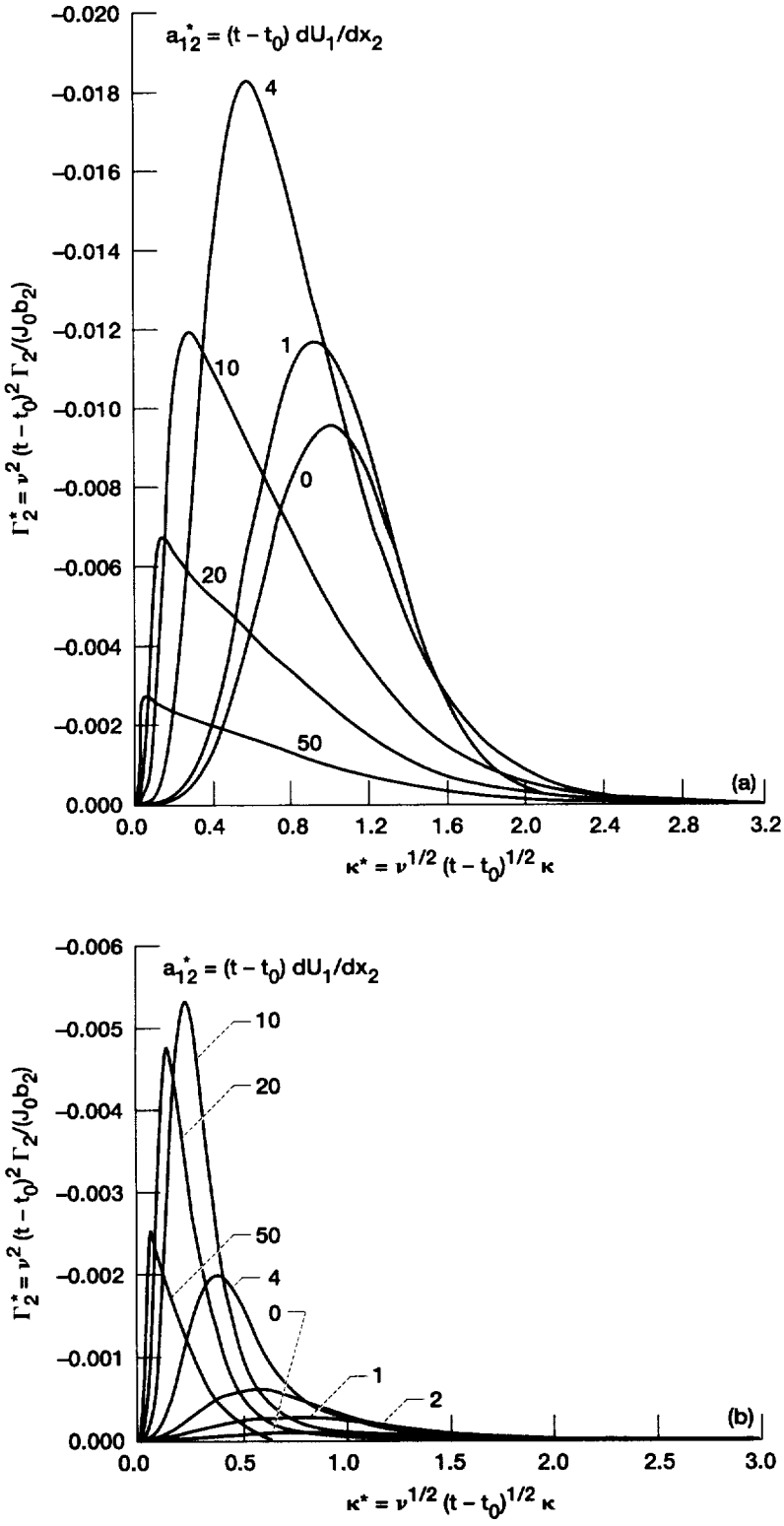

Figure 5-75.—Dimensionless spectra of $\overline{\tau u_2}$ for uniform transverse velocity and temperature gradients. (a) Prandtl number, 1. (b) Prandtl number, 0.01.

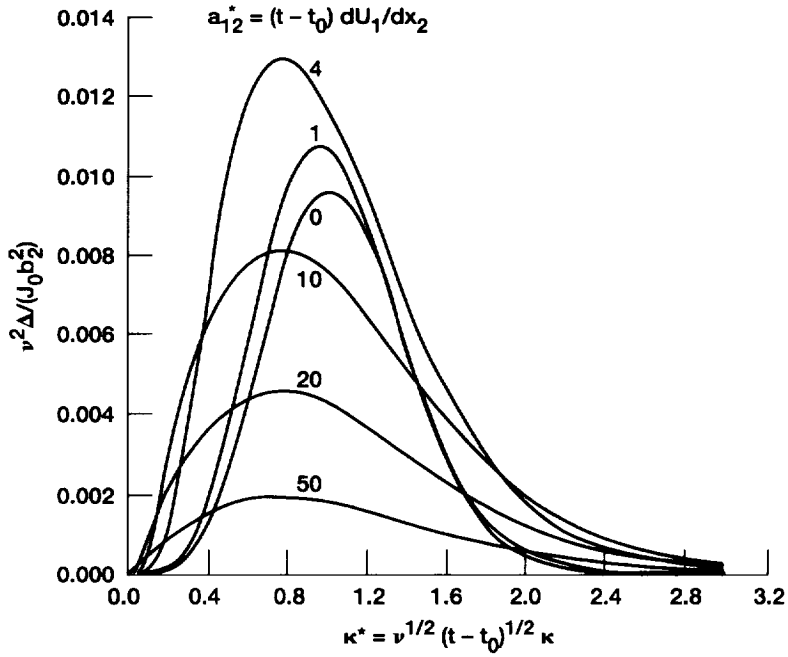

Figure 5-76.—Dimensionless spectra of $\overline{\tau^2}$ for uniform transverse velocity and temperature gradients. Prandtl number, 1.

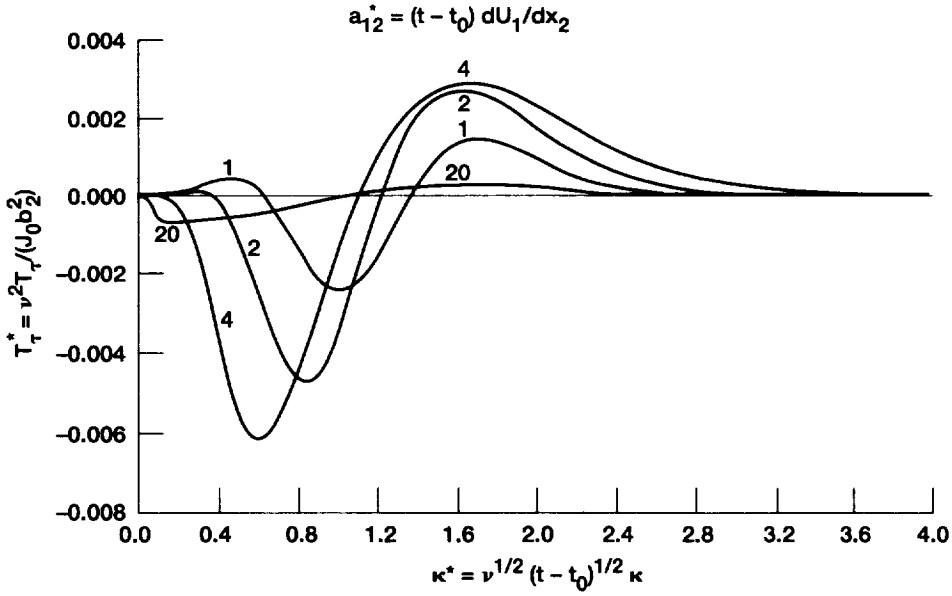

Figure 5-77.—Dimensionless spectra of transfer term due to mean velocity gradient in spectral equation for $\overline{\tau^2}$. Prandtl number, 1.

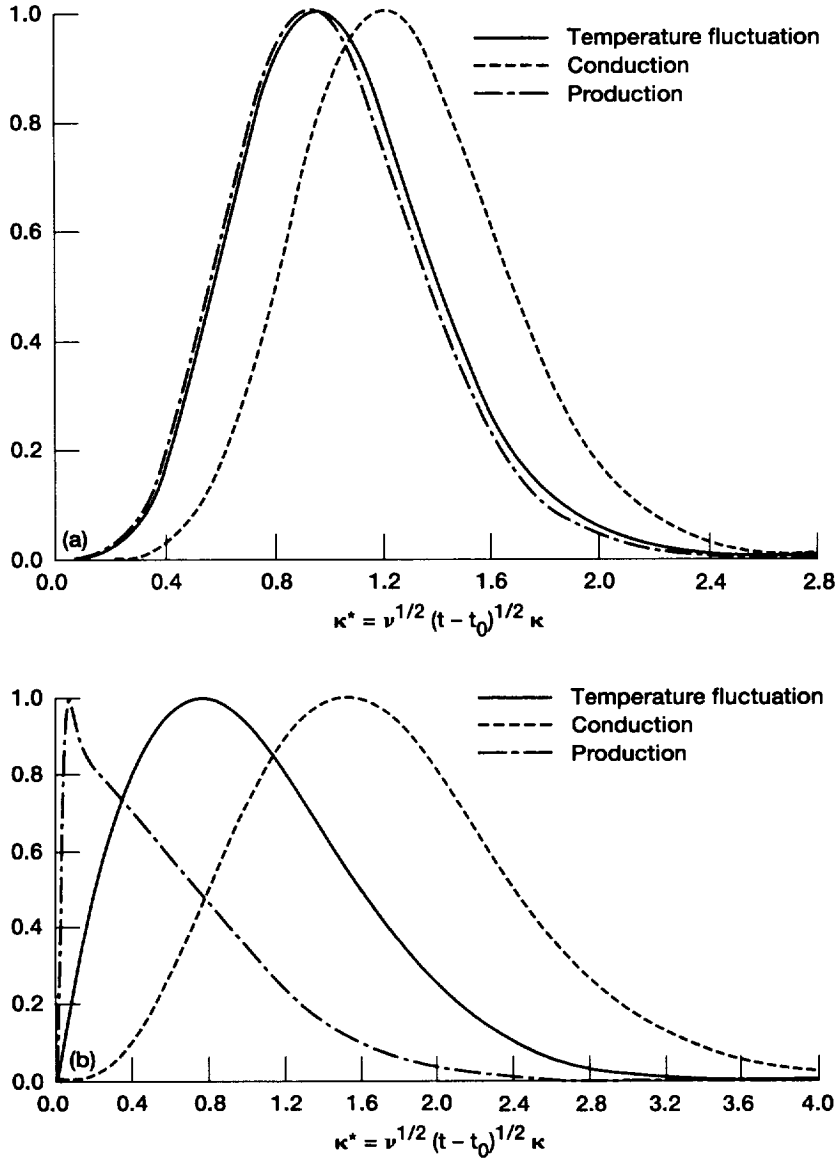

Figure 5-78.—Comparison of production, temperature fluctuation, and conduction spectra from spectral equation for $\overline{\tau u_2}$. Prandtl number, 1. Curves are normalized to same height. (a) $a_{12}^* = (t - t_0)\, dU_1/dx_2 = 1$. (b) $a_{12}^* = (t - t_0)\, dU_1/dx_2 = 50$.

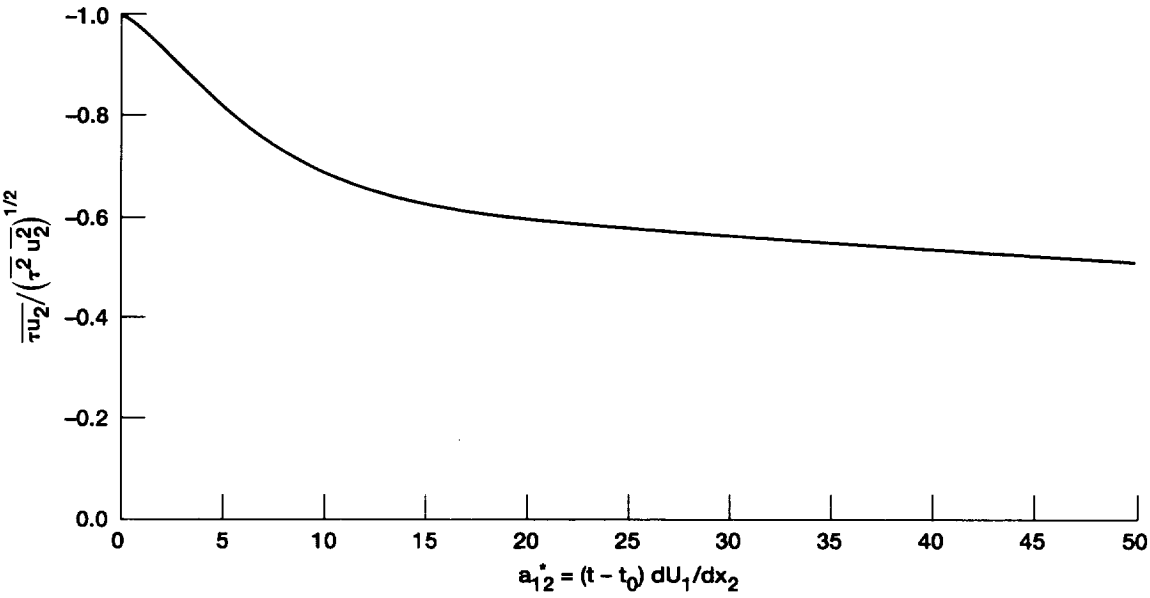

Figure 5-79.—Variation of temperature-velocity correlation coefficient with dimensionless velocity gradient. Prandtl number, 1.

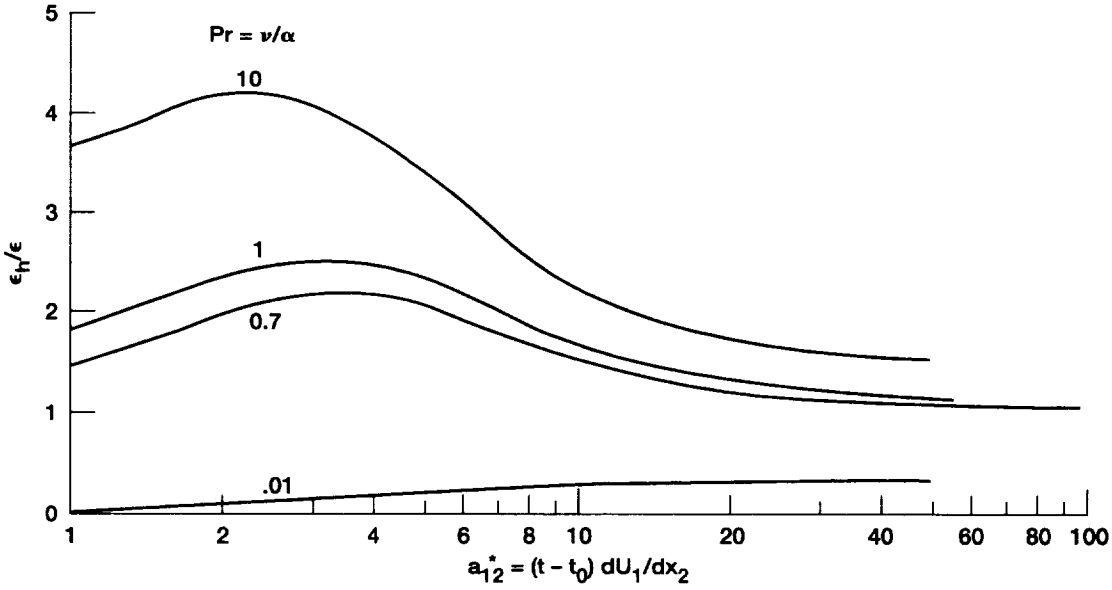

Figure 5-80.—Variation of ratio of eddy diffusivity for heat transfer to that for momentum transfer with dimensionless velocity gradient.

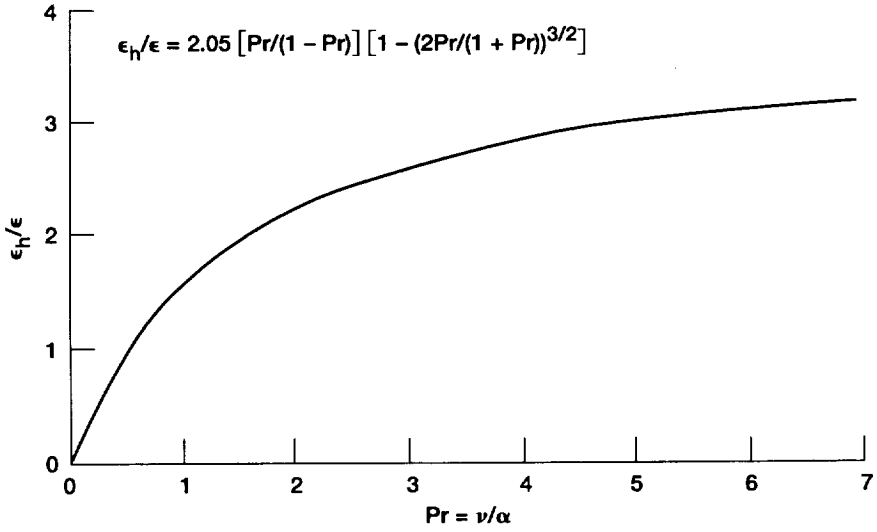

Figure 5-81.—Variation of ϵ_h/ϵ with Prandtl number for isotropic turbulence with velocity gradient = 0.

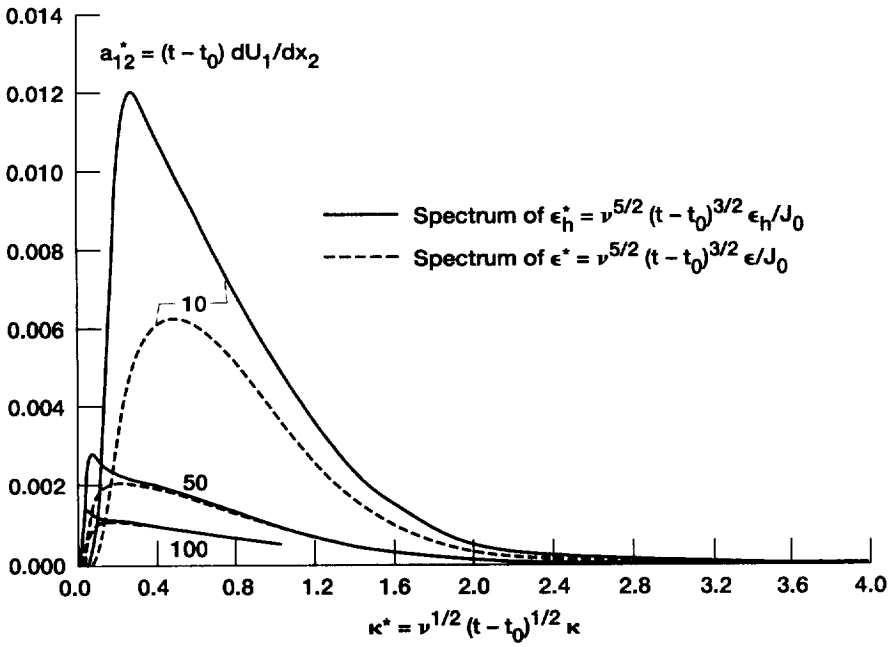

Figure 5-82.—Comparison of spectra of ϵ_h with those of ϵ. Prandtl number, 1.

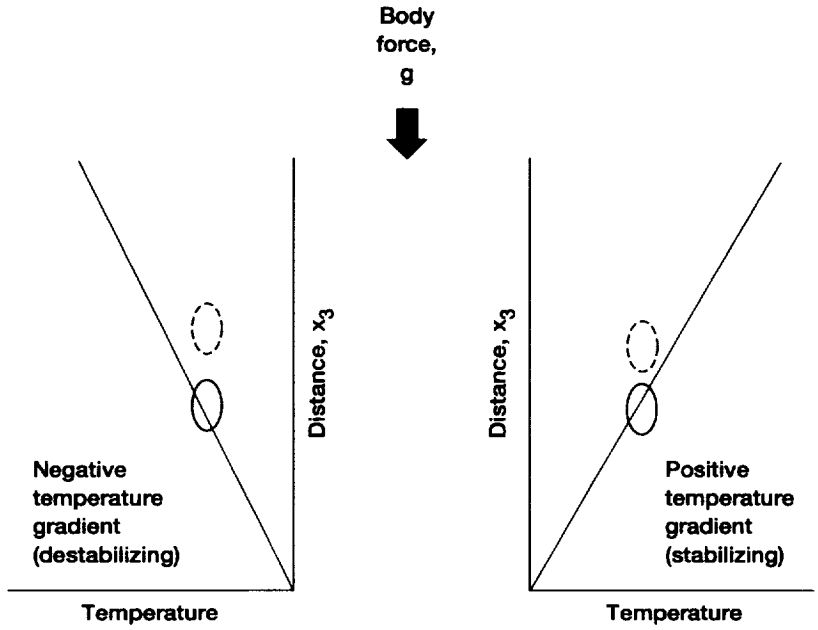

Figure 5-83.—Expected effects of buoyancy forces on turbulent eddy.

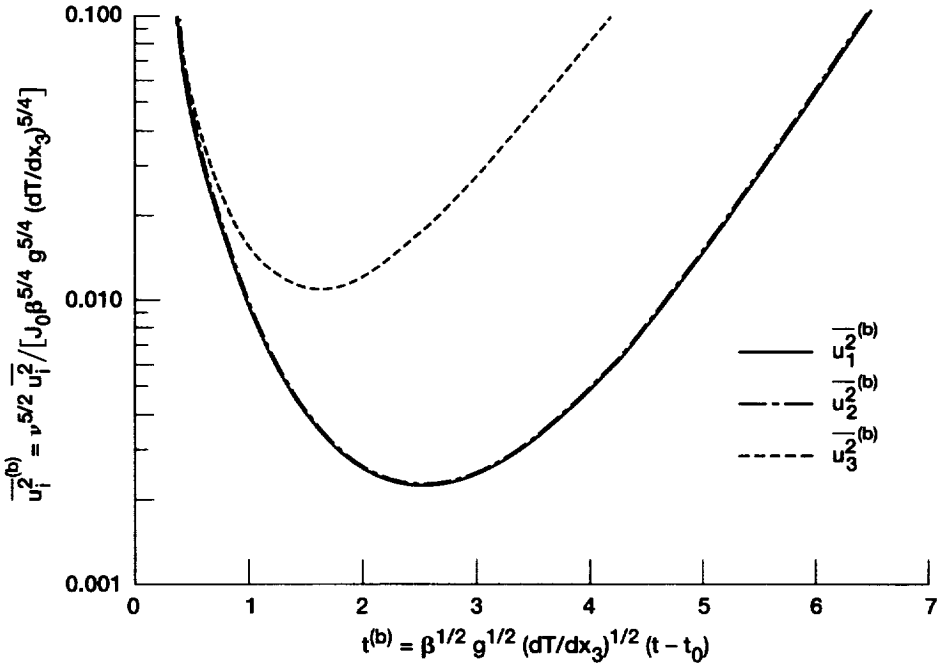

Figure 5-84.—Evolution of homogeneous turbulence in a flow with destabilizing buoyancy. Prandtl number, 0.7.

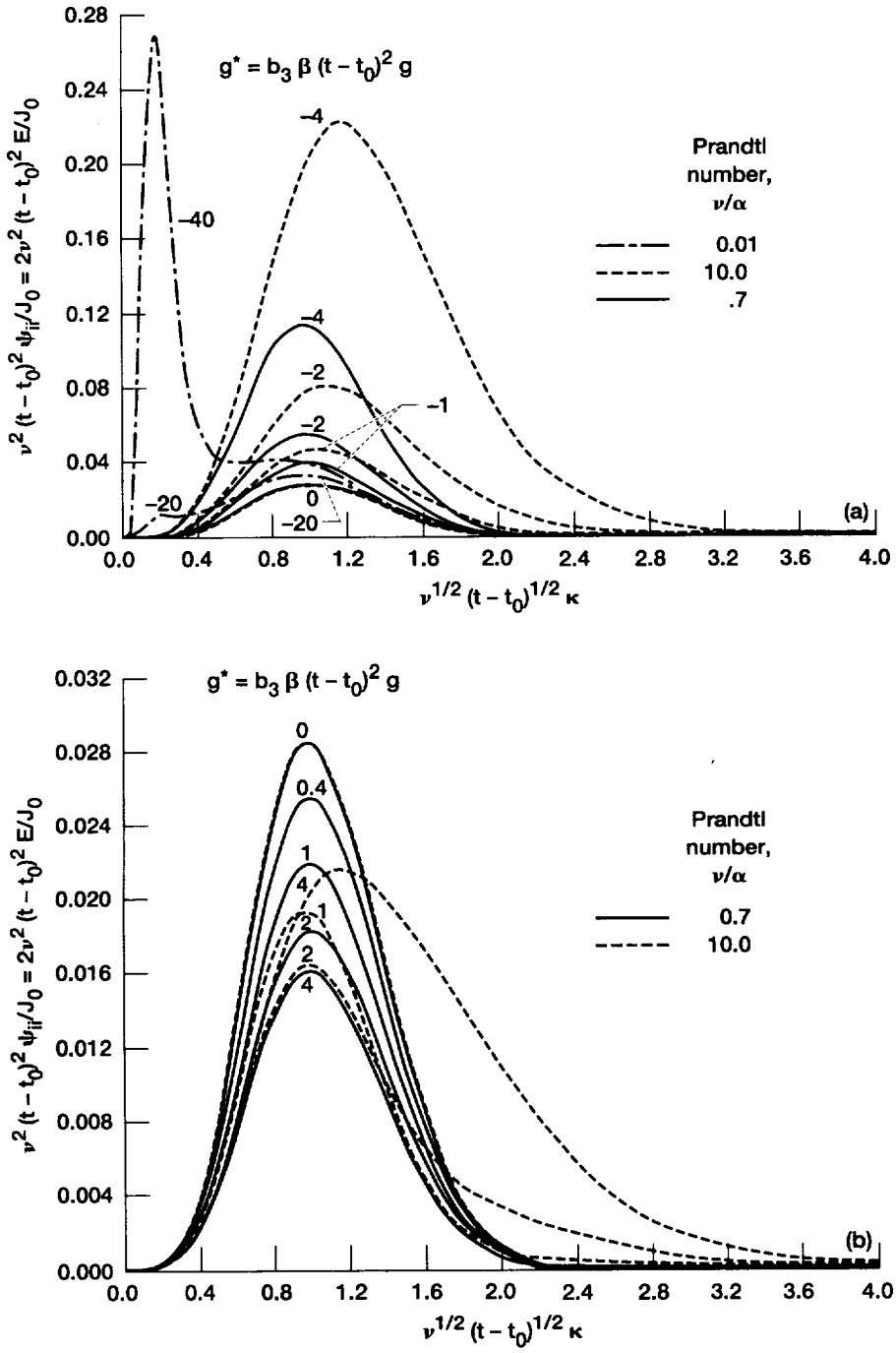

Figure 5-85.—Dimensionless spectra of $\overline{u_i u_i}$ (energy spectra). (a) With buoyancy forces destabilizing. (b) With buoyancy forces stabilizing.

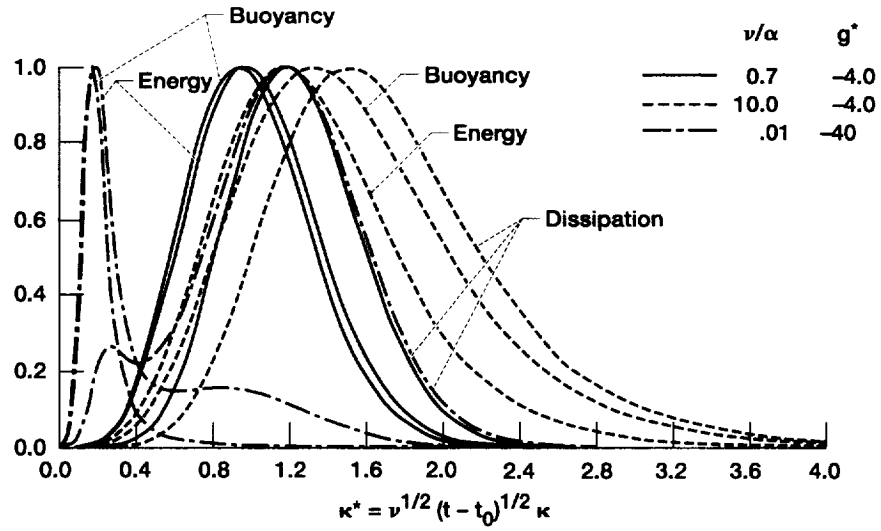

Figure 5-86.—Comparison of normalized energy, dissipation, and buoyancy spectra with buoyancy forces destabilizing.

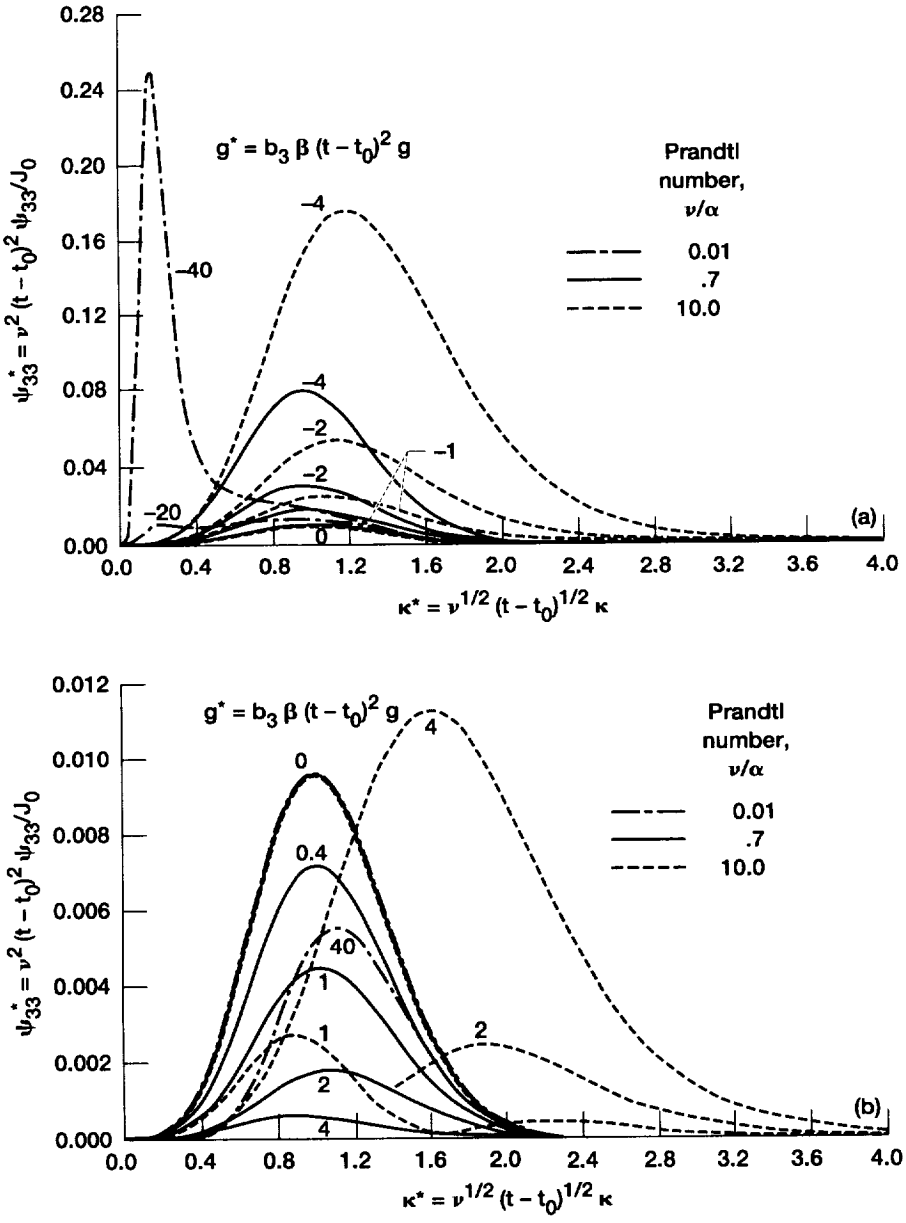

Figure 5-87.—Dimensionless spectra of $\overline{u_3^2}$. (a) With buoyancy forces destabilizing. (b) With buoyancy forces stabilizing.

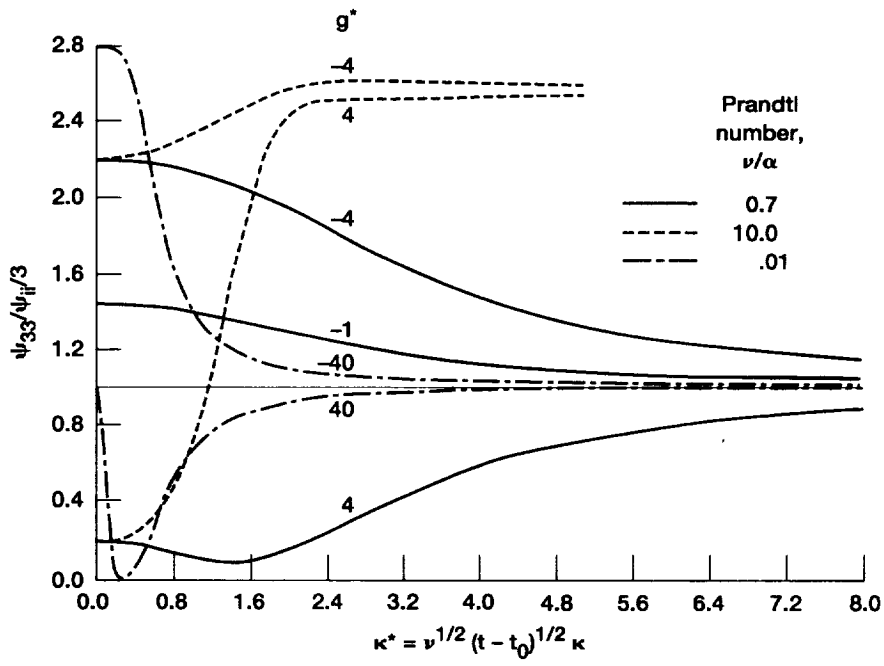

Figure 5-88.—Curves showing ratio of spectrum curves for $\overline{u_3^2}$ to those for $\overline{u_i u_i}/3$.

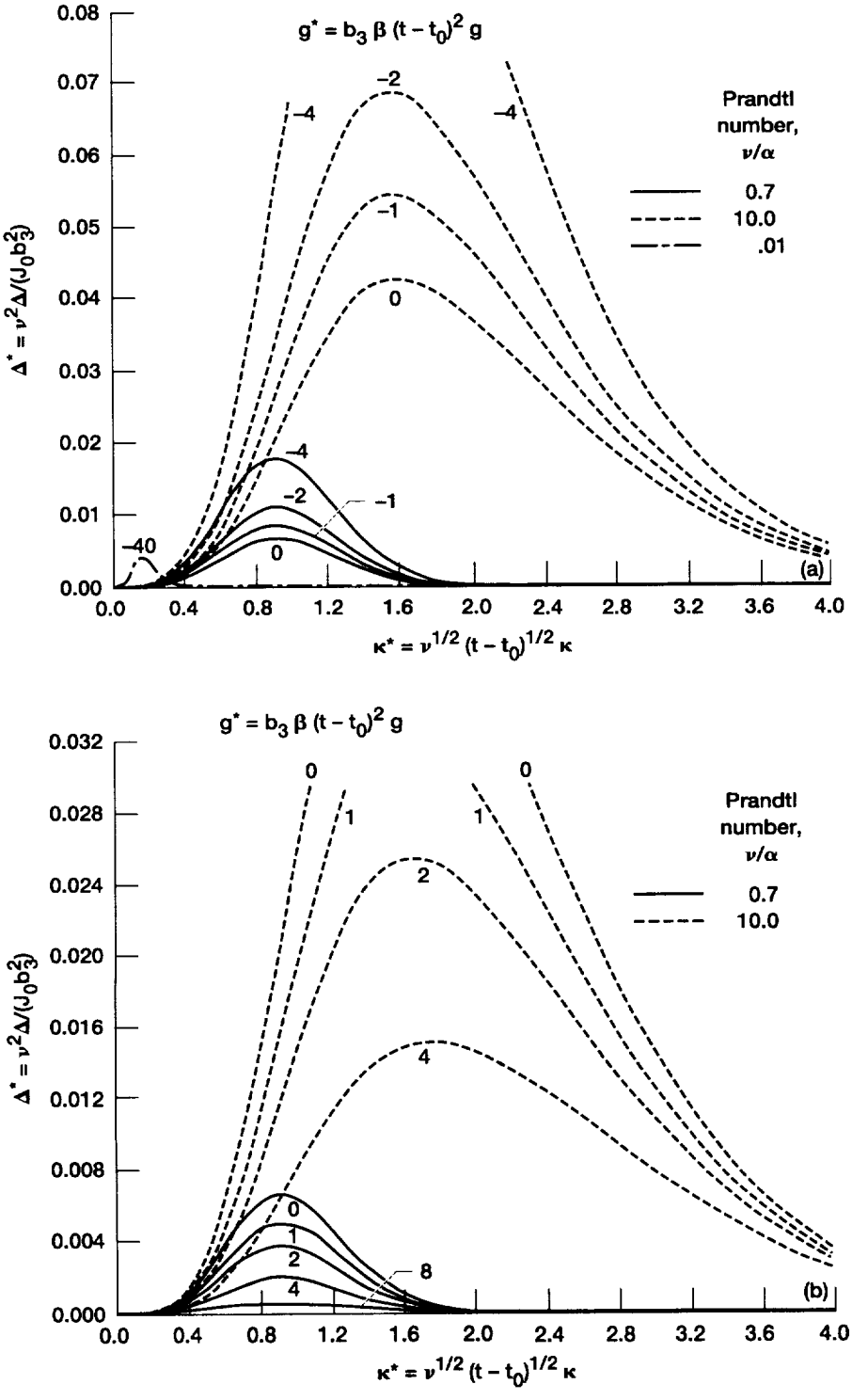

Figure 5-89.—Dimensionless spectra of temperature variance $\overline{\tau^2}$. (a) With buoyancy forces destabilizing. (b) With buoyancy forces stabilizing.

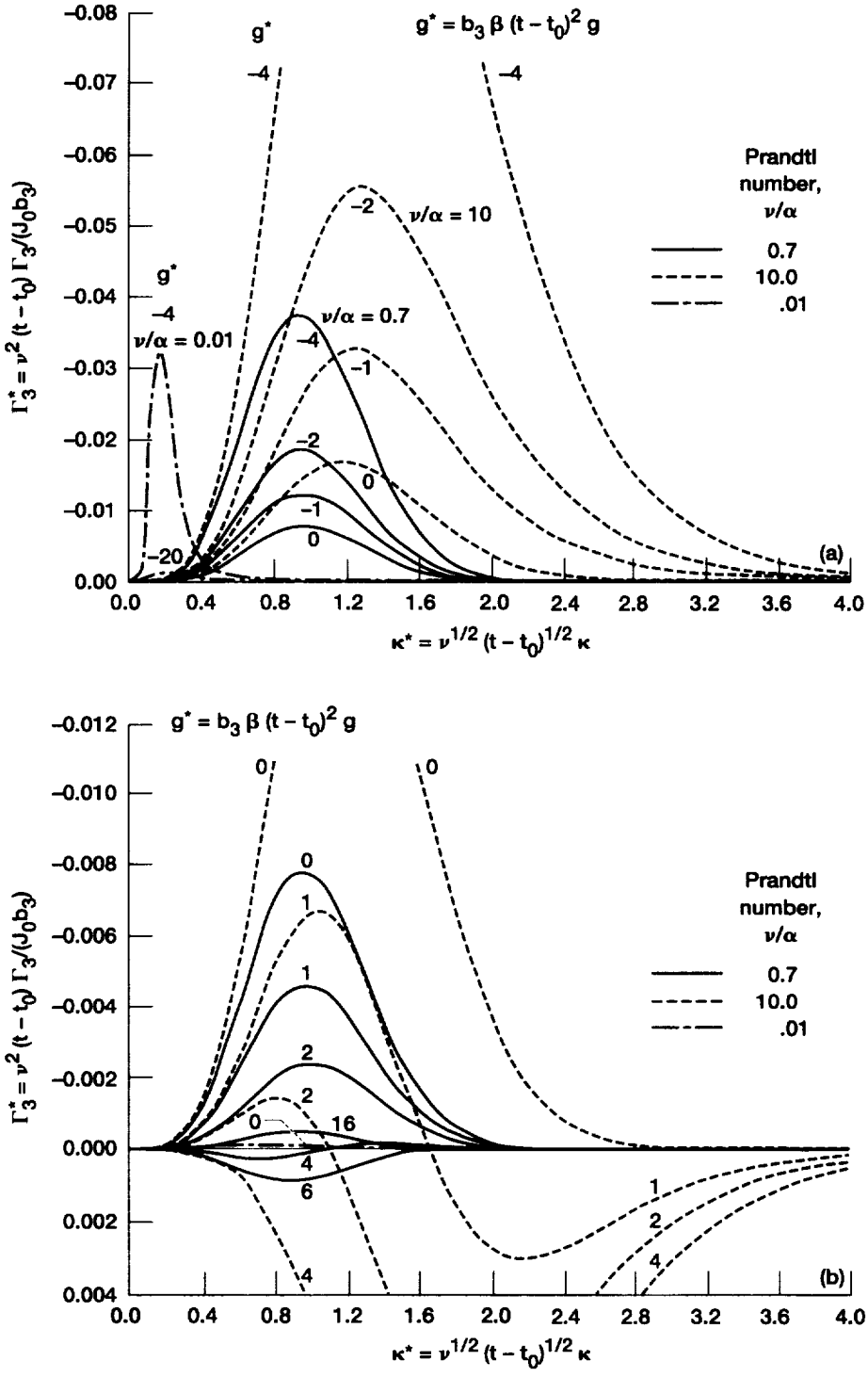

Figure 5-90.—Dimensionless spectra of temperature-velocity correlations $\overline{\tau u_3}$. (a) With buoyancy forces destabilizing. (b) With buoyancy forces stabilizing.

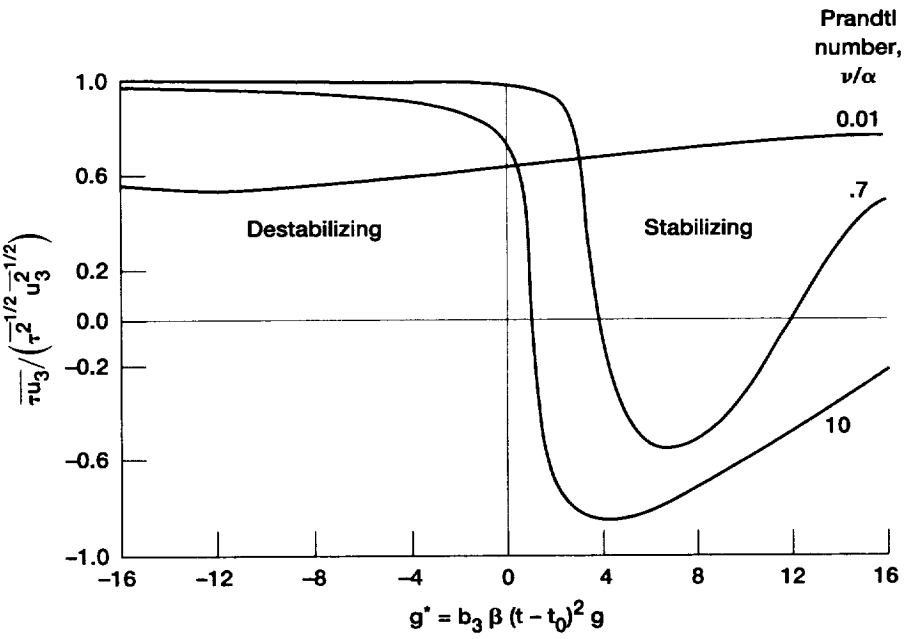

Figure 5-91.—Temperature-velocity correlation coefficient as a function of buoyancy parameter.

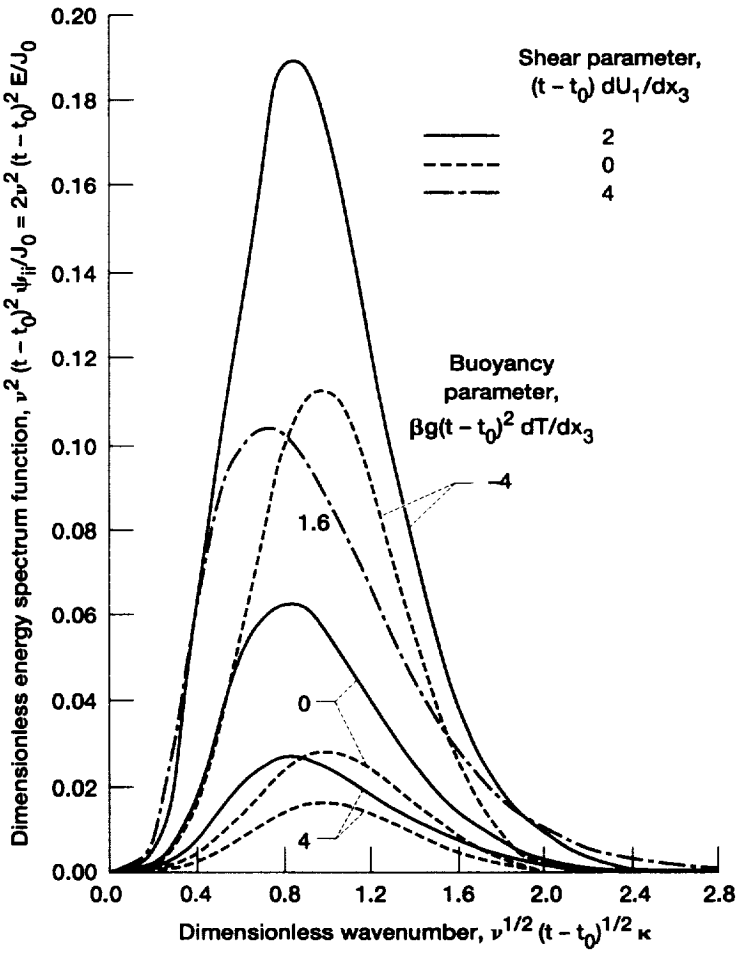

Figure 5-92.—Dimensionless spectra of turbulent energy $\overline{u_i u_i}$. Prandtl number, 0.7.

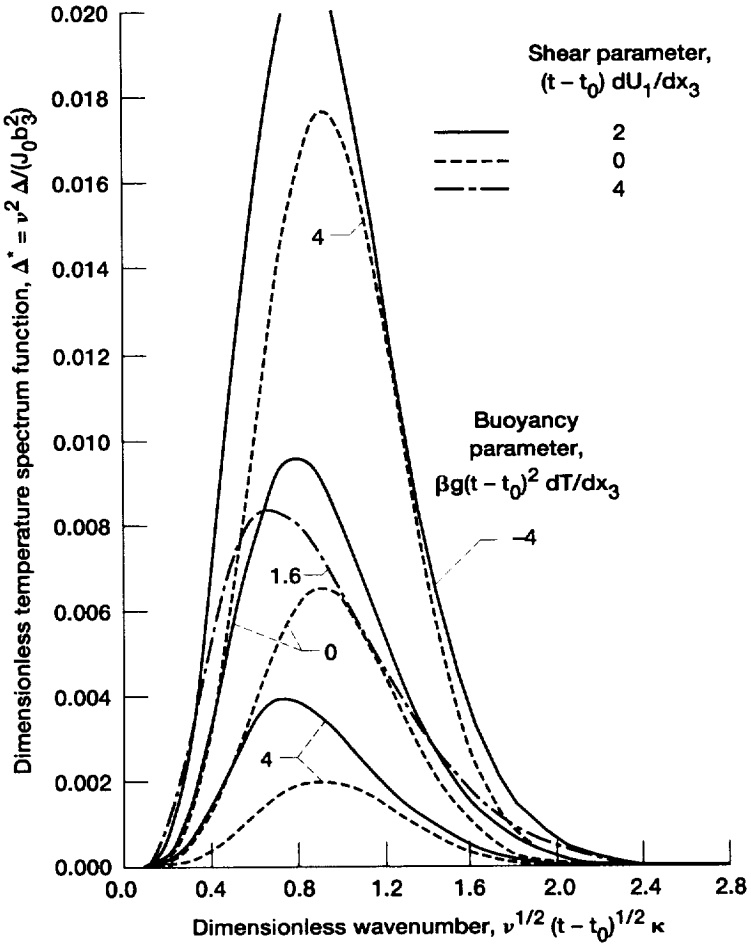

Figure 5-93.—Spectra of dimensionless temperature variance $\overline{\tau^2}$. Prandtl number, 0.7.

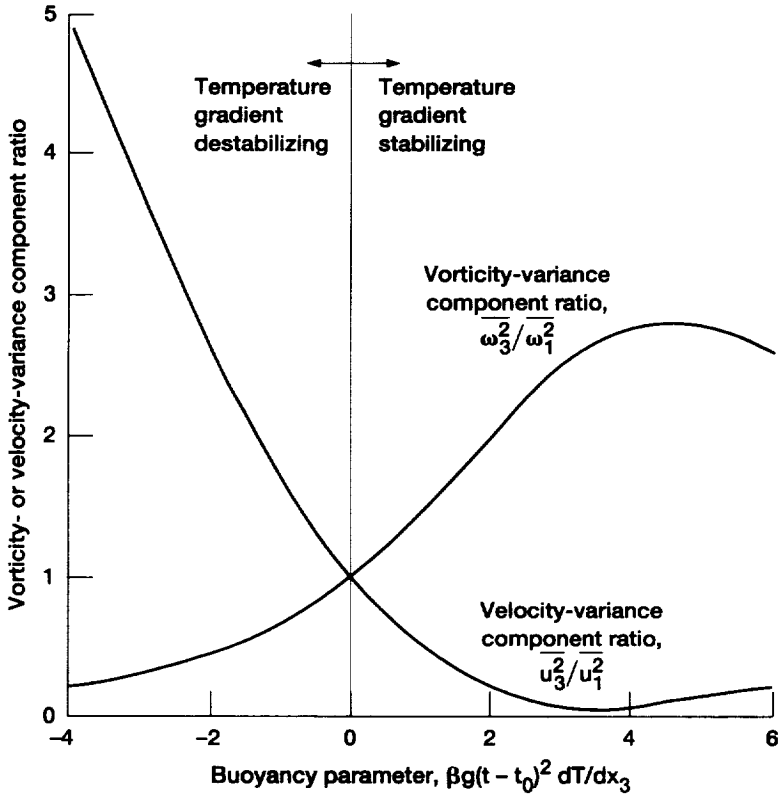

Figure 5-94.—Velocity- and vorticity-variance component ratios plotted against buoyancy parameter for case of no shear. Prandtl number, 0.7.

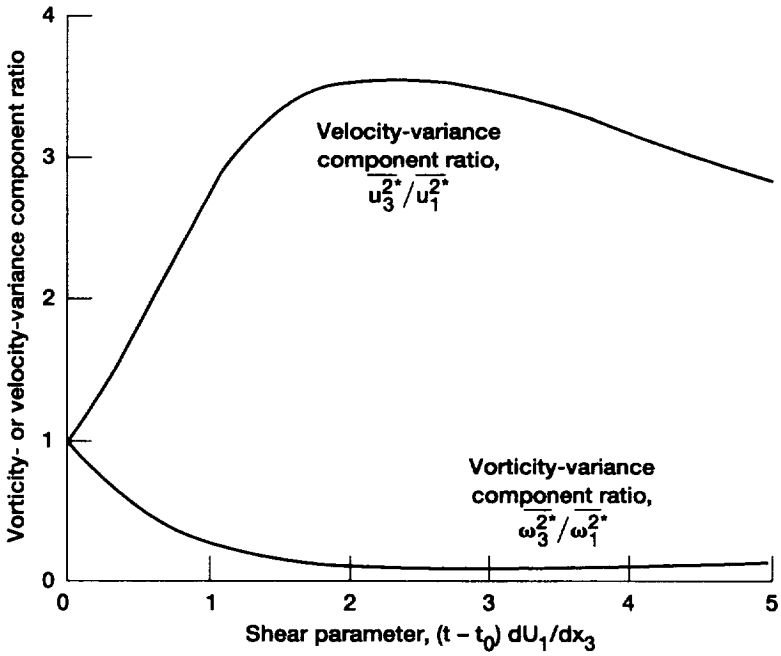

Figure 5-95.—Velocity- and vorticity-variance component ratios in coordinate system rotated 45° plotted against shear parameter for case of no buoyancy effects.

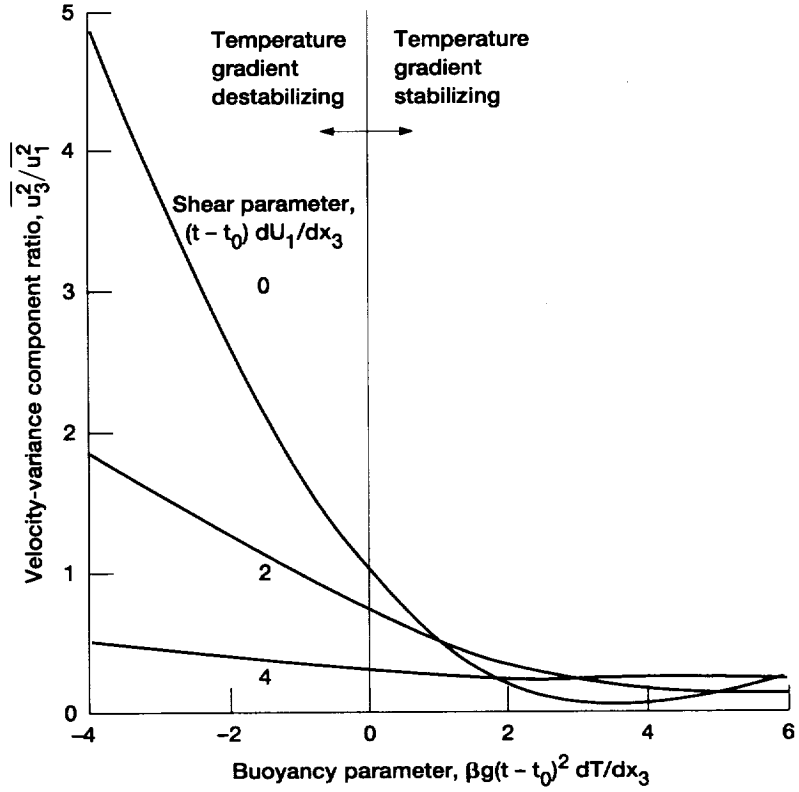

Figure 5-96.—Plot showing velocity-variance component ratio $\overline{u_3^2}/\overline{u_1^2}$ as a function of buoyancy and shear parameters. Prandtl number, 0.7.

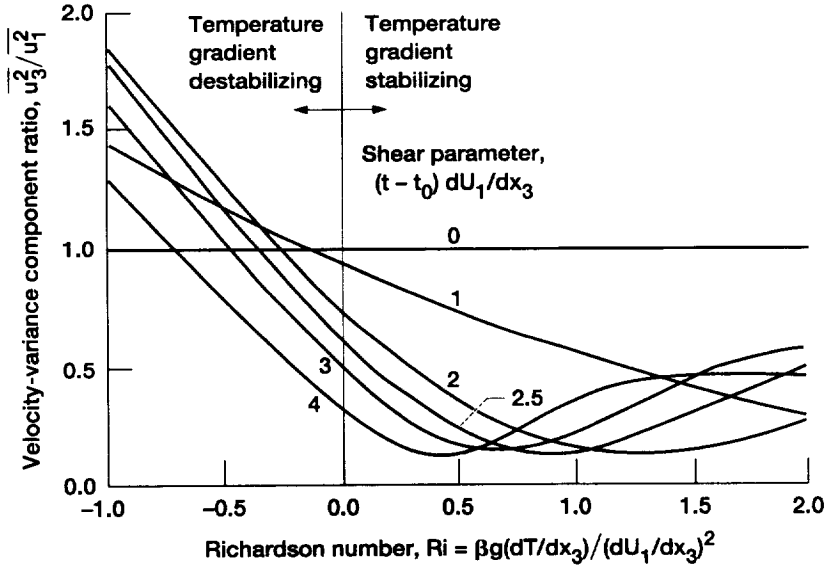

Figure 5-97.—Plot showing velocity-variance component ratio $\overline{u_3^2}/\overline{u_1^2}$ as a function of Richardson number and shear parameter. Prandtl number, 0.7.

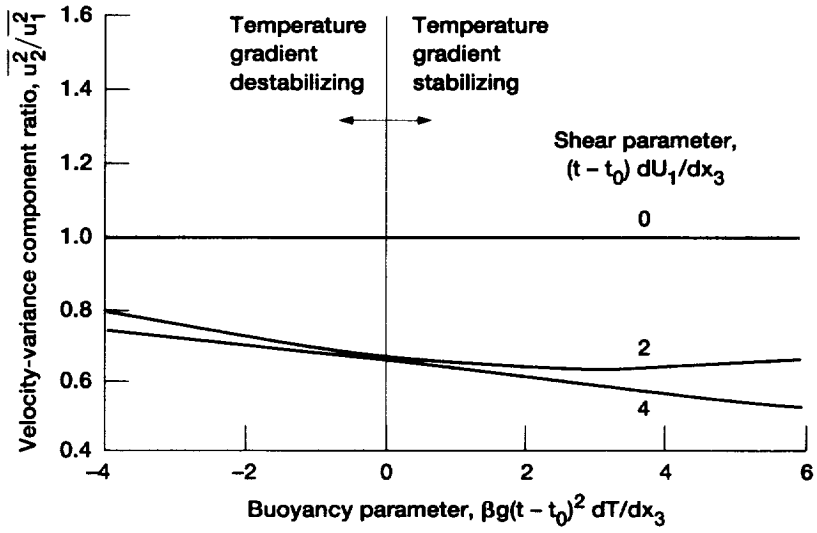

Figure 5-98.—Plot showing velocity-variance component ratio $\overline{u_2^2}/\overline{u_1^2}$ as a function of buoyancy and shear parameters.

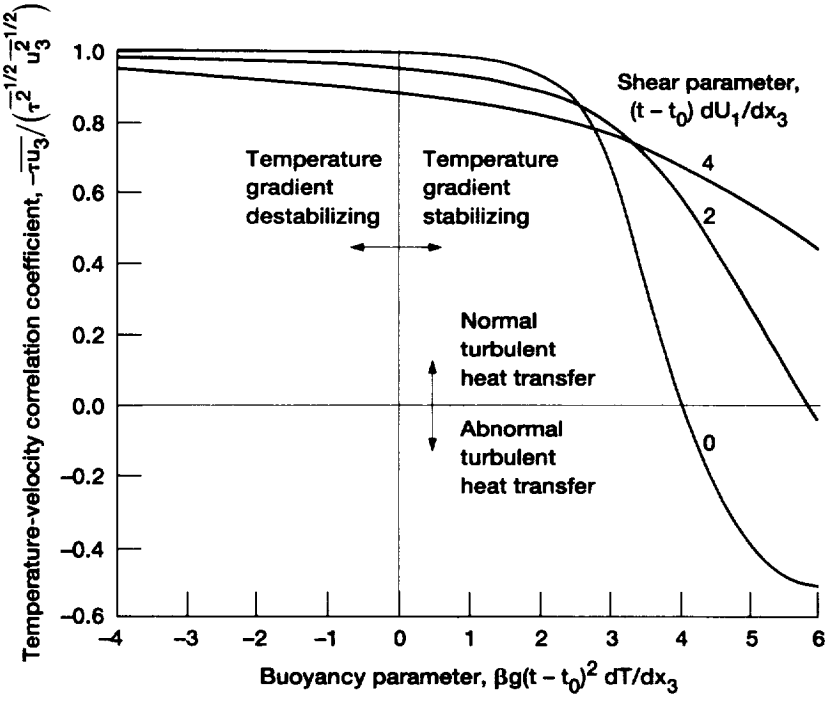

Figure 5-99.—Plot showing temperature-velocity correlation coefficient $-\overline{\tau u_3}/\left(\overline{\tau^2}^{1/2}\,\overline{u_3^2}^{1/2}\right)$ as a function of buoyancy and shear parameters. Prandtl number, 0.7.

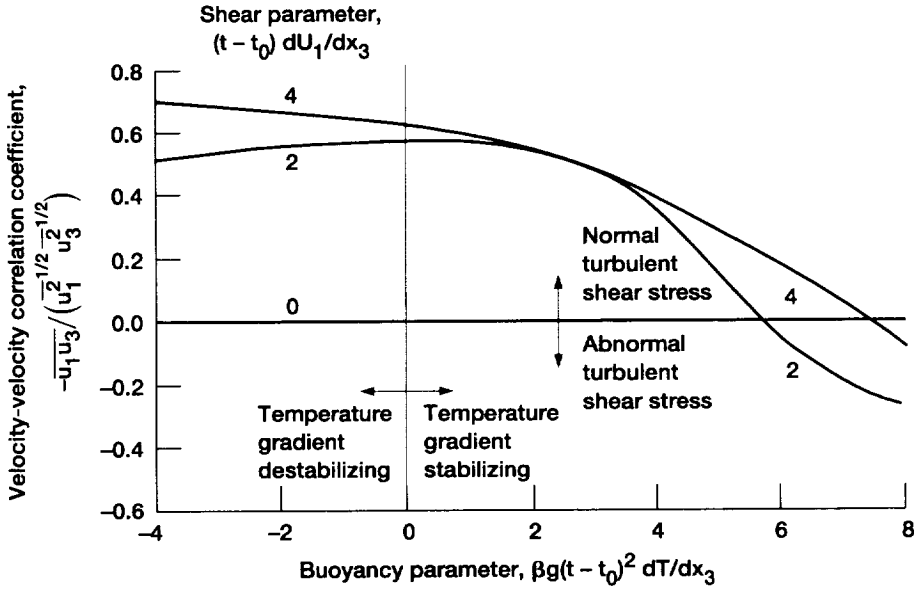

Figure 5-100.—Plot showing velocity-velocity correlation coefficient $-\overline{u_1 u_3}/\left(\overline{u_1^2}^{1/2}\,\overline{u_3^2}^{1/2}\right)$ as a function of buoyancy and shear parameters.

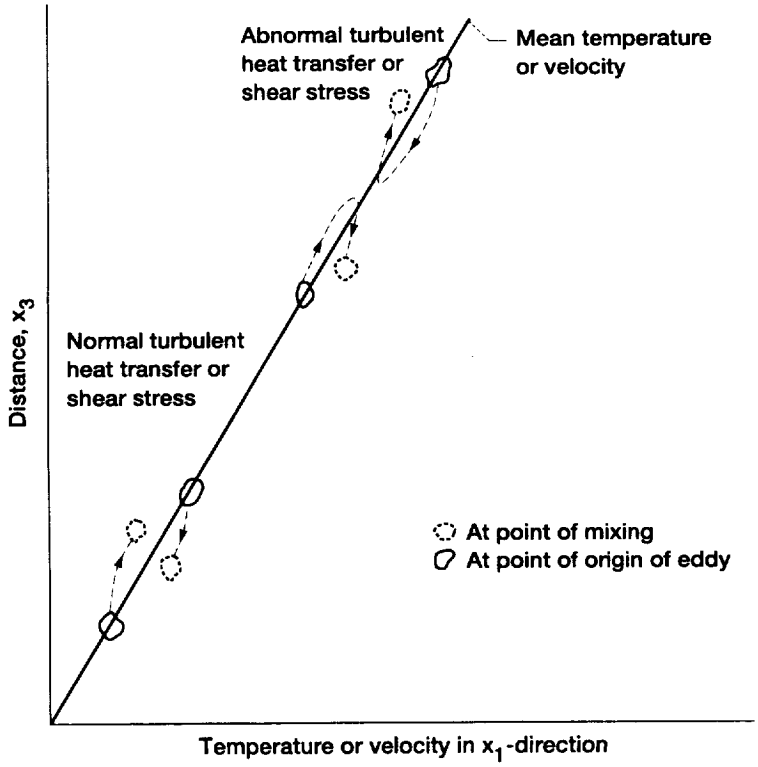

Figure 5-101.—Sketch illustrating possible mechanism for producing negative eddy conductivity and viscosity.

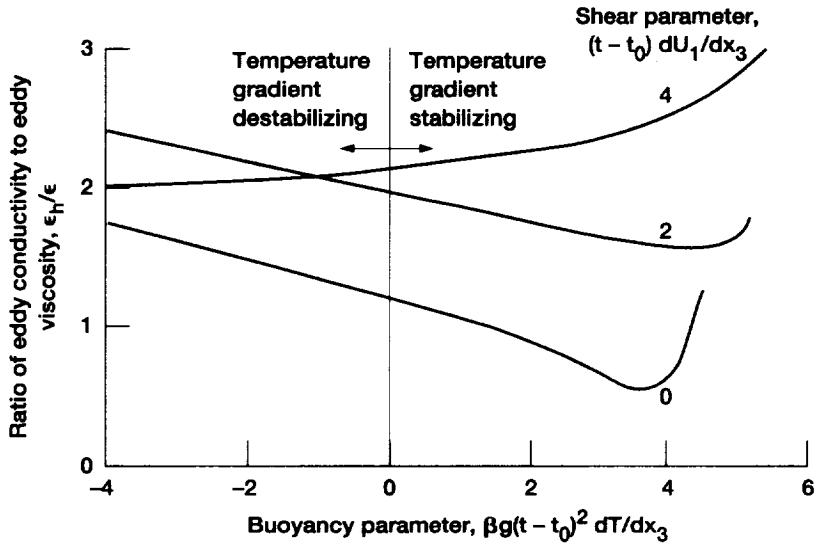

Figure 5-102.—Plot showing ratio of eddy conductivity to eddy viscosity as a function of buoyancy and shear parameters. Prandtl number, 0.7.

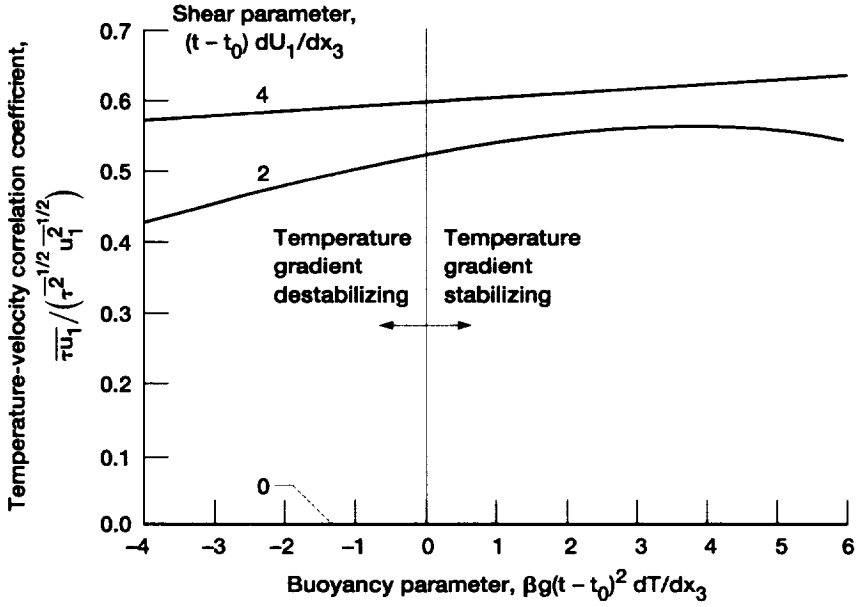

Figure 5-103.—Plot showing correlation coefficient $\overline{\tau u_1}/\left(\overline{\tau^2}^{1/2}\, \overline{u_1^2}^{1/2}\right)$ as a function of buoyancy and shear parameters. Prandtl number, 0.7.

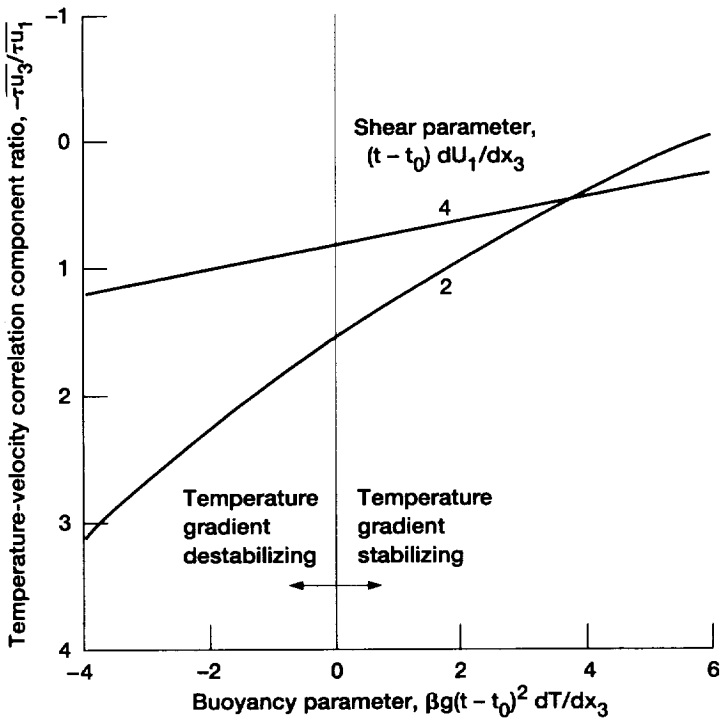

Figure 5-104.—Plot showing temperature-velocity correlation component ratio $-\overline{\tau u_3}/\overline{\tau u_1}$ as a function of buoyancy and shear parameters.

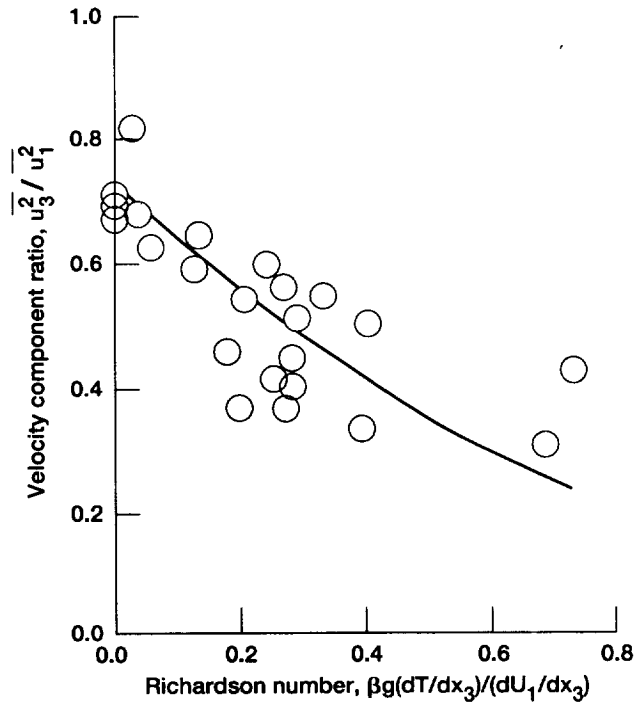

Figure 5-105.—Some analytical and experimental results for station 5 (ref. 116) with a shear parameter $(t - t_0)\, dU_1/dx_3$ of 2.

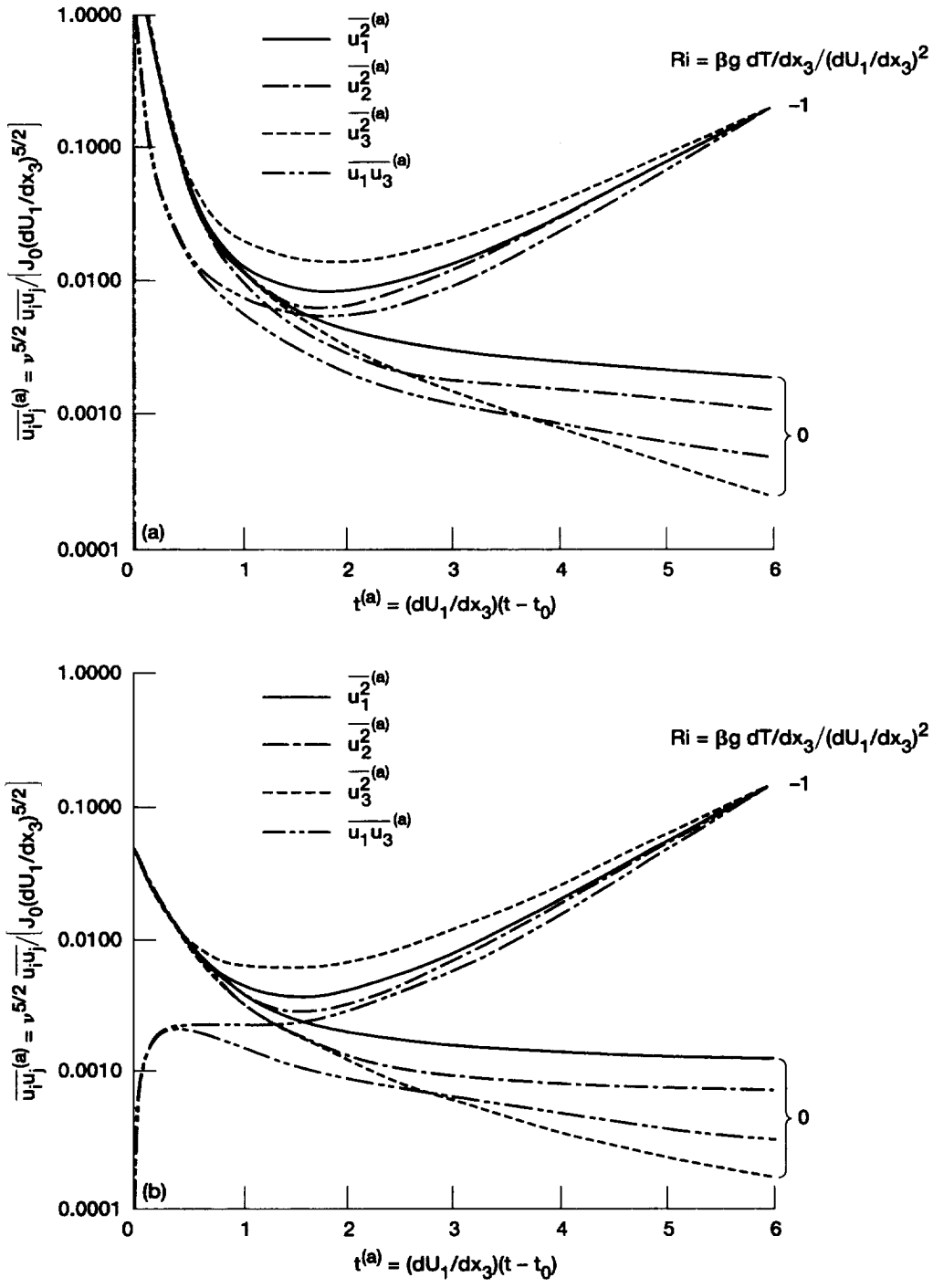

Figure 5-106.—Effect of destabilizing buoyancy on the variation with time of turbulence in a uniform shear flow. Prandtl number, 0.7. (a) $\kappa_0^{(a)} = \nu^{1/2}\kappa_0/(dU_1/dx_3)^{1/2} = \infty$. (b) $\kappa_0^{(a)} = \nu^{1/2}\kappa_0/(dU_1/dx_3)^{1/2} = 1$.

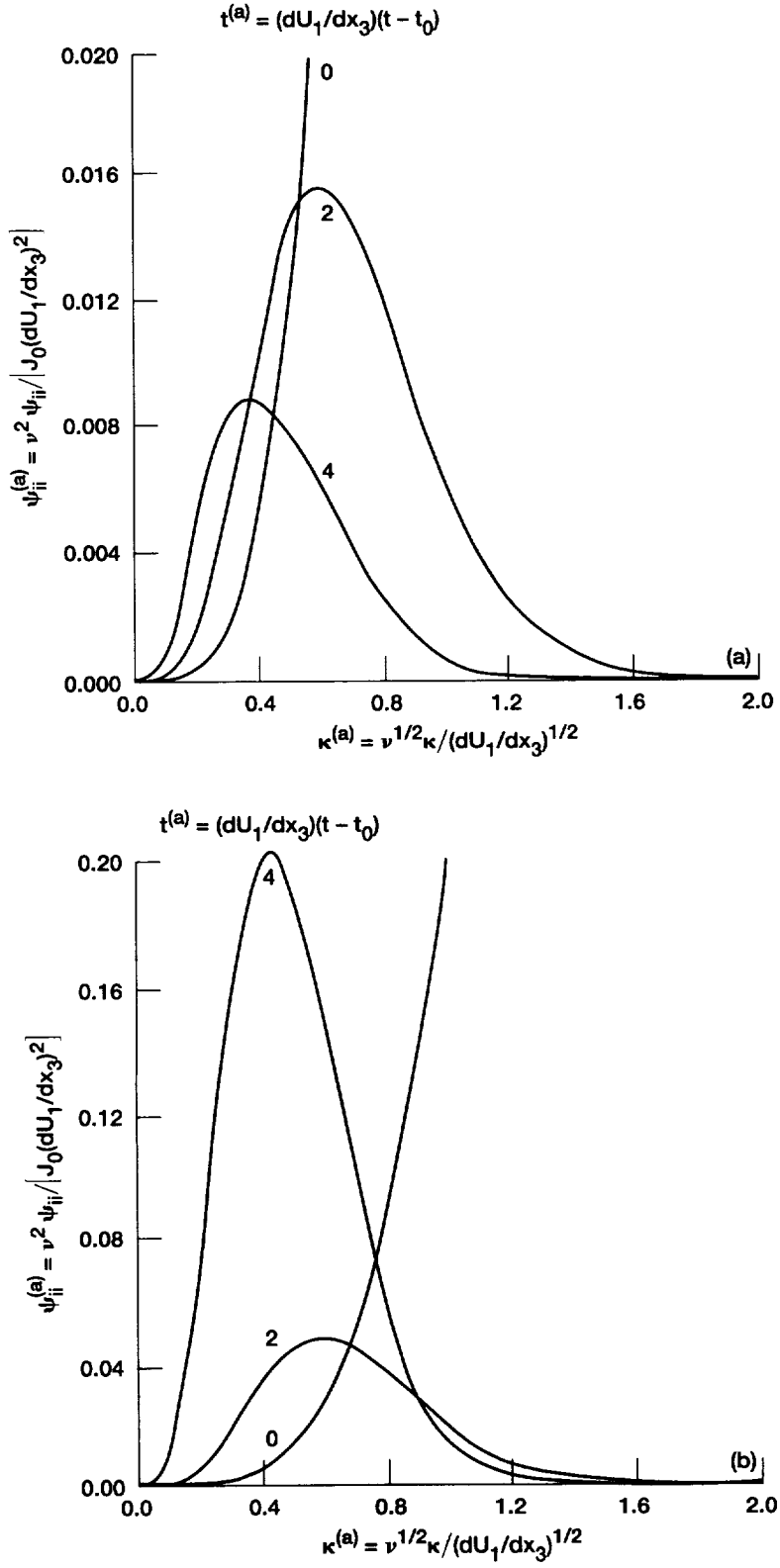

Figure 5-107.—Variation with time of turbulent energy spectra (spectra of $\overline{u_i u_i}$). Prandtl number, 0.7. (a) Ri = 0. (b) Ri = –1.

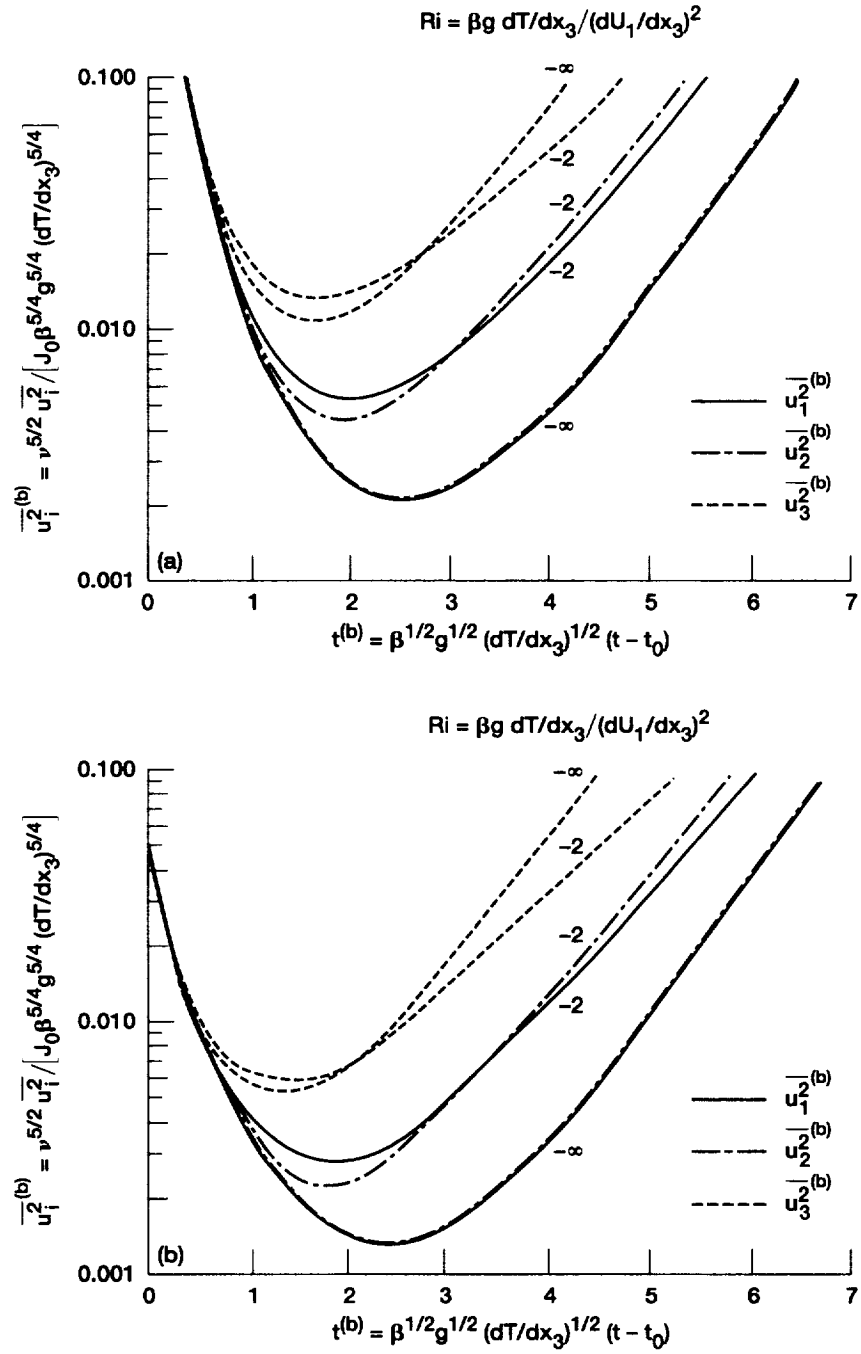

Figure 5-108.—Effect of a uniform shear on the variation with time of turbulence in a flow with destabilizing buoyancy. Prandtl number, 0.7.
(a) $\kappa_0^{(b)} = \nu^{1/2}\kappa_0 / \left|(-dT/dx_3)^{1/4}\,\beta^{1/4}g^{1/4}\right| = \infty$. (b) $\kappa_0^{(b)} = \nu^{1/2}\kappa_0 / \left|(-dT/dx_3)^{1/4}\,\beta^{1/4}g^{1/4}\right| = 1$.

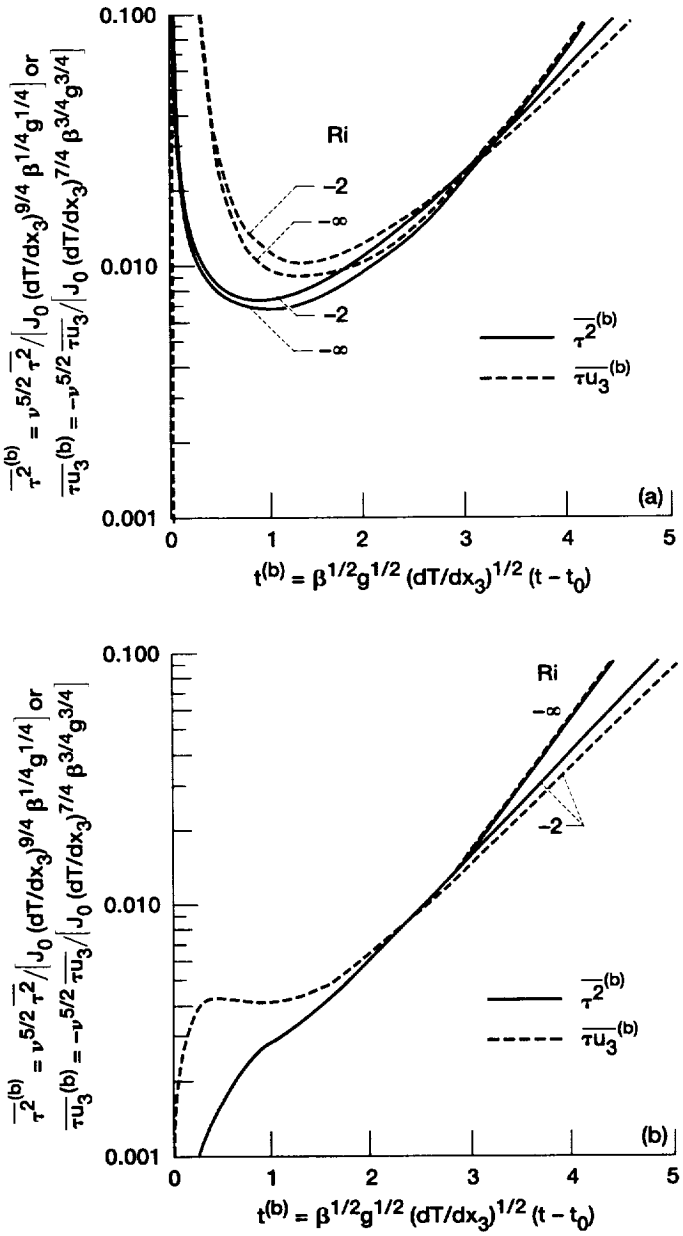

Figure 5-109.—Effect of a uniform shear on the variation with time of temperature fluctuations and temperature-velocity correlations in a flow with destabilizing buoyancy. Prandtl number, 0.7.

(a) $\kappa_0^{(b)} = \nu^{1/2}\kappa_0/\left|(-dT/dx_3)^{1/4} \beta^{1/4} g^{1/4}\right| = \infty$.

(b) $\kappa_0^{(b)} = \nu^{1/2}\kappa_0/\left|(-dT/dx_3)^{1/4} \beta^{1/4} g^{1/4}\right| = 1$.

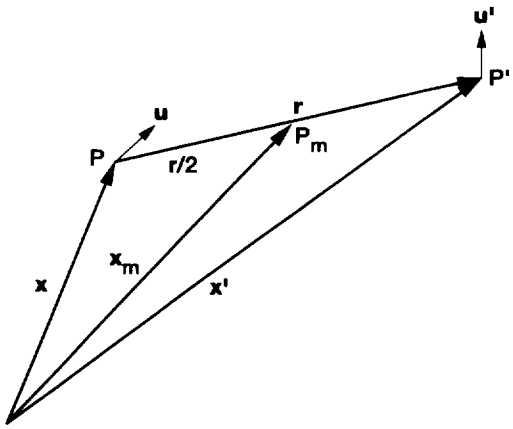

Figure 5-110.—Vector configuration for two-point correlation equations.

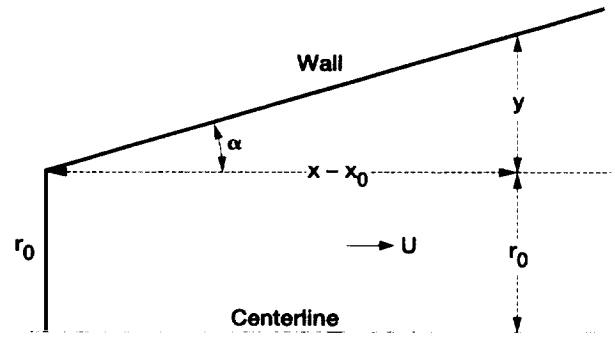

Figure 5-111.—Section of cone considered in analysis. Flow cross section is arbitrary; α can be positive or negative.

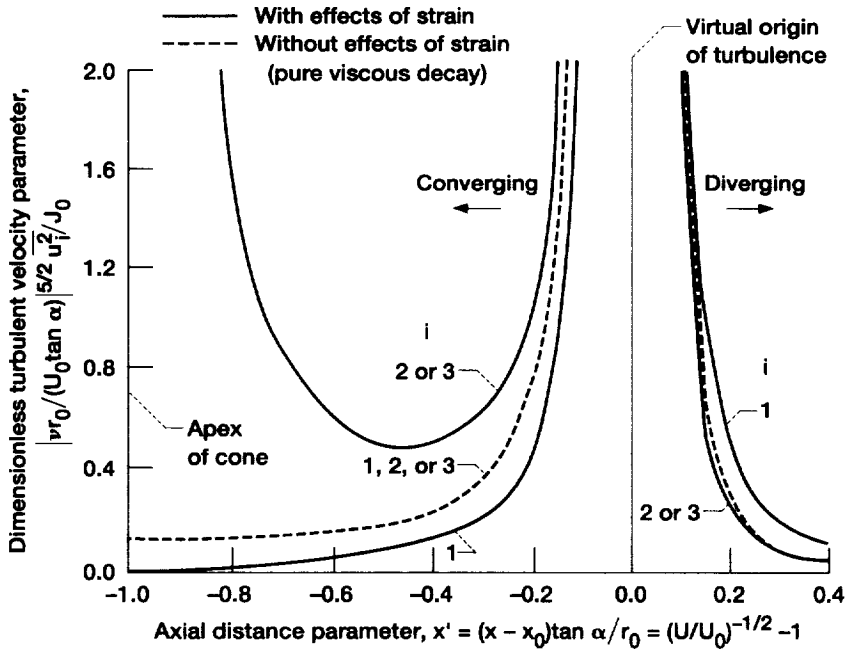

Figure 5-112.—Variance of turbulent velocity components for flow through cone.

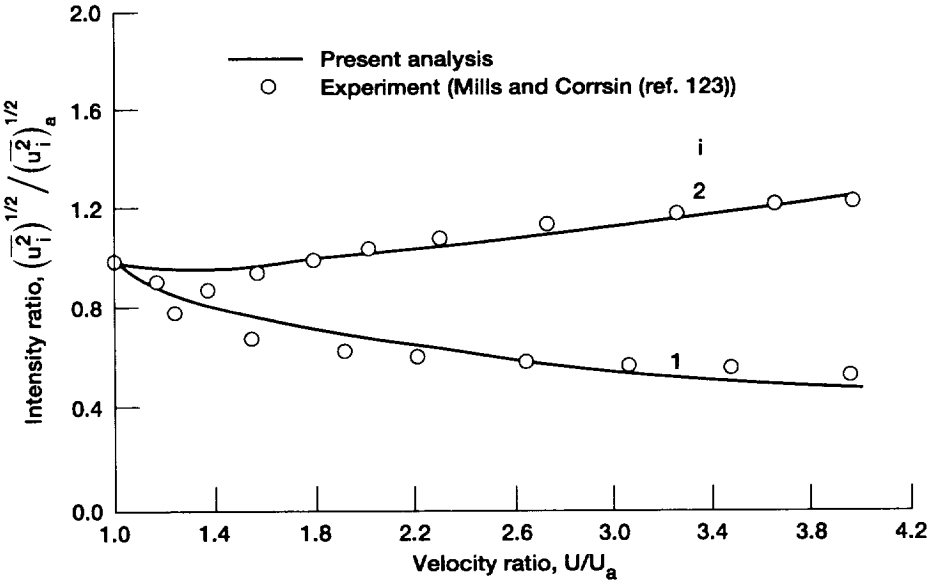

Figure 5-113.—Present analysis compared with experiment for converging flow.

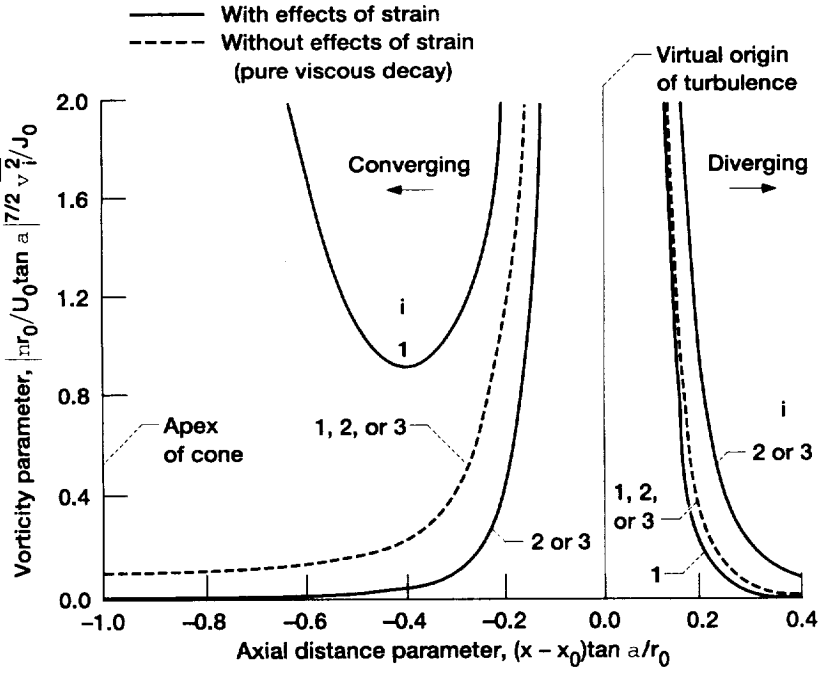

Figure 5-114.—Variance of turbulent vorticity components for flow through cone.

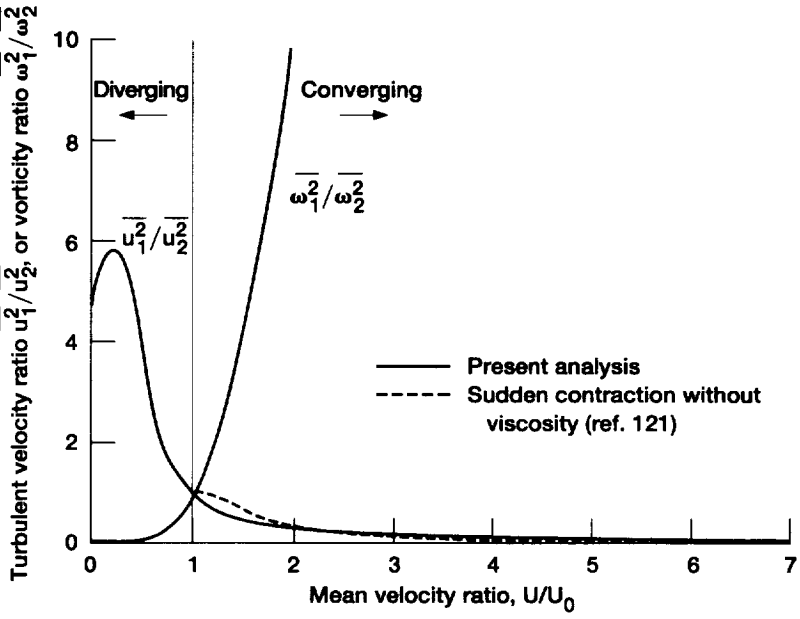

Figure 5-115.—Plot of $\overline{u_1^2}/\overline{u_2^2}$ and $\overline{\omega_1^2}/\overline{\omega_2^2}$ against velocity ratio.

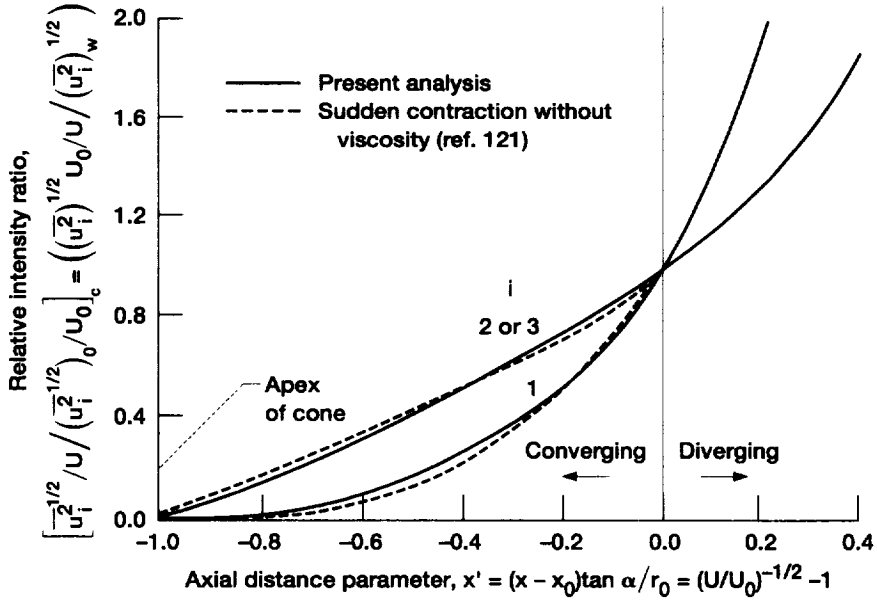

Figure 5-116.—Relative intensity ratios for turbulent components corrected to eliminate decay.

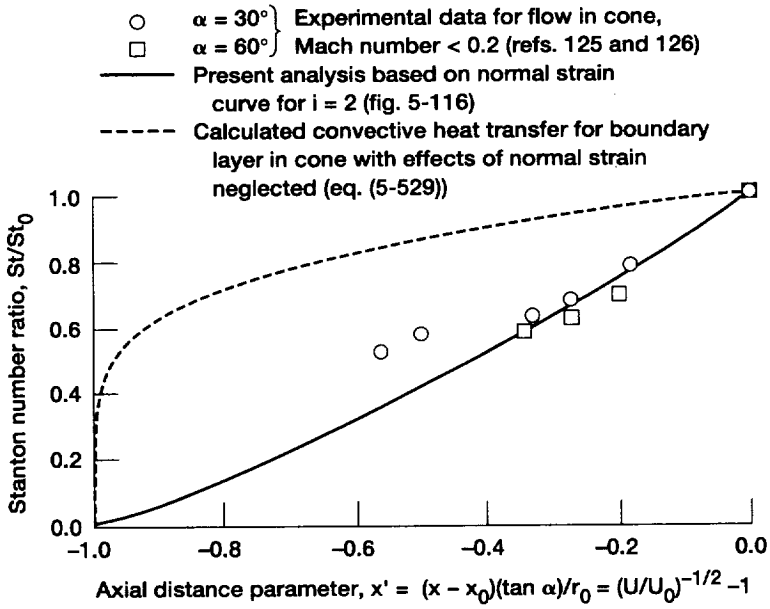

Figure 5-117.—Approximate calculation of heat transfer between cone wall and fluid and comparison with experiment. Angle α (in degrees) in figure is angle between cone generator and flow direction.

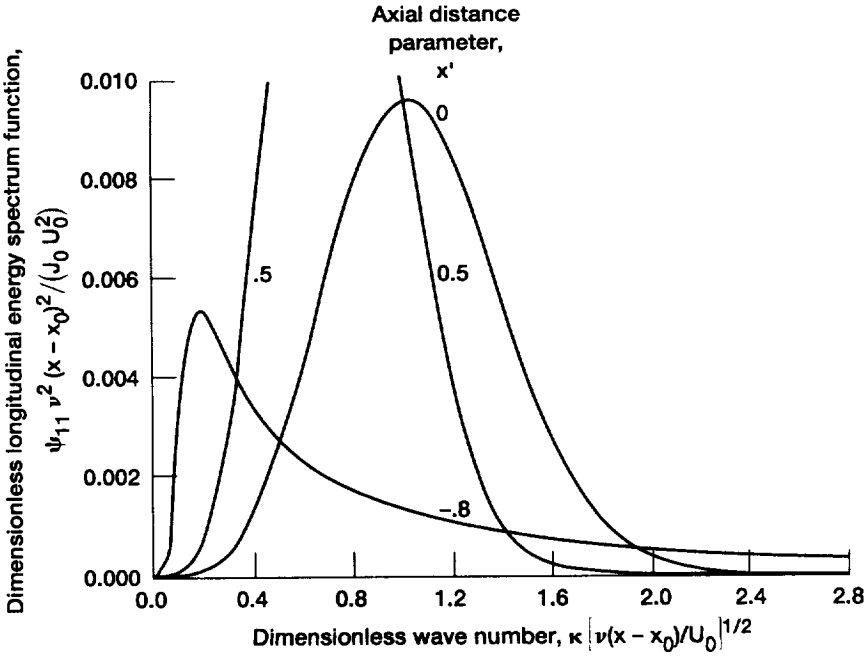

Figure 5-118.—Spectra of dimensionless $\overline{u_1^2}$.

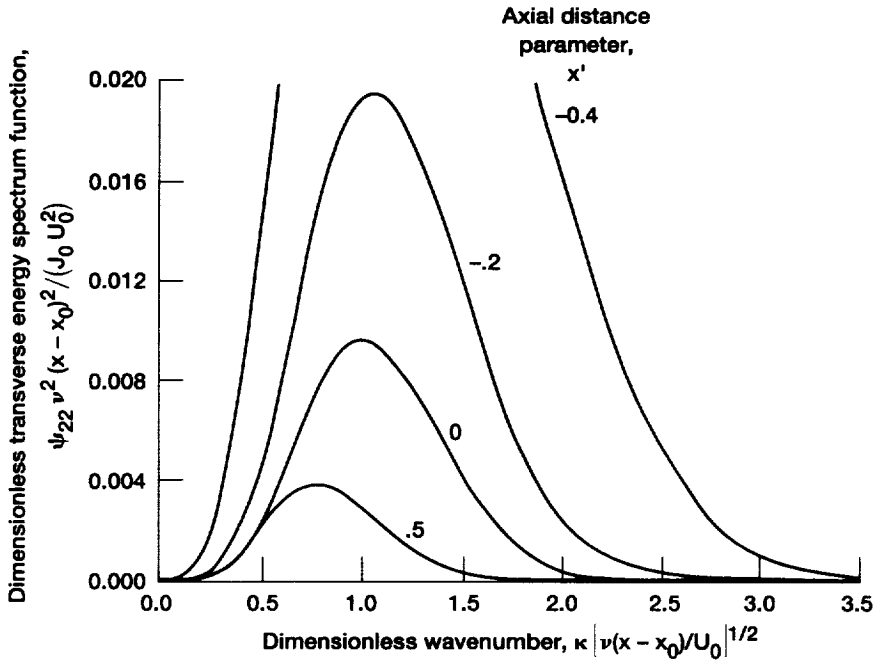

Figure 5-119.—Spectra of dimensionless $\overline{u_2^2}$ (see fig. 5-112 for definition of x').

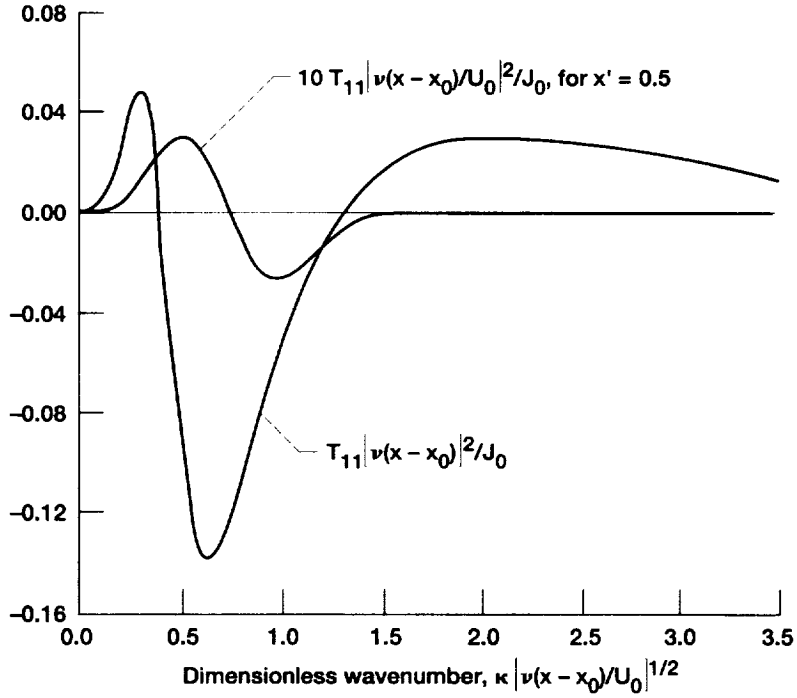

Figure 5-120.—Dimensionless transfer spectra. x' is axial distance parameter (see fig. 5-112).

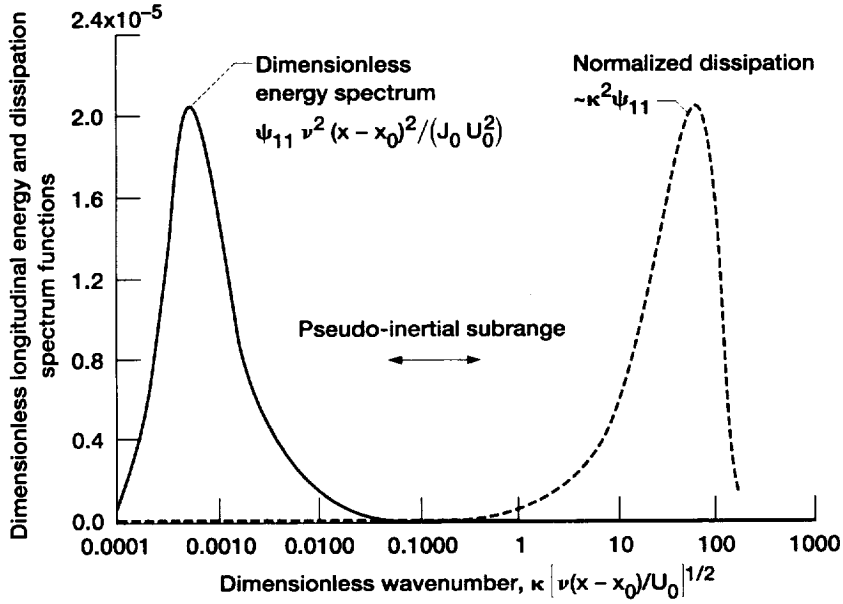

Figure 5-121.—Energy and dissipation spectra for dimensionless $\overline{u_1^2}$ for x' = –0.99. Dissipation spectrum normalized to height of dimensionless ψ_{11} spectrum.

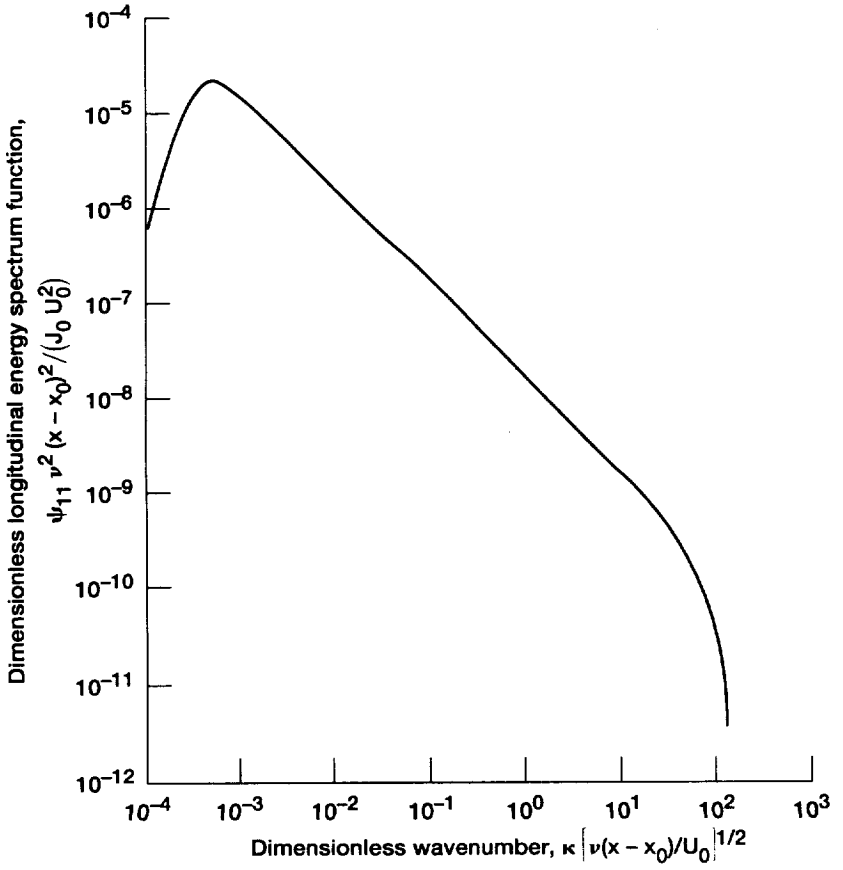

Figure 5-122.—Log-log plot of spectrum of dimensionless $\overline{u_1^2}$ for x' = –0.99.

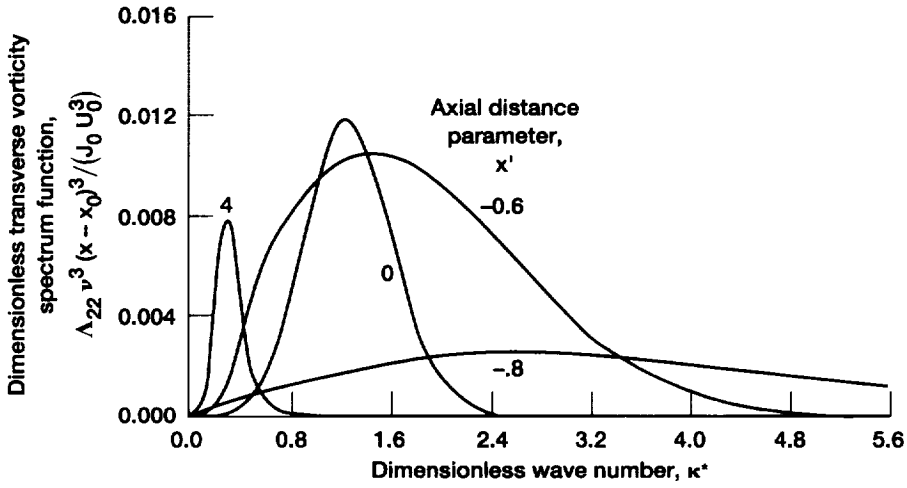

Figure 5-123.—Spectra of dimensionless $\overline{\omega_2^2}$.

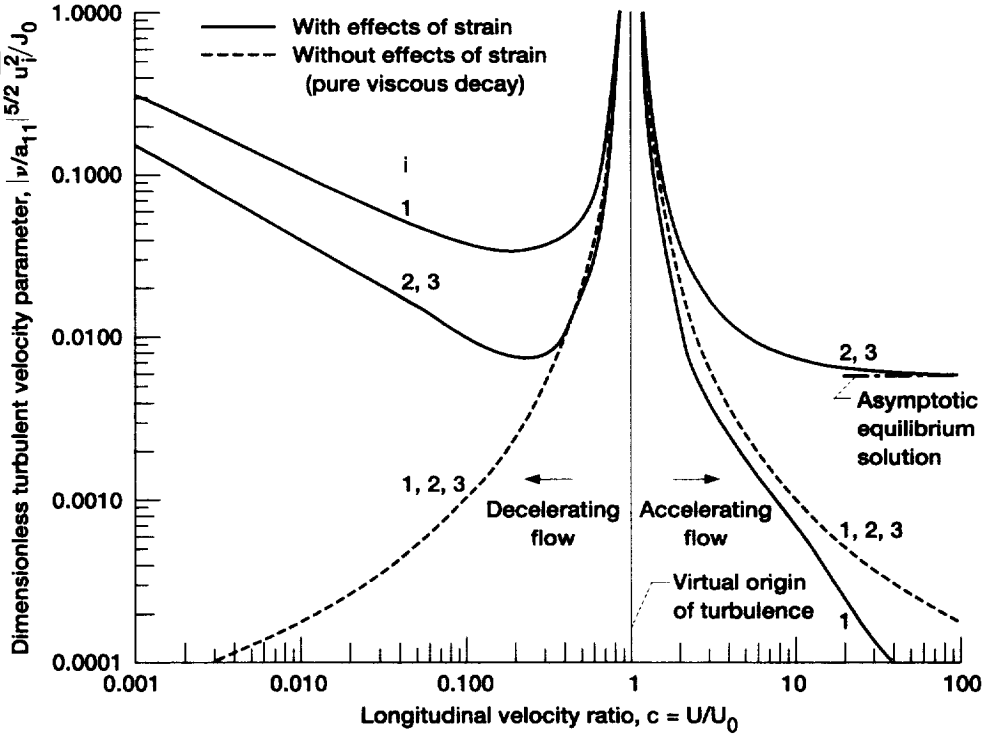

Figure 5-124.—Dimensionless variance of turbulent velocity components for uniform incompressible strain.

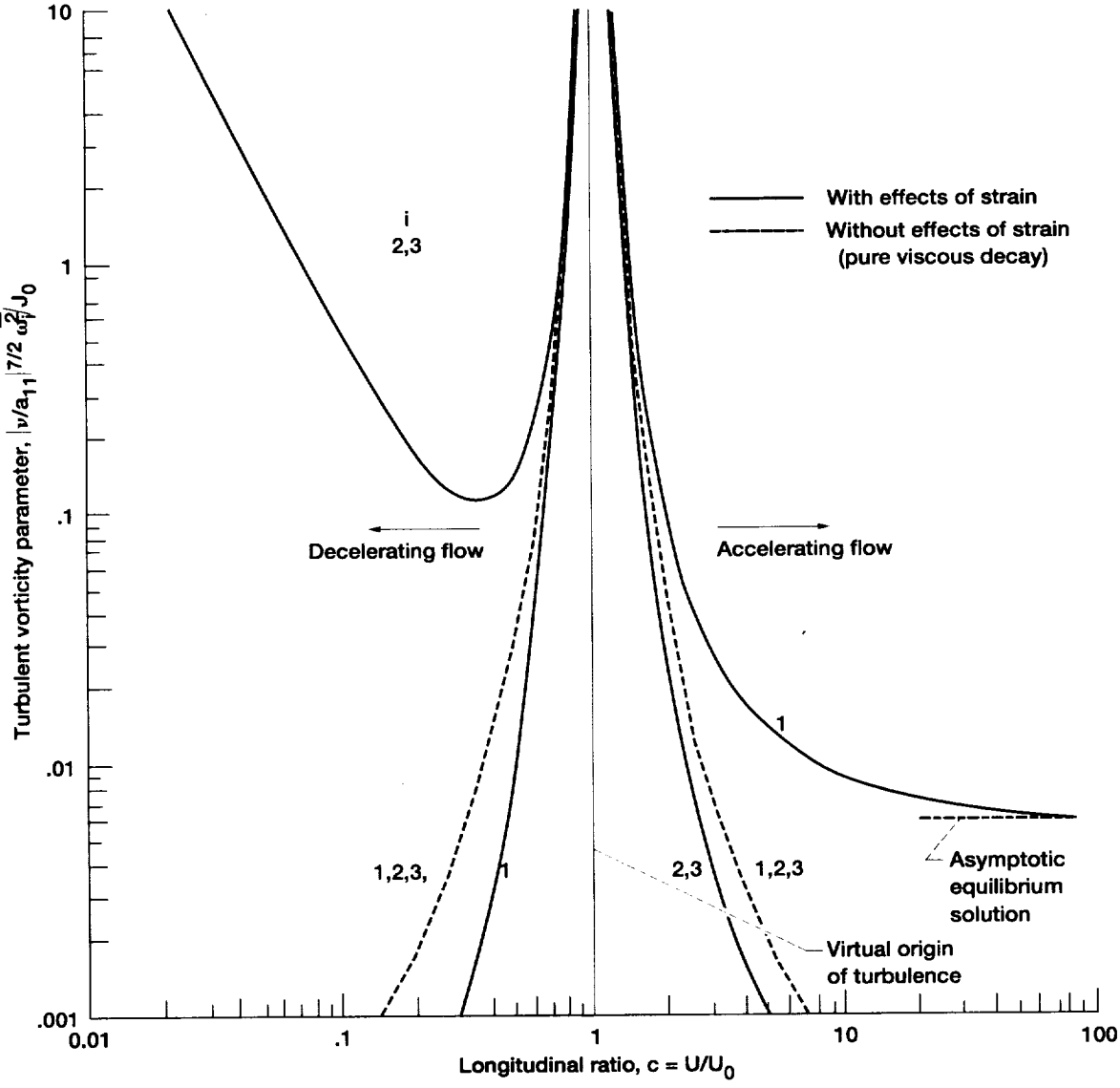

Figure 5-125.—Dimensionless variance of turbulent vorticity components for uniform incompressible strain.

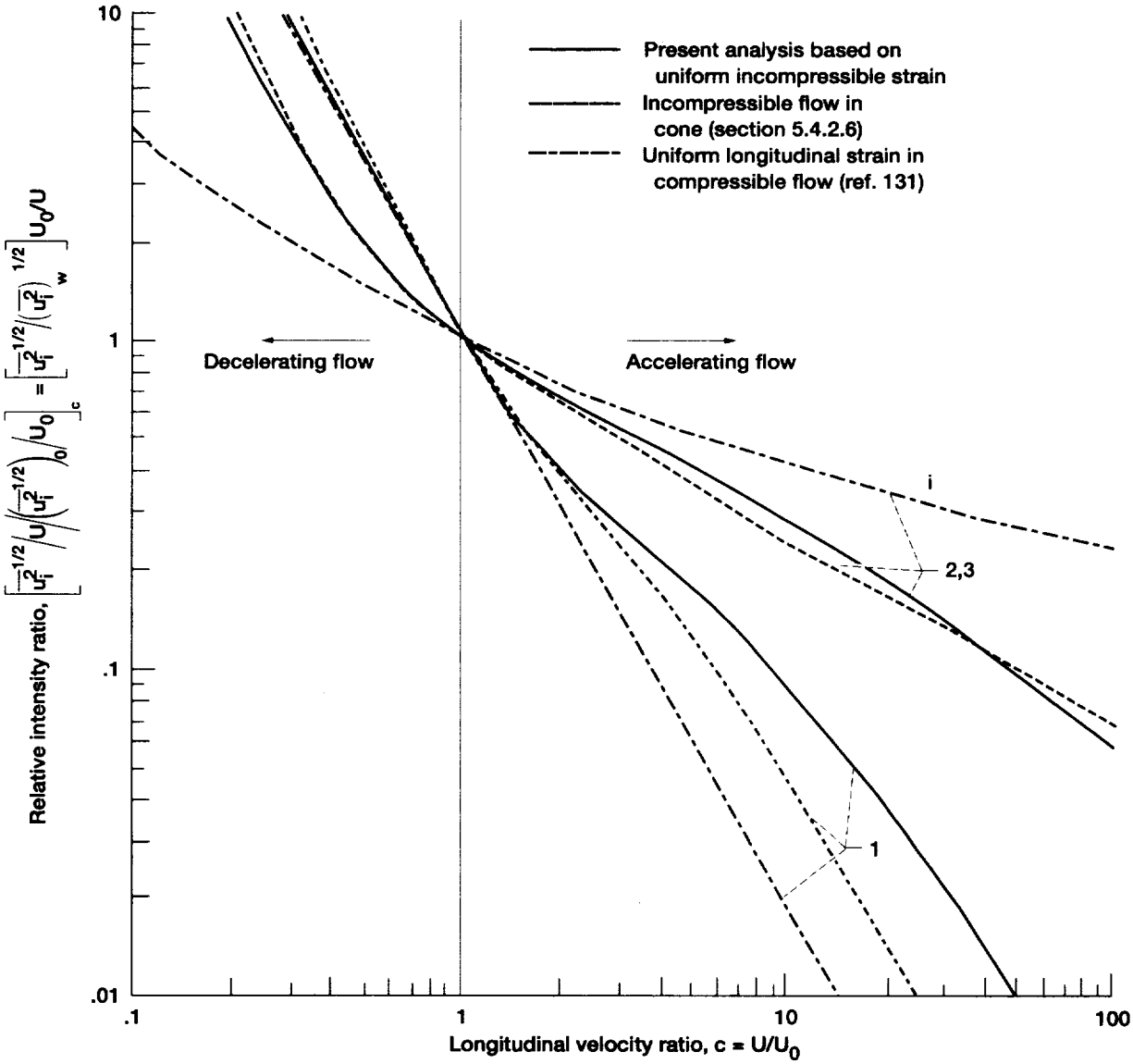

Figure 5-126.—Comparison of relative intensity ratios for turbulent components corrected to eliminate decay for several situations. The subscript c means corrected. The subscript w means without strain.

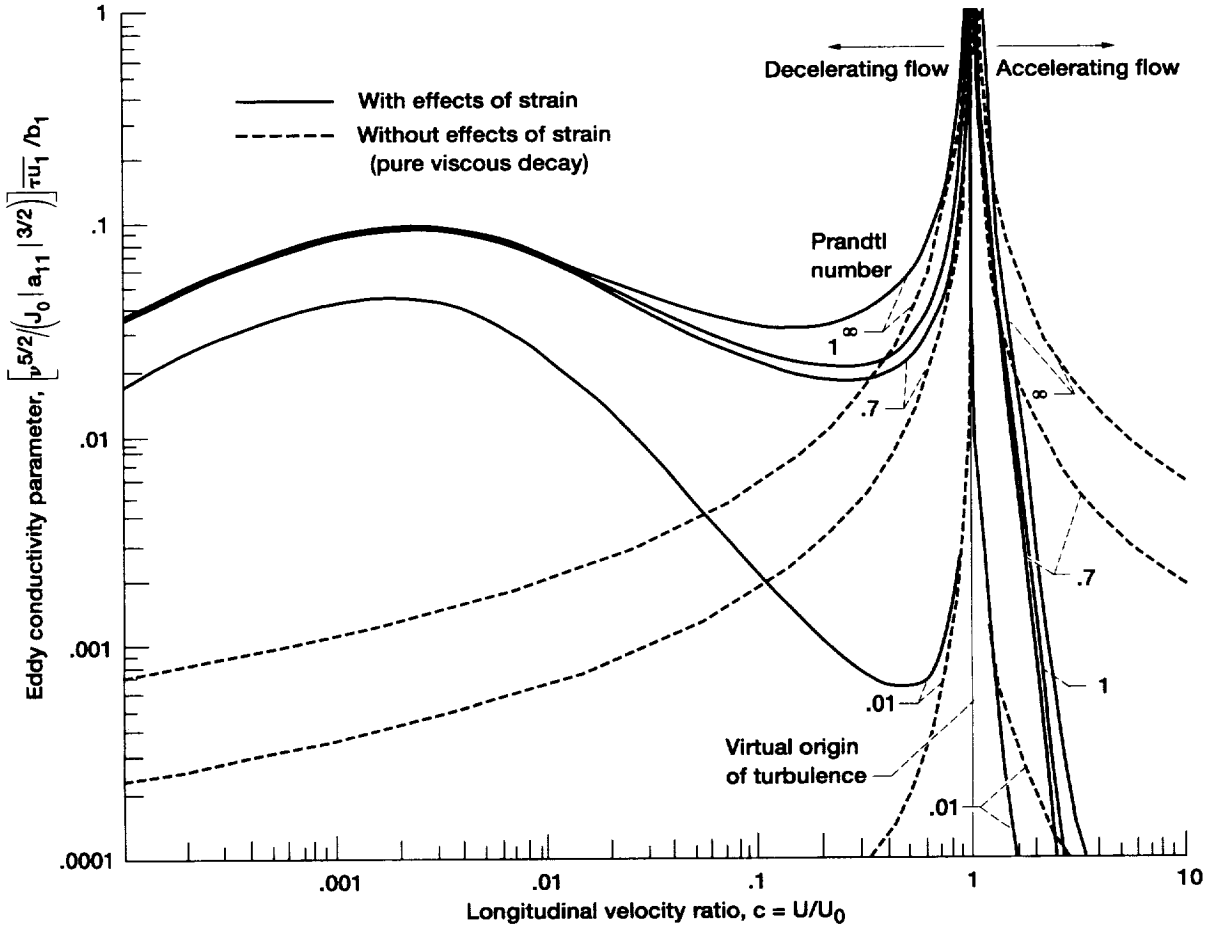

Figure 5-127.—Dimensionless longitudinal eddy conductivity for uniform incompressible strain.

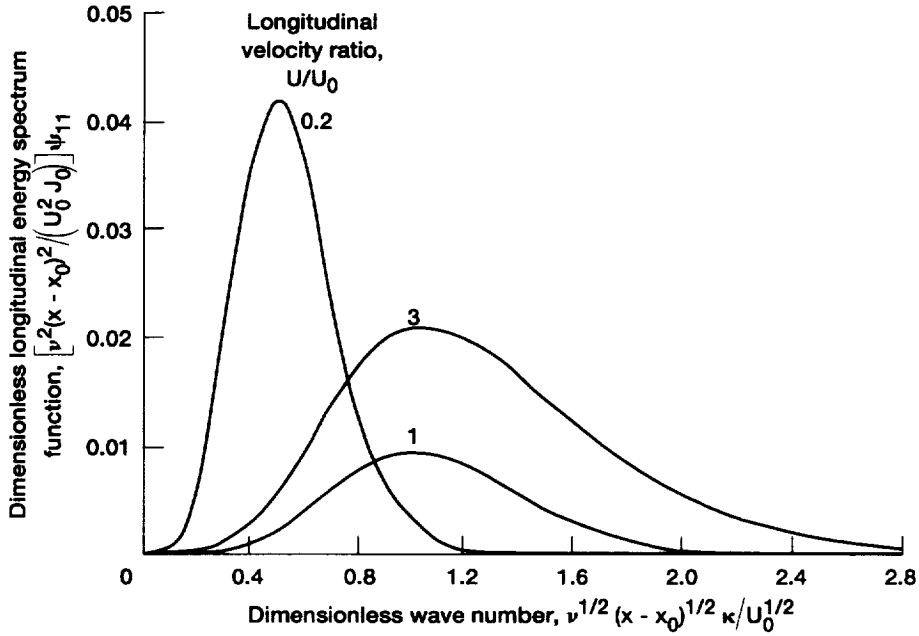

Figure 5-128.—Spectra of dimensionless longitudinal velocity variance $\overline{u_1^2}$.

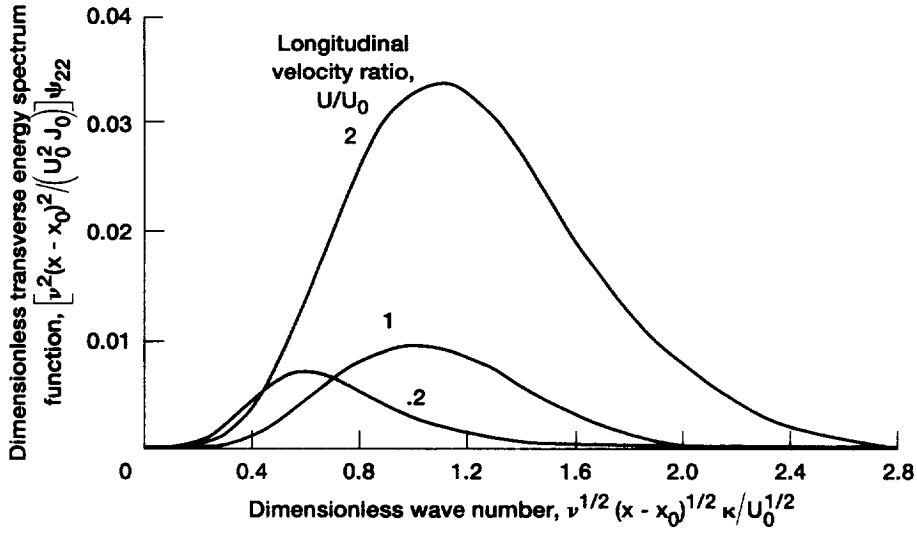

Figure 5-129.—Spectra of dimensionless transverse velocity variance $\overline{u_2^2}$.

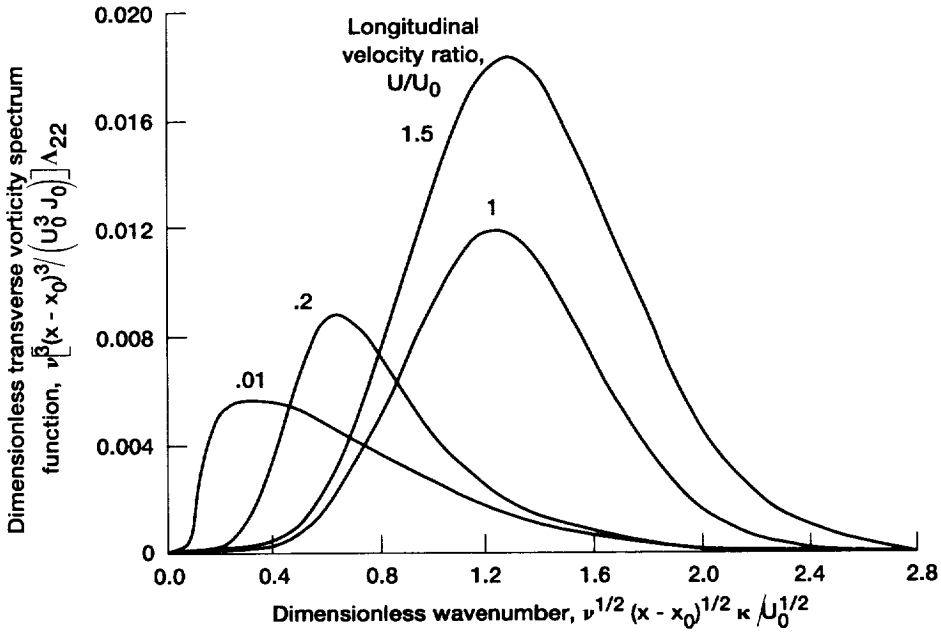

Figure 5-130.—Spectra of dimensionless transverse vorticity variance $\overline{\omega_2^2}$.

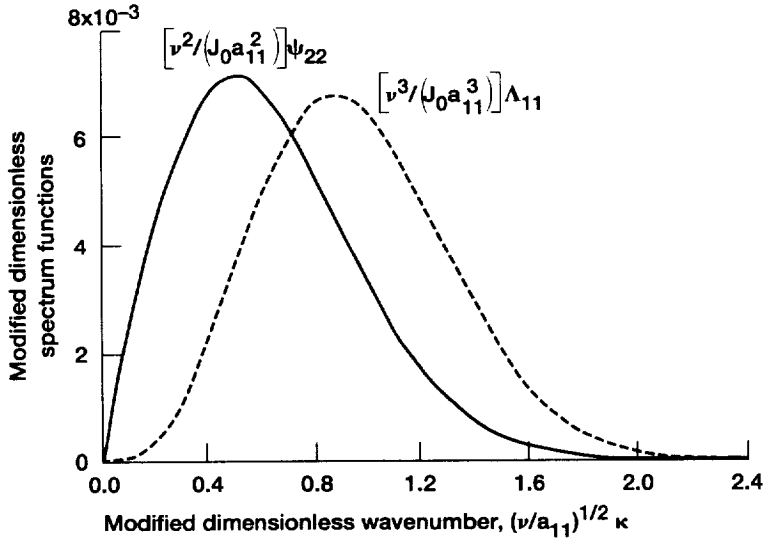

Figure 5-131.—Asymptotic equilibrium spectra for longitudinal velocity ratio $U/U_0 \to \infty$

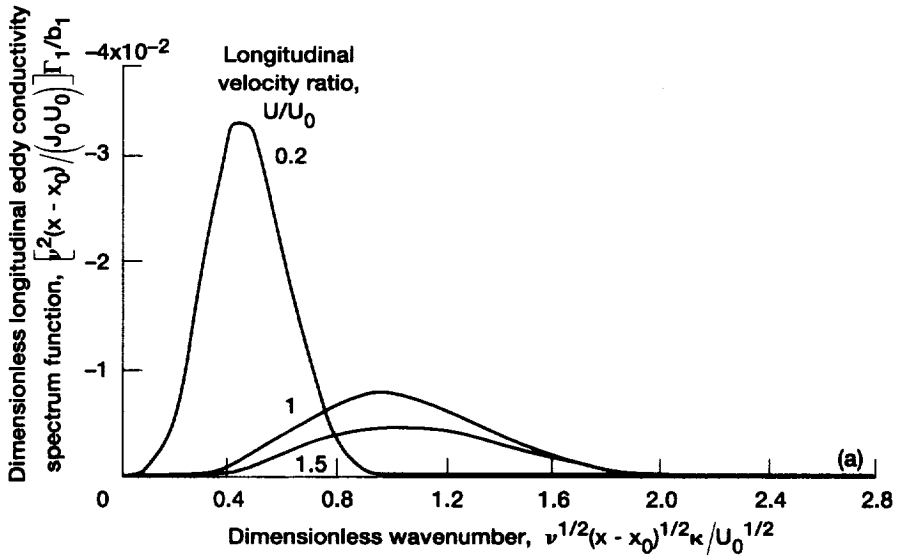

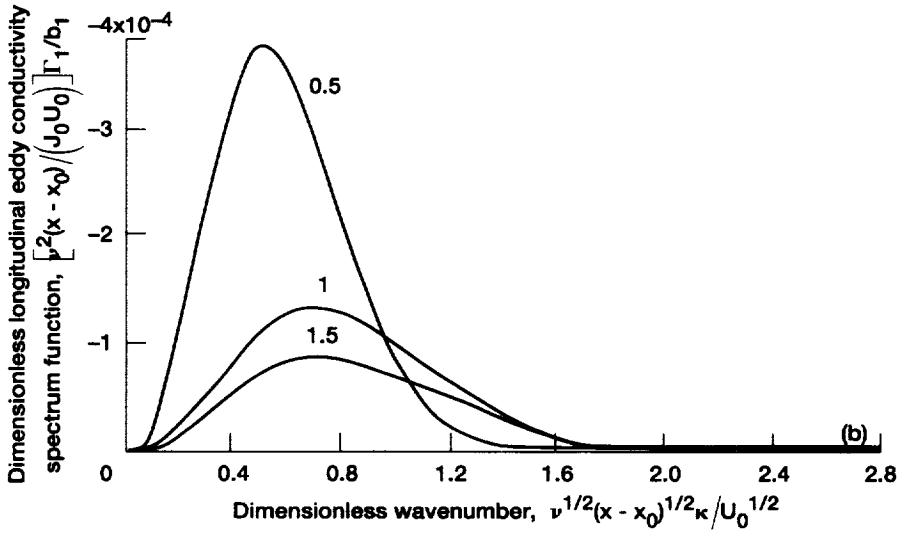

Figure 5-132.—Spectra of dimensionless longitudinal eddy conductivity $\overline{\tau u_1}$.
(a) Prandtl number, 0.70. (b) Prandtl number, 0.01.

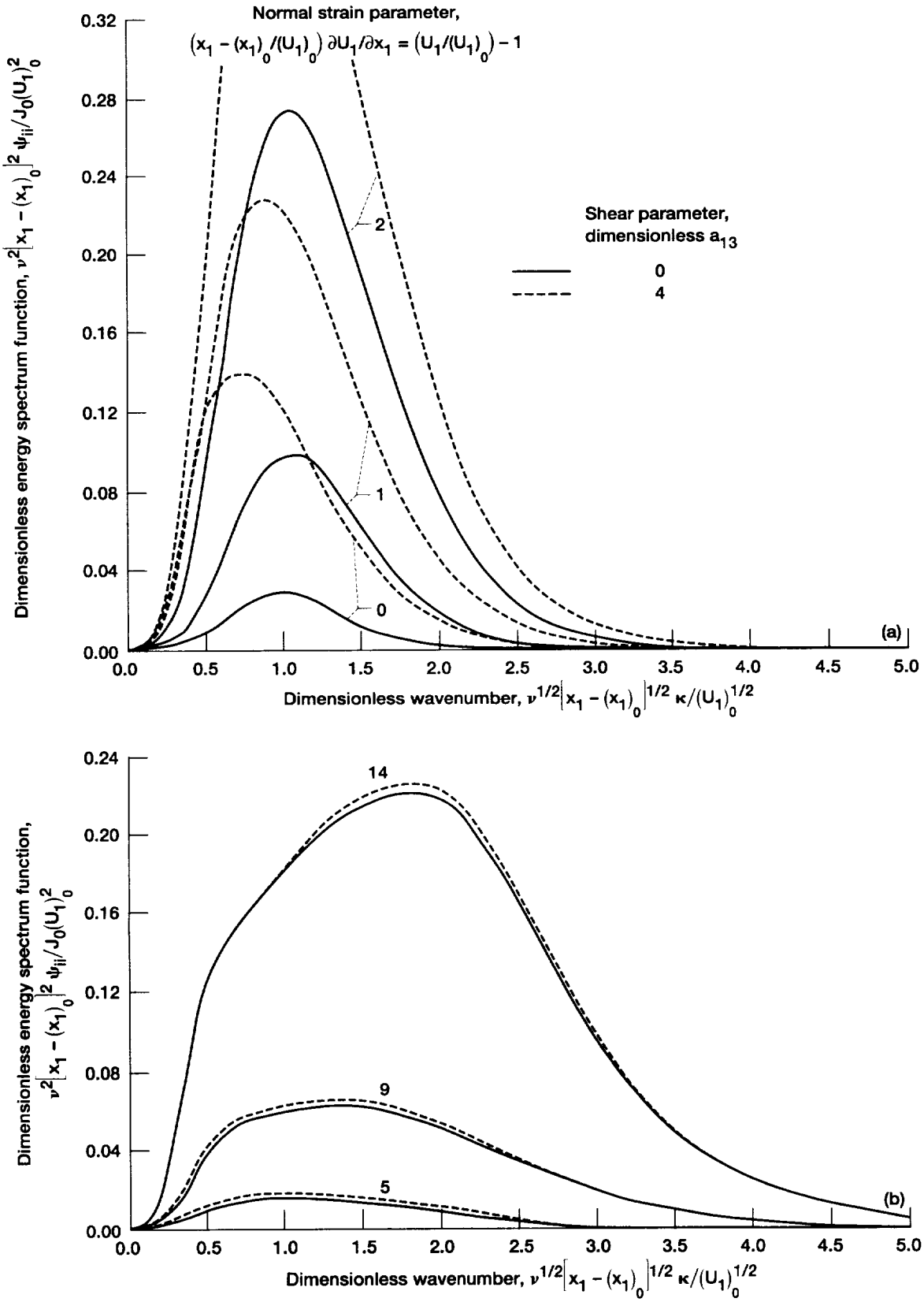

Figure 5-133.—Effects of uniform shear and normal strain on spectra of dimensionless turbulent energy. (a) Low values of normal strain parameter. (b) High values of normal strain parameter.

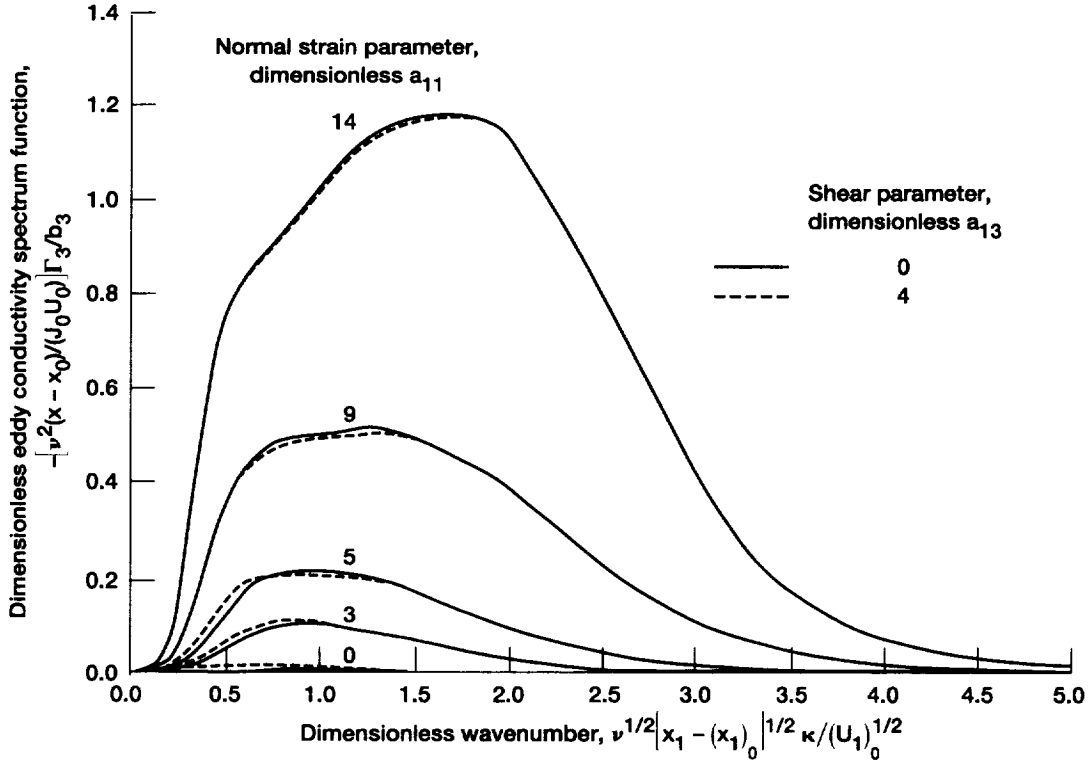

Figure 5-134.—Effects of uniform shear and of normal strain on spectra of dimensionless eddy conductivity; Prandtl number, 0.7.

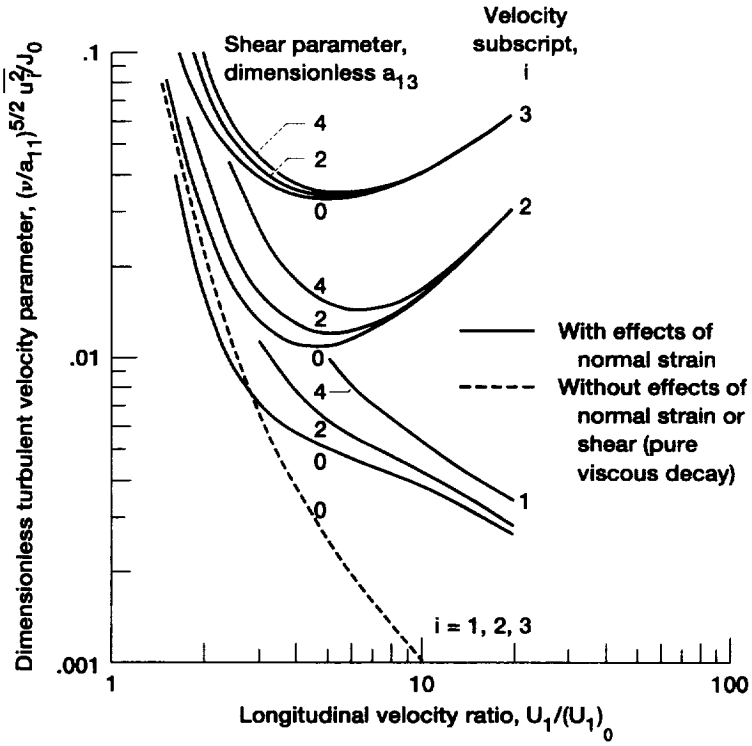

Figure 5-135.—Effect of uniform shear and of normal strain (or velocity ratio) on dimensionless variance of turbulent velocity components.

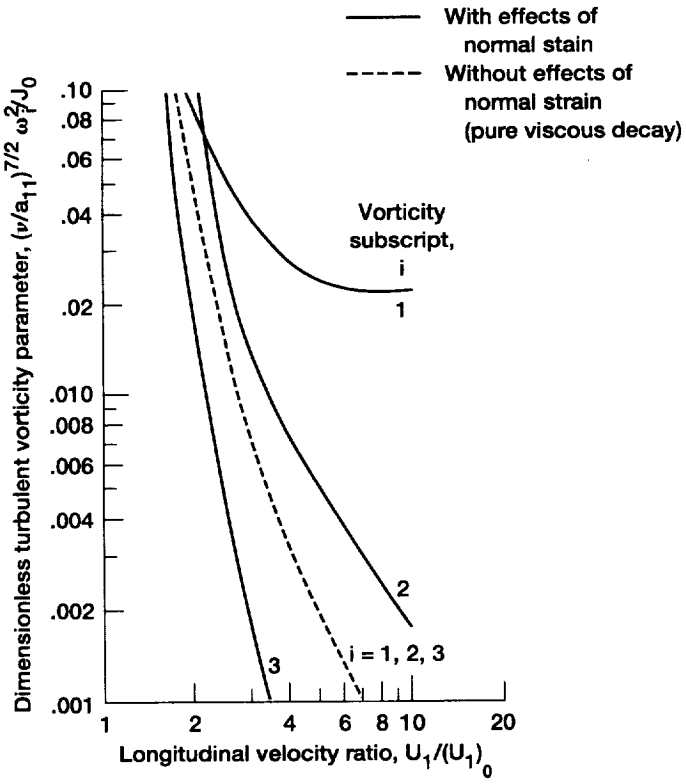

Figure 5-136.—Effect of uniform normal stain (or velocity ratio) on dimensionless variance of turbulent vorticity components; shear parameter, 0.

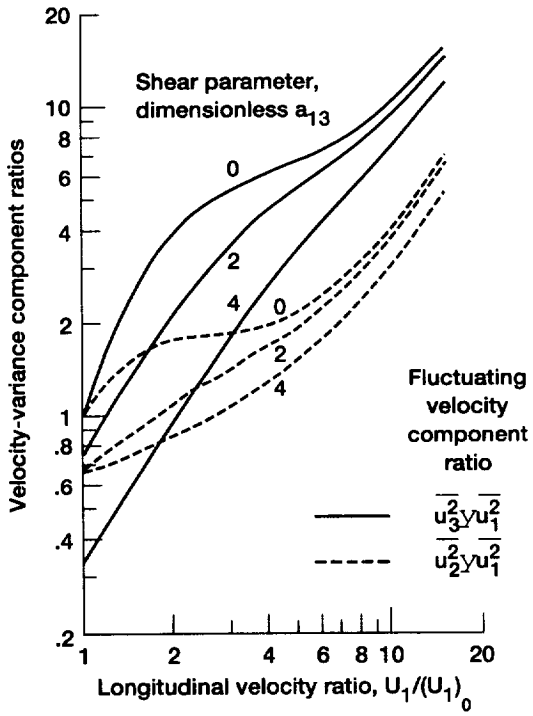

Figure 5-137.—Effect of uniform shear and of normal strain (or velocity ratio) on velocity-variance component ratios.

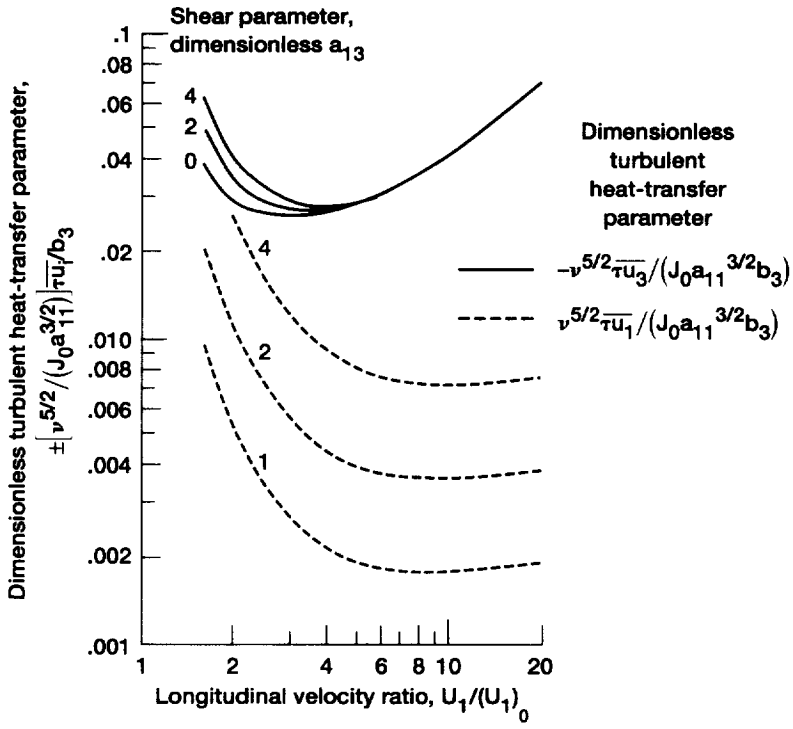

Figure 5-138.—Effect of uniform shear and of normal strain (or velocity ratio) on dimensionless temperature-velocity correlations; Prandtl number, 0.7.

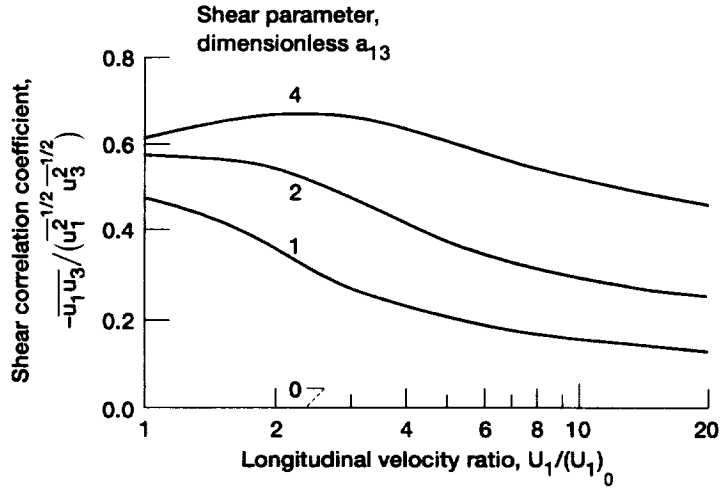

Figure 5-139.—Effect of uniform shear and of normal strain (or velocity ratio) on shear correlation coefficient.

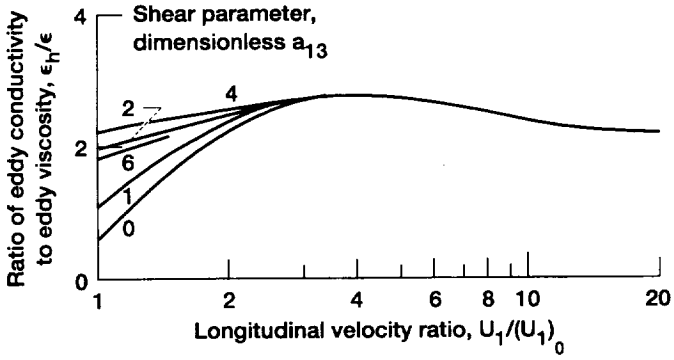

Figure 5-140.—Effect of uniform shear and of normal strain (or velocity ratio) on ratio of eddy conductivity to eddy viscosity; Prandtl number, 0.7.

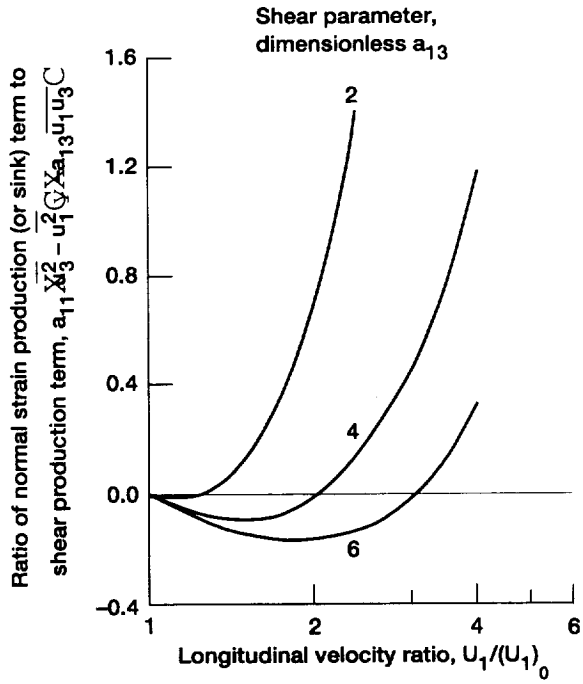

Figure 5-141.—Ratio of normal strain production (or sink) term to shear production term in turbulent energy equation (second and third terms in eq. (5-603) multiplied by ξ_1 and integrated over all wave numbers) as function of shear and of normal strain (or velocity ratio).

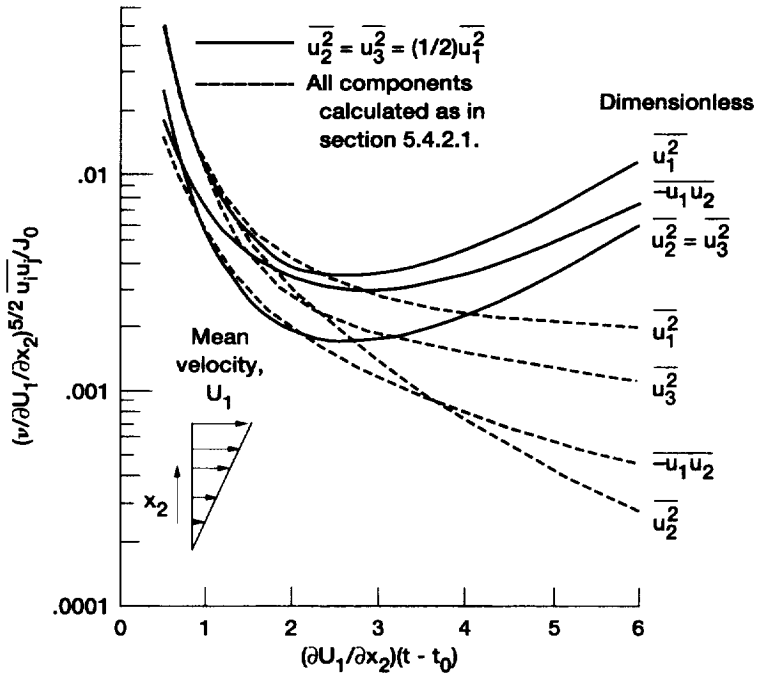

Figure 5-142.— Growth due to shear of weak , locally homogeneous turbulence when $\overline{u_2^2} = \overline{u_3^2} = (1/2)\overline{u_1^2}$, and comparison with case for all components calculated as in section 5.4.2.1, where energy is allowed to drain out of transverse components.

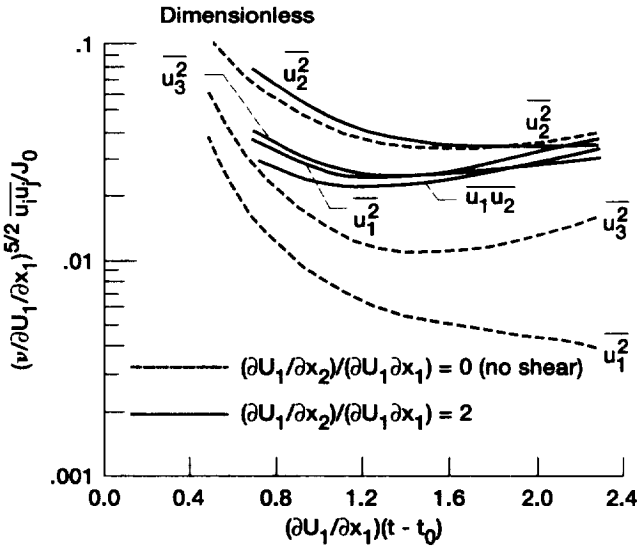

Figure 5-143.—Growth due to shear of weak, locally homogeneous turbulence with normal strain.

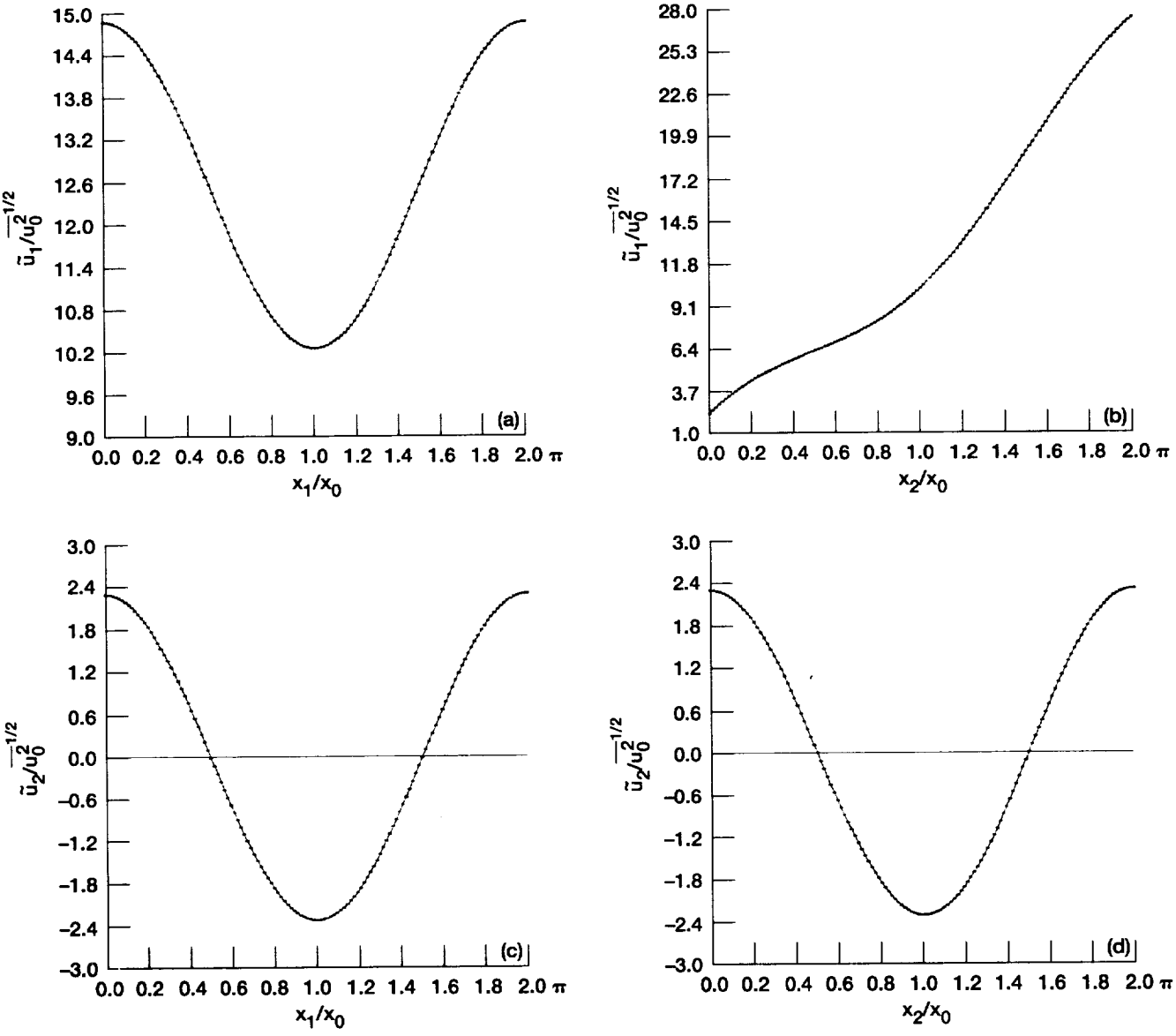

Figure 5-144.—Instantaneous profiles of velocity components $\tilde{u}_i$. Initial Reynolds number $R_0 = \overline{u_0^2}^{1/2} x_0/\nu = 34.68$, $(x_0^2/\nu)\, dU_1/dx_2 = 138.7$. (a) $(\nu/x_0^2)\, t = 0$, $x_2/x_0 = x_3/x_0 = \pi$. (b) $(\nu/x_0^2)\, t = 0$, $x_1/x_0 = x_3/x_0 = \pi$. (c) $(\nu/x_0^2)\, t = 0$, $x_2/x_0 = x_3/x_0 = \pi$. (d) $(\nu/x_0^2)\, t = 0$, $x_1/x_0 = x_3/x_0 = \pi$.

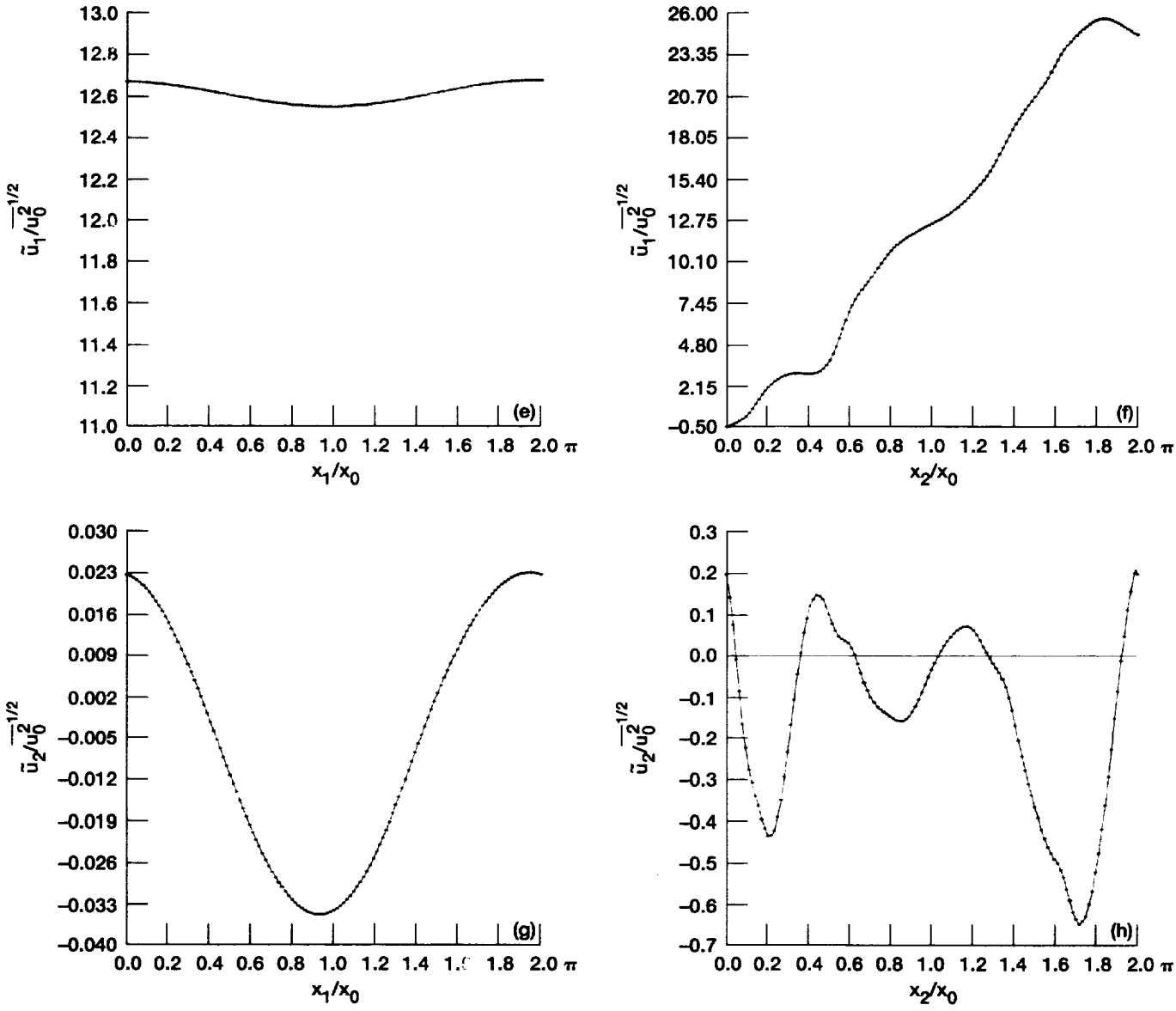

Figure 5-144.—Continued. (e) (ν/x_0^2) t = 0.1010, $x_2/x_0 = x_3/x_0 = \pi$. (f) (ν/x_0^2) t = 0.1010, $x_1/x_0 = x_3/x_0 = \pi$. (g) (ν/x_0^2) t = 0.1010, $x_2/x_0 = x_3/x_0 = \pi$. (h) (ν/x_0^2) t = 0.1010, $x_1/x_0 = x_3/x_0 = \pi$.

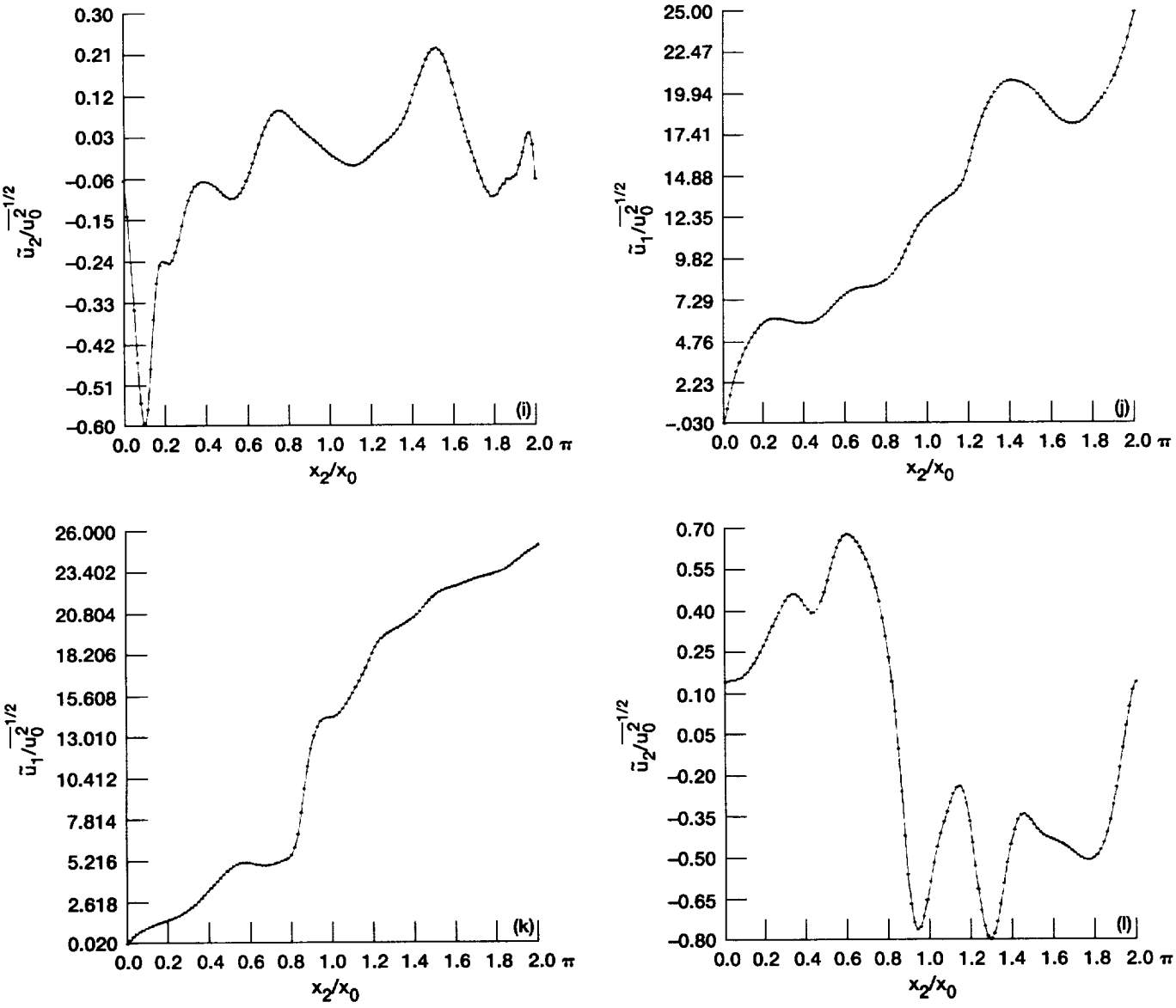

Figure 5-144.—Continued. (i) (ν/x_0^2) t = 0.1010, $x_1/x_0 = (37/32)\ \pi$, $x_3/x_0 = (47/32)\ \pi$. (j) (ν/x_0^2) t = 0.310, $x_1/x_0 = x_3/x_0 = \pi$. (k) (ν/x_0^2) t = 0.310, $x_1/x_0 = (37/32)\ \pi$, $x_3/x_0 = (47/32)\ \pi$. (l) (ν/x_0^2) t = 0.310, $x_1/x_0 = (37/32)\ \pi$, $x_3/x_0 = (47/32)\ \pi$.

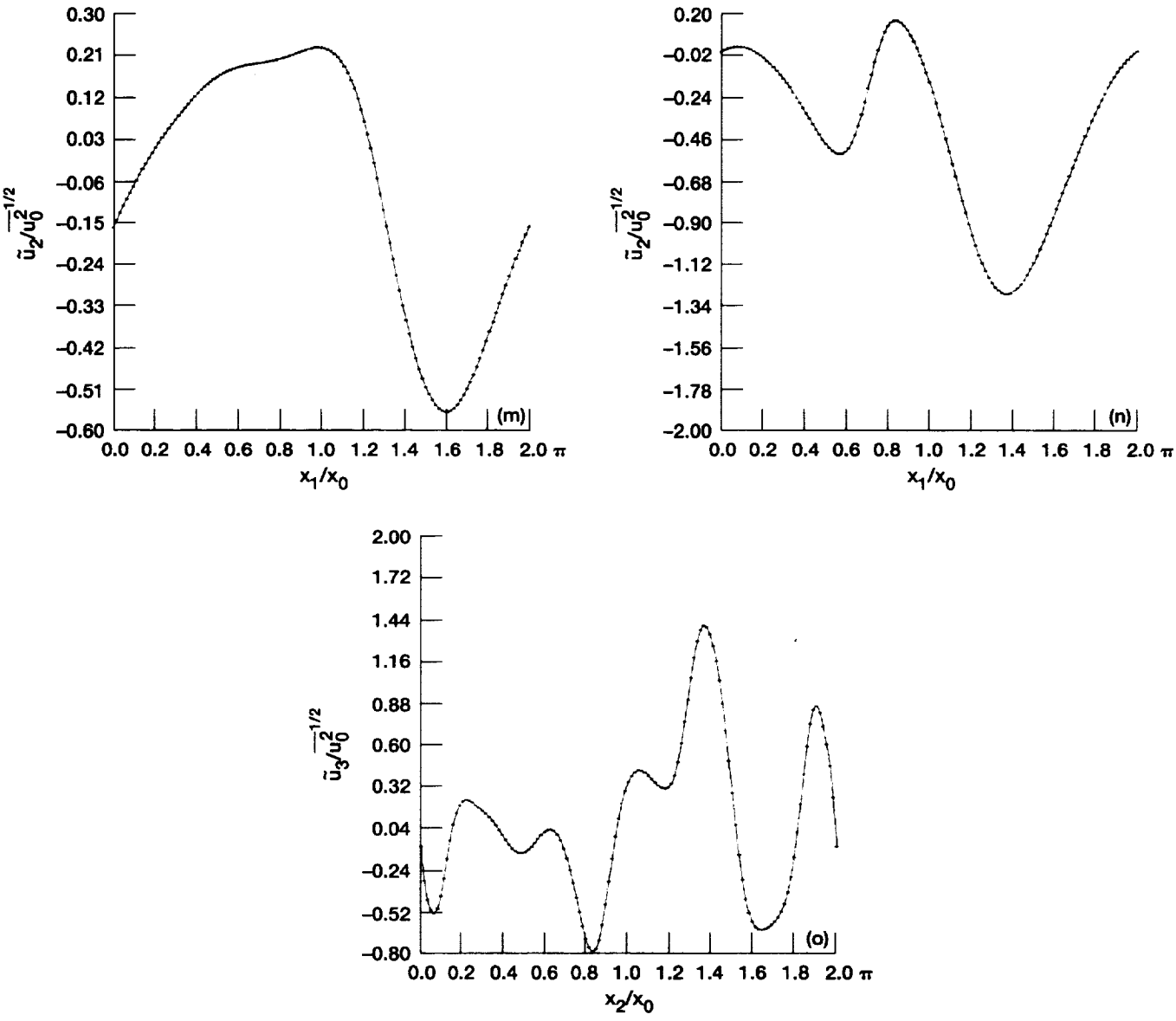

Figure 5-144.—Concluded. (m) $(\nu/x_0^2)\ t = 0.310$, $x_2/x_0 = \pi$, $x_3/x_0 = \pi$. (n) $(\nu/x_0^2)\ t = 0.310$, $x_2/x_0 = (41/32)\ \pi$, $x_3/x_0 = (47/32)\ \pi$. (o) $(\nu/x_0^2)\ t = 0.310$, $x_1/x_0 = \pi$, $x_3/x_0 = \pi$.

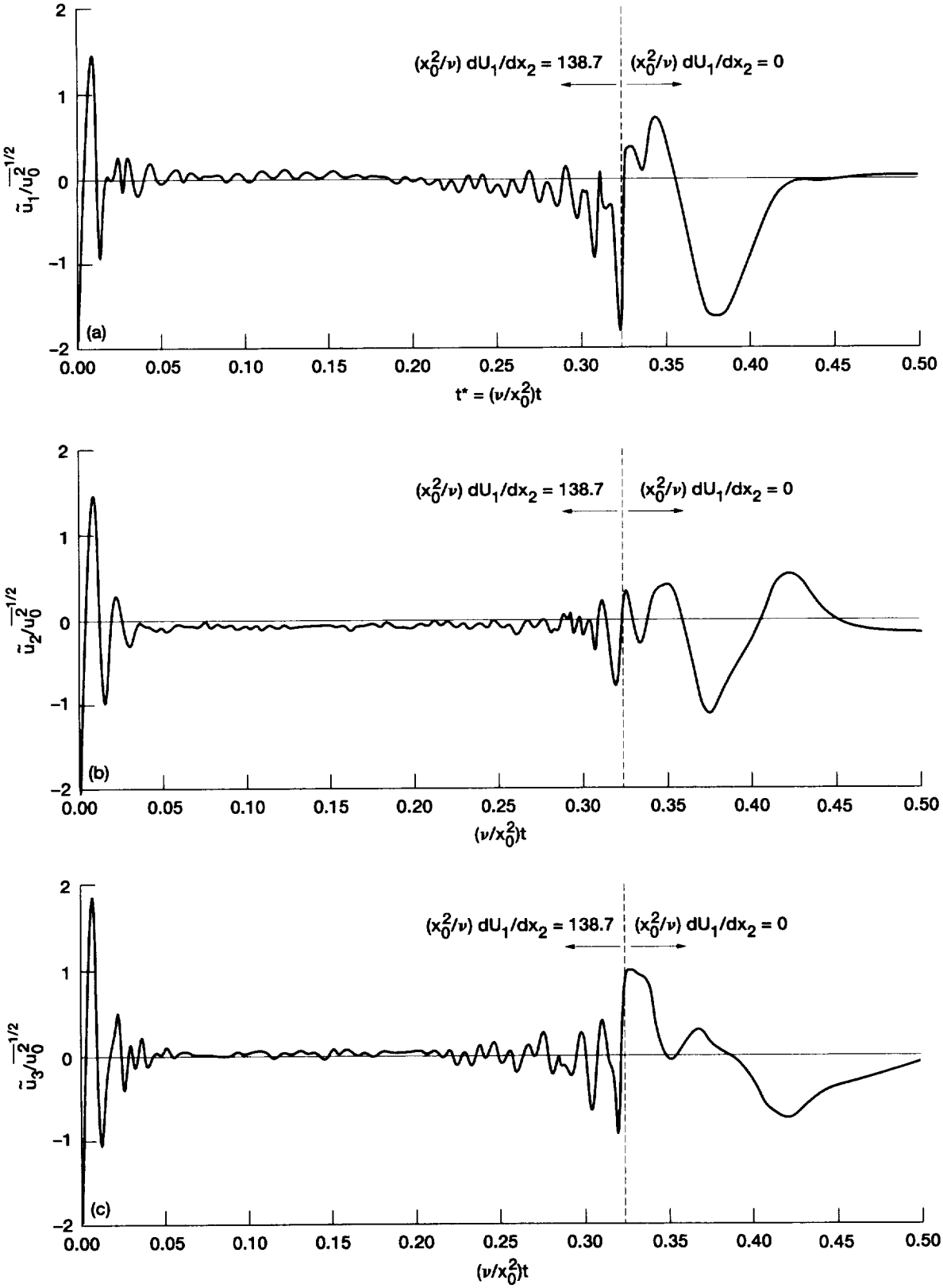

Figure 5-145.—Evolution of instantaneous velocity components at center of computational grid. $R_0 = \overline{u_0^2}^{1/2}$ $x_0/\nu = 34.68$. Mean shear removed at $t^* = 0.325$.

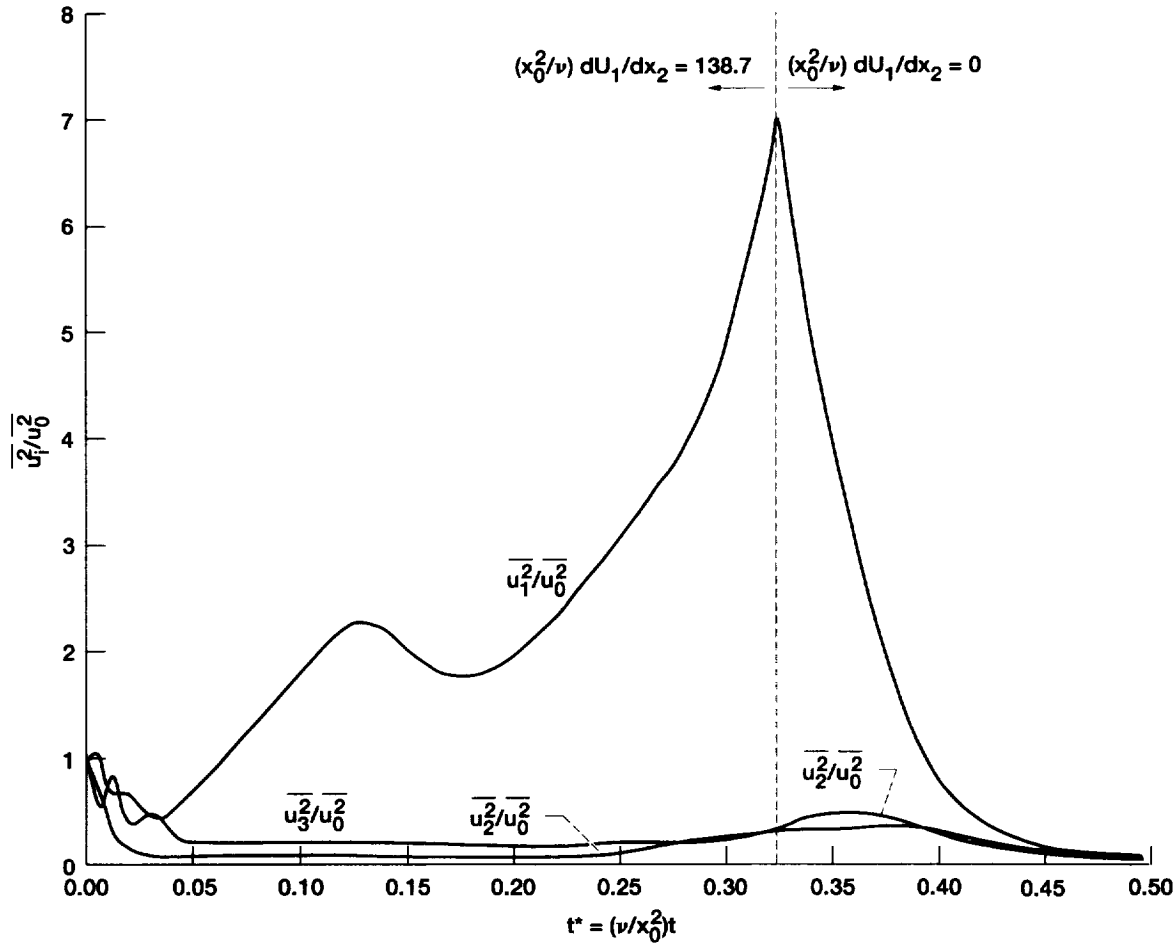

Figure 5-146.—Evolution of mean-square velocity components. $R_0 = \overline{u_0^2}^{1/2}\, x_0/\nu = 34.68$. Mean shear removed at $t^* = 0.325$.

REPORT DOCUMENTATION PAGE

Form Approved
OMB No. 0704-0188

1. AGENCY USE ONLY (*Leave blank*)	2. REPORT DATE	3. REPORT TYPE AND DATES COVERED
	August 1996	Technical Memorandum

4. TITLE AND SUBTITLE
Turbulent Fluid Motion V—Fourier Analysis, the Spectral Form of the Continuum Equations, and Homogeneous Turbulence

5. FUNDING NUMBERS
WU-505-90-53

6. AUTHOR(S)
Robert G. Deissler

7. PERFORMING ORGANIZATION NAME(S) AND ADDRESS(ES)
National Aeronautics and Space Administration
Lewis Research Center
Cleveland, Ohio 44135-3191

8. PERFORMING ORGANIZATION REPORT NUMBER
E-9374

9. SPONSORING/MONITORING AGENCY NAME(S) AND ADDRESS(ES)
National Aeronautics and Space Administration
Washington, D.C. 20546-0001

10. SPONSORING/MONITORING AGENCY REPORT NUMBER
NASA TM-106825

11. SUPPLEMENTARY NOTES
Responsible person, Robert G. Deissler, organization code 0130, (216) 433-5823.

12a. DISTRIBUTION/AVAILABILITY STATEMENT
Unclassified - Unlimited
Subject Category 34

This publication is available from the NASA Center for Aerospace Information, (301) 621-0390.

12b. DISTRIBUTION CODE

13. ABSTRACT (*Maximum 200 words*)

Background material on Fourier analysis and on the spectral form of the continuum equations, both averaged and unaveraged, are given. The equations are applied to a number of cases of homogeneous turbulence with and without mean gradients. Spectral transfer of turbulent activity between scales of motion is studied in some detail. The effects of mean shear, heat transfer, normal strain, and buoyancy, are included in the analyses.

14. SUBJECT TERMS
Turbulence; Fourier analysis; Spectrum; Homogeneous

15. NUMBER OF PAGES
250

16. PRICE CODE
A11

17. SECURITY CLASSIFICATION OF REPORT	18. SECURITY CLASSIFICATION OF THIS PAGE	19. SECURITY CLASSIFICATION OF ABSTRACT	20. LIMITATION OF ABSTRACT
Unclassified	Unclassified	Unclassified	